THE JOURNAL OF PHYSICAL CHEMISTRY

VOLUME 67, NUMBER 3 MARCH, 1963

COMMUNICATION TO THE EDITOR

AUTHOR INDEX

THE JOURNAL OF
PHYSICAL CHEMISTRY

(Registered in U. S. Patent Office)

VOLUME 67, NUMBER 3 MARCH 15, 1963

THE EFFECT OF BENZENE MODERATOR ON THE (n,γ) ACTIVATED REACTIONS OF BROMINE ATOMS WITH ETHYL BROMIDE

BY MIRIAM MILMAN

Ecole Normale Supérieure, Laboratoire de l'Accélérateur Linéaire B.P. 5, Orsay (Seine et Oise), France

Received January 11, 1962

The nature of the chemical reactions following neutron capture in mixtures of ethyl bromide and benzene were studied. After having ascertained the own reactivity of the benzene moderator, it was possible to determine the contribution of "hot" and "diffusive" reactions to the yield of organic activity. A tentative description of the nature of reactions following radiative neutron capture in the solid system is proposed.

Introduction

A nucleus absorbing a thermal neutron emits the excess energy in the form of one or more γ-rays. As a result of the radiative emission the atom acquires recoil energy, positive charge due to internal conversion or Auger electron emission, and also can be left in an excited state. The activated atom can enter stable chemical combinations after having lost some of its excess energy in successive collisions with the surrounding molecules; the experimental evidence seems to point out[1] that if the medium is closely packed (liquid or solid phase) charge and excitation energy also are lost in this process.

The atoms having a kinetic energy higher than the thermal energy of the environment are called "hot atoms" and their chemical reactions are known as "hot reactions"; they have the following characteristic features which distinguish them from the reactions of the same atom at thermal energies: (a) Their yield is temperature independent. (b) Since they take place after only a limited number of collisions of the recoiling atom, their yield is not affected by small concentrations of scavengers added to remove thermalized free radicals. The use of scavengers in the study of the chemical effects of nuclear transformations helped to give a measure of the yield of reactions taking place in the immediate vicinity of the capture event and of those taking place further away, after the active atom and free radicals start diffusing ("diffusive reactions").[2] (c) Hot reactions are sensitive to additives (moderators) that remove the kinetic, vibrational, or electronic energy of the excited species.

Recent studies[3] of the hot hydrogen reactions in gaseous hydrocarbons have led to the development of a model that was successfully applied to tritium and methane reactions moderated by inert gases, and also was used[4] to estimate the contribution of reactions due to the kinetic energy of hot bromine and iodine in methane.

Unless inert gases are used as moderators, the reactions of the hot atom with the additive further complicate the interpretation of the results.

The work described in this paper was undertaken to investigate the influence of the addition of benzene moderator on the organic yield in liquid and solid ethyl bromide.

Experimental

Materials.—Ethyl bromide (chemically pure, Touzard and Matignon) was purified as described previously.[5] The retention (percentage of the total activity in organic combinations) of 32%, now generally admitted for neutron irradiated ethyl bromide in the presence of about 10^{-5} molar fraction of bromine, was used as a criterion for the desired purity of the material.

The benzene (Merck p.p.a.) was stored in daylight with elementary bromine for about 30 min., to saturate olefinic impurities. To avoid extensive addition of bromine to benzene this treatment must not be prolonged, and further processing is necessary. After extraction of excess bromine with aqueous bisulfite and drying over magnesium sulfate, the benzene was shaken with successive portions of concentrated sulfuric acid (until the acid remained colorless) followed by extractions with sodium bicarbonate solutions and water. The material was dried over magnesium sulfate, filtered, and distilled in a column (50-cm. length, 1.5-cm. diameter) packed with glass helices. The middle 50% was retained and passed dropwise (directly from the condenser attached to the distillation column) through a chromatographic column (50-cm. length, 1.5-cm. diameter) filled with silica gel (chromatographic grade). The benzene obtained in this way was recrystallized from an ice bath, discarding about 15%.

(1) M. Milman, *Radiochim. Acta*, **1**, 15 (1962).

(2) (a) F. S. Rowland and W. F. Libby, *J. Chem. Phys.*, **21**, 1495 (1953); (b) L. Friedman and W. F. Libby, *ibid.*, **17**, 647 (1949); (c) F. Goldhaber, R. S. Chiang, and J. E. Willard, *J. Am. Chem. Soc.*, **73**, 2271 (1951); (d) G. Levey and J. E. Willard, *ibid.*, **74**, 6161 (1952); (e) M. Milman and P. F. D. Shaw, *J. Chem. Soc.*, 1303 (1957); (f) N. Knight, G. E. Miller, and P. F. D. Shaw, *J. Inorg. Nucl. Chem.*, **23**, 15 (1961).

(3) P. J. Estrup and R. Wolfgang, *J. Am. Chem. Soc.*, **82**, 2661, 2665 (1960).

(4) (a) E. P. Rack and A. A. Gordus, *J. Chem. Phys.*, **34**, 1855 (1961); (b) *J. Phys. Chem.*, **65**, 944 (1961).

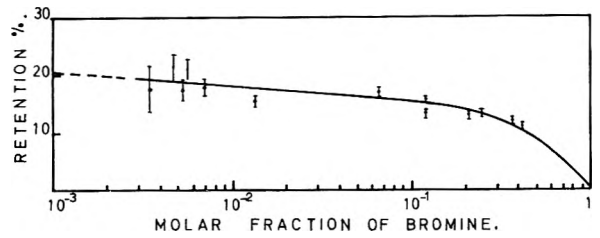

Fig. 1.—Scavenger effect of bromine on the reactions of Br^{80} activated by the (n,γ) process with benzene (semi-log plot).

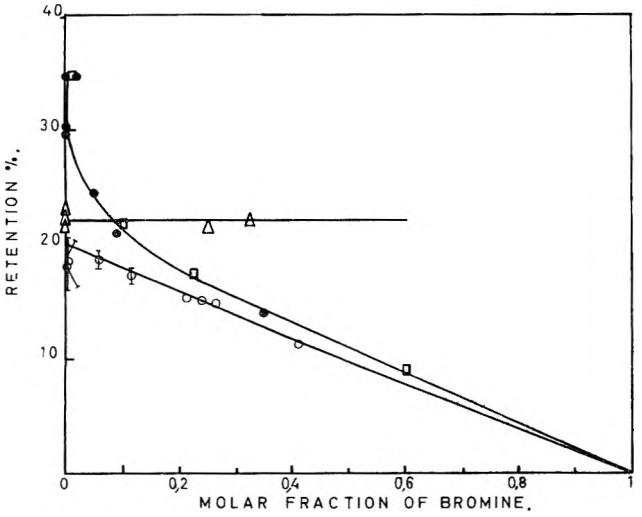

Fig. 2.—Scavenger effect of bromine on the reactions of Br^{80} with: O, benzene (liquid); △, benzene (solid); ●, hexane (liquid); □, cyclohexane (liquid).

The hexane and cyclohexane were purified using the same procedure as for benzene.

Neutron Irradiations and Determination of Organic Yields.—The irradiations were performed with a 1.5-curie polonium–beryllium neutron source. The geometry and experimental procedure after irradiation have been described in an earlier work.[5] The samples were irradiated for 40 min. and only Br^{80} (half-life of 18 min.) was studied; for longer irradiations, or for delayed counting of the activity, second measurements were made in order to account for the presence of any Br^{80m} (half-life of 4.4 hr.). The results were corrected for density variations and, when necessary, for dilution.

Results and Discussion

Reactivity of Moderators.—It was found previously[6] that the presence of pentane, hexane, heptane, and decane in neutron-irradiated ethyl bromide and iodide leads to an increase of the organic retention (in the order mentioned above), and that this increase was practically independent of the presence of scavenger. This was interpreted to mean that the higher the molecular size of the solvent the more effective is the caging of fragments in the recoil volume, hence the higher the yield due to "hot reactions".[7] On the other hand, the organic yield of bromine from irradiated carbon tetrabromide dissolved in ethyl alcohol was found in an early experiment to fall to zero at high dilutions.[8]

This apparent contradiction shows the complexity of the problem and suggests that the sensitivity of the solvent to hot halogen atom attack has to be ascertained before drawing conclusions about mechanisms of moderation and dilution.

(5) M. Milman, *J. Am. Chem. Soc.*, **80**, 5592 (1958).
(6) S. Aditya and J. E. Willard, *ibid.*, **79**, 3367 (1957).
(7) The term "hot reactions" as used in ref. 6 applies to direct displacement reactions as well as to the thermal recombination reactions of the tagged atom with radicals it has formed in the slowing down process. For a detailed discussion of this interpretation see ref. 1.
(8) W. F. Libby, *J. Am. Chem. Soc.*, **62**, 1930 (1940).

In order to determine the specific reactivity of the moderators, the scavenger curves (the organic yield as a function of bromine concentration) for benzene, hexane, and cyclohexane were established, and are shown in Fig. 1 and 2. A comparison of the behavior of the three hydrocarbons clearly shows that in the case of benzene there is no sharp fall of the retention for small concentrations of bromine scavenger.

The retention obtained from the extrapolation of the scavenger curve to zero bromine concentration was taken as the extent to which the moderator reacts with halogen in the absence of scavenger. Using the least mean squares method, the value obtained for benzene was R [liquid benzene] = 20.5 ± 0.2%.

Similar irradiations of quickly frozen mixtures of benzene and bromine gave an organic yield of 22.0 ± 0.4% that remained constant (within experimental error) over the range of scavenger concentrations studied (Fig. 2).

In all the cases in which a radical scavenger is present during the irradiation of an organic bromide or iodide, small concentrations of additive cause a large drop of the organic retention, indicating its interference with the formation of radiohalides by diffusion controlled reactions. As the scavenger concentration is increased, the fall of retention is less abrupt and is attributed to the presence of the molecular halogen at the very site of the capture event.[2] In the case of bromine and hydrocarbon mixtures, an extremely small fraction of the halogen (about 10^{-14} molar fraction) is activated by the capture process and the rest acts as an ordinary scavenger. In consequence the scavenger curves of such systems should have the usual shape. This was found to be the case for bromine and hexane or cyclohexane mixtures and also for other hydrocarbon halogen systems.[9] As can be seen from Fig. 1 and 2 benzene seems to be an exception, as the retention is independent of bromine concentration over quite a big range (3×10^{-3} to 7×10^{-2}), and falls linearly with higher concentrations of scavenger (10^{-1} to 1 molar fraction). The absence of a marked scavenger effect in benzene and bromine (or iodine[9b]) systems indicates that no organic radicals are available for diffusive reactions with the tagged atom. This can be due to the known stability of the benzene molecule; its low G-values are currently[10] attributed to a self-protection effect characteristic of the highly resonant structure, so that any excitation energy is distributed immediately over the whole molecule without any decomposition. It is quite possible that benzene shows the same inertia to the collisions with hot halogen atoms.

On the other hand it was found by Evans[11] that 85% of the organic retention of active bromine in benzene is due to the formation of bromobenzene, the rest being dibromo compounds. Hence, the only radical apparently involved is the phenyl radical (to a lesser extent the bromophenyl radical). This radical can be removed either by immediate recombination with the active bromine atom

$$C_6H_5\cdot + Br^* \longrightarrow C_6H_5Br^*$$

or by the reaction

$$C_6H_5\cdot + C_6H_6 \longrightarrow C_6H_5\cdot C_6H_5 + H\cdot$$

(9) (a) C. E. McCauley and R. Schuler, *J. Phys. Chem.*, **62**, 1364 (1958); (b) P. F. D. Shaw, private communication.
(10) S. Gordon and M. Burton, *Discussions Faraday Soc.*, **12**, 88 (1952).
(11) J. B. Evans, Ph.D. Thesis, University of Wisconsin, 1957.

a type of reaction with is known to occur[9b,12] only in aromatic systems. The result of the competition between the two reactions would be that the phenyl radicals would react to become diphenyl before having a chance to meet the thermalized active bromine atom.

Effect of Moderator. (a) **Liquid Phase.**—The effect of benzene moderator on the retention of activity in liquid mixtures of ethyl bromide and benzene (in the presence of 3×10^{-3} molar fraction of bromine) is shown in the upper curve of Fig. 3. To estimate the contribution of hot reactions to the total organic yield in benzene and ethyl bromide mixtures, it was necessary to establish the scavenger curves for a number of specific mixtures of the two components. The results are given in Table I. The part of the retention due to hot reactions is given by the intercept on the axis (at zero scavenger concentration) of the back-extrapolated scavenger curves at high bromine concentration.[2e] These values as well as those obtained from the irradiation of ethyl bromide and benzene (at vanishingly small scavenger concentration) were corrected for the presence of 3×10^{-3} molar fraction of bromine during the irradiation of the moderated systems studied and are plotted in Fig. 3, curve h.

Table I

Molar fraction of benzene	Molar fraction of Br_2	Retention, %	Retention due to hot reactions, %[a]
0	6.0×10^{-4}	30.0	18.4
	2.4×10^{-1}	14.0	
	3.7×10^{-1}	11.4	
	5.0×10^{-1}	9.3	
1.8×10^{-1}	6.0×10^{-4}	29.0	19.2
	2.4×10^{-1}	14.7	
	3.8×10^{-1}	12.0	
	4.5×10^{-1}	10.6	
3.7×10^{-1}	6.0×10^{-4}	28.0	19.7
	2.4×10^{-1}	15.0	
	3.9×10^{-1}	12.2	
	4.5×10^{-1}	10.8	
7.8×10^{-1}	2.4×10^{-1}	14.9	20.0
	4.0×10^{-1}	12.5	
1	2.5×10^{-1}	15.2	20.5[b]
	4.0×10^{-1}	12.2	

[a] Determined using the back-extrapolation method.[2e] [b] See also Fig. 1 and 2.

For a system of two components it is probable that the retention due to thermal diffusive reactions should be a sum of two independent terms

$$R \text{ (diffusive)} = \text{mol. fr.}_1 \cdot R_1 + \text{mol. fr.}_2 \cdot R_2$$

where R_1 and R_2 are the diffusive retentions for the pure substance and mol. fr.$_1$ and mol. fr.$_2$ their respective molar fractions.

It was shown in the first paragraph of the Discussion that in the case of benzene there are hardly any thermal diffusive reactions. Consequently we expect the thermal retention in a mixture of ethyl bromide–benzene to be a function of the concentration of ethyl bromide only. In other words benzene acts as a diluent and the yield of such reactions will be proportional to (1 − molar fraction of benzene). This was verified to be the case by subtracting the experimentally determined retention due to hot reactions (see Table I) from the total retention. The result is the linear plot starting at R (diffusive) = 9.6% for pure ethyl bromide and decreasing linearly to R (diffusive) = 0 for pure benzene.

(12) (a) For review see D. R. Augood and G. H. Williams, *Chem. Rev.*, **57**, 123 (1957); (b) W. A. Waters, "The Chemistry of Free Radicals," Second Ed., Oxford Clarendon Press, 1950, p. 149

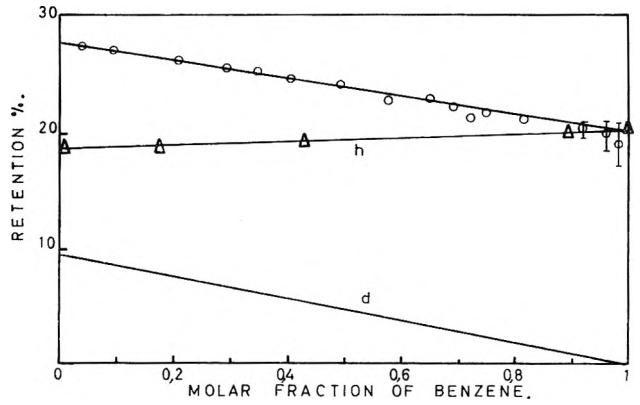

Fig. 3.—Liquid phase: effect of benzene moderator on the reactions following the (n,γ) process in ethyl bromide (3×10^{-3} molar fraction bromine scavenger present): curve h, retention due to "hot" reactions; curve d, retention due to "diffusive" reactions.

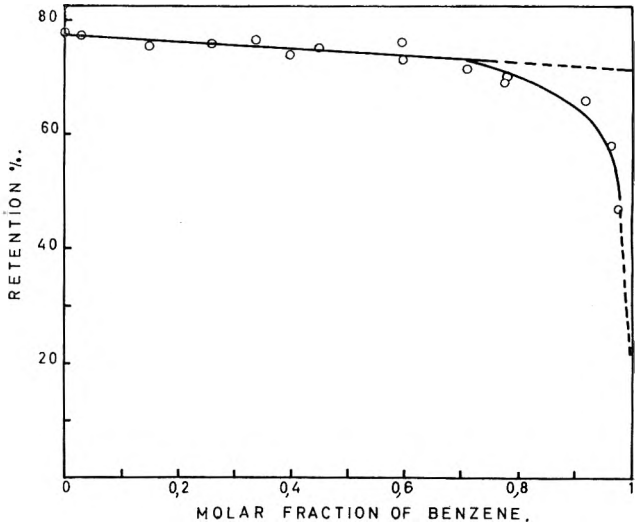

Fig. 4.—Solid phase: effect of benzene moderator on the reactions following the (n,γ) process in ethyl bromide (3×10^{-3} molar fraction bromine scavenger present). The irradiations were performed at −196°.

(b) **Solid Phase.**—Any conclusions drawn from the radiolytic or radiochemical studies of solid mixtures are subject to the condition of homogeneity. Owing to the scarcity of data available on the parameters of molecular crystals and even more so about mixtures of substances forming molecular crystals, it is difficult to affirm with certainty that quickly frozen mixtures of hydrocarbons, organic halides, and halogen have kept the same homogeneity as in the liquid phase.

In the following study it is assumed that the extremely small size of the crystals obtained by abrupt freezing is a sufficient condition to establish a homogeneous distribution of the reagents. This is evidently an approximation confirmed only by the results of the Laue X-ray back reflection analysis[5] and by the reproducibility of our results for a given mixture. Having this restriction in mind, the interpretation of the results from solid phase (n,γ) reactions in C_2H_5Br and C_6H_6 mixtures is only tentative.

It was found previously that diffusion controlled reactions hardly contribute to the total organic yield in solid ethyl bromide[6] and the retention of activity in solid benzene is independent of bromine concentration up to about 3×10^{-1} molar fraction of scavenger (Fig. 2). There are thus very good reasons to believe that the chemical reactions following neutron capture in solid ethyl bromide–benzene mixtures are confined to isolated regions in the immediate vicinity of the recoil. It is expected that the organic yield of the system should decrease from $R = 78\%$ for pure ethyl bromide to 22% for pure benzene.

As can be seen from Fig. 4 the retention seems to vary linearly to an extrapolated value of 71.5%, but the experimental points fall abruptly for benzene concentrations greater than 0.8 molar fraction to a value of presumably 22% characteristic for pure solid benzene.

The abrupt change in retention for the addition of small amounts of ethyl bromide to benzene can be explained either by energy transfer from excited benzene molecules to ethyl bromide that can decompose further, or by competition between reactions of the type

$$C_6H_5\cdot + C_6H_6 \longrightarrow C_6H_5\cdot C_6H_5 + H\cdot \quad (1)$$

which does not produce radicals susceptible to contribute to organic retention, and

$$C_6H_5\cdot + C_2H_5Br \longrightarrow C_6H_5Br + C_2H_5\cdot \quad (2)$$

which produces ethyl radicals.

Similar reactions have been postulated to account for retentions in solutions of ethyl iodide and iodine in benzene.[13]

The phenyl radicals involved in these reactions probably were created by the hot halogen atom while slowing down to energies where stable chemical compounds can be formed. It was proved and it is immediately obvious that because of the dilution and the high diffusion coefficients involved, the hot atom has no chance of recombining with any of these fragments in scavenged gaseous systems. It can be shown that the great majority of the available data from liquid halides can be rationalized without involving these fragments.[1] In solids, the radicals so formed are frozen, probably very near the site of hot reactions. In the experimental procedure it is necessary to melt the system before performing the reductive extraction; the inorganic species containing the radioactive atom are in this way given the opportunity of reacting thermally with the fragments found in their vicinity. Such reactions are only apparently "hot" in the sense that they are localized and only a high concentration of scavenger would affect them but are in fact "thermal," as they are subject to normal kinetics.[14]

Acknowledgments.—The author wishes to express her gratitude to Professors H. Halban and A. J. Blanc Lapierre for encouragement and to Professor R. Wolfgang for many helpful discussions. Financial support from the "Commissariat à l'Energie Atomique" is gratefully acknowledged.

(13) P. F. D. Shaw and J. Macrae, private communication.

(14) Such "post effects" also could be partly responsible for the increase of retention through annealing.[15]

(15) M. M. de Maine, A. G. Maddock, and K. Taugbol, *Discussions Faraday Soc.*, **23**, 211 (1957).

DIFFUSION IN THE THREE COMPONENT LIQUID SYSTEM METHYL ALCOHOL–*n*-PROPYL ALCOHOL–ISOBUTYL ALCOHOL

BY F. O. SHUCK[1] AND H. L. TOOR

Department of Chemical Engineering, Carnegie Institute of Technology, Pittsburgh 13, Pennsylvania

Received June 12, 1962

The diffusion behavior of the system methyl alcohol–*n*-propyl alcohol–isobutyl alcohol was studied at 30°. The diffusion coefficients for the binary systems which form the borders of the ternary system as well as those for the ternary system were measured using the diaphragm cell method. The binary as well as the four ternary diffusion coefficients were found to be linear functions of mass or volume fraction.

Introduction

A study of the diffusion behavior in completely miscible ternary liquid systems was recently undertaken in these Laboratories. The behavior of a relatively ideal system of this type has already been reported.[2] As a continuation of this program the diffusion behavior of the system methyl alcohol–*n*-propyl alcohol–isobutyl alcohol has been examined over the full concentration range.

Experimental

The diffusion coefficients for the system were measured using a modification of the diaphram cell method which was described previously.[2] The methyl and *n*-propyl alcohols used were "certified" reagent grade obtained from the Fisher Scientific Company and the isobutyl alcohol was obtained from the Matheson, Coleman and Bell Division of the Matheson Company. These alcohols were used without further purification. Concentrations were measured by gas–liquid chromatography, using a Beckman GC-2A instrument with helium as a carrier gas. A six foot, 1/4 inch diameter column packed with 15 weight % of polyethylene glycol (carbowax 600—Union Carbide Chemicals Company) on 40/60 mesh firebrick gave reasonable resolution and short elution times.

The accuracy of analysis depended upon the sample composition. The amount of a component present in a sample could in general be determined to within 1.0 to 0.2% of the amount present.

The cell factors, β, for the four cells which were used (β is defined by eq. 1) were determined by calibrating with 0.5 *N* HCl diffusing into pure water at 25.0°. The results of several replicas and the 95% confidence ranges are

$$\beta_0(\text{cell } 0) = 0.1685 \pm 0.0046 \text{ cm.}^{-2}$$

$$\beta_1(\text{cell } 1) = 0.2121 \pm 0.0042 \text{ cm.}^{-2}$$

$$\beta_2(\text{cell } 2) = 0.1990 \pm 0.0046 \text{ cm.}^{-2}$$

$$\beta_3(\text{cell } 3) = 0.2602 \pm 0.0042 \text{ cm.}^{-2}$$

(1) Department of Chemical Engineering, Iowa State University, Ames, Iowa.

(2) J. K. Burchard and H. L. Toor, *J. Phys. Chem.*, **66**, 2015 (1962).

Binary Systems.—The mutual diffusion coefficients for the binary systems—methyl alcohol–*n*-propyl alcohol; *n*-propyl alcohol–isobutyl alcohol; and methyl alcohol–isobutyl alcohol—which form the borders of the ternary system, were measured at 30° for several mean concentrations over the binary concentration ranges. In most cases two duplicate measurements were made at each average concentration. The mass densities of these binary systems were found to be very nearly constant so the usual equation[3] for the diffusion coefficient takes the form

$$\frac{1}{\beta t} \ln \frac{\Delta w_i^0}{\Delta w_i^f} = \bar{\mathfrak{D}}_{ij} \qquad (1)$$

where w_i is the mass fraction of component i, t is the duration of the run in seconds, superscript 0 refers to initial conditions ($t = 0$), superscript f to final conditions ($t = t$), and Δw_i is the difference between the mass fraction in one cell chamber and that in the other. Since volume changes on mixing are negligible, $\bar{\mathfrak{D}}_{ij}$ is the integral binary diffusion coefficient in the volume reference frame. Since the two bulbs in each cell are of about equal volume, and $\mathfrak{D}_{ij}$ is close to linear in w_i over the concentration range used in an experiment, $\bar{\mathfrak{D}}_{ij}$ may be taken to be the differential coefficient at the arithmetic average composition of the experiment.

From these measurements it was found that the diffusion coefficients for these binary systems are linear functions of mass fraction. (Mass fraction in these systems of nearly constant density is very nearly equal to the volume fraction.) The data were treated statistically and it was found that in all cases the coefficients of the higher order terms in w_i were not significantly different from zero at the 95% confidence level. Moreover when correlated with mole fraction two of the systems (methyl, *n*-propyl and *n*-propyl, isobutyl) were found to have coefficients of x^2 which were significantly different from zero. In these cases the quadratic function of mole fraction was found to be virtually the same "curve" as the linear function of mass fraction. In the methyl–isobutyl alcohol system the correlation with mole fraction was found to be statistically linear as was the correlation with mass fraction. However, this result was felt to be a consequence of the small number of data points and since the system is similar to the other two which were found to be linear in mass fraction the linear correlation in terms of mass fraction is reported.

The results are shown in Table I and Fig. 1, 2, and 3 where the diffusion coefficients are shown as functions of mole fraction. The points in the figures are generally the average of two runs. The equations for the diffusion coefficients which are linear in mass fraction are given in the figures and are also plotted. The original data are given by Shuck.[4]

Figure 1 also shows the correlation of $\mathfrak{D}_{MP}/(1 + d \ln \gamma_M/d \ln x_M)$ which is linear in mole fraction. (Indistinguishable lines are given by a linear regression or by dividing the $\mathfrak{D}_{MP}$ which are obtained as a linear function of w_M by the activity correction.) For this plot the activity coefficient data of Hill and Van Winkle[5] were used.

The confidence ranges for the correlations shown in Fig. 1, 2, and 3 vary considerably for the different sys-

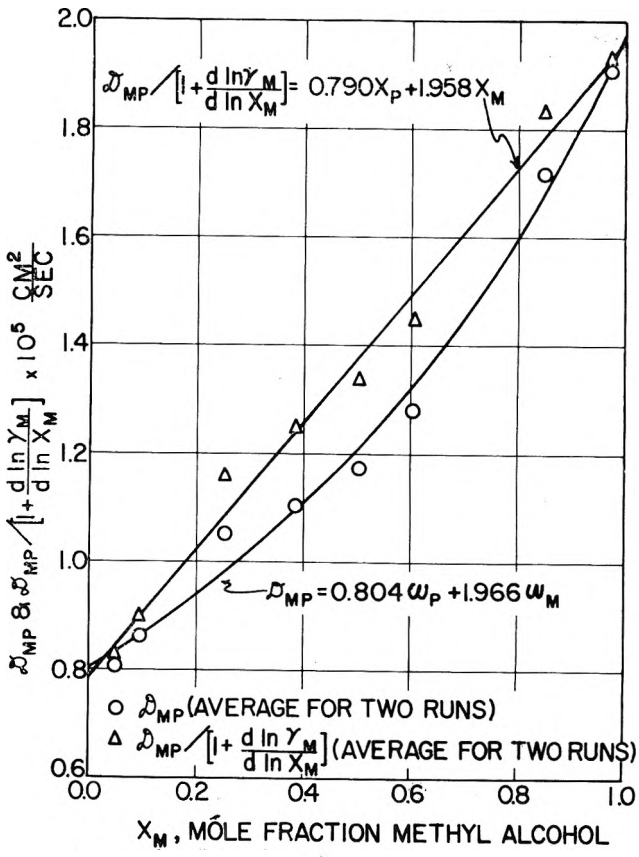

Fig. 1.—Binary diffusion coefficients—methyl alcohol–*n*-propyl alcohol.

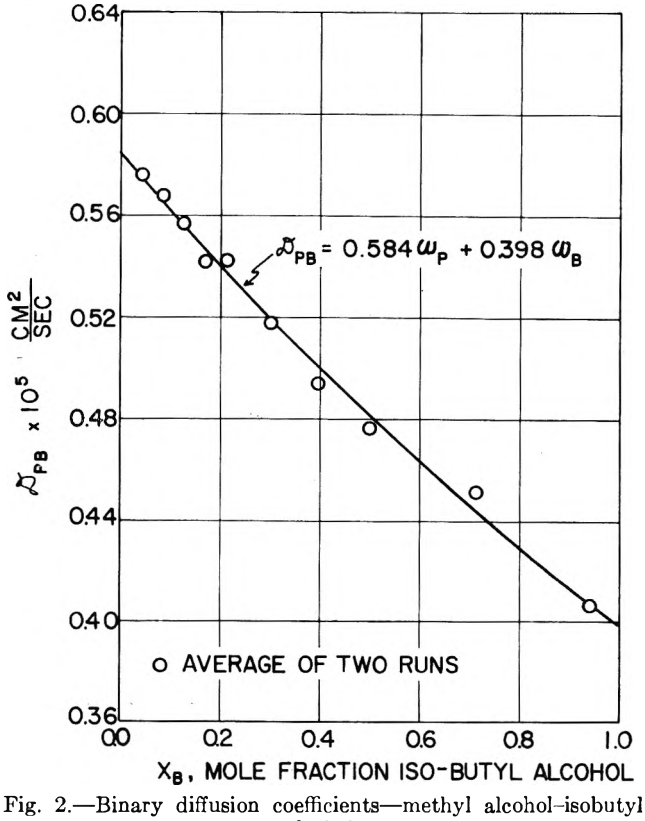

Fig. 2.—Binary diffusion coefficients—methyl alcohol–isobutyl alcohol.

(3) A. R. Gordon, *Ann. N. Y. Acad. Sci.*, **46**, 285 (1945).

(4) F. O. Shuck, Ph.D. Thesis, Carnegie Institute of Technology, Pittsburgh, Pa. (1962).

(5) W. D. Hill and M. Van Winkle, *Ind. Eng. Chem.*, **44**, 2450 (1952).

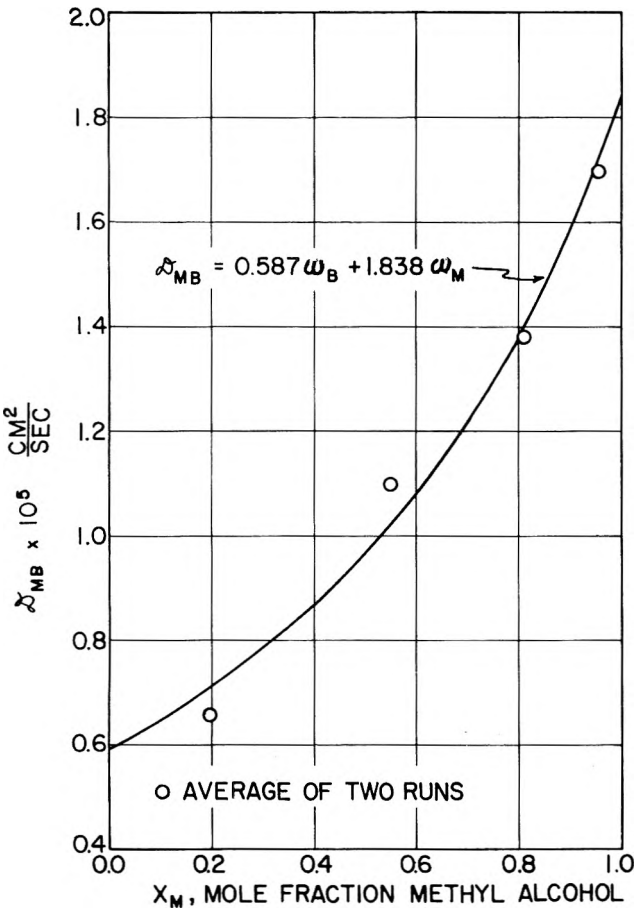

Fig. 3.—Binary diffusion coefficients—isobutyl alcohol–*n*-propyl alcohol.

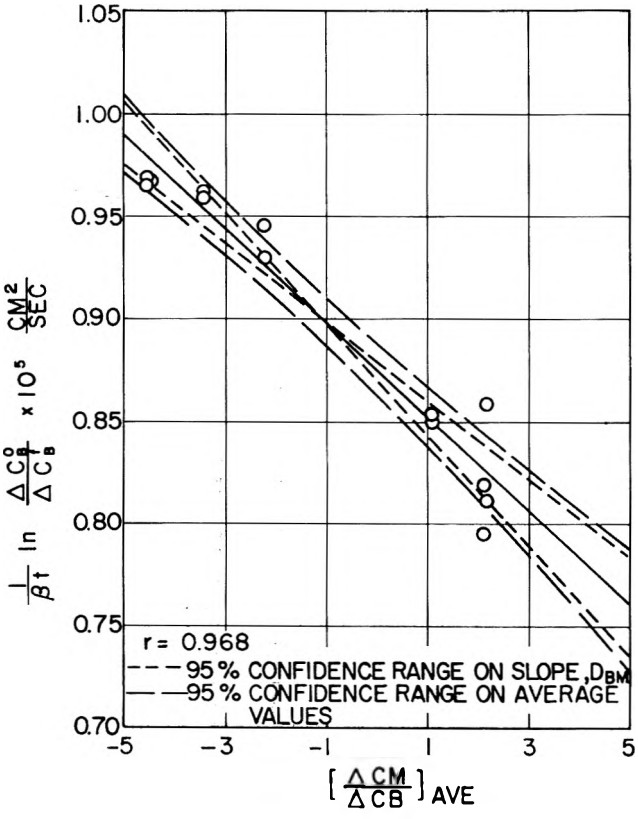

Fig. 4.—Determination of D_{BB} and D_{BM} at concentration C_1.

tems. The differences result largely from the differences in the precision with which the various systems could be analyzed. From the 95% confidence envelopes it was determined that the average values of the

Table I

Binary Diffusion Coefficients

x_M	$\mathcal{D}_{MP}$[a]	x_M	$\mathcal{D}_{MB}$	x_B	$\mathcal{D}_{BP}$
0.0464	0.799	0.1989	0.651	0.0417	0.574
.0467	.819	.1989	0.664	.0416	.579
.0911	.856	.5491	1.114	.0859	.568
.0926	.867	.5500	1.087	.1258	.547
.2512	1.049	.8096	1.412	.1272	.567
.2539	1.054	.8098	1.350	.1684	.545
.3851	1.143	.9531	1.668	.1690	.539
.3859	1.063	.9536	1.726	.2135	.545
.5022	1.218			.2123	.540
.5027	1.128			.3039	.522
.6053	1.266			.3036	.514
.6076	1.292			.3975	.495
.8478	1.726			.3981	.493
.8485	1.707			.4975	.477
.9726	1.863			.4977	.476
.9734	1.948			.7106	.456
				.7098	.447
				.9394	.407
				.9388	.406

[a] All values of $\mathcal{D}_{ij}$ are in cm.²/sec. ($\times 10^5$).

diffusion coefficients given by these correlations are reliable to within about

methyl, *n*-propyl alcohol	±4%
n-propyl, isobutyl alcohol	±1%
methyl, isobutyl alcohol	±8%

The values of the diffusion coefficients at infinite dilution were determined by extrapolation and are shown with their 95% confidence ranges in Table II. $\mathcal{D}_{ij}^0$ refers to the diffusion coefficient for dilute i in concentrated j. These values are also compared with those predicted by the empirical correlation of Wilke and Chang.[6] Although the relative magnitudes of the predicted coefficients are in agreement with the experimental values, the Wilke and Chang equation gives values which are consistently higher than experiment.

Table II

Binary Diffusion Coefficients at Infinite Dilution

	$\mathcal{D}_{ij}^0$ (exp.) × 10^5, cm.²/sec.	$\mathcal{D}_{ij}^0$ (calcd.) × 10^5, cm.² /sec.[a]
$\mathcal{D}_{MP}^0$	0.804 ± 0.041[b]	1.148
$\mathcal{D}_{PM}^0$	1.966 ± .059	2.492
$\mathcal{D}_{BP}^0$	0.584 ± .005	0.619
$\mathcal{D}_{PB}^0$	.398 ± .007	.481
$\mathcal{D}_{MB}^0$	.587 ± .105	.771
$\mathcal{D}_{BM}^0$	1.838 ± .106	2.153

[a] Calculated from the equation of Wilke and Chang.[6] [b] Indicates 95% confidence range of correlation at the end point.

Ternary System.—The four diffusion coefficients to be measured are defined by the equations[2]

$$J_M = -D_{MM}\nabla C_M - D_{MB}\nabla C_B \quad (2)$$

$$J_B = -D_{BM}\nabla C_M - D_{BB}\nabla C_B \quad (3)$$

where J_i is the molar flux of species i with respect to the volume average velocity and C_i is the concentration of species i in moles per unit volume. Subscripts M and B refer to methyl and butyl alcohol, respectively.

It was shown earlier that in a diaphragm cell these equations lead to the working equations[2,7]

(6) C. R. Wilke and P. Chang, *A.I.Ch.E. J.*, **1**, 264 (1955).

TABLE III

TERNARY DIFFUSION COEFFICIENTS

	Concentration ω_M	Concentration ω_B	$\bar{D}_{MM}$[a]	$\bar{D}_{MB}$	$\bar{D}_{BM}$	$\bar{D}_{BB}$
c_1	0.2941	0.3533	1.039 ± 0.042[b]	0.032 ± 0.023	−0.023 ± 0.004	0.875 ± 0.012
c_2	.1487	.1493	0.909 ± .038	.030 ± .040	− .009 ± .005	.721 ± .021
c_3	.1478	.7016	0.765 ± .031	.027 ± .032	− .039 ± .008	.624 ± .038
c_4	.6995	.1504	1.505 ± .117	.211 ± .139	− .004 ± .007	1.383 ± .017

[a] All $\bar{D}$'s are in cm.²/sec. × 10^5. [b] 95% confidence range.

$$\frac{1}{\beta t}\ln\frac{\Delta C_M^0}{\Delta C_M^f} = \bar{D}_{MM} + \bar{D}_{MB}\left(\frac{\Delta C_B}{\Delta C_M}\right)_{ave} \quad (4)$$

$$\frac{1}{\beta t}\ln\frac{\Delta C_B^0}{\Delta C_B^f} = \bar{D}_{BM}\left(\frac{\Delta C_M}{\Delta C_B}\right)_{ave} + \bar{D}_{BB} \quad (5)$$

where the overbars refer to integral average values of the diffusion coefficients and the average of the ratio of the concentration differences is the arithmetic average of the initial and final values.

In order to cover the ternary concentration range the diffusion behavior of this system was investigated at four average concentrations using the same diffusion cells as were used in the binary studies. Several runs were made at each concentration. From the measured concentration changes the four ternary diffusion coefficients were calculated from eq. 4 and 5.

Equations 4 and 5 indicate that $(1/\beta t)\ln(\Delta C_i^0/\Delta C_i^f)$ should vary linearly with $(\Delta C_j/\Delta C_i)_{ave}$ at a constant average concentration. Thus several runs at each average concentration were made with varying initial values of the ratio of concentration differences. (Hence the average values of this ratio also varied for the different runs.) From all the data at a given average concentration the coefficients were calculated by computing the quantities $1/\beta t \ln(\Delta C_i^0/\Delta C_i^f)$ and $(\Delta C_j/\Delta C_i)_{ave}$ and using the method of least squares to determine the slope and intercept of the best straight line through the data. An example is shown in Fig. 4. Using this method the confidence ranges of the coefficients could also be calculated readily. The diffusion coefficients obtained are shown with their confidence ranges in Table III. The main diffusion coefficients, D_{MM} and D_{BB}, were found to be significantly different from one another, that is, the only overlap of the confidence ranges of these coefficients is the slight overlap at concentration c_4. Furthermore, the cross diffusion coefficients, D_{MB} and D_{BM}, although much smaller than the main coefficients, were found to differ significantly from zero in many cases.

The measured coefficients were employed in the equation of Miller[8] which constitutes a test of the Onsager reciprocal relations. Although the lack of activity data for the ternary system made it necessary to use a form of Miller's equation which applies to ideal systems, the measured coefficients are seen to be consistent with this relation within the range of experimental error (see Table IV). The uncertainties given in the table were calculated from the uncertainties in D_{ij}. Because non-ideality effects are neglected the agreement may be fortuitous.

TABLE IV

CONSISTENCY OF EXPERIMENTAL DIFFUSION COEFFICIENTS WITH THE EQUATION OF MILLER[8]

Concn.	LHS (× 10^5)	RHS (× 10^5)
c_1	0.915 ± 0.040[a]	0.951 ± 0.058
c_2	.829 ± .166	.822 ± .087
c_3	.655 ± .076	.663 ± .052
c_4	1.504 ± .096	1.490 ± .145

$$\text{LHS} = \frac{A}{B}\bar{D}_{MB} + \bar{D}_{BB}$$

$$\text{RHS} = \bar{D}_{MM} + \frac{D}{B}\bar{D}_{BM}$$

$$A = \left(1 + \frac{C_M\bar{v}_M}{C_P\bar{v}_P}\right)\frac{1}{C_M} - \frac{1}{C}\left(1 - \frac{\bar{v}_M}{\bar{v}_P}\right)\left(1 + \frac{C_M + C_B}{C_P}\frac{\bar{v}_M}{\bar{v}_P}\right)$$

$$B = \frac{\bar{v}_B}{C_P\bar{v}_P} - \frac{1}{C}\left(1 - \frac{\bar{v}_M}{\bar{v}_P}\right)\left(1 + \frac{C_M + C_B}{C_P}\frac{\bar{v}_B}{\bar{v}_P}\right)$$

$$D = \left(1 + \frac{C_B\bar{v}_B}{C_P\bar{v}_P}\right)\frac{1}{C_B} - \frac{1}{C}\left(1 - \frac{\bar{v}_B}{\bar{v}_P}\right)\left(1 + \frac{C_M + C_B}{C_P}\frac{\bar{v}_B}{\bar{v}_P}\right)$$

[a] Refers to 95% confidence range.

An attempt was made to relate the ternary diffusion coefficients to the binary coefficients using Bearman's results.[9] In the end, however, an assumption was needed in order to complete the relationship. When the same assumption was made as that made by Burchard and Toor[2] when they attempted to apply the Maxwell–Stephan equations to a similar situation, the results obtained (neglecting effects of non-ideality) were considerably inferior to those obtained below, as were the results obtained when the Maxwell–Stephan equations were used in the manner of Burchard and Toor.[2]

From a consideration of eq. 2 and 3 the following limiting values of the ternary diffusion coefficients may be obtained.[10]

$$\lim_{C_j \to 0} D_{ii} = \mathfrak{D}_{iP} = \mathfrak{D}_{Pi}, \quad i,j = M,B;\ j \neq i \quad (6a)$$

$$\lim_{C_i, C_P \to 0} D_{ii} = \mathfrak{D}_{ij}^0, \quad i,j = M,B;\ j \neq i \quad (6b)$$

$$\lim_{C_i \to 0} D_{ij} = 0, \quad i,j = M,B;\ j \neq i \quad (6c)$$

$$\lim_{C_j, C_P \to 0} D_{ij} = (\mathfrak{D}_{Pi}^0 - \mathfrak{D}_{ji}^0)\frac{\bar{v}_j}{\bar{v}_i}, \quad i,j = M,B;\ j \neq i \quad (6d)$$

(7) The assumptions necessary to obtain these relations are (1) a quasi-steady state is obtained in the diaphragm cell, (2) the diffusion may be treated as though it were uni-directional, (3) the diffusion occurs only within the fluid in the diaphragm, (4) the volumetric average velocity within the diaphragm is zero, (5) the contents of the constant volume cell chambers are completely mixed, (6) the $\bar{D}_{ij}$ are constant over a run, (7)

$$\beta t\left[\left(\frac{\bar{D}_{BB} - \bar{D}_{MM}}{2}\right)^2 + \bar{D}_{MB}\bar{D}_{BM}\right]^{1/2} \ll 1$$

and (8)

$$\beta t\left[\frac{D_{ii} - D_{ij}}{2} - D_{ji}\frac{\Delta C_i^0}{\Delta C_j^0}\right] \ll 1 \quad i,j = M,B;\ i \neq j$$

Assumptions 1 to 6 inclusive lead to two unwieldly equations in the $\bar{D}_{ij}$ and assmptions 7 and 8 allow simplification to eq. 4 and 5. The errors caused by the use of eq. 4 and 5 in place of the more cumbersome equations were found to be negligible in this study.

(8) D. G. Miller, *J. Phys. Chem.*, **63**, 570 (1959).

(9) R. J. Bearman, *ibid.*, **65**, 1961 (1961).

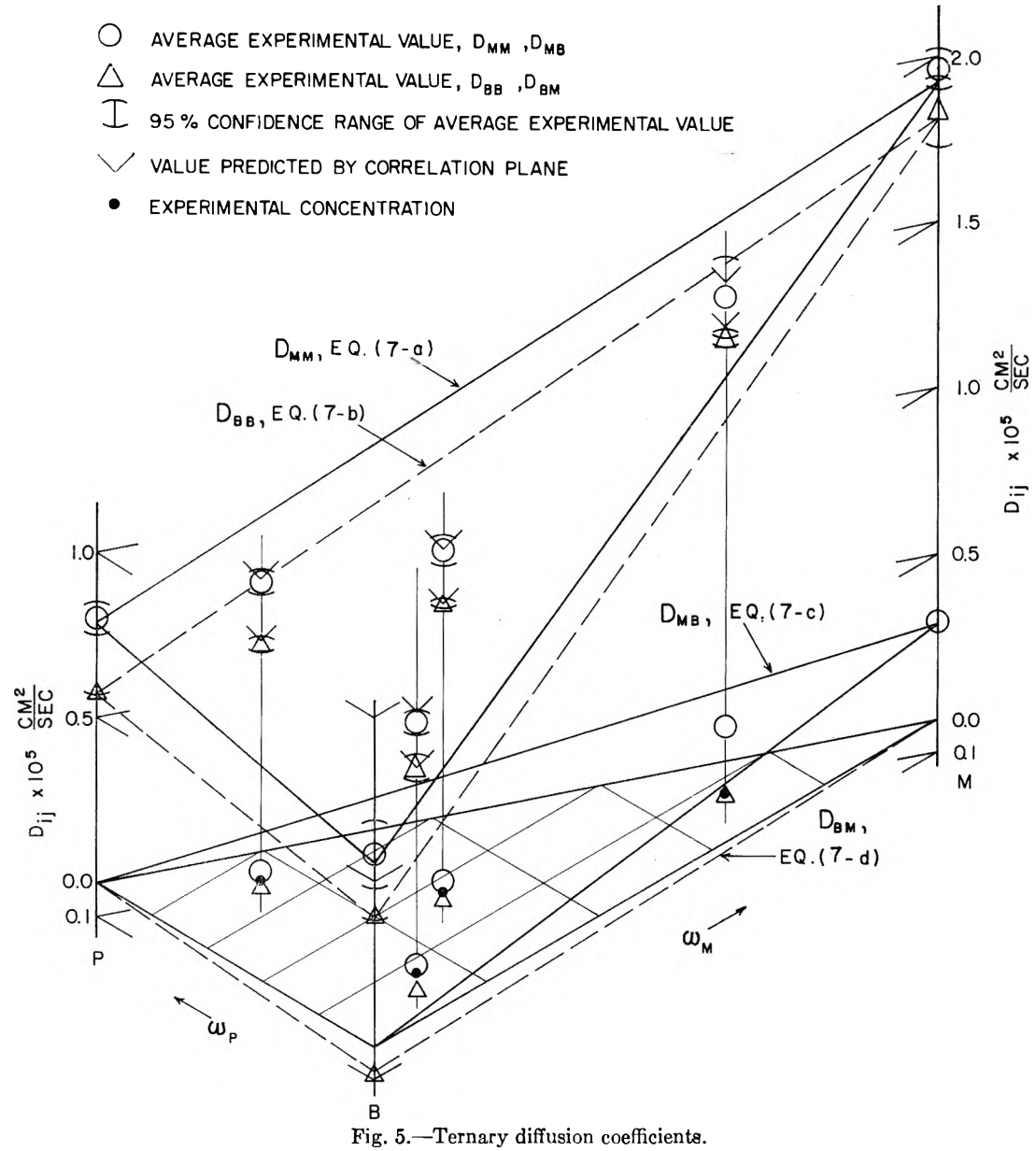

Fig. 5.—Ternary diffusion coefficients.

Using the measured binary diffusion coefficients in conjunction with eq. 6 and the measured diffusion coefficients at the four interior points of the ternary concentration field, it is empirically found that the ternary diffusion coefficients may be treated as linear functions of mass fraction, as was the case with the binary diffusion coefficients. The resulting planes with their correlation coefficients, r, are[11]

$$D_{MM} = 1.928w_M + 0.557w_B + 0.784w_P, \; r = 0.998 \quad (7a)$$

$$D_{BB} = 1.815w_M + 0.390w_B + 0.573w_P, \; r = 0.999 \quad (7b)$$

$$D_{MB} = 0.285w_M, \; r = 0.974 \quad (7c)$$

$$D_{BM} = 0.072w_B, \; r = 0.963 \quad (7d)$$

These planes are drawn in Fig. 5. The correlation is highly significant. The diffusion coefficients which are given by these equations at the interior concentration points are compared to experiment in Table V.

Since eq. 6 gives the value of each of the four ternary diffusion coefficients along one binary border of the ternary concentration field, as well as at the corner opposite to this border, the binary diffusion coefficients alone may be used to calculate planes for each ternary diffusion coefficient. Using eq. 6 and the result that

(10) Equations 6a and 6c are obtained by noting that eq. 2 and 3 must reduce to the appropriate binary equations at the borders of the ternary concentration field and that the flux of species i must go to zero as the concentration of species i goes to zero. Equation 6c has been obtained elsewhere (I. J. O'Donnel and L. J. Gosting, "The Structure of Electrolytic Solutions," John Wiley and Sons, Inc., New York, N. Y., 1957, p. 160).

Equations 6b and 6d follow from a development given by Burchard and Toor[2] or from the auxiliary relationship

$$\lim_{C_P \to 0} D_{ii} - D_{ij}\frac{\bar{v}_i}{\bar{v}_j} = \mathfrak{D}_{ij}, \quad \begin{matrix} i,j, = M, B \\ j \neq i \end{matrix} \quad (6e)$$

and eq. 6a and 6c. Equation 6e is obtained from eq. 2 and 3 and the condition

$$\Sigma \bar{v}_i \nabla C_i = 0$$

(11) In order to avoid biasing the correlation with a large number of binary points eq. 6a was replaced by the equations

$$\lim_{C_j,\, C_P \to 0} D_{ii} = \mathfrak{D}_{iP}^0, \; i,j = M,B \quad (j \neq i)$$

$$\lim_{C_j,\, C_i \to 0} D_{ii} = \mathfrak{D}_{iP}^0, \; i,j = M,B \quad (j \neq i)$$

so the only binary diffusion coefficients which were used in the statistical determination of eq. 7 were the dilute values in Table II.

TABLE V

COMPARISON OF EXPERIMENTAL AND CALCULATED TERNARY DIFFUSION COEFFICIENTS

Concn.	D_{ij}[a]	Exptl.	Calcd. eq. 7	Calcd. eq. 8
c_1	MM	1.039	1.040	1.069
	MB	0.032	0.084	0.087
	BM	− .023	− .025	− .029
	BB	.875	.874	.887
c_2	MM	.909	.920	.944
	MB	.030	.042	.044
	BM	− .009	− .011	− .012
	BB	.721	.730	.743
c_3	MM	.765	.794	.823
	MB	.027	.042	.044
	BM	− .039	− .051	− .057
	BB	.621	.628	.639
c_4	MM	1 505	1.550	1.584
	MB	0.211	0.199	0.207
	BM	−0.004	−0.011	−0.012
	BB	1.383	1.414	1.433

[a] All values of D_{ij} are in cm.²/sec. ($\times 10^5$).

the binary diffusion coefficients may be taken as linear in w

$$D_{ii} = \mathfrak{D}_{Pi}{}^0 w_i + \mathfrak{D}_{ij}{}^0 w_j + \mathfrak{D}_{iP}{}^0 w_P, \quad \begin{matrix} i,j = M,B \\ i \neq j \end{matrix} \qquad (8a)$$

$$D_{ij} = w_i(\mathfrak{D}_{Pi}{}^0 - \mathfrak{D}_{ji}{}^0)\frac{\bar{v}_j}{\bar{v}_i}, \quad \begin{matrix} i,j = M,B \\ i \neq j \end{matrix} \qquad (8b)$$

These equations were used with the values of the dilute binary diffusion coefficients in Table II to compute the ternary diffusion coefficients at the interior points of the concentration field. The results are given in Table V. The differences between the computed and measured values are in all cases within experimental error.

It is interesting to note that the diffusion coefficients in this constant mass density system are also linear functions of volume fraction. In the toluene–chlorobenzene–bromobenzene system the main diffusion coefficients were reported as linear functions of mole fraction,[2,12] but since this was a constant molar density system these coefficients are also linear in volume fraction. Thus, both systems are described by eq. 8a[13] if w is taken as volume fraction. This gratifying behavior which allows for estimation of the ternary coefficients from the dilute binary coefficients alone is not to be expected in less thermodynamically ideal systems.

Acknowledgment.—The authors are grateful to the National Science Foundation for its financial support of this work.

(12) The precision of measurement of the cross diffusion coefficients was not great enough to determine the concentration dependence of the cross diffusion coefficients in that system.

(13) The T-C-B system is described by a degenerate form of eq. 8a for in this system $\mathfrak{D}_{ij}{}^0 \cong \mathfrak{D}_{kj}{}^0$ so there is only "one" main diffusion coefficient.

MICROCALORIMETRIC STUDIES OF THE DISTRIBUTION OF SURFACE ENERGY IN CHEMISORPTION

BY V. KEVORKIAN AND R. O. STEINER

Esso Research & Engineering Co., Process Research Division, Linden, N. J.

Received July 5, 1962

Surface energy distributions of a series of oxide catalysts were measured using NH_3 adsorbate in a differential isothermal microcalorimeter at 50°. The catalysts studied were Al_2O_3 calcined at 1100 and 1600°F., SiO_2, $KOH–Al_2O_3$, $Pt–Al_2O_3$, and $SiO_2–MgO$. It was found that Al_2O_3 (1100°F.) has a heterogeneous distribution of surface energy which is not destroyed by high temperature calcination. SiO_2, on the other hand, has a fairly homogeneous surface energy distribution. Alumina's energy distribution may be altered by impregnation, *e.g.*, with KOH or Pt. When a co-gel of MgO and SiO_2 is formed, its surface is more energetic and its surface energy distribution more heterogeneous than that of SiO_2 alone.

Adsorption on a catalyst surface occurs on so-called adsorption sites. These sites vary in affinity for a given adsorbate, and the surface of the adsorbent is therefore said to be heterogeneous. When gas molecules are adsorbed on a clean catalyst surface, the highest energy sites tend to be covered first, the lower energy sites last. Consequently, the heat of interaction released generally falls off as successive doses of gas are adsorbed. Microcalorimetry is one of the best methods known for measuring accurately the differential heats of adsorption and so of characterizing a catalyst by the energy distribution of its surface sites. The major portion, by far, of microcalorimetric investigations has been devoted to physical adsorption (*e.g.*, ref. 1), and to chemisorption on metals (*e.g.*, ref. 2). This study, therefore, turned to the important area of supported metal catalysts and common catalyst supports. It is concerned with microcalorimetric studies of the chemisorption of ammonia on various catalyst surfaces.

(1) R. A. Beebe, B. Millard, and J. Cynarski, *J. Am. Chem. Soc.*, **75**, 839 (1953).

(2) R. A. Fisher, Jr., "Adsorption Properties of Hydrogen and Oxygen on Platinum Black and Carbon Supported Platinum from 20 to 300 Degrees Kelvin," Ph.D. Thesis, Department of Chemistry, The Pennsylvania State University, 1961.

Experimental

To measure differential heats of adsorption, or surface energy distributions, a small amount of catalyst, between 1 and 2 g., was loaded into a calorimeter which then was inserted into a high vacuum system. A thermocouple was attached to the calorimeter to measure the heat release, for adsorption is always exothermic. The calorimeter and thermocouple reference junctions were contained in the same constant temperature bath. The catalyst was outgassed overnight at a temperature of 450° until a pressure of 5×10^{-5} mm. was achieved at 450°. The calorimeter then was cooled and immersed in the constant temperature bath at 50° under a pressure of 10^{-6} mm. About 0.7 mm. of helium was added to the calorimeter to facilitate the heat measurements. A small measured dose of NH_3 was adsorbed on the catalyst, liberating about 1 cal. of heat which generated an e.m.f. of several microvolts in the thermocouple (Pt/Pt, 13% Rh). This signal was amplified and sent to a recorder. The

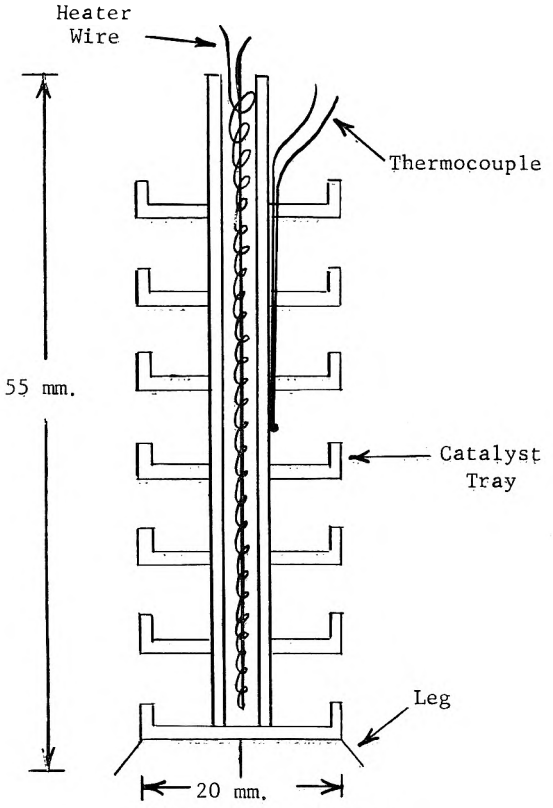

Fig. 1.—Microcalorimeter.

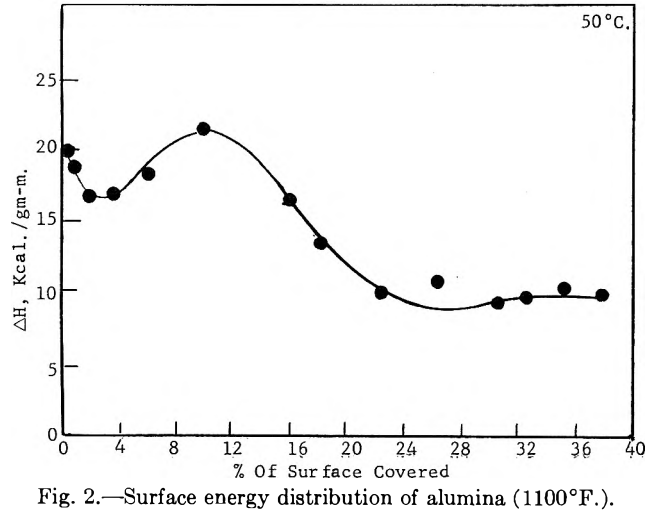

Fig. 2.—Surface energy distribution of alumina (1100°F.).

recorder pen followed a straight vertical line when the catalyst and thermocouple reference junction were at the same temperature. The heat of adsorption caused the pen to be deflected sharply away from this equilibrium position. As the catalyst slowly lost the adsorption heat to its surroundings, a cooling curve was traced out by the recorder pen. After thermal equilibrium was re-established, a calibration was made by sending a known amount of electrical energy through a heater wire in the calorimeter, generating another heating–cooling curve. The area under the calibration curve was measured with a planimeter and compared to that under the adsorption curve to determine quantitatively the adsorption heat release. The amount of NH_3 which adsorbed, and caused this heat release, was determined by measurement of the equilibrium pressure. This process then was repeated numerous times by adsorbing more small doses until an appreciable part of the surface was covered. In this way, data were obtained which are necessary to calculate the surface energy distribution of the catalyst.

The adsorption system associated with the calorimeter has two high vacuum manifolds which operate over a pressure range of 10^{-6} to 1 mm. One manifold is used to prepare the adsorbate and the other to outgas the catalyst. A high pressure manifold (10^{-1} to 10^{3} mm.) is used for measuring BET surface areas of the catalysts.

The constant temperature bath is doubly thermostated and designed to operate over a temperature range of 30–200 ± 0.01°. Sensitive temperature control was achieved in the central bath by use of a helix which contained glycerol. The glycerol either expanded against, or contracted from, a mercury column to achieve the temperature control. Three centrifugal pumps (Eastern Model DH-11) circulated the water of the inner and outer baths to eliminate temperature gradients.

The large bath and two electric furnaces (Hevi-Duty) were mounted on a hydraulic platform which moved on wheels and rails for correct positioning. Special shielding and an isolation transformer were installed to eliminate stray electrical charges which might affect the e.m.f. measurements.

A tray-type calorimeter was specially designed for this study so that it would have a minimum of heat transfer, mass transfer, and diffusional limitations. One already has been described[3] for use in an adiabatic calorimeter system used for the measurement of specific heats of high polymers. A cut-away side view of the one used in this study is shown in Fig. 1. Seven shallow trays are gold-soldered to a hollow, heavy-walled, central shaft. The entire calorimeter is made of platinum–rhodium (3.5%) alloy. Inside the shaft is the nichrome heater wire (39.2 ohms resistance), and spot-welded to its side is the thermocouple. The very broad area of contact between the trays and the shaft should result in good heat transfer to the thermocouple. Since the catalyst beds on the trays were only about 2 mm. deep, spurting of the catalyst during outgassing did not occur. Also, diffusional limitations were reduced to a minimum and should not have affected the measured energy distributions because of non-selective adsorption.

Current for the calibration was supplied by a 6-volt storage battery. A standard electric timer, which could be read to ±0.05 sec., was used to measure the length of the calibration period. Voltage and current were read with a d.c. voltmeter (Weston Model 1) and a d.c. ammeter (Weston Model 1). The thermocouple e.m.f. was amplified by a Beckman d.c. breaker amplifier (Model 14) and recorded on a 0–10 mv. Brown recorder.

Preparation of Adsorbates.—Helium of 99.99% min. purity was obtained from the Matheson Co. Before use, it was passed over activated carbon maintained at liquid nitrogen temperatures. Anhydrous ammonia of 99.99% min. purity also was obtained from the Matheson Co. It was admitted to an evacuated system, liquefied at −78°, and distilled into a 3-l. storage flask. Prepurified nitrogen was obtained from the Matheson Co. with a purity of 99.996% min. and was used "as is."

Preparation of Adsorbents. Alumina.—Adsorptive aluminas were prepared by calcining β-alumina trihydrate in an atmosphere of dry nitrogen at 1100°F. for 4 hr.—Al_2O_3 (1100°F.)—and at 1600°F. for 8 hr.—Al_2O_3 (1600°F.). These catalysts, like all others investigated, were ground to a small particle size.

Potassium Hydroxide–Alumina.—β-Alumina trihydrate was treated with a solution containing KOH to provide 5 moles of KOH/100 moles of alumina and calcined at 1100°F.—KOH–Al_2O_3.

Platinum–Alumina.—Al_2O_3 (1100°F.) was wet with enough of a solution of "P salt" ($Pt(NH_3)_2(NO_2)_2$) to deposit 0.3 wt. % Pt. This wet mixture was dried at 250°F. overnight and finally calcined 1 hr. at 1100°F. Although Debye and Chu[4] have shown the deposited platinum to be highly dispersed, its exact nature (atomic or ionic) is unknown.

Silica.—The silica gel was a pure sample supplied by the Esso Research Laboratories of Baton Rouge, La. It was heated for 3 hr. at 850°F. before shipment.

Silica–Magnesia.—This catalyst also was supplied by the Esso Research Laboratories of Baton Rouge, La. Sodium silicate was mixed with sulfuric acid solution maintained below 60°F. Powdered Westvaco Co. magnesia then was sprinkled in with rapid stirring to form a stiff co-gel. It was broken up and water washed. The catalyst then was calcined overnight at 1000°F. and for 3 hr. at 1250°F. The resulting catalyst consisted of 70% silica and 30% magnesia.

Results

The catalysts studied, and their BET surface areas, measured with nitrogen adsorbate at liquid nitrogen temperatures, are listed in Table I.

(3) A. E. Worthington, P. C. Marx, and M. Dole, *Rev. Sci. Instr.*, **26**, 698 (1955).

(4) P. Debye and B. Chu, *J. Phys. Chem.*, **66**, 1021 (1962).

TABLE I

Catalyst	Surface area, m.²/g.
Al_2O_3 (1100°F.)	296
SiO_2	572
Al_2O_3 (1600°F.)	75
$KOH-Al_2O_3$	250
$Pt-Al_2O_3$	220
SiO_2-MgO	536

The surface energy distributions are shown in Fig. 2–8. Heats of adsorption in kilocalories per gram-mole ammonia adsorbed are plotted against the degree of surface coverage by ammonia. Surface coverage was calculated assuming the surface of the outgassed catalyst to be bare and a cross sectional area of 16 Å.² for the NH_3 molecule. It was assumed further that multi-layer adsorption did not occur and that NH_3 did not displace any other adsorbed species. The surface coverage corresponding to a given heat measurement was taken as the mid-point of the incremental increase in surface coverage due to the dose.

To determine the precision of the data, heat measurements were made using three different samples of Al_2O_3 (1100°F.). The maximum spread in the data was ±8%.

Discussion

The surface energy distributions (Fig. 2–8) are plotted assuming that the catalyst surfaces were completely cleaned by outgassing (*i.e.*, they start at zero surface coverage). However, since the calorimeter housing was made of Pyrex, the maximum outgassing temperature was 450°. Molecular water is removed by outgassing at 150° but hydrogen atoms and hydroxyl groups remain chemisorbed to the surface. Weight loss experiments as a function of outgassing temperature showed that there are enough of these species remaining at 450° to cover about 36% of the surfaces.

From Fig. 2, it is seen that when the surface energy distribution of Al_2O_3 (1100°F.) is plotted as differential heats of adsorption *vs.* surface coverage, the resulting curve has three distinct regions. The first region, which is due to adsorbate–adsorbent interaction, consists of high initial heats of about 20 kcal./g. mole. ΔH continuously drops off to a minimum value as surface coverage increases. The heats of the first region of the energy distribution curve may be due to either or both of two causes. First, the initial ammonia doses are adsorbed on the strongest available Lewis acid sites, forming strong bonds with the surface (due to electron transfer), and liberating large heats. It is also known from associated infrared spectroscopy studies of this and other laboratories that strongly hydrogen-bonded hydroxyl groups are present on this surface. Thus, the adsorbed ammonia might react with surface protons to form ammonium ions. This is a measure of the Brönsted, or protonic acidity of the surface. As Lewis sites of decreasing strength are covered by the succeeding doses, the curve drops to a minimum. At the minimum in the distribution curve, all of the surface acidity, both Lewis and Brönsted, is probably neutralized by the basic ammonia. If the surface coverage due to surface protons and hydroxyl groups is included, it is seen that the minimum occurs at about 40% coverage.

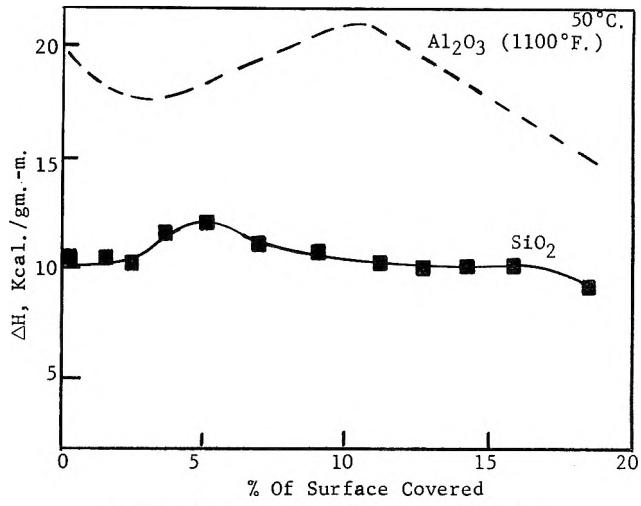

Fig. 3.—Surface energy distribution of SiO_2.

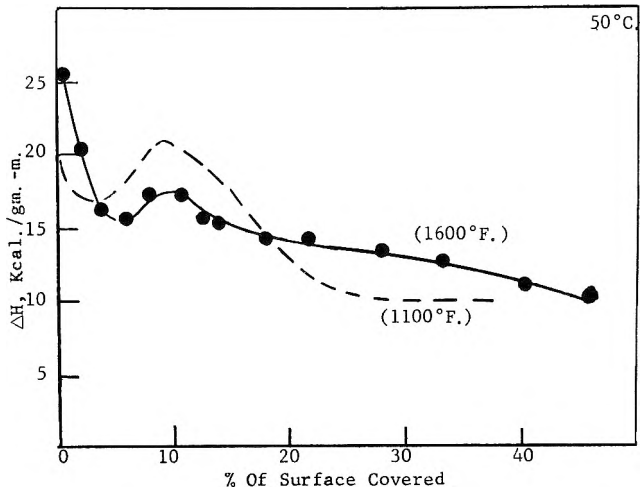

Fig. 4.—Surface energy distribution of Al_2O_3 (1600°F.).

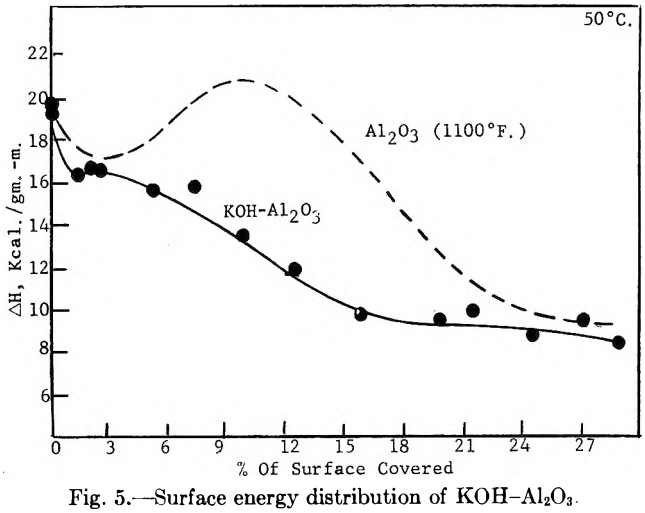

Fig. 5.—Surface energy distribution of $KOH-Al_2O_3$.

The second distinct region of the distribution curve is the portion rising about 2–3 kcal. above the minimum, probably representing adsorbate–adsorbate interaction. This rise, which has been reproducibly measured (see also ref. 5 for another example of minima and maxima in surface energy distributions) is too great to be ascribed to simple van der Waals adsorbate interaction, which should cause a rise of no more than about 1 kcal. However, it could be due to hydrogen bonding of the NH_3 to surface hydroxyl groups, the formation

(5) A. V. Kiselev, *Quart. Rev.*, **15**, 99 (1961).

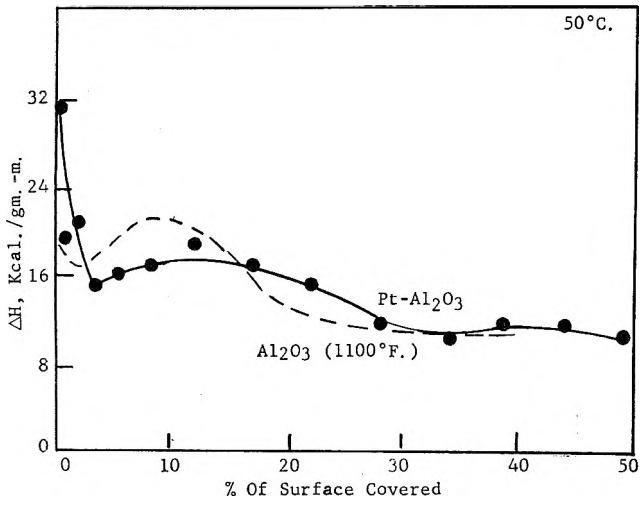

Fig. 6.—Surface energy distribution of Pt–Al_2O_3.

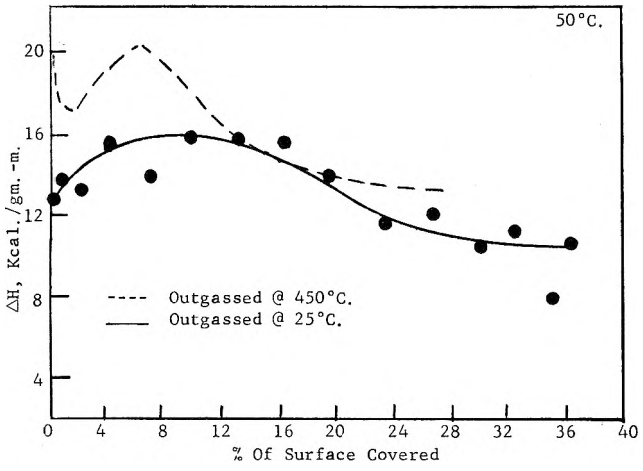

Fig. 7.—Effect of outgassing temperature on surface energy distribution of Al_2O_3 (1100°F.).

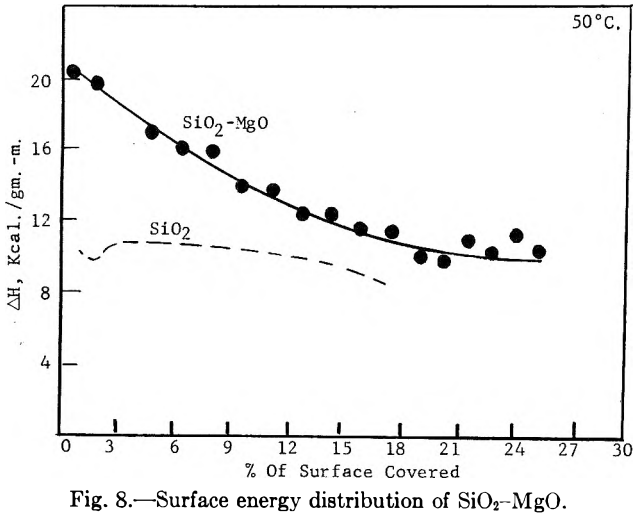

Fig. 8.—Surface energy distribution of SiO_2–MgO.

of surface coördination complexes, or perhaps capillary condensation. Thus, if the rise is due to surface coördination complexes, ammonia molecules of succeeding doses after the minimum could be forming these complexes with ammonium ions and highly polarized ammonia molecules already on the surface. These complexes would result in coulombic forces which are much stronger than the relatively weak van der Waals interaction forces. Additional effort would be needed to determine which of the possible explanations, if any, for the rise is the correct one. Both the shape and extent of the second adsorption region are most probably dependent on the adsorbate being used to measure the energy distribution.

The third adsorption region is the drop-off from the maximum. The heats probably would approach the heat of liquefaction of ammonia, 5–6 kcal., at higher surface coverages.

The surface energy distribution of silica gel was measured and compared to that of alumina (1100°F.) to see whether the microcalorimeter is sensitive enough to differentiate between various surfaces (Fig. 3). Since the initial heats for silica are only about 60% of those for alumina, it is clear that the microcalorimeter differentiates between catalyst surface types.

These microcalorimetric data are in agreement with results of infrared spectrometric studies of this Laboratory[6] on the two catalysts where only one type of OH group was found on silica, compared to three on alumina (1100°F.). This would indicate a more homogeneous energy distribution as far as OH groups are concerned. It was also observed that all the ammonia could be very easily desorbed from the silica surface simply by evacuation at room temperature, implying that the bonds formed between adsorbed ammonia and the silica surface are weak. About 600° is necessary to desorb NH_3 under similar conditions from some of the aluminas.

Substantiating the above, heats of adsorption for silica were found to be much lower (about 10 kcal.) than for alumina. Also, the silica energy distribution is considerably more uniform. This may indicate a correlation between surface energy distribution and OH surface structure.

The surface energy distribution of Al_2O_3 (1600°F.) was measured and compared to that of Al_2O_3 (1100°F.) (Fig. 4). Although calcination at the higher temperature reduced the surface area by a factor of $1/4$, the heterogeneity of Al_2O_3 (1100°F.) was not destroyed. Some of the high energy sites after the first minimum in the curve have been weakened by about 3 kcal. because of calcination at the higher temperature. However, the sites above 18% coverage seem to be appreciably stronger than those of alumina calcined at 1100°F. Calcination at different temperatures, therefore, does not merely affect the catalyst surface area, but also the surface energy distribution.

Impregnation was investigated to learn whether it would be a good technique for altering the surface energy distribution (Fig. 5). Impregnation with KOH at 1100°F. slightly weakened the strong sites of Al_2O_3 (1100°F.) at initial coverages. The minimum and maximum of the energy distribution curve of untreated alumina also are almost eliminated by the impregnation. Between coverages of 5–22%, sites of the treated alumina are much weaker than those of Al_2O_3 (1100°F.). These data indicate that energy distributions may be conveniently altered by impregnation in a way which is quantitatively measurable in the microcalorimeter.

Addition of Pt to the Al_2O_3 (1100°F.) surface lowered both the minimum in the distribution curve by about 2 kcal. and the second adsorption region by several kcal. (Fig. 6). The Pt–Al_2O_3 surface between 17 and 35% coverage is more energetic by several kcal. than that of Al_2O_3 (1100°F.).

(6) R. O. Steiner, unpublished results.

A sample of Al_2O_3 (1100°F.) was outgassed at room temperature in order to determine the effect of adsorbed water on the surface energy distribution (Fig. 7). After outgassing at 25°, this catalyst had sufficient water to form 1.5 monolayers, compared with 36% surface coverage when outgassed at 450°. The heats are sharply reduced on the "wetter" sample. Actually, these heats, 13–15.5 kcal., represent the heat of solution of ammonia in water adsorbed on the alumina surface. They may be compared with the value for solution in water, 8.5 kcal.

The addition of MgO to SiO_2 causes a change in the surface energy distribution (Fig. 8). SiO_2–MgO has high initial heats of about 20 kcal. which drop off regularly to 10.5 kcal. at 25% coverage. SiO_2 by itself has a more homogeneous surface, whose sites do not differ appreciably from each other in energy.

Acknowledgment.—The authors wish to acknowledge gratefully the helpful suggestions of Dr. P. J. Lucchesi and the assistance of Messrs. W. Bracht and J. L. Carter, who performed the microcalorimetry and infrared experiments, respectively.

TRANSIENT MEASUREMENTS OF PHOTOCHEMICAL PROCESSES IN DYES. II. THE MECHANISM OF THE PHOTOSENSITIZED OXIDATION OF AQUEOUS PHENOL BY EOSIN[1]

BY E. F. ZWICKER AND L. I. GROSSWEINER

Department of Physics, Illinois Institute of Technology, Chicago 16, Illinois

Received July 16, 1962

The mechanism for the oxidation of aqueous phenol as photosensitized by eosin has been investigated by flash-photolytic and continuous-irradiation methods. Oxygen quenches triplet eosin and also reacts with it in a slower permanent oxidation. In the absence of oxygen, phenol reduces triplet eosin to a semiquinone, producing the neutral phenoxy radical. The radical products disappear primarily by fast back-reactions, with competing permanent decomposition from dismutation of semi-reduced eosin and bimolecular reaction of phenoxy radical. The basic form of semi-reduced eosin undergoes debromination. The dissociation constant of semi-reduced eosin was determined from the dependence of the rate of radical back-reaction on acidity. Numerical rate constants for the elementary reactions were calculated and the absorption spectra and extinction coefficients of the unstable species were measured.

I. Introduction

The identification of the short-lived intermediate species produced by the photosensitized oxidation of aqueous phenol in the presence of fluorescein or its halogenated derivatives was reported in earlier publications.[2] Flash spectra obtained by the irradiation of phenol and dye solutions with visible light, absorbed only by the dye, showed that the primary act is the oxidation of phenol by triplet dye, to give phenoxy radical and semi-reduced dye. Flash bleaching showed that the dye triplet molecules decay in a fast bimolecular quenching reaction and that the radical products disappear in fast bimolecular processes. This paper includes additional flash photolysis and continuous-irradiation experiments, which further establish the reaction mechanism, and reports numerical values for the rate constants of the elementary processes.

II. Experimental Details

A. Chemicals.—Commercial eosin Y (National Aniline, C.I. no. 768) was purified chromatographically following the method of Koch.[3] The impure dye was dissolved in 0.03% ammonium hydroxide and adsorbed on a column consisting of activated alumina (1 part by wt.) and talc (3 parts by wt.). Elution with water separated four distinct bands. The eosin phase was recovered by breaking the column and dissolving the dye in ammonium hydroxide. Acidic eosin was precipitated with glacial acetic acid, filtered, washed, and dried. The maximum extinction coefficient obtained in lightly buffered aqueous solution at pH 9 is $9.15 \pm 0.15 \times 10^4\ M^{-1}\ \text{cm.}^{-1}$ at 516 mμ. Previous values of 8.0×10^4 and 8.2×10^4 were reported by Imamura[4] and Adelman and Oster,[5] respectively, where chromatography had not been employed. A comparable 10% increase in the extinction coefficient of fluorescein was obtained by Lindqvist[6] by means of chromatographic purification. The other dye phases on the column were identified from their absorption spectra as tribromofluorescein (0.45%), dibromofluorescein (0.06%), and fluorescein (0.02%)—all wt.% organic matter.

The determination of the dissociation constant of aqueous eosin by spectrometric titration of dilute solutions (10 μ*M*) was inconclusive. The absorption spectrum is unchanged from pH 12 to pH 4.4. Between pH 4.4 and 3.7 there is a gradual shift of the peak wave length from 516 to 520 mμ and a corresponding 30% decrease in extinction. Near pH 3 a colloidal suspension could be detected, and finally, a colored gelatinous precipitate was formed at lower pH. Since the basic dye solution is di-anionic, the wave length shift observed is opposite to the expected direction for the production of the mono-anion. Additional information was obtained by potentiometric titration of more concentrated (2 m*M*) eosin solutions. A single broad plateau occurred at pH 4.3 and a colored colloidal suspension was produced below pH 4. The observations can be explained by the influence of bromine substitution on the dissociation of aqueous fluorescein. Noting that Lindqvist[6] obtained p*K* 4.4 and 6.7 for neutral fluorescein and the mono-anion, respectively, the plateau obtained with eosin probably represents a composite of the two dissociations. The colored precipitate indicates that the eosin mono-anion is insoluble in water and that the hydroxyl group is partially ionized in the solid. This form may resemble the *o*-quinonoid zwitterion of fluorescein proposed by Nash.[7] Recently Oster, Oster, and Karg[8] have reported a value of 3.6 for the eosin p*K*, as obtained from the optical method. The present authors found the results of the optical method to be ambiguous at the low dye concentrations which had to be employed, because of the difficulty in distinguishing spectral changes due to dissociation from those due to the formation of a colloid. Therefore, we favor the potentiometric results at higher eosin concentrations which gave a p*K* of 4.3 for the mono-anion. All photochemical measurements reported below were made with the di-anionic dye.

(1) Supported by the U. S. Atomic Energy Commission.

(2) (a) L. I. Grossweiner and E. F. Zwicker, *J. Chem. Phys.*, **31**, 1141 (1959); (b) **34**, 1411 (1961).

(3) L. Koch, *J. Assoc. Offic. Agr. Chemists*, **39**, 397 (1956).

(4) M. Imamura, *J. Inst. Polytech. Osaka City Univ.*, **5**, 85 (1956).

(5) A. H. Adelman and G. Oster, *J. Am. Chem. Soc.*, **78**, 3977 (1956).

(6) L. Lindqvist, *Arkiv Kemi.*, **16**, 79 (1960).

(7) T. Nash, *J. Phys. Chem.*, **62**, 1574 (1958).

(8) G. Oster, G. K. Oster, and G. Karg, *ibid.*, **66**, 2514 (1962).

The solutions were made with doubly-distilled water and buffered with analytical grade potassium acid phosphate salts. Buffer concentrations were 1 M from pH 6 to 8 and 0.1 M otherwise. Analytical grade phenol (Merck) was used without further purification. The dye and phenol solutions were stored in the dark and were mixed immediately before each run.

B. **Continuous Photobleaching.**—The quantum efficiency for the photobleaching of eosin solutions under continuous irradiation was measured for aerobic and evacuated conditions. The samples were contained in a cylindrical Pyrex cell, 2.5 cm. in diameter and 1.0 cm. long, with a side bulb to facilitate degassing. The cell was immersed in a thermostated water bath and irradiated with a 500-watt projection lamp, through a glass filter transmitting from 450 to 600 mμ. The bleaching rate was determined by intermittent measurements of the optical absorption of the cell with the Beckman DU spectrophotometer. Aerobic conditions were maintained by passing water-saturated air continuously through the cell. For vacuum runs, the air was removed by vigorously shaking the solution while it was maintained below 1×10^{-5} mm. at 1° to minimize evaporation. The air-free eosin solutions showed negligible bleaching after 3 hr. of irradiation. The bleaching light intensity was maintained constant by photoelectric monitoring.

Although Imamura[4] determined the quantum efficiency for aerobic photobleaching of aqueous eosin, it was deemed desirable to repeat this measurement with our purified dye and experimental arrangement, since this quantity was used to calculate the light-absorption rate for the vacuum-photobleaching runs. For this purpose, the incident light was filtered by a narrow-band interference filter with a 506 mμ maximum and a full width of 21 mμ at half height. The light intensity passed by the filter was measured with an Epply bismuth-silver junction, windowless thermopile. The rate of photon absorption in the dye was calculated by integrating numerically the product of the spectral distribution of the tungsten lamp (as calculated from the filament temperature and the spectral emissivity of tungsten), the filter transmission, and the dye absorption. The quantum efficiency for the aerobic photobleaching of 14 μM eosin from pH 5.5 to 7.2 was found to be 0.00026 at 26.3 ± 0.2° which is in good agreement with Imamura's value of 0.00025. The average rate of light absorption for the vacuum photobleaching runs was 3.8×10^{16} photons per sec.

C. **Flash Photolysis.**—The flash spectroscopy results reported here were obtained with the apparatus and methods described in ref. 2b. The earlier kinetic spectrophotometry results have been extended under improved conditions for the determination of the reaction rate constants of the elementary processes. The irradiations were performed in cylindrical Pyrex cells from 10 to 30 cm. in length. The flash irradiation source consisted of two xenon-filled lamps adjacent to the reaction cell inside a polished aluminum reflector. They were energized at 500 to 1000 watt-sec. and 10 kv., to give a 25 μsec. light flash. Transmission changes were measured with a Hilger E720 photoelectric scanning unit on a Hilger E498 "medium" quartz prism spectrograph. The 1P28 photomultiplier signal was coupled directly to a Tektronix 545 oscilloscope with a 53/54K preamplifier. The monitoring lamp for all runs was an Osram HBO 109 mercury arc with suitable filters. The incident flash irradiation was filtered with a standard green Cellophane, which transmitted only from 460 to 600 mμ.

Transmission changes after flash irradiation were measured both at the peak of the unexcited dye absorption band and in the absorption regions of the short-lived intermediate species. It was found that spurious rate data were obtained unless the initial dye concentration was below 2 μM for measurements on the dye peak and below 5 μM for measurements on the transient spectra. This was shown to be due to a non-uniform light absorption across the cell at higher dye concentrations. Because of a permanent decomposition of eosin on flash irradiation, which is discussed below, all data reported are for the initial flash irradiation of fresh solutions.

The transient optical density change is related to the concentration of transient substance by

$$\Delta O.D. = C^*(\epsilon^0 - \epsilon^*)L = \log (V_s + \Delta V)/V_s \quad (1)$$

where ϵ^0 and ϵ^* are the molar extinction coefficients of the initial and transient substances at the wave length of measurement, L is the length of the irradiation cell, C^* is the molar concentration of transient substance (assuming that each reacted molecule gives one molecule of transient), V_s is the steady photoelectrical signal, and ΔV is the change in the photoelectric signal at any instant.

When the transient substance disappears in a first-order process, the measured rate is independent of the cell length and relative extinction coefficients, in which case information cannot be obtained about the latter. However, for second-order decay

$$(dC^*/dt) = -k(C^*)^2$$

the optical density change should depend on time according to

$$(\Delta O.D.)^{-1} = \text{constant} \pm [k/(\epsilon^0 - \epsilon^*)L]t \quad (2)$$

so that measurements made on the unexcited dye peak and on the transient spectra make it possible to calculate both the bimolecular rate constants and extinction coefficients of the unstable intermediates.

III. Results

The elementary processes which are used to explain the photochemical reactions of aqueous eosin with oxygen and with phenol are given in Table I. The proposed reaction scheme is based to a large extent on the previous work of Oster and Adelman[9], Imamura and Koizumi,[10] Lindqvist,[5] and Grossweiner and Zwicker.[2b] The following discussion is organized according to the "chronological" order of events subsequent to light absorption by eosin.

A. **Photoexcitation of Eosin.**—The states of aqueous eosin of photochemical importance are the ground state (D), the lowest excited-singlet state (D′), and the lowest triplet state (D*). If it is assumed that the excited singlet state decays by fluorescence (k_1), radiationless deactivation to the ground state (k_1'), and transitions to the triplet state (k_2), then the rate constants are related to experimental quantities by

$$\tau = (k_1 + k_1' + k_2)^{-1}; \quad \phi_{fl} = k_1\tau; \quad \phi_{max} = k_2\tau$$

where τ is the experimental fluorescence lifetime [1.6×10^{-9} sec.; Brody[11]], ϕ_{fl} is the fluorescence efficiency [0.20; Forster and Dudley[12]], and ϕ_{max} is the maximum efficiency for an irreversible oxidation induced by the eosin triplet state [0.092; Adelman and Oster[5]]. Parker and Hatchard[13] have shown that the long-lived, weak, visible luminescence of eosin at room temperature is actually delayed fluorescence due to a temperature-dependent transition from the triplet to the excited-singlet state. However, the rate must be considerably smaller than k_2 and this process should not alter appreciably the above relationships. The numerical values are listed in Table I. The intersystem crossing rate k_2 is the same order as obtained by Parker and Hatchard[13] for eosin in glycerol (4×10^7 sec.$^{-1}$) and in ethanol (1×10^7 sec.$^{-1}$).

The excited-singlet state fluorescence is not quenched by oxygen, although it is strongly quenched by halide ions and organic compounds.[14] On the other hand, triplet eosin is deactivated by oxygen as inferred from the absence of the slow luminescence in air-saturated solutions[15,16] and the strong oxygen-retardation of flash bleaching.[2b]

(9) G. Oster and A. H. Adelman, *J. Am. Chem. Soc.*, **78**, 913 (1956).
(10) M. Imamura and M. Koizumi, *Bull. Chem. Soc. Japan*, **29**, 899 (1956).
(11) S. S. Brody, *Rev. Sci. Instr.*, **28**, 1021 (1957).
(12) L. S. Forster and D. Dudley, private communication.
(13) C. A. Parker and C. G. Hatchard, *Trans. Faraday Soc.*, **57**, 1894 (1961).
(14) P. Pringsheim, "Fluorescence and Phosphorescence," Interscience Publishers, Inc., New York, N. Y., 1949, pp. 323, 332, 333.
(15) S. Boudin, *J. chim. phys.*, **27**, 785 (1930).
(16) H. Kautsky and A. Hirsch, *Chem. Ber.*, **64**, 2677 (1931).

TABLE I

ELEMENTARY REACTIONS OF THE EOSIN-PHOTOSENSITIZED OXIDATION OF PHENOL

	$I = 10^3 I'$ (einstein/cm.²-sec.)/L(cm.)
D + light → D′	
(1) D′ → D + light	$k_1 = 1.3 \times 10^6$ sec.$^{-1}$
(1′) D′ → D + heat	$k_1' = 4.4 \times 10^8$ sec.$^{-1}$
(2) D′ → D*	$k_2 = 5.8 \times 10^7$ sec.$^{-1}$
(3) D* → D + light and heat	$k_3 = 420$ sec.$^{-1}$
(3′) D* + D* → 2D	$2k_3' = 2.4 \times 10^9\ M^{-1}$ sec.$^{-1}$
(4) D′ + C_6H_5OH → D + C_6H_5OH	$k_4 = 1.4 \times 10^{10}\ M^{-1}$ sec.$^{-1}$ (Stern–Volmer)
(5) D* + O_2 → D + O_2	$k_5 = 1.6 \times 10^6\ M^{-1}$ sec.$^{-1}$
(6) D* + O_2 → products	$k_6 = 9.1 \times 10^3\ M^{-1}$ sec.$^{-1}$
(7) D* + C_6H_5OH → DH· + C_6H_5O·	$k_7 = 1.5 \times 10^5\ M^{-1}$ sec.$^{-1}$
(8) DH· + C_6H_5O· → D + C_6H_5OH	$k_8 = 6.0 \times 10^9\ M^{-1}$ sec.$^{-1}$
(9) D·$^-$ + C_6H_5O· → D + C_6H_5OH	$k_9 = 3.5 \times 10^9\ M^{-1}$ sec.$^{-1}$
H^+	
(10) DH· + DH· → D + DH_2	$2k_{10}2k_{11} = 1.4 \times 10^{16}$
(11) C_6H_5O· + C_6H_5O· → products	
(12) C_6H_6O· + H· → C_6H_5OH	$2k_{11} + k_{12} \approx 6 \times 10^9\ M^{-1}$ sec.$^{-1}$

B. Triplet Eosin.—Flash-irradiation of aqueous, air-free eosin temporarily bleaches the ground state absorption spectrum and produces a transient spectrum which was assigned to the eosin triplet.[2b] Figure 1 shows the absorption spectrum of triplet eosin obtained from the flash photolysis of 14 μM aqueous eosin at pH 5.4, as corrected for the absorption of the remaining unexcited dye; the dashed line is an interpolation in the spectral region where the unexcited dye is strongly absorbing. The ordinate was obtained by fitting the extinction coefficients calculated from the spectrum plate to values measured by kinetic spectrophotometry at selected wave lengths.

The triplet spectrum is unchanged from pH 4 to pH 12, indicating that pK of triplet eosin is below 4. This is consistent with the conclusion of Lindqvist[6] that pK of the triplet fluorescein mono-anion is almost the same as for the unexcited fluorescein mono-anion. Furthermore, Jackson and Porter[17] have shown that the acidity constants of a number of aromatic triplet molecules are comparable to their ground states, while that of the first excited-singlet state differs by a factor of 10^6 in each case.

The previous flash bleaching experiments showed that triplet eosin disappears predominantly in a fast bimolecular quenching reaction under flash photolysis conditions.[2b] In order to determine the first-order decay rate, the experiments were extended to lower eosin concentrations in cells of longer optical path. Since the return of dye coloration measures the total rate of all reversible bleaching processes, the kinetic spectrophotometry measurements were made on the eosin triplet absorption band at 436 mμ to minimize interference from other reactions. Figure 2 shows the decay of the transient absorption obtained by irradiating oxygen-free, 1.4 μM eosin at pH 9. The slow exponential contribution has a first-order rate constant of 15 sec.$^{-1}$, which is at least a power of ten smaller then would be expected for the dye triplet decay, by comparison to aqueous and non-aqueous solutions of xanthene dyes and other aromatic triplets. Furthermore, a triplet lifetime of this order leads to a value for the oxygen-quenching rate constant which is inconsistent with other measurements (see below). Therefore, the slow first-order decay is attributed to transient absorption by another product, leading to the corrected decay curve shown in the figure. The exponential decay of the latter at long times gives a rate constant of 420 sec.$^{-1}$, which is taken to be the first-order triplet decay. In order to determine the second-order rate constant, the corrected data were subjected to the differential analysis derived by Linschitz and Sarkanen[18] leading to the equation

$$-\mathrm{d}\ln(\Delta\mathrm{O.D.})/\mathrm{d}t = k_3 + [2k_3'/(\epsilon^* - \epsilon^0)L](\Delta\mathrm{O.D.}) \quad (3)$$

The corrected optical density changes taken from Fig. 2 plotted according to eq. 3 give a straight line of non-zero slope and positive intercept, verifying that the re-

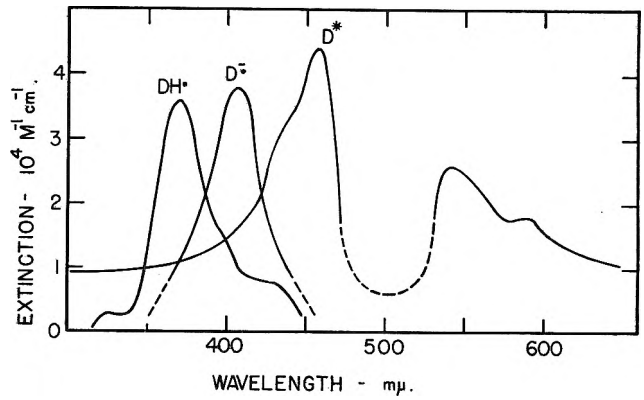

Fig. 1.—Absorption spectra of unstable species as determined from flash spectroscopy. The triplet spectrum (D*) was obtained from oxygen-free 1.4 μM eosin at pH 5.4; the semi-reduced radical spectra were obtained from oxygen-free eosin (5.4 μM) and phenol (1 mM) at pH 11.7 (D·$^-$) and from oxygen-free eosin (5.4 μM) and phenol (10 mM) at pH 5.9 (DH·).

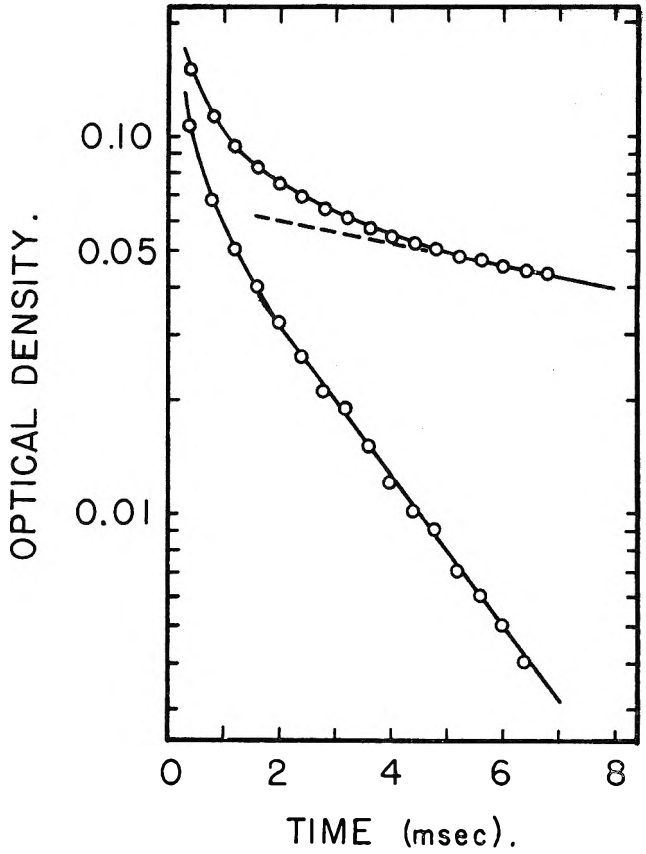

Fig. 2.—Decay of triplet eosin as measured by kinetic spectrophotometry at 436 mμ. The lower plot was derived from the upper by subtracting the long-lived process.

(17) G. Jackson and G. Porter, *Proc. Roy. Soc.* (London), **A260**, 13 (1961).

(18) H. Linschitz and K. Sarkanen, *J. Am. Chem. Soc.*, **80**, 4826 (1958).

sultant data represent simultaneous first and second-order decay processes. The intercept gives a value for k_3 close to that obtained directly in Fig. 2. The slope gives $2k'_3 = 2.8 \times 10^9\ M^{-1}$ sec.$^{-1}$, where the triplet extinction coefficient was taken from Fig. 1 at 436 mμ. This result is in agreement with a number of kinetic spectrophotometry measurements made at 516 mμ for various acidities and eosin concentrations and in cells of 1 to 30 cm. path length, which give $2k_3' = 2.4 \pm 0.4 \times 10^9\ M^{-1}$ sec.$^{-1}$. The origin of the 15-sec.$^{-1}$ decay is not known. It probably is due to another transient product whose spectrum overlaps that of triplet eosin, because the separation employed would fail if the process subtracted from the integrated rate were a decay of triplet eosin.

C. Reactions of Triplet Eosin. (1) Photolysis of Eosin Solutions.—Although oxygen-free eosin solutions are completely stable under continuous irradiation, there was always some permanent decomposition after flash-lamp irradiation. This effect could not be eliminated by any modification of the degassing procedure and is not due to residual oxygen. Comparative absorption spectra were obtained by exposing 4 μM eosin solutions to five successive flash irradiations of 500 watt-sec. each. The incident light was restricted to the visible region with a green filter. At pH 5.5, flash irradiation converts oxygen-free eosin to a colorless product and the addition of oxygen inhibits the extent of bleaching. When phenol was present in oxygen-free solutions, the amount of permanent bleaching was enhanced. The inhibitory effect of oxygen on the extent of permanent bleaching was also evident at pH 9.0. However, with the addition of phenol to oxygen-free solutions at the higher pH, the predominant effect of irradiation was a shift of the absorption peak to shorter wave lengths, indicating that debromination had occurred. It is clear that two different processes are involved. The permanent bleaching inhibited by oxygen probably is a reaction of triplet eosin, since there is no indication that excited-singlet eosin reacts with oxygen at the concentrations employed. Lindqvist[6] noted a comparable permanent change on flash irradiation of oxygen-free fluorescein solutions and suggested that it is due to a photooxidation of triplet dye *via* a two-step process. The marked dependence of debromination on acidity indicates that it takes place from the reaction product of triplet eosin with phenol, *i.e.*, semi-reduced eosin. As shown below, pK for this semiquinone species is 6.8, so that it is the di-anion which dehalogenates. This is in agreement with the observations of Imamura and Koizumi,[19] who showed that air-free solutions of eosin in 10% ethanol–water are photodebrominated and noted that a small amount of acetic acid inhibits the reaction. Recently, Oster, Oster, and Karg[8] investigated the photochemical dehalogenation of various halogenated fluorescein dyes in the presence of tertiary amines and postulated a semiquinone intermediate which decomposes spontaneously to yield the partially dehalogenated species.

(2) Steady-State Reactions of Triplet Eosin.—The photolysis of oxygen-free eosin and phenol solutions gives information on the primary reaction between triplet eosin and phenol, and the rate of aerobic reaction gives information on the competition between oxygen-quenching of triplet eosin and the reaction of triplet eosin with either oxygen or phenol. In relating the experimental quantities to rate constants, it was necessary to evaluate carefully the approximations employed, since the rates of triplet disappearance by various processes can be competitive. Quenching of excited singlet eosin by phenol should be significant only above 10 mM phenol. The previously determined[2b] Stern–Volmer quenching constant of 22 M^{-1}, which equals τk_4, gives $1.4 \times 10^{10}\ M^{-1}$ sec.$^{-1}$ for k_4. Although the interpretation of this quantity as a diffusion-controlled rate constant is a considerable simplification, the result indicates that phenol is a very efficient quencher of excited singlet eosin.

In the absence of quenching agents, the steady-state concentration of triplet eosin is determined by

$$I\phi_{max} - k_3\mathrm{D}^* - 2k_3'(\mathrm{D}^*)^2 = 0$$

where I is the rate of light absorption in the irradiated volume. (Chemical symbols are used to designate molar concentrations in rate equations, except where ambiguity would result.) Substitution of the experimentally determined light intensity (1.6×10^{-5} einstein/l.-sec.) and the rate constants in Table I gives $\mathrm{D}^* = 4 \times 10^{-9}\ M$, so that the rate of first-order triplet decay exceeds that of second-order decay by a factor of 50 and the latter can be neglected in this work.

a. Aerobic Photobleaching.—In phenol-free aerobic solutions, the quantum efficiency for photobleaching is given by

$$\phi_a^0 = k_6^0\phi_{max}/(k_3 + k_5^0 + k_6^0) \qquad (4)$$

where the superscript 0 denotes the product of the rate constant and the molar concentration of oxygen in air-saturated water. Substitution of the experimentally determined quantum efficiency for the photobleaching of 14 μM eosin at pH 5.5 and 25° gives $k_5 + 1.8 \times 10^6 = 367k_6$.

When phenol is present, the photobleaching rate is retarded by a competitive reaction with triplet eosin giving

$$(\phi_a)^{-1} = (\phi_a^0)^{-1} + k_7C/k_6^0\phi_{max} \qquad (5)$$

where C is the molar phenol concentration and reaction 4 has been neglected. The data for retardation give a straight line when plotted according to eq. 5, as shown in Fig. 3, and the slope gives $k_7/k_6 = 16.4$.

b. Vacuum Photobleaching.—The steady-state conditions for the vacuum photobleaching of aqueous eosin, where the acidic semiquinone is stable, are

$$k_7\mathrm{D}^*C - k_8(\mathrm{DH}\cdot)(\mathrm{C_6H_5O}\cdot) - 2k_{10}(\mathrm{DH}\cdot)^2 = 0$$

$$k_7\mathrm{D}^*C - k_8(\mathrm{DH}\cdot)(\mathrm{C_6H_5O}\cdot) - 2k_{11}(\mathrm{C_6H_5O}\cdot)^2 = 0 \qquad (6)$$

The quantum efficiency is

$$\phi_v = (k_{10}k_7\mathrm{D}^*C/I)[(k_8/p) + 2k_{10}]^{-1} \qquad (7)$$

where $p = (2k_{11}/2k_{10})^{1/2}$. When reaction 3′ is neglected, $\mathrm{D}^* = I\phi_{max}/(k_3 + k_7C)$ and

$$(\phi_v)^{-1} = (\phi_v^\infty)^{-1}[(k_3/k_7C) + 1] \qquad (8)$$

where

$$(\phi_v^\infty) = k_{10}\phi_{max}/[2k_{10} + (k_8/p)] \qquad (9)$$

(19) M. Imamura and M. Koizumi, *Bull. Chem. Soc. Japan*, **29**, 913 (1956).

Figure 4 shows the data for the vacuum photobleaching of 14 μM eosin at pH 5.5 and 25° plotted according to eq. 8. The intercept gives $\phi_v^\infty = 0.89 \times 10^{-3}$, which is 10^{-2} times the value of ϕ_{max} as obtained from the vacuum photobleaching of eosin in the presence of allyl thiourea,[9] proving that the oxidation of phenol by triplet eosin is largely reversible. It is concluded that radical recombination is the predominant process by which the semiquinone product disappears and that the permanent bleaching is due to slower reactions, probably dismutation. From Fig. 4 and the value for k_3, it is found that $k_7 = 1.50 \times 10^5\ M^{-1}$ sec.$^{-1}$ and that $2k_{10}2k_{11} = 1.4 \times 10^{16}$, where the value for k_8 has been taken from the flash photolysis data reported below. The values for k_5 and k_6 reported in Table I were calculated from these results.

D. Free Radical Reactions.—It was reported previously that flash spectra taken of air-free dye and phenol solutions show two distinct transient spectra.[2b] One spectrum was constant for the various halogenated fluorescein dyes and was identical with the spectrum identified by Grossweiner and Mulac as the phenoxy radical-ion.[20] The wave length maxima of the other spectra are shifted to longer wave lengths with increasing halogenation and they were identified with the semi-reduced dye radicals. The spectra of semi-reduced eosin in acidic and basic solutions are shown in Fig. 1. The extinction coefficients were calculated from kinetic spectrophotometry measurements at the unexcited dye peak and at the radical transient absorption bands, according to eq. 2. The average values obtained from runs with various dye concentrations and cell lengths are $3.6 \pm 0.4 \times 10^4\ M^{-1}$ cm.$^{-1}$ for the mono-anion (DH·) at 369 mμ, and $3.8 \pm 0.4 \times 10^4\ M^{-1}$ cm.$^{-1}$ for the di-anion (D·$^-$) at 405 mμ. The DH· spectrum is very similar to the transient absorption first obtained by Kato and Koizumi[21] on flash photolysis of eosin in ethanol, which they identified as the semiquinone radical of eosin.

Grossweiner and Mulac[20] originally assigned the phenoxy radical spectrum to the cation and Grossweiner and Zwicker[22] assigned to the neutral phenoxy radical a different spectrum obtained by flash photolysis of aqueous phenol at pH 14. Subsequently, Land, Porter, and Strachan[23] showed that the latter was due to photolysis of a reaction product of phenol. We have re-investigated the flash photolysis of aqueous phenol from pH 1 to pH 14 and concur that only the neutral phenoxy radical is stable in this acidity range. Kinetic spectrophotometry measurements of 1 mM phenol solutions at pH 7 showed that the phenoxy radical disappearance is bimolecular during the initial stages with a ratio of rate constant to extinction coefficient at 399 mμ of $5.8 \pm 1.5 \times 10^5$/cm.-sec.$^{-1}$. Estimating an extinction coefficient of 10^4 from the strong absorption[24] gives $2k_{11} + k_{12} = 6 \times 10^9\ M^{-1}$ sec.$^{-1}$.

Kinetic spectrophotometry of air-free phenol and eosin solutions showed that the rate constants for the disappearance of acidic and basic semi-reduced eosin depend on pH. (The measurements were made at 360 and 410 mμ to give a better separation of the two spectra.) The variation is due to dissociation equilibrium. This effect was investigated by determining the reaction rate over a range of acidity established by strong phosphate buffers. Lindqvist[6] and Jackson and Porter[17] have pointed out that the time required to establish equilibrium in unbuffered aqueous solution is too long for flash photolysis measurements, particularly from pH 6 to 8. The results are shown in Fig. 5. The rate constant for the disappearance of DH· is relatively constant in acidic solution and increases rapidly in basic solution; the converse is true for D·$^-$. This variation can be analyzed by an approach which was used previously to explain the dependence of the decay rate of I_2^- on iodide ion concentration[25]; it is as-

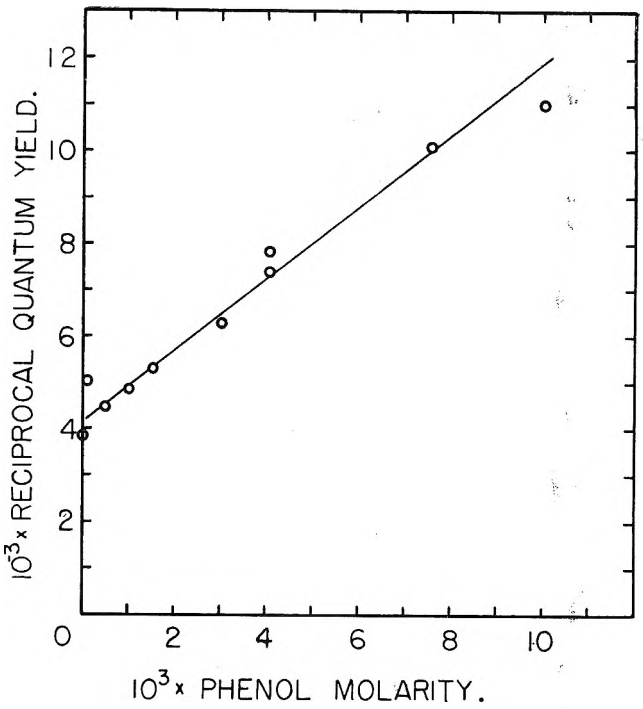

Fig. 3.—The retardation of the aerobic photobleaching of 14 μM eosin at pH 5.5 by phenol.

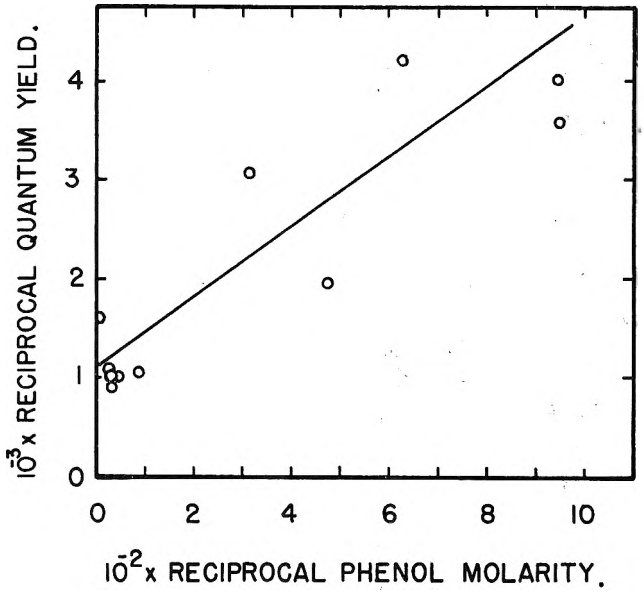

Fig. 4.—The dependence of the vacuum photobleaching quantum efficiency on phenol concentration, for 14 μM eosin at pH 5.5 and 25°.

(20) L. I. Grossweiner and W. A. Mulac, *Radiation Res.*, **10**, 515 (1959).
(21) S. Kato and M. Koizumi, *Nature*, **184**, 1620 (1959).
(22) L. I. Grossweiner and E. F. Zwicker, *J. Chem. Phys.*, **32**, 305 (1960).
(23) E. J. Land, G. Porter, and E. Strachan, *Trans. Faraday Soc.*, **57**, 1885 (1960).
(24) L. I. Grossweiner, *J. Chem. Phys.*, **24**, 1255 (1956).
(25) L. I. Grossweiner and M. S. Matheson, *J. Phys. Chem.*, **61**, 1089 (1957).

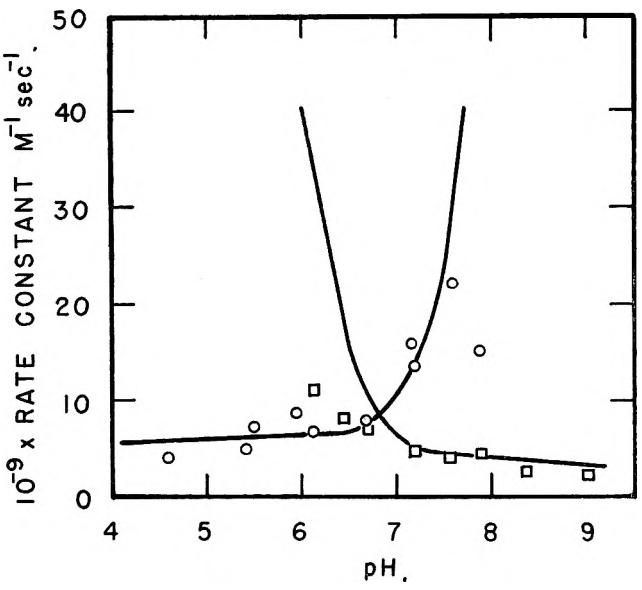

Fig. 5.—The dependence of the rate constant for the bimolecular reaction of semi-reduced eosin on acidity. The disappearance of DH· was measured at 360 mμ and that of D·⁻ at 410 mμ. The solid lines were calculated from eq. 10 for pK = 6.8.

sumed that the reactions that establish dissociation equilibrium are much faster than the rate at which the unstable radicals disappear, a good approximation for the buffered solutions used in these measurements.

Dissociation equilibrium of semi-reduced eosin with the buffer gives

$$DH\cdot + B^- \underset{k'}{\overset{k}{\rightleftharpoons}} D\cdot^- + BH$$

where the equilibrium constant (k/k') is equal to the ratio of the dissociation constant of semi-reduced eosin to the dissociation constant of the buffer. It can be assumed that the phenoxy radical concentration approximately equals the total concentration of semi-reduced eosin, giving

$$d(DH\cdot)/dt = -k_8(DH\cdot)[(DH\cdot) + (D\cdot^-)] - k(DH\cdot)(B^-) + k'(D\cdot^-)(BH)$$

$$d(D\cdot^-)/dt = -k_9(D\cdot^-)[(DH\cdot) + (D\cdot^-)] - k'(D\cdot^-)(BH) + k(DH\cdot)(B^-)$$

Addition of the above equations and substitution on the equilibrium condition gives

$$d(DH\cdot)/dt = -(k_8 + qk_9)(DH\cdot)^2 = -k_8'(DH\cdot)^2$$

$$d(D\cdot^-)/dt = -(k_9 + q^{-1}k_8)(D\cdot^-)^2 = -k_9'(D\cdot^-)^2 \quad (10)$$

where $q \equiv K/(H^+) = k_8'/k_9'$.

The extent of approximation in this analysis can be clarified by noting that eq. 10 are not exactly compatible with the equilibrium relation. Integration of eq. 10

$$1/(DH\cdot) = 1/(DH\cdot)_0 + k_8't$$

$$1/(D\cdot^-) = 1/(D\cdot^-)_0 + k_9't$$

and elimination of the time gives

$$K = \frac{(H^+)(D\cdot^-)}{(DH\cdot)}\left[\frac{1 - \dfrac{(DH\cdot)}{(DH\cdot)_0}}{1 - \dfrac{(D\cdot)^-}{(D\cdot^-)_0}}\right]$$

Therefore, the "instantaneous" equilibrium constant as derived from the dependence of the observed rate constants on acidity is exact only at long decay times. The two parts of eq. 10 were applied to the data by taking as the true rate constants the measured values at high and low acidity. Accordingly, the solid line in Fig. 5 was calculated from eq. 10 for $k_8 = 6.0 \times 10^9$ and $k_9 = 3.5 \times 10^9$ and a trial and error value pK = 6.8, which was selected for a best fit to the data. The agreement between the calculated and experimental rate constants is sufficiently good to establish that dissociation equilibrium of semi-reduced eosin is the major factor leading to a dependence of the measured rate constants on pH. However, the discrepancy at high and low pH shows that this simple theory is not quantitatively accurate over the entire acidity range.

IV. Discussion

In solutions where the phenolate ion is stable, the primary photochemical act is almost certainly an electron-transfer from the phenolate ion to triplet eosin. In more acidic solutions, it could not be determined whether the primary act is an electron or a hydrogen atom transfer. However, since the result of the former would be a fast dissociation of the phenol radical-cation, the distinction between the two processes is not clearly delineated. The mechanism of the primary act can be taken as

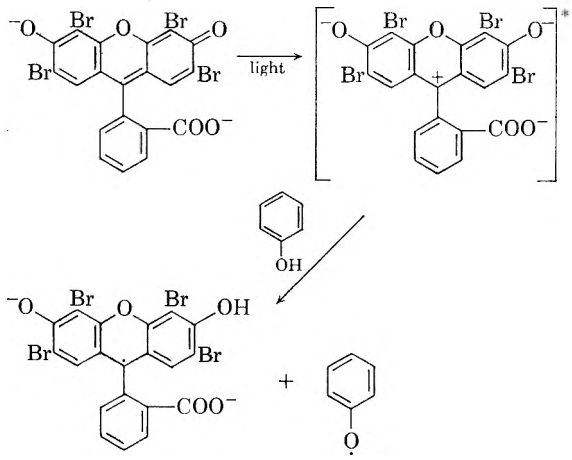

The semiquinone structure with the unpaired electron at carbon 9 is based on the e.p.r. measurements of Bubnov and co-workers,[26] and the triplet structure indicated is one of a number of possible resonance forms.

Table II shows a summary of the results with eosin compared with those obtained by Lindqvist for fluorescein.[6] An unexplained variation is that the triplet spectra differ appreciably in wave length maxima and extinction coefficients. Another significant difference between eosin and fluorescein involves the reactions of the triplet dye. Lindqvist proposed that first-order deactivation competes with quenching by the unexcited dye and with an electron-transfer reaction be-

(26) N. N. Bubnov, L. A. Kibalko, V. F. Tsepalov, and V. Ya. Shliapintokh, *Opt. i Spektroskopiya*, **7**, 117 (1959).

TABLE II

COMPARISON OF FLUORESCEIN AND EOSIN

Unexcited di-anion	Fluorescein[a]	Eosin[b]
Absorption maximum (mμ)	491	516
Maximum extinction (M^{-1} cm.$^{-1}$)	8.8×10^4	9.2×10^4
pK (of mono-anion)	6.7	≈4.3
Triplet di-anion		
Absorption maximum (mμ)	520, >950	459, 540
Maximum extinction (M^{-1} cm.$^{-1}$)	8×10^3	4.4×10^4
pK (of mono-anion)	7.0	<4
1st-order decay rate (sec.$^{-1}$)	50	420
2nd-order decay rate (M^{-1} sec.$^{-1}$)	1.7×10^{9c}	2.4×10^9
Basic semi-reduced radical		
Absorption maximum (mμ)	394	405
Maximum extinction (M^{-1} cm.$^{-1}$)	5×10^4	3.8×10^4
Acidic semi-reduced radical		
Absorption maximum (mμ)	355	369
Maximum extinction (M^{-1} cm.$^{-1}$)	3×10^4	3.6×10^4
pK (of mono-anion)	9.5	6.8

[a] Taken from the work of Lindqvist, ref. 6. [b] Taken from ref. 2 and this work. [c] Total rate of all second-order processes.

tween triplet molecules, producing semi-reduced and semi-oxidized radical species. On the other hand, our measurements show that first-order triplet decay competes only with bimolecular self-quenching. Furthermore, flash spectra taken of oxygen-free eosin solutions from pH 4 to 12 show no indication of semi-reduced eosin and, subsequently, the triplet–triplet electron-transfer reaction cannot be significant for eosin. (We did obtain the band identified by Lindqvist as semi-oxidized fluorescein on flash spectra taken of aqueous fluorescein.) It must be concluded that bromination of fluorescein changes markedly the electronic properties of the triplet state. The charge-separation structure shown above is consistent with an extensive alteration of the charge distribution by the strongly electronegative substituents.

The first-order triplet lifetime of 2.4 msec. is in agreement with the work of Parker and Hatchard,[13] who obtained 2.7 and 1.7 msec. in glycerol and ethanol solutions, respectively, at 25°. The rate constant for oxygen-quenching of triplet eosin is in approximate agreement with the measurements of Imamura,[4] showing that the quantum yield for aerobic photobleaching is negligible below 2×10^{-5} M oxygen and giving $k_6/k_3 \approx 5 \times 10^4$, which can be compared to 4×10^3 from Table I. Triplet eosin is 1000 times more stable against oxygen quenching than triplet anthracene, although their first-order decay constants are comparable.[27]

The extent of reversibility of the dye-photosensitized process depends on the relative rate of the radical back-reaction compared to the dismutation of semi-reduced dye and reactions of the oxidized substrate and not on the primary reaction with triplet dye. For example, the rate constant for the reversible oxidation of phenol by triplet eosin is 1.5×10^5 M^{-1} sec.$^{-1}$, while that for the reversible oxidation of p-phenylenediamine by triplet fluorescein is 5×10^9 M^{-1} sec.$^{-1}$.[6] On the other hand, the irreversible oxidation of allyl thiourea by triplet fluorescein proceeds at a rate of 2×10^5 M^{-1}sec.$^{-1}$.[6] The vacuum photobleaching results show that $2k_{10} \ll 6 \times 10^9$. An unambiguous value for the rate of the dismutation reaction cannot be obtained from our data because the results on the flash photolysis of aqueous phenol give only $2k_{11} + k_{12}$ and the mechanism for the disappearance of phenoxy radical is not known. If the photooxidation of phenol is largely reversible, then $2k_{10} \approx 10^7$ to 10^9. However, if reaction 11 predominates over reaction 12, then $2k_{10} \approx 10^6$. Hatchard and Parker[28] have shown that the dismutation rate constant of aqueous semi-reduced thionine is 2.4×10^9 M^{-1} sec.$^{-1}$, suggesting that the former case is more likely. The work of Tsepalov and Shliapintokh[29] on the photostationary eosin and ascorbic acid system in pyridine is interesting in this connection, in that it was proposed that semi-reduced eosin not only dismutes, but also is further reduced to the leuco base by ascorbic acid. Ascorbic acid is a much stronger reducing agent than phenol and this process probably does not contribute to the permanent reduction of eosin by phenol.

Acknowledgment.—The authors wish to acknowledge the contributions of the following undergraduate research participants supported by a National Science Foundation Undergraduate Science Education Program: David Brewe, Peter DePerro, Richard Powers, and Paul Wattelet.

(27) G. Jackson, R. Livingston, and A. C. Pugh, *Trans. Faraday Soc.*, **56**, 1635 (1960).

(28) C. G. Hatchard and C. A. Parker, *ibid.*, **57**, 1093 (1961).

(29) V. F. Tsepalov and V. Ya. Shliapintokh, *Izv. Akad. Nauk SSSR, Otd. Khim. Nauk*, **4**, 637 (1959).

THE STATISTICAL MECHANICS OF MICELLES[1]

BY R. H. ARANOW

RIAS, Baltimore 12, Maryland

Received July 23, 1962

A theory of micelle statistics is developed using the extended theory of dilute solutions, the dielectric continuum model of the solvent, and the statistical mechanical treatment of physical clusters at constant pressure, and a connection is made between the mass action approach and the two-phase approach currently in use for examining micelle behavior. Both ionic and non-ionic micelles are treated. A discussion is given for non-ionic micelles of the meaning of averages, fluctuations in size, ideality, and variation of c.m.c. with temperature. A more general theory of micelle statistics is formulated by the elimination of the continuum model of the solvent and the extended theory of dilute solutions. Reich's model for non-ionic micelles is used to illustrate the theory.

Introduction

Micelles, large clusters of molecules in equilibrium, are sometimes treated theoretically as a product of the reaction of single molecules to form clusters with an associated equilibrium constant.[2,3] Sometimes the micelles are considered to be a different phase and the thermodynamics of phase equilibria is invoked.[4,5] Hoeve and Benson,[6] in a treatment which can be considered as a simplification of Hill's theory of molecular clusters of imperfect gases,[7] studied the statistical mechanics of micellar systems using the canonical ensemble.

The purpose of this report is to develop a more general theoretical treatment of micelle statistics using Hill's theory of physical clusters and the ensemble natural for constant temperature, pressure and quantity of solvent. The more general theory provides a common foundation for previous different approaches and reveals the relationship between them as well as the source of some of the uncertainty underlying the interpretation of micelle behavior.

Some of the problems which arise in the study of micelles are the meaning of the temperature variation of the critical micelle concentration, the effect of interaction of micelles upon the distribution of micelle sizes, the meaning of "ideality," the nature of the spread of micelle sizes about the average value, and whether or not consideration of a single micellar size can be used as a basis for a theoretical treatment of micelles. We shall endeavor to answer some of these questions or at least to state the question in a quantitative manner. In section I of this paper we shall present a more general ensemble for non-ionic systems using the physical cluster theory of Hill, the extended theory of dilute solutions of Fowler and Guggenheim,[8] and the assumption of incompressibility. This ensemble yields information about osmotic pressure and the effect of interaction of clusters. The meaning of the law of mass action and phase equilibrium will be stated.

In section II several useful relationships for non-ionic micelles will be derived concerning fluctuations in micelle size and the effect of dimerization on quantities related to the critical micelle concentration.

In section III ionic micelles will be treated using a modified constant pressure ensemble, the physical cluster theory of Hill, the continuum model of the solvent, and the extended theory of dilute solutions.

Suggestions for a more general treatment of micellar statistics will be discussed in section IV.

In section V calculations for an analytically tractable model proposed by Reich will be presented in order to demonstrate the relationships developed in preceding parts of this report.

I. Constant Pressure Solution Theory.—In order to develop a more general formal structure for studying micelle systems, we use the ensemble suitable for constant pressure, constant temperature, and constant amount of solvent which Hill considered for a constant pressure solution theory.[9] The partition function for this ensemble is

$$\Gamma(N_\alpha, p, T, \mu_\beta) = e^{-N_\alpha\mu_\alpha/kT} = \sum_{N_\beta \geq 0} \Delta_{N\beta}(N_\alpha, p, T) e^{N_\beta\mu_\beta/kT} \quad (1)$$

where

$$\Delta_{N\beta} = \sum_V Q(N_\alpha, N_\beta, V, T) e^{-pV/kT}$$

and $Q(N_\alpha, N_\beta, V, T)$ is the canonical ensemble partition function. N is the number of molecules, μ is the chemical potential, V is the volume, p is the pressure, and T is the absolute temperature. Subscript α refers to the solvent and subscript β to the solute. We restrict our discussion to a binary non-ionic system. The leading term, Δ_0, of the sum in (1) refers to the pure solvent.

The extended theory of dilute solutions[8] requires that the total free energy be the sum of the free energy of the component parts and the partition function for a binary solution must be the product of two partition functions of the form

$$Q_{\text{solution}} = Q_{\text{solvent}}(T, V - N_\beta v_\beta, N_\alpha) \times Q_{\text{solute}}(N_\alpha, N_\beta, V, T) \quad (2)$$

where Q_{solute} contains all solute–solvent interaction terms and v_β is the partial molar volume of a molecule of solute. If both the solvent and solution are regarded as incompressible and the extended theory of dilute solutions applies we have

$$Q(N_\alpha, N_\beta = 0, V, T) = Q_0(N_\alpha, V, T)\delta(V - V_0)$$

(1) This research was supported by the United States Air Force through Directorate of Chemical Sciences, Air Force Office of Scientific Research, under Contract Number AF 49(638)-735. Reproduction in whole or in part is permitted for any purpose of the United States Government.

(2) (a) I. Reich, *J. Phys. Chem.*, **60**, 257 (1956); (b) D. Stigter, *Rec. trav. chim.*, **73**, 593 (1954).

(3) M. J. Vold, *J. Colloid Sci.*, **5**, 506 (1950).

(4) K. Shinoda, *Bull. Chem. Soc. Japan*, **26**, 101 (1953).

(5) (a) E. Matijevic and B. A. Pethica, *Trans. Faraday Soc.*, **54**, 587 (1958); (b) E. Hutchinson, A. Inaba, and L. G. Baily, *Z. physik. Chem.*, **5**, 344 (1955); (c) G. Stainsby and A. E. Alexander, *Trans. Faraday Soc.*, **46**, 587 (1950); (d) K. Shinoda and E. Hutchinson, *J. Phys. Chem.*, **66**, 577 (1962).

(6) C. A. J. Hoeve and G. C. Benson, *ibid.*, **61**, 1149 (1957).

(7) T. L. Hill, *J. Chem. Phys.*, **23**, 617 (1955).

(8) R. Fowler and E. A. Guggenheim, "Statistical Thermodynamics," Cambridge, 1956, Chapter VIII, p. 372.

(9) T. L. Hill, *J. Am. Chem. Soc.*, **79**, 4885 (1957); *J. Chem. Phys.*, **30**, 93 (1959).

and

$$Q(N_\alpha, N_\beta, V, T) = Q_0(N_\alpha, V - N_\beta v_\beta, T) \times \delta(V - [V_0 + N_\beta v_\beta])Q_{N\beta}(N_\alpha, N_\beta, V,T) \quad (3)$$

where δ is the Dirac δ-function.

Substituting these relations into eq. 1 we have

$$\Gamma = \sum_{N\beta \geqq 0} e^{-p(V_0+N\beta v\beta)/kT} Q_0 Q_{N\beta} e^{N\beta\mu\beta/kT} = e^{-pV_0/kT} Q_0 \sum_{N\beta \geqq 0} Q_{N\beta} \lambda_\beta{}^{N\beta} \quad (4)$$

where λ_β is a constant quantity for the ensemble and is, by definition, $\exp(\mu_\beta - pv_\beta)/kT$. Let us introduce the following notation

$$\mu_s = s(\mu_\beta)$$
$$v_s = s(v_\beta)$$
$$\lambda_s = (\lambda_\beta)^s \quad (5)$$

Using the methods developed by Hill in the theory of molecular clusters in imperfect gases the partition function $Q_{N\beta}$ can be written in a way in which the clusters appear explicitly

$$Q_{N\beta} = \sum_{\mathbf{N}} Q_{\mathbf{N}} \quad (6)$$

where $Q_{\mathbf{N}}$ refers to the partition function for a set of clusters $\mathbf{N} = N_1, N_2, \ldots N_s, \ldots$ and the summation is taken over all possible sets subject to the restriction

$$\sum_{s=1}^{\infty} sN_s = N_\beta \quad (7)$$

The product $Q_{N\beta}\lambda_\beta{}^{N\beta}$ can then be rewritten as

$$Q_{N\beta}\lambda^{N\beta} = \sum_{\mathbf{N}} Q_{\mathbf{N}} (\prod_s \lambda_s{}^{N_s}) \quad (8)$$

where the N_s is from the set $\mathbf{N}$. Then

$$\sum_{N\beta \geqq 0} Q_{N\beta}\lambda_\beta{}^{N\beta} = \sum_{\mathbf{N} \geqq 0} Q_{\mathbf{N}} (\prod_s \lambda_s{}^{N_s}) \quad (9)$$

where the summation is over all cluster sets corresponding to all possible values of N_β and the relationship between Q_N and $Q_{\mathbf{N}}$ is displayed, for example, by

$$Q_1 = Q_{100\ldots}$$
$$Q_2 = Q_{200\ldots} + Q_{010\ldots}$$
$$Q_3 = Q_{300\ldots} + Q_{110\ldots} + Q_{001\ldots} \quad (10)$$

The subscript notation on the right reveals the nature of the distribution. The position in the sequence reveals the number of particles in the cluster, *i.e.*, s, while the number in that position reveals N_s.

The equilibrium or average number of s clusters is obtained by applying

$$\bar{N}_s = \lambda_s \frac{\partial \ln \Gamma}{\partial \lambda_s} \quad (11)$$

to eq. 4 using eq. 9. After the differentiation we set $\lambda_s = \lambda_\beta{}^s$. This gives

$$\bar{N}_1 = \lambda_\beta Q_{100\ldots} + \lambda_\beta{}^2 (2Q_{200\ldots} - Q_{100}{}^2\ldots) + \ldots$$
$$\bar{N}_2 = \lambda_\beta{}^2 Q_{010\ldots} + \lambda_\beta{}^3 (Q_{110\ldots} - Q_{100\ldots}Q_{010\ldots}) + \ldots$$
$$\bar{N}_n = \lambda_\beta{}^n Q_{000\ldots1} + \lambda_\beta{}^{n+1}(Q_{100\ldots1} - Q_{100\ldots}Q_{000\ldots1}) + \ldots \quad (12)$$

When the clusters are non-interacting as in the theory of Hoeve and Benson, only the leading terms appear. The Q's of the leading terms are the partition functions for single clusters in the system. The interaction of the cluster with the solvent but not with other clusters is contained in the leading term. When the first interaction term is included, the effect of interaction of monomer with cluster is taken into account.

The set of eq. 12 leads to "law of mass action" equilibrium quotients

$$\frac{\bar{N}_1{}^n}{\bar{N}_n} = \frac{Q_{100\ldots1}{}^n}{Q_{000\ldots1}{}^n} \left\{1 + \lambda_\beta \left[\frac{2nQ_{200\ldots}}{Q_{100\ldots}} - (n-1)Q_{100\ldots} - \frac{Q_{100\ldots1}}{Q_{000\ldots1}}\right] + \ldots\right\} \quad (13)$$

where the first term in λ_β accounts for interaction of monomer with monomer and with the cluster of size n.

Extension of the development to ideal mixed micelles can be made by considering the clusters themselves to be ideal (perfect) solutions[11] internally at constant temperature and pressure. Then the summation in $\Gamma(N_\alpha,p,T,\mu_\beta,\mu_\gamma)$ would be taken over all values of N_β and N_γ and then over all cluster distributions $\mathbf{N}$ where each distribution corresponds to a particular combination, $N_\beta + N_\gamma$. Since no further concepts are introduced, the methods are essentially the same as we have discussed and the assumptions are equivalent to those of the two phase treatment by Shinoda[12] and the mass action treatment of Mysels and Otter,[13] we shall not consider this topic further.

II. Applications.—One further result of constant pressure solution theory which is useful in micelle studies is the relationship of the ensemble to osmotic pressure.[9]

Noting that

$$N_\alpha\mu_\alpha(p,T,0) = -kT \ln \Delta_0 \quad (14)$$

where $\mu_\alpha(p,T,0)$ is the chemical potential of pure solvent and defining

$$\mu_\alpha'(p,T,\bar{N}_\beta) = \mu_\alpha(p,T,\bar{N}_\beta) - \mu_\alpha(p,T,0) \quad (15)$$

we have

$$-\frac{\mu_\alpha'(p,T,\bar{N}_\beta)}{kT} = \frac{1}{N_\alpha} \ln \frac{\Gamma}{\Delta_0} \quad (16)$$

But for osmotic equilibrium between a solution at $p,T,\bar{N}_\beta$, and the pure solvent at $p - \Pi$, T, we have

$$\mu_\alpha(p,T,\bar{N}_\beta) = \mu_\alpha(p - \Pi,T,0) \quad (17)$$

and

$$\mu_\alpha(p,T,0) - \mu_\alpha(p - \Pi,T,0) = \frac{-\mu_\alpha'}{kT}(p,T,\bar{N}_\beta) = \int_{p-\Pi}^{p} v_\alpha(p',T)dp' \quad (18)$$

(10) B. D. Flockhart, *J. Colloid Sci.*, **16**, 484 (1961).
(11) R. Fowler and E. A. Guggenheim, ref. 8, Chap. VIII, p. 353.
(12) K. Shinoda, *J. Phys. Chem.*, **58**, 541 (1954).
(13) K. J. Mysels and R. J. Otter, *J. Colloid Sci.*, **16**, 474 (1961).

Using the same assumption of incompressibility we used to develop the form of Γ we have the relationships

$$\frac{-\mu_\alpha'}{kT} = \frac{\Pi v_\alpha}{kT} = \frac{1}{N_\alpha} \ln \frac{\Gamma}{\Delta_0} = \frac{1}{N_\alpha} \ln \left(\sum_{\mathbf{N} \geq 0} Q_{\mathbf{N}} \left(\prod_s \lambda_s^{N_s} \right) \right) \tag{19}$$

Therefore, the ensemble sum has a clear physical interpretation. When the maximum term method can be used for N_β and for **N** and micelles do not interact, the expected result for an ideal dilute solution can be deduced that

$$\frac{\Pi v_\alpha}{kT} = \sum_s \frac{N_s^*}{N_\alpha} \tag{20}$$

where the asterisk denotes values in the most probable (maximum) distribution. Let us return now to the distribution of average micelle sizes in order to compare the statistical treatment to a two-phase equilibrium problem. For the non-ionic detergent, ignoring cluster interactions we have, letting $Q_{000\ldots1} = \mathrm{Q}_s$

$$\bar{N}_s = e^{\frac{s(\mu_\beta - pv_\beta)}{kT}} \mathrm{Q}_s \tag{21}$$

For the monomer we compute

$$\mu_\beta = pv_\beta - kT \ln \mathrm{Q}_1 + kT \ln \bar{N}_1 \tag{22}$$

For the cluster

$$s\mu_\beta = sv_\beta - kT \ln \mathrm{Q}_s + kT \ln \bar{N}_s \tag{23}$$

At the maximum $\bar{N}_s$ in the distribution, $\bar{N}_s^*$, where the asterisk denotes the maximum value

$$\frac{\partial \ln \bar{N}_s^*}{\partial s} = 0 \tag{24}$$

Thus

$$\mu_\beta = pv_\beta - kT \frac{\partial \ln \mathrm{Q}_s^*}{\partial s} \tag{25}$$

Equating 22 to 25 we have the relationship

$$-kT \frac{\partial \ln \mathrm{Q}_s^*}{\partial s} = -kT \ln \mathrm{Q}_1 + kT \ln \bar{N}_1 \tag{26}$$

At the critical micelle concentration when dimers have not formed appreciably $\bar{N}_1/V$ is the critical micelle concentration. This relationship is comparable to the one used by Shinoda[4] in his treatment of the effect of chain length on critical micelle concentration. (See section III of this paper.) Shinoda's energy calculations for the micelle "phase" clearly are related to the energy changes involved in adding or removing a molecule from the most probable micelle. This relationship displays the reason for the success in some calculations of theories which postulate only a single micelle size: only the most probable micelle need be considered in any calculation involving chemical potential. (Vold[3] has discussed other aspects of this problem for ionic micelles in terms of the mass action law.) When dimers are appreciably formed at the critical micelle concentration, we need only substitute the relationship N/V = c.m.c. $= (\bar{N}_1 + 2\bar{N}_2)/V$ to obtain

$$-kT \frac{\partial \ln \mathrm{Q}_s^*}{\partial s} = -kT \ln \mathrm{Q}_1 + kT \ln [(\text{c.m.c.})V - 2\bar{N}_2] \tag{27}$$

The interpretation of the changes of c.m.c. with temperature is clear for the case in eq. 26.

$$-\left(\frac{\partial \left(\frac{\partial \ln \mathrm{Q}_s^*}{\partial s} \right)}{\partial T} \right)_{p, N_\alpha, \bar{N}_\beta} = -\left(\frac{\partial \ln \mathrm{Q}_1}{\partial T} \right)_{p, N_\alpha, \bar{N}_\beta} + \left(\frac{\partial \ln V\,(\text{c.m.c.})}{\partial T} \right)_{p, N_\alpha, \bar{N}_\beta} \tag{28}$$

For eq. 27 a similar computation may be made.

Deviations of heats of micellization computed using eq. 28 from those found calorimetrically are sometimes attributed to non-ideality or to dimerization.[10] Equations 12 indicate the nature of the terms which must be considered to include monomer and cluster interactions if these are the source of non-ideality.

The fluctuation of micelle size about the average of the distribution for non-interacting clusters of non-ionic detergents can be related to experimental observables. Using the definitions

$$\bar{\mathbf{N}} = \sum_s \bar{N}_s = \sum_s \lambda_\beta^s \mathrm{Q}_s$$
$$\bar{N}_\beta = \sum_s s\bar{N}_s = \sum_s S\lambda_\beta^s \mathrm{Q}_s \tag{29}$$

we compute $\partial(\bar{\mathbf{N}}/\bar{N}_\beta)/\partial\lambda_\beta$. For experiments where λ_β is varied only by the introduction of more solute, Q_s is not an implicit function of λ_β as long as the system is still dilute. The result is

$$\frac{\partial(\bar{\mathbf{N}}/\bar{N}_\beta)}{\partial \ln \lambda_\beta} = -\frac{\overline{(s - \bar{s})^2}}{\bar{s}^2} \tag{30}$$

Now

$$\frac{\bar{\mathbf{N}}}{\bar{N}} = \frac{1}{\bar{s}} \text{ and } \ln \lambda_\beta = \frac{\mu_\beta - pv_\beta}{kT}$$

At ordinary pressures pv_β/kT is constant and negligible. Thus

$$\frac{\overline{(s - \bar{s})^2}}{\bar{s}^2} = -\frac{\partial(1/\bar{s})}{\partial(\mu_\beta/kT)} \tag{31}$$

In the ordinary micellar system the activity and the average micelle size change very little above the critical micelle concentration; hence, very sensitive measurements would be required to determine the fluctuation.

III. Derivation of the Constant Pressure Ensemble for Ionic Detergents.—Development of a comparable cluster theory for ionic detergents is attended by certain difficulties which are part of the general problem of electrolyte theory. Among these difficulties is the necessity of assuring weak interaction among the members of the statistical ensemble while allowing the number of molecules of a charged species to vary from zero to infinity. Clearly, the condition exists that some members of the ensemble will have infinite charge and in this case will interact strongly with other members of the ensemble.

In order to avoid these problems of interaction we shall assume the restriction of the members of the ensemble to electrically neutral systems or to systems of some arbitrary closeness to electrical neutrality. By the use of this restriction we assure the condition that the members of a statistical ensemble be weakly inter-

acting. The resultant restricted ensemble is no longer the same as that for the non-ionic case but is a hybrid constructed by the sum over canonical, incompressible, almost neutral, and neutral ensembles. When the fluctuation of charge of the real system about the neutral point is very small, the resultant hybrid ensemble should give a correct representation of properties.

The extended theory of dilute solutions applies only to non-electrolytes. We find an analog of this theory, however, in the continuum model of the solvent in an electrolyte system described by Fowler and Guggenheim.[14] The statistical mechanics of the system is studied by considering the solvent to be a dielectric continuum of dielectric constant ϵ. The ions which interact are immersed thus in a continuum and the effect of the solvent on the interaction of the ions is contained in the term ϵ. The effect of the solvent on the ions themselves is assumed constant for all configurations of the ions. If we generalize these definitions and require that the effect of the solvent on the potential energy due to charge and the effect of the solvent on the potential energy of the remaining part of the ion be separable, then the effect of the solvent on the potential energy due to charge can be treated as constant for all configurations of the ions while the remaining potential energy can be treated just as in the case of non-ionic molecules. The Helmholtz free energy of a system then can be expressed as

$$F = F_{\substack{\text{solvent} \\ \text{in ideal soln.}}}(N_\alpha,\ V - \sum_s N_s v_s,\ T) + \sum_s F_{s\ \substack{\text{uncharged} \\ \text{solute}}} + F^{el} \quad (32)$$

where s refers to all solute species. The additional free energy of the electrolyte, F^{el} will be a function of the volume. The assumption of incompressibility will again be applied although the assumption of additivity of volume is a poorer assumption for electrolyte solutions.

The use of the continuum model for electrolyte solutions as well as the use of the extended theory of dilute solutions for non-ionic solutions obviously is incorrect for members of the ensemble where the amount of solute is of the same order or much greater than the amount of solvent. However, for systems where $\bar{N}_s$ corresponds to a highly dilute system, the contribution of such concentrated members of the ensemble to the ensemble is negligible. Hence, the use of these models for concentrated ensemble members has a negligible effect on the averages but is a great convenience mathematically.

In the derivation that follows, we shall consider only one type of solution for the sake of simplicity: namely, an ionic detergent and uni-univalent salt with a common ion in aqueous solution. The application to other types of systems is obvious.

Ionic detergents shall be treated as systems where each type of ion is regarded as a different species. The following notation shall be used

α = solvent species
β = detergent ion
γ = detergent counterion and added counterion from a simple salt
η = ion from simple salt of same charge as detergent ion

The ions all are treated as solutes at constant pressure. The ensemble sum as in eq. 4 is

(14) R. Fowler and E. A. Guggenheim, ref. 8, Chap. IX, p. 383.

$$\Gamma(N_\alpha,p,T,\mu_\beta,\mu_\gamma,\mu_\eta) = Q_0 e^{-\frac{pV_0}{kT}} \sum_{N_\beta,N_\gamma,N_\eta} Q(N_\alpha,N_\beta,N_\gamma,N_\eta,V,T) \times e^{\frac{N_\beta(\mu_\beta - pv_\beta) + N_\gamma(\mu_\gamma - pv_\gamma) + N_\eta(\mu_\eta + pv_\eta)}{kT}} \quad (33)$$

where Q_0 no longer represents the complete partition function of the solvent but rather the partition function of the solvent in a solution of discharged ions.

$Q(N_\alpha,N_\beta,N_\gamma,N_\eta,V,T)$ represents the product of the partition function of the discharged solute and the additional term, Q^{el}, due to presence of charge. Thus

$$\sum_s F_s \text{ (discharged solute)} + F^{el} = -kT \ln Q(N_\alpha,N_\beta,N_\gamma,N_\eta,V,T) \quad (34)$$

We use the following definitions

$$\lambda_\beta = \exp(\mu_\beta - pv_\beta)/kT$$
$$\lambda_\gamma = \exp(\mu_\gamma - pv_\gamma)/kT$$
$$\lambda_\eta = \exp(\mu_\eta - pv_\eta)/kT \quad (35)$$

As in eq. 6

$$Q(N_\alpha,N_\beta,N_\gamma,N_\eta,V,T) = \sum_{\mathbf{N}} Q_{\mathbf{N}} \quad (36)$$

where $Q_{\mathbf{N}}$ is the partition function for the grouping, **N**, of N_β, N_σ, N_η molecules into a particular arrangement (set) of various size clusters. The summation over **N** is the summation over all possible sets consistent with the restriction that the total amount of molecules of β, γ and η be N_β, N_γ, and N_η, respectively.

Let us decompose the product $\lambda_\beta{}^{N\beta}\ \lambda_\gamma{}^{N\gamma},\ \lambda_\eta{}^{N\eta}$ into a product of terms of the type $\lambda_\beta{}^{s\beta}\ \lambda_\gamma{}^{s\gamma}\ \lambda_\eta{}^{s\eta}$ which correspond to clusters containing s_β β-ions and s_γ γ-ions and s_η η-ions. Then the summation in eq. 33 is taken over all cluster sets, where the cluster sets range over all values of N_β, N_γ, N_η but restricted to set values close to electrical neutrality. If we then define the variable

$$\lambda_{s\beta s\gamma s\eta} = \lambda_\beta{}^{s\beta}\lambda_\gamma{}^{s\gamma}\lambda_\eta{}^{s\eta} \quad (37)$$

we have the relationship as in eq. 11

$$\bar{N}_{s\beta,s\gamma,s\eta} = \lambda_{s\beta s\gamma s\eta}\frac{\partial \ln \Gamma}{\partial \lambda_{s\beta s\gamma s\eta}} \quad (38)$$

Thus from the ensemble sum using eq. 36 we can express the properties of the system taking all possible clusters into account explicitly. In general, the average number of systems $\bar{N}_{s\beta,s\gamma,s\eta}$ as derived using eq. 38 will be infinite series involving terms of the type

$$\lambda_\beta{}^{n\beta}\lambda_\gamma{}^{n\gamma}\lambda_\eta{}^{n\eta}$$

where $n_\beta \geq s_\beta$, $n_\gamma \geq s_\gamma$, and $n_\eta \geq s_\eta$. In particular a term of the type

$$\lambda_\beta{}^{s\beta}\lambda_\gamma{}^{s\gamma+1}\lambda_\eta{}^{s\eta}$$

accounts for the interaction of a cluster (s_β s_γ s_η) with a single monomer ion of γ.

We shall now focus attention on terms of the type $\bar{N}_{s\beta,s\gamma}$ where s_β is equal in number to s_γ. The distribution of terms of this type can be represented as lying in a plane of the distribution space where the axes cor-

respond to $s = s_\beta = s_\gamma$ and $\bar{N}_{s_\beta s_\gamma}$. Terms of this type correspond to uncharged clusters and hence interaction terms with other particles and clusters should be relatively small, particularly in dilute solution.

Thus we have approximately

$$\bar{N}_{s_\beta s_\gamma} \cong \lambda_\beta^{s_\beta} \lambda_\gamma^{s_\gamma} Q_{000\ldots1}^{(s_\beta, s_\gamma)}, \quad s_\beta = s_\gamma \tag{39}$$

where the partition function $Q_{000\ldots1}^{(s_\beta, s_\gamma)}$ is the partition function for a single cluster of size $s_\beta + s_\gamma$. If we now differentiate the logarithm of eq. 39 with respect to $s = s_\beta = s_\gamma$, we obtain

$$\frac{\partial \ln \bar{N}_{s_\beta s_\gamma}}{\partial s} = \ln (\lambda_\beta \lambda_\gamma) + \frac{\partial \ln Q_{000\ldots1}^{(s_\beta, s_\gamma)}}{\partial s}, \quad s_\beta = s_\gamma = s \tag{40}$$

In the plane defined by $\bar{N}_{s_\beta s_\gamma}$ and s, the existence of a maximum, $\bar{N}^*_{s_\beta s_\gamma}$, leads to the relationship

$$\ln (\lambda_\beta \lambda_\gamma) = -\frac{\partial \ln Q_{000\ldots1}^{(s_\beta, s_\gamma)*}}{\partial s}, \quad s_\beta = s_\gamma = s \tag{41}$$

The average number of monomer particles is given by equations of the type

$$\bar{N}_{1\beta} = \lambda_\beta [Q_{100}^{(1\beta)} + \sum_{l,m,n} A_{lmn} \lambda_\beta^{\,l} \lambda_\gamma^{\,m} \lambda_\eta^{\,n}], \quad A_{030} = 0 \tag{42}$$

When the interaction terms are assumed negligible, which would be the case for ideally dilute solution, we have

$$\begin{aligned} \bar{N}_{1\beta} &\cong \lambda_\beta Q_{100\ldots}^{(1\beta)} \\ \bar{N}_{1\gamma} &\cong \lambda_\gamma Q_{100\ldots}^{(1\gamma)} \end{aligned} \tag{43}$$

Combining eq. 43 and 41 we have the relationship

$$\ln \lambda_\beta \lambda_\gamma = \ln \bar{N}_{1\beta} \bar{N}_{1\gamma} - \ln Q_{100\ldots}^{(1\beta)} Q_{100\ldots}^{(1\gamma)} = -\frac{\partial \ln Q_{000\ldots1}^{(s_\beta s_\gamma)*}}{\partial s}, \quad s_\beta = s_\gamma \tag{44}$$

This result can be compared with the two-phase uncharged micelle model of Shinoda and Hutchinson[5d] which assumes monomer ideality.

Define the standard state by the equations

$$\begin{aligned} (\mu_\beta - pv_\beta)^0 &\equiv -kT \ln Q_{100\ldots}^{(1\beta)} + kT \ln V \\ (\mu_\gamma - pv_\gamma)^0 &\equiv -kT \ln Q_{100\ldots}^{(1\gamma)} + kT \ln V \end{aligned} \tag{45}$$

Thus

$$(\mu_\beta - pv_\beta)(\mu_\gamma - pv_\gamma) = kT \ln \left(\frac{\bar{N}_{1\beta}}{V}\right)\left(\frac{\bar{N}_{1\gamma}}{V}\right) + (\mu_\beta + pv_\beta)^0 (\mu_\gamma + pv_\gamma)^0 \tag{46}$$

At ordinary pressures the pv terms are negligible. Thus

$$\mu_\beta \mu_\gamma \cong kT \ln \left(\frac{\bar{N}_{1\beta}}{V}\right)\left(\frac{\bar{N}_{1\gamma}}{V}\right) + \mu_\beta^0 \mu_\gamma^0 \tag{47}$$

The equation

$$\mu_\beta \mu_\gamma = \left(\mu_{\frac{\beta}{\gamma}}\right)$$

defines a mean chemical potential, $\left(\mu_{\frac{\beta}{\gamma}}\right)$. Thus if β refers to the positive species and γ to the negative species, we have

$$(\mu_\pm) = kT \ln \left(\frac{\bar{N}_+}{V}\right)\left(\frac{\bar{N}_-}{V}\right) + (\mu_\pm)^0 \tag{48}$$

This relationship may be compared with eq. 8 from the paper of Shinoda and Hutchinson which differs only in the use of mole fraction in place of $\bar{N}/V$. Obviously, this difference depends upon the definition (45). Definition 45 is used here since it is analogous to the relationship used for ideal gases

$$\frac{\mu(\rho)}{kT_{\rho \to 0}} = \ln \left(\frac{V}{Q_1}\right) \tag{49}$$

We also have the relationship

$$(\mu_\pm) \cong \frac{-\partial\, kT \ln Q_{000\ldots1}^{(s_\beta, s_\gamma)*}}{\partial s}, \quad s_\beta = s_\gamma = s \tag{50}$$

Since $-kT \ln Q_{000\ldots1}^{(s_\beta s_\gamma)*}{}_{,s_\beta = s_\gamma}$ may be interpreted as the Helmholtz free energy of the maximum neutral micellar cluster, the derivative with respect to s may be interpreted as the chemical potential of the "mean" particle which is removed from the micelle leaving the micelle in an uncharged state. Calculation of temperature changes of all these quantities follows according to the derivation given by Shinoda and Hutchinson. However, it must be observed that the maximum in the distribution may be a function of T. Thus, in the interpretation of the quantity $\partial \mu_\pm / \partial T$, consideration of the shift of the maximum of the distribution cannot be ignored.

We shall now comment on the comparison of the ensemble to the mass action model. For uncharged micelle clusters the mass action quotients derived as for eq. 13 should have negligible interaction terms. These quotients therefore have a constant value and the mass action approach is a good one. For charged micelle clusters, the interaction terms most certainly will not be negligible and deviations from ideality may be considerable. As a first approximation to a correct distribution, interaction with gegenion only might be considered. Then we would have for the distribution an expression of the form

$$\bar{N}_{s_\beta s_\gamma} = \lambda_\beta^{s_\beta} \lambda_\gamma^{s_\gamma} [Q_{000\ldots1}^{(s_\beta s_\gamma)} + \sum_l A_l \lambda_\gamma^{\,l}] \tag{51}$$

where the term in brackets represents an effective single cluster partition function as a function of gegenion concentration. One might also consider a fully charged micelle

$$\bar{N}_{s_\beta} = \lambda_\beta^{s_\beta} (Q_{000\ldots1}^{(s_\beta)} + \sum_{lmn} A_{lmn} \lambda_\gamma^{\,l} \lambda_\beta^{\,m} \lambda_\eta^{\,n}] \tag{52}$$

When terms due to interaction of micelle cluster with particles and clusters of the same charge as the micelle may be considered negligible, the term in the brackets may be considered independent of β and η and the distribution becomes

$$\bar{N}_{s_\beta} = \lambda_\beta^{s_\beta} Q_{\text{eff}}(\lambda_\gamma) \tag{53}$$

Equations of the type of (23)–(26) may also be derived for this case. Estimation of $Q_{\text{eff}}(\lambda_\gamma)$ by a particular model of electrical interaction leads to the charged phase separation model of Shinoda and Hutchinson.

IV. Improvement of Statistical Treatment.—Two methods for improving the statistical treatment of micelles are suggested. Either more and more interaction terms may be included as in eq. 12 or the separation of the solvent and solute partition functions may be abandoned. In the latter case the ensemble sum in (4) would take the form

$$\Gamma = e^{\frac{-pV_0}{kT}} \sum_{N_\beta \geq 0} Q'(N_\alpha, N_\beta, V_0 + N_\beta v_\beta, T)\, \lambda_\beta^{N_\beta} \quad (54)$$

where Q' is the canonical ensemble partition function for the solute and the solvent. An equation of the type of (9) can still be written

$$Q'(N_\alpha, N_\beta, V_0 + N_\beta v_\beta, T)\lambda_\beta^{N_\beta} = \sum_{\mathbf{N}} Q_{\mathbf{N}}'\left(\prod_s \lambda_s^{N_s}\right) \quad (55)$$

but the $Q_{\mathbf{N}}'$ is to be interpreted as the partition function for a particular arrangement of solute molecules *and* the solvent. We still have the relationship

$$\bar{N}_s = \lambda_s \frac{\partial \ln \Gamma}{\partial \lambda_s} \quad (56)$$

Then since Γ may be written as

$$\Gamma = e^{\frac{-pV_0}{kT}} Q'(N_\alpha, 0, V_0, T)\left(1 + \left\{\frac{\lambda_\beta Q'(N_\alpha, 1, V_0 + v_\beta, T)}{Q'(N_\alpha, 0, V_0, T)} + \ldots\right\}\right) \quad (57)$$

if the sum of the λ_β power series terms in the brackets, $\{\ \}$, is less than unity, then the inverse of Γ may be expanded in a power series in $\{\ \}$. Thus

$$\frac{1}{\Gamma} = \frac{1}{e^{\frac{-pV_0}{kT}} Q'(N_\alpha, 0, V_0, T)}\left[1 - \{\ \} + \{\ \}^2 + \ldots\right] \quad (58)$$

Thus after differentiation as in eq. 56 using eq. 55, changing λ_s to λ_β^s and after collection of terms in λ_β^n we have for example

$$\bar{N}_1 = \lambda_\beta \frac{Q'_{100\ldots}}{Q_0} + \lambda_\beta^2\left(\frac{2Q'_{200\ldots}}{Q_0} - \left(\frac{Q'_{100\ldots}}{Q_0}\right)^2\right) + \ldots \quad (59)$$

where $Q'(N_\alpha, 0, V_0, T) = Q_0$

Formally the new series may be generated from the series in equation 12 with the substitution, for example, $Q'_{000\ldots 1}/Q_0$ for $Q_{000\ldots 1}$. This formulation enables explicit account to be taken of specific interactions of the solvent with the micelle (such as hydration). A similar derivation may be given for the ionic system.

V. Model Calculations.—Reich's model for explaining stability of micelles is based upon a law of mass action treatment.[1] The equilibrium ratio of concentrations for formation of a micelle of size s is given by

$$\frac{[N_s]}{[N_1]^s} = e^{\frac{s\{S_0T + \epsilon(1 - s^{-1/3})\}}{kT}} \quad (60)$$

where S_0 is the entropy change per molecule when a cluster of size s is formed from monomer, $s\epsilon$ is the internal energy change and $\epsilon s^{2/3}$ is the surface energy change. As we have seen from eq. 13, this ratio in the ideal case corresponds to

$$\frac{Q_s}{Q_1^s} V^{s-1} \quad (61)$$

and then

$$\bar{N}_s = \lambda_\beta^s Q_s = \lambda_\beta^s \frac{Q_1^s}{V^{s-1}} e^{\frac{s(S_0T + \epsilon(1 - s^{-1/3}))}{kT}} \quad (62)$$

Let us now consider this problem from the "two-phase equilibrium" viewpoint.

$$\frac{\partial \ln \bar{N}_s}{\partial s} = \ln \lambda \frac{Q_1}{V} + \frac{S_0T + \epsilon(1 - s^{-1/3})}{kT} + \frac{\epsilon s^{-1/3}}{3kT} \quad (63)$$

Then

$$0 = \ln \lambda \frac{Q_1}{V} + \frac{S_0T + \epsilon(1 - s^{*-1/3})}{kT} + \frac{\epsilon s^{*-1/3}}{3kT} \quad (64)$$

where $s^* = s_{\max}$.

But

$$\bar{N}_1 = \lambda Q_1$$

Then

$$\ln \frac{\bar{N}_1}{V} = -\frac{(S_0T + \epsilon)}{kT} + \frac{2}{3}\frac{\epsilon}{kT} s^{*-1/3} \quad (65)$$

At the critical micelle concentration $\bar{N}_1$ can be considered the total solute. We also have

$$\frac{\partial\, kT \ln \frac{\bar{N}_1}{V}}{\partial T} = -S_0 - \frac{2}{9}\epsilon s^{*-4/3}\frac{\partial s^*}{\partial T} \quad (66)$$

According to Reich, phase separation (P.S.) occurs when

$$\ln\left(\frac{\bar{N}_1}{V}\right)_{\text{P.S.}} = -\frac{(\epsilon + S_0T)}{kT} = \ln \lambda_0 \frac{Q_1}{V} \quad (67)$$

where λ_0 is the value of λ when phase separation occurs. Thus, just before phase separation

$$\ln\left(\frac{\bar{N}_1}{V}\right) = -\frac{(\epsilon + S_0T)}{kT} + \tau \quad (68)$$

where $e^\tau = \lambda/\lambda_0$ and τ is negative and close to zero. Then

$$\frac{\bar{N}_1}{V} = \lambda \frac{Q_1}{V} = e^{-(\epsilon + S_0T)/kT + \tau} \quad (69)$$

and

$$\frac{\bar{N}_s}{V} = e^{s\tau} e^{-(\epsilon/kT)s^{2/3}} \quad (70)$$

When τ approaches zero the exponential, $e^{s\tau}$, may be expanded in a power series in τ and higher terms ignored. Then

$$\bar{N}_s \cong V(1 + s\tau)e^{-(\epsilon/kT)s^{2/3}} \quad (71)$$

We can also compute the maximum value of $\bar{N}_s$ in terms of τ.

$$\frac{\partial \ln \bar{N}_s}{\partial s} = 0 = \tau - \frac{2}{3}\frac{\epsilon}{kT} s^{*-1/3} \qquad (72)$$

But, as we have seen, τ is equivalent to $\ln (\lambda/\lambda_0)$ or

$$\tau = \left(\frac{\mu_s - pv_\beta}{kT}\right) - \left(\frac{\mu_\beta - pv_\beta}{kT}\right)_0 \qquad (73)$$

Since the pv_β term is negligible and for all practical purposes constant, we have

$$\tau \cong \frac{\mu_\beta - \mu_{\beta 0}}{kT} \qquad (74)$$

where $\mu_{\beta 0}$ is the chemical potential when phase separation occurs. We also observe

$$\frac{\partial \ln \sum_s \bar{N}_s}{\partial \tau} = \bar{s} \qquad (75)$$

It can be deduced using eq. 71 and replacing the summation by an integration that $\sum_s \bar{N}_s$ is a linear function of τ of the form $A + B\tau$ where A and B are non-zero coefficients. Thus

$$\bar{s} = \frac{B}{A + B\tau} \qquad (76)$$

From eq. 72 we have

$$s^* = \left(\frac{2}{3}\frac{\epsilon}{kT}\frac{1}{\tau}\right)^3 \qquad (77)$$

As expected, the average value and the maximum value are quite different. Reich has discussed his model extensively from a mass action viewpoint. We shall not restate his argument. It has been our purpose to illustrate, using Reich's model, the results which are to be obtained when Reich's model is analyzed from the two-phase viewpoint and from the constant temperature and pressure ensemble viewpoint.

Conclusions.—The general statistical approach contains within it the various models used for the study of micelles and the relationship between these models. The nature of the approximations involved is laid bare. The appropriate interaction terms necessary for improving existing theory are displayed in the general distribution equations for $\bar{N}_s$.

The basic assumptions of incompressibility and additivity of volumes and the assumption of separability of partition functions used to separate solvent and solute contributions to Γ are of course inexact. However, they enable us to simplify the ensemble sum and do lead to results in accord with existing theoretical treatments. The separability of solvent and solute contributions can be eliminated easily in the formulation, leading to equations which represent an improvement over existing treatments.

Acknowledgment.—The author wishes to express sincere appreciation and gratitude to Dr. Louis Witten and Dr. John Gryder for many helpful and stimulating discussions and to the Chemical Directorate of the Air Force Office of Scientific Research for their support of this work.

FREE RADICAL REACTIONS INITIATED BY IONIZING RADIATIONS. III. PARAFFIN REACTIVITIES IN HYDROGEN ATOM ABSTRACTION REACTIONS

BY KANG YANG

Radiation Laboratory, Continental Oil Company, Ponca City, Oklahoma

Received July 27, 1962

Rate constants, $k = BT^{1/2}\exp(-\epsilon/RT)$, for these reactions $H + M \rightarrow H_2 + R$ have been determined by investigating the temperature dependence of hydrogen yields in the γ-radiolysis of paraffin–propylene systems. Assuming $\epsilon = 2.2$ kcal./mole for the hydrogen atom addition reaction with propylene, the following ϵ values are estimated: ethane, 8.6; propane, 7.0; *n*-butane, 6.3; isobutane, 4.7. The LCBO treatment of an assumption that the energy required for isolating two electrons in a bond to be broken from the rest of the σ-electron system plays the decisive role in determining paraffin reactivities leads to the expression: $\epsilon = \xi + N_{CH}\eta$. Here N_{CH} is the number of additional CH bonds formed by the carbon atom that forms the CH bond to be broken. Two constants, ξ and η, have these meanings: ξ is the activation energy for the hydrogen atom abstraction reaction involving diatomic CH molecules; and η represents the major structural contribution to the reactivity and comes from the fact that the bond to be broken undergoes stabilizing interactions with neighboring CH bonds. Examination of experimental data in the light of the above equation indicates that each such interaction contributes 2.0 kcal./mole to the activation energy, thus reducing the paraffin reactivity about 30-fold at room temperature.

Introduction

Structurally similar compounds often exhibit markedly different reactivities in a series of similar radical reactions.[1] In the case of radical addition reactions with carbon–carbon double bonds, this difference is attributable to a difference in the energy, E_{loc}, required for localizing a π-electron at the reaction center[2–6]; thus it is demonstrated that[7]

$$\epsilon = aE_{loc} - b \qquad (E\text{-}1)$$

where ϵ is the activation energy for the hydrogen atom addition reactions in gas phase, and two constants, a and b, are expressible in terms of parameters characterizing potential changes involved in these reactions. Attempts have been made to extend this successful localization energy concept to the case of abstraction

(1) See, for example, M. Szwarc, *J. Phys. Chem.*, **61**, 40 (1957).
(2) G. W. Wheland, *J. Am. Chem. Soc.*, **64**, 900 (1942).
(3) C. A. Coulson, *J. Chem. Soc.*, 1435 (1955).
(4) J. H. Binks and M. Szwarc, *J. Chem. Phys.*, **30**, 1494 (1959).
(5) S. Sato and R. J. Cvetanovic, *J. Am. Chem. Soc.*, **81**, 3223 (1959).
(6) K. R. Jennings and R. J. Cvetanovic, *J. Chem. Phys.*, **35**, 1233 (1961).
(7) K. Yang, *J. Am. Chem. Soc.*, **84**, 3795 (1962).

reactions involving σ-electron systems.[4] Here the corresponding localization energy may be defined as the energy required for isolating two electrons in a bond to be broken from the rest of the σ-electron systems. The present paper describes an experimental and theoretical test of (E-1) in which E_{loc} is defined as above.

The experimental work consists essentially of accurate determinations of activation energy differences in a series of simple gas-phase reactions

$$H + M \xrightarrow{k_m} H_2 + R \qquad (1)$$

where M denotes ethane, propane, butane, or isobutane. The main reason for this choice is that solvent effects are absent, and there can be little steric hindrance; also, although somewhat controversial,[8] the required information is available for the corresponding D atom reactions.[9] In the case of the H atom reactions, reliable data obtained directly from temperature dependence of relative rates seem to be absent from the literature.

The experimental method has been described in detail in part I[10] and part II[7] of the present series (hereafter denoted as part I or part II).[11] It employs hydrogen atoms produced in the γ-radiolysis of M. These atoms undergo competitive reactions 1 and 2

$$H + C_3H_6 \xrightarrow{k_s} C_3H_7 \qquad (2)$$

propylene being added initially.

The decrease in hydrogen yield resulting from reaction 2 is then determined at very low conversion ($\sim 10^{-3}$%) of M. Under this condition, $[C_3H_6]$ can be considered as constant throughout the radiolysis and the following rate equation results[10]

$$r_s = \frac{k_m}{k_s}\frac{[M]}{[S]}(r_0 - r_s) + r_2 \qquad (E\text{-}2)$$

Here r_0 and r_s denote the hydrogen yields in the absence and presence of propylene, and r_2 is the hydrogen yield from processes in which the thermalized H atoms do not participate.[12] In this method, hydrogen atoms are produced at a controlled rate and the reaction temperature can be varied widely (50–250°). This is essential for obtaining accurate activation energy data. Disadvantages of the present method are, in general, that the radiolysis mechanism is quite complicated and that other non-radical processes are conceivable by which olefins may reduce the hydrogen yield.[7] In spite of these, relative rates estimated by the present method agree well with that obtained by photochemical method.[7,11] In addition, temperature dependence of inhibition effect strongly suggests that the above radical mechanism is correct.[7]

In the case of substitution reactions involving σ-electron systems, the localization energy concept has been treated theoretically.[13] There, E_{loc} was calculated by using a mobile σ-electron model[14] which regards hydrocarbons as composed of carbon skeletons only, thus neglecting the influence of CH bonds. Obviously, such an approach is incapable of treating abstraction reactions. In the present paper, E_{loc} is estimated by using the linear combination of bond orbitals (LCBO) method.[15–17] The result, which explains the experimental data quite well, indicates that the major structural factor governing paraffin reactivities in abstraction reactions is the stabilization of the bond to be broken by neighboring CH bonds.

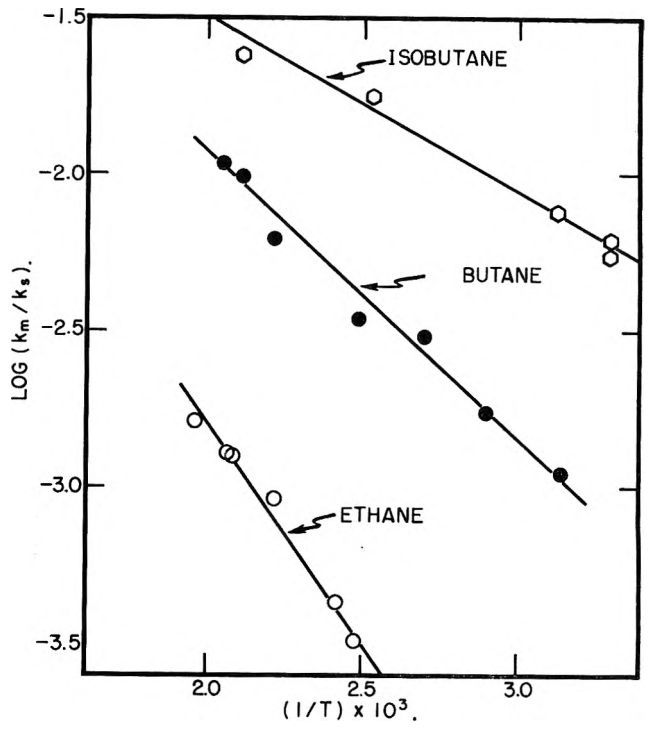

Fig. 1.—The temperature dependence of the rate constant ratios, k_m/k_s, for the reactions $H + M \xrightarrow{k_m} H_2 + R$ and $H + C_3H_6 \xrightarrow{k_s} C_3H_7$.

Experimental

Phillips research grade hydrocarbons were used. All gases were degassed and distilled except for ethane, which was subject to additional bromine treatment in a high-pressure steel vessel.[18] The concentration of added propylene did not exceed 3%. Other experimental details have been described previously.[7,10]

Results

The rate constant ratios, k_m/k_s, were obtained by plotting r_s against $(r_0 - r_s)[M]/[S]$ as shown in (E-2). Kinetic data were similar to the ones given in part I and part II, and good straight lines resulted in all cases. Figure 1 summarizes temperature dependence of the resulting ratios. From least squares treatment, we obtained these relations

$$\log k(\text{ethane})/k_s = (-0.01 \pm 0.18) - (6{,}380 \pm 370)/2.3RT \qquad (E\text{-}3)$$

$$\log k(\text{propane})/k_s = (0.15 \pm 0.05) - (4{,}800 \pm 100)/2.3RT \qquad (E\text{-}4)[19]$$

(8) For example, see S. W. Benson, "The Foundations of Chemical Kinetics," McGraw-Hill Book Co., New York, N. Y., 1960, p. 293, footnote g.

(9) B. de B. Darwent and R. Roberts, *Discussions Faraday Soc.*, **14**, 55 (1953).

(10) K. Yang, *J. Am. Chem. Soc.*, **84**, 719 (1962).

(11) See the following references also: (a) R. A. Back, *J. Phys. Chem.*, **64**, 124 (1960); (b) T. J. Hardwick, *ibid.*, **65**, 101 (1961); (c) **66**, 291 (1962).

(12) L. M. Dorfman, *ibid.*, **62**, 29 (1958).

(13) K. Fukui, H. Kato, and T. Yonezawa, *Bull. Chem. Soc. Japan*, **33**, 1201 (1960).

(14) H. Yoshizumi, *Trans. Faraday Soc.*, **53**, 123 (1957).

(15) G. G. Hall, *Proc. Roy. Soc.* (London), **A205**, 541 (1951).

(16) R. D. Brown, *J. Chem. Soc.*, 2615 (1953).

(17) For a recent review, see R. Daudel, R. Lefebvre, and C. Moser, "Quantum Chemistry," Interscience Publishers, Inc., New York, N. Y., 1959.

(18) K. Yang and P. L. Gant, *J. Phys. Chem.*, **65**, 1861 (1961).

(19) This relation is taken from part I.[10]

$$\log k(\text{butane})/k_s = (-0.18 \pm 0.14) - (4{,}070 \pm 250)/2.3RT \quad \text{(E-5)}$$

$$\log k(\text{isobutane})/k_s = (-0.44 \pm 0.13) - (2{,}470 \pm 200)/2.3RT \quad \text{(E-6)}$$

where uncertainties are indicated in terms of standard deviations. By assuming

$$k_s = 10^{12.0}T^{1/2}\exp(-2{,}200/RT) \quad \text{(E-7)}$$

we computed the k_m values given in Table I. In estimating (E-7), k_s at 31° is taken to be 4.8×10^{11} cc./mole-sec.[20] and the activation energy to be 2.2 kcal./mole. As indicated in part II, published ϵ values range from 1.3[21] to 4.2[9]; hence the present choice introduces average deviations of about 1.5 in the data listed in Table I. With this in mind, it is of interest to compare the present results with published data.

TABLE I

RATE CONSTANTS, k_m (CC./MOLE-SEC.), FOR THE REACTIONS

$$H + M \xrightarrow{k_m} H_2 + R$$

$$k_m = BT^{1/2}\exp(-\epsilon/RT)$$

M	log B	$\epsilon \times 10^{-3}$
Ethane	12.0	8.6
Propane	12.2	7.0
Butane	11.8	6.3
Isobutane	11.6	4.7

Berlie and LeRoy[22] investigated the ethane reaction using hydrogen atoms generated by Wood's method and reported that $k(\text{ethane}) = 10^{11.01}T^{1/2}\exp(-6{,}400/RT)$. In view of the present result, their ϵ value seems to be too low. With presently available information alone, it is difficult to ascertain the exact source of the discrepancy.

When isotope effects are neglected, Darwent and Roberts' data[9] on the D atom reactions can be compared also. For this purpose, it is desirable to recalculate their results to give $\epsilon = 2.2$ for the hydrogen atom addition reaction with propylene. When this is done, the following data result

M	Ethane	Propane	Butane	Isobutane
ϵ	7.0	5.2	5.1	4.3

Except for the isobutane reaction, ϵ values seem to be too low. Benson[8] suggested that their data may contain contributions from hot atom reactions. This could be partially responsible for the present discrepancy.

The uncertainties in the present absolute ϵ values do not appreciably weaken the forthcoming discussion, because the major importance is the activation energy differences whose standard deviations do not exceed 0.4.

In discussing radiolysis mechanism, r_0 and r_2 values are important. These are given in Table II in terms of $G(H_2)$ (molecules/100 e.v.). The r_0 values were reproducible within ±3%; for the present purpose of relative rate determinations, variations of r_0 with temperature may be regarded as quite small. Because of uncertainties in the intercept, deviations in r_2 values

(20) A. B. Callear and J. C. Robbs, *Trans. Faraday Soc.*, **51**, 638 (1955).
(21) M. D. Sheer and R. Klein, *J. Phys. Chem.*, **65**, 375 (1961).
(22) M. R. Berlie and D. J. LeRoy, *Discussions Faraday Soc.*, **14**, 50 (1953).

TABLE II

THE YIELDS (MOLECULES/100 E.V.) OF HYDROGEN IN HYDROCARBON RADIOLYSIS AT VARIOUS TEMPERATURES[a]

	r_0[b]			r_2[b]
M	50°	150°	240°	50–240°
Ethane	8.8	8.9	9.3	3.3
Propane	6.4	6.5	6.7	1.6
Butane	5.4	5.5	5.8	1.8
Isobutane	5.4	5.4	5.5	1.8

[a] For dosimetry, see reference 18. [b] r_0 is total yield while r_2 is molecular yield.

are relatively high (~10%). Within this limit, r_2 values did not depend on temperature.

Discussion

To examine the data in Table I in light of the localization energy concept, we make this assumption: (E-1) is applicable in the case of abstraction reactions also. In estimating E_{loc}, Brown's LCBO treatment[15] of paraffins may be used. Although his approach has been described carefully, the following derivation of an expression for E_{loc} in a form suitable for reactivity discussion is quite helpful in understanding our arguments below. As an example, we consider the ethane reaction

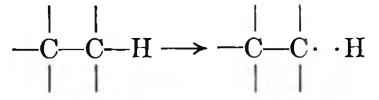

The eigenfunction of the reactant is represented by the linear combination of six CH bond orbitals, Y_{CH}, and one CC bond orbital, Y_{CC}. In the localized structure, two electrons in the bond to be broken are isolated from the rest of the σ-electron system. The energy difference between these two structures gives E_{loc}. For the matrix elements, we use this notation

$$\alpha_{CC} = \int Y_{CH}HY_{CH}\,d\tau;\quad \beta = \int Y_{CH}HY_{CH'}\,d\tau$$

$$\beta' = \int Y_{CH}HY_{CC}\,d\tau;\quad S = \int Y_{CH}Y_{CH}\,d\tau$$

$$\gamma = 4(\beta - S\alpha_{CC});\ \text{and}$$

$$\Delta\alpha = \alpha_C + \alpha_H - 2\alpha_{CC} \quad \text{(E-8)}$$

When a pair of CH bonds do not originate from the same carbon, β is taken to be zero. The term $\alpha_C + \alpha_H$ in $\Delta\alpha$ denotes the energy of two electrons in the bond to be broken. By using the variation method and expanding[16] the resulting secular equation in a power series in S, it can be shown that

$$E_{loc} = \Delta\alpha + 2S\gamma \quad \text{(E-9)}$$

In obtaining (E-9), we neglect terms containing second or higher powers of S. It is also assumed that $(\beta'/\beta)^2 \simeq 0$, which seems reasonable in view of a value $\beta'/\beta \simeq 0.2$ obtained by investigating ionization potentials of paraffins by the LCBO method.[15]

An extension of the above argument leads to the generalization

$$E_{loc} = \Delta\alpha + N_{CH}S\gamma \quad \text{(E-10)}[23]$$

Here N_{CH} denotes the number of CH bonds surrounding the bond to be broken. For example, it is unity in case of the propane reaction. From (E-1) and (E-10)

(23) An equation similar to (E-10) has been successfully used by Brown[15] in treating bond energy data.

$$\epsilon = \xi + N_{CH}\eta \qquad \text{(E-11)}$$

where $\xi = a\Delta\alpha - b$, and $\eta = aS\gamma$.

The present E_{loc} is different from bond strength, D, in two respects. First, the term $\alpha_C + \alpha_H$ in E_{loc} may contain a significant contribution from the interaction of two electrons in the bond to be broken, while this is not so in the case of D. Secondly, structural differences between alkyl radicals in isolated and bound states affect D but not E_{loc}. For these reasons it is quite possible that $E_{loc} < D$. If these differences are assumed to make a constant contribution to ϵ in a series of similar reactions, then E_{loc} and D may be used interchangeably. In this case, (E-1) implies a well known and successful expression[24-28]

$$\epsilon = \alpha_m D - \beta_m \qquad \text{(E-12)}$$

where α_m and β_m are constants. In the present paper, however, it is not necessary to use (E-12). As shown below, a correlation of activation energy data is achieved without using bond energy data. This is worth emphasizing because, in discussing relative reactivity, the use of (E-12) demands ΔD values on which available information often contains a large per cent of errors.

According to (E-11), a straight line should result when ϵ in Table I is plotted against N_{CH}. Figure 2 confirms this prediction. In Fig. 2 only those bonds having the highest reactivities are considered, and the experimental data are assumed to correspond with the reaction involving such a bond. Actually, in the temperature ranges investigated here, some less reactive bonds are also likely to participate. In view of the linearity shown in Fig. 1, however, uncertainties in ϵ from such sources are not likely to exceed 0.4.

From Fig. 2, we estimate the ϵ value for the reaction

$$H + CH_4 \longrightarrow H_2 + CH_3 \qquad (3)$$

to be 10.3. Recently Fenimore and Jones[29] investigated this reaction in a flame and reported that k(methane) $= 2 \times 10^{13} \exp(-11{,}500/RT)$. This corresponds to an ϵ value of 10, in excellent agreement with the present estimation.

From the data in Fig. 2, we obtain

$$\xi = 4.7 \qquad \eta = 2.0 \qquad \text{(E-13)}$$

We now examine the physical significances of these two constants.

In the case of the reaction

$$H + i\text{-}C_4H_{10} \longrightarrow H_2 + t\text{-}C_4H_9 \qquad (4)$$

$N_{CH} = 0$; hence $\epsilon = \xi$. The same relation results when the present theory is applied to the reaction involving an isolated CH bond.

$$H + CH \longrightarrow H_2 + C \qquad (5)$$

Reactions 4 and 5 thus should have about the same activation energy. In such a reaction involving three

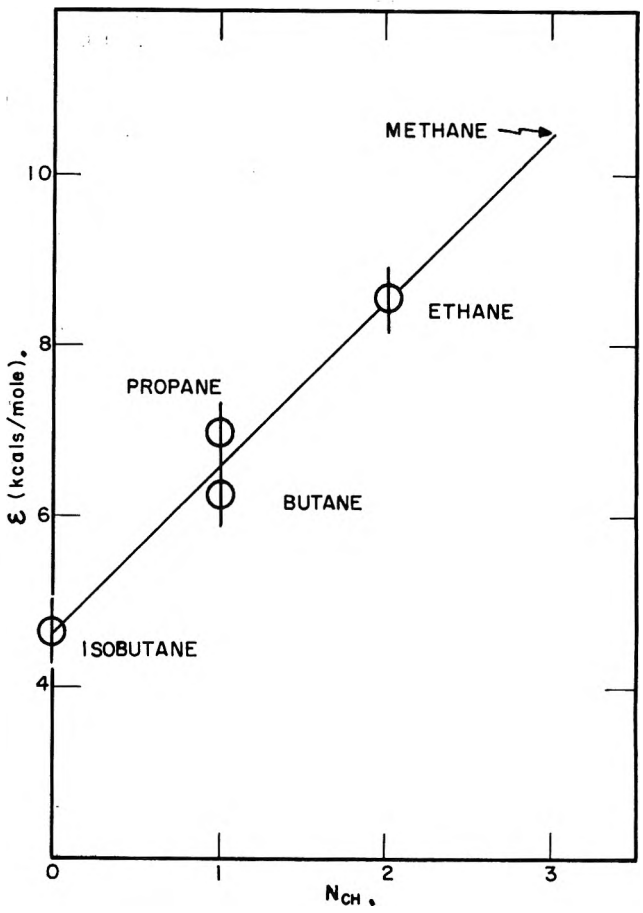

Fig. 2.—Activation energy, ϵ, for the hydrogen atom abstraction reactions as a function of the number, N_{CH}, of additional CH bonds formed by the carbon atom that forms CH bond to be broken.

atoms, Eyring and his co-workers' semi-empirical method[30] can be used to estimate ϵ. Hirschfelder[31] has shown that, when the interactions between two outer atoms are neglected, this method yields a simple expression for ϵ

$$\epsilon = \frac{D}{2}[2 - 3n - (3(1 - 2n))^{1/2}] \qquad \text{(E-14)}$$

where D is the CH bond strength in an isolated CH bond, and n signifies the ratio of coulombic energy to total binding energy and is usually taken to be 0.14. Here, D is different from D(C–H) in diatomic molecules, because the effective Hamiltonian in ξ is not the same as that needed in treating the CH molecules. For the present purpose, it is more appropriate to use D(C–H) (= 94 kcal./mole[33]) in isobutane[32]; then ϵ becomes 5.2, in good agreement with the ξ value of 4.7 ± 1.5. Unfortunately, ϵ estimated from (E-14) seems to be not better than ±5, and the above agreement only indicates that the present ξ value is not inconsistent with the transition state theory.

The physical significance of η is equally clear-cut. It is the major structural factor governing the activation energy differences (hence the relative reactivity also)

(24) A. F. Trotman-Dickenson, *Discussions Faraday Soc.*, **10**, 111 (1951).
(25) A. F. Trotman-Dickenson, "Gas Kinetics," Butterworths Scientific Publications, Ltd., London, 1955, p. 199.
(26) E. Warburst, *Quart. Rev.*, **5**, 44 (1951).
(27) R. E. Dodd, *J. Chem. Phys.*, **26**, 1353 (1959).
(28) K. Otozai, *Sci. Papers Osaka Univ.*, 20 (1951); *Bull. Chem. Soc. Japan*, **24**, 218, 257, 262 (1951); also see ref. 8, p. 317.
(29) C. P. Fenimore and C. W. Jones, *J. Phys. Chem.*, **65**, 2200 (1962).
(30) S. Glasstone, K. J. Laidler, and H. Eyring, "The Theory of Rate Processes," McGraw-Hill Book Co., Inc., New York, N. Y., 1941.
(31) J. Hirschfelder, *J. Chem. Phys.*, **9**, 645 (1941).
(32) We express our appreciation for the referee who brought this point to our attention.
(33) T. L. Cottrell, "The Strength of Chemical Bonds," Academic Press, Inc., New York, N. Y., 1954, p. 272.

and comes from a stabilizing interaction of neighboring CH bonds with the bond to be broken. Equation (E-12) indicates that each such interaction contributes 2.0 to the activation energy, thus reducing the paraffin reactivity about 30-fold at room temperature.

Acknowledgment.—We express our appreciation to Dr. F. H. Dickey, Dr. L. O. Morgan, and Mr. C. L. Hassell for their valuable discussion and to Mr. P. L. Gant and Mr. J. D. Reedy for helping with the experimental work.

DILUTE SOLUTION PROPERTIES OF BRANCHED POLYMERS. POLYSTYRENE TRIFUNCTIONAL STAR MOLECULES[1]

BY T. A. OROFINO AND FRANZ WENGER[2]

Mellon Institute, Pittsburgh, Pennsylvania

Received July 30, 1962

The results of intrinsic viscosity, second virial coefficient and related thermodynamic measurements on samples of polystyrene trifunctional star molecules are reported. These branched polymers were synthesized by means of a coupling reaction between essentially monodisperse polystyryllithium and 1,2,4-tris-(chloromethyl)-benzene. The homogeneity of the materials obtained with regard to molecular weight and functionality was established by fractionation, sedimentation, and absolute molecular weight determinations. Intrinsic viscosities and second virial coefficients in both poor and good solvent media were found to be less for these materials than for linear polystyrenes of comparable molecular weights. The Huggins viscosity constant k' in good solvents was unaffected by branching; in poor solvent media, an augmentation of k' with branching was noted. The results of these and other dilute solution studies are discussed from the point of view of current theoretical interpretations. An attempt is made to extend them in applicability to more general branched polymer systems.

Introduction

The interpretation of dilute solution data obtained on branched polymer systems to date has been complicated to varying degrees by structural and molecular weight heterogeneity present in the samples investigated. Although some general conclusions[3,4] concerning the effect of branching have been deduced from the considerable quantity of experimental data accumulated, the lack of adequate sample characterization has in large part precluded attempts at quantitative evaluation of the results.

A general method for the controlled synthesis of branched polymers has recently been outlined by one of us,[5] the initial application of which has led to the preparation of polystyrene trifunctional star molecules—branched polymers formed by three linear polystyrene chains joined at one end through a common junction. The skeletal structure of these materials involves only carbon–carbon linkages, coupling of the three constituent linear chains in each molecule being achieved through use of a suitable low molecular weight aromatic compound. The virtual chemical identity of the branched chains with linear polystyrene, together with their homogeneity in regard to functionality and molecular weight, make them ideally suited for physical measurements, the results of which in comparison with known properties of their linear counterparts can be attributed unequivocally to the branched nature of the chains.

The principal aim of the present investigation thus has been to determine the dilute solution properties of the model branched structures described and to compare these with the corresponding properties of chemically identical, linear polymers of the same molecular weights. The significance of this undertaking rests directly upon the degree to which three essentially independent aspects of the investigation can be pursued in an accurate and internally consistent manner. These are (1) the establishment of the physical constitutions of the branched samples selected for study, (2) the detailed investigation of the solution properties of these, and (3) the evaluation of the corresponding solution properties of their linear counterparts.

In addition to the analyses of primary measurements utilized to establish the architectural structure of the particular materials selected for investigation, the data presented here include the detailed results of osmotic pressure, light scattering, and viscometric studies as functions of temperature in both poor and good solvent media. In a separate study pursued by one of us[6] the corresponding solution properties of a (reference) linear polystyrene sample have been extensively examined. The results of that investigation, coupled with other relevant studies carried out on linear polystyrenes in the course of the present project, provide the principal basis upon which the solution properties of the trifunctional star structures and their linear analogs of the same molecular weight are herein compared. Also, we have included in our presentation a summary of results obtained on a mixture of star and linear polystyrenes. These data provide a supplementary measure of the degree to which various dilute solution parameters are affected by branching of the kind here considered.

The results of our investigation are discussed from the point of view of various prevalent theoretical developments appropriate to the analysis of branched polymer systems.

(1) The results of this investigation were presented at the 141st American Chemical Society National Meeting, March, 1962, Washington, D. C.

(2) Data obtained on earlier branched polymer samples have been reported in previous communications (a) F. Wenger, Discussion Contribution No. 187. Paper A41, International Symposium on Macromolecular Chemistry, July, 1961, Montreal, Canada—see *J. Polymer Sci.*, **57**, 481 (1962); (b) T. A. Orofino and F. Wenger, Division of Polymer Chemistry, American Chemical Society, Preprints 3, 274 (1962). These results have since been supplemented through more extensive studies on better characterized materials, data for which are herein reported.

(3) C. D. Thurmond and B. H. Zimm, *J. Polymer Sci.*, **8**, 477 (1952).

(4) W. H. Stockmayer and M. Fixman, *Ann. N. Y. Acad. Sci.*, **57**, 334 (1953).

(5) F. Wenger and S.-P. S. Yen, presented at the 141st American Chemical Society National Meeting, March, 1962, Washington, D. C. (to be published). See also, Division of Polymer Chemistry, American Chemical Society, Preprints 3, 162 (1962).

(6) T. A. Orofino, Division of Polymer Chemistry, American Chemical Society, Preprints, 2, 161 (1961); T. A. Orofino and J. W. Mickey, Jr., *J. Chem. Phys.*, **38**, in press.

Finally, in the concluding sections of this communication we have attempted to interpret our findings in terms of two characteristics distinguishing branched materials from the corresponding linear polymers, *viz.*, coil size in dilute solution and segment density distribution. Insofar as seems justifiable, these interpretations are extended to more general branched polymer systems.

Experimental

The various experimental procedures employed in sample characterization and in the detailed solution studies are described below. The solvents used in this investigation were Fisher Certified Reagent grade. In the case of cyclohexane, which constitutes a Θ-solvent mixture with polystyrene (*cf. seq.*), the solvent was freshly distilled prior to the series of measurements.

1. **Intrinsic Viscosity.**—Intrinsic viscosities in benzene and toluene were determined with a Ubbelohde viscometer (flow time for benzene, *ca.* 80 sec.) maintained at temperature by means of a water bath controlled to ±0.02°. Solutions were prepared individually, diluted in volumetric flasks at 25°, and filtered directly into the viscometer through grade "C" glass frits. The observed flow times were corrected for kinetic energy. Intrinsic viscosities in cyclohexane were determined with another Ubbelohde viscometer yielding a flow time for solvent of *ca.* 250 sec. at 35°. This solvent medium constitutes a Θ-mixture with polystyrene at about 35° and special precautions were therefore necessary to avoid phase separation. Each solution was individually prepared in the following manner: the desired amount of polymer was accurately weighed into a volumetric flask to which sufficient cyclohexane was then added to effect eventual solution. The flask and contents were stored for about 16 hr., with periodic shaking, in a small oven maintained at 40 ± 2°. The oven was equipped with an insulated front cover fitted with a double-wall glass window and access ports permitting observation and manipulation of the contents without disruption of temperature control. After complete solution was effected, the flask, still in the oven, was diluted to the mark with cyclohexane stored in the oven prior to use. The temperature of dilution was recorded and subsequently used to correct (volume) concentrations to measurement temperatures. The solution then was filtered into a second volumetric flask through a coarse glass frit (all apparatus maintained at oven temperature), temporarily insulated, and transferred quickly to the constant temperature water bath containing the dry viscometer. Solution was admitted into the viscometer, maintained at this stage at the highest temperature of measurement, by means of a preheated syringe and needle inserted into the warm environment of the filling tube.

The flow times of each solution at the various temperatures studied were obtained by successive lowering of the bath settings, maintained in all cases to within ±0.002° as read from Beckmann thermometers calibrated against a National Bureau of Standards resistance thermometer. For the solvent and one solution, flow times at the highest temperature were reconfirmed at the end of the series by raising the bath setting to this level and repeating the measurements. No difficulties with erratic flow times were experienced over the range of concentration and temperature investigated.

All flow times were corrected for kinetic energy. Solution concentrations were corrected in each case to measurement temperature through use of the empirical density relationship established from previous data[6] on (linear) polystyrene–cyclohexane solutions

$$\rho(t,c) = 0.774 - (1.1)10^{-3}(t - 25) + (3.2)10^{-3}c \quad (1)$$

$$20 \leq t \leq 45° \qquad 0 \leq c \leq 2$$

where c is expressed in g./100 cc. Owing to the relatively high concentrations employed in this polymer–solvent system it was considered desirable to correct the viscosity data for solution density. We therefore included in the equation for the relative viscosity η_{rel} of each solution

$$\eta_{rel} = \eta/\eta_0 = (\rho/\rho_0)[t - \beta'/\alpha' t]/[t_0 - \beta'/\alpha' t_0] \quad (2)$$

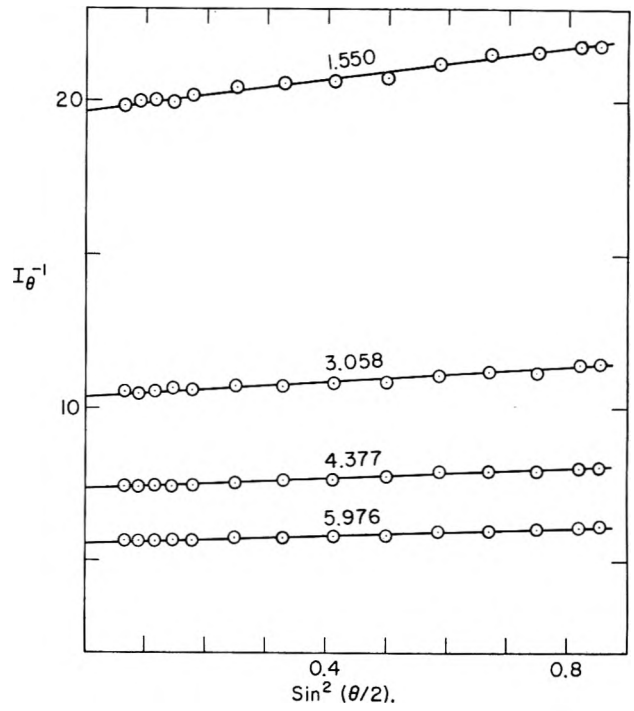

Fig. 1.—Plots of reciprocal excess scattering intensities *vs.* $\sin^2(\theta/2)$ for star polystyrene in cyclohexane at 40.22°. Polymer concentrations indicated are in (g./cc.) × 10^3.

where β'/α' is the kinetic energy constant, t is flow time, and the subscript zero denotes the solvent; values of the densities ρ computed from eq. 1.

2. **Light Scattering.**—The photometer used in our work was a Brice–Phoenix unit, Series 1250, suitably modified for temperature control of the scattering solutions. The thermostat consists of two pieces: a hollow base upon which the cylindrical glass cell rests, and a double walled cylindrical jacket which fits over the cell and rests upon the base. The jacket is designed to provide for the uninterrupted passage of the incident and scattered beams. Water from an external source of large capacity is circulated through both sections of the thermostat, directed, in the upper section, by suitable baffles. The thermostat and supply conduits are heavily insulated to minimize heat loss. Temperature control, as judged from measurements of entrance and exit temperatures of the circulating fluid under equilibrium conditions, was ±0.002° deviation from a stable temperature gradient of less than ±0.02° within the cell, at the highest temperature employed.

Angular alignment of the cell over the range 30–135° was ascertained by measurement of light intensities from fluorescein solution. Calibration constants for the instrument–cell combinations were derived from measurements on a series of narrowly distributed linear polystyrene samples, absolute molecular weights and weight-to-number average ratios (*ca.* 1.05) of which had been previously determined from osmometry and fractionation data.[7] All solution measurements reported were made with unpolarized blue light (4358 Å.).

The preparation and handling of solutions was essentially as described in section 1 (intrinsic viscosity). Satisfactory clarification of liquids was achieved by filtration through ultrafine glass frits under dry nitrogen pressure. In the case of the cyclohexane measurements, the entire operation was carried out in the small oven described earlier.

Intensity data obtained as a function of scattering angle were treated according to the extrapolation method. A typical plot of reciprocal excess scattering intensity I_θ^{-1} (instrument units) *vs.* $\sin^2(\theta/2)$ for one of the series of cyclohexane measurements carried out on star sample 8-III$_2$ (*cf. seq.*) is shown in Fig. 1.

(7) The method described for absolute calibration of the photometer gave a result in agreement with that provided by 90° scattering measurements on the Cornell Polystyrene in toluene. The use of the latter calibration constant in the treatment of data obtained on polystyrene samples dissolved in media other than toluene, however, required inclusion of an empirical refractive index correction in the light scattering equations. The procedure adopted avoided this difficulty, providing direct reference to the absolute molecular weight scale.

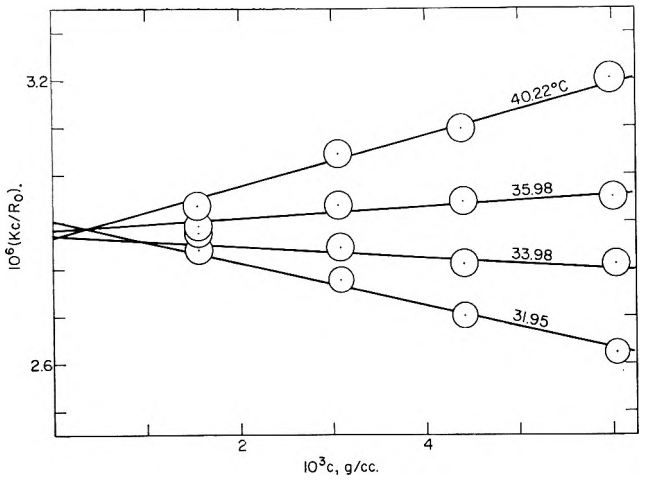

Fig. 2.—Plots of reduced reciprocal scattering intensities at zero angle as a function of concentration for star polystyrene in cyclohexane at various temperatures.

The angular dissymmetries exhibited by all solutions investigated, although too small to provide an accurate measure of coil dimensions ($I_{45}/I_{135} < 1.1$) were of sufficient magnitude to warrant the corrections to molecular weight and thermodynamic parameters provided by the angular extrapolation procedure employed.

3. Osmotic Pressure.—The osmometer used in our work was an all brass block instrument with a membrane-capillary ratio area of 1.7×10^4. Details of construction have been described elsewhere.[8] The measuring tubes were matched in regard to capillary rise of solvent.

The membranes employed were wet regenerated cellulose, gage 300, conditioned to solvent in the osmometer. Normal quilibration behavior with solvent and absence of dissymmetry were ascertained prior to solution measurements. Half times were of the order of 30 min.

Individually prepared cyclohexane solutions of known polymer concentration were used to rinse and fill the osmometer which was maintained at all times at *ca.* 35°. During the actual measurements, the osmometer was contained in a water bath, the temperature of which was controlled to within ±0.001°. The heights of the capillary levels as a function of time were read by means of a properly aligned cathetometer calibrated in units of 0.001 cm.

The stable differences between solution and solvent levels in each measurement were observed from initial settings less than and greater than the equilibrium difference in height. The two values agreed to within 1%, and their mean, multiplied by solution density, was taken as the osmotic pressure of the solution.

At the termination of each measurement the polymer content of the solvent compartment was determined by dry weight analysis. Values thus obtained were zero within the weighing error, indicating absence of appreciable diffusion of low molecular weight components through the membrane.

Characterization of Polymer Samples

The parent branched polymer samples from which the fractions employed in this investigation were isolated were synthesized by means of a coupling reaction between polystyryl-lithium of narrow molecular weight distribution (weight-to-number average ratio *ca.* 1.02) and 1,2,4-tris(chloromethyl)-benzene. The details of the preparative procedure are outlined in another communication.[5]

The primary sample (fraction 8-III$_2$) employed in the current study was separated from the whole polymer mixture through repeated stepwise fractionation from methyl ethyl ketone–methanol mixtures at 30°. These conventional procedures have been found sufficient for the eventual separation of the desired trifunctional species from other components[9] of the whole polymer mixtures, the assessment of which through ultracentrifuge studies will be treated in detail in another publication.[5]

Molecular weight characterization data for sample 8-III$_2$ are compiled in Table I. The weight average value $\bar{M}_w$ for this sample was obtained in the course of detailed light scattering studies described in the following section; the molecular weight of the linear starting material ($\bar{M}_{w_0}$) was determined from light scattering studies in cyclohexane at 35°. The number average molecular weight $\bar{M}_n$ of the star sample was derived from the results of osmotic pressure measurements in accordance with the relation

$$\Pi/c = (RT/\bar{M}_n)(1 + \Gamma_2 c + \ldots) \qquad (3)$$

where Π is osmotic pressure, R is the gas constant, T is absolute temperature, and Γ_2 is the second virial coefficient. In the solvent medium selected for these measurements, cyclohexane at 34.8°, the value of the latter parameter was found to be zero (*cf. seq.*).

The weight-to-number average molecular weight ratio and the ratio of $\bar{M}_w$ to $\bar{M}_{w_0}$ listed in Table I for the polystyrene trifunctional star sample are, within experimental error, unity and three, respectively, in accord with expectations.

TABLE I

CHARACTERIZATION DATA

POLYSTYRENE STAR SAMPLE 8-III$_2$

$\bar{M}_w = 3.48 \times 10^5$

$\bar{M}_n = 3.51 \times 10^5$	$\bar{M}_{w_0} = 1.12 \times 10^5$
$\bar{M}_w/\bar{M}_n = 0.99\ (1.00)$	$\bar{M}_w/\bar{M}_{w_0} = 3.11$

Results

The results of the principal dilute solution measurements on star sample 8-III$_2$ carried out subsequent to the preliminary characterization studies described in the preceding section are summarized below.

1. Light Scattering.—Light scattering intensities in cyclohexane at 40.2, 36.0, 34.0, and 32.0° were determined. The extrapolated zero angle data were treated in accordance with the familiar virial relationship

$$Kc/R_0 = 1/\bar{M}_w + 2(\Gamma_2/\bar{M}_w)c + \ldots \qquad (4)$$

where R_0 is Rayleigh's ratio at zero angle and K is the optical constant. The results are shown graphically in Fig. 2. The radius of the circle surrounding each of the experimental points represents 1% of the ordinate value plotted. Polymer concentrations are in all cases expressed in volume units appropriate to the measurement temperatures indicated.

Values of the second virial coefficient for the branched sample $\Gamma_{2,b}$, derived from the slopes and intercepts of the curves in Fig. 2, are compiled in column 2 of the first part of Table II. In the third column are listed the ratios of the observed virial coefficients to those calculated for linear polystyrene ($\Gamma_{2,l}$) of the same molecular weight, dissolved in the same solvent media. The required values for the latter systems were deduced from results of a similar study on cyclohexane solutions of a reference linear polystyrene sample[6]

(8) W. R. Krigbaum and P. J. Flory, *J. Am. Chem. Soc.*, **75**, 1775 (1953).

(9) The whole polymers obtained in these syntheses contain, in addition to the principal trifunctional star components, deactivated linear chains and discrete, coupled products of other functionalities. The narrow molecular weight range encompassed by the primary chains, and therefore by multifunctional products derived therefrom, greatly facilitates component separation.

($\bar{M}_w = 4.06 \times 10^5$), corrected for the slight difference in molecular weight from that of the branched polymer with the aid of Krigbaum's published data[10] on his fraction H2–8.

The second virial coefficient data obtained on the branched polystyrene–cyclohexane system have been utilized to compute the Θ-temperature[11] of the pair, taking as the operational definition[11,12] of the latter the

TABLE II

DILUTE SOLUTION PARAMETERS FOR POLYSTYRENE TRIFUNCTIONAL STAR MOLECULES (SAMPLE 8-III$_2$)

$\bar{M}_w = 3.48 \times 10^5$

1 t, °C.	2 $\Gamma_{2,b}$ (cc./g.)	3 $\Gamma_{2,b}/\Gamma_{2,l}$	4 $[\eta]_b$ (dl./g.)	5 g'	6 k'_b
		Cyclohexane			
40.22	9.4	0.70	0.471	0.82_1	0.53
35.98	2.2	0.63			
(34.8)[θ]	(0)		(0.435)	(0.85_1)	(0.5^0)
34.30			0.432	0.85_4	0.59
33.98	−2.0	0.71			
31.95	−7.6	0.67	0.416	0.87_0	0.60
		Benzene			
25.0	...	...	1.052	0.87_4	0.37
		Toluene			
30.0	115	0.86[a]	0.976	0.88_2	0.39

[a] The value listed derives from $\Gamma_{2,l}$ computed in accordance with the relationship of Krigbaum and Flory.[8] Employing instead the $\Gamma_{2,l}$ value derived from the data of Cowie, Worsfold, and Bywater,[13] we compute the ratio 0.92.

temperature at which Γ_2 in eq. 4 vanishes. In Fig. 3 a plot of second virial coefficient *vs.* reciprocal absolute temperature is shown. We interpolate from this curve at $\Gamma_{2,b}$ equal to zero the value Θ = 308.0°K. = 34.8°C. The dashed curve in Fig. 3, constructed from previous data, represents the corresponding temperature relationship for linear polystyrene of the same molecular weight.

In addition to the light scattering series in cyclohexane described above, measurements on star sample 8-III$_2$ in the good solvent, toluene at 30°, also have been carried out. These data appear plotted in Fig. 4. The upper (curve) represents the customary treatment of the light scattering results in accordance wih eq. 4; the lower (line) describes the same data treated in accordance with the square root relationship.[14] The radii of the circles surrounding the points in the two constructions denote one and one-half per cent, respectively, of the ordinate values plotted. The value of $\Gamma_{2,b}$ for the star sample in toluene, derived from the square root plot of Fig. 4, is listed in column 2 of the last section of Table II.

2. Intrinsic Viscosity.—Intrinsic viscosity measurements have been carried out on star sample 8-III$_2$ in cyclohexane at three temperatures near the Θ-point, in benzene at 25°, and in toluene at 30°. The data, shown plotted in Fig. 5 and 6, were treated in accordance with the complementary relationships for intrinsic viscosity $[\eta]$

(10) W. R. Krigbaum, *J. Am. Chem. Soc.*, **76**, 3758 (1954).

(11) P. J. Flory, "Principles of Polymer Chemistry," Cornell University Press, Ithaca, N. Y., 1953.

(12) T. A. Orofino and P. J. Flory, *J. Chem. Phys.*, **26**, 1067 (1957).

(13) J. M. G. Cowie, D. J. Worsfold, and S. Bywater, *Trans. Faraday Soc.*, **57**, 705 (1961).

(14) The acceptance of linearity in the plot of $(Kc/R_0)^{1/2}$, derived from eq. 4, rests upon the assumption that Γ_3 appearing in the c^2 term of this relationship may be satisfactorily approximated by $(\Gamma_2^2/3)$, higher terms being negligible.

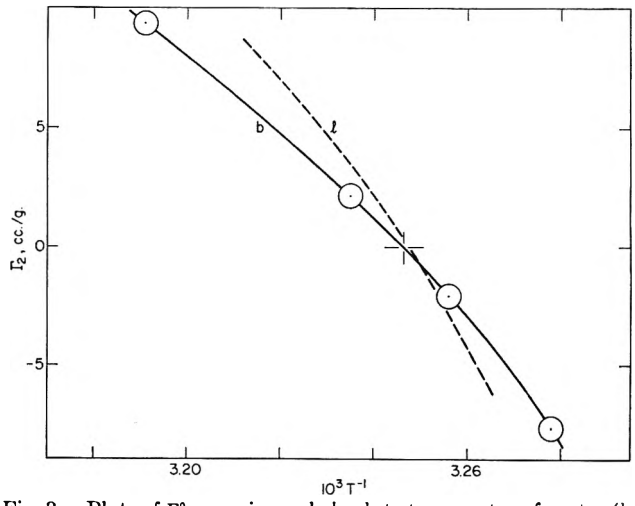

Fig. 3.—Plots of Γ^0 *vs.* reciprocal absolute temperature for star (b) and linear (l) polystyrene in cyclohexane.

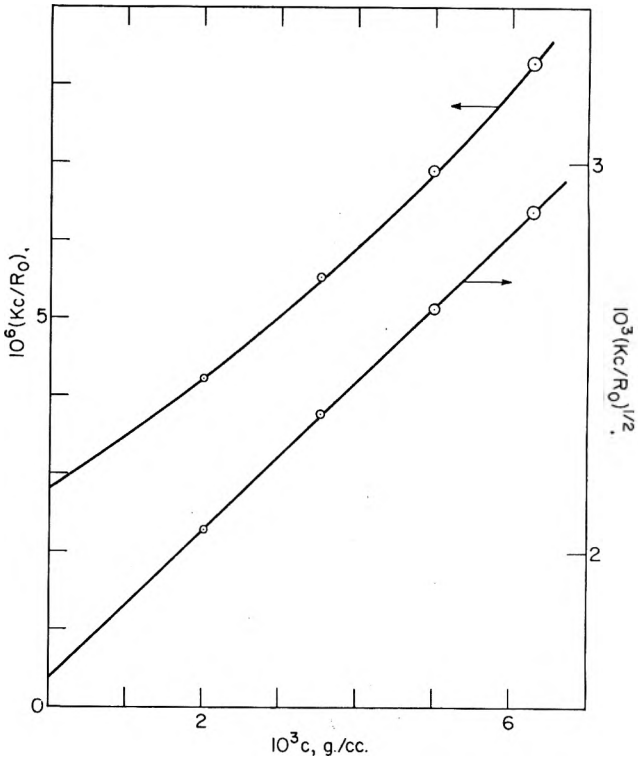

Fig. 4.—Linear and square root plots of reduced reciprocal scattering intensity at zero angle *vs.* concentration for star polystyrene in toluene at 30°.

$$\eta_{sp}/c = [\eta] + k'[\eta]^2c + \ldots \qquad (5)$$

$$(\ln \eta_{rel})/c = [\eta] + k''[\eta]^2c + \ldots$$

where η_{sp} is the specific viscosity, k' is the Huggins constant, and k'' is the corresponding parameter for the logarithmic form. The circle radii in these figures denote 1% of the ordinate data. The parameters $[\eta]_b$ and k_b' derived therefrom are listed in columns 4 and 6 of Table II, together with the interpolated values for the cyclohexane system at the Θ-temperature of the polymer–solvent pair.

In column 5 of Table II are listed values of the ratio[15] g' defined

$$g' \equiv [\eta]_b/[\eta]_l \qquad (6)$$

where $[\eta]_l$ denotes the intrinsic viscosity of the linear

(15) B. H. Zimm and R. W. Kilb, *J. Polymer Sci.*, **37**, 19 (1959).

TABLE III

COMPARISON OF DILUTE SOLUTION PARAMETERS

Sample	$10^{-5}M_w$	% Star	$\bar{M}_w/\bar{M}_{w_0}$	Θ-solvent: Θ, °K.	ψ_1	g_Θ'	k_Θ'	Good solvents: g'	k'	$\Gamma_2/\Gamma_{2,1}$
Linear reference	4.06	0	1.00	308.0	0.38	1.00	0.50	1.00	0.38	1.00
10-III	3.12[c]	(50)	2.55	307.5	.25	0.91	.56	0.94	.36	...
8-III$_2$	3.48	(100)	3.11	308.0	.24	0.85	.59	0.88	.38	0.86

[a] The molecular weights of the trifunctional star and (difunctional) linear components are *ca.* 3.7 and 2.4 × 10^5, respectively.

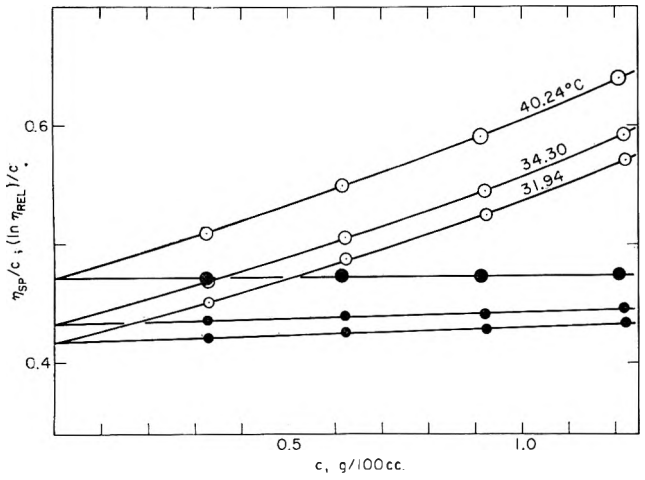

Fig. 5.—Plots of η_{sp}/c (open circles) and (ln η_{rel})/c (solid circles) *vs.* c for star polystyrene in cyclohexane at various temperatures.

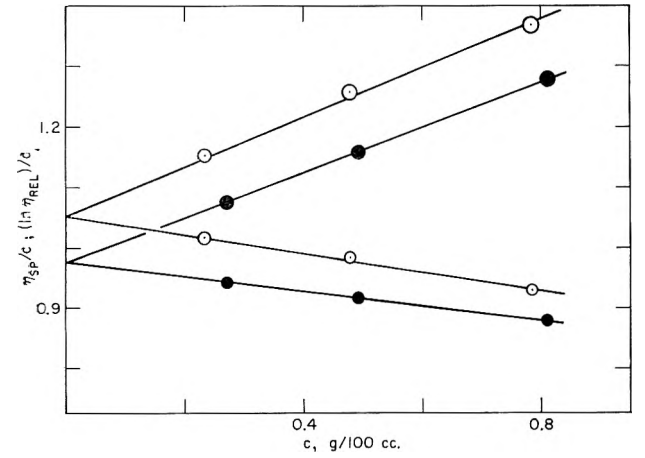

Fig. 6.—Plots of η_{sp}/c and (ln η_{rel}/c) *vs.* c for star polystyrene in benzene at 25° (open circles) and in toluene at 30° (solid circles).

polymer of the same molecular weight dissolved in the same solvent medium.

The g' entries for the cyclohexane systems were calculated with the aid of $[\eta]_l$ values derived from data[6] on the reference linear polystyrene sample at the same measurement temperatures, through multiplication of the latter by the square root of the ratio of the branched polymer molecular weight to that of the linear sample in question. The justification for this procedure rests upon the assumption that the proportionality[11] between $[\eta]_l$ and $M^{1/2}$, properly utilized in the calculation of g' at the (common) Θ-temperature of the branched and linear molecules, may also be extended to data at temperatures a few degrees above and below Θ. Owing to the proximity of the molecular weights involved, the error introduced is in fact of no consequence.

The value of $[\eta]_l$ required in the evaluation of g' for the benzene system was computed from the relationship

$$[\eta]_l = 0.918 \times 10^{-4}\bar{M}_w^{0.743} \qquad (7)$$

derived from data on a number of linear polystyrene samples studied in our Laboratory. The g' entry for the toluene datum was similarly computed, utilizing eq. 7 and the relationship between intrinsic viscosities in benzene and toluene reported by Bawn, *et al.*[16]

3. Summary of Results.—The data presented in Table II and in the foregoing text provide a detailed compilation of the results of our dilute solution studies on polystyrene trifunctional star molecules. Our principal findings may be more compactly summarized by resolution of the data and additional parameters derived therefrom into two important categories, *viz.*, those appropriate to characteristics of the star structures in Θ-solvent media (cyclohexane at 34.8°) and those pertaining to solution behavior in good solvents (benzene or toluene). Our results arranged in accordance with this classification are compiled in the last line of Table III. Entered for later reference is the cyclohexane value of the parameter ψ_1 appearing in the Flory–Krigbaum theory[11] for the second virial coefficient, applicable in form to branched or linear polymer systems (*cf. seq.*). An operational procedure for derivation of ψ_1 from virial coefficient–temperature data has been described previously.[10]

Included in Table III are entries corresponding to the above for the reference linear polystyrene previously cited. Also listed are data on sample 10-III, a mixture of trifunctional star and linear polystyrene approximately 50–50% by weight (as deduced from sedimentation studies). We shall make no attempt to interpret quantitatively the data on the latter mixture in subsequent sections; they are included here only to indicate in more detail the sensitivity of the various parameters entered to the branched chain content of the samples.

All of the derived quantities listed in Table III are unlikely to be sensitive to variations in polymer molecular weight over the relatively narrow range encompassed by the three samples. The values of the parameters derived may accordingly be compared from the viewpoint of the effect of trifunctional branching in the molecular weight range 3–4 × 10^5.

Discussion

1. Intrinsic Viscosities and Intramolecular Interaction Parameters.—Inspection of the values of g' (eq. 6) entered in Table II and in the last line of Table III shows that the intrinsic viscosities of the branched samples investigated, both in poor and in good solvent media, are significantly less than those calculated for their linear counterparts of the same molecular weights. The observed diminution in $[\eta]$ accompanying the introduction of branching at fixed molecular weight may no doubt be attributed to the smaller volume pervaded by the relatively compact branched chain.

(16) C. E. H. Bawn, R. F. J. Freeman, and A. R. Kamaliddin, *Trans. Faraday Soc.*, **46**, 1107 (1950).

An important theoretical treatment of the viscosity ratio g' of certain branched polymer systems was presented a few years ago by Zimm and Kilb.[15] They calculated g' for various uniform and irregular star-shaped molecules obeying random flight statistics and, in addition, observed that the values obtained could be reasonably well approximated by $g_\Theta^{1/2}$, the random flight (Θ-solvent) ratio of root-mean-square radii of gyration of the branched molecules and linear molecules of the same molecular weights.[17] Thus, on the basis of their computations the authors concluded, with what appears to be a justifiable generalization, that for all star-shaped molecules the particular variant of our eq. 6 appropriate to Θ-solvent mixtures may be explicitly expressed

$$g_\Theta' \equiv [\eta]_{\Theta,b}/[\eta]_{\Theta,l} \simeq g_\Theta^{1/2} \qquad (8)$$

For the special class of p-functional star molecules of uniform branch length, the parameter g_Θ is given by the expression[17,18]

$$g_\Theta = 3/p - 2/p^2 \qquad (9)$$

It is of interest to note that the value of g_Θ' (0.85) determined in the present investigation is in fair agreement with either the calculated ratio (0.90) given by Zimm and Kilb for these trifunctional star structures or, in accordance with the approximation suggested by them, the corresponding value of $g_\Theta^{1/2}$ (0.882) computed from eq. 9. The observed discrepancy between the results of experiment and either of the theoretical predictions, however, is probably significant. We would conclude on this basis that in the case of trifunctional star molecules the Zimm–Kilb treatment somewhat underestimates the effect of branching on viscometric properties.

The values of g_Θ' listed in Tables II and III for the good solvent systems polystyrene–benzene and toluene (0.87–0.88) can be considered to lie in excellent agreement with the theoretical quantity $g_\Theta^{1/2}$ if, as implied by Zimm and Kilb, eq. 8, unrestricted to Θ-solvent conditions, may be extended to good solvent data as well. The foregoing extension, however, neglects the possibly important influence of relative intramolecular expansion of branched and linear polymers in good solvent media (*cf. seq.*). We would tend to regard the formal coincidence of g' and $g_\Theta^{1/2}$ observed in these cases as fortuitous, emphasizing instead the more significant indication from our studies, *viz.*, that g' for star structures is augmented by increase in solvent power of the medium.

An alternate theoretical expression for g'

$$g' \equiv [\eta]_b/[\eta]_l \simeq g^{3/2} \qquad (10)$$

supposedly applicable to all branched structures in poor and good solvents, was originally proposed a number of years ago.[3,11] This formulation follows by straightforward generalization of the Flory–Fox equation for linear polymers[19]

$$[\eta]_l = 6^{3/2}\Phi(\bar{s^2})^{3/2}/M \qquad (11)$$

where $\bar{s^2}$ is the mean-square radius of gyration of the polymer molecule (not necessarily dissolved in a Θ-solvent) and Φ is a constant stipulated to be independent of molecular weight, solvent and temperature. The relationship (11) has enjoyed considerable success in correlating the viscosity behavior of linear polymers; its proposed extension to branched systems merely involves identification of $\bar{s^2}$ with the mean square radius of the branched molecule, thus leading to the expression for g' given in eq. 10. Unfortunately, however, the latter convenient relationship has not been borne out by experimental data obtained on branched systems to date. The results of the present measurements are likewise in disagreement with eq. 10, as is evident, for example, by comparison of our g_Θ' value with $g_\Theta^{3/2}$ (0.686) computed from eq. 9.

Notwithstanding the discrepancies noted, the extension of eq. 11 to branched systems involves a most reasonable and singularly attractive supposition; namely, that the intrinsic viscosity of a branched polymer is proportional to some measure of the molecular volume. If we accept the formal applicability of eq. 11 to linear polymers, together with its logical extension to branched systems, failure of the relationship 10 to describe adequately experimental results must arise from a dependence of the viscosity constant Φ on branching. The latter presumably has its origin in the effect of branched structure on the segment density distribution of the polymer coil, affecting the flow behavior of solvent through the molecule, and thus the relationship between $(\bar{s^2})^{1/2}$ and the effective hydrodynamic radius.[4,20] This notion is not new, of course, but we consider it worthwhile to pursue the argument in somewhat more quantitative fashion in the analysis of our viscosity data.

We assume that (1) the intrinsic viscosity of any branched structure may be expressed by an equation of the form (11) with the coefficient Φ replaced by Φ_b, now regarded as a function of chain branching. We assume further that (2) the value of Φ_b does not depend on the solvent in which a particular branched molecule is dissolved. Thus, as in the case of linear polymers, augmentation of chain dimensions resulting from segment–solvent interactions are assumed to have negligible effect on the proportionality between $(\bar{s^2})^{1/2}$ and hydrodynamic radius.[21] On the basis of assumption (1) we arrive at the revised version[22] of eq. 10

$$g' = (\Phi_b/\Phi_l)[(\bar{s_\Theta^2})_b^{3/2}/(\bar{s_\Theta^2})_l^{3/2}](\alpha_b^3/\alpha_l^3) \qquad (12)$$
$$= g_\Theta^{3/2}(\Phi_b/\Phi_l)(\alpha_b^3/\alpha_l^3)$$

where α^3 for the branched (b) or linear (l) molecule expresses the expansion of molecular dimensions from the random flight values, denoted by the subscript Θ.

With assumption (2) we may define for a given branched molecule dissolved in a non-ideal solvent

$$[\eta]_b/[\eta]_{\Theta,b} \equiv \alpha_b^3 \simeq (\bar{s^2})_b^{3/2}/(\bar{s_\Theta^2})_b^{3/2} \qquad (13)$$

(17) B. H. Zimm and W. H. Stockmayer, *J. Chem. Phys.*, **17**, 1301 (1949).

(18) T. A. Orofino, *Polymer*, **2**, 305 (1961).

(19) P. J. Flory and T. G Fox, *J. Am. Chem. Soc.*, **73**, 1904 (1951).

(20) F. Bueche, *J. Polymer Sci.*, **41**, 549 (1959).

(21) Although it is not required in the present application, an additional approximation might be proposed, namely that (3) Φ_b is constant with respect to systematic variations in a suitable structural parameter characterizing a homologous branched polymer series, which variations do not seriously alter the form of the segment density profile of the molecule. Examples are variations in branch length of p-functional star molecules and variation in backbone length of regular comb polymers (see ref. 18).

(22) G. C. Berry (Thesis, University of Michigan, Ann Arbor, Michigan (1960)) has employed a similar relation in the interpretation of his data on comb-branched polyvinyl acetate.

where all quantities refer to the same polymer molecular weight. Equation 13 is identical in form with the corresponding expression for linear polymers.[11]

As pointed out earlier, our data on polystyrene star molecules indicate a slight increase in the viscosity ratio g' with solvent power of the medium. In the preceding development leading to eq. 12 and 13 we have attributed this variation in g' to concomitant variations in the ratio α_b^3/α_l^3. This is more directly evident from inspection of eq. 12 in which $g_\Theta^{3/2}$ and the Φ ratio contained therein are, by definition or assumption, taken to be independent of solvent power.

Values of α_b^3 for the various branched systems investigated, calculated in accordance with eq. 13, are listed in Table IV. We shall have occasion to refer to these in a subsequent section. Also listed in Table IV are values of the ratio α_b^3/α_l^3, which, in accordance with eq. 12, may be directly obtained from the equivalent ratio g'/g_Θ'. Although in all cases the expansion factor ratio departs only slightly from unity, it is of interest to note that the deduced relative change in coil expansion of the branched polymer in the good solvents benzene and toluene is in the direction indicated by theory.[23]

The suppositions involved in the foregoing, provisional interpretation of our intrinsic viscosity data embodied in the eq. 12 and 13 could be subjected to direct experimental test. For this purpose light scattering

TABLE IV

INTRAMOLECULAR EXPANSION FACTORS FOR POLYSTYRENE TRIFUNCTIONAL STAR MOLECULES

Solvent medium	α_b^3 (eq. 13)	α_b^3/α_l^3
Cyclohexane, 31.95°	0.956	1.02
33.98	(0.989)	
34.8$_\Theta$	1.000	1.00
35.98	(1.018)	
40.22	1.083	0.97
Toluene, 30.0°	2.24	1.04
Benzene, 25.0°	2.42	1.03

radii of gyration, coupled with $[\eta]$ values, would be required for evaluation of Φ_b. Because of the lack of sufficient precision otherwise associated with determination of the former quantities, such measurements would most profitably be confined to well characterized star molecule samples of substantially higher molecular weights than those here considered. In defense of the proposals at the present time, we should like to point out that mere acceptance of the proportionality of $[\eta]_b$ to the cube of a coil dimension, coupled with the predictions of the Zimm–Kilb relation (8) with which our Θ-solvent data are in semiquantitative accord, unequivocally entail a substantial modification of Φ_b over Φ_l. For star molecules this takes the form $\Phi_b \simeq \Phi_l/g_\Theta$.

In conclusion of this section, we may make some remarks in regard to the values of the Huggins constant k' (eq. 5) listed in Tables II and III.

Our viscosity data in the good solvent media benzene and toluene yield values of k' experimentally indistinguishable from those obtained in our Laboratories and reported in the literature[11] for linear polystyrene in the same or comparable media. Thus, we have found no indication that k' in good solvents is significantly affected by branching of the type considered here.

Our viscosity data obtained in the cyclohexane Θ-solvent mixture yield a value of k' more or less comparable to those observed[6,24] for cyclohexane solutions of the linear polymer. The value 0.59 listed in Table III is, however, slightly larger than the value 0.50 found in our Laboratories for the corresponding linear polystyrene–cyclohexane system. Although curvature in the η_{sp}/c *vs.* c plots in each case renders specification of k' somewhat uncertain, the difference observed probably is significant, inasmuch as the viscometer, procedure, and treatment of data were identical for both the branched and linear systems compared. We conclude on this basis that for polystyrene star molecules, k' near Θ is augmented by branching.

2. Second Virial Coefficients and Intermolecular Interaction Parameters.—The second virial coefficient Γ_2 appearing in eq. 3 for the osmotic pressure and in eq. 4 for reciprocal light scattering intensity, each of which is equally applicable to linear or branched polymers, is a measure of the extent of intermolecular segment–segment interactions in dilute solution. In recent years several theories relating Γ_2 for linear polymers to molecular weight, coil size and interaction parameters have been advanced. Some of these developments also have been extended to branched polymer systems, the application of which to our relevant dilute solution data provides the subject matter of this section. Values of Γ_{2b} obtained in the present studies on branched polymers are listed in Table II. In the analyses following, it will be convenient to consider separately the results for the cyclohexane (poor solvent media) and the toluene (good solvent medium) systems.

The data obtained on sample 8-III$_2$ in cyclohexane at various temperatures constitute a limited, but systematic study of the second virial coefficient over a narrow range of polymer interactions which includes the Θ-solvent conditions established here. On this account, it is of interest to compare our data with the predictions of some exact theoretical developments applicable over a restricted range of segment excluded volume. The results of the exact treatment for the second virial coefficient of branched or linear polymers[4,25] may be expressed in the general form

$$\Gamma_2 = (N\beta M/2M_0^2)(1 + b_1 z + \ldots) \qquad (14)$$

where M and M_0 are polymer and segment molecular weight, respectively, and N is Avogadro's number. The parameter β represents segment excluded volume, equal to zero for Θ-solvent mixtures and increasing in value with increasing segment interactions; the parameter z is defined in terms of β through the relationship

$$z = \beta(M/M_0)^{1/2}(3/2\pi b_0^2)^{3/2} \qquad (15)$$

where b_0 is the length of one segment.[26]

(23) An earlier calculation (a) M. Fixman, *J. Chem. Phys.*, **23**, 1656 (1955), of the initial effect of segment excluded volume on coil dimensions of tetrafunctional star molecules has led to the conclusion that α is diminished by branching; (b) T. A. Orofino (to be published) recently has revised and extended the development cited to the general class of p-functional star molecules. The results, contrary to the above, support the notion that α is augmented by star branching for all values of p; see also: (c) O. B. Ptitsyn, *J. Gen. Chem. U.S.S.R.*, **29**, 396 (1955), and (d) W. R. Krigbaum and Q. A. Trementozzi, *J. Polymer Sci.*, **28**, 295 (1958).

(24) T. G Fox and P. J. Flory, *J. Am. Chem. Soc.*, **73**, 1915 (1951).

(25) B. H. Zimm, *J. Chem. Phys.*, **14**, 164 (1946).

(26) In applications to real systems, M_0 and b_0 refer to the statistical or equivalent polymer segment defined in part through the familiar random flight relationship for linear polymers $\overline{s_0^2} = (M/M_0)(b_0^2/6)$. The left-hand side of this equation represents, for any given polymer, a definite, measurable quantity whose value is independent of the foregoing theoretical considerations.

Numerical values of the first coefficient b_1 appearing in eq. 14 have been computed for both linear and tetrafunctional star polymers, the latter containing four branches of equal length. More recently,[27] the calculations have been extended to the general class of p-functional star molecules. The b_1 values for linear and trifunctional star polymers are -2.865 and -3.279, respectively.

Equation 14 is of limited use in the quantitative interpretation of experimental data, owing to the slow convergence of the series involved and the lack of a precise correspondence between the interaction parameter z (or β) and experimentally accessible quantities. Qualitatively, however, one may conclude from the relative values of b_1 cited above that, at least for z very small and positive, the second virial coefficient for a trifunctional star molecule is less than the corresponding Γ_2 for a linear polymer of the same molecular weight. This expectation is borne out by our virial coefficient data in cyclohexane, as may be seen from the values of the ratio $\Gamma_{2,b}/\Gamma_{2,l}$ listed for these systems in column 3 of Table II. A somewhat more critical test of these data, however, is provided below.

The series development[23a,28] for the intramolecular expansion factor $\alpha_{(s)}$, the companion expression to eq. 14 for an isolated polymer coil, may be written

$$\alpha_{(s)}^2 \equiv \bar{s}^2/\bar{s}_\Theta^2 = 1 + a_1 z + a_2 z^2 - \ldots \quad (16)$$

where for linear and trifunctional star molecules[23b] the first coefficient a_1 has the values 1.276 and 1.298, respectively. (The precise definition of $\alpha_{(s)}$ as the ratio of root-mean-square radii given above should not be confused with the operational definition of the expansion factor α in eq. 13, written without parenthetical subscript.) The series equation 16 may be combined[28] with eq. 14 through elimination of z to yield the expression

$$\Gamma_2 = (4\pi^{3/2}N/a_1)[(\bar{s}_\Theta^2)_l^{3/2}/M][(\alpha_{(s)}^2 - 1) + c_1(\alpha_{(s)}^2 - 1)^2 + \ldots] \quad (17)$$

$$c_1 = (a_1 b_1 - a_2)/a_1^2$$

Equation 17, as written, is applicable to branched or linear polymers. The mean square radius $(\bar{s}_\Theta^2)_l$ appearing therein, however, refers in either case to a *linear* chain of molecular weight M.

In Fig. 7 values of Γ_{2b} for the trifunctional star–cyclohexane system appear plotted *vs.* $\alpha^2 - 1$. The latter quantities were computed from eq. 13 (see Table IV) on the assumption that this relation provides an adequate estimate of the mean square radius expansion factor defined by eq. 16 and contained in eq. 17. According to the latter relation, the slope of the dashed line is proportional to $(\bar{s}_0^2)_l^{3/2}/M$. With the known M value for this sample, we derive from Fig. 7 the molecular weight independent ratio (for linear chains) $(\bar{s}_\Theta^2)_l/M = 0.93 \times 10^{-17}$. This may be compared with the value 0.96×10^{-17} determined from application of eq. 17 to similar data on the linear reference polystyrene–cyclohexane system[6] cited previously. Either of the values is in acceptable agreement with the experimental ratio determined by direct measurement,[11,29] *ca.* $0.85 \pm 0.1 \times 10^{-17}$.

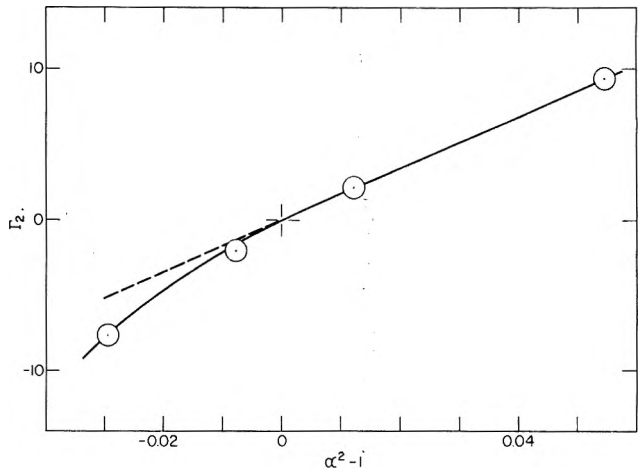

Fig. 7.—Plot of $\Gamma_{2,b}$ *vs.* $\alpha^2 - 1$ for star polystyrene 8-III$_2$ in cyclohexane (see text).

It is of interest to note that through the above procedure a reasonable estimate of the branched polymer dimensions can be obtained from our data, even though the molecular size in this instance is too small to permit direct evaluation from the light scattering envelope. The general consistency of the $(\bar{s}_\Theta^2)_l/M$ values obtained in the various ways described lends some support to the interpretation of viscometric data advanced in the preceding section, at least for small deviations from θ-solvent conditions.

One further aspect of the virial coefficient results in cyclohexane may be considered, *viz.*, a comparison of some interaction parameters evaluated from our data on branched polystyrene with values of the corresponding parameters found for the linear polymer.

In Table III are listed values of the intermolecular interaction parameters Θ and ψ_l appearing in the Flory–Krigbaum[11,12] expression for the second virial coefficient, which with neglect of higher terms assumes the form

$$\Gamma_2 = (16\pi/3^{3/2})[N(\bar{s}^2)^{3/2}/M] \ln [(\pi^{1/2}/4)X_1 + 1] \quad (18)$$

The theoretical development employed in the derivation of the latter relation does not explicitly depend upon the linear nature of the polymer chain. The form of the relationship 18 thus is equally appropriate for the description of branched or linear polymer systems (subject, of course, to any common limitations which might be inherent in the model chosen). The parameter X_1 appearing in eq. 18 is defined for linear polymers through the relationship

$$X_{1,l} = (3^{3/2}/4\pi^{3/2})(\bar{v}^2/V_1 N)[M^2/(\bar{s}^2)_l^{3/2}]\psi_1(1 - \Theta/T) \quad (19)$$

where $\bar{v}$ is the partial specific volume of polymer and V_1 is molar volume of solvent.

Adaptation of eq. 19 to branched chains would require replacement of $(\bar{s}^2)_l$ appearing therein by the corresponding mean square radius $(\bar{s}^2)_b$. In addition, the numerical coefficient of the right-hand side of this equation may possibly require revision inasmuch as the

(27) E. F. Casassa, *J. Chem. Phys.*, **37**, 2176 (1962).

(28) B. H. Zimm, W. H. Stockmayer, and M. Fixman, *ibid.*, **21**, 1716 (1953).

(29) W. R. Krigbaum and D. K. Carpenter, *J. Phys. Chem.*, **59**, 1166 (1955).

value of X_1 depends upon the distribution of segments about the molecular center of mass adopted for any particular structure.

The parameters Θ and ψ_1 appearing in eq. 18 and 19, and in the analogous form of the latter for branched polymers, are primarily dependent upon *segment*–solvent interactions. Thus, to a first approximation, their magnitudes should not reflect details of the over-all molecular architecture. The values of Θ found for polystyrene–cyclohexane mixtures (308.0°K.), for both branched and linear systems, are in accord with this expectation. While it is conceivable that the disparity in values of the parameter ψ_1 listed in Table III is attributable to experimental error, the possibility of significant second-order effects of structure cannot be discounted.

We consider next the single virial coefficient datum for star sample 8-III$_2$ in the good solvent, toluene at 30°. An estimate of the value of $\Gamma_{2,b}/\Gamma_{2,l}$ to be expected for this system may be obtained from the relations 18 and 19, with suitable revision of the latter to take into account the branched nature of the chains. For this purpose, we merely replace $(\bar{s^2})_l$ appearing therein by the corresponding mean square radius of the star molecule (the sole modification which would result if, in the analogous derivation[4] of $X_{1,b}$ for branched chains, the segment density distribution were represented by a single gaussian function, normalized to the correct radius of gyration). With the additional, implicit assumption that Θ and ψ_1 appearing in the foregoing relations assume identical values for toluene solutions of branched and linear polystyrene, we have

$$\Gamma_{2,b}/\Gamma_{2,l} = g_\Theta^{3/2}(\alpha^3_{(s),b}/\alpha^3_{(s),l}) \times \{\ln[(\pi^{1/2}/4)X_{1,b} + 1]\}/\{\ln[(\pi^{1/2}/4)X_{1,l} + 1]\}$$

$$X_{1,b}/X_{1,l} = g_\Theta^{-3/2}(\alpha^3_{(s),l}/\alpha^3_{(s),b}) \quad (20)$$

All quantities for the two structures refer of course to the same polymer molecular weight. The parameter $X_{1,l}$ may be conveniently estimated through the correspondence

$$X_{1,l} = 2(\alpha^2_{(s),l} - 1) \simeq 2[([\eta]_l/[\eta]_{\Theta,l})^{3/2} - 1] \quad (21)$$

obtained by combination of eq. 19 with the Flory relationship for the expansion factor of linear chains.[30] The intrinsic viscosity ratio appearing above may be computed from data on linear polystyrene cited earlier. We calculate for $X_{1,l}$ the value[31] 1.35. The quantity $X_{1,b}$ may now be computed from the second of the eq. 20, since the other parameters appearing therein can again be deduced from data previously given (*e.g.*, taking for $\alpha^3_{(s),b}$ the intrinsic viscosity ratio listed in Table IV). We find for $X_{1,b}$ the value 1.89. The calculated ratio $\Gamma_{2,b}/\Gamma_{2,l}$ now follows directly from the first of the eq. 20. The value arrived at in this manner, 0.93, stands in good agreement with the corresponding ratio obtained directly from experimental data (see last entry, column 3, Table II, and its footnote). We conclude that the observed diminution in Γ_2 with branching in good solvents observed in the present study can be satisfactorily accounted for by straightforward extension of the Flory–Krigbaum theory. As viewed in this comparative connection, however, other treatments[27] appropriately extended to branched systems may be equally applicable.

(30) P. J. Flory, *J. Chem. Phys.*, **17**, 303 (1949).

(31) About the same value may be derived through direct application of eq. 18 and 19 to pertinent dilute solution data on linear polystyrene–toluene solutions (see ref. 12).

Conclusions

We have presented in this communication the results of pertinent experimental measurements designed to elucidate some of the dilute solution characteristics of polystyrene trifunctional star molecules. Particular emphasis has been directed to comparison of the observed solution properties with those of linear molecules of the same chemical composition and polymer molecular weight. With an object toward extending the applicability of our results to more general systems, we shall now endeavor to interpret the various differences and similarities noted in terms of two aspects of prime importance in the distinction between linear molecules and any branched structures, *viz.*, coil size and segment density distribution in dilute solution. It will also be of interest to compare the results of our study with some of those reported for other branched polymer systems.

One important conclusion drawn from the present investigation is, of course, the significant diminution of $[\eta]$ accompanying introduction of trifunctional branching in polystyrene. A considerable amount of experimental data[3,22,32] attests to the applicability of this general correspondence in regard to other branched polymers and their linear analogs. Although the decrease in $[\eta]$ with branching at fixed molecular weight observed in the present investigation may be readily attributed to a concomitant reduction in hydrodynamic volume of the molecule, the ratio of the latter to the cube of the radius of gyration differs for the branched and linear polymers compared. In this respect, the significant role of segment density distribution determining the ratio in each case is particularly emphasized. On theoretical grounds, the effect of branching is perhaps most clearly illustrated by the Zimm–Kilb relationship which requires a substantial modification in the value of Φ if the Flory–Fox equation is to be formally extended to star polymer systems.

We have chosen to interpret our viscosity results, for both poor and good solvent media, in accordance with a modified form of the Flory–Fox equation in which the parameter Φ is regarded as a specific function of chain branching. The adequacy of the assumption that Φ_b is independent of the solvent power of the medium, adopted in subsequent estimations of the expansion factor $\alpha_{(s),b}$, cannot be assessed independently from our studies. Values of the latter parameter deduced in this manner from our cyclohexane data near the Θ-temperature, however, are consistent with the predictions of the exact series developments for small excluded volume. We conclude on this basis that the ratio $([\eta]_b/[\eta]_{\Theta,b})^{1/3}$, in analogy with the corresponding expression for linear chains—and to the same degree of approximation[33]—may be retained as a satisfactory measure of the radius of gyration expansion factor for star molecules. Since the assumptions involved in ar-

(32) M. Cantow, G. Meyerhoff, and G. V. Schulz, *Makromol. Chem.*, **49**, 1 (1961).

(33) The compatibility of values of the ratio $(s\Theta^2)_l/M$ derived from our data on branched and linear polymers in accordance with the exact series treatments is preserved, if, as recently suggested for linear molecules (M. Kurata, H. Yamakawa, and H. Utiyama, *Makromol. Chem.*, **34**, 139 (1959)), the ratio $[\eta]/[\eta]\Theta$ in each case is identified with $\alpha_{(s)}{}^{2.43}$.

riving at this identification do not relate specifically to star structures, the same relationship should be applicable to other branched molecules as well.

Our findings in regard to the effect of trifunctional branching on the values of the Huggins constant k' in poor and good solvent media are in accord with some results reported[3,22,34,35] for other branched polymer systems.[36] While no attempt has been made to analyze the results of the present investigation in detail, it would appear that our observations are in qualitative conformity with the related behavior of linear polymer–solvent systems. Thus, the observed insensitivity of k' in good solvents to details of the molecular architecture, *i.e.*, branching, may be considered to parallel, in the case of the corresponding linear systems, the approximate constancy of this parameter with respect to variations in polymer molecular weight. For Θ-solvents, however, where k' for the same linear polymer may deviate appreciably from its value in more strongly interacting media, and indeed, may vary with the specific nature of the Θ-solvent,[6] it is not unreasonable to expect additional, superimposed effects of branching as observed in the present study.

The coincidence of the values of Θ characteristic of cyclohexane solutions of star and linear polystyrene molecules established in the course of this investigation parallels the findings of Thurmond and Zimm,[3] who observed an analogous correspondence in the case of linear and randomly branched polystyrenes in mixed solvent media. Our data, however, do indicate a dependence upon branching of the temperature coefficient of Γ_2 at $T = \Theta$. In terms of the Flory–Krigbaum theory, this effect is evidenced in the values of the parameter ψ_1 calculated for linear and branched polymers. The disparity in ψ_1 values noted may arise from higher order effects of molecular structure on local segment interactions. An analogous phenomenon has been observed in the case of linear polymers where, in general, both ψ_1 and Θ may depend somewhat upon over-all chain length.[12]

We have found that the values of the second virial coefficient $\Gamma_{2,b}$ for polystyrene trifunctional star molecules, in both poor and good solvent media, are less than those characteristic of the corresponding linear polymer–solvent systems. The observed effect of branching on Γ_2 is quite in accord with qualitative theoretical expectations, which have in fact received ample substantiation through earlier studies.[3,22,23d,37]

The various theoretical developments by means of which we have here attempted to describe our virial coefficient results also provide some interesting predictions in regard to branched polymer systems in general. While for the most part these pertain to data beyond the scope of the experimental portion of the present investigation, it is nevertheless of interest to examine them in some detail.

The exact series formulation (17) for the second virial coefficient of branched or linear polymers, as well as the approximate closed forms expressed through relations 18 and 19 and appropriate variants thereof, suggest the phenomenological resolution[12] of Γ_2 into two multiplicative factors: the first of these, represented by the cube of the polymer radius in either eq. 17 or 18, expresses the dominant role of coil size in determining the extent of polymer–polymer interaction, and thus the magnitude of Γ_2; the second, expressed, for example, by the logarithmic term in eq. 18, may be regarded as an interpenetration factor whose value denotes the degree to which bimolecular encounters of the more or less spherically distributed segment domains are rendered effective in augmenting Γ_2.

With equivalent generality, the quantity $\Gamma_{2,b}/\Gamma_{2,l}$ may be expressed as the product of the ratios of the same constituent factors designated above. For sufficiently high molecular weight polymers dissolved in good solvents, the values of the segment–solvent interaction parameters, appearing in both the series expression 14 and in the closed form (18), should be independent of branching. With this provision, the ratio $\Gamma_{2,b}/\Gamma_{2,l}$, expressed for example in terms of the latter relationship, assumes the relatively simple form contained in the first of the eq. 20. The systems to which eq. 20 should most appropriately apply—high molecular weight polymers dissolved in strongly interacting media—are characterized by large values of the parameter X_1. Accordingly, the normally moderating influence of the relative interpenetration (logarithmic) factors in these cases is of minimal consequence, the ratio $\Gamma_{2,b}/\Gamma_{2,l}$ being primarily determined by the $g^{3/2}$ term. The value of the latter factor, of course, is quite sensitive to alterations in molecular structure. We would on this account anticipate a corresponding sensitivity of $\Gamma_{2,b}/\Gamma_{2,l}$ to branching even greater than that exhibited through the viscosity ratio g', in which the factor $g^{3/2}$ also appearing therein is partially compensated by opposing hydrodynamic effects (see eq. 12).

Finally, we wish to call to the reader's attention the close parallel of the present investigation to one recently reported by Morton, *et al.*,[38] in which dilute solution properties of silicon-linked polystyrene star molecules are described. Although the findings of the two studies are in conceptual accord, disagreement as to detail on several important points is readily apparent. The results of Morton, *et al.*, however, are not accompanied by the necessary experimental particulars which any attempt here at critical analysis of the origin of our dissenting conclusions would require.

Acknowledgment.—The authors wish to acknowledge the assistance of Mrs. S.-P. S. Yen and Mr. John W. Mickey, each of whom has contributed significantly to the experimental portions of this work. In addition, our appreciation is extended to the Aeronautical Systems Division, Wright–Patterson Air Force Base, Dayton, Ohio, which has provided financial support for this undertaking through contractural arrangements with Mellon Institute.

(34) P. J. Flory and J. R. Schaefgen, *J. Am. Chem. Soc.*, **70**, 2709 (1948).

(35) J. A. Manson and L. H. Cragg, *J. Polymer Sci.*, **33**, 193 (1958).

(36) Contrary to our findings, however, pronounced effects of branching on k' in good solvents have been reported for some systems (H. W. Melville, F. W. Peaker, and R. L. Vale, *ibid.*, **30**, 29 (1958); *Makromol. Chem.*, **28**, 140 (1958)).

(37) P. Doty, M. Brownstein, and W. Schlener, *J. Phys. Colloid Chem.*, **53**, 213 (1949).

(38) M. Morton, T. E. Helminiak, S. D. Gadkary, and F. Bueche, *J. Polymer Sci.*, **57**, 471 (1962).

HYDROLYTIC TENDENCIES OF FERRIC CHELATES[1]

BY RICHARD L. GUSTAFSON AND ARTHUR E. MARTELL

Departments of Chemistry of Clark University, Worcester, Massachusetts, and the Illinois Institute of Technology, Chicago, Ill.

Received August 1, 1962

Potentiometric equilibrium measurements are reported for the hydrolysis and polymerization of Fe(III) complexes of ethylenediaminetetraacetic acid (EDTA), cyclohexanediaminetetraacetic acid (CDTA), N-hydroxyethylethylenediaminetriacetic acid (HEDTA), and nitrilotriacetic acid (NTA), which have a 1:1 molar ratio of ligand to metal ion. Equilibrium constants are reported for the formation of monohydroxo mononuclear complexes, and for their conversion to μ-dihydroxo binuclear chelates. Heats and entropies of reaction for the formation of EDTA and CDTA mono- and binuclear dihydroxo species were calculated from temperature coefficient data. The results are interpreted on the basis of the probable structures of the metal complexes formed.

Introduction

The purpose of the work described in this paper was to extend to the Fe(III) chelates the studies previously carried out in these Laboratories on the hydrolytic behavior of chelate compounds of copper(II),[2,3] oxouranium(VI),[4,5] thorium(IV),[4,6,7] and zirconium(IV).[8,9] Schwarzenbach and co-workers have reported the first and second hydrolysis constants of ferric chelates of ethylenediaminetetraacetic acid,[10] N,N-ethylenediaminediacetic acid,[11] N-hydroxyethyliminodiacetic acid,[11] and nitrilotriacetic acid.[12] Skochdopole and Chaberek[13] have studied the hydrolysis of N-hydroxyethylethylenediaminetriacetato-iron(III). In these studies, the possibility of formation of polynuclear ferric chelates was not investigated. Chaberek, *et al.*,[14] suggested the formation of an unhydrolyzed binuclear Fe(III) chelate of N,N-dihydroxyethylglycine but did not calculate equilibrium constants for the reactions involved. Recently, Richard, *et al.*,[4] demonstrated the existence of a binuclear diolated species containing two moles of 8-hydroxyquinoline-5-sulfonate per mole of ferric ion.

The ferric chelates studied in this investigation are those of ethylenediaminetetraacetic acid (EDTA), trans-1,2-diaminocyclohexanetetraacetic acid (CDTA), N-hydroxyethyliminodiacetic acid (HIMDA), dihydroxyethylglycine (HXG), N-hydroxyethylethylenediaminetriacetic acid (HEDTA), and nitrilotriacetic acid (NTA).

Experimental

Reagents.—A 0.3 *M* solution of Baker's Analyzed Reagent grade $Fe(NO_3)_3$ was prepared such that the solution was also 0.1 *M* in HCl. Standardization was carried out by titration with standard 0.200 *M* disodium salt of EDTA in the presence of 0.2 *M* acetate buffer with salicylic acid as an indicator, in a modification of the method outlined by Sweetser and Bricker.[15] Determination of the amount of free acid in the stock solution was carried out on the basis of potentiometric titrations of solutions containing equimolar amounts of ferric ion and the disodium salt of EDTA. The difference between the quantity of base required to reach the midpoint of the first inflection corresponding to formation of the ferric EDTA chelate, and the quantity calculated to neutralize the two moles of acid liberated from the ligand, was a measure of the amount of free acid present. Disodium EDTA was obtained from Distillation Products Industries, Rochester 3, N. Y. A Sample of CDTA was kindly donated by the Geigy Chemical Co., Ardsley, N. Y., and samples of HEDTA, NTA, HIMDA, and HXG were supplied through the courtesy of the Dow Chemical Co., Midland, Mich. Establishment of purity of the various ligands was carried out on the basis of potentiometric titration of dried samples with standard NaOH, with and without the addition of excess calcium ion. Standard carbonate-free sodium hydroxide was prepared by the usual procedure from a saturated NaOH solution.

Potentiometric Measurements.—Calculation of the various equilibrium constants was carried out from data obtained from potentiometric measurements of 1:1 ferric chelates over a concentration range 8×10^{-3} to 8×10^{-2} *M*. The hydrogen ion concentration was recorded with a Beckman Model G pH meter fitted with extension glass and calomel electrodes. Measurements were carried out under a nitrogen atmosphere in a medium 1.00 *M* in KCl. The details of calibration of the electrode system have been described in a previous publication.[3] In the cases of ferric chelates of NTA, HIMDA, and HXG, equilibrium was reached slowly and it was not possible to complete a series of measurements within a single day. In these cases solutions containing appropriate amounts of metal, ligand, KCl and NaOH were allowed to equilibrate in sealed glass containers at constant temperature for extended periods of time. The pH values of the various solutions were measured at appropriate intervals varying from one day to several months.

Mathematical Treatment of Data.—The solution equilibria may be expressed in terms of the equations

$$FeL^{3-n} \overset{K_a}{\rightleftharpoons} Fe[OH]L^{2-n} + H^+$$

$$K_a = \frac{[Fe[OH]L^{2-n}][H^+]}{[FeL^{3-n}]} \quad (1)$$

$$2FeL^{3-n} \overset{K_D}{\rightleftharpoons} (Fe[OH]L)_2^{4-2n} + 2H^+$$

$$K_D = \frac{[(Fe[OH]L)_2^{4-2n}][H^+]^2}{[FeL^{3-n}]^2} \quad (2)$$

$$2Fe[OH]L^{2-n} \overset{K_d}{\rightleftharpoons} (Fe[OH]L)_2^{4-2n}$$

$$K_d = \frac{[(Fe[OH]L)_2^{4-2n}]}{[Fe[OH]L^{2-n}]^2} \quad (3)$$

(1) This work was supported by the U. S. Atomic Energy Commission under Contracts AT-(30-1)-1823 (Clark University), and AT-(11-1)-1020 (Illinois Institute of Technology).

(2) R. C. Courtney, R. L. Gustafson, S. Chaberek, and A. E. Martell, *J. Am. Chem. Soc.*, **81**, 519 (1959).

(3) R. L. Gustafson and A. E. Martell, *ibid.*, **81**, 525 (1959).

(4) C. F. Richard, R. L. Gustafson, and A. E. Martell, *ibid.*, **81**, 1033 (1959).

(5) R. L. Gustafson, C. F. Richard, and A. E. Martell, *ibid.*, **82**, 1526 (1960).

(6) R. F. Bogucki and A. E. Martell, *ibid.*, **80**, 4170 (1958).

(7) R. L. Gustafson and A. E. Martell, *ibid.*, **82**, 5610 (1960).

(8) B. J. Intorre and A. E. Martell, *ibid.*, **82**, 358 (1960).

(9) B. J. Intorre and A. E. Martell, *ibid.*, **83**, 3618 (1961).

(10) G. Schwarzenbach and J. Heller, *Helv. Chim. Acta*, **34**, 576 (1951).

(11) G. Anderegg and G. Schwarzenbach, *ibid.*, **38**, 1940 (1955).

(12) G. Schwarzenbach and J. Heller, *ibid.*, **34**, 1889 (1951).

(13) R. Skochdopole and S. Chaberek, *J. Inorg. Nucl. Chem.*, **11**, 222 (1959).

(14) S. Chaberek, R. C. Courtney, and A. E. Martell, *J. Am. Chem. Soc.*, **75**, 2185 (1953).

(15) P. B. Sweetser and C. E. Bricker, *Anal. Chem.*, **26**, 195 (1954).

$$\mathrm{Fe[OH]L^{2-n}} \overset{K_b}{\rightleftharpoons} \mathrm{Fe[OH]_2L^{1-n}} + \mathrm{H^+}$$

$$K_b = \frac{[\mathrm{Fe[OH]_2L^{1-n}}][\mathrm{H^+}]}{[\mathrm{Fe[OH]L^{2-n}}]} \quad (4)$$

$$2\mathrm{Fe[OH]_2L^{1-n}} + 2\mathrm{H^-} \overset{K_c}{\rightleftharpoons} (\mathrm{Fe[OH]L})_2^{4-2n}$$

$$K_c = \frac{[(\mathrm{Fe[OH]L})_2^{4-2n}]}{[\mathrm{Fe[OH]_2L^{1-n}}]^2[\mathrm{H^+}]^2} \quad (5)$$

Here H_nL represents the organic ligand. Thus FeL^{3-n} is an unhydrolyzed metal chelate, $Fe[OH]L^{2-n}$ and $Fe[OH]_2L^{1-n}$ would represent mono- and dihydroxo chelates, respectively, and $(Fe[OH]L)_2^{4-2n}$ indicates a binuclear diolated chelate. Combination of the above equations with the usual material balance and electroneutrality relations gives

$$\frac{[\mathrm{H^+}](T_{\mathrm{OH}} + [\mathrm{H^+}] - [\mathrm{OH^-}])}{[\mathrm{FeL^{3-n}}]} = K_a + 2K_D\frac{[\mathrm{FeL^{3-n}}]}{[\mathrm{H^+}]} \quad (6)$$

where $[FeL^{3-n}] = T_M - T_{OH} - [H^+] + [OH^-]$, T_{OH} is the total concentration of NaOH added beyond the formation of the normal ferric chelate, FeL^{3-n}. A plot of $[H^+](T_{OH} + [H^+] - [OH^-])/FeL^{3-n}]$ as ordinate *vs.* $2[FeL^{3-n}]/[H^+]$ as absicssa will yield a straight line of slope K_D and intercept K_a if the binuclear diolated species is the only polynuclear chelate present in appreciable concentration. If the concentration of FeL^{3-n} is sufficiently small, K_c and K_b may be expressed by the relationship

$$\frac{T_M - [\mathrm{Fe[OH]_2L^{1-n}}]}{[\mathrm{H^+}][\mathrm{Fe[OH]_2L^{1-n}}]} = 2K_c[\mathrm{H^+}][\mathrm{Fe[OH]_2L^{1-n}}] + \frac{1}{K_b} \quad (7)$$

where T_M is the total concentration of Fe(III) in all forms. Here a plot similar to that described above will give a slope equal to K_c and an intercept equal to $1/K_b$.

Values of ΔH^0 and ΔS^0 for the various reactions involved were calculated with the usual thermodynamic relationships.

Results

Fe(III)-EDTA.—Potentiometric measurement of a solution containing equimolar quantities of ferric salt and the disodium salt of EDTA (H_2L^{2-}) produces an inflection at $m = 2$, followed by a buffer region terminating in a second inflection at $m = 3$. Here m is equal to the number of moles of standard NaOH added per mole of metal ion. The first buffer region corresponds to the reaction

$$\mathrm{Fe^{3+}} + \mathrm{H_2L^{2-}} \rightleftharpoons \mathrm{FeL^{1-}} + 2\mathrm{H^+}$$

whereas the second buffer region corresponds to the reaction

$$\mathrm{FeL^{1-}} \rightleftharpoons \mathrm{Fe[OH]L^{2-}} + \mathrm{H^+}$$

and possibly also to an olation reaction. Potentiometric data obtained over a tenfold concentration range at 25° are shown in Fig. 1. Here $m = 0$ corresponds to the unhydrolyzed chelate, FeL^{1-}. Beyond $m = 1$ precipitation was observed in all solutions in the concentration range studied (8.5×10^{-3} to 8.2×10^{-2} M).

A plot of eq. 6 demonstrating the presence of a binuclear diolated ferric EDTA species is shown in Fig. 2 for data obtained at 25°. Data from experiments carried out at other temperatures did not exhibit such

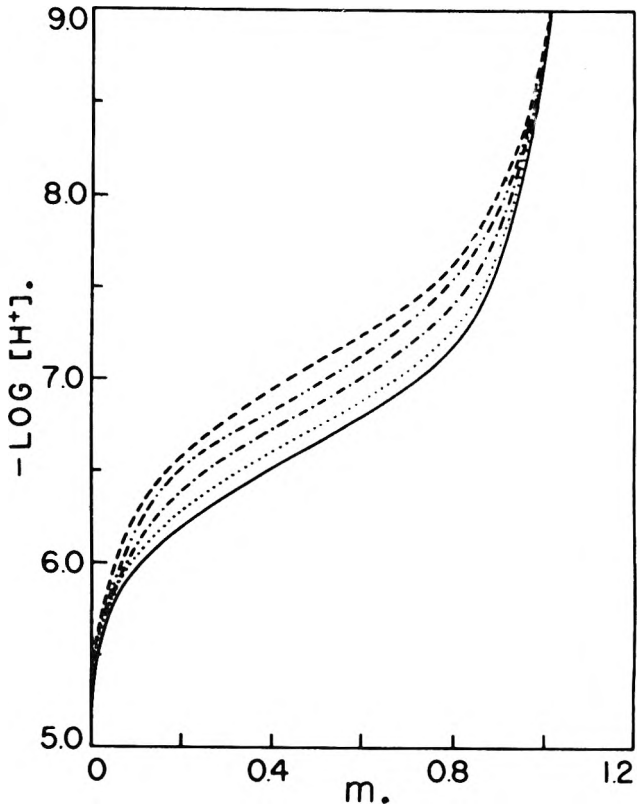

Fig. 1.—Potentiometric titration of 1:1 Fe(III)-EDTA chelate. Concentrations: ———, 8.5×10^{-2} M; . . . . . , 5.6×10^{-2} M; - - - -, 3.0×10^{-2} M; - - - - - -, 1.6×10^{-2} M; – – – –, 8.2×10^{-3} M. m = moles of base added per gram ion of Fe(III), $m = 0$ corresponds to complete formation of normal Fe(III)-EDTA chelate, $t = 25.0°$, $\mu = 1.0$ (KCl).

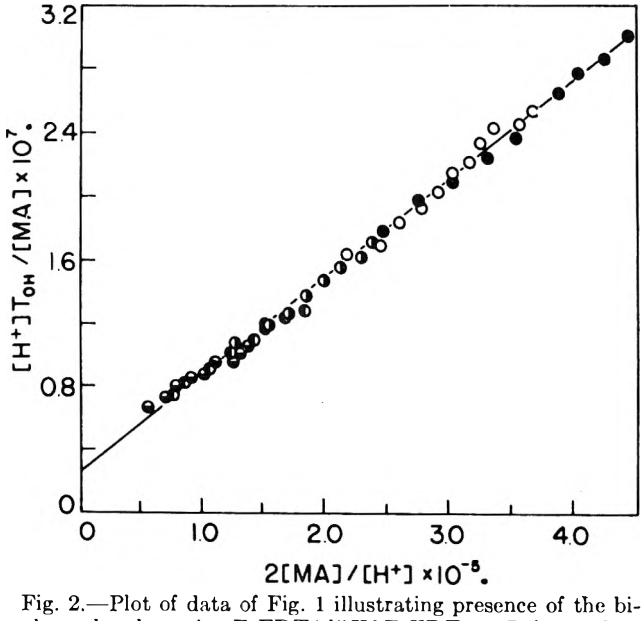

Fig. 2.—Plot of data of Fig. 1 illustrating presence of the binuclear olated species FeEDTA[OH]$_2$FeEDTA. Points calculated from data obtained at the following concentrations: ●, 8.5×10^{-2} M; ○, 5.6×10^{-2} M; ◓, 3.0×10^{-2} M; ◒, 1.6×10^{-2} M; ◑, 8.2×10^{-3} M.

small deviations as those shown in Fig. 2, although the average deviations of the experimental points from the best straight line corresponded to an error of only ±0.02 pH unit.

Equilibrium constants obtained at several temperatures are shown in Table I.

Since the value for log K_d is determined by the relationship

$$\log K_d = 2pK_a - pK_D$$

where there is a relatively large uncertainty in the intercept K_a, values of log K_d sometimes show discrepancies

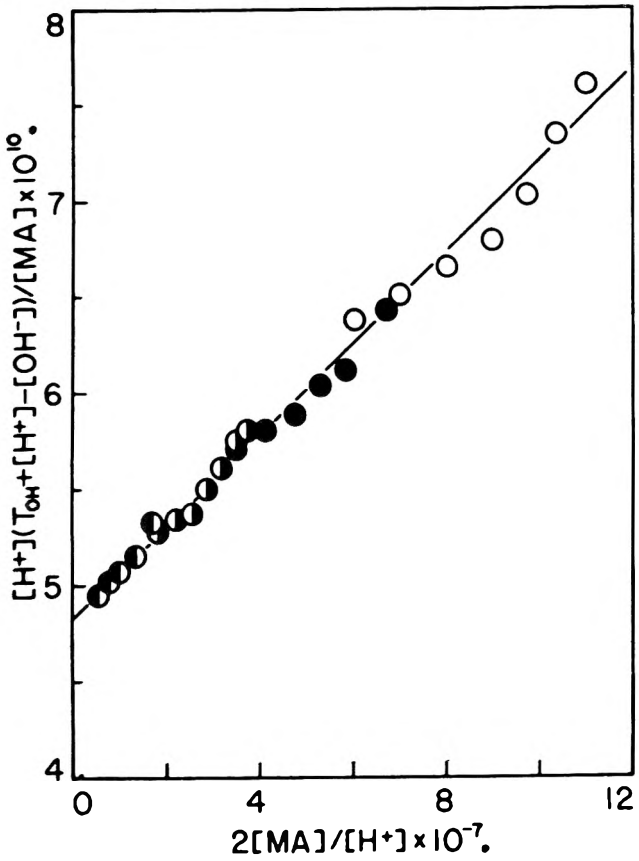

Fig. 3.—Plot of data illustrating the formation of the binuclear diolated Fe(III)–CDTA chelate. Points calculated from data obtained at the following concentrations: ○ $7.3 \times 10^{-2} M$; ●, $3.8 \times 10^{-2} M$; ◑, $2.0 \times 10^{-2} M$; ◐, $8 \times 10^{-3} M$. $t = 25.0°$, $\mu = 1.0$ (KCl).

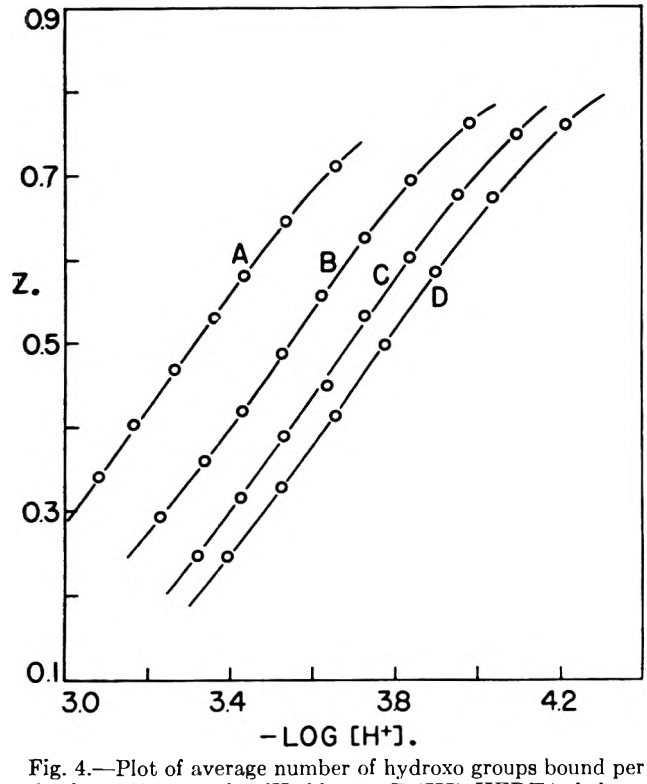

Fig. 4.—Plot of average number of hydroxo groups bound per mole of metal ion *vs.* $-\log [H^+]$ for 1:1 Fe(III)–HEDTA chelates at various concentrations: A, $9.0 \times 10^{-2} M$; B, $3.6 \times 10^{-2} M$; C, $1.9 \times 10^{-2} M$; D, $1.0 \times 10^{-2} M$. $t = 25.0°$, $\mu = 1.0$ (KCl).

TABLE I

HYDROLYSIS AND OLATION OF Fe(III)–EDTA

t, °C.	pK_a	pK_D	log K_d
0.4	7.97	12.71	3.23
13.7	7.80	12.37	3.24
25.0	7.58	12.21	2.95
42.4	7.11	12.04	2.18

such as that for the value obtained at 0.4° in Table I. Data obtained at 13.7, 25.0, and 42.4° gave nearly linear plots of log K *vs.* $1/T$ and data at these three temperatures were employed in calculating ΔH^0 for the various reactions involved. A summary of thermodynamic constants pertaining to the hydrolysis and olation reactions of Fe(III)–EDTA are shown in Table II. Here it may be seen that the reaction of two moles of monohydroxo chelate to form one mole of a binuclear species proceeds because of a favorable enthalpy change.

TABLE II

VALUES OF ΔF^0, ΔH^0, AND ΔS^0 FOR HYDROLYSIS AND OLATION REACTIONS OF Fe(III)–EDTA

Reaction	ΔF^0 (25°), kcal./mole	ΔH^0, kcal./mole	ΔS^0 (25°), cal./mole deg.
$FeL^{1-} \rightleftharpoons Fe[OH]L^{2-} + H^+$	+10.3	+10 ± 1	− 2
$2FeL \rightleftharpoons (Fe[OH]L)_2^{4-} + 2H^+$	+16.7	+4.7 ± 0.4	−40
$2Fe[OH]L^{2-} \rightleftharpoons (Fe[OH]L)_2^{4-}$	− 4.0	−15 ± 3	−36

Fe(III)–CDTA.—Potentiometric measurements of equimolar mixtures of ferric ion and CDTA over a tenfold concentration range resulted in a family of curves similar to that shown in Fig. 1. A plot of data according to eq. 8 gave the straight line shown in Fig. 3, indicating that a binuclear diolated species is the predominant polynuclear chelate. The equilibrium constants obtained at the three temperatures studied are given in Table III.

TABLE III

HYDROLYSIS AND OLATION OF Fe(III)–CDTA

t, °C.	pK_a	pK_D	log K_d
1.0	9.95	18.58	1.31
25.0	9.32	17.62	1.01
42.3	8.90	16.92	0.89

Thermodynamic constants for reactions 1–3 for Fe(III)–CDTA are presented in Table IV. As in the case of the analogous EDTA compound, the driving force in the reaction $2Fe[OH]L^{2-} \rightleftharpoons (Fe[OH]L)_2^{4-}$ is a favorable enthalpy change whereas the entropy change is −9 e.u. at 25°.

TABLE IV

THERMODYNAMIC CONSTANTS FOR HYDROLYSIS AND OLATION REACTIONS OF Fe(III)–CDTA

Reaction	ΔF^0 (25°), kcal./mole	ΔH^0, kcal./mole	ΔS^0, cal./mole deg.
$FeL^{1-} \rightleftharpoons Fe[OH]L^{2-} + H^+$	+12.7	+10.0 ± 0.2	− 9
$2FeL^{1-} \rightleftharpoons (Fe[OH]L)_2^{4-} + 2H^+$	+24.0	+16.1 ± 0.9	−27
$2Fe[OH]L^{2-} \rightleftharpoons (Fe[OH]L)_2^{4-}$	− 1.4	− 3.9 ± 0.6	− 9

Fe(III)–HEDTA.—Potentiometric measurements of equimolar amounts of Fe(III) and N-hydroxyethylethylenediaminetriacetic acid (HEDTA), H_3L, results in a curve of $-\log [H^+]$ *vs.* m which has a steep inflection

after the addition of four moles of base per mole of metal chelate. This corresponds to the formation of a monohydroxo chelate and corresponding polymerization products. Sillén,[16-18] in his treatment of polynuclear complexes, has shown that in many cases a plot of $Z = T_{OH} + [H^+] - [OH^-]$ as ordinate *vs.* $-\log [H^+]$ as abscissa produces a family of parallel curves for potentiometric titration data obtained at various metal ion concentrations. A plot of $-\log T_M$ *vs.* $-\log [H^+]$ for data obtained at constant Z values then yields a straight line plot, the slope of which is equal to t in the general "core plus links" type complex, $M(M[OH]_t)_n$. As may be seen in Fig. 4, a plot of Z *vs.* $-\log [H^+]$ for Fe(III)–HEDTA at 25° in the region $m = 3$–4 produces a series of curves which are essentially parallel. The plots of Fig. 5 show that an average value of $(\partial \log T_M/\partial \log [H^+])_Z = 2.14$ is obtained, suggesting that a polymer of the general type $ML(M[OH]_2L)_n^{2n-}$ is obtained. The only polymer which is consistent with the fact that one mole of hydroxide ion is bound per mole of metal chelate is the dimer where $n = 1$. It should be pointed out that the presence of significant amounts of monohydroxo species in equilibrium with the dimer would tend to give values of $(\partial \log T_M/\partial \log [H^+])$ in excess of 2.0. The fact that a value of 2.14 is obtained indicates that the dimer is by far the most predominant hydrolyzed species in solutions in the concentration range studied.

In Fig. 6, plots of $[H^+](T_{OH} + [H^+])/[ML]$ *vs.* $2\cdot[ML]/[H^+]$ obtained from the same data as those used in Fig. 4 and 5 show a definite drift toward higher intercept values as the concentration of metal chelate increases. In calculating the best straight line through the data, values obtained at the highest concentration ($8.9 \times 10^{-2} M$) were not used since these data also did not conform with the straight lines in Fig. 5. No apparent explanation can be offered for this inconsistency on the basis of the information now available. It had earlier been noted that stock solutions of Fe(III)–HEDTA decomposed on standing, with the result that plots similar to those of Fig. 6 yielded curves which nearly doubled back on themselves at high $[ML]/[H^+]$ values. This difficulty was eliminated by carrying out each titration with a freshly prepared chelate solution. The equilibrium constants obtained for the hydrolysis and olation of the Fe(III)–HEDTA chelate compound are listed in Table V.

TABLE V

EQUILIBRIUM CONSTANTS FOR HYDROLYSIS AND OLATION REACTIONS OF Fe(III)–HEDTA AT 25° IN 1 *M* KCl

$$K_a = \frac{[Fe[OH]L^{1-}][H^+]}{[FeL]} = 10^{-4.11 \pm 0.07}$$

$$K_D = \frac{[(Fe[OH]L)_2^{2-}][H^+]^2}{[FeL]^2} = 10^{-5.84 \pm 0.01}$$

$$K_d = \frac{[(Fe[OH]L)_2^{2-}}{[Fe[OH]L^{1-}]^2} = 10^{-2.38 \pm 0.08}$$

$$K_b = \frac{[Fe[OH]_2L^{2-}][H^+]}{[Fe[OH]L^{1-}]} = 10^{-8.69 \pm 0.02}$$

$$K_c = \frac{[(Fe[OH]L)_2^{2-}]}{[Fe[OH]_2L^{2-}]^2[H^+]^2} = 10^{12.5 \pm 0.2}$$

Data obtained in the buffer region from $m = 4$–5 were plotted according to eq. 7. Because of the considerable scatter of points, it was difficult to determine the intercept, which is equal to $1/K_b$. Hence an algebraic determination of K_b was employed. Combination of eq. 3, 4, and 7 leads to the equation

(16) L. G. Sillén, *Acta Chem. Scand.*, **8**, 299 (1954).
(17) L. G. Sillén, *ibid.*, **8**, 318 (1954).
(18) S. Hietanen and L. G. Sillén, *ibid.*, **8**, 1607 (1954).

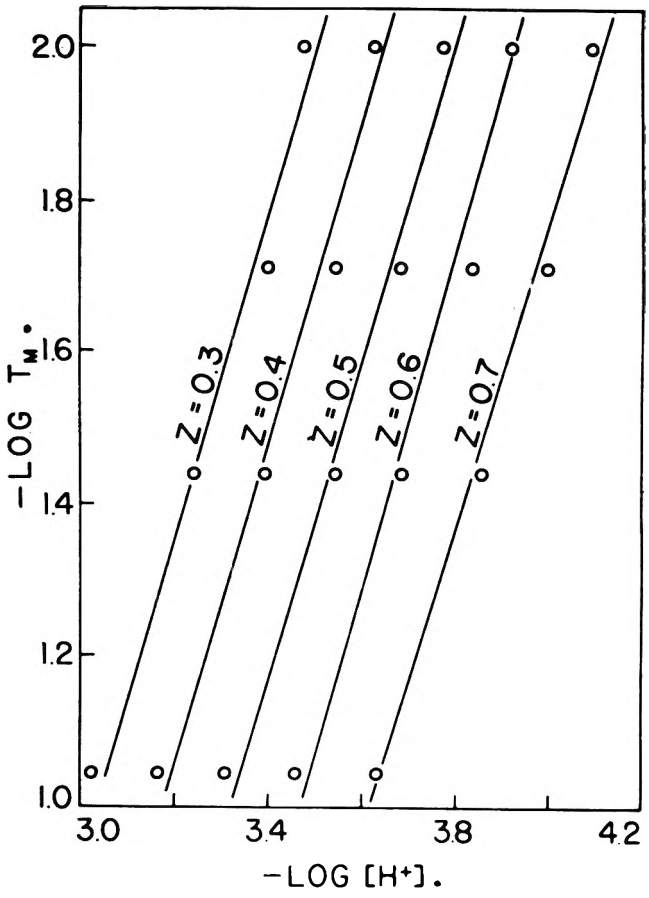

Fig. 5.—Plot of $-\log T_M$ *vs.* $-\log [H^+]$ at constant Z based on data shown in Fig. 4 for Fe(III)–HEDTA chelates.

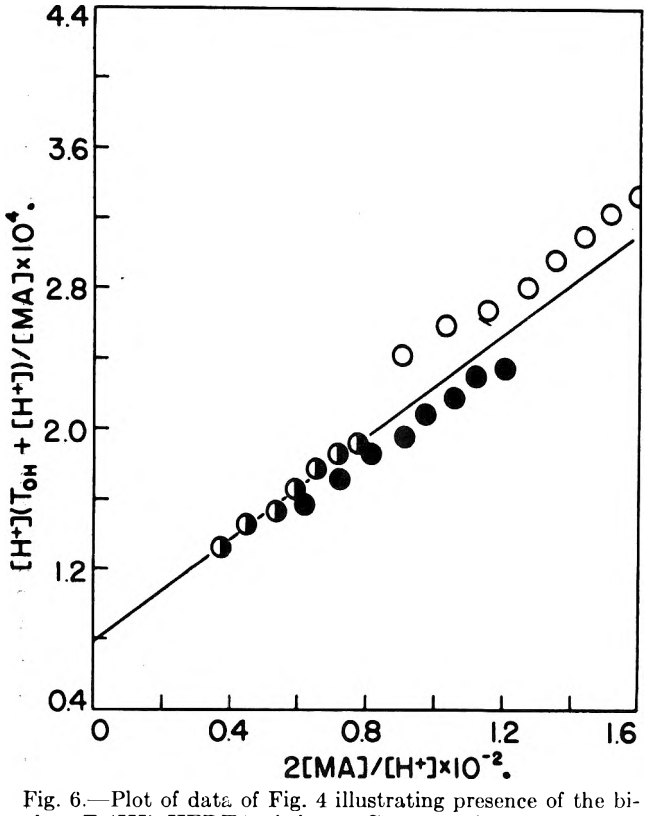

Fig. 6.—Plot of data of Fig. 4 illustrating presence of the binuclear Fe(III)–HEDTA chelate. Concentrations: ○, $3.6 \times 10^{-2} M$; ◑, $1.9 \times 10^{-2} M$; ●, $1.0 \times 10^{-2} M$.

$$K_b = \frac{4K_d[H^+](T_{OH} - T_M + [H^+] - [OH^-])}{-1 \pm \sqrt{1 + 8K_d(2T_M - T_{OH} - [H^+] + [OH^-])}} \quad (8)$$

The average value of pK_b obtained for 20 experimental points is included in Table V. The value of K_c was obtained from previously calculated constants by the relationship

$$K_c = K_D/K_a^2K_b^2$$

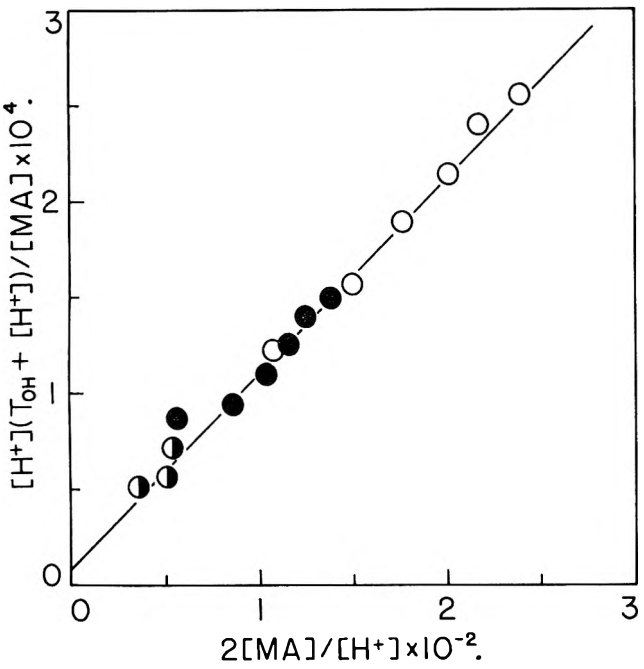

Fig. 7.—Plot of data illustrating presence of the binuclear diolated Fe(III)–NTA chelate. Points calculated from data obtained at the following concentrations: ○, 5.3 × 10^{-2} M; ●, 1.8 × 10^{-2} M; ◑, 6 × 10^{-3} M. t = 25.0°, μ = 1.0 (KCl).

Fe(III)–NTA.—Potentiometric measurement of $-\log [H^+]$ *vs.* m for the 1:1 Fe(III)–NTA chelate system results in a steep inflection, followed by precipitation, after the addition of one mole of hydroxide ion per mole of chelate, indicating the formation of monohydroxo chelate and its corresponding binuclear form. Because equilibrium was reached slowly, the titration procedure was modified by using a number of sealed glass vessels containing equal aliquots of metal chelate and supporting electrolyte to which varying amounts of standard hydroxide were added. Plots of titration data based on the assumption of formation of a monohydroxo chelate and its corresponding dimer are shown in Fig. 7 for samples which were allowed to equilibrate for 1, 2, and 5 days, respectively. The results indicate the probable formation of a binuclear chelate although the following equilibrium constants may be considered to be only approximate

$$pK_a = 5.0$$
$$pK_D = 6.0$$
$$\log K_d = 4.0$$

Upon standing for 2 to 3 months, precipitation, presumably of ferric hydroxide, was observed in all of the solutions employed in the measurements which are summarized in Fig. 7.

Fe(III)–HIMDA and Fe(III)–HXG.—Solutions of ferric chelates of N-hydroxyethyliminodiacetic acid (HIMDA) and dihydroxyethylglycine (HXG), containing up to two moles of hydroxide ion per mole of chelate, were allowed to stand for several months. The recorded pH values showed a continuous drift, resulting in eventual precipitation in the Fe(III)–HXG solutions. Mathematical treatment of data obtained within the first few days of equilibration indicated the formation of polynuclear chelates in both cases, although calculation of even approximate values of the equilibrium constants was not possible.

Discussion

The data in Table I provide a new, more precise, concept of the aqueous chemistry of Fe(III)–EDTA chelate compounds. Interpolation of values of pK_a gives a value of 7.68 at 20° in 1 M KCl, whereas Schwarzenbach and Heller[10] obtained a value of pK_a = 7.49 at 20° in 0.1 M KCl under conditions where the metal chelate concentration was approximately 1.5 × 10^{-3} M. Part of the discrepancy is accounted for by the differences in the supporting electrolyte concentrations and the corresponding changes in activity coefficients. However, the higher value of $10^{-7.49}$ also was caused by the fact that the presence of polynuclear hydroxo species was overlooked and that all of the reacting hydroxide ion was assumed to be utilized in forming Fe[OH]EDTA. Titrations carried out using 1.6 × 10^{-3} M Fe(III)–EDTA in 0.1 M KNO_3 yielded values of pK_a having average deviations of less than 0.01 pH unit over a wide pH range, even though contributions by binuclear species were neglected. Such small deviations would usually indicate that the reaction assumed in the calculation procedure was in fact the only one taking place in the experimental solution. Only by increasing the ferric–EDTA concentration markedly was it possible to detect the existence of the binuclear chelate species.

It is noteworthy that the tendency of Fe(III)–CDTA to hydrolyze and polymerize is much less than that of Fe(III)–EDTA as may be seen by comparison of results in Tables I and III. This may be due to the fact that the more stable Fe(III)–CDTA chelate has a weaker affinity for an additional donor group such as a hydroxyl ion than does its EDTA analog; *i.e.*, the ferric ion in the CDTA chelate is less acidic than that in the EDTA chelate. This may be illustrated by comparison of the dissociation constants of the two ligands (EDTA: pK_1 = 1.99; pK_2 = 2.67; pK_3 = 6.16; pK_4 = 10.26 in 0.1 M KCl at 25°. CDTA: pK_1 = 2.43; pK_2 = 3.52; pK_3 = 6.12; pK_4 = 11.70 in 0.1 in 0.1 M KCl at 25°) where it may be seen that the donor groups of CDTA are considerably more basic than those of EDTA. The difference in dimerization constants also correlates with the difference in hydrolytic tendencies of the Fe(III)–EDTA and CDTA chelates. Thus the much higher pK of the CDTA chelate (9.32 *vs.* 7.58) indicates a lower affinity of the Fe(III) ion in this complex for the hydroxyl ion. Since this indicates greater coördination saturation for the Fe(III) ion when combined to CDTA, one would therefore expect that the hydroxyl ion would also be less effective in forming hydroxo bridges in the presence of this ligand. These two metal chelates therefore provide good examples of the relationships between basicity of the ligand, stability of

the chelate, tendency to form hydroxo mononuclear derivatives of the chelate, and the tendency to form binuclear chelates through hydroxo bridges (olation).

It is of interest to compare the thermodynamics of dimerization of Fe(III)–EDTA and Fe(III)–CDTA chelates with the results obtained for dimerization of a number of Cu(II) chelates of substituted diamines.[3] The summary in Table VI indicates that in the cases of the Cu(II) chelates of DMEN, TMEN, and HEN, the reaction

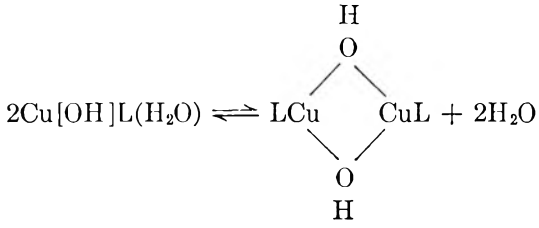

TABLE VI

THERMODYNAMIC CONSTANTS FOR REACTION

$$2M[OH]L \rightleftharpoons (M[OH]L)_2$$

Metal	Ligand	ΔH^0, kcal./mole	ΔS^0 (25°), cal./mole deg.
Cu(II)	DMEN[a,e]	+1.0	+21
Cu(II)	TMEN[b,e]	+3	+28
Cu(II)	HEN[c,e]	+4	+23
Cu(II)	2-HEN[d,e]	−1	+ 3
Fe(III)	EDTA[f]	−15	−36
Fe(III)	CDTA[f]	−3.9	− 9

[a] N,N′-Dimethylethylenediamine; [b] N,N,N′,N′-Tetramethylethylenediamine; [c] N-Hydroxyethylethylenediamine; [d] N,N′-Dihydroxyethylethylenediamine; [e] In 0.1 *M* KNO_3; [f] In 0.1 *M* KCl.

proceeds because of a large favorable entropy change produced by the increase in translational entropy upon release of the coördinated water molecules when dimerization occurs. In the cases of Fe(III)–EDTA and Fe(III)–CDTA chelates, where there probably are no coördinated water molecules involved in the reactions, negative entropy changes are observed.

It might be expected that if the dimerization reaction occurs between I and II rather than between III and IV, a negative value of ΔS^0 would be observed. The fact that a slightly positive value of ΔS^0 is obtained for dimerization of the hydrolyzed Cu(II)–2-HEN chelate suggests that there may be a contribution by both reactions and that the equilibrium between I and III favors the former structure.

No explanation is apparent for the fact that the entropy change associated with the dimerization of Fe(III)–CDTA is more favorable than that of the analogous EDTA chelate.

The hydrolysis and dimerization constants shown in Table V for the Fe(III)–HEDTA chelate indicate that although the tendency toward hydrolysis is considerably greater than in the case of the analogous Fe(III)–EDTA chelate, the tendency to polymerize is somewhat less. The low value of pK_a suggests that binding probably takes place through the hydroxyethyl group and that the hydrolysis reaction is the conversion of V to VI. The binuclear complex may also involve bridging by alkoxide groups of the ligand, as is indicated by VII and VIII. On the basis of evidence now available, it is, of course, impossible to distinguish between the alternative arrangements in I and III, V and VI, and VII and VIII.

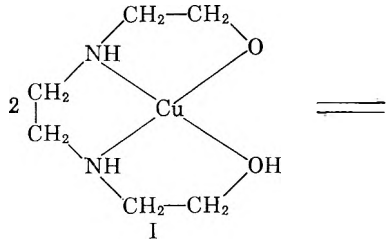

I

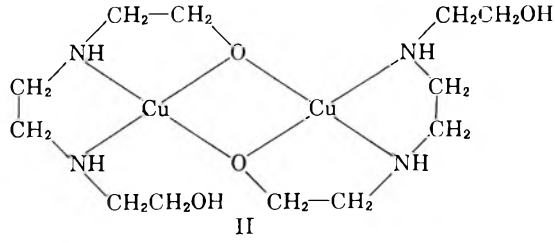

II

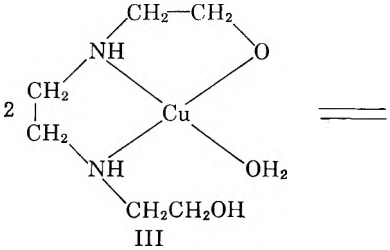

III

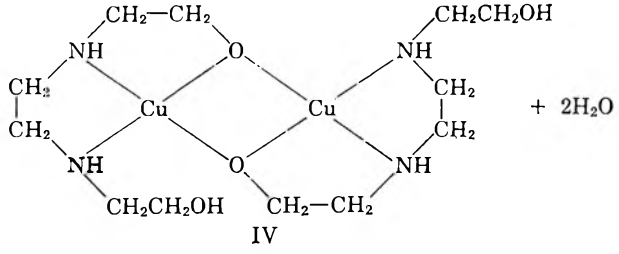

IV

The reactions of Fe(III)–HEDTA are similar to those studied previously in the cases of Cu(II)–diamine systems[3] where it has been shown that further hydrolysis of binuclear olated chelates results in depolymerization and the formation of monodentate dihydroxo complexes at elevated pH.

The degree of polymerization of the hydroxo derivative of the 1:1 Fe(III)–NTA chelate is greater than that of any of the ferric chelates described above. This is undoubtedly due to the fact that only four coördination positions are occupied by donor groups of NTA, leaving two aquated coördination positions available for hydrolysis and olation.

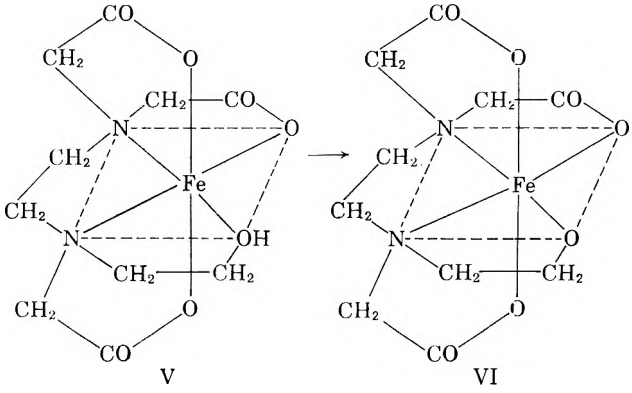

V VI

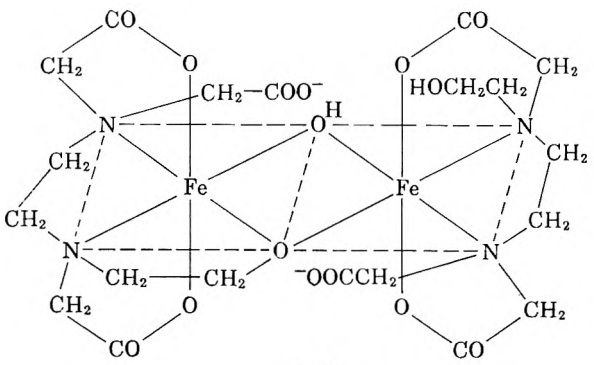

VII

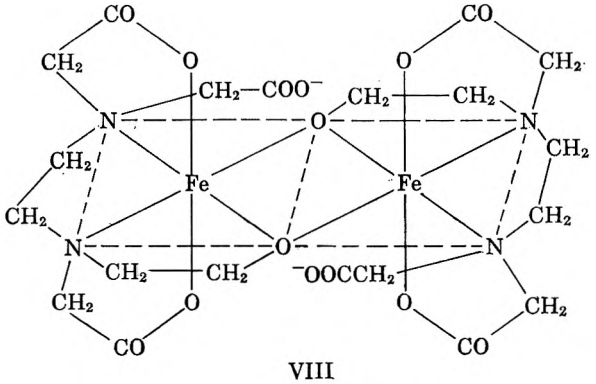

VIII

CATALYTIC HYDROLYSIS OF SALICYL PHOSPHATE IN THE PRESENCE OF COPPER(II) CHELATES[1]

BY YUKITO MURAKAMI[2a] AND ARTHUR E. MARTELL[2b]

Departments of Chemistry, Clark University, Worcester, Massachusetts, and Illinois Institute of Technology, Chicago, Illinois

Received August 1, 1962

Rates of hydrolysis of salicyl phosphate (SP) in the present investigation generally followed first-order kinetics. Studies of the catalytic hydrolysis of SP at 30.0° were carried out at an ionic strength of 0.100 *M*. The 1:1 hydroxyethylethylenediamine–Cu(II) (HEN–Cu(II)) catalyzed hydrolysis of SP was carried out in the middle pH range ($-\log[H^+]$ = 4.00, 5.50, 6.00, 6.50, and 7.00). The increased hydrolysis rate is attributed to interaction of the diionic and the triionic species of the substrate with Cu(II) ion. The Cu(II)–dipyridyl system was found to be inactive as a catalyst in the hydrolysis of SP. The interactions of salicyl phosphate with Cu(II) ion and the dipyridyl–Cu(II) chelate were studied by means of potentiometric measurements, and the formation constants of the Cu(II)–SP chelate and the Cu(II)–dipyridyl–SP chelate are reported.

A qualitative investigation on the catalytic hydrolysis of salicyl phosphate (SP) has been carried out recently[3] with a series of copper chelate and vanadyl chelate compounds. In order to explore further the mechanism for the catalytic hydrolysis of SP, more extensive study on the hydrolysis catalyzed by Cu(II)–hydroxyethylethylenediamine (HEN) and dipyridyl (DIPY) has been performed.

Experimental

Salicyl phosphate (*o*-carboxyphenylphosphate, SP) was purchased from the California Foundation for Biochemical Research, Los Angeles, California. The purity of the compound, which was established by phosphorus analysis and potentiometric titration, was sufficiently high so that further purification was not necessary.

N-Hydroxyethylthylenediamine (HEN), purchased from the Eastman Kodak Co., was isolated as the dihydrochloride after two recrystallizations from methanol solution.

α,α'-Dipyridyl, obtained from the S.A.F. Hoffman-La Roche and Co., Ltd., Basel, Switzerland, was used without further purification.

Copper(II) solution was prepared from its nitrate salt and was standardized by titration with standard disodium salt of ethylenediaminetetraacetic acid, with murexide as an indicator.[4]

The procedures employed for the potentiometric measurements, kinetic measurements, and phosphorus analysis were described in the previous paper.[3] The potentiometric measurements were carried out at 10.1 ± 0.05° in aqueous media of an ionic strength of 0.100 *M* with KNO_3 as supporting electrolyte. All the kinetic studies were carried out at 30.0 ± 0.05° by maintaining an ionic strength at 0.100 *M* with KNO_3.

(1) This investigation was supported by a grant from the Esso Education Foundation, Linden, New Jersey.

(2) (a) Department of Organic Synthesis, Faculty of Engineering, Kyushu University, Japan; (b) Department of Chemistry, Illinois Institute of Technology, Chicago 16, Illinois.

(3) R. Hofstetter, Y. Murakami, G. Mont, and A. E. Martell, *J. Am. Chem. Soc.*, **84**, 3041 (1962).

(4) G. Schwarzenbach, "Die Komplexometrische Titration," Ferdinand Enke, Stuttgart, 1955 p. 68.

Results

Interaction between SP and Cu(II).—To obtain information about the chelating tendency of salicyl phosphate with cupric ion, potentiometric titration of the SP–Cu(II) system was carried out over an eightfold concentration range, as is shown in Fig. 1. These curves, together with the comparison in Fig. 2 of the titration curves of salicyl phosphate in the presence and in the absence of an equivalent concentration of Cu(II) ion, give a clear picture of the nature of the interaction between SP and Cu(II). Since SP undergoes hydrolysis at or above room temperature, the measurements were carried out quickly at 10.1 ± 0.05°. Under these conditions the degree of hydrolysis of SP was observed to be negligible even after a titration had been completed. Since a precipitate was observed beyond m = 3.0, calculation of the formation constant, carried out algebraically in the usual way from data obtained below m = 2.60, indicated appreciable interaction between metal ion and ligand. Under these conditions the reactions are expressed by the following equilibrium constants:

Dissociation of SP

$$H_2A^- \rightleftharpoons HA^{2-} + H^+ \quad K_2 = 10^{-3.63}$$

$$HA^{2-} \rightleftharpoons A^{3-} + H^+ \quad K_3 = 10^{-6.37}$$

where H_3A represents the acid form of salicyl phosphate.

Formation Constant

$$Cu^{2+} + A^{3-} \rightleftharpoons CuA^- \quad K_{CuA} = 10^{3.64}$$

Interaction between SP and Cu(II)–DIPY.—Potentiometric titrations of solutions containing a 1:1:1 molar

ratios of Cu(II):DIPY:SP were carried out at 10.1 ± 0.05° to avoid the hydrolysis of SP. Actually, no significant hydrolysis of SP was observed in the short period of time during which the titrations were carried out. The concentration of the solutions titrated was varied over a tenfold range. In Fig. 2 it is seen that there is interaction between the Cu(II)–DIPY chelate and SP between $m = 2.0$ and 3.0 where the predominant species of SP are the dinegative and trinegative anions. The concentration effect for this mixed chelate system is shown in Fig. 3.

The equilibrium constants were calculated for this system, with the aid of the assumption that the following reaction takes place

$$CuL^{2+} + A^{3-} \rightleftarrows CuLA^{-} \quad K_{CuLA} = \frac{[CuLA^{-}]}{[CuL^{2+}][A^{3-}]} \tag{1}$$

According to the equilibrium constants for the Cu(II)–DIPY system obtained previously,[5] the concentration of free cupric ion is very small above $-\log [H^+] = 4.00$ (1.3 mole % at $-\log [H^+] = 4.00$) and small enough above $-\log [H^+] = 5.00$ to be neglected in this calculation of the equilibrium constants. The following stoichiometric relationships hold for this system

$$T_M = [CuL^{2+}] + [CuLA^{-}] \tag{2}$$

$$T_{SP} = [H_2A^{-}] + [HA^{2-}] + [A^{3-}] + [CuLA^{-}] \tag{3}$$

$$[H^+] - [OH^-] = [H_2A^{-}] + 2[HA^{2-}] + 3[A^{3-}] + 3[CuLA^{-}] - mT_M \tag{4}$$

$$[H_2A^{-}] = \frac{[H^+]}{K_2}[HA^{2-}] \tag{5}$$

$$T_M = T_{SP} \tag{6}$$

where T_M and T_{SP} represent the total concentrations of metal and salicyl phosphate species, respectively, and m = moles of base added per mole of metal salt present. From the above relationships, the quantities, $[A^{3-}]$, $[CuL^{2+}]$, and $[CuLA^{-}]$, are expressed in terms of measurable and known quantities.

$$[HA^{2-}] = \frac{((3 - m)T_M - [H^-])K_2}{(K_2 + 2[H^+])} \tag{7}$$

$$[A^{3-}] = \frac{K_3}{[H^+]}[HA^{2-}] \tag{8}$$

$$[CuL^{2+}] = [H_2A^{-}] + [HA^{2-}] + [A^{3-}] \tag{9}$$

$$[CuLA^{-}] = T_M - [CuL^{2-}] \tag{10}$$

The value of K_{MLA} determined from these relationships is $10^{4.08}$.

The family of titration curves in the higher buffer region beyond $m = 3.0$ behave in a manner different from that usually observed in metal chelate systems. No significant amounts of H_2A^- and HA^{2-} are expected above $-\log [H^+] = 8.50$, as is seen in the titration curve of SP in Fig. 2. In order to explain the potentiometric titration curve above $m = 3.0$, two competing reactions are proposed

(5) R. L. Gustafson and A. E. Martell, *J. Am. Chem. Soc.*, **81**, 525 (1959).

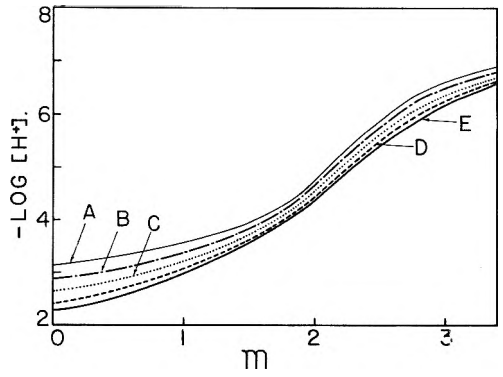

Fig. 1.—Potentiometric titration curves of the 1:1 salicyl phosphate–Cu(II) system at 10.1° and 0.10 ionic strength (KNO_3). Concentrations of Cu(II): A, $5.37 \times 10^{-4} M$; B, $1.04 \times 10^{-3} M$; C, $1.86 \times 10^{-3} M$; D, $3.15 \times 10^{-3} M$; E, $4.20 \times 10^{-3} M$. m = moles of base added per mole of metal on.

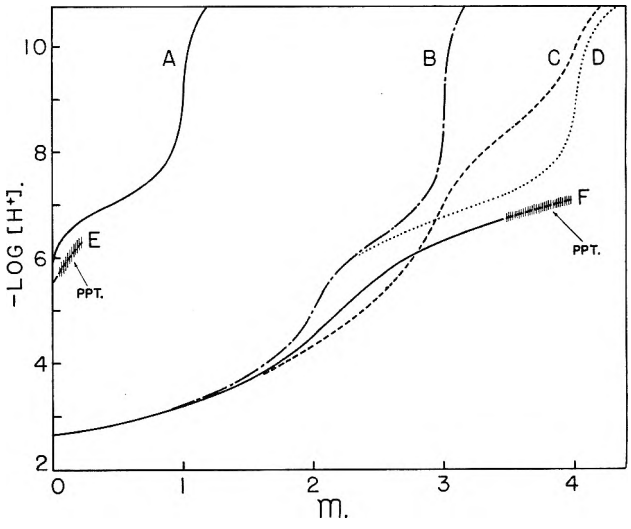

Fig. 2.—Potentiometric titration curves of copper(II) chelates at 10.1°; m = moles of base added per mole of metal ion: total concentration of salicyl phosphate for B, C, D, and F and total concentration of Cu(II) for A, C, D, E, and F are $1.86 \times 10^{-3} M$; A, Cu(II)–DIPY 1:1; B, salicyl phosphate; C, Cu(II)–DIPY-SP (1:1:1); D, (calculated from A and B), Cu(II)–DIPY–salicyl phosphate (1:1:1); E, Cu(II); F, Cu(II)–salicyl phosphate (1:1).

$$CuLA^{-} \rightleftarrows CuL(OH)^{+} + A^{3-} + H^{+} \quad (K^{H}_{MLA})$$

$$2CuLA^{-} \rightleftarrows (CuL(OH))_2^{2+} + 2A^{3-} + 2H^{+} \quad (K'_D)$$

These reactions are suggested by the behavior of the dipyridyl–Cu(II) chelate, which has already been described.[5] The following stoichiometric relationships may be set up on the basis of these reactions

$$T_M = [CuL(OH)^{+}] + 2[(CuL(OH))_2^{2+}] + [CuLA^{-}] \tag{11}$$

$$T_{SP} = [A^{3-}] + [CuLA^{-}] \tag{12}$$

$$[H^+] - [OH^-] = [CuL(OH)^{+}] + 2[CuL(OH))_2^{2+}] - T_{OH} \tag{13}$$

$$T_{OH} = (m - 3)T_M \tag{14}$$

where T_{OH} is total moles of base added per liter of solution beyond $m = 3$. Equation 13 may be rearranged to give

$$\frac{T_{OH} + [H^+] - [OH^-]}{[CuLA^-]/[H^+][A^{3-}]} = K^H_{ML(OH)} + 2K_D' \frac{[CuLA^-]}{[H^+][A^{3-}]} \quad (15)$$

where

$$[CuLA^-] = T_M - T_{OH} + [OH^-] \quad (16)$$

$$[A^{3-}] = T_{OH} - [OH^-] \quad (17)$$

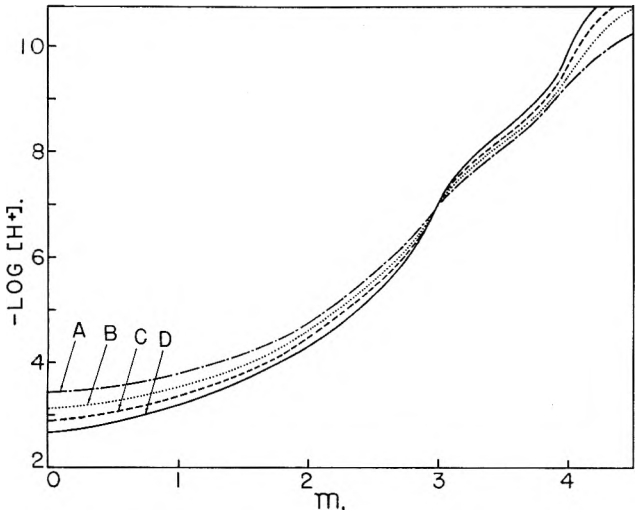

Fig. 3.—Potentiometric titration curves of the (1:1:1) Cu(II)–DIPY–salicyl phosphate system at 10.1° and ionic strength of 0.10 M (KNO_3), m = moles of base added per mole of metal ion. Concentrations of Cu(II): A, 2.38×10^{-4} M; B, 5.33×10^{-4} M; C, 1.05×10^{-3} M; D, 1.86×10^{-3} M.

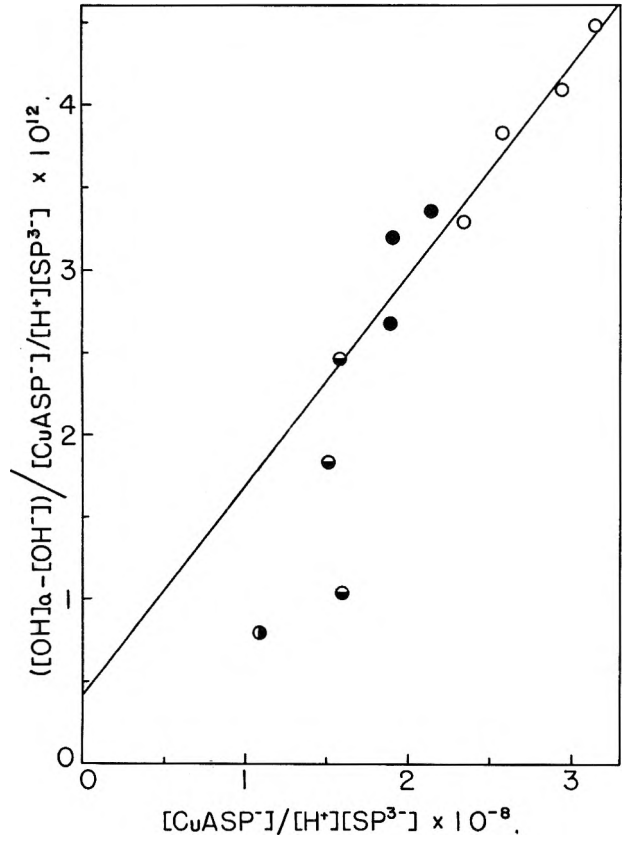

Fig. 4.—Graphical determination of the substitution reaction of the 1:1:1 Cu(II)–DIPY–salicyl phosphate complex in the higher pH region at 10.1°; concentrations of Cu(II): ○, 1.86×10^{-3} M; ●, 1.05×10^{-3} M; ◒, 5.53×10^{-4} M; ◑, 2.38×10^{-4} M.

$$[OH^-] = 4.63 \times 10^{-15}[H^+]^{-1} \text{ (at } 10°, \mu = 0.1\ M) \quad (18)^6$$

$$K^H_{MLA} = \frac{[CuL(OH)^+][A^{3-}][H^+]}{[CuLA^-]} \quad (19)$$

$$K_D' = \frac{[CuL(OH)_2][A^{3-}]^2[H^+]^2}{[CuLA^-]^2} \quad (20)$$

Therefore, if the reactions assumed for this system actually occur, a straight line would be expected when $(T_{OH} + [H^+] - [OH^-])/([CuLA^-]/[H^+][A^{3-}])$ is plotted against $[CuLA^-]/[H^+][A^{3-}]$. The slope of this line would be equal to $2K_D'$ and the intercept at $[CuLA^-]/[H^+][A^{3-}] = 0$ would be equal to K^H_{MLA}. As is shown graphically in Fig. 4, the linear relationship was established. Some scattering of the points in the lower region was obtained from the calculations for the lower concentrations. Such deviations are expected because the experimental data are less accurate at low concentrations. The equilibrium constants K^H_{ML} and K_D' obtained from Fig. 4 are

$$pK^H_{MLA} = 12.40$$

$$pK_D' = 20.19$$

Recently, Gustafson and Martell[5] reported the hydrolysis constants of a number of copper chelates of diamines. The hydrolysis constants which they obtained for dipyridyl–Cu(II) at three different temperatures, 0.3, 25.0, and 42.5°, make it possible to estimate the values at 10.1° by interpolation. In this way, the following constants are obtained

$$CuL^{2+} + H_2O \rightleftarrows CuL(OH)^+ + H^+: \quad pK^H_{ML} = 8.13$$

$$2CuL^{2+} + 2H_2O \rightleftarrows (CuL(OH))_2^{2+} + 2H^+: \quad pK_D = 11.32$$

Since K_{MLA}, the formation constant of the Cu–DIPY–SP chelate, was obtained in the lower buffer region, K^H_{MLA} and K_D' may be calculated from the equations

$$pK^H_{MLA} = pK^H_{ML} + \log K_{MLA} = 12.21 \quad (21)$$

$$pK_D' = pK_d + 2 \log K_{MLA} = 19.48 \quad (22)$$

The agreement between the values calculated above and the estimated values is sufficient to provide support for the reactions proposed for the higher buffer regions of the titration curves in Fig. 3.

Effect of Dipyridyl–Cu(II).—The investigations of the catalytic effect of Cu–DIPY on the hydrolysis of SP indicated a negative effect at pH values near that of the maximum rate for the spontaneous hydrolysis of SP. Some of the results are summarized in Table I.

TABLE I

HYDROLYSIS OF SALICYL PHOSPHATE IN THE PRESENCE OF DIPY–Cu(II) AT 30.0° AND μ = 0.1 M (KNO_3)

−log [H+]	T_M, M[b]	Obsd. first-order rate, sec.$^{-1}$ Spontaneous	Catalyzed
5.10	1.02×10^{-3}	3.59×10^{-5}	2.97×10^{-5}
5.60	1.06×10^{-3}	3.26×10^{-5}[a]	2.69×10^{-5}

[a] Data by R. Hofstetter, *et al.*[3] [b] T_M = total concentration of dipyridyl–Cu(II).

(6) H. S. Harned and B. B. Owen, "The Physical Chemistry of Electrolytic Solutions," Reinhold Publ. Corp., New York, N. Y., 1950, pp. 485, 578.

The rate constant of the DIPY–Cu(II)-catalyzed reaction is smaller than that of the spontaneous reaction. Since this observed rate is comparable to that of the spontaneous reaction, it seems reasonable to propose two competing reactions, the spontaneous hydrolysis reaction and the formation of relatively unreactive side product involving reaction of the salicyl phosphate with Cu(II)–DIPY.

Hydroxyethylthylenediamine–Cu(II).—The HEN–Cu(II) catalyzed hydrolysis of SP was measured at $-\log [H^+]$ values of 4.00, 5.50, 6.00, 6.50, and 7.00. First-order rates were obtained with respect to free SP concentration except for the reactions catalyzed by higher concentrations of the Cu(II) chelate compound at $-\log [H^+]$ values of 6.50 and 7.00, as shown in Table II. These reactions were probably exceptional because of poisoning of the catalyst by secondary reactions between the HEN–Cu(II) chelate and the products of the hydrolysis reaction. This conclusion was indicated by a plot of log $T_{SP}/[SP]$ against time, in which the experimental points were found to deviate progressively further from linearity with increasing time.

The results of studies on the concentration effect of Cu(II)–HEN at $-\log [H^+] = 4.00$, 5.50, and 6.00 are summarized in Table II and are shown graphically in Fig. 5.

TABLE II

CATALYTIC HYDROLYSIS OF SALICYL PHOSPHATE IN THE PRESENCE OF N-HYDROXYETHYLETHYLENEDIAMINE–Cu(II) AT 30.0°, $\mu = 0.1\ M$ (KNO_3)

$-\log [H^+]$	$T_{Cu\cdot HEN} \times 10^3$, M	$k_{obsd} \times 10^5$, sec.$^{-1}$
4.00	0	(2.58)[a]
	0.237	3.56
	0.593	4.39
	1.18	5.71
	1.77	6.31
	2.35	7.13
5.50	0	(3.36)[a]
	0.239	5.72
	0.593	7.27
	0.885	8.06
	1.17	8.41
	1.74	9.43
	2.29	9.75
6.00	0	2.66
	0.238	3.87
	0.590	4.79
	1.17	5.78
	1.73	6.62
	2.27	6.98
6.50	0	1.62
	0.588	2.79
	1.11	3.74
	1.72	(4.65)[b]
7.00	0	(0.889)[a]
	0.564	1.69
	1.11	(2.33)[b]

[a] Calculated value. [b] Calculated for the initial part of the rate curve.

The concentration of five metal chelate species which are in equilibrium in the experimental solution were calculated as a function of concentrations of metal ion and ligand, and of hydrogen ion concentration, in accordance with equations 23–26.

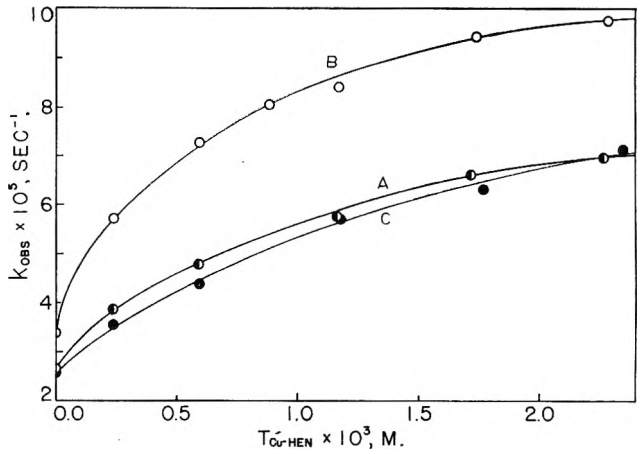

Fig. 5.—HEN–Cu(II)-catalyzed hydrolysis of salicyl phosphate at 30.0°: values of log $[H^+]$: ●, 4.00; ○, 5.50; ◐, 6.00; μ = 0.10 (KNO_3).

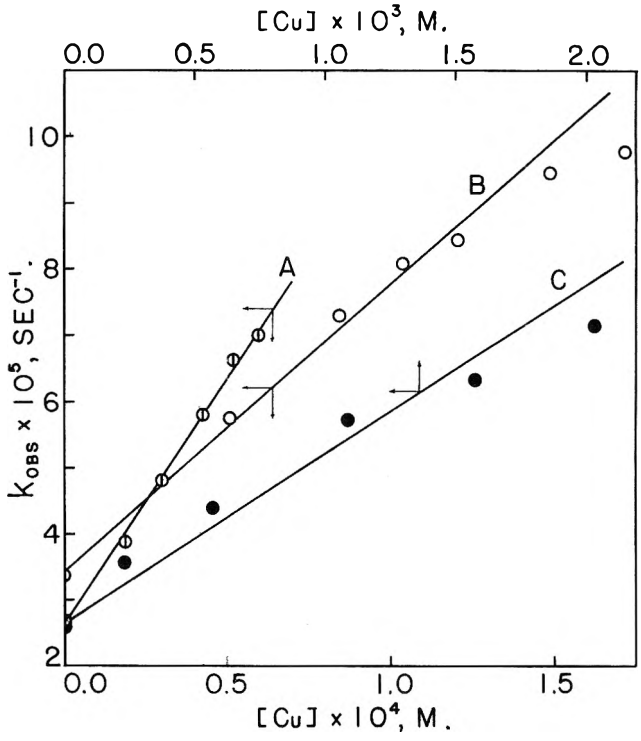

Fig. 6.—Graphical evaluation of the rate constants of the hydrolysis of salicyl phosphate catalyzed by Cu(II) ion in the presence of the 1:1 HEN–Cu(II) complex at 30.0° and $-\log [H^+]$ values of: A, 6.00; B, 5.50; C, 4.00; μ = 0.10 (KNO_3).

$$[Cu] = [CuL]^{1/2}\left(\frac{[H^+]^2 + K_1[H^+] + K_1K_2}{K_{ML}K_1K_2}\right)^{1/2} \quad (23)$$

$$[Cu(OH)L^+] = \frac{K^H_{ML}}{[H^+]}[CuL^{2+}] \quad (24)$$

$$[Cu(OH)_2L] = \frac{K^H_{M(OH)L}}{[H^+]^2}[CuL^{2+}] \quad (25)$$

$$[(Cu(OH)L)_2^{2+}] = \frac{K_D}{[H^+]}[CuL^{2+}]^2 \quad (26)$$

The equilibrium constants employed here were interpolated from the data obtained by Gustafson and Martell.[5] The calculated results are summarized in Table III.

TABLE III

MOLAR CONCENTRATIONS OF Cu(II) AND HEN–Cu(II) CHELATE SPECIES AT 30.0° AND μ = 0.1 M (KNO_3)

$-\log [H^+]$	T_M	$[Cu^{2+}]$	$[CuL^{2+}]$	$[Cu(OH)L^+]$	$[Cu(OH)_2L]$	$[(Cu(OH)L^{2+})_2]$
4.00	2.37×10^{-4}	2.33×10^{-4}	4.19×10^{-6}	2.41×10^{-9}	3.82×10^{-15}	8.83×10^{-16}
	5.93×10^{-4}	5.68×10^{-4}	2.49×10^{-5}	1.43×10^{-8}	2.27×10^{-14}	3.11×10^{-14}
	1.18×10^{-3}	1.09×10^{-3}	9.19×10^{-5}	5.29×10^{-8}	8.48×10^{-14}	4.24×10^{-13}
	1.77×10^{-3}	1.58×10^{-3}	1.93×10^{-4}	1.11×10^{-7}	1.76×10^{-13}	1.86×10^{-12}
	2.35×10^{-3}	2.03×10^{-3}	3.18×10^{-4}	1.83×10^{-7}	2.90×10^{-13}	5.05×10^{-12}
5.50	2.39×10^{-4}	5.11×10^{-5}	1.84×10^{-4}	3.35×10^{-6}	1.66×10^{-10}	1.70×10^{-9}
	5.93×10^{-4}	8.44×10^{-5}	5.00×10^{-4}	9.10×10^{-6}	4.56×10^{-10}	1.25×10^{-8}
	8.85×10^{-4}	1.04×10^{-4}	7.66×10^{-4}	1.39×10^{-5}	6.98×10^{-10}	1.25×10^{-8}
	1.17×10^{-3}	1.21×10^{-4}	1.03×10^{-3}	1.88×10^{-5}	9.40×10^{-10}	2.84×10^{-8}
	1.74×10^{-3}	1.49×10^{-4}	1.56×10^{-3}	2.84×10^{-5}	1.42×10^{-9}	1.22×10^{-7}
	2.29×10^{-3}	1.72×10^{-4}	2.08×10^{-3}	3.79×10^{-5}	1.90×10^{-9}	2.17×10^{-7}
6.00	2.38×10^{-4}	1.89×10^{-5}	2.07×10^{-4}	1.19×10^{-5}	1.89×10^{-9}	2.15×10^{-8}
	5.90×10^{-4}	3.01×10^{-5}	5.30×10^{-4}	3.05×10^{-5}	4.83×10^{-9}	1.40×10^{-7}
	1.17×10^{-3}	4.28×10^{-5}	1.07×10^{-3}	6.16×10^{-5}	9.76×10^{-9}	5.73×10^{-7}
	1.73×10^{-3}	5.23×10^{-5}	1.59×10^{-3}	9.16×10^{-5}	1.45×10^{-8}	1.27×10^{-6}
	2.27×10^{-3}	6.00×10^{-5}	2.09×10^{-3}	1.20×10^{-4}	1.91×10^{-8}	2.19×10^{-6}
6.50	5.88×10^{-4}	1.13×10^{-5}	4.87×10^{-4}	8.86×10^{-5}	4.44×10^{-8}	1.19×10^{-6}
	1.11×10^{-3}	1.55×10^{-5}	9.25×10^{-4}	1.68×10^{-4}	8.43×10^{-8}	4.29×10^{-6}
	1.72×10^{-3}	1.93×10^{-5}	1.43×10^{-3}	2.60×10^{-4}	1.30×10^{-7}	1.02×10^{-5}
7.00	5.64×10^{-4}	4.4×10^{-6}	3.51×10^{-4}	2.02×10^{-4}	3.20×10^{-7}	6.2×10^{-6}
	1.11×10^{-3}	6.1×10^{-6}	6.85×10^{-4}	3.95×10^{-4}	6.25×10^{-7}	2.4×10^{-5}

The total rate of the catalyzed reaction is the summation of rates of individual catalyzed reactions and the rate of the spontaneous reaction.

$$k_{obsd} = k^0 + k_{Cu}[Cu^{2+}] + k_{CuL}[CuL^{2+}] + k_{Cu(OH)L}[Cu(OH)L^+] + k_{Cu(OH)_2L}[Cu(OH)_2L] + k_{(Cu(OH)L)_2}[(Cu(OH)L)_2^{2+}] \quad (27)$$

General treatment of the data requires the estimation of the catalytic effects of all the species present in the system. The four normal coördination sites of each copper(II) ion in the dimer species are satisfied by combination with donor groups. Thus the dimer species would be rendered less reactive than other species by coördination and by steric effects which hinder its approach to a substrate. In addition to these two factors, the concentration of the dimer species is much lower in the case of HEN than was true of the DIPY–Cu(II) chelate system described above. For these reasons, the catalytic effect of the dimer HEN–Cu(II) on the hydrolysis of SP was neglected. The attempt to assign a catalytic effect to each species, Cu(II), HEN–Cu(II), and the two hydroxo-complexes, failed to give reasonable results with the aid of eq. 27.

As an alternative, analysis of data was made to find out whether copper(II) ion might be the only active species present. Thus the following kinetic equation could apply

$$k_{obsd} = k^0 + k_{Cu}[Cu^{2+}] \quad (28)$$

This relationship seems to hold satisfactorily for the data obtained at the values of $-\log [H^+]$ of 4.00, 5.50, and 6.00, as is shown in Fig. 6. The relationships obtained at these three hydrogen ion concentrations are described below

At $-\log [H^+] = 4.00$ $k_{Cu} = 2.6 \times 10^{-2}$

$$0.344k^{I}_{Cu} + 0.656k^{II}_{Cu} = 2.6 \times 10^{-2} \quad (29)$$

At $-\log [H^+] = 5.50$ $k_{Cu} = 0.44$

$$0.909k^{II}_{Cu} + 0.091k^{III}_{Cu} = 0.44 \quad (30)$$

At $-\log [H^+] = 6.00$ $k_{Cu} = 0.72$

$$0.763k^{II}_{Cu} + 0.237k^{III}_{Cu} = 0.72 \quad (31)$$

k^{I}_{Cu}, k^{II}_{Cu}, and k^{III}_{Cu} stand for the rate constants of copper-catalyzed hydrolysis of the mono-, di-, and trinegative ions of salicyl phosphate, respectively. Equations 29, 30, and 31 are obtained by substituting the available data into the equation

$$k_{Cu} = M_I k^{I}_{Cu} + M_{II} k^{II}_{Cu} + M_{III} k^{III}_{Cu} \quad (32)$$

M_I, M_{II}, and M_{III} are the fraction of the total SP concentration in the monoionic, diionic, and triionic forms, respectively. If the copper(II) ion were active as a catalyst in the hydrolysis of the monoionic form, one would expect to observe a catalytic effect in the lower pH region where the main substrate species is the monoionic form. The HEN–Cu(II) chelate compound is almost completely dissociated. The experimental results obtained in this Laboratory[3] under such conditions are shown in Table IV.

TABLE IV

CATALYTIC EFFECTS OF AQUOCOPPER(II) ION AND HEN–COPPER(II) ION

$-\log [H^+]$	M_I	Catalyst	k_{obsd}, sec.$^{-1}$	k^0, sec.$^{-1}$
3.3	0.723	Cu(II)	1.25×10^{-5}	1.35×10^{-5}
3.8	.454	Cu(II)	3.3×10^{-5}	2.22×10^{-5}
3.8	.454	1:1 Cu(II)–HEN	3.5×10^{-5}	2.22×10^{-5}

From the results in Table IV it seems reasonable to assume that copper(II) ion does not contribute to the hydrolysis of H_2A^- as an active catalyst. Therefore, the catalytic effect observed at $-\log [H^+] = 4.00$ would be due most likely to the effect of Cu(II) on the hydrolysis of HA^{2-}. The rate constant k^{II}_{Cu}, calculated by the aid of eq. 29, is 4.0×10^{-2}. Evaluation of k^{III}_{Cu} by means of eq. 30 and 31 gives values of 4.4 and of 3.0, respectively. The difference between these values presumably is caused by the fact that the concentration of A^{3-} is low at $-\log [H^+] = 5.50$, and also the fact that at $-\log [H^+] = 6.00$, the concentration of free Cu(II) ion is relatively low in comparison to other

species present in the system. Thus, the average value of 3.7 may be taken as an approximate value for k^{III}_{Cu}.

Discussion

The fact that both the dipyridyl and N-hydroxyethylethylenediamine chelate compounds containing one mole of ligand per gram-ion of Cu(II) are not catalytically active may be due to a number of reasons. There are several ways in which the metal ion may form a mixed chelate compound with the substrate and dipyridyl. Two possible arrangements of ligand are illustrated by I and II: In the case of I, the carboxylate and phosphate groups are both bound to the metal ion, so that the intramolecular nucleophilic attack of the carboxylate ion on the phosphorus atom would be prevented. For the arrangement shown in II, one would expect that the intramolecular attack of the phosphorus atom would still be possible; in fact, the coördination shown would increase the electrophilic activity of the phosphorus over that of the trinegative species, so that a catalytic effect would be expected relative to the pure substrate at high pH. In view of the negative effect of Cu(II) dipyridyl in the pH range 5–6, structure I is preferred for the mixed chelate.

On the other hand, the reduced rate is not incompatible with II, since its activity should be compared with those of the species present in the low pH range, rather than with that of the trinegative species which is not the predominant form under the experimental conditions. Since the influence of the Cu(II) ion on the electrophilic reactivity of the phosphate group would be much less than that of the one or two protons which it replaces, there should be a drop in reaction rate on the addition of the HEN–Cu(II) chelate, even though its catalytic effect were of appreciable magnitude (*i.e.*, it would be a less effective catalyst than the proton).

The lack of activity of the HEN–Cu(II) chelate compound III may be due to its greater thermodynamic stability, and the terdentate nature of the ligand. Hall and Dean[7] and Martell and co-workers[8] suggested that in the Cu(II)–HEN chelate, three of the four coördination sites of Cu(II) chelate are occupied by the three donor groups of the ligand. Such an arrangement of donor groups of the ligand would reduce the tendency of copper(II) to combine with salicyl phosphate. The Cu(II) ion in this complex would be coördinatively more saturated and would be expected, therefore, to have less catalytic activity than the Cu(II)–dipyridyl complex. The low stability of the latter would lead one to expect it to have some catalytic effect, and its lack of activity at low pH must be due to the special properties of the mixed salicyl phosphate–dipyridyl chelate, as mentioned above. At high pH, one would expect the 1:1 dipyridyl–Cu(II) and N-hydroxyethylethylenediamine–Cu(II) chelates to be active as catalysts for the hydrolysis of the trinegative form of the substrate. The conversion of these complexes to hydroxo forms (such as III and IV) at high pH makes it impossible to demonstrate such activity experimentally.

In accordance with the absence (or very low values) of the catalytic activities of the metal chelates, the

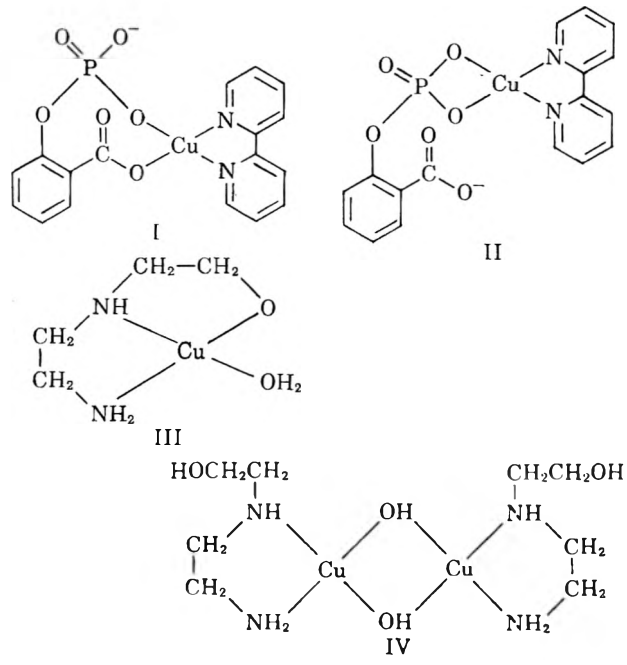

principal function of the ligands used in this investigation is to control the concentration of the Cu(II) ion, the main catalytically active species. The resulting metal buffer systems maintain the metal ion concentrations at sufficiently low values to prevent precipitation of the metal hydroxide, thus making possible kinetic measurements of the specific catalytic activities of the metal ion on the various substrate species present.

For Cu(II) ion catalysis, the probable structures of the transition state through which the reaction proceeds are indicated by V and VI. The type of interaction indicated by V would be relatively weak and would necessitate nucleophilic attack on the phosphorus atom by water or hydroxyl ion. Structure VI, on the other

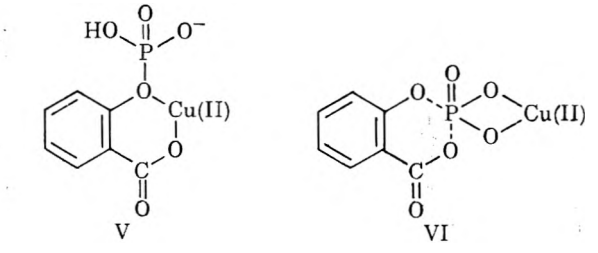

hand, would allow the intramolecular nucleophilic attack to take place, in accordance with the mechanism of the spontaneous reaction. It would seem, therefore, that transition state VI is favored as the more reactive form. The nature of the mechanism of metal ion catalysis will be described in greater detail in a subsequent publication.

(7) J. L. Hall and W. E. Dean, *J. Am. Chem. Soc.*, **80**, 4183 (1958).

(8) R. C. Courtney, R. L. Gustafson, S. Chaberek, Jr., and A. E. Martell, *ibid.*, **81**, 519 (1959).

CURRENT-POTENTIAL CHARACTERISTICS FOR ELECTRODE PROCESSES WITH SPECIFIC ADSORPTION OF REACTANT AND/OR PRODUCT

BY DAVID M. MOHILNER[1] AND PAUL DELAHAY

Coates Chemical Laboratory, Louisiana State University, Baton Rouge 3, Louisiana

Received August 6, 1962

A general current–potential characteristic is derived for electrode processes controlled by charge transfer kinetics and equilibrium for specific adsorption of reactant and product. The supporting electrolyte is supposed not to be specifically adsorbed. Particular forms of this equation are derived (a) for processes with specific adsorption of a single substance and (b) specific adsorption of a single substance obeying the logarithmic Temkin isotherm. A simple experimental criterion is derived which involves the study of the variations of the apparent exchange current density with the activities of reactant and product. Processes with control by charge transfer equilibrium and adsorption kinetics are briefly treated. Experimental and theoretical studies suggested by this work are indicated.

Current–potential characteristics have been discussed for a number of electrode processes with specific adsorption of reactant and/or product, *e.g.*, hydrogen ion discharge and hydrogen evolution,[2,3] metal deposition.[4] Relaxation methods have also been analyzed for such processes: potentiostatic and galvanostatic methods,[5] faradaic impedance and rectification.[6] The problem is attacked here in a new way by application of recent ideas[7] on adsorption kinetics at electrodes and use of Parsons' treatment of electrode kinetics.[8] A criterion is derived for the detection and, possibly, quantitative study of adsorption. Stoichiometric number and coefficients are assumed to be equal to unity but results can easily be modified when this assumption cannot be made. It is further assumed that the supporting electrolyte is not specifically adsorbed. Mass transfer polarization is not considered.

Control by Adsorption Equilibrium and Charge Transfer Kinetics

General Equation.—We consider the over-all process $O^z + ne = R^{z'}$ which is decomposed in the following consecutive steps

$$O^z + S = A_O \quad (1)$$

$$A_O + ne = A_R \quad (2)$$

$$A_R = R^{z'} + S \quad (3)$$

There, O^z and $R^{z'}$ of ionic valency z and z', respectively, are soluble in the electrolyte (possibly R in the electrode, *e.g.*, amalgam electrode); A_O and A_R are the specifically adsorbed forms of O^z and $R^{z'}$, S represents the adsorption sites. It is assumed that sites are equally available to either O^z and $R^{z'}$. This formalism is inspired from our previous paper[7] on adsorption kinetics. We define the states

I: O^z(bulk) + ne(electrode) + S

II: A_O + ne(electrode)

III: A_R

IV: $R^{z'}$ (bulk) + S

The corresponding standard free energies are

$$G_I^0 = \mu_O^0 + n\mu_e^M - nF\phi^M + \mu_S^n + \mu_S^q \quad (4)$$

$$G_{II}^0 = \mu_{A_O}^n + \mu_{A_O}^q + n\mu_e^M - nF\phi^M \quad (5)$$

$$G_{III}^0 = \mu_{A_R}^n + \mu_{A_R}^q \quad (6)$$

$$G_{IV}^0 = \mu_R^0 + \mu_S^n + \mu_S^q \quad (7)$$

where the μ^0's are the standard chemical potentials; the μ^n's the charge-independent parts of the standard electrochemical potentials; the μ^q's the charge-dependent parts of the standard electrochemical potentials; and ϕ^M is the inner potential of the electrode referred to the potential in the bulk of the solution. The division of the electrochemical potentials of species A_O, A_R, and S into charge-independent and charge-dependent parts was previously used by us.[7] This division is nonoperational but this is immaterial because (a) the current-potential characteristics derived below include only *differences* of the charge-dependent parts of the electrochemical potentials, and (b) these differences can be determined by experiment. The "electrical" (as opposed to "neutral") parts of the standard free energies are

$$(G_I^0)_e = -nF\phi^M + \mu_S^q \quad (8)$$

$$(G_{II}^0)_e = -nF\phi^M + \mu_{A_O}^q \quad (9)$$

$$(G_{III}^0)_e = \mu_{A_R}^q \quad (10)$$

$$(G_{IV}^0)_e = \mu_S^q \quad (11)$$

We now postulate similarly to Parsons[8] that the electrical part of the standard free energy of the activated complex $(G_\ddagger^0)_e$ is such that

$$(G_\ddagger^0)_e - (G_{II}^0)_e = \alpha\,[(G_{III}^0)_e - (G_{II}^0)_e] \quad (12)$$

(1) Postdoctoral fellow, 1960–1962.

(2) (a) A detailed review of some aspects of this problem (and also the influence of adsorption of foreign ions) is given by A. N. Frumkin, "Advances in Electrochemistry and Electrochemical Engineering," Vol. 3, P. Delahay, editor, Interscience Division, John Wiley and Sons, Inc., New York, N.Y., in course of publication. (b) See also K. J. Vetter, "Elektrochemische Kinetik," Springer-Verlag, Berlin, 1961, pp. 468–474.

(3) (a) For *recent* work, *cf.*, R. Parsons, *Trans. Faraday Soc.*, **54**, 1053 (1958). (b) H. Gerischer, *Bull. soc. chim. Belges*, **67**, 506 (1958). (c) L. Krishtalik, *Zh. Fiz. Khim.*, **33**, 1715 (1959); **34**, 117 (1960). (d) J. G. N. Thomas, *Trans. Faraday Soc.*, **57**, 1603 (1961).

(4) For a review, *cf.*, *e.g.*, H. Gerischer, *Ann. Rev. Phys. Chem.*, **12**, 227 (1961).

(5) H. Matsuda and P. Delahay, *Collection Czechoslov. Chem. Commun.*, **25**, 2977 (1960). It is assumed that adsorption follows a Langmuir isotherm at equilibrium as in earlier analyses of the faradaic impedance for processes with specific adsorption. This analysis is superseded by that of ref. 6.

(6) M. Senda and P. Delahay, *J. Am. Chem. Soc.*, **65**, 1580 (1961). See previous work of other authors therein.

(7) P. Delahay and D. M. Mohilner, *J. Phys. Chem.*, **66**, 959 (1962) (Communication); *J. Am. Chem. Soc.*, in press. Adsorption of neutral substances is treated but results can readily be transposed to adsorption of ions. It suffices to introduce in the expression for the adsorption exchange rate a Frumkin type of correction for the activity of the adsorbed species in the outer Helmholtz plane.

(8) R. Parsons, *Trans. Faraday Soc.*, **47**, 1332 (1951).

$$= \alpha\,[\mu_{A_R}{}^q - (\mu_{A_O}{}^q - nF\phi^M)]$$

where α ($0 < \alpha < 1$) is the transfer coefficient. Likewise

$$(G_{\ddagger}{}^0)_e - (G_{II}{}^0)_e = (\alpha - 1)\,[(G_{III}{}^0)_e - (G_{II}{}^0)_e] \quad (13)$$
$$= (\alpha - 1)\,[\mu_{A_R}{}^q - (\mu_{A_O}{}^q - nF\phi^M)]$$

The standard free energy of activation for the forward processes is

$$\vec{\Delta G}_{\ddagger}{}^0 = G_{\ddagger}{}^0 - G_I{}^0 \quad (14)$$
$$= (\vec{\Delta G}_{\ddagger}{}^0)_n - (\Delta G_{\ddagger}{}^0)_e$$
$$= (\vec{\Delta G}_{\ddagger}{}^0)_n + (G_{\ddagger}{}^0)_e - (G_I{}^0)_e$$
$$= (\vec{\Delta G}_{\ddagger}{}^0)_n + \alpha\Delta G_R{}^q + (1 - \alpha)\Delta G_O{}^q + \alpha nF\phi^M$$

where $(\vec{\Delta G}_{\ddagger}{}^0)_n$ is the charge-independent part of $\vec{\Delta G}_{\ddagger}{}^0$, and $\Delta G_O{}^q$ and $\Delta G_R{}^q$ are defined by

$$\Delta G_O{}^q = \mu_{A_O}{}^q - \mu_S{}^q \quad (15)$$
$$\Delta G_R{}^q = \mu_{A_R}{}^q - \mu_S{}^q \quad (16)$$

Likewise, one has for the backward process

$$\overleftarrow{\Delta G}_{\ddagger}{}^0 = G_{\ddagger}{}^0 - G_{IV}{}^0 = (\overleftarrow{\Delta G}_{\ddagger}{}^0)_n + \alpha\Delta G_R{}^q + (1 - \alpha)\Delta G_O{}^q - (1 - \alpha)\,nF\phi^M \quad (17)$$

The current densities for the forward and backward reactions are, respectively

$$\vec{I} = nF(kT/h)[\exp(-\vec{\Delta G}_{\ddagger}{}^0/RT)]a_O a_S \quad (18)$$

$$\overleftarrow{I} = nF(kT/h)\,[\exp(-\overleftarrow{\Delta G}_{\ddagger}{}^0/RT)]a_R a_S \quad (19)$$

where the a_O and a_R are the activities of O^z and $R^{z'}$ in the bulk of the solution and a_S is the activity of the sites S; the other symbols are as usual. At equilibrium $\vec{I} = \overleftarrow{I} = I_a{}^0$, where $I_a{}^0$ is the *apparent exchange current density* ("apparent" because $I_a{}^0$ is an over-all quantity which does not pertain solely to charge transfer between A_O and A_R). One has by analogy with the treatment of electrode kinetics in the absence of specific adsorption[9]

$$I_a{}^0 = nFk^0 a_O{}^{1-\alpha} a_R{}^\alpha a_S \exp[-\alpha(\Delta G_R{}^q)_r/RT]\exp[-(1 - \alpha)(\Delta G_O{}^q)_r/RT] \quad (20)$$

where the *standard rate constant* k^0 is

$$k^0 = (kT/h)\exp[-(\vec{\Delta G}_{\ddagger}{}^0)_n/RT]\exp[-\alpha nF\phi^M/RT]$$
$$= (kT/h)\exp[-(\overleftarrow{\Delta G}_{\ddagger}{}^0)_n/RT]\exp[(1 - \alpha)nF\phi_0{}^M/RT] \quad (21)$$

There $\phi_r{}^M$ is the equilibrium potential, $\phi_0{}^M$ is the standard potential for the reaction $O^z + ne = R^{z'}$, and $(\Delta G_O{}^q)_r$ and $(\Delta G_R{}^q)_r$ are the values of $\Delta G_O{}^q$ and $\Delta G_R{}^q$ at $\phi_r{}^M$. The current density–potential characteristic ($I \gtrless 0$ for a net cathodic or anodic current, respectively) is

$$I = I_a{}^0\,\{\exp\{-\alpha[\Delta G_R{}^q - (\Delta G_R{}^q)_r]/RT\}\exp\{-(1 - \alpha)\,[\Delta G_O{}^q - (\Delta G_O{}^q)_r]/RT\}\} \times \{\exp[-\alpha nF\eta/RT] - \exp[(1 - \alpha)nF\eta/RT] \quad (22)$$

where $\eta = \phi^M - \phi_r{}^M$ is the overvoltage, and $\Delta G_R{}^q$ and $\Delta G_O{}^q$ are taken at ϕ^M. It can readily be shown that eq. 22 reduces to the Nernst equation for $\phi^M = \phi_r{}^M$.

Equation 22 includes the factors (between the second pair of braces) showing the well known dependence of I on overvoltage and it should account, together with eq. 20 for $I_a{}^0$, for the influence of specific adsorption. Application of the general equations 20 and 22 requires the explicit form of a_S and the knowledge of the variations of $\Delta G_O{}^q$ and $\Delta G_R{}^q$ with ϕ^M. Application will be limited here to processes in which only one species—either O^z or $R^{z'}$—is specifically adsorbed and the logarithmic Temkin isotherm is obeyed at equilibrium.

Case of a Single Specifically Adsorbed Substance.—We assume that substance O^z is specifically adsorbed and $R^{z'}$ is not. States III and IV now are

III: $R^{z'}$ (outer Helmholtz plane) + S

IV: $R^{z'}$ (bulk) + S

The corresponding standard free energies are

$$G_{III}{}^0 = \mu_R{}^0 + z'F\phi^h + \mu_S{}^n + \mu_S{}^q \quad (23)$$
$$G_{IV}{}^0 = \mu_R{}^0 + \mu_S{}^n + \mu_S{}^q \quad (24)$$

where $\mu_R{}^0$ is the standard chemical potential of $R^{z'}$ and ϕ^h is the inner potential in the outer Helmholtz plane referred to the inner potential in the bulk of the solution. Equations 10 and 11 now become

$$(G_{III}{}^0)_e = z'F\phi^h + \mu_S{}^q \quad (25)$$
$$(G_{IV}{}^0)_e = \mu_S{}^q \quad (26)$$

and consequently (*cf.* eq. 12)

$$(G_{\ddagger}{}^0)_e - (G_{II}{}^0)_e = \alpha\,[z'F\phi^h + \mu_S{}^q - (\mu_{A_O}{}^q - nF\phi^M)] \quad (27)$$

$$(G_{\ddagger}{}^0)_e - (G_{III}{}^0)_e = (\alpha - 1)\,[z'F\phi^h + \mu_S{}^q - (\mu_{A_O}{}^q - nF\phi^M)] \quad (28)$$

Hence (*cf.* eq. 14 and 17)

$$\vec{\Delta G}_{\ddagger}{}^0 = (\vec{\Delta G}_{\ddagger}{}^0)_n + (1 - \alpha)\Delta G_O{}^q + \alpha z'F\phi^h + \alpha nF\phi^M \quad (29)$$

$$\overleftarrow{\Delta G}_{\ddagger}{}^0 = (\overleftarrow{\Delta G}_{\ddagger}{}^0)_n + (1 - \alpha)\Delta G_O{}^q + \alpha z'F\phi^h - (1 - \alpha)\,nF\phi^M \quad (30)$$

The exchange current density is

$$I_a{}^0 = nFk^0 a_O{}^{1-\alpha}\,a_R{}^\alpha\,a_S \exp\,[-\alpha z'F\phi_r{}^h/RT] \times \exp[-(1 - \alpha)\,(\Delta G_O{}^q)_r/RT \quad (31)$$

where k^0 is defined by eq. 21 and $\phi_r{}^h$ is the value of ϕ^h at $\phi_r{}^M$. It is seen that the effect of non-specific adsorption of $R^{z'}$ corresponds to a purely electrostatic term of the Frumkin correction type (*cf.* ref. 10). The I–η characteristic is

$$I = I_a{}^0\,\{\exp\{-\alpha z'F\,(\phi^h - \phi_r{}^h)/RT\} \times \exp\{-(1 - \alpha)\,[\Delta G_O{}^q - (\Delta G_O{}^q)_r]/RT\} \times \{\exp[-\alpha nF\eta/RT] - \exp[(1 - \alpha)\,nF\eta/RT]\} \quad (32)$$

(9) For a review, *cf.*, *e.g.*, P. Delahay in "Advances in Electrochemistry and Electrochemical Engineering," Vol. 1, P. Delahay, editor, Interscience Division, John Wiley and Sons, Inc., New York, N. Y., 1961, pp. 233–318.

Single Specifically Adsorbed Substance Obeying the Logarithmic Temkin Isotherm.—The logarithmic Temkin isotherm is[10]

$$b\Gamma = -\Delta G^0 - RT \ln a \qquad (33)$$

where b is a characteristic parameter of the adsorbed substance under given conditions, Γ the surface concentration, ΔG^0 the standard free energy of adsorption, and a the activity in solution for the adsorbed substance. This isotherm represents quite well, *as a first approximation*, data on adsorption of ions[11,12] and some organic substances[13] on an ideal polarized electrode at constant charge density and provides a convenient starting point in this treatment. One then has

$$a_S = \exp[-(\lambda b/RT)\Gamma] \qquad (34)$$

where λ is the *coverage parameter* introduced by Temkin.[10] In view of eq. 33, one has for adsorption equilibrium

$$a_S = (a_O)^{-\lambda} \exp[-\lambda(\Delta G^n + \Delta G^q)/RT] \qquad (35)$$

where ΔG^n and ΔG^q are the charge-independent and charge-dependent components of the standard free energy of adsorption ΔG^0, respectively. $I_a{}^0$ and the I–η characteristic are

$$I_a{}^0 = nF(k^0)'a^{1-\alpha-\lambda}a_R{}^\alpha \exp[-\alpha z'F\phi_r{}^h/RT] \times \exp[(\alpha - \lambda + 1)\,\Delta G_r{}^q/RT] \qquad (36)$$

$$I = I_a{}^0 \{\exp\{-\alpha z'F[\phi^h - \phi_r{}^h]/RT\} \times \exp[(\alpha - \lambda - 1)(\Delta G^q - \Delta G_r{}^q)/RT]\} \times \{\exp[-\alpha nF\eta/RT] - \exp[(1-\alpha)\,nF\eta/RT]\} \qquad (37)$$

where ΔG^q and $\Delta G_r{}^q$ correspond to ϕ^M and $\phi_R{}^M$, respectively, and $(k^0)' = k^0 \exp(\lambda\Delta G^0/RT)$ (*cf.* eq. 21). It is seen from eq. 37 that $I_a{}^0$ includes two terms depending on ϕ^M: the term in $\phi_r{}^h$ which corresponds to the Frumkin correction for the non-specifically adsorbed substance $R^{z'}$, and the term in $\Delta G_r{}^q$ resulting from specific adsorption of O^z.

More quantitative data are needed on the dependence of $\Delta G_r{}^q$ on ϕ^M at the present, and only a preliminary conclusion can be reached. Thus, it was shown by Parsons[12] that ΔG^q varies linearly with the charge density q for adsorption of Cl^-, Br^-, and I^- on an ideal polarized Hg electrode. As a *crude* approximation q varies linearly with ϕ^M not too near the point of zero charge, and consequently the exponential containing $\Delta G_r{}^q$ in eq. 36 is equivalent to an exponential function of ϕ^M. The dependence of $\Delta G_r{}^q$ on q for organic substances is more involved but can be determined experimentally.[13]

Experimental Criterion for Specific Adsorption.—In addition to the usual methods applied to ideal polarized electrodes for the detection of specific adsorption, eq. 36 supplies a simple criterion based on the measurement of $I_a{}^0$. One has by analogy with processes without specific adsorption[9]

$$\left(\frac{\partial \ln I_a{}^0}{\partial \ln a_O}\right)_{a_R} = (1 - \alpha - \lambda) - \alpha\frac{z'}{n}\left(\frac{\partial \phi_r{}^h}{\partial \phi_r{}^M}\right)_{a_R} + \frac{1 + \alpha - \lambda}{nF}\left(\frac{\partial \Delta G_r{}^q}{\partial \phi_r{}^M}\right)_{a_R} \qquad (38)$$

$$\left(\frac{\partial \ln I_a{}^0}{\partial \ln a_R}\right)_{a_O} = \alpha + \alpha\frac{z'}{n}\left(\frac{\partial \phi_r{}^h}{\partial \phi_r{}^M}\right)_{a_O} - \frac{1 + \alpha - \lambda}{nF}\left(\frac{\partial G_r{}^q}{\partial \phi_r{}^M}\right)_{a_O} \qquad (39)$$

For a given pair of a_O and a_R one has

$$\left(\frac{\partial \ln I_a{}^0}{\partial \ln a_O}\right)_{a_R} + \left(\frac{\partial \ln I_a{}^0}{\partial \ln a_R}\right)_{a_O} = 1 - \lambda \qquad (40)$$

In the absence of specific adsorption, the left-hand members of eq. 38 and 39 are equal to $1 - \alpha$ and α, respectively, whereas this is not the case when there is specific adsorption of one reactant. The sum in eq. 40 is equal to 1 in the former case and is comprised between 0 and 1 ($0 < \lambda < 1$) in the latter case. This provides a simple experimental criterion for detection of specific adsorption. This criterion should not be used without discrimination since other causes than adsorption (complexity of reaction, etc.) may cause the sum of eq. 40 to differ from unity.

Control by Charge Transfer Equilibrium and Adsorption Kinetics

We assume that $R^{z'}$ is not adsorbed and that O^z is adsorbed according to the logarithmic Temkin isotherm at equilibrium. Further, eq. 1 is supposed to be slow and equilibrium prevails for eq. 2. We consider the states

I: O^z(bulk) + ne(electrode) + S

II: O^z(outer Helmholtz plane) + ne(electrode) + S

III: A_O + ne(electrode)

IV: $R^{z'}$ (bulk) + S

We proceed as before and postulate that

$$(G_{\neq}{}^0)_e - (G_{II}{}^0)_e = \rho[(G_{III}{}^0)_e - (G_{II}{}^0)_e] \qquad (41a)$$

$$(G_{\neq}{}^0)_e - (G_{III}{}^0)_e = (\rho - 1)\,[(G_{III}{}^0)_e - (G_{II}{}^0)_e] \qquad (41b)$$

where ρ is the *charge parameter* previously introduced[7] in the treatment at adsorption kinetics. Thus

$$I_a{}^0 = nF(k^0)''a_O{}^{1-\alpha} \exp[-(1-\rho)zF\phi_r{}^h/RT] \times \exp[(\lambda - \rho)\,\Delta G_r{}^q/RT] \qquad (42)$$

with

$$(k^0)'' = (kT/h)\exp[-(\overrightarrow{\Delta G}_{\neq}{}^0)_n/RT]\exp[\lambda\Delta G^n/RT] = (kT/h)\exp[-(\Delta G_{\neq}{}^0)_n/RT]\exp[\lambda\Delta G^n/RT] \times \exp[-\Delta G_r{}^0/RT] \qquad (43)$$

where $\Delta G_r{}^0$ is the change in standard free energy for the over-all reaction $O^z + ne = R^{z'}$. Equation 42 is quite similar to that for the adsorption exchange rate previously derived[7] except that the effect of the charge transfer process following adsorption is now included. The I–η characteristic can be written provided that functions $\phi^h(\phi^M)$ and $\Delta G^q(\phi^M)$ are known or can be postulated.

We also considered the general case of control by the kinetics of adsorption and charge transfer but the resulting equations are too involved to be of practical use.

(10) M. I. Temkin, *Zh. fiz. Khim.*, **15**, 296 (1941). Translation available.

(11) D. C. Grahame, *J. Am. Chem. Soc.*, **80**, 4201 (1958).

(12) (a) R. Parsons, *Proc. 2nd Int. Congress Surface Activity*, **3**, 38 (1957); (b) R. Parsons, *Trans. Faraday Soc.*, **55**, 999 (1959).

(13) D. M. Mohilner, P. Delahay, and T. H. Tidwell, unpublished investigation.

Conclusion

Electrode processes with specific adsorption of reactant and/or product can be analyzed rather rigorously by the method of this paper. Further progress requires experimental studies on (a) adsorption isotherms, (b) determination of the standard free energy of adsorption as a function of charge density, and (c) application of the experimental criterion deduced in this paper.

Acknowledgment.—This investigation was supported by the National Science Foundation.

PROTON RESONANCE STUDIES OF *ORTHO*-SUBSTITUTED PHENOLS

BY E. A. ALLAN AND L. W. REEVES

Department of Chemistry, University of British Columbia, Vancouver 8, B. C.

Received August 8, 1962

The formation of a *cis–trans* dimer of *ortho*-halo-phenols in dilute solution in CS_2 has been studied by n.m.r. Values of the dimerization equilibrium constant are obtained.[1] The temperature dependence of the –O–H chemical shift in 2,6 substituted halo-phenols is interpreted in terms of the asymmetry of the 2-fold internal rotation barrier of the C–O–H group. The ring proton spectra of these compounds have been analyzed and values of chemical shifts and absolute values of coupling constants obtained.

Introduction

In a recent paper[1] the study of intramolecular hydrogen bonds by proton resonance methods gave quantitative information about the enthalpy of formation of the hydrogen bonds in *ortho*-chloro-, bromo-, and iodophenol. The changes in chemical shift of the –OH proton on formation of an internal hydrogen bond have been shown to be approximately linearly related to the change in the OH infrared stretching frequency.[1-3]

In studies of 2-hydroxybenzophenones similar correlations have been noted.[4] Careful work by Gutowsky and co-workers[5] has shown that chelated hydrogen bonds in derivatives of phenol, β-naphthol, and 9-phenanthrol show –OH proton resonances shifted to lower field from the parent compound by an amount proportional to $\Delta\nu$ (C=O) in the infrared spectra and the bond multiplicity of the C=C bond in the chelate ring. Further work on intermolecular hydrogen bonded association between phenols and solvent molecules has indicated a correlation between hydrogen bond strength and change in chemical shift.[6]

The object of the present work has been to extend conclusions on intramolecular hydrogen bonds in *ortho*-halo-phenols to include the formation of O–H---O hydrogen bonds at finite concentrations by intermolecular association.[1] A study of 2,6-substituted *ortho*-halo-phenols also is made and some work on the ring proton resonances in these compounds is included.

Experimental

Spectra were recorded on a Varian V.4300B high resolution spectrometer at 40 Mc. Small modifications to improve the precision of chemical shift measurements have been described in the previous paper.[1] For the work involving ring spectrum analysis, a Varian 60 Mc. A-60 analytical spectrometer was used. The chemical shift of the –OH proton at room temperature obtained with this instrument agreed with the results obtained at 40 Mc.

2-Fluoro-4,6-diiodo-, 2-chloro-4,6-diiodo-, and 2-bromo-4,6-diiodophenol were prepared according to the procedure of Baker and Kaeding.[7] The products were recrystallized several times from *n*-heptane. 2-Fluoro-4,6-dibromo- and 2-chloro-4,6-dibromophenol were prepared by the method of Raiford and Le Rosen.[8] The remaining substituted phenols used in this work were Eastman Kodak White Label materials further purified by successive recrystallization from redistilled *n*-hexane. The carbon disulfide was fractionally distilled reagent grade material. A small amount of tetramethylsilane (~1%) was added to serve as an internal reference peak.

Results

Solutions of the 2,6-substituted halo-phenols were made up at 2 and 4 mole % in carbon disulfide and sealed in 5 mm. o.d. sample tubes. An independently prepared duplicate set of solutions also was prepared and measured as a check. The –O–H proton resonance in these solutions was measured with respect to tetramethylsilane at temperatures between 0 and 100°. The standard deviation of 10 measurements on each solution varied but was never greater than ±0.5 c.p.s.

The chemical shift of the –OH proton resonance was the same for the 4 and 2 mole % solutions within experimental error. The variation of the chemical shift with respect to cyclohexane at various temperatures is given in graphical form in Fig. 1. The results are given in cycles per second from cyclohexane for comparison with previous results.[1] A study of 2,4,6-trichlorophenol in various solvents also was carried out. Values obtained for the –OH proton resonance were −4.32 p.p.m. in CS_2, CCl_4, and cyclohexane, −4.24 p.p.m. in $CHCl_3$, −3.83 p.p.m. in benzene, and −8.94 p.p.m. in acetone. These results show that the –O–H proton is not sufficiently sterically hindered to prevent interaction with solvent.

Analysis of the ring proton spectra in these compounds also was made and these are included in Table I. No spectrum analyzed was more complex than an ABX case.[9] A complete summary of these analyses is given in Table I.

Discussion

Formation of *cis–trans* Dimers.—The data in the previous paper[1] showed that the concentration dependence of the –OH chemical shift in three singly substituted *ortho*-halo-phenols was linear from 0–4 mole % between −50 and +100°; and the infinite dilution chemical shift of the –OH proton resonance in these phenols has been used to determine the *cis–trans* equilibrium constant. At any finite concentration the

(1) E. A. Allan and L. W. Reeves, *J. Phys. Chem.*, **66**, 613 (1962).
(2) L. W. Reeves, *Can. J. Chem.*, **38**, 748 (1960).
(3) L. W. Reeves, E. A. Allan, and K. O. Strømme, *ibid.*, **38**, 1249 (1960).
(4) J. R. Merrill, *J. Phys. Chem.*, **65**, 2023 (1961).
(5) A. L. Porte, H. S. Gutowsky, and I. M. Hunsberger, *J. Am. Chem.* **82**, 5057 (1960).
(6) L. Grannacher, *Helv. Phys. Acta*, **34**, 272 (1961).
(7) A. W. Baker and W. W. Kaeding, *J. Am. Chem. Soc.*, **81**, 5904 (1959).
(8) L. C. Raiford and A. L. Le Rosen, *ibid.*, **66**, 2080 (1944).
(9) J. A. Pople, W. G. Schneider, and H. J. Bernstein, "High Resolution Nuclear Magnetic Resonance Spectroscopy," McGraw-Hill Book Co., New York, N. Y., 1959.

TABLE I

CHEMICAL SHIFTS AND COUPLING CONSTANTS FOR SEVERAL SUBSTITUTED PHENOLS AT 25°[a]

Compound (~5 mole % in CS_2)[b]	δ_{OH}, p.p.m.	δ_A, p.p.m.	δ_B, p.p.m.	δ_X, p.p.m.	J_{AB}, cycles/sec.	J_{AX}, cycles/sec.	J_{BX}, cycles/sec.
2-Chloro-4,6-diiodophenol	5.80	7.55	7.86	...	2.0	...	...
2-Chloro-4,6-dibromophenol	5.74	7.34	7.45	...	2.3	...	...
2,3,4,6-Tetrachlorophenol	5.87	...	7.33	...	...	...	...
2-Iodo-4,6-dichlorophenol	5.72	7.52	7.26	...	2.4	...	...
2-Iodo-4,6-dibromophenol	5.68	7.66	7.46	...	2.2	...	...
2-Fluoro-4,6-diiodophenol	5.47	7.28	7.60	...	2.0	9.2	1.9
2-Fluoro-4,6-dibromophenol	5.28	7.10	7.31	...	2.2	9.4	1.9
2-Nitro-4-chlorophenol (X proton at positon 6)	...	7.74	7.20	6.78	2.5	0.48	9.0
2,6-Dimethoxyphenol (protons *meta* to –OH designated as A, *para* as B)	5.43	6.40	6.58	...	8.8	...	...

[a] All chemical shifts are given from tetramethylsilane as internal standard (~1 mole %). [b] Except where noted, the proton at position three is designated as the A proton, that at position 5 and the B proton.

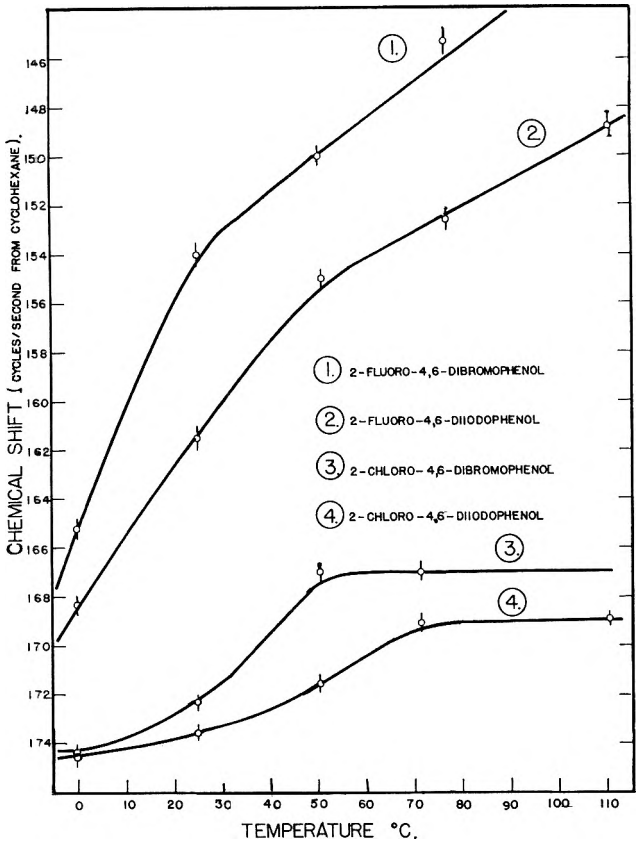

Fig. 1.—Temperature dependence of chemical shifts in *o*-halo phenol solutions in CS_2. The shifts are downfield with respect to cyclohexane.

linear change of chemical shift to low field can be interpreted as due to the formation of dimers joined by an OH---O hydrogen bond. The *trans*-form of *ortho*-chloro-, bromo-, and iodophenol is in low concentration in dilute solutions in CS_2 because of the small values obtained for $K_1 = [trans]/[cis]$.[1] The *trans* form of these molecules is the only species which has a free –OH to form hydrogen bonds. In view of its small concentration it is considered that the dimers form between *cis* and *trans* molecules since the former have a much higher concentration.

Suppose we assume the low concentration of dimers does not appreciably alter the value of K_1 at a finite concentration in CS_2. If we have initially "a" moles of phenol, "m_s" moles of CS_2, "m_c" moles of the *cis* form, m_D moles of dimer, where $(a - m_c)/m_c = K_1$,

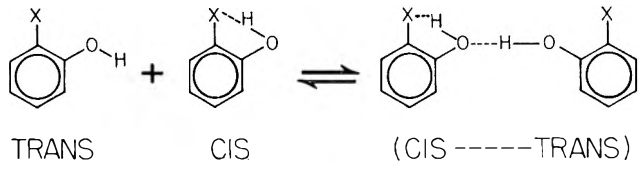

then at a finite concentration we may write the moles of each form present at equilibrium

	Moles	Mole fraction
trans	$(a - m_c - m_D)$	$\frac{(a - m_c - m_D)}{(a - m_D) + m_s}$
cis	$(m_c - m_D)$	$\frac{(m_c - m_D)}{(a - m_D) + m_s}$
cis–trans dimer	m_D	$\frac{m_D}{(a - m_D) + m_s}$

We can define a K_2 in mole fraction units

$$K_2 = \frac{[cis\text{–}trans]}{[cis][trans]} = \frac{m_D(a - m_D + m_s)}{(a - m_c - m_D)(m_c - m_D)} \quad (1)$$

If we have chemical shifts as follows: δ_{mc} = measured chemical shift at a finite concentration "c"; δ_T, δ_c = chemical shift in *trans* and *cis* forms; respectively, δ_{TD} and δ_{cD} = chemical shift in dimer forms of the *trans* and *cis* molecules, respectively, the following relationship for the measured chemical shift holds[10]

$$\delta_{mc} = \left(\frac{(a - m_c - m_D)}{a - m_D}\right)\delta_T + \left(\frac{(m_c - m_c)}{(a - m_D)}\right)\delta_c + \left(\frac{m_D}{a - m_D}\right)\delta_{TD} + \left(\frac{m_D}{a - m_D}\right)\delta_{cD} \quad (2)$$

If $\delta_{cD} \cong \delta_c$; assuming only small perturbation of the *cis*-OH proton in the dimer, we may combine the values for δ_c and δ_{cD}. From the previous paper[1] the expression

$$\delta_{M_\infty} = \left(\frac{a - m_c}{a}\right)\delta_T + \frac{m_c}{a}\delta_c \quad (3)$$

gives the infinite dilution chemical shift.

$\delta_{M_0} \longrightarrow \delta_{M_\infty}$ as $m_D \longrightarrow 0$, providing $(a - m_D) \cong a$

(10) H. S. Gutowsky and A. Saika, *J. Chem. Phys.*, **21**, 1688 (1953).

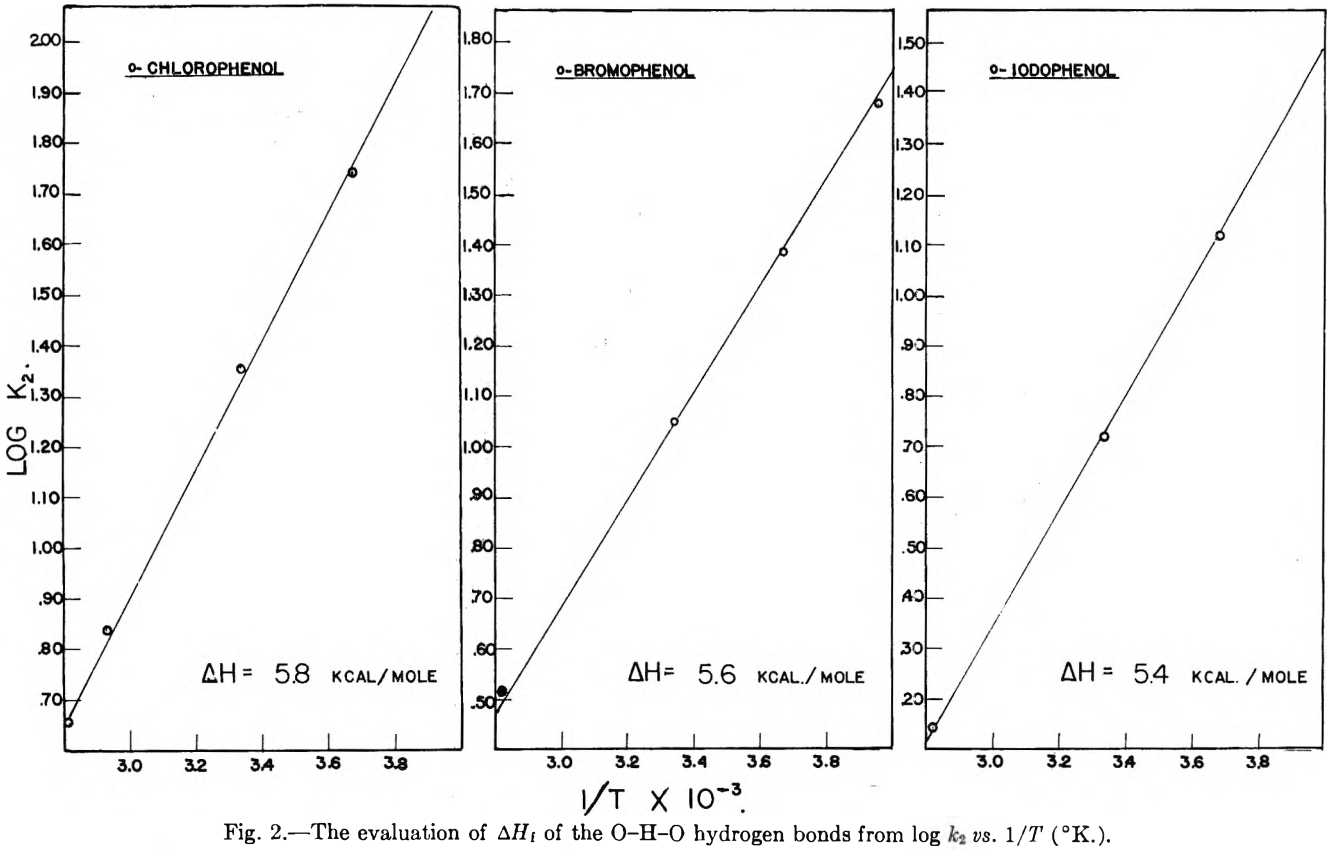

Fig. 2.—The evaluation of ΔH_f of the O–H–O hydrogen bonds from log k_2 *vs.* $1/T$ (°K.).

From (2) we can obtain

$$m_D = \frac{(\delta_{Mc} - \delta_{M\infty})a}{(\delta_{TD} - \delta_T) + (\delta_{Mc} - \delta_{M\infty})} \qquad (4)$$

Let

$$A = \left[\frac{(\delta_{Mc} - \delta_{M\infty})}{(\delta_{TD} - \delta_T) + (\delta_{Mc} - \delta_{M\infty})}\right]$$

Expression 4 shows that the moles of dimer formed is approximately proportional to the number of moles of phenol, "*a*." If the value of m_D in eq. 4 is substituted into the K_2 expression (1), noting that

$$m_c = \left(\frac{a}{1 + K_1}\right)$$

the value of K_2 becomes (neglect term in K_1^2 and A^2)

$$K_2 = \frac{A(1 + 2K_1)}{K_1} \times \left[\frac{(a + m_s)}{a}\right]$$

The values of A and K_1 can be obtained from the experimental data in the previous paper.[1] The magnitude of $(\delta_{TD} - \delta_T)$ is taken as 8 p.p.m. (320 c.p.s.) from the chemical shift change accompanying the formation of an O–H---O hydrogen bond.[1] The K_2's obtained at the lower temperatures are shown in Table II for a concentration of 1 mole %. The value of the enthalpy of formation of the dimer OH---O hydrogen bond should be independent of the *ortho*-halo-phenol if the analysis is correct. The slope of the chemical shift–concentration curve with temperature is quite small at the higher temperatures and so the best values of ΔH_f are obtained from the lower temperatures.[1] The values obtained from data in Table II for *ortho*-chloro-, bromo-, and iodophenol in CS_2 are shown in Fig. 2. These have an uncertainty of approximately 500 cal./mole^{-1}.

These values are appropriate for O–H---O hydrogen bonds and are remarkably independent of the particular phenol.

The Variable Temperature Studies of 2,6-Substituted Phenols.—In phenol itself the rotation of the –OH group about the C–O bond is hindered because of conjugation effects with the π-electrons in the ring. The twofold barrier has been estimated by infrared methods to be 3.3 kcal. mole^{-1}.[11] In the *ortho*-halo-phenols[1] the twofold barrier becomes unsymmetrical because the energy of the *cis* form is lowered by the binding energy of the intramolecular hydrogen bond. In a non-polar solvent at infinite dilution phenol should have a temperature invariant –OH chemical shift. The chemical shift is strongly concentration dependent because of intermolecular hydrogen bonding.[12] The singly substituted

TABLE II

VALUES OF EQUILIBRIUM CONSTANTS FOR DIMERIZATION OF *ortho*-HALO PHENOLS IN DILUTE CARBON DISULFIDE SOLUTION

Compound	Temp., °K.	$K_2 = \frac{[cis\text{–}trans\ \text{dimer}]}{[cis][trans]}$ mole fraction units
o-Chlorophenol	355	4.54
	341	7.04
	300	23.48
	272	55.08
o-Bromophenol	300	11.22
	272	24.10
	253	46.89
o-Iodophenol	355	1.42
	300	5.24
	272	12.9

(11) J. C. Evans, *Spectrochim. Acta*, **16**, 1382 (1960).

(12) C. M. Huggins, G. C. Pimmentel, and J. N. Shoolery, *J. Phys. Chem.*, **60**, 1311 (1956).

ortho-halo-phenols also form intermolecular associations *via* the *trans* form but the competition with the intramolecular hydrogen bonds makes the concentration dependence of chemical shift much smaller.[1] The unsymmetrical twofold barrier causes the value of $\delta_{M\infty}$ to vary with temperature,[1] even in the case of fluorophenol where the intramolecular hydrogen bond is difficult to detect. In a symmetrical 2,6-disubstituted phenol the twofold internal barrier to rotation is again symmetrical. Intermolecular hydrogen bonding is blocked by steric effects so that no concentration or temperature dependence of chemical shift is expected. In unsymmetrical 2,6-substituted halo phenols no concentration dependence of chemical shift is observed but the temperature dependence arises because the twofold barrier to C–O–H rotation is not symmetric. The temperature dependence is a function of the difference in energy of the two possible intramolecular hydrogen bonds. The strength of the intramolecular hydrogen bonds has been determined.[1] These are 1650 cal. mole^{-1} in *o*-iodophenol, 2141 cal. mole^{-1} in *o*-bromophenol, and 2356 cal. mole^{-1} in *o*-chlorophenol. The barrier to rotation will be nearly symmetrical in the case of 2-chloro-4,6-dibromophenol and 2-chloro-4,6-diiodophenol and so the temperature dependence is quite small. The temperature independent region above 50–70° can be ascribed to equal population of two torsional levels whose energies differ by less than 500 cal.$^{-1}$ in a high temperature approximation. It is significant that the temperature invariant chemical shift occurs at a lower temperature for 2-chloro-4,6-dibromophenol, where the energy difference of the two hydrogen bonds is smallest.

The temperature dependence of chemical shifts in the 2-fluoro-4,6-dibromo- and 2-fluoro-4,6-diiodophenols is much greater. *o*-Fluorophenol has an internal hydrogen bond which has such low binding energy that its presence may only be inferred by a slight temperature dependence of the infinite dilution shift in CS_2.[1] The twofold barrier will differ in minimum energy by approximately 2000 cal. mole^{-1} and this results in a greater temperature dependence of chemical shift, as shown in Fig. 1.

Acknowledgment.—This research was supported by a grant from the Petroleum Research Fund of the American Chemical Society (to L. W. R.).

SELF-DIFFUSION OF OXYGEN IN LEAD OXIDE[1]

BY BARBARA A. THOMPSON

General Engineering Laboratory, General Electric Company, Schenectady, N. Y.

AND ROBERT L. STRONG

Department of Chemistry, Rensselaer Polytechnic Institute, Troy, N. Y.

Received August 10, 1962

Self-diffusion coefficients for oxygen ions in solid PbO have been determined at various temperatures between 500 and 650°. The method employed was the measurement of the rate of isotopic exchange between the solid oxides and oxygen gas enriched in the stable isotope of mass 18. The exchange rates were determined using mass spectrometry. The anion diffusion coefficients were compared with published data on cation diffusion to characterize the defect structure of the oxide and to establish the mechanism of oxidation of metallic lead. The diffusion coefficients can be expressed in terms of the Arrhenius equation: $D^{O}_{PbO} = (5.39 \times 10^{-5}) \exp(-22{,}400/RT)$ cm.^{2}/sec. The data show that in PbO, anions are one or more orders of magnitude more mobile than cations and indicate that the oxidation of liquid lead is controlled by diffusion of anions, probably by a vacancy mechanism, through the solid PbO coating.

Introduction

The determination of self-diffusion coefficients in solid oxides not only leads to greater understanding of the nature of the defect structures of the oxides, but also provides a means of correlating the theoretical mechanisms for diffusion-controlled oxidation of metals with experimental rate data. Many cation self-diffusion coefficients have been determined using radioactive tracer techniques, but no anion measurements were made until fairly recently because no long-lived radioactive isotope of oxygen exists. With the increased availability of oxygen enriched in the stable isotope of mass 18, anion self-diffusion coefficients have been determined in a number of oxides, including CdO,[2] Cu_2O,[3] Fe_2O_3,[4] and MgO,[5] as well as others. For those oxides whose cation diffusion coefficients were already known, it was possible to correlate theoretical rate constants for the diffusion-controlled oxidation of the particular metal with experimental results and thus check proposed mechanisms. It was the purpose of this work to determine anion self-diffusion coefficients for lead oxide whose cation diffusion has been studied,[6,7] comparing the combined data with current theories of the nature of the defect structure and the mechanism of oxidation of metallic lead. This oxide is of particular interest because the observed cation diffusion rate is too low to explain observed rates of oxidation of lead.

Experimental Procedures

General Principles.—Diffusion coefficients were determined by measuring the rate of isotopic exchange between oxygen gas enriched in oxygen-18 and the solid oxide having the normal oxygen isotopic ratio. It is assumed that the rate-limiting step is solid-state diffusion of the oxide ions and not surface exchange. This is the same general method used for the anion diffusion measurements cited above.[2-5] Crank[8] has published solutions to Fick's

(1) Based on a thesis submitted by Barbara A. Thompson to the Graduate School, Rensselaer Polytechnic Institute, in partial fulfillment of the requirements for the degree of Doctor of Philosophy. (Available from University Microfilms, Ann Arbor, Michigan.)

(2) R. Haul and D. Just, *Z. Elektrochem.*, **62**, 1124 (1958).

(3) W. J. Moore, Y. Ebisuzaki, and J. A. Sluss, *J. Phys. Chem.*, **65**, 1438 (1958).

(4) W. D. Kingery, D. C. Hill, and R. P. Nelson, *J. Am. Ceram. Soc.*, **43**, 473 (1960).

(5) Y. Oishi and W. D. Kingery, *J. Chem. Phys.*, **33**, 480 (1960).

(6) R. Lindner, *Arkiv Kemi*, **4**, 385 (1952).

(7) R. Lindner and H. N. Terem, *ibid.*, **7**, 273 (1954).

law for these experimental conditions which he calls "uptake of a solute from a stirred solution of limited volume." The sample geometries for which he has developed solutions include spheres of known radius, cylinders of known radius, and infinite plane sheets of known thickness. For the latter, the solution, expressed in terms of M_t, the total amount of solute in the sheet at time t, as a fraction of M_∞, the amount of solute in the sheet at infinite time, is

$$\frac{M_t}{M_\infty} = 1 - \sum_{n=1}^{\infty} \frac{2\alpha(1+\alpha)}{1+\alpha+\alpha^2 q_n^2} e^{-Dq_n^2 t/a^2} \quad (1)$$

where $2a$ is the thickness of the sheet, the q_n are the non-zero positive roots of

$$\tan q_n = -\alpha q_n \quad (2)$$

and α is the ratio of volumes of the solution and the sheet. Crank has plotted a family of curves showing M_t/M_∞ as a function of $(Dt/a^2)^{1/2}$ for various values of the fraction of the solute finally taken up by the sheet. Similar families of curves are given for cylinders and spheres. Thus values of Dt/a^2 can be obtained for each experimental value of M_t/M_∞. A plot of these as a function of time yields a straight line whose slope is D/a^2. The linearity of this curve provides a check of whether the exchange is diffusion controlled.

Preparation of Materials.—Small spheres of PbO were prepared in a manner similar to that described by Kingery and co-workers.[9] The pure, reagent grade powder was dropped vertically from a spatula through the horizontal flame of a gas–oxygen glassblowing torch. In passing through the flame some of the powder fused into small spheres. After flaming, the oxide powder was graded by passing through a series of standard mesh screens. The spheres were then separated from the unfused powder by means of an inclined plane. The diameters of the spheres ranged from 90 to 160 μ. The range in diameter within each batch was less than $\pm 10\%$.

Each batch of spheres was annealed by heating for at least 24 hr. in air at the temperature of the diffusion experiments. X-Ray diffraction analysis confirmed that the lead oxide was in the yellow high-temperature or orthorhombic form in all cases.

Enriched oxygen containing about 6% oxygen-18 was obtained in the form of water from the Weizmann Institute of Science. Conversion to oxygen gas was accomplished electrolytically, following the addition of a small amount of sodium hydroxide to provide conductivity. Mass spectrometric analysis of the gas showed the presence of traces of hydrogen, water, and air.

Determination of Exchange Rates.—The apparatus used for the determination of exchange rates was very similar to that of Haul and Just.[2] The oxide sample was placed in a mullite furnace tube which was sealed to the rest of the system with Apiezon black wax. The tube was heated in air to the desired temperature using a small Nichrome-wound tube furnace. The mullite tube was used because of the high rate of oxygen exchange with quartz.[2,9] Heating was continued for several hours or overnight to assure that a constant temperature was attained. The temperature was controlled to $\pm 3°$ with a Leeds and Northrup Micromax controller–recorder. After the initial heating period, the system was evacuated to a pressure of about 1 μ and enriched oxygen was introduced from the reservoir to a pressure of about 100 mm. Gas samples were taken at intervals by means of an incompletely bored stopcock. The sample volume removed in this way was about 0.1% of the total gas volume so that a number of samples could be removed without appreciably changing the amount of gas present in the system. The procedure thus meets the conditions necessary for application of the Crank solutions.

The gas samples were analyzed with a General Electric analytical mass spectrometer. The isotopic content was determined by taking the ratio of the peaks at masses 34 and 32. To compensate for fluctuations in the instrument, at least five duplicate measurements of the 34 and 32 peaks were made for each sample. In general, the precision thus obtained was $\pm 0.05\%$ or better. "Blank" runs carried out with no oxide present showed that up to 1000° no appreciable exchange occurred with the mullite tube so that it was not necessary to correct the data for "background."

Diffusion coefficients were determined from the experimental isotopic ratios in the following way. Since diffusion took place rapidly, it was feasible to let the exchange continue until equilibrium was complete and thus determine experimentally the oxygen-18 concentration at infinite time. The ratios M_t/M_∞ needed for the Crank solutions were then calculated from the relationship

$$\frac{M_t}{M_\infty} = \frac{C_0 - C_t}{C_0 - C_\infty} \quad (3)$$

where C_0, C_t, and C_∞ are the isotopic ratios at zero time, time t, and infinite time, respectively. In this case it is unnecessary to know the weight of oxide or any of the dimensions of the apparatus. The only information required in addition to the isotopic ratios is the radius of the spheres.

In addition to these ratios it is also necessary to know the final fractional uptake of oxygen-18, which is given by

$$F = \frac{C_0 - C_\infty}{C_0} \quad (4)$$

Values of $(Dt/a^2)^{1/2}$ corresponding to each value of M_t/M_∞ can now be found readily from Crank's curves and D determined from the slope of a plot of Dt/a^2 *vs.* t.

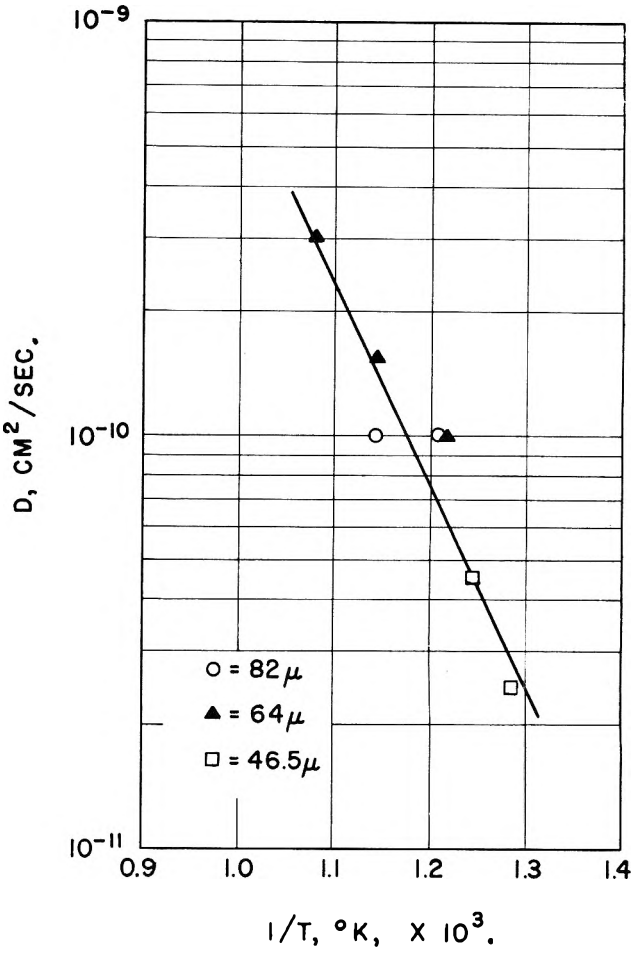

Fig. 1.—Self-diffusion coefficient of oxygen in PbO as a function of temperature. The legend refers to sphere diameter.

Results

Seven separate diffusion runs were made with PbO spheres at temperatures from 500 to 650°. The transition temperature between the orthorhombic PbO used and the red, tetragonal form is 488° and no experiments were carried out below this temperature. In every case a plot of Dt/a^2 as a function of time gave a straight line showing that the exchange was controlled by diffusion within the solid and not by surface effects or other extraneous factors. Three sets of spheres of different diameters were used for these experiments. Within the experimental error the results are inde-

(8) J. Crank, "Mathematics of Diffusion," Clarendon Press, Oxford, 1956.
(9) W. D. Kingery, J. Pappis, M. E. Doty, and D. C. Hill, *J. Am. Ceram. Soc.*, **42**, 393 (1959).

pendent of sphere diameter, providing further evidence that solid-state diffusion controlled the rate of exchange. In Fig. 1 the D values obtained in each experiment have been plotted as a logarithmic function of $1/T$. A least squares fit yields a straight line whose equation is

$$D^{O}_{PbO} = (5.39 \times 10^{-5}) \exp(-22{,}400/RT) \text{ cm.}^2/\text{sec.}$$

The probable errors in the activation energy and in D_0 are ± 1 kcal. and $\pm 0.45 \times 10^{-5}$ cm.^{2}/sec., respectively.

Discussion

The diffusion coefficients for oxygen in lead oxide are in every case at least one order of magnitude higher than those found by Lindner and Terem[7] for diffusion of lead in lead oxide. Lindner and Terem have shown that cation diffusion takes place too slowly to account for the observed oxidation rates of lead. Thus, the results of the present study immediately suggest that anion diffusion may be rate limiting. To test this hypothesis, rate constants were calculated for several temperatures by both the Wagner[10] and Mott–Gurney[11] methods. The Wagner equation for rate of growth of oxide film in equivalents/cm. sec. is

$$\frac{dn}{dt} = c_{eq} \int_{a_x'}^{a_x''} \left[\frac{Z_c}{|Z_A|} D_c + D_A \right] d \ln a_x \quad (5)$$

where

$c_{eq} = Z_c C_c = Z_A C_A$ = concn. of metal or non-metal ions in equiv./cc.; D_i is the self-diffusion coefficient of particles of type i; Z_i is the charge of particles of type i; a_x' is the activity of oxygen at metal–oxide interface; and a_x'' is the activity of oxygen at oxide–gas interface.

For purposes of calculation, a_x'' is taken as the experimental oxygen pressure and a_x' as the dissociation pressure of the oxide at the temperature of the experiment. This can be converted readily to units of k_p since[12]

$$\frac{dn}{dt} = {}^1/_2 \, V_{eq} \left[\frac{Z_A}{M_A} \right]^2 k_p \quad (6)$$

where V_{eq} is the volume of one equivalent of oxide and M_A is the atomic weight of oxygen. The PbO dissociation pressures required for this calculation were determined from thermodynamic data.[13]

The Mott–Gurney equation is

$$k_p = 4 D_i \rho^2 f_O^2 \quad (7)$$

where D_i is the diffusion coefficient for particles of type i; ρ is the density of the oxide; and f_0 is the weight fraction of oxygen in the oxide. Anion diffusion was assumed to predominate for calculations using this equation. Calculated and experimentally observed rate constants are listed in Table I. The agreement is not exact but is reasonably good in view of the assumptions involved and the variations in the literature values of k_p. Thus the conclusion that oxidation of lead is controlled by anion diffusion appears justified.

(10) C. Wagner, in "Atom Movements," Am. Soc. for Metals, Cleveland, Ohio, 1951, pp. 153–173.

(11) N. F. Mott and R. W. Gurney, "Electronic Processes in Ionic Crystals," 2nd Ed., Clarendon Press, Oxford, 1948, pp. 249–255.

(12) O. Kubaschewski and B. E. Hopkins, "Oxidation of Metals and Alloys," Butterworths Scientific Publications, London, 1953, pp. 120–124.

(13) W. M. Latimer, "Oxidation Potentials," 2nd Ed., Prentice-Hall, Inc., Englewood Cliffs, New Jersey, 1952, p. 152.

TABLE I

PARABOLIC RATE CONSTANTS FOR OXIDATION OF LEAD

	k_p (g.^{2} cm.$^{-4}$ sec.$^{-1}$)		
T, °C.	Observed	Calcd. according to eq. 7	Calcd. according to eq. 5 and 6
500	7.9×10^{-11}[a]	5.0×10^{-11}	2.7×10^{-11}
525	9.3×10^{-11}[a]	8.4×10^{-11}	4.5×10^{-11}
550	2.0×10^{-10}[a]; 1.9×10^{-9}[b]	1.6×10^{-10}	8.6×10^{-11}
600	6.1×10^{-9}[b]; 8×10^{-10}[c]	3.8×10^{-10}	1.6×10^{-10}

[a] Reference 14. [b] Reference 15. [c] Reference 7.

The value of 22.4 kcal. obtained for the activation energy for anion diffusion is unusually low and deserves some comment. The activation energy for diffusion in solids is generally considered to be the sum of the energy required for defect formation and the energy required to move the defect. The former has been determined for a variety of types of crystals to be of the order of 0.5–0.7 e.v. Assuming a comparable energy for defect formation in PbO leads to a value for the energy of motion which is extremely low. The crystal structure of PbO is an unusual one, consisting of layers of lead ions and oxide ions. Evidently, motion of oxide ions through this layer structure requires little energy. Since the activation energies for anion and cation diffusion are quite different (22.4 and 66 kcal., respectively), different mechanisms seem to be involved.

It is of interest to know whether diffusion is occurring by means of vacancies or by an interstitial mechanism. Very few conductivity data are available in the literature on which to base a decision. From the value of 22.4 kcal. for the activation energy for anion diffusion, which is much lower than that reported for zinc in ZnO[16,17] whose defect structure is believed to consist of interstitial zinc ions, and is more nearly comparable to the values reported for Co^{+2} in CoO and Fe^{+2} in FeO[18] where a vacancy mechanism is believed to predominate, it appears likely that oxygen diffusion in PbO takes place by a vacancy mechanism. However, further work on the pressure dependence of diffusion and conductivity would be very helpful in establishing the nature of the defect structure more precisely.

It is fairly unusual to observe anion diffusion in solid oxides occurring more rapidly than cation diffusion; however, it should be noted that, in contrast to most of the oxides studied to date, the ionic radii of the Pb^{+2} and O^{-2} ions are identical, the usual situation being a cation with a much smaller ionic radius. Thus, in PbO, considerations of size and mass alone would lead us to expect more rapid anion diffusion.

Conclusions

The gas–solid exchange technique has been shown to be a very satisfactory method of determining anion self-diffusion coefficients in solid oxides. The method has great experimental simplicity as compared to the more familiar sectioning techniques.

The results show that for PbO the anions are much more mobile than the cations and that the oxidation

(14) W. Gruhl, *Z. Metallkunde*, **40**, 225 (1949).

(15) E. Weber and W. M. Baldwin. *Trans. AIME*, **194**, 854 (1952).

(16) E. A. Secco and W. J. Moore, *J. Chem. Phys.*, **26**, 942 (1957).

(17) W. J. Moore and E. L. Williams, *Discussions Faraday Soc.*, **28**, 86 (1959).

(18) R. E. Carter and F. D. Richardson, *Trans. AIME*, **200**, 1244 (1954)

of lead is controlled by anion diffusion. The low value of the activation energy indicates that diffusion proceeds by a vacancy mechanism rather than by motion of interstitial oxygen ions. However, further work on the pressure dependence of diffusion and conductivity should be carried out to provide greater insight into the defect structure of this oxide.

Acknowledgment.—The authors acknowledge with thanks much helpful advice and criticism given by Professor W. H. Bauer, Rensselaer Polytechnic Institute, and by G. P. Schacher, J. R. Gambino, and W. C. Hagel, of the General Electric Company. It is a pleasure to thank C. B. Murphy and H. R. Schmidt for their encouragement and support.

AN EXPERIMENTAL STUDY OF ADSORPTION CHROMATOGRAPHY WITH A NON-LINEAR ISOTHERM USING THE SYSTEM ISOBUTYLENE–ACTIVATED ALUMINA

BY R. D. OLDENKAMP AND G. HOUGHTON

Chemical Engineering Department, Division of Engineering Research, University of Pittsburgh, Pittsburgh, Pennsylvania

Received August 13, 1962

The effects of temperature, flow rate, sample size, and weight of adsorbent on retention time and exit composition are investigated experimentally in gas–solid chromatography for the system isobutylene–alumina. The observed phenomena are interpreted by a model that takes into account the curvature of the adsorption isotherm at low surface coverages.

Introduction

The measurement of transport times in gas–solid chromatography[1-4] as a function of temperature has been used to determine heats of adsorption at low coverages while similar measurements in gas–liquid chromatography[5] have been used to obtain heats of solution. In these chromatographic methods it is assumed that the partial pressures of solute in the mobile phase are so low that Henry's law is obeyed. However, for the non-uniform surface of a high area powder the distribution of sites of various energy conceivably could produce a detectable non-linearity in the adsorption isotherm, even at the low coverages expected in gas–solid chromatography. Such curvature as well as stepwise adsorption has been observed by Lopez-Gonzalez, *et al.*,[6] whose measurements for N_2 and A on graphite were carried out at relative pressures ranging from unity to as low as 10^{-8}, corresponding to extremely low coverages. In this connection a recent theoretical analysis[7] has shown that a non-linearity in the adsorption isotherm can have an appreciable effect on the shape and position of the elution band at low adsorbate concentrations if the elution time is long enough, which is true for most practical cases. The purpose of the present work therefore was to investigate some of the factors affecting the use of the chromatographic method for the measurement of heats of adsorption. The system isobutylene-alumina was used since the isotherms at low coverages are concave toward the pressure axis and the isosteric heats of adsorption already have been obtained by static measurements[8] for surface coverages as low as 6%.

(1) S. A. Greene and H. Pust, *J. Phys. Chem.*, **62**, 55 (1958).
(2) P. E. Eberly, Jr., *ibid.*, **65**, 68 (1961).
(3) P. E. Eberly, Jr., and E. H. Spencer, *Trans. Faraday Soc.*, **57**, 289 (1961).
(4) S. Ross, J. K. Saelens, and J. P. Olivier, *J. Phys. Chem.*, **66**, 696 (1962).
(5) J. E. Funk and G. Houghton, *J. Chromatog.*, **6**, 193, 281 (1961).
(6) J. de D. Lopez-Gonzalez, F. G., Carpenter, and V. R. Deitz, *J. Phys. Chem.*, **65**, 1112 (1961).
(7) G. Houghton, *ibid.*, **67**, 84 (1963).
(8) R. D. Oldenkamp and G. Houghton, *ibid.*, **67**, 303 (1963).

Theory

In the evaluation of heats of adsorption by chromatography it is assumed that a linear isotherm of the form $n = K_0 + K_1C$ is operative, where n represents the moles of adsorbate per unit volume of packed adsorbent and C is the moles of solute per unit volume of mobile phase. The retention time, t_{RO}, for linear chromatography is then found to be of the form[2-5,7]

$$t_{RO} = \frac{L}{U} = \frac{L}{u}\left(1 + \frac{K_1}{\epsilon}\right) \qquad (1)$$

where L is the length of the column, ϵ the void fraction, and u is the interstitial fluid velocity. Thus $U = u/(1 + K_1/\epsilon)$ is the velocity of the solute peak through the adsorption column. The apparent retention time t_{RO} thus is inversely proportional to the eluent velocity and directly proportional to the length (weight) of adsorbent.

For a non-linear isotherm of the type $n = K_0 + K_1C + K_2C^2$ it has been shown that, in the absence of axial dispersion, a fully developed chromatogram has a triangular shape with leading or trailing edges that are sharp, depending upon whether K_2 is negative or positive, respectively (*cf.* Houghton,[7] Fig. 2c). The peak or apex of the triangular band is defined by the point (ξ_3, C_3) where $\xi = z - Ut$, with z as the axial distance from the center of the initial pulse. Since most adsorption isotherms encountered in practice will be of type II and concave to the C-axis at low coverages, then K_2 will be negative, so that setting $z = L$ and taking $\lambda = 2K_2/\epsilon(1 + K_1/\epsilon) < 0$ in eq. 22 given by Houghton,[7] the retention time, $t = t_{R-}$, for the apex of the triangular band is readily found to be

$$t_{R-} = \frac{L}{u}\left(1 + \frac{K_1}{\epsilon}\right) - \left[\frac{(2|\lambda|C_0Ut_{R-}L_0)^{1/2} - {}^1/_2L_0}{u}\right]\left(1 + \frac{K_1}{\epsilon}\right) \qquad (2)$$

For a fully developed elution band $(2\ |\lambda|C_0\ Ut_{R-}\ L_0)^{1/2}$

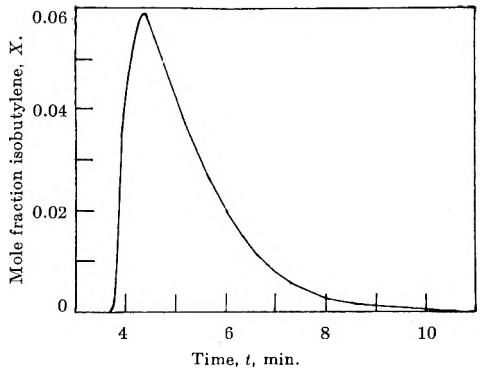

Fig. 1.—Typical elution curve at 60° for a 5-cc. sample with Q = 58.8 cc./min., w = 8.98 g., and X_0 = 1.00.

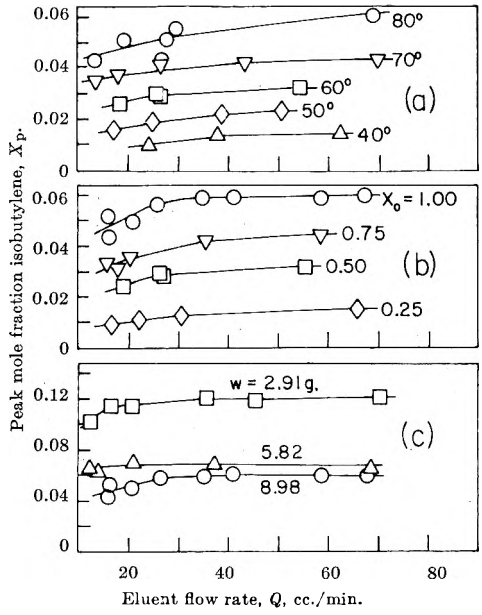

Fig. 2.—Peak mole fractions of isobutylene, X_p, as a function of flow rate, Q, for 5-cc. samples: (a) effect of temperature for w = 8.98 g. and X_0 = 0.50; (b) effect of mole fraction isobutylene in the initial sample, X_0, at 60° for w = 8.98 g.; (c) effect of weight of alumina, w, at 60° for X_0 = 0.50.

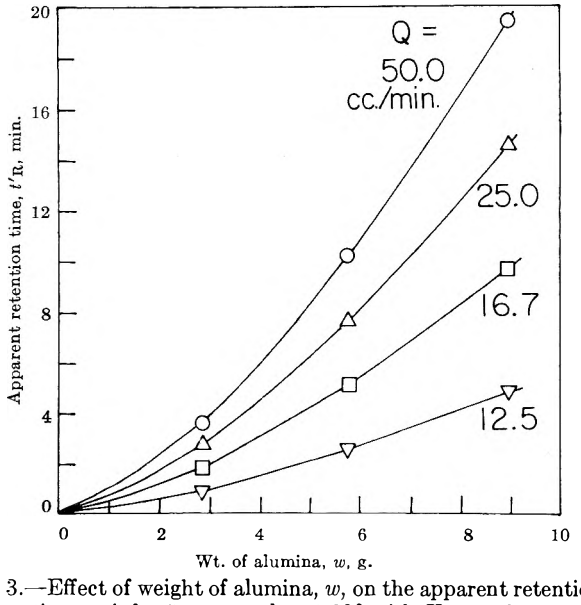

Fig. 3.—Effect of weight of alumina, w, on the apparent retention time, t_R', for 5-cc. samples at 60° with X_0 = 1.00.

> $^1/_2L_0$, so that the peak for a negative K_2 will appear earlier than a peak with $K_2 = 0$. However, the effects of both partial development and axial dispersion[7] will be to cause the residence time to become greater than t_{R-} when $\lambda < 0$. Thus the residence time, t_R, actually observed in practice for a type II isotherm at low coverages will lie in the interval $t_{R-} \leqslant t_R \leqslant t_{RO}$, where t_{RO} and t_{R-} are given by eq. 1 and 2, respectively. It is important to observe from eq. 2 that the residence time for an adsorbate with a non-linear isotherm is a complicated function of the non-linearity represented by the parameter λ, the initial concentration C_0, and the initial pulse length L_0. Although eq. 2 is only valid for $|\lambda C_0| << 1$, non-linear effects can still be appreciable if the residence time, t_{R-}, is long enough.[7] Furthermore, because of the presence of t_{R-} on both sides of eq. 2, the residence time for a non-linear isotherm probably will not be a linear function of column length L, and hence weight of adsorbent, as predicted by eq. 1.

Experimental

With the exception of the sample injection system, the apparatus used to measure residence times for the isobutylene–alumina system was the same as that described previously.[5]

The chromatographic column was a 7 mm. i.d. Pyrex tube about 100 cm. long. The alumina rested on a plug of glass wool and the remainder of the column was filled with 20–30 mesh glass beads that exhibited no detectable adsorption of isobutylene under the experimental conditions. The carrier gas, helium, flowed continuously through the bed at rates in the range 7–70 cc./min., the flow being measured to within 0.5% by a soap bubble flow meter. To virtually eliminate measurement lags and avoid distortion of the pulse shape, the thermal conductivity detector was the bare tungsten filament of a Westinghouse No. 1819 miniature light bulb located directly in the gas stream only 3.5 cm. from the end of the packed section. A similar filament was placed about 100 cm. downstream in the same tube to compensate for flow variations. The two filaments formed two arms of a chopper-stabilized Wheatstone bridge, the unbalance voltage being recorded on a Leeds and Northrup Azar recorder with a time constant of 1 sec. and a chart speed of 0.5 in./min. The column and detectors were surrounded by a water jacket provided with water circulating from a thermostated bath; the column temperature could be adjusted and maintained at any temperature in the range 20–80° to within ±0.05°.

By making separate measurements of the pressure drop across the column completely filled with glass beads and then completely filled with alumina using a water manometer, it was possible to ascertain that corrections for pressure drop were less than 1%. Nevertheless, the flow rates, Q, in cc./min. were corrected to the mean pressure (usually close to 76 cm.) and temperature in the adsorbent section.

The transport times for a non-adsorbing gas were first measured as a function of flow rate by injecting samples of nitrogen directly into the glass beads at the top of the column using a 10 cc. hypodermic syringe. Retention times, as a function of flow rate, were then measured by injecting samples of pure isobutylene and isobutylene–helium mixtures into the same column. Apparent retention times, t_R', were calculated by subtracting the nitrogen transport times, L/u, from the retention times, t_R, observed for isobutylene at the same flow rate. The present method of injecting the samples into glass beads was found to be very reproducible and an improvement over the unpacked slug-chamber used previously,[5] the reason presumably being that the flow pattern in the slug-chamber will be the parabolic velocity distribution of an open tube rather than that of a packed bed, so that the sample may enter the column unmixed, perhaps in the form of a "Poiseuille tongue."

The adsorbent was the same as that used by Oldenkamp and Houghton[8] for the measurement of the isosteric heats of adsorption of isobutylene, being 28–48 mesh Alcoa F1 alumina with a BET area of 199 m.²/g. Each sample of alumina was heated to 200° for 2 hr. and cooled in a desiccator before it was introduced into the column. The column was filled with the aid of a vibrator to ensure the same degree of packing in each case. Weights of 2.91, 5.82, and 8.98 g. of alumina corresponding to packed heights of 6.3, 9.3, and 18.5 cm., respectively, were used in the various experiments. The adsorbate was Matheson C.P. grade isobutylene (2-methylpropene). Mixtures containing 25, 50, and 75 volume % isobutylene with helium were prepared over mercury in a gas buret.

Because the thermal conductivity detector was a bare tungsten filament directly exposed to the main carrier gas stream, it was subject to the effects of local random disturbances in the flow. In order to optimize the sensitivity in relation to the effects of local fluid turbulence over the complete ranges of temperature and flow rate, it was found that the lower limit of sample size was 1 cc. for 100% isobutylene and 5 cc. for 25% isobutylene in helium. Nevertheless, the use of a bare filament close to the exit of the column made it possible to obtain a close representation of the true shape of the band.

Results and Discussion

Figure 1 is a typical elution curve of mole fraction isobutylene leaving the column *vs.* time showing a leading edge that is steeper than the trailing edge, indicating that the adsorption isotherm is concave toward the C-axis, confirming both the theoretical analysis[7] and the static adsorption measurements for the isobutylene–alumina system.[8] Although the elution curves tended to become more symmetrical at lower temperatures, lower flow rates, and lower initial mole fractions of isobutylene in the sample, Fig. 1 is quite representative of the shapes observed in practice, being calculated by first calibrating the recorder scale with samples of isobutylene of known initial size.

The peak mole fractions, X_p, leaving the column are shown in Fig. 2 and indicate that lower coverages are obtained at lower temperatures and flow rates for large column lengths. The effect of adsorbent weight (column length), w, on peak mole fraction is non-linear, with a larger difference between the 2.91 and 5.82 g. columns than between the 5.82 and 8.98 g. columns, indicating that most of the reduction in concentration occurs near the top of the bed. It would appear that as the sample enters the column, the adsorbate partial pressure is rapidly reduced by adsorption and then decreases only slowly for the rest of the bed. Thus the surface coverage can be expected to be relatively small throughout most of the bed. The peak compositions of Fig. 2 combined with the static adsorption measurements obtained previously[6] show that for the 8.98 g. bed of alumina the surface coverages are less than about 12, 10, 8, and 4%, respectively, for initial samples containing 100, 75, 50, and 25 mole % isobutylene for all temperatures in the range 40–80°. Another interesting effect in Fig. 2b is that of dilution of the initial sample, in which the peak mole fractions leaving the column, $X_0 = 22{,}400C_0$, are roughly in proportion to the mole fraction of isobutylene at the inlet, a relationship that should be exactly true for a linear isotherm as discussed previously.[5]

That the apparent retention time, t_R', is a non-linear function of the column length or weight of alumina in Fig. 3 also indicates that the non-linearity of the isotherm is having an appreciable effect even at coverages below 8%. Similarly, the variation of retention time, t_R', with sample volume, V_s, in Fig. 4 also is explainable by the non-linearity, since any error in transport time due to the location of the center of the sample in the injection procedure is less than 0.2 min. compared with a total variation of 2.7 min. For a linear adsorption isotherm with instantaneous equilibrium and no axial dispersion, the residence time should be independent of the sample size.

The plots of t_R *vs.* $1/Q$ in Fig. 5 are linear within experimental error where the carrier gas flow rate, Q, is related to the interstitial velocity, u, and the cross-sectional area of the column, A, by $Q = u\epsilon A$. This

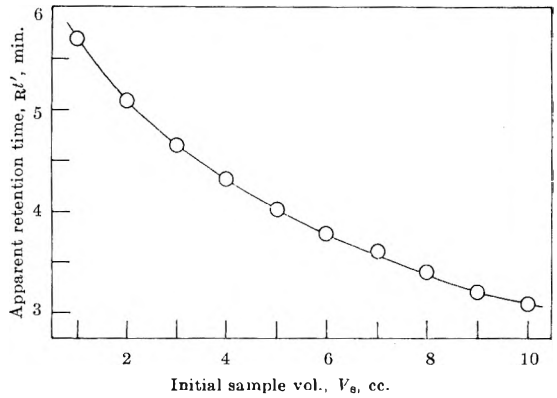

Fig. 4.—Effect of initial sample volume, V_s, on the apparent retention time, t_R', at 60° with Q = 49.2 cc./min., w = 8.98 g., and X_0 = 1.00.

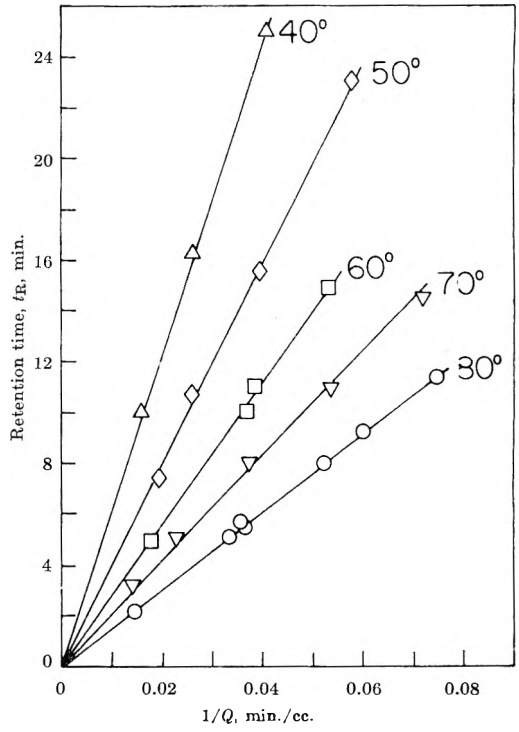

Fig. 5.—Plot of retention time, t_R, *vs.* reciprocal flow rate, $1/Q$, for 5-cc. samples with w = 8.98 g. and X_0 = 0.50.

linearity is in accordance with eq. 2; the product Ut_{R-} in the term arising from the non-linearity will be insensitive to velocity u and hence flow rate Q since, to a first approximation, U is directly proportional to u while t_{R-} is inversely proportional to u. However, the non-linearity in the adsorption isotherm will cause the slopes of the plots in Fig. 5 to be lower than those predicted by eq. 1 for a linear isotherm.

Figure 6 is a plot of log (V_R'/T) *vs.* $1/T$, where $V_R' = t_R'Q/w$ represents the specific retention volume. Since isosteric heats of adsorption are obtained from static measurements by plotting log p *vs.* $1/T$ for fixed volumes, V (at S.T.P.), of gas adsorbed where p is the partial pressure, then for a linear isotherm $LK_1/u\epsilon = kp_0 \cdot Tw/QT_0$ with T_0 and p_0 corresponding to standard temperature (0°) and pressure (76 cm.). The constant k is the slope of the linear adsorption isotherm of V *vs.* p and is given by $k = B\exp(-q/RT)$. Thus by subtracting the transport time, L/u, eq. 1 may be rearranged into the following form, corresponding to the plots of Fig. 6.

$$\frac{V_R'}{T} = \frac{t_R'Q}{wT} = \frac{p_0B}{T_0}\exp(-q/RT) \qquad (3)$$

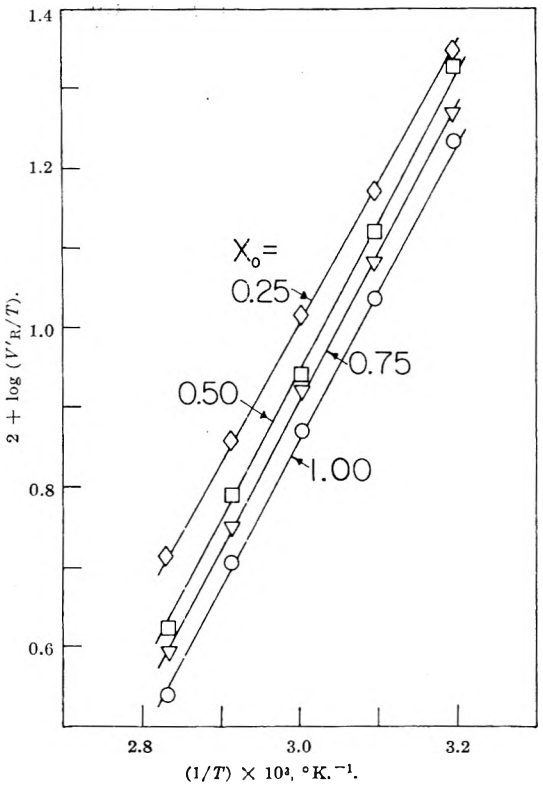

Fig. 6.—Plot of log (V_R'/T) *vs.* $1/T$ for 5-cc. samples with w = 8.98 g.

Thus the slopes of Fig. 6 are $q/2.303R$ if the isotherms are linear and eq. 1 is valid. For samples initially containing 0.25, 0.50, 0.75, and 1.00 mole fraction of isobutylene the corresponding values of the heat of adsorption, q, are 8.1, 8.5, 8.5, and 8.5 kcal./g. mole, respectively, indicating that the slope is relatively unaffected by the non-linearity. However, inspection of Fig. 6 shows that the retention volume and hence the apparent retention time increases as the initial sample becomes more dilute. This finding is in keeping with the shapes of the adsorption isotherms obtained by static methods[8] which show that the slope increases as the adsorbate partial pressure decreases. The exit mole fractions for the initial samples containing 50 and 25 mole % isobutylene correspond to static surface coverages of less than 8 and 4%, respectively, indicating that the isotherms are still appreciably curved at these low coverages. Furthermore, even though the slopes of the log (V_R'/T) *vs.* $1/T$ plots of Fig. 6 do not seem to change much with coverage, yielding heats of adsorption of 8.1–8.5 kcal./g. mole corresponding to maximum coverages in the range 4–12%, these results are only in rough agreement with the values of 9.8–9.5 kcal./g. mole for coverages of 0–12% found in the static measurements of the isosteric heats of adsorption of isobutylene on alumina.[8] The reason for the lower slopes in the chromatographic experiments is probably the correction term in eq. 2 for the non-linearity of the isotherm, which itself is a complicated function of temperature.

Acknowledgment.—R. D. O. is indebted to the Westinghouse Corporation for a Graduate Fellowship.

DIFFUSION RELATIONSHIPS IN THE SYSTEM BENZENE–DIPHENYL AT 25°

BY REGINALD MILLS

Research School of Physical Sciences, Australian National University, Canberra, Australia

Received August 18, 1962

The tracer-diffusion[1] coefficients of both benzene and diphenyl have been measured at 25° in benzene–diphenyl mixtures in the range 0 to 0.33 mole fraction of diphenyl. Use of liquid scintillation counting has enabled coefficients of high precision (±0.3%) to be determined. Various proposed equations relating the mutual and the tracer-diffusion coefficients for binary systems have been tested. A critical analysis of the derivations and limits of validity of these equations is given.

In recent years, a number of equations have been proposed which claim to relate, directly or indirectly, the tracer-diffusion coefficients of the components of binary non-electrolyte mixtures to the corresponding mutual diffusion coefficients. A survey of the literature in this field indicates, however, that there exist no tracer-diffusion data of a sufficiently precise nature to test these various formulations. In part, this is due to the difficulty in counting carbon-14, which is commonly used to label non-electrolytes, with any degree of precision. Most studies where this isotope has been used report coefficients with possible errors of ±5%. Therefore it has been one of the aims of this work to improve the precision of tracer-diffusion measurements by at least an order of magnitude, by employing modern counting techniques.

The benzene–diphenyl system was chosen for study for several reasons. Sandquist and Lyons[2] have measured the differential coefficients of diphenyl in benzene–diphenyl mixtures using an optical method, and these data probably are reliable to ±0.1%. The system also has been studied extensively with regard to its thermodynamic properties by Tompa[3] and Everett and Penney.[4]

Other simplifying features are that association would be expected to be negligible and the molar volumes are practically constant over the concentration range studied.[3]

(1) The use of the term "tracer-diffusion" is to be preferred to "self-diffusion" for describing the diffusion of the labeled components in mixtures. A trace component in an otherwise uniform mixture can diffuse by exchange with components other than its own kind. "Self-diffusion" connotes the exchange of identical species and should be confined to diffusion in the pure component.

(2) C. L. Sandquist and P. A. Lyons, *J. Am. Chem. Soc.*, **76**, 4641 (1954).

(3) H. Tompa, *J. Chem. Phys.*, **16**, 292 (1948).

(4) D. H. Everett and M. F. Penney, *Trans. Roy. Soc.* (London), **A212**, 164 (1952).

Experimental

Materials.—Analar benzene was used without further purification in most experiments. A gas chromatographic analysis of this grade of benzene showed that negligible amounts of impurities were present. For some check experiments, however, Analar benzene was fractionated on a column of 17 theoretical plates and only the middle fraction boiling at the range 79.9–80.1° was collected. The diffusion coefficients measured with the purified benzene were indistinguishable, within experimental error, from those employing the Analar solvent. Sandquist and Lyons[2] also concluded that for diffusion measurements, rigid purification of materials appears to be unnecessary. B.D.H. laboratory reagent grade diphenyl was finely ground and then thoroughly dried in a vacuum desiccator. Its melting point was 69 ± 0.2°.

Two samples of C^{14}-labeled benzene were used and compared, one from the Radiochemical Centre, Amersham, England, and the other from Tracerlab Inc., Waltham, Mass., U.S.A. Labeled diphenyl was supplied by Merck, Sharpe and Dohme of Canada Ltd., Montreal, Canada.

Diphenyl solutions were made up approximately by weight and a pycnometer then was used to measure their density accurately. The concentrations were determined by interpolation on a large graph of the concentration density function for 25° reported by Sandquist and Lyons.[2]

$$d = 0.873141 + 0.024030C - 0.00011007C^2$$

Apparatus.—The magnetically stirred diaphragm cell as developed by Stokes[5] was used for all measurements. Some modifications to the normal type of cell were necessary, however, due to the high volatility of benzene. The bottom compartment was sealed by a polythene stopper which had a fine capillary drilled through it. This capillary widened at its outer end to take a very small plug of the same material. Withdrawal of this small plug at the end of an experiment did not draw liquid through the diaphragm. The top compartment was closed by a finely-ground glass capillary stopper which could be closed with a small ground cap. A glass cup was sealed to the lip of the cell socket which was filled with mercury after the stopper was inserted, thus effectively sealing the ground joint to benzene evaporation. Without this precaution, bubbles were liable to appear in the top compartment. The general filling and sampling procedures were essentially similar to those described by Robinson and Stokes.[6]

Calibration.—The diaphragm cell constant was determined in the normal manner as described in ref. 6 by allowing a solution of 0.5 *M* KCl to diffuse into pure water. After diffusion, the concentrations of the cell compartments were determined very precisely by conductance measurements on a Jones bridge. Duplicate values of these constants agreed to within ±0.1%. There is a slight variation with time, however, due to diaphragm wear and calibrations were made after every eight runs and the constants for individual runs were obtained by interpolation.

Up to this time, it has been assumed that the type of calibration described above should hold for diffusion measurements involving non-aqueous solvents. Our measurements now have confirmed the correctness of this assumption. We have used as a calibrating point the limiting value of the mutual diffusion coefficient of diphenyl in benzene which ought to be identical with the limiting tracer-diffusion coefficient of diphenyl in this solvent. Sandquist and Lyons[2] have made very precise measurements of the mutual coefficients for this system using a Gouy diffusiometer and their values in dilute solution extrapolate to give $D_{AB}^0 = 1.558 \times 10^{-5}$ cm.²/sec., which probably is accurate to ±0.2% (A, diphenyl; B, benzene). In this work, using solutions approximately 1.3×10^{-4} *M* in diphenyl, we have obtained for three runs an average value of $1.554 \times 10^{-5} \pm 0.3\%$ for D_A^*, which is in very good agreement with the mutual value.

Counting Techniques.—Liquid scintillation counting was used because of its precision and high efficiency. The scintillator solution was prepared by dissolving 3 g. of DPO (diphenyloxazole) and 0.3 g. of POPOP (1,4-bis-2-[5-phenylaxozolyl]-benzene) in 1 l. of benzene. For light pulse collection, an EMI 9514S photomultiplier tube was used in conjunction with a Franklin linear amplifier and a Tracerlab "Compumatic" scaler.

All power supplies were highly stabilized. Samples were counted in an air-conditioned room and at night, to ensure that fluctuations due to temperature change and from the mains were at a minimum. By these measures and by appropriate settings of the discriminator levels on the linear amplifier, the background rate could be kept to less than 0.5% of the counting rate. Total counts on a given sample were always greater than 10^6 so that statistical counting error would be expected to be less than ±0.1%.

The glass counting vials used in this technique vary slightly in shape and transparency so that solutions to be compared should be counted in the same vial. In our procedure, 5-ml. aliquots of one of the compartment solutions were transferred with a siliconed pipet to four counting vials, each of which contained 10 ml. of scintillator solution. Weight checks show that the reproducibility of these volumes was better than ±0.05%. When a vial had been counted it was immediately emptied, rinsed, refilled with scintillator and solution from the remaining compartment, respectively, and recounted. Errors due to long-term drift in the counting equipment were obviated in this way. Four diffusion coefficients were calculated separately, one from the data for each vial. The high precision gained by these precautions was reflected in the agreement among the four coefficients, the root mean square deviation of which averaged ±0.2%.

Results

The results of the tracer-diffusion measurements are shown in Table I together with other relevant data.

TABLE I

TRACER-DIFFUSION COEFFICIENTS OF DIPHENYL AND BENZENE IN BENZENE–DIPHENYL MIXTURES AT 25°

C_A, moles/l. Diphenyl	N_A Diphenyl	N_B Benzene	$D_A^* \times 10^5$, cm.²/sec.	$D_B^* \times 10^5$, cm.²/sec.	η/η_0	$D_A^*\eta/\eta_0$	$D_B^*\eta/\eta_0$
0	0	1		2.247	1		2.247
1.3×10^{-4}	~0	~1	1.554		~1	1.554	
0.4562	0.0419	0.9581	1.440	2.062	1.104	1.590	2.276
0.9501	.0901	.9099	1.307	1.911	1.217	1.591	2.327
1.980	.2008	.7992	1.091	1.590	1.544	1.685	2.455
2.931	.3176	.6824		1.311	1.956		2.564
2.996	.3261	.6738	0.890		1.988	1.769	

As stated in the Experimental section, the average counting error was of the order ±0.2% and as diaphragm cell measurements usually can be reproduced to ±0.1%, the total error is estimated to be ±0.3%. Replicate measurements at the same concentration agreed within this error.

In Table II, values for the self-diffusion coefficient of benzene which have been reported in the literature are compared with the figure obtained in this study.

TABLE II

SELF-DIFFUSION COEFFICIENT OF BENZENE AT 25°

Investigators	$D_B^* \times 10^5$	Estimated precision, %	Isotope used	Method
Graupner and Winter[7]	2.15	±2–3	H^2	Diaphragm cell
Johnson and Babb[8]	2.18	±6	C^{14}	Capillary
Hiraoka, Osugi, and Jono[9]	2.13	±3	C^{14}	Capillary
Rathbun and Babb[10]	2.21	±5	C^{14}	Capillary
This work	2.247	±0.3	C^{14}	Diaphragm cell

It will be observed that our value is considerably higher than those obtained by other workers, although in one or two cases it falls within their quoted limits of error. The intercalibration of our cells with the KCl diffusion data of Harned and Nuttall[11] and Gosting[12]

(5) R. H. Stokes, *J. Am. Chem. Soc.*, **72**, 763 (1950).

(6) R. A. Robinson and R. H. Stokes, "Electrolyte Solutions," 2nd Ed., Butterworths, London, 1959, p. 253.

(7) K. Graupner and E. R. S. Winter, *J. Chem. Soc.*, 1145 (1952).

(8) P. A. Johnson and A. L. Babb, *J. Phys. Chem.*, **60**, 14 (1956).

(9) H. Hiraoka, J. Osugi, and W. Jono, *Rev. Phys. Chem., Japan*, **28**, 52 (1958).

(10) R. E. Rathbun and A. L. Babb, *J. Phys. Chem.*, **65**, 1072 (1961).

(11) H. S. Harned and R. L. Nuttall, *J. Am. Chem. Soc.*, **69**, 736 (1947); **71**, 1460 (1949).

(12) L. J. Gosting, *ibid.*, **72**, 4418 (1950).

and the diphenyl figure of Sandquist and Lyons[2] would lead one to assume that there is no systematic error in our experimental procedure. The only other source of error would be from possible radioactive impurities in the labeled benzene. As a means of testing this possibility, we have obtained labeled benzene from two different suppliers on the assumption that as these samples were synthesized in different laboratories, it is unlikely that both would contain the same impurities in the same proportions. Benzene labeled with carbon-14 therefore was obtained from the Radiochemical Centre, Amersham, England, and Tracerlab Inc., Waltham, Mass., U.S.A. Diffusion runs on two samples gave

U.K. sample $D_B^* = 2.250 \times 10^{-5}$ cm.^{2}/sec.

U.S. sample $D_B^* = 2.245 \times 10^{-5}$ cm.^{2}/sec.

the results agreeing within the experimental error of the measurements.

Discussion

Several equations have been proposed relating the processes of mutual and tracer-diffusion in binary non-electrolyte mixtures. These equations will now be listed, tested with our data, and then critically examined. In the derivations of these equations, two main approaches can be distinguished. One type, characterized by the treatments of Hartley and Crank[13] and Adamson,[14] adduces a direct thermodynamic relationship between the mutual and tracer-diffusion coefficients. In effect, the mutual coefficient (erroneously termed an "intrinsic" coefficient in the original derivations) is equated to the tracer coefficient corrected by an activity term. Hartley and Crank's equation is of the form

$$D_{AB} = RT/N \frac{\partial \ln a_A}{\partial \ln N_A}\left(\frac{N_B}{\sigma_A \eta} + \frac{N_A}{\sigma_B \eta}\right) \quad (1)$$

where $\sigma_i\eta$ is a resistance coefficient, σ_i being some function of molecular size and shape. Equation 1 has been extended by Carman and Stein,[15] who equate $RT/N\sigma_A\eta$ to D_A^* and so obtain the expression

$$D_{AB} = (N_B D_A^* + N_A D_B^*)\left(\frac{\partial \ln a_A}{\partial \ln N_A}\right) \quad (2)$$

Adamson's treatment [14] differed from the above in that the rational activity term, instead of the concentration-based one, was used to couple the tracer and mutual diffusion coefficients directly. This modification gives the final equation

$$D_{AB} = (\phi_A D_B^* + \phi_B D_A^*)\left(\frac{\partial \ln a_A}{\partial \ln N_A}\right) \quad (3)$$

where ϕ_i is the volume fraction of component i.

The other group exemplified by the derivations of Bearman,[16] Lamm,[17] and Adamson and Irani[18] is based on both molecular and thermodynamic approaches. Their main characteristic is the use of friction coefficients, specific for interaction between diffusing molecules. Bearman's equations, when restricted to diffusion in regular solutions, take the form

$$D_A^*/D_B^* = V_B/V_A \quad (4)$$

where V_i is the partial molar volume of component i, and

$$D_{AB} = (N_B D_A^* + N_A D_B^*)\left(\frac{\partial \ln a_A}{\partial \ln N_A}\right) \quad (5)$$

which is identical with the Hartley–Crank extension, eq. 2.

Lamm's general equations cannot be tested directly experimentally, but he has given an approximation[19] which can be used

$$D_{AB} = N_A\left(\frac{D_B^* D_B^{*0}}{D_B^{*0} - \phi_B D_B^*}\right)\left(\frac{\partial \ln a_B}{\partial \ln C_B}\right) \quad (6)$$

where D_B^{*0} is the limiting tracer coefficient of B in pure A.

Adamson and Irani give a similar kind of approximation for experimental testing

$$D_{AB} = (D_B^* - \phi_B D_B^{*0}\eta_B^0/\eta)/\phi_A \frac{\partial \ln a_B}{\partial \ln C_B} \quad (7)$$

In Table III below, the experimental mutual diffusion coefficients of Sandquist and Lyons[2] are compared with those calculated from eq. 2–7 above. The ratios D_B^*/D_A^* also are listed. Figure 1 illustrates graphically the extent of agreement of some of these equations.

TABLE III

C_A, mole/l.	D_{AB}, obsd.[4]	D_{AB}, eq. 2, 5	D_{AB}, eq. 3	D_{AB}, eq. 6	D_{AB}, eq. 7	D_B^*/D_A^*
0.5	1.450	1.421	1.439	0.615	1.521	1.45
1.0	1.342	1.301	1.331	.610	1.390	1.45
1.5	1.242	1.200	1.241	.603	1.309	1.45
2.0	1.147	1.103	1.148	.604	1.205	1.46
2.5	1.062	1.021	1.066	.584	1.115	1.46
3.0	0.977	0.940	0.984	.570	1.006	1.46

Table III shows also that the ratio D_B^*/D_A^* is virtually constant over the concentration range measured. It is noteworthy that Carman and Stein's[15] data for tracer-diffusion in the ethyl iodide–*n*-butyl iodide system as quoted by Bearman[20] also show constancy over a similar concentration range. Further, as shown in Table IV, the ratios of V_A/V_B to D_B^*/D_A^* for the two systems are fairly comparable.

TABLE IV

Component	V	V_A/V_B	D_B^*/D_A^*	$\frac{V_A D_A^*}{V_B D_B^*}$
Benzene (B)	89.44	1.67	1.45	1.15
Diphenyl (A)	149			
Ethyl iodide (B)	80.51	1.41	1.14	1.24
n-Butyl iodide (A)	113.87			

Analysis of Diffusion Equations.—Before commenting on the agreement between the experimental evidence and the above equations, it is proposed to examine critically the derivations of the latter and the limits of their validity. There appears to be some confusion in the literature as to the applicability of some equations, particularly those of the Hartley–Crank type. Bear-

(13) G. S. Hartley and J. Crank, *Trans. Faraday Soc.*, **45**, 801 (1949).
(14) A. W. Adamson, *J. Phys. Chem.*, **58**, 514 (1954).
(15) P. C. Carman and L. H. Stein, *Trans. Faraday Soc.*, **52**, 619 (1956).
(16) R. J. Bearman, *J. Phys. Chem.*, **65**, 1961 (1961).
(17) O. Lamm, *ibid.*, **51**, 1063 (1947).
(18) A. W. Adamson, *Trans. AIME*, **219**, 158 (1960).
(19) O. Lamm, *Acta Chem. Scand.*, **8**, 1120 (1954).
(20) R. J. Bearman, *J. Chem. Phys.*, **32**, 1308 (1960).

man,[16] in a recent and valuable paper, has clarified some of the issues.

In the first place, we shall look at an equation used in the derivation of eq. 1 by Hartley and Crank[13] and also in the treatments of Prager[21] and Adamson.[14] This equation is supposed to relate the so-called intrinsic diffusion coefficients of the two components of a binary mixture to the volume-frame mutual coefficient. It is of the form

$$D_{AB} = \phi_A D_B + \phi_B D_A \qquad (8)$$

where D_A is termed the intrinsic coefficient of component A. We shall show in a very direct way that these intrinsic coefficients have no real meaning.

An essential requirement in the description of a diffusing system is the frame of reference against which the diffusion coefficient, D, can be defined. We shall follow the procedure and formulations given in a recent paper by Kirkwood, *et al.*[22] In deriving eq. 8, Hartley and Crank define a volume-fixed frame of reference in the usual way by the restriction that there is no net volume flow across it, *i.e.*

$$J_A{}^V V_A + J_B{}^V V_B = 0 \qquad (9)$$

where $J_A{}^V, J_B{}^V$ are the volume fluxes. They then go on to say that in a closed vessel with no *over-all* change of volume, this frame will be fixed with respect to the cell. In other words, the volume-fixed and cell-fixed frames will coincide.

They next state that if one component of a binary mixture diffuses at a faster rate than the other, then a hydrostatic pressure will be built up in the region originally containing the slower component and that this pressure will be relieved by a bulk flow of the whole solution. Therefore, on a cell-fixed frame there will be transport due to both diffusive flow and macroscopic flow. Intrinsic diffusion coefficients, intended to separate pure diffusive flow from the other, then were defined on a frame of reference which moved so that there was no bulk flow through it and then were related by a velocity term to the supposedly coinciding cell- and volume-fixed frames.

What Hartley and Crank failed to take into account was the fact that *if* there is such a pressure effect and resultant bulk flow in the diffusing system, then the molar volumes of the two components will not be constant throughout the cell. The *total* volume may remain constant but due to changes in free space in the liquid, the molar volumes must change. Therefore, to keep eq. 9 valid, if such a pressure gradient exists, the volume-frame must move away from the cell frame and in fact can be identified with the bulk-flow frame of Hartley and Crank. It follows that these intrinsic coefficients are identical and are in fact equal to the single mutual diffusion coefficent on the volume-frame. These coefficients then have no separate existence and the term intrinsic diffusion coefficient should be dropped. It should perhaps be emphasized that eq. 8 is still valid, even though it is trivial, since $D_{AB} = D_A = D_B$. This means that it does not render invalid subsequent equations in which it is used.

Bearman[16] also came to these conclusions from other considerations but analyzed the above aspect of Hartley and Crank's derivation wrongly. Admittedly their mass-flow frame was badly defined. Bearman misinterpreted this frame as one through which there was no net mass flow, *i.e.*

$$J_A{}^M + J_B{}^M = 0 \qquad (10)$$

In other words there is no net *diffusive* flow of mass and Hartley and Crank did not mean this. He then, of course, finds that there is only one diffusion coefficient in this system, the mutual coefficient on the mass frame which is simply related to the mutual one on the volume frame. As a result of this analysis he finds that the intrinsic coefficient $D_A = D_{AB}{}^V V/V_B$. However, from other considerations, he finds later in his paper that $D_A = D_B = D_{AB}{}^V$) thus contradicting his former result. Our explanation clears this matter up.

Since eq. 8 does not in fact correct for bulk flow, there remains the question of whether there is a pressure difference of the type postulated and how it can be treated when using an experimental or cell-fixed frame. It is not proposed to elaborate on this problem here except to say that pressure gradients have been observed in gaseous systems[23] and bulk movement in solids.[24] However, there is as yet no evidence of an analogous effect in homogeneous liquid systems. If it does exist, its description will of course depend on the boundary conditions of the diffusion experiment and would need to be formulated in terms of equations given in ref. 22. Thus the cell frame would be related to the volume frame by the equation

$$(J_A)_C = (J_A)_V + C_A u_{VC} \qquad (11)$$

where

$$u_{VC} = (J_A)_C V_A + (J_B)_C V_B$$

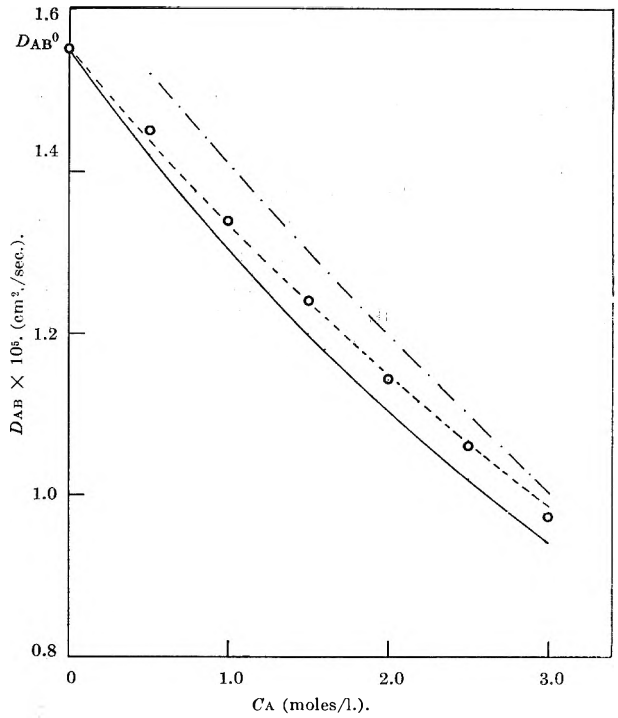

Fig. 1.—Comparison of experimental data of Sandquist and Lyons for D_{AB} with those calculated from theoretical equations in benzene–diphenyl system at 25°: O, experimental data; ———, eq. 2, 5; – – – –, eq. 3; — · —, eq. 7.

(21) S. Prager, *J. Chem. Phys.*, **21**, 1344 (1953).

(22) J. G. Kirkwood, R. L. Baldwin, P. J. Dunlop, L. J. Gosting, and G. Kegeles, *ibid.*, **33**, 1505 (1960).

(23) K. P. McCarty and E. A. Mason, *Phys. Fluids*, **3**, 908 (1960).

(24) A. D. Le Claire, *Progr. Metal Phys.*, **1**, 306 (1949).

A practical flow equation then can be obtained by finding a suitable integral expression for u_{VC} and substituting into eq. 11, see for example eq. 51 of ref. 22.

The next sensitive point in the Hartley–Crank type of formulation is the approximation that the mutual diffusion coefficient is equal to the tracer coefficient suitably corrected by a thermodynamic factor. The derivation of this relationship uses the standard procedure of equating the diffusion velocity of a component to its mobility multiplied by a force, this force being the gradient of its chemical potential. Equations as below then are obtained[13,15]

$$D_{AB} = D_A^* \frac{\partial \ln a_A}{\partial \ln C_A} \qquad (12a)$$

$$= D_B^* \frac{\partial \ln a_B}{\partial \ln C_B} \qquad (12b)$$

In point of fact Hartley and Crank[13] did not put in the tracer coefficient D_A^* but their eq. 1 was extended by Carman and Stein[15] to give the equivalent of (12). These workers used the intrinsic coefficients, however, and we have substituted the mutual coefficient which is the valid one. An important consequence of the amended formulation as given by (12) emerges from the fact that since

$$D_{AB} = D_A^* \frac{\partial \ln a_A}{\partial \ln C_A} = D_B^* \frac{\partial \ln a_B}{\partial \ln C_B} \qquad (13)$$

and since

$$\frac{\partial \ln a_A}{\partial \ln C_A} \Big/ \frac{\partial \ln a_B}{\partial \ln C_B} = V_A/V_B$$

then

$$D_A^*/D_B^* = V_B/V_A$$

which is precisely the same coupling as expressed in eq. 5, as proposed by Bearman.[16]

Adamson[14] employs a variation of eq. 12. In this equation, it is assumed that the statistical movements at a given concentration are the same for both tracer and mutual diffusion except that in the latter process a bias is imposed by the non-ideality of the gradient of chemical potential. Adamson argued that in an ideal dilute solution both types of diffusion should be exactly the same with the thermodynamic facto requal to unity. Since the concentration-based thermodynamic factor $\partial \ln a_A/\partial \ln C_A$ is not unity in an ideal solution, he therefore substituted the rational thermodynamic factor $\partial \ln a_A/\partial \ln N_A$. In consequence his final equation is (3) instead of (2). However since we have shown that the proper treatment of the Hartley–Crank approach leads to the identity $D_{AB} = D_A = D_B$, then

$$D_{AB} = D_A^* \frac{\partial \ln a_A}{\partial \ln N_A} = D_B^* \frac{\partial \ln a_B}{\partial \ln N_B}$$

so that $D_A^* = D_B^*$, which is obviously wrong.

Bearman[16] has pointed out that since the Hartley–Crank equations as modified in (2) are the same as his own and since the latter are restricted to regular solutions, then the former also are only applicable to such solutions. One can also see directly the essential factor which limits such equations to regular solutions. In order to equate D_A^* with $RT/N\sigma_A\eta$, in deriving eq. 2, Carman and Stein[15] assume that at a given concentration of A and B, the mobility of A in mutual diffusion, u_A, is the same as the mobility u_A^* of the tagged species A^* in tracer diffusion. We may expect this equality to have very limited applicability, however. In mutual diffusion, transport through the solution is governed only by the exchange of A and B molecules. In tracer diffusion, such transport depends on exchange of A* with both A and B molecules. In regular solutions where the radial distribution functions are independent of composition, molecules of A and B are expected to have similar size, shape, and interaction potentials.[16] In this particular case, the mobilities will be approximately equal for the two types of exchange and Carman and Stein's approximation is then justified.

One may conclude from the foregoing that the Hartley–Crank type of formulation would be valid only for regular solutions. As the system benzene–diphenyl is not regular, the equations would not be expected to apply and as seen in Fig. 1, eq. 2 does not. The unexpected agreement with eq. 3 must be regarded as fortuitous. Possibly the arbitrary replacement of the concentration-based by the rational thermodynamic factor has introduced a compensating error.

Turning now to the other approaches, those of Bearman,[16] Lamm,[17] and Adamson and Irani,[18] it is evident that these do take account of all possible types of exchange. At the moment, although equations involving the mobilities or their inverse, the friction coefficients, for all types of interaction can be formulated, they cannot be tested experimentally. This is because there is no obvious way of measuring directly the mobility corresponding to AA* interaction in the presence of B. A very similar stage has been reached in diffusion studies in metals.[24]

By restricting his formulas to regular solutions, Bearman has obtained eq. 4 and 5. It is seen that neither equation represents the data in the irregular benzene–diphenyl system. Both Lamm and Adamson and Irani give the approximate equations, (6) and (7). In each case the approximation is made that during tracer diffusion in a mixture of A and B, specific AA* interaction is unaltered by change of concentration of B molecules. Table III shows that eq. 6 is in error by a factor of 2 and (7) shows only fair agreement.

It is therefore apparent from the above analysis that the only equations that can be tested experimentally are restricted to a narrow class, that of regular solutions. It is also apparent that any widening of this class will probably come from the more general second approach, and in particular, the statistical mechanical treatment of Bearman.[16,20] The most fruitful field of study at the moment may be the study of AA* interaction as a function of concentration for various systems. Experimental evidence of this type may lead to extension of the statistical mechanical equations to non-regular solutions.

A few comments follow on the viscosity aspect. In regular solutions it is expected that the product of viscosity and tracer-diffusion coefficients will be constant and several equations have been proposed embodying this relationship. In our system such constancy is not expected and not evidenced. It is of interest, however, to recall that Onsager[25] predicted

(25) L. Onsager, *Ann. N. Y. Acad. Sci.*, **46**, 253 (1945).

that "...a positive deviation from Raoult's law corresponds to local segregation of the components, which might well facilitate diffusion and yet impede viscous flow." Benzene–diphenyl is a system showing such positive deviations and it is evident from Table I that the viscosity increases more rapidly than the diffusion rate of either component decreases, which is in accord with this prediction.

Acknowledgments.—The author is indebted to Professor R. H. Stokes for helpful discussions.

THE LIQUID PHASE REACTION OF METHYL RADICALS WITH METHANOL[1]

BY MARK CHER

Research Department of Atomics International, A Division of North American Aviation, Inc., Canoga Park, Cal.

Received August 17, 1962

The liquid phase photolysis ($\lambda > 2900$ Å.) of acetone-d_6 in the presence of CH_3OH and CD_3OH has been studied at 30.0° by measuring the isotopic composition of the resulting methanes. The results are interpreted in terms of hydrogen abstraction reactions of methyl-d_3 radicals with substrate molecules. The conclusions are: the rate constant for the abstraction of hydrogen from the methyl group in methanol is (a) 45 times greater than the rate constant for the abstraction of hydrogen from the hydroxyl group in methanol, (b) 8.7 times greater than the rate constant for the abstraction of deuterium from CD_3OH, and (c) 0.56 times as large as the rate constant for the abstraction of deuterium from acetone-d_6. The disproportionation reaction between methyl and acetyl radicals to form methane and ketene is shown to be unimportant except at light intensities much higher than that used in the measurements.

There is general agreement at present that hydrogen atoms are produced when methanol is decomposed by ultraviolet photolysis,[2] mercury photosensitization,[3,4] or radiolysis.[5,6] There is some question, however, as to which of the two types of hydrogen in methanol actually is involved in the subsequent abstraction reaction producing hydrogen gas. In order to answer this question directly we have photolyzed mixtures of acetone-d_6 in both CD_3OH and in CH_3OH, and measured the isotopic composition of the product methane, the assumption being that methyl radicals and hydrogen atoms behave similarly in the abstraction from methanol. Since our interest was directed mainly in trying to correlate results in the liquid phase radiolysis of methanol,[6] we chose to work first with liquid mixtures. Studies of the liquid phase photolysis of acetone, alone[7] and in the presence of various solvents,[8–10] already have indicated that decomposition proceeds by way of free radicals with reactions analogous to those known to occur in the gas phase.

Experimental

Because of the high cost of the deuterated materials, about 0.3 cc. was photolyzed in each run. Reaction cells of approximately 1-mm. path length were constructed from thin parallel rectangular strips of quartz, 14 mm. wide and 35 mm. long, fused to one arm of a stopcock. The temperature was maintained at 30.0 ± 0.1° by circulating water through a glass jacket surrounding the reaction cell. The light source was a Hanovia mercury arc type A. A flat Pyrex glass window was cemented to the wall of the jacket to limit the effective light to wave lengths above 2900–3000 Å., well above the absorption limit of methanol.

The experimental procedure was to pipet 0.3 cc. of solution, which had been prepared by weight, to a tube in the vacuum line, degas by the freeze–pump–thaw technique, and then vacuum distil the entire sample into the reaction cell. After photolysis the mixture was distilled into a Dry Ice trap, the non-condensable gas was toeplered through a liquid nitrogen trap into a calibrated volume where the pressure was read, and then it was transferred into a sealed container for analysis, using a modified C.E.C. 21-620 mass spectrometer.

Materials.—Methanol-d_3 (CD_3OH), 99% stated isotopic purity, and acetone-d_6, 99.5% stated isotopic purity, were purchased from Volk Radiochemical Company. The methanol-d_3 was chemically pure by gas chromatography, but the acetone-d_6 contained a few per cent of unidentified chemical impurities in some but not all of the purchased samples. The CD_3H/CD_4 yield ratio from the photolysis or γ-radiolysis of various samples of acetone-d_6 alone ranged from 0.093 to 0.28; purification by gas chromatography of a previously radiolyzed sample decreased the CD_3H/CD_4 yield ratio from 0.23 to 0.084. Both unpurified and purified (by gas chromatography) acetone-d_6 were used in our measurements; the spread of the data in Fig. 2 probably is due largely to this cause. The methanol was Mallinckrodt reagent grade. It was dried with "Drierite" and purified by bulb to bulb distillation at −80°.

Results

The main gaseous products of the reaction were CD_4, CD_3H, and CO. Trace amounts of other isotopic methanes also were observed. The yields of methane corresponded to not more than 2% acetone decomposition. The CD_4/CD_3H ratio was determined from the heights of the mass peaks 20 and 19 after suitable corrections for the C-13 isotope contribution and on the assumption of equal spectrometer sensitivity. The CD_4/CD_3H ratio was plotted against the initial acetone/methanol concentration ratio with results as shown in Fig. 1 and 2.

An attempt to increase the gas yields by substituting a Vycor filter for the Pyrex filter resulted in anomalously high yields of CD_4. Consequently, the effect of varying the light intensity on the CD_4/CD_3H yield ratio in the photolysis of a mixture of CD_3COCD_3 and CH_3OH was studied using the Vycor filter by inserting wire screens of varying transmittance between the lamp and the cell. The average rate of gas production was taken as a measure of the relative light intensity. The results are shown in Fig. 3. The experimental points denoted by solid circles are based on the photolysis experiments using the Pyrex filter, and were estimated by interpolation from the data shown in Fig. 1.

(1) Work performed under AEC contract AT(11-1)-GEN-8.

(2) R. P. Porter and W. A. Noyes, Jr., *J. Am. Chem. Soc.*, **81**, 2307 (1959).

(3) M. K. Phibbs and B. de B. Darwent, *J. Chem. Phys.*, **18**, 495 (1950).

(4) (a) R. F. Pottie, A. G. Harrison, and F. P. Lossing, *Can. J. Chem.*, **39**, 102 (1961); (b) A. R. Knight and H. E. Gunning, *ibid.*, **39**, 1231 (1961).

(5) J. H. Baxendale and F. W. Mellows, *J. Am. Chem. Soc.*, **83**, 4720 (1961).

(6) J. G. Burr, Proceedings of the IAEA Symposium on the Uses of Tritium, Vienna, May, 1961.

(7) R. Pieck and E. W. R. Steacie, *Can. J. Chem.*, **33**, 1304 (1955).

(8) D. B. Peterson and G. J. Mains, *J. Am. Chem. Soc.*, **81**, 3510 (1959).

(9) D. H. Volman and L. W. Swanson, *ibid.*, **82**, 4141 (1960).

(10) R. Doepker and G. J. Mains, *ibid.*, **83**, 294 (1961).

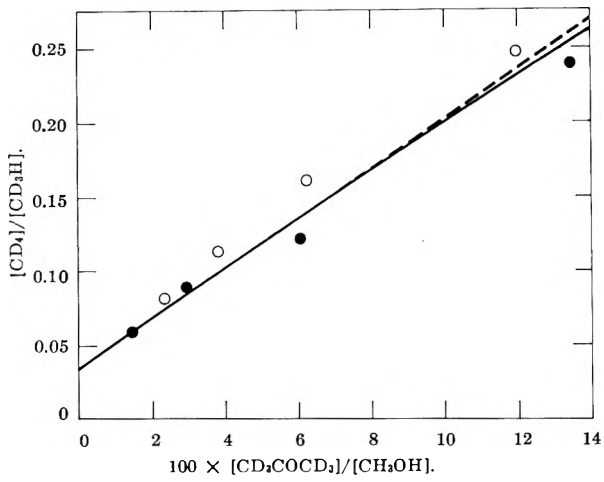

Fig. 1. –The isotopic composition of methane in the photolysis of CD_3COCD_3–CH_3OH mixtures: O, unpurified acetone-d_6; ●, acetone-d_6 purified by gas chromatography.

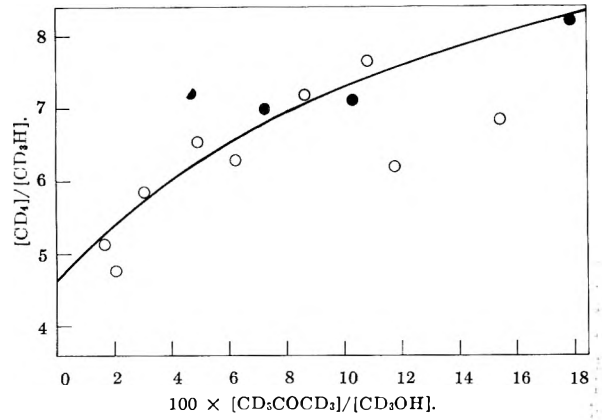

Fig. 2.—The isotopic composition of methane in the photolysis of CD_3COCD_3–CD_3OH mixtures: O, unpurified acetone-d_6; ● acetone-d_6 purified by gas chromatography. Notice that the scale of the Y-axis is different from that of Fig. 1.

Discussion

In the photolysis of mixtures of acetone-d_6 and methyl-d_3 alcohol the only important reactions leading to the formation of CD_4 and CD_3H are assumed to be

$$CD_3 + CD_3COCD_3 \xrightarrow{k_1} CD_4 + CD_2COCD_3 \quad (1)$$

$$CD_3 + CD_3OH \xrightarrow{k_2} CD_4 + CD_2OH \quad (2)$$

$$CD_3 + CD_3OH \xrightarrow{k_3} CD_3H + CD_3O \quad (3)$$

$$CD_3 + CD_2HCOCD_3 \xrightarrow{k_4} CD_3H + CD_2COCD_3 \quad (4)$$

$$CD_2H + CD_3COCD_3 \xrightarrow{k_1} CD_3H + CD_2COCD_3 \quad (5)$$

$$CD_2H + CD_3OH \xrightarrow{k_2} CD_3H + CD_2OH \quad (6)$$

Reactions 4, 5, and 6 are included because of the presence of acetone-d_5 in the acetone-d_6. They are needed to account for the decrease in the slope in Fig. 2 as the acetone concentration is increased, and also to account for the finite CD_4/CD_3H yield ratio in the photolysis of acetone alone.

If light methanol is substituted for methanol-d_3,

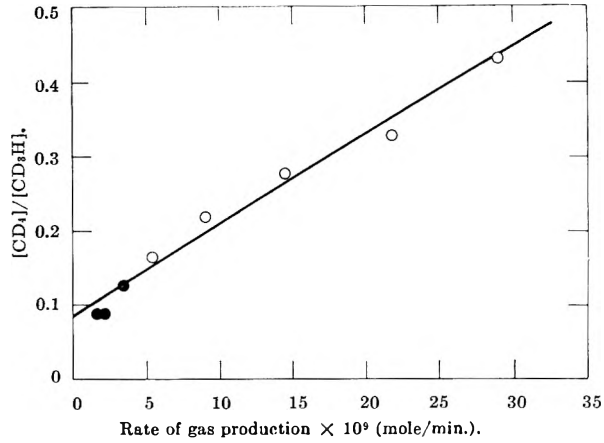

Fig. 3.—Effect of light intensity on the isotopic composition of methane in the photolysis of a mixture of CD_3COCD_3 and CH_3OH; mole fraction CD_3COCD_3 = 0.0273; O, Vycor filter; ●, Pyrex filter.

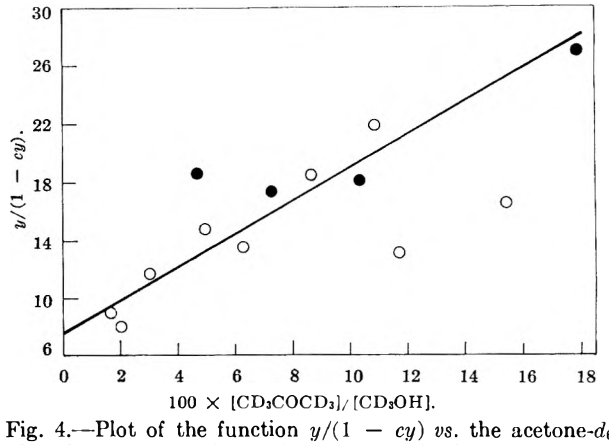

Fig. 4.—Plot of the function $y/(1 - cy)$ *vs.* the acetone-d_6/methanol-d_3 concentration ratio: O, unpurified acetone-d_6; ●, acetone-d_6 purified by gas chromatography.

we must assume the following reactions, analogous to (2) and (3)

$$CD_3 + CH_3OH \xrightarrow{k_7} CD_3H + CH_2OH \quad (7)$$

$$CD_3 + CH_3OH \xrightarrow{k_3} CD_3H + CH_3O \quad (8)$$

In the case of CD_3OH, consideration of reactions 1 through 6 gives for the ratio of the rates of production of CD_4 to CD_3H

$$\frac{R_{CD_4}}{R_{CD_3H}} \equiv y = \frac{1 + ax}{b + acx} \quad (9)$$

where x is the mole fraction ratio of acetone ($d_5 + d_6$) to methanol, the constants a, b, and c are defined as

$$a = (1 + \alpha)^{-1}(k_1/k_2)$$

$$b = (k_3/k_2) + \alpha/(2 + \alpha)$$

$$c = \alpha[(k_4/k_1) + 1/(2 + \alpha)]$$

and α is the acetone-d_5/acetone-d_6 concentration ratio. In deriving eq. 9 we assume that $k_5 = k_1$, $k_6 = k_2$, and also that the CD_2H/CD_3 concentration ratio is given by $\alpha/(2 + \alpha)$, since acetone-d_5 can decompose to form either CD_3 or CD_2H with nearly equal probability. Equation 9 may be rearranged to give the linear form

$$y/(1 - cy) = (b - c)^{-1} + a(b - c)^{-1}x \quad (10)$$

inasmuch as the value of c can be estimated from the CD_4/CD_3H yield in "pure" acetone-d_6. Figure 4 shows the data of Fig. 2 plotted according to eq. 10, using $c = 0.085$.

With solutions containing CH_3OH, consideration of reactions 1, 4, 5, 7, and 8, and assuming $k_8 = k_3$, gives the expression

$$y = px(1 + pcx)^{-1} \quad (11)$$

where

$$p = (1 + \alpha)^{-1}k_1/(k_7 + k_3)$$

Equations 10 and 11 permit us to determine the numerical, values of the interesting rate constant ratios, namely, k_7/k_3, k_7/k_2, and k_7/k_1, from the initial slope in Fig. 1 [initial slope = p] and from the slope and intercept in Fig. 4. In these calculations we take $\alpha = 0.05$, as estimated from gas chromatography and mass spectrometer measurements of the acetone-d_6. The results are as follows: $k_7/k_3 = 45 \pm 12$; $k_7/k_2 = 8.7 \pm 2.8$; and $k_7/k_1 = 0.56 \pm 0.05$. An indication of the goodness of the fit may be obtained by noting that the solid curves in Fig. 1 and 2 were calculated on the basis of eq. 9 and 11 using the constants given above, except that in Fig. 1 the entire curve was shifted upward by 0.038 unit in order to fit the observed intercept. This latter point is discussed below.

Qualitatively, the ratio $k_7/k_3 = 45 \pm 12$ means that the abstraction of a hydrogen atom from CH_3OH by methyl radicals occurs mainly (98% probability) at the methyl group. Moreover, this value probably is too low since in our treatment we have neglected entirely the effect of CD_2HOH impurity in the CD_3OH. This result is consistent with the observation by Porter and Noyes[2] that in the gas phase photolysis of CD_3OH as much as 20% of the product hydrogen is H_2, since a high intrinsic probability that photolytic H atoms abstract from the methyl group to produce HD is partially offset by the isotope effect tending to retard abstraction of D atoms relative to H atoms,[11] as suggested below.

The ratio $k_7/k_2 = 8.7 \pm 2.8$ is a measure of the isotope effect corresponding to the abstraction of hydrogen or deuterium from the methyl group in methanol. This result may be compared with a calculated value[12] of 6.0 at 30°, based on published[13] C–H and C–D stretching frequencies for CH_3OH and CD_3OH.

The ratio $k_7/k_1 = 0.56 \pm 0.05$ is a measure of the relative rates of abstraction by CD_3 radicals of hydrogen from the methyl group in methanol and deuterium from acetone-d_6. This ratio would no doubt be even smaller if light acetone were being compared to methanol. This means that in the liquid phase the rate of abstraction from acetone is greater than that from methanol, whereas in the gas phase the opposite is true.[14]

The interpretation of the experimental measurements as presented here is based on the assumption that all the reactions producing CD_4 or CD_3H have been included in the mechanism.[15] There is considerable evidence[7-9] that in the liquid phase photolysis of acetone the reaction

$$CD_3 + CD_3CO = CD_4 + CD_2CO \quad (12)$$

is of importance. The increase in the CD_4/CD_3H yield ratio with increasing light intensity constitutes additional evidence for the occurrence of this reaction.[16] In our measurements using the Pyrex filter, however, reaction 12 need not be considered in view of the fact that the CD_4/CD_3H yield ratio in Fig. 3 extrapolated to zero intensity, where this reaction is certainly not important, differs from the observed CD_4/CD_3H ratio in the Pyrex experiments by less than 10%.[17] The small but real positive intercept in Fig. 1 may be due to the contribution of reaction 12 occurring partly homogeneously in the solution and partly as a cage reaction. Correction for the excess CD_4 would tend to shift all the experimental points downward, and thus the intercept, which was not predicted by eq. 11, conceivably might be eliminated.

Acknowledgment.—The author is indebted to Mr. R. A. Meyer for the mass spectroscopic analyses.

(11) In our experiments the ratio of relative rates of abstraction by CD_3 radicals from the methyl and hydroxyl groups in CD_3OH is $k_2/k_3 = 5.2$. Thus we calculate that 16% of the methane originating in the abstraction from CD_3OH is CD_3H.

(12) L. Melander, "Isotope Effects on Reaction Rates," Ronald Press Co., New York, N. Y., 1960, p. 20.

(13) M. Falk and E. Whalley, *J. Chem. Phys.*, **34**, 1554 (1961).

(14) A. F. Trotman-Dickenson, "Gas Kinetics," Butterworths Scientific Publications, London, 1955, pp. 201–202.

(15) Isotopic exchange between methanol and acetone-d_6 is not considered important in view of the very small yields of CD_2H_2. Furthermore, photolysis of liquid mixtures of acetone in D_2O indicated no deuterium in the methane product.

(16) The dependence of the rate of this reaction on intensity implies that the reaction takes place mainly homogeneously in the liquid phase rather than in a "cage" following the primary dissociation step.

(17) The fact that the results based on the Pyrex filter experiments fall reasonably close to the straight line drawn through the points based on the Vycor filter experiments suggests that the essential difference between these two sets of experiments is in the total over-all intensity entering the reaction cell, rather than in the difference in spectral distribution.

REACTION BETWEEN 1-HEXENE AND HYDROGEN AND DEUTERIUM ON COPPER–CHROMIUM OXIDE CATALYST

BY ISAO MATSUZAKI AND ROBERT L. BURWELL, JR.

Department of Chemistry, Northwestern University, Evanston, Illinois

Received August 17, 1962

Reaction of hydrogen and deuterium with 1-hexene has been investigated in a vapor phase, flow reactor on copper–chromium oxide catalyst at temperatures of from 50 to 150°. The catalyst was pretreated with hydrogen at 325°. There are three primary reactions, hydrogenation, isomerization to *trans*- and *cis*-2-hexene which appear in a ratio of about 10, and formation of isotopically exchanged 1-hexene. The last reaction is the fastest and, as shown by n.m.r., it involves almost exclusively exchange at carbon atom-2 to form 1-hexene-2-*d*. The activation energy for isomerization is about 5 kcal. greater than that for hydrogenation. The rates of the two reactions are equal at about 90°. At 60°, presence of 1-hexene almost completely inhibits hydrogenation of 2-hexene but it does not inhibit isomerization of 2- to 3-hexene. The isotopic distribution pattern of the hexane formed at low conversions seems to result from the addition of two (H,D) atoms to a mixture of 1-hexene and 1-hexene-2-*d* formed by previous exchange. Thus, during the course of hydrogenation, there seems to be little tendency for reversion of diadsorbed hexane to monoadsorbed. Isotopic distribution patterns for *trans*-2-hexene are presented and difficulties in the application of the Horiuti–Polanyi mechanism to olefin isomerization and exchange are discussed.

The Adkins copper–chromium oxide catalyst is the catalyst of choice for the hydrogenation of esters to alcohols. Although it has been used extensively for preparative purposes in this and certain other reactions,[1,2] its fundamental catalytic characteristics have been little examined. The chemical composition of the active catalyst is not entirely clear. In its preparation, a basic cupric ammonium chromate is decomposed at about 400° to give a mixture of cupric oxide and cupric chromite. Except in his last paper[3] Adkins used this material directly. Adkins considered that the active ingredient was unreduced copper oxide[1-3] but it is clear that the copper oxide is reduced to metallic copper under the reaction conditions.[4-7] The actual catalyst probably is copper supported on copper chromite or chromium oxide. Although the reduced copper–chromium oxide catalyst seems to have properties somewhat similar to those of copper catalysts,[7] the two are not identical in catalytic behavior.[8]

In his last paper,[3] Adkins reported that pretreatment of the catalyst suspended in alcohol with high pressure hydrogen at above 100° permitted certain catalytic reactions to occur at much lower temperatures.[9] Little is known about the hydrogenation of olefins except for Adkins' resport[1] that temperatures of about 150° were necessary. One might suspect that olefin hydrogenation would occur at much lower temperatures on a pre-activated catalyst.

We report here a study of the vapor phase reactions between 1-hexene and hydrogen and deuterium on the copper–chromium oxide catalyst. This system was chosen because it would permit comparison with the catalytic behavior of chromium oxide and of metallic catalysts.

Experimental

Materials.—Electrolytic hydrogen was obtained from the Matheson Company, deuterium, from General Dynamics. 1-Hexene (Phillips Petroleum Company, pure grade) was fractionally distilled. It was refluxed for 2 hr. with sodium–potassium alloy before fractionation for the work reported in Table I.

The copper–chromium oxide catalyst was prepared according to the method for HJS 2 given by Adkins, Burgoyne, and Schneider.[3] The original precipitate was decomposed in a Woods metal bath at 350°, leached with 10% acetic acid at room temperature, washed with water, and dried at 125°. It was pelleted at 3200 kg./cm.^{2}, crushed, and sieved to 40–60 mesh.

Apparatus.—The apparatus was similar to one previously used by Dr. August Hell in these Laboratories. 1-Hexene was fed to a vaporizer from a motor-driven syringe of 10-cc. capacity. The syringe was of stainless steel, the packings of Teflon. The hexene was delivered to the top of a tube at the bottom of which the hydrogen or deuterium feed was supplied. This tube and that leading to the catalyst chamber were warmed by a resistance wire winding. The apparatus terminated in a soap-film flow meter by means of which the hydrogen flow rate could be computed. The motor driving assembly was provided with a set of changeable gears. Previous calibration gave the feed rate of hexene.

Hydrogen was purified by passage through a Deoxo unit followed by a charcoal trap cooled with liquid nitrogen. Deuterium was passed over nickel–kieselguhr kept at 400°, calcium chloride, Linde Molecular Sieve 4A, and nickel–kieselguhr at room temperature, and a charcoal trap cooled with liquid nitrogen.

The catalyst chamber consisted of a tube of 6 mm. inside diameter into which a thermocouple well of 3 mm. outside diameter projected. The catalyst was contained partly in the annular space between the two tubes and partly in the region into which the thermocouple well did not project. The vapor stream from the catalyst chamber was condensed in a Dry Ice trap. Hydrogen sample collection tubes were provided between the trap outlet and the soap-film flow meter.

Procedure.—In all experiments except preliminary ones, the catalyst was diluted with about 2 cc. of 40 mesh glass beads so as to reduce the temperature rise in the catalyst bed. The quantity of catalyst was varied from 5 to 150 mg. according to the temperature employed and the conversion desired. The catalyst chamber was immersed in a thermostated oil or water bath during runs. The mole ratio of hydrogen or deuterium to hexene was 2.0. Samples of condensed product were removed about every 12 min. from the trap and analyzed by gas chromatography. Most of the analyses were performed on a silver nitrate–glycol column. In runs with deuterium, the product was separated on silver nitrate–glycol into three portions: (1) hexane, (2) *trans*-2- and *trans*-3-hexene, and (3) 1-hexene and *cis*-2- and *cis*-3-hexene. These were analyzed for deuterium distribution on a Consolidated 21-130 mass spectrometer provided by a matching grant to this department from the National Science Foundation.

Experimental Results.—No reaction between 1-hexene and hydrogen occurred on the unactivated catalyst at 100° but extensive reaction occurred at 200 and 300°. Following use at 300°, the catalyst was active at 75°. This suggests that heating in hydrogen might activate the catalyst. Accordingly, the effect of activation temperature upon activity measured at 50° was determined. In two series of runs, activity measurements were

(1) H. Adkins, "Reactions of Hydrogen," University of Wisconsin Press, Madison, Wis., 1937.

(2) H. Adkins, "Organic Reactions," Vol. VIII, John Wiley and Sons, Inc., New York, N. Y., 1954, Chapter 1.

(3) H. Adkins, E. E. Burgoyne, and H. J. Schneider, *J. Am. Chem. Soc.*, **72**, 2626 (1950).

(4) J. D. Stoupe, *ibid.*, **71**, 569 (1949).

(5) P. W. Selwood, F. N. Hill, and H. Boardman, *ibid.*, **68**, 2055 (1946).

(6) I. Rabes and R. Schenck, *Z. Elektrochem.*, **52**, 37 (1948).

(7) R. Miyake, *J. Pharm. Soc. Japan*, **68**, 18, 22, 26, 33 (1948).

(8) D. G. Manly and A. P. Dunlop, *J. Org. Chem.*, **23**, 1093 (1958).

(9) See also ref. **7** and **8**.

TABLE I

REACTION BETWEEN HYDROGEN OR DEUTERIUM AND 1-HEXENE

Wt., mg. catalyst[a]	Composition of hydrocarbon fraction, mole %					
	Hexane	1-Hexene	*cis*-2-	*trans*-2-	*cis*-3-	*trans*-3-
			62.5° and hydrogen			
20A	9.0	85.3	0.5	5.0	0.0	0.2
50A	26.5	58.5	2.2	12.2	.0	0.6
100A	45.0	29.8	3.5	19.5	.2	2.0
150A	63.9	0.55	5.3	21.6	.85	7.8
		(0.55)	(7.9)	(16.2)	(3.3)	(8.1)[b]
			100° and hydrogen			
5B	4.7	88.1	0.6	6.2	0.0	0.4
10B	12.0	70.9	1.2	14.5	.0	1.4
10A	28.6	37.95	3.1	25.8	.55	4.0
20A	48.4	1.5	9.9	27.7	1.9	10.6
30A	65.0	0.5	6.3	19.0	1.2	8.0
		(0.7)	(8.5)	(15.0)	(3.5)	(7.3)[b]
			150° and hydrogen			
5B	15.0	53.5	3.0	23.0	1.0	4.5
10B	34.3	15.8	7.6	30.4	1.8	10.1
10A	44.7	2.4	10.8	27.4	2.6	12.1
20A	60.9	0.5	8.1	19.1	2.4	9.0
		(1.0)	(10.2)	(15.8)	(4.3)	(7.7)[b]
			60° and deuterium			
120A	8.5	83.6	0.73	6.8	0.0	0.34
			140° and deuterium			
15A	6.9	81.7	1.26	9.6	0.0	0.5

[a] Flow rate designated by A is 0.0108 mole of 1-hexene per hour; B is 0.0216 mole per hour. Hydrogen flow rates in moles were twice those of 1-hexene. [b] Parenthetical figures are equilibrium values computed from F. D. Rossini, "Selected Values of Physical and Thermodynamic Properties of Hydrocarbons," Carnegie Press, Pittsburgh, Pa., 1953.

alternated with treatment with flowing hydrogen for 1 hr. at successively higher temperatures. As shown in Fig. 1, activation at about 325° provided maximum activity. In subsequent experiments, the catalyst was activated for 1.5 hr. at 325° before use. The original brownish color of the catalyst changed to black during decomposition at 350° and then remained unaltered during all subsequent experiments.

The hydrogenation of 1-hexene was examined at 62.5, 100, and 200° using 1-hexene which had been purified merely by fractionation. Results were nearly the same as those shortly to be described except that the catalytic activity declined to about half of its initial value in 15 to 75 min. Refluxing the 1-hexene with sodium–potassium alloy before fractionation greatly decreased

TABLE II

ISOTOPIC DISTRIBUTION OF DEUTERIUM[a]

	Hexane, %	1- + *cis*-2- + *cis*-3-ene, %	*trans*-2- + *trans*-3-ene, %
	60°		
d_0	27.6	86.9	46.9
d_1	58.9	12.8	46.2
d_2	11.5	0.3	4.55
d_3	1.2		2.06
d_4	0.0		0.29
d_5	.51		
d_6	.20		
d_{av}[b]	.89	0.134	0.63
	140°		
d_0	21.4	49.0	42.4
d_1	34.1	49.3	43.5
d_2	30.4	1.7	12.5
d_3	13.3		1.1
d_4	0.4		0.35
d_5	.3		.18
d_6	...		...
d_{av}[b]	1.38	0.53	0.74

[a] See Table I for hydrocarbon composition. [b] Average number of deuterium atoms in sample.

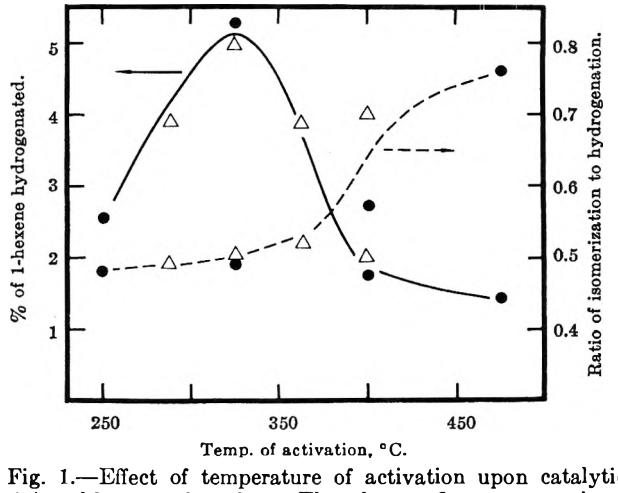

Fig. 1.—Effect of temperature of activation upon catalytic activity of 0.031 g. of catalyst. The 1-hexene flow rate was about 0.01 mole/hr. Data for two samples of catalyst are shown, △ and ●.

the rate of loss of activity. For example, in one run at 62.5°, over a 5-hr. period the fraction of 1-hexene hydrogenated declined slowly and continuously from 0.64 to 0.59. In another at 200°, the fraction declined from 0.565 to 0.515 over the same period. We do not know the origin of these slow declines in activity. Two further attempted purifications were without effect: passage of 1-hexene in a stream of nitrogen over the catalyst at 100°, introduction of a charcoal trap cooled by liquid nitrogen into the hydrogen line (the use of the trap was nevertheless continued).

Experiments were run at a reaction temperature of 200° in which the catalyst was omitted and another in which the usual catalyst was employed but hydrogen was replaced by nitrogen. Neither hydrogenation nor isomerization was detected in either case.

The interaction between hydrogen and purified 1-hexene on the activated catalyst was examined at 62.5, 100, and 150°. Results are presented in Table I. Runs with deuterium were made at 60 and 140°. Composition data are given in Table I and isotopic

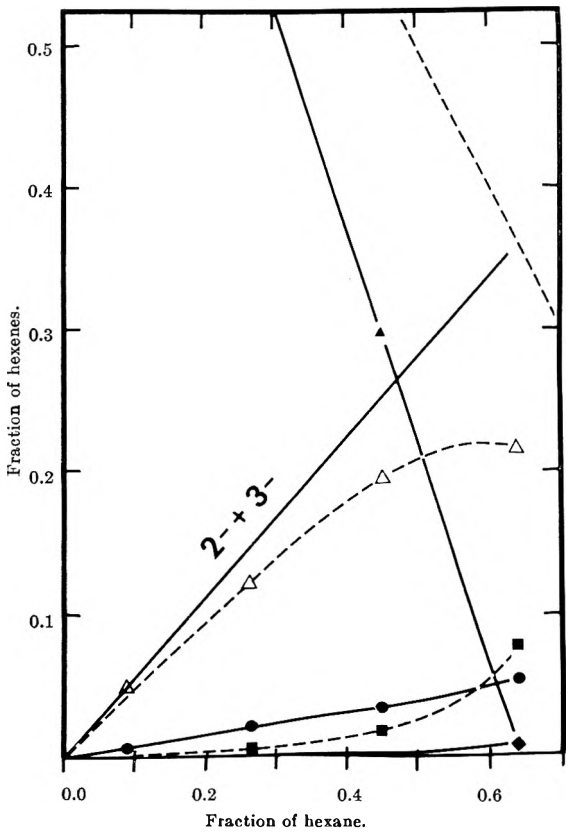

Fig. 2.—Product distribution in reaction between 1-hexene and hydrogen at 62.5°: broken line at upper right is total hexenes; 2- + 3- is the sum of 2- and 2-hexenes; ▲, 1-hexene; ●, *cis*-2-hexene; △, *trans*-2-hexene; ◆, *cis*-3-hexene; ■, *trans*-3-hexene.

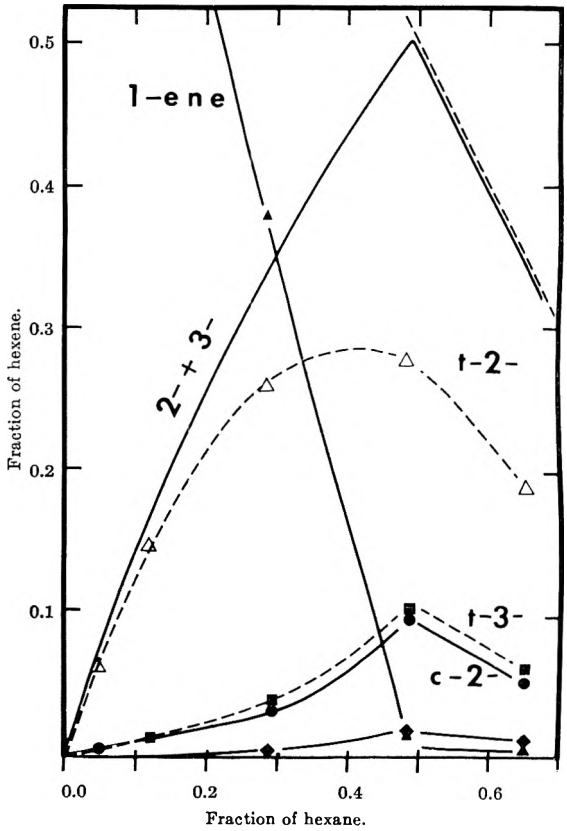

Fig. 3.—Product distribution in reaction between 1-hexene and hydrogen at 100°; the symbols are the same as in Fig. 2.

distribution data, in Table II. Because of slight interference by 1-hexene, the values for both *cis*-enes are somewhat less precise at large values of 1-hexene.

The 1-hexene + *cis*-2-hexene fraction of the 140° run with deuterium was examined by nuclear magnetic resonance. As may be seen from Tables I and II, the sample was 98.3% 1-hexene. Except for 1.7% of hexene-d_2, it was a nearly equal mixture of hexene-d_0 and hexene-d_1. The absorption bands for the olefinic hydrogen atoms of standard 1-hexene at positions 1 and 2 were identical with those reported and assigned for 4,6,8-trimethylnonene-1.[10] In the deuteriated sample, the intensity of the band assigned to the hydrogen atom at position 2 had declined to one-half of its original value; the intensities of the other bands were nearly unchanged. Thus, the 1-hexene-d_1 is predominantly 1-hexene-2-*d*.

Discussion

Consider first reaction of 1-hexene at 62.5° (Fig. 2 and Table I). The rate of isomerization of 1-hexene to other hexenes is 0.56 of its rate of hydrogenation. *trans*-2-Hexene and *cis*-2-hexene are initial products but *cis*-3-hexene is not. Little if any *trans*-3-hexene is made initially. The initial ratio of *cis*- to *trans*-2-hexene is about 0.1. Since the equilibrium ratio is about 0.5, *trans*-2-hexene is formed stereo-selectively.

As shown in Fig. 2, the plot of total 2- and 3-hexenes is a straight line, *i.e.*, the sum of 2- and 3-hexenes is a constant fraction of the hexane formed. Thus, negligible amounts of 2- and 3-hexenes are hydrogenated as long as more than a few % of 1-hexene remains unreacted.

Although hydrogenation of *trans*-2-hexene is suppressed by the presence of 1-hexene, its isomerization is not. *trans*-2-Hexene reacts to form the other hexenes, particularly, *trans*-3-hexene, throughout the course of the reaction. At the point at which 1-hexene has nearly disappeared, the 2- and 3-hexenes are present in nearly their equilibrium ratio (see Table I).

At 100° (Fig. 3 and Table I), the ratio of the initial rates of isomerization and hydrogenation is larger, about 1.5. Further, the hydrogenation of 1-hexene *vs.* the other hexenes is no longer completely selective as is shown by the curvature of the plot of the sum of the 2- and 3-hexenes against hexane in Fig. 3. The relative rate of isomerization of *trans*-2-hexene also is larger, as shown by the greater curvature of its plot against hexane. Beyond the point of near disappearance of 1-hexene, the 2- and 3-hexenes are present in proportions at or not far from the equilibrium ones (see Table I).[11] Thus the relative rates of hydrogenation of the 2- and 3-hexenes must be nearly the same. *cis*- and *trans*-2-hexene are formed in about the same initial ratio as at 62.5°. *cis*-3-Hexene is essentially a secondary product but owing to the augmented relative rate of isomerization of *trans*-2-hexene it is difficult to decide about *trans*-3-hexene.

At 150°, the initial ratio of isomerization to hydrogenation is about 2.6. Since the curvature of the plot of 2- + 3- hexenes *vs.* hexane is considerably larger than at 100°, selectivity for hydrogenation of 1-hexene is further reduced. The curvature of the plot of *trans*-2-hexene also is larger. The data do not give a good test as to whether or not *cis*- and *trans*-3-hexene are primary products.[12]

(10) N. S. Bhacca, L. F. Johnson, and J. N. Shoolery, "NMR Spectra Catalog," Varian Associates, Palo Alto, Calif., 1962, spectrum 298.

(11) T. M. O'Grady, R. M. Alm, and M. C. Hoff, Preprints, Division of Petroleum Chemistry, American Chemical Society, Vol. 4, No. 4, p. B-65, have reported a study of the direct equilibration of the hexenes at 0° with a sodium-on-alumina catalyst. Their values deviate from those computed from the data of Rossini (see Table I) in much the same way as our results at high conversions. In particular the computed value of *cis*-3-hexene appears to be too large, that of *trans*-2-hexene, too small.

The results of a preliminary examination of the reaction between deuterium and 1-hexene at 60 and 140° are given in Tables I and II. Conversions were as low as practicable. The product was separated into three fractions for mass spectroscopy: 1-hexene (contaminated with about 1% *cis*-2-hexene), *trans*-2-hexene (plus about 5% *trans*-3-hexene), and hexane.

During the course of the reaction with deuterium, D_2 adsorbs on the catalyst to give *-D which can undergo isotopic exchange with adsorbed hydrocarbon to form *-H. Let the ratio *-D/*-H be a/b. At 140°, the average deuterium content of the total product was 0.61 atom per mole whereas the total addition of hydrogen and deuterium atoms was twice the hexane fraction, $2 \times 0.069 = 0.138$. Considerable exchange must have occurred between gas phase deuterium and hydrogen atoms of the hydrocarbon. The computed deuterium content of effluent deuterium is 88%. Thus, the rate of desorption of HD was rather large. At 60°, the relative rate of HD desorption was much less: the average deuterium content of product was 0.234 *vs.* 0.17 for addition.

Any particular hydrocarbon desorbs from any particular section of the catalyst surface with various fractions of its hydrogen atoms equilibrated with the surface H–D pool. Let N_x represent the fraction of the particular hydrocarbon in which x atoms have been equilibrated, *i.e.*, the fraction of hydrocarbon-$(h,d)_x$.[13] The species, hydrocarbon-$(h,d)_x$, will be distributed as hydrocarbon-d_0, hydrocarbon-d_1, ... hydrocarbon-d_x according to the local value of a/b.[13]

1-Hexene undergoes isotopic exchange to form 1-hexene-*d* faster than it isomerizes or hydrogenates. At 60°, formation of 1-hexene-*d* is 1.5 times faster than hydrogenation, at 140°, 7.2 times faster. As shown by n.m.r. only the single hydrogen atom at position-2 exchanges with any rapidity. This accords with the simple isotopic distribution pattern of 1-hexene: only very small amounts of species with more than one deuterium atom. Thus, for exchanged 1-hexene, $N_1 = 1.0$. Since a/b will have been less than infinity, some "exchanged" 1-hexene was formed as 1-hexene-d_0 and the gross rate of exchange was greater than the mere rate of formation of 1-hexene-2-*d*.

Our deuterogenation data are inadequate for a detailed treatment along the lines given for a similar investigation on platinum.[13] However, for the hexane product of Table II, it is clear that N_2 and N_3 are the only N's which can have substantially non-zero values (N_0 and N_1 are necessarily zero). The patterns may well result from the addition of two (D,H) atoms to the mixture of unreacted 1-hexene and the 1-hexene-d_0 and -d_1 which results from the exchange reaction. At 140°, it appears possible that the average value of a/b was about 1.0 and that the exchange and hydrogenation both occurred on the same sections of the catalyst. This requires almost all of the 1-hexene to have "exchanged," *i.e.*, $N_3 = 1.0$ for hexane and the average $a/b \simeq 1.0$.[14]

The interpretation of the isotopic distribution patterns of *trans*-2-hexene is less clear. Since most conceivable mechanisms would require the isotopic equilibration of one position on carbon atom-1 to accompany isomerization, we assume that $N_0 = 0$. If only one position is equilibrated, $N_1 + N_2 = 1.00$, the non-zero value of N_2 arising from isomerization of 1-hexene-2-*d*. Such a process could largely account for the data of Table II. The species more exchanged than d_2 might result from non-zero values of N_3 formed *via* exchange of the olefinic hydrogen atom at carbon atom-3 and from the contaminating content of *trans*-3-hexene. At 140°, if the two olefinic hydrogen atoms of 2-hexene exchange on the same sections of the surface as 1-hexene, they must exchange to a much lesser extent since such exchange alone would make $d_{av} = 1.0$. However, the situation is not so clear that we can establish that 1-hexene inhibits the exchange of 2-hexene although, as we have seen, 1-hexene clearly inhibits the hydrogenation of 2-hexene.

Mechanism.—The conventional representation of reactions between hexenes and deuterium on metallic surfaces would be

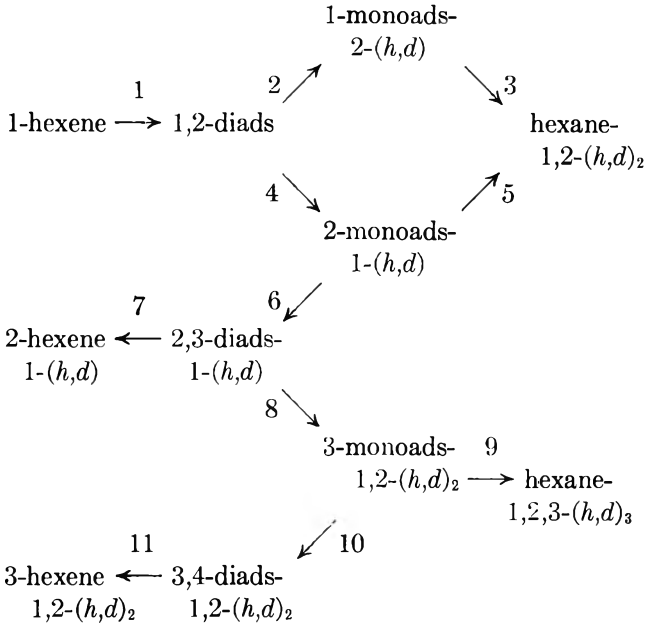

and let a prime on a step number indicate the reverse of that shown in the diagram.

The straight-through reactions, 1-2-3 or 1-4-5, operating on a mixture of 1-hexene and 1-hexene-2-(h,d) would give the type of distribution we observe in the hexane product. Step 4′ cannot occur to any significant extent. Step 2′ might occur in minor degree since it would merely generate hexane-1,2,2-$(h,d)_3$, the same species formed in starting from 1-hexene-2-(h,d). On the whole, however, conversion of monoadsorbed to diadsorbed hexane must be assumed negligible. On most metallic catalysts, a much broader isotopic distribution pattern results from addition of deuterium to olefins,[15] and transformation of mono-

(12) If concentration gradients were severe within the catalyst particles, their centers would be devoid of 1-hexene. 2-Hexene could, then, hydrogenate in this region. At 62.5°, the high selectivity for hydrogenation of 1-hexene demonstrates the absence of severe gradients. At higher temperatures, the lowered selectivity might be the result of the intrusion of severe concentration gradients. Such gradients also would confuse the decision as to whether the 3-hexenes were primary products. See J. Newham and R. L. Burwell, Jr., *J. Phys. Chem.*, **66**, 1431 (1962).

(13) G. V. Smith and R. L. Burwell, Jr., *J. Am. Chem. Soc.*, **84**, 925 (1962).

(14) Presumably, the product hexane is a mixture of that formed at different distances from the entrance to the catalyst bed and the value of a/b varied along the catalyst bed. This will lead to a less peaked isotopic distribution than that computed from an average a/b.

(15) G. C. Bond, "Catalysis by Metals," Academic Press, London, 1962, p. 261, *et seq.*

adsorbed to diadsorbed alkanes must occur with some facility. The situation on copper chromite bears more resemblance to that on chromium oxide gel, on which reversion of monoadsorbed to diadsorbed alkanes is unlikely.[16]

It has been commonly assumed that isomerization and hydrogenation occur on metallic catalysts by interlinked mechanisms on the same sites. In the reaction scheme given above, hydrogenation of 1-hexene would involve steps 1-2-3 or 1-4-5; isomerization of 1- to 2-hexene would involve 1-4-6-7; and isomerization of 2- to 3-hexene, 7′-8-10-11. Since 1-hexene inhibits the hydrogenation of 2-hexene but not its isomerization, one would be required to assume that the presence of 1-hexene inhibits steps 5 and 9 but not 3. If this is unpalatable and if one wishes to retain a Horiuti–Polanyi mechanism, one must assume that isomerization of 2-hexene and hydrogenation of 1-hexene involve different sections of the surface. Alternatively, olefin isomerization might occur by a different mechanism.[17]

If formation of 1-hexene-2-*d* is to occur *via* a Horiuti–Polanyi mechanism on the same sites as those involved in hydrogenation, the sequence must be 1-2-2′-1- and step 4 must be minor since otherwise one would get multiply exchanged 1-hexene and much of the deuterium would be on carbon atom-1. In the reaction alkane ⟶ monoadsorbed alkane on metallic catalysts, formation of a 2-monoadsorbed alkane usually seems to be favored over 1-monoadsorbed alkane.[18] One then might expect that reaction 4 would be preferred over 2. However, it has been argued that a 1,2-diadsorbed alkane would preferably convert to a 1-monoadsorbed alkane, *i.e.*, step 2 would be favored over step 4.[19] The situation is far from clear and a completely different mechanism might be involved, for example, the formation and desorption of 2-monoadsorbed 1-hexene (the Farkas dissociatively adsorbed olefin). On platinum,

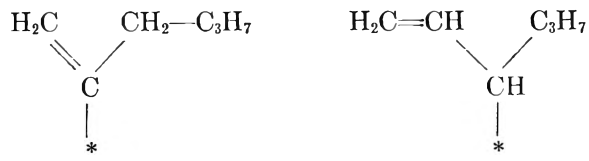

formation and desorption of an allylicly monoadsorbed olefin has been established for $\Delta^{9,10}$-octalin.[13] The analogous formation and desorption of 3-monoadsorbed 1-hexene is, however, of no importance in the present set of reactions.

Acknowledgment.—Acknowledgment is made to the donors of the Petroleum Research Fund, administered by the American Chemical Society, and to the Army Office of Research (Durham) for the support of this research.

(16) R. L. Burwell, Jr., A. B. Littlewood, M. Cardew, G. Pass, and C. T. H. Stoddart, *J. Am. Chem. Soc.*, **82**, 6272 (1960).

(17) *vic*-Diadsorbed alkanes probably exist in eclipsed conformations (R. L. Burwell, Jr., B. K. C. Shim, and H. C. Rowlinson, *J. Am. Chem. Soc.* **79**, 5142 (1957). Step 6 generates two enantiomeric 2,3-diadsorbed hexanes which may be called *cis*- and *trans*-. Steric interference would favor formation of *trans*-2,3-diadsorbed hexane which then desorbs as *trans*-2-hexene. If step 6 is a slow step, the Polyanyi–Horiuti mechanism predicts isomerization preferably to the *trans*-olefin. We observe a high preference for *trans*-2-hexene. However, the hydrogen-switch mechanism (J. Turkevich and R. K. Smith, *J. Chem. Phys.*, **16**, 466 (1948)) also would favor formation of *trans*-2-hexene.

(18) See T. I. Taylor, "Catalysis," Vol. V, P. H. Emmett, Ed., Reinhold Publ. Corp., 1957, pp. 323 and 334; see also ref. 16, p. 6278.

(19) S. Siegel and G. V. Smith, *J. Am. Chem. Soc.*, **82**, 6087 (1960).

CARBON-14-CONTAINING COMPOUNDS PRODUCED BY THE PILE NEUTRON IRRADIATION OF α-CYANOACETAMIDE[1]

BY THOMAS W. LAPP AND ROBERT W. KISER

Department of Chemistry, Kansas State University, Manhattan, Kansas

Received August 20, 1962

We have investigated the nature and relative quantities of the radiocarbon-labelled compounds obtained from the dissolution in water of pile-neutron irradiated α-cyanoacetamide. Succinamide and α-cyanoacetamide were found to contain 23 and 9%, respectively, of the total carbon-14 activity induced in the α-cyanoacetamide sample. A polymeric material, $(>CHC(O)NH-)_x$, was found to contain 44% of the total carbon-14 activity. Little activity was found in twelve other chemical species investigated. Possible paths are suggested leading from the matrix-stabilized species to the final products observed in solution.

Introduction

The capture of a thermal neutron by a nitrogen atom results in the formation of a carbon-14 atom possessing a recoil energy of approximately 40,000 e.v. This large excess of kinetic energy results in complete rupture of all chemical bonds attached to the recoil atom and in projection of the atom into its surroundings. The excess kinetic energy possessed by the recoil carbon-14 atom is dissipated to its surroundings during the course of its movement through the crystalline matrix. The energy dissipation results in the formation of radicals and ions in a region near the recoil path. The fragmentation and recombination processes involving the recoil carbon-14 atom result in a diverse mixture of carbon-14 labeled products. This complex mixture of labeled chemical species, made still more complex because of the gamma radiation accompanying the neutron flux, is evidenced by the products produced in the neutron irradiations.

The formation of carbon-14-labelled products resulting from the neutron irradiation of crystalline acetamide has been studied by Wolf and co-workers[2] and by Lapp and Kiser.[3] The results of these studies indicate that the radical, $\cdot CH_2C(O)NH_2$, produced by the

(1) This work was supported in part by the U. S. Atomic Energy Commission, under contract no. AT(11-1)-751 with Kansas State University, and is a portion of a dissertation to be presented by T. W. Lapp to the Graduate School of Kansas State University in partial fulfillment for the degree of Doctor of Philosophy in Chemistry.

(2) A. P. Wolf, C. S. Redvanly, and R. C. Anderson, *J. Am. Chem. Soc.*, **79**, 3717 (1957).

(3) T. W. Lapp and R. W. Kiser, *J. Phys. Chem.*, **66**, 1730 (1962).

carbon-14 recoil atom and/or by the accompanying γ-radiation, may play an important role in the formation of the neutron-irradiation products observed in solution. Miyagawa and Gordy[4] have studied the production of free radicals in crystalline acetamide by X-irradiation and have shown from their electron spin resonance studies that the principal free radical produced is the $\cdot CH_2C(O)NH_2$ radical.

In an effort to obtain a better understanding of the actual processes occurring during the recombination period, we have extended these studies further. We have irradiated α-cyanoacetamide and subsequently studied the various carbon-14 containing compounds present when the target compound was dissolved in water. In the previous studies of the pile neutron irradiation of crystalline acetamide,[2,3] it was postulated that the formation of those compounds, containing the highest percentage of the total activity isolated, occurred through the intermediate formation of a radiocarbon-labeled $\cdot CH_2CONH_2$ radical. It was anticipated that the neutron irradiation (and simultaneous γ-irradiation) of α-cyanoacetamide might also form the radiocarbon-labeled $\cdot CH_2CONH_2$ radical, in much the same manner as that postulated in the studies of acetamide. If this radical is formed, it should be possible to explain the production of the various carbon-14-containing compounds which one would experimentally observe in the pile-neutron irradiated sample as arising from reactions involving the radio-labeled $\cdot CH_2CONH_2$ radical. We present in this paper our experimental approaches and findings, and attempt to utilize the results in the discussion of possible reactions producing the observed radio-labeled products.

Experimental

Sample Preparation and Irradiation.—White, crystalline α-cyanoacetamide (Eastman Red Label) was held for 1 hr. at 100° and 4.993 g. of the sample was placed in a quartz ampoule which was then attached to a vacuum system. The ampoule and contents were repeatedly flushed with argon and evacuated to less than 1 μ to exclude rigorously oxygen not trapped or dissolved in the solid from the sample. The quartz ampoule was sealed off under vacuum with a hand torch while the contents of the ampoule were maintained at liquid nitrogen temperature. The irradiations were carried out at Oak Ridge National Laboratories in the graphite reactor; pertinent data are as follows: neutron flux of approximately 5×10^{11} cm.$^{-2}$ sec.$^{-1}$; irradiation time of 670 hr.; γ-ray flux of 4.9×10^5 r. hr.$^{-1}$; maximum sample temperature of 80°. The sample was stored for 36 months following irradiation; the ampoule was opened and the extremely dark, shiny appearing contents of the ampoule were transferred to a Pyrex storage bottle. The sample was maintained in a desiccator over $CaCl_2$ during the course of the experimental study.

Preliminary Experiments.—Each carrier or its derivative isolated from the aqueous solution of a portion of the irradiated α-cyanoacetamide was dissolved either directly or by means of a suitable solvent into a scintillator solution. All carbon-14-radioactivity measurements were made using a Packard Tri-Carb liquid scintillation spectrometer. The counting efficiency and scintillator solution used in this study have been described previously.[5] The total carbon-14 activity was determined by dissolution of known portions of the irradiated α-cyanoacetamide in water. Aliquots were taken and the total activity determined by liquid scintillation counting. An average value for three determinations was 14.2 ± 0.4 microcuries for the 4.993-g. sample; *i.e.*, 2.84 ± 0.1 μc./g.

To establish the distribution of the carbon-14 activity among the various species likely to result from the neutron irradiation and the subsequent dissolution of the sample in water, solutions of irradiated α-cyanoacetamide were subjected to analysis for the chemical species listed in Table I.

Chemical Separations.—Analyses usually were made for one carrier in each solution of the target material; in a few cases, two or more carriers were added and analyzed per solution of target sample. The separation of the various activities free from contamination was the principal problem encountered in the procedures employed in this study. Therefore, all compounds and derivatives isolated were purified to constant specific activity by repeated recrystallizations or distillation in an attempt to achieve radiochemical purity.

Separation techniques for essentially all of the chemical species listed in Table 1 have been described previously.[3,5] We note briefly here only those analytical procedures which are new and pertinent to this study.

α-Cyanoacetamide.—α-Cyanoacetamide was separated by multiple recrystallizations from 95% ethanol and dissolved directly into the scintillator solution.

Glycinamide.—Glycinamide was separated by formation of its derivative with phenylisothiocyanate. The derivative was repeatedly recrystallized from water and then dissolved directly into the scintillator solution.

Polymeric Material.—Upon dissolution of a sample of the irradiated α-cyanoacetamide in distilled water, a brown-black material was found to remain undissolved. It was also found that the material was insoluble in many other common solvents, *i.e.*, acetone, ethanol, benzene, chloroform, carbon tetrachloride, etc. However, it was found to be soluble in N,N-dimethylformamide (DMF) as well as soluble in a 10% NaOH solution

TABLE I

CARBON-14 DISTRIBUTION AMONG VARIOUS COMPOUNDS RESULTING FROM PILE NEUTRON IRRADIATION OF α-CYANOACETAMIDE

Fraction	% of total activity	
	Average	Values obtained
HCHO	1.4	1.5, 1.7, 0.9
HCOOH	0.1	0.1, 0.2, 0.0
CH_3OH	.1	.0, 0.2, 0.1
CH_3CN	.2	.2, 0.3, 0.2, 0.0
CH_3NH_2	.1	.0, 0.0, 0.3
CH_3CH_2OH	.0	.0, 0.0, 0.0
$CH_3C(O)CH_3$	.1	.2, 0.0, 0.1
$CH_3C(O)NH_2$	.4	.6, 0.0, 0.9, 0.0, 0.1, 1.0
$NH_2C(O)NH_2$	.1	.1, 0.0, 0.1
$CH_3CH_2C(O)NH_2$	.5	.5, 0.3, 0.8, 0.5
$NH_2CH_2C(O)NH_2$	.1	.0, 0.2
$NCCH_2C(O)NH_2$	9.1	9.6, 8.6, 9.2
$NH_2C(O)CH_2C(O)NH_2$	1.4	1.7, 1.1, 1.4
$NH_2C(O)CH_2CH_2C(O)NH_2$	22.7	22.5, 24.0, 21.7
Polymer	44.2	43.9, 41.1, 47.5

The dark brown material, separated from aqueous solution by centrifugation, was found to have a melting point >342°. Using semiquantitative procedures, we determined that 0.16 g. of this polymeric material was present in 1.00 g. of the irradiated sample. This result does not consider any finite solubility of the polymer in water.

An infrared analysis of the material in a KBr pellet was obtained using a Perkin–Elmer Model 137 Infracord spectrophotometer. The dark polymeric material showed absorptions at 3.0–3.1 μ and 6.1–6.3 μ, which would correspond to a structure of the type $(\rangle CHC(O)NH\text{-})_x$. Using a Cary Model 11 recording spectrophotometer, a sample of the polymeric material dissolved in 10% NaOH did not show any characteristic absorption maxima in the visible or ultraviolet regions. Because of the very limited solubility of the polymeric material in a variety of solvents, an osmometric determination of the molecular weight of the polymer was not possible.

Anal. Calcd. for $(\rangle CHC(O)NH\text{-})_x$: C, 42.86; H, 3.60; N, 24.99; O, 28.55. Found: C, 42.66; H, 3.92; N, 25.24[6]; O, 28.18 (by difference).

A sample of the polymeric material was dissolved in 10% NaOH and added directly to the scintillator solution. This material was found to contain 44% of the total activity.

Evolved Gases.—Upon opening the quartz ampoule containing

(4) I. Miyagawa and W. Gordy, *J. Am. Chem. Soc.*, **83**, 1036 (1961).
(5) T. W. Lapp and R. W. Kiser, *J. Phys. Chem.*, **66**, 152 (1962).
(6) Galbraith Laboratories, Inc., Knoxville, Tennessee.

the target material, the gaseous products, produced by the pile-neutron irradiation, were collected and analyzed by mass spectrometric techniques. The principal products were found to be hydrogen and methane. A quantitative determination of the relative amounts of the gases produced was not obtained, nor was the carbon-14 radioactivity present in these gases determined.

Results of Analyses.—The results obtained by the procedures described above are given in Table I. In all cases the data reported are based on specific activity measurements and the percentage activity is based on the total activity of aliquots of aqueous solutions of the original irradiated α-cyanoacetamide sample.

The total activity isolated in this study was 80.5% of the total carbon-14 activity induced in the α-cyanoacetamide sample by neutron irradiation. Nearly 95% of the total activity isolated in this study occurred in three compounds: α-cyanoacetamide, succinamide, and the polymeric material.

Discussion

The results obtained from the investigation of the system presented in this paper have afforded an interesting insight into possible solid matrix-stabilized species produced during the neutron irradiation of crystalline nitrogen-containing compounds.

By means of the procedures utilized in this investigation, we have considered only the final chemical form of the various species incorporating the recoil carbon-14 atom. It has been suggested previously[7] that many chemical species containing the recoil carbon-14 atom are present within the solid matrix following irradiation. During the subsequent dissolution in water of the crystalline irradiated material, these matrix-stabilized species may undergo decomposition, rearrangement, or other types of reactions. Since only the final form assumed by the recoil carbon-14 atom is actually determined, the chemical species, stabilized within the crystalline matrix, can be estimated only by a critical analysis of the results obtained from a particular determination and the proposition of reasonable intermediates to yield the products experimentally observed.

An important result of this study is that the recoil carbon-14 atom in α-cyanoacetamide does not appear to be stabilized within the solid matrix in the form of a "simple" chemical species or in a form that would undergo a chemical change, such as decomposition or rearrangement, in the presence of water to produce a "simple" compound. This observation has been noted previously in the investigation of the chemical compounds containing the recoil carbon-14 atom which were produced by the neutron irradiation of solid acetamide.[3] The small degree of carbon-14 labeling found in the "simple" compounds suggests the radiocarbon labeling process occurs primarily as a result of reactions with other α-cyanoacetamide molecules within the solid matrix in which the C^{14} atom undergoes a replacement reaction with a carbon atom in the α-cyanoacetamide unlabeled molecule. As a result of this reaction, a fragmentation of the molecule occurs in which only one or two chemical bonds are broken and the multiple rupture of bonds to produce small fragments containing only one carbon atom does not occur to any significant extent. This suggestion is supported by the results observed in the neutron irradiation of crystalline acetamide and by the results reported in the present work. From the results of this study, it is concluded that the $\cdot CH_2C(O)NH_2$ radical plays an important role in the production of the final chemical species incorporating the recoil carbon-14 atom. The production of this radical may occur by a replacement reaction with an α-cyanoacetamide molecule within the solid matrix, after the recoil atom has been slowed down to the point where it is stable toward recombination. This reaction results in the rupture of a carbon–hydrogen bond, in the case of acetamide, and a C–CN bond, in the case of α-cyanoacetamide. This leads to the formation of the radio-labeled $\cdot CH_2C(O)NH_2$ radical, which may then undergo reactions with other molecules of the matrix to produce the final chemical compounds observed. If this process occurs, then the formation of "simple" compounds, containing the recoil carbon-14 atom, would not be expected to take place to any large extent. This result has been verified by the studies performed on acetamide and the results obtained in this study.

An additional and very interesting result of this study is that nearly half of the total activity produced in the pile-neutron irradiation was found in the form of a polymer. The formation of this polymer may be postulated to occur by eq. 1, 2, and 3

$$NCCH_2C(O)NH_2 \xrightarrow{(n,p)} \text{recoil carbon-14} + \text{molecular fragments} \quad (1)$$

$$\text{recoil carbon-14} + NCCH_2C(O)NH_2 \longrightarrow \cdot C^{14}H_2C(O)NH_2 \text{ or } \cdot CH_2C^{14}(O)NH_2 + \cdot CN \quad (2)$$

and

$$\cdot C^{14}H_2C(O)NH_2 \text{ or } \cdot CH_2C^{14}(O)NH_2 \xrightarrow{\gamma\text{-ray}} :C^{14}HC(O)NH\cdot \text{ or } :CHC^{14}(O)NH\cdot \quad (3)$$

The carbon-14-containing radicals might further react with other similar inactive radicals, produced by the recoil carbon-14 atom passing through the matrix and/or by the action of the accompanying γ-radiation.

If a $-G$(α-cyanoacetamide) of 5 is assumed for the γ-damage of α-cyanoacetamide, the radiation damage of the sample is calculated to be about 15%. We have determined experimentally that the polymeric material comprises approximately 16% by weight of the sample. This would imply, however, that all of the α-cyanoacetamide decomposed by the γ-radiation is utilized in the formation of the polymeric material. The formation of radiocarbon-labeled succinamide is also reported in this study, as discussed below. Although the specific quantity was not determined experimentally, we estimate that measurable quantities of succinamide were also formed as a result of the γ-radiation accompanying the neutron flux. Therefore, we estimate a $-G$(α-cyanoacetamide) of >5 as a lower limit, for the γ-damage of α-cyanoacetamide. Tolbert[8] has stated that many compounds have decomposition coefficients (G-values) of 5–10 for irradiation of pure materials *in vacuo*, which is in agreement with our estimated values of > 5.

The results of this study have shown that, in addition to the polymeric material, significant levels of activity were found in only two other compounds, succinamide (23%) and α-cyanoacetamide (9%). The formation of succinamide may be suggested to occur in the same

(7) P. E. Yankwich and W. R. Cornman, Jr., *J. Am. Chem. Soc.*, **77**, 2096 (1955).

(8) B. M. Tolbert, *Nucleonics*, **18**, [8] 74 (1960).

manner as previously reported in the studies of the pile-neutron irradiation of acetamide.[2,3] A possible method for the formation of α-cyanoacetamide, the parent compound, is

$$\cdot C^{14}H_2C(O)NH_2 \text{ or } \cdot CH_2C^{14}(O)NH_2 + \cdot CN \longrightarrow NCC^{14}H_2C(O)NH_2 \text{ or } NCCH_2C^{14}(O)NH_2 \quad (4)$$

Certainly, alternate possibilities for the formation of the three chemical species described above could be written, about which we could only speculate further.

Degradation studies of succinamide, α-cyanoacetamide, and the polymeric material, which would indicate the percentage of carbon-14 labeling at each carbon position, were not performed, so we are unable to indicate specifically the more abundant carbon-14 positions in the product molecules.

The results of this study have shown that the neutron irradiation of crystalline α-cyanoacetamide does not cause the incorporation of carbon-14 into the "simpler" molecules. We would suggest that the incorporation of the recoil carbon-14 atom into the more complex chemical species occurs *via* replacement reactions of the recoil carbon-14 atom with the α-cyanoacetamide molecules of the matrix to produce the $\cdot CH_2C(O)NH_2$ radical. This radical then further reacts with other species present in the matrix to produce the final products observed. The significant effect of the accompanying γ-radiation cannot be disregarded and future studies of the (n,p) processes in the absence of large γ-fluxes would enable further clarification of this suggestion.

Acknowledgments.—The initial stage of this research was supported in part by a grant from the Petroleum Research Fund administered by the American Chemical Society. Grateful acknowledgment hereby is made to the donors of the fund.

SURFACE TENSION AND ADSORPTION IN GAS–LIQUID SYSTEMS AT MODERATE PRESSURES[1]

BY W. L. MASTERTON, J. BIANCHI, AND E. J. SLOWINSKI, JR.

University of Connecticut, Storrs, Connecticut

Received August 21, 1962

Surface tensions at pressures from 1–120 atmospheres have been measured for the following systems: nitrogen–water, nitrogen–*n*-hexane, argon–water, argon–*n*-hexane, argon–*n*-octane, and argon–methanol. Surface tension lowerings are interpreted in terms of surface excesses, $\Gamma_2^{(1)}$ and $\Gamma_2^{(V)}$ of gaseous adsorbents. The data are consistent with a surface structure consisting of a monomolecular layer about 4 Å. thick. This layer appears to be only about 25–40% complete at the highest pressures reached.

Introduction

The investigations of Kundt[2] and Hough[3] on the effect of pressurizing gases on the surface tensions of liquids indicate a strong dependence on the condensability of the gas. This effect was confirmed by work done in this Laboratory,[4] where it was found that the surface tensions of water and *n*-hexane were lowered in progressively greater amounts by hydrogen (b.p. −253°), nitrogen (b.p. −196°), methane (b.p. −161°), ethane (b.p. −89°), and carbon dioxide (subl. temp. −78°).

For the gas–liquid systems listed above, the surface tensions appeared, at least at low pressures, to be a linear function of pressure. At a given gas pressure, the surface tension lowering in dynes/cm. was nearly the same for the two liquids used. The present investigation, which represents a refinement of our earlier work, was designed to establish more exactly: (1) the functional dependence of surface tension upon pressure in representative gas–liquid systems and (2) the influence of the nature of the liquid upon the surface tension lowerings observed with a given gas.

The lowering of liquid surface tensions by pressurizing gases can be attributed qualitatively to adsorption of gas at the liquid surface. Rice[5] has discussed the thermodynamic relationship between surface tension lowering and surface concentration of gaseous adsorbent, based upon the fundamental derivations of Gibbs.[6] The physical interpretation of surface excesses and their calculation from experimentally measurable quantities have been developed in a particularly straightforward manner by Guggenheim.[7] We have chosen to follow Guggenheim's treatment, adapting the relationship derived for liquid–liquid systems to the gas–liquid systems studied in this investigation.

Experimental

Surface tension measurements were made by the capillary-rise technique, using the cell and pressurizing apparatus previously described.[4] The pressure bomb was surrounded by an air bath maintained at a temperature of 30.0 ± 0.1°. Heights were measured with a cathetometer read to ±0.001 cm. Readings were taken at ascending pressures at intervals of approximately 100 p.s.i. To ensure the attainment of equilibrium at each point, the column of liquid in the cell capillary was caused to oscillate 1–2 cm. in both directions before taking a measurement. Duplicate runs were made for each system studied; height readings at corresponding pressures showed an average deviation between runs of ±0.003 cm.

Surface tensions were calculated from the relation[8]

$$\gamma = {}^1/_2 rg\left(h + \frac{r}{3}\right)(\rho_l - \rho_g) \quad (1)$$

(1) Taken in part from an M.S. thesis presented by J. Bianchi, June, 1962. Work supported by the National Science Foundation under NSF-G-10010.

(2) A. Kundt, *Ann. physik. Chem.*, **12**, 538 (1881).

(3) E. W. Hough, B. B. Wood, and M. J. Rzasa, *J. Phys. Chem.*, **56**, 996 (1952).

(4) E. J. Slowinski, Jr., E. E. Gates, and C. E. Waring, *ibid.*, **61**, 808 (1957).

(5) O. K. Rice, *J. Chem. Phys.*, **15**, 333 (1947).

(6) J. W. Gibbs, "Collected Works," Vol. I, Yale University Press, New Haven, Conn., 1948, pp. 219–269.

(7) E. A. Guggenheim and N. K. Adams, *Proc. Roy. Soc.* (London), **A139**, 218 (1933).

(8) A. Weissberger, "Physical Methods of Organic Chemistry," Interscience Publishers, New York, N. Y., 1959, 3rd Ed., Part I, pp. 767–769.

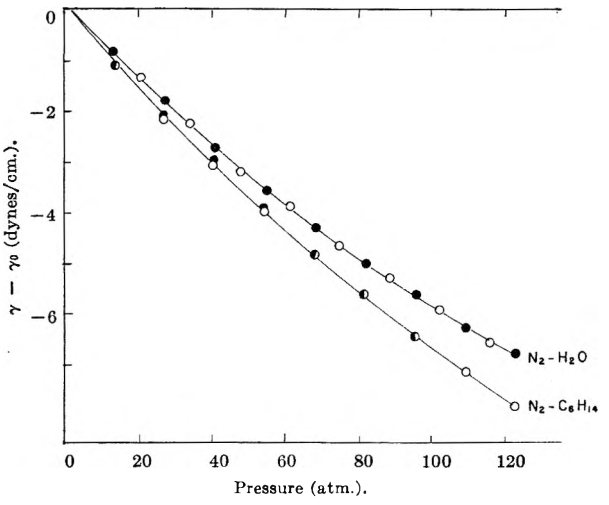

Figure 1.

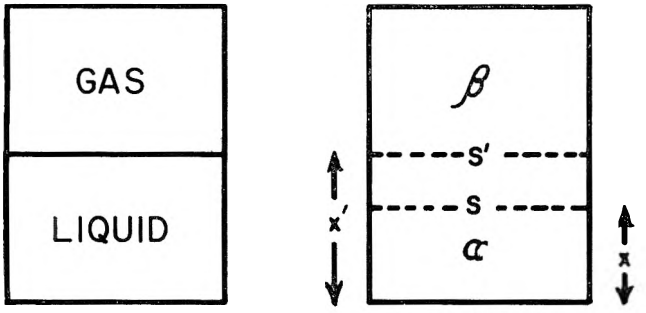

Figure 2.

where γ is the surface tension, r the capillary radius, g the acceleration of gravity, h the capillary rise, ρ_l the density of the liquid phase, and ρ_g the density of the gas phase. The radius (average value = 0.02410 cm.) was determined to ±0.1% at 0.2-cm. intervals along the capillary from capillary rise measurements carried out at atmospheric pressure using water and benzene as calibrating liquids. Liquid densities for the systems involving organic solvents were determined by a closed float method.[9] For the nitrogen–water and argon–water systems, the density of the liquid phase was taken to be that of pure water at the same pressure. Gas densities were calculated from the Beattie–Bridgman equation, making a small correction for the effect of solvent vapor.

The nitrogen and argon used as pressurizing gases were of 99.9 mole % purity. The organic solvents were of 99.6 mole % purity or better. Laboratory distilled water was used without further purification. All solvents were degassed before use by refluxing. Measured surface tensions at 30.0° and atmospheric pressure (71.18, 17.45, 20.72, and 21.81 dynes/cm. for water, *n*-hexane, *n*-octane, and methanol, respectively) agreed with literature values within at least 0.2 dyne/cm.

Results

The surface tension data obtained at 30.0° for the six systems studied may be represented by the quadratic equations

$$N_2\text{–water: } \gamma = \gamma_0 - 0.0732(p - p_0) + 1.42 \times 10^{-4}(p - p_0)^2 \quad (2)$$

$$N_2\text{–}n\text{-hexane: } \gamma = \gamma_0 - 0.0813(p - p_0) + 1.42 \times 10^{-4}(p - p_0)^2 \quad (3)$$

$$\text{Ar–water: } \gamma = \gamma_0 - 0.0733(p - p_0) + 1.27 \times 10^{-4}(p - p_0)^2 \quad (4)$$

$$\text{Ar–}n\text{-hexane: } \gamma = \gamma_0 - 0.0840(p - p_0) + 1.20 \times 10^{-4}(p - p_0)^2 \quad (5)$$

$$\text{Ar–}n\text{-octane: } \gamma = \gamma_0 - 0.0860(p - p_0) + 1.32 \times 10^{-4}(p - p_0)^2 \quad (6)$$

$$\text{Ar–methanol: } \gamma = \gamma_0 - 0.0772(p - p_0) + 1.49 \times 10^{-4}(p - p_0)^2 \quad (7)$$

where γ is in dynes/cm., p in atm., γ_0 = surface tension at atmospheric pressure p_0.

The average deviation of an experimentally determined surface tension from the value predicted by the above equations is ±0.04 dyne/cm. The precision of the measurements is indicated by the reproducibility of the data obtained from duplicate runs on the same system (Fig. 1).

It may be noted that in each case (eq. 2–7), the slope of the plot of γ *vs.* p decreases with increasing pressure; the deviation from a linear relationship is particularly noticeable at high pressures. Surface tension loweringings at a given gas pressure are somewhat greater for the hydrocarbon solvents than for water. The curve for the argon–methanol system lies between that for argon–water and argon–*n*-hexane, closely approaching the former at high pressures. It appears that for these systems there is a qualitative relationship between surface tension lowering and gas solubility in the liquid phase. Nitrogen and argon are nearly 100 times as soluble in solvents such as *n*-hexane and *n*-octane as in water; the solubility of argon in methanol is intermediate between that in non-polar solvents and in water. The qualitative dependence of surface tension lowering on solubility is hardly surprising in view of the direct relation between surface tension lowering and adsorption; one might expect the extent of adsorption of a gas at a liquid surface to parallel to some extent its solubility in the liquid phase.

Interpretation

Surface Excesses.—For a two-component, two-phase system, the relationship between surface tension (γ) and the chemical potentials (μ_1, μ_2) of the components is given by the Gibbs adsorption isotherm which in its most general form may be written

$$d\gamma = -\Gamma_1 d\mu_1 - \Gamma_2 d\mu_2 \quad (8)$$

The quantities Γ_1 and Γ_2 are commonly referred to as "surface excesses" of solvent and solute, respectively. They represent the difference, per cm.^{2} of surface, between the number of moles of a component in the actual system and in a hypothetical system in which the two phases are imagined to be homogeneous up to a mathematical plane drawn parallel to the physical surface.

The numerical magnitudes of Γ_1 and Γ_2 depend upon the position at which one chooses to draw the dividing line in the hypothetical system. The most common choice, and the one which lends itself most readily to the direct calculation of surface excesses from surface tension data, is to draw the line at a position (x in Fig. 2) such that Γ_1 becomes zero. (For a gas–liquid system, this will ordinarily require that the line be drawn somewhat below the physical surface, within the liquid phase.) Adopting this convention, designated by the

(9) W. L. Masterton, D. A. Robins, and E. J. Slowinski, Jr., *J. Chem. Eng. Data*, **6**, 531 (1961).

superscript (1) to conform to Guggenheim's notation, eq. 8 simplifies to

$$d\gamma = -\Gamma_2^{(1)} d\mu_2 \qquad (9)$$

For a gas–liquid system in which the pressure is changing, $d\mu_2$ is given to an excellent degree of approximation by the expression $V_2^0 dp$, where V_2^0 is the molar volume of the pure gas. Therefore

$$d\gamma = -\Gamma_2^{(1)} V_2^0 dp \text{ or } \Gamma_2^{(1)} = \frac{-1}{V_2^0}\frac{d\gamma}{dp} \qquad (10)$$

Equation 10 was used to calculate the values of $\Gamma_2^{(1)}$ reported in Table I; $d\gamma/dp$, obtained in dynes cm.$^{-1}$ atm.$^{-1}$ from eq. 2–7 was converted to cm., while V_2^0 in cm.^{3} mole^{-1} was calculated from the Beattie–Bridgman equation.

More meaningful expressions for Γ may be obtained by drawing the dividing line in the hypothetical system at a point x' such that the geometric surface S' coincides exactly with the limit of homogeneity of the gas phase, β. The surface excess $\Gamma_2^{(V)}$ defined on the basis of this convention becomes the number of moles of solute per cm.^{2} in the surface region minus the number of moles of solute in an equal volume of the bulk liquid phase. The surface excess of solvent, $\Gamma_1^{(V)}$, may be given an analogous interpretation.

To relate $\Gamma_2^{(V)}$ and $\Gamma_1^{(V)}$ to $\Gamma_2^{(1)}$ for a gas–liquid system, it is convenient to start with Guggenheim's general relation (eq. 6 in ref. 7)

$$\Gamma_i' = \Gamma_i + (x' - x)(C_i^\beta - C_i^\alpha) \qquad (11)$$

This gives for the solute the relation

$$\Gamma_2^{(V)} = \Gamma_2^{(1)} + (x' - x)(C_2^\beta - C_2^\alpha) \qquad (12)$$

and for the solvent, where C_1^β is very small compared to C_1^α and $\Gamma_1^{(1)}$ is by definition zero

$$\Gamma_1^{(V)} = -(x' - x)C_1^\alpha \qquad (13)$$

Eliminating the quantity $(x' - x)$ between eq. 12 and 13 gives

$$\Gamma_2^{(V)} = \Gamma_2^{(1)} - \Gamma_1^{(V)}\frac{(C_2^\beta - C_2^\alpha)}{C_1^\alpha} \qquad (14)$$

It is readily shown that, provided the partial molal volumes of solute and solvent, $\bar{V}_2$ and $\bar{V}_1$, have the same values in the surface region as in the interior of the liquid, $\Gamma_2^{(V)}$ and $\Gamma_1^{(V)}$ are related by the simple expression

$$\Gamma_1^{(V)} = -\frac{\bar{V}_2}{\bar{V}_1}\Gamma_2^{(V)} \qquad (15)$$

Substituting (15) in (14) and rearranging, one obtains

$$\Gamma_2^{(V)} = \frac{\Gamma_2^{(1)}}{1 - \frac{\bar{V}_2}{\bar{V}_1}\frac{(C_2^\beta - C_2^\alpha)}{C_1^\alpha}} \qquad (16)$$

Equation 16 was used to calculate the values of $\Gamma_2^{(V)}$ given in Table I from the corresponding values for $\Gamma_2^{(1)}$. Concentrations of solute and solvent in the liquid phase at the various pressures were calculated from solubilities at 1 atm.[10–13] using Henry's law.

(10) F. L. Boyer and L. J. Bircher, *J. Phys. Chem.*, **64**, 1330 (1960).

(11) H. L. Clever, R. Battino, J. H. Saylor, and P. M. Gross, *ibid.*, **61**, 1078 (1957).

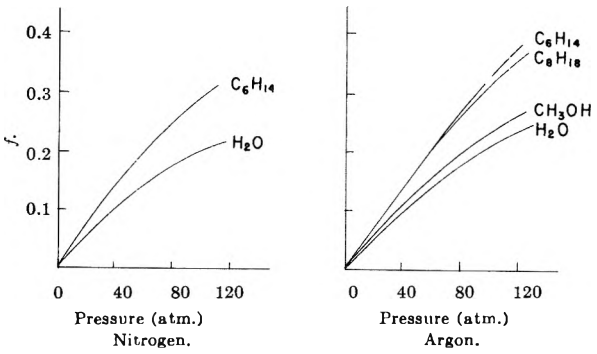

Fig. 3.—Fraction of surface covered by solute molecules.

Partial molal volumes for the systems involving organic solvents were taken from density data previously reported.[9] The partial molal volumes of nitrogen and argon in water were estimated to be about 40 and 35 cc., respectively.[14]

Structure of the Surface.—In order to calculate the number of moles, n_i, of a component in unit area of the surface, it is necessary to add to the surface excess, $\Gamma_i^{(V)}$, an amount equal to the number of moles in an equal volume of the bulk liquid phase. That is

$$n_2 = \Gamma_2^{(V)} + C_2^\alpha t \qquad (17)$$

$$n_1 = \Gamma_1^{(V)} + C_1^\alpha t \qquad (18)$$

where t is the thickness of the surface. To evaluate t, one must choose a suitable model for the surface region. The simplest choice, which will be shown to be consistent with the data, is to take the surface layer to be one molecule thick. On this basis

$$A_1 n_1 + A_2 n_2 = 1 \qquad (19)$$

where A_1 and A_2 are the areas per mole of the components in the unimolecular layer.

Solving eq. 17–19 simultaneously gives

$$t = \frac{1 - A_1\Gamma_1^{(V)} - A_2\Gamma_2^{(V)}}{A_1 C_1^\alpha + A_2 C_2^\alpha} \qquad (20)$$

To evaluate t and thereby n_1 and n_2, areas estimated from adsorption measurements on solids[15] were substituted in eq. 20. In view of the fact that these areas are subject to considerable uncertainty, particularly insofar as their variation with pressure is concerned, it is rather remarkable that the values of t calculated by eq. 20 agree so closely with those obtained from the relation[16]

$$t = \left(\frac{\bar{V}_2}{N}\right)^{1/3} \qquad (21)$$

for the thickness of an argon or nitrogen molecule. This agreement must to some extent be fortuitous; nevertheless it lends support to the concept of a monomolecular surface layer. Only in the two systems involving water as a solvent are there serious discrepancies (Table II). Fortunately, in these systems the value of t is not critical for the calculation of n_2, since

(12) J. C. Gjaldeback and J. H. Hildebrand, *J. Am. Chem. Soc.*, **71**, 3147 (1949).

(13) "International Critical Tables," Vol. III, McGraw-Hill Book Co., New York, N. Y., 1928, pp. 255–256.

(14) J. H. Hildebrand and R. L. Scott, "The Solubility of Non-Electrolytes," 3rd Ed., Reinhold Publ. Corp., New York, N. Y., 1950, p. 247.

(15) H. K. Livingston, *J. Colloid Sci.*, **4**, 447 (1949).

(16) F. E. Bartell and F. C. Benner, *J. Phys. Chem.*, **46**, 847 (1942).

TABLE I

SURFACE EXCESSES IN MOLES/CM.^{2} $\times 10^{11}$

	N_2–water		N_2–*n*-hexane		Ar–water		Ar–*n*-hexane		Ar–*n*-octane		Ar–methanol	
p(atm.)	$\Gamma_2^{(1)}$	$\Gamma_2^{(V)}$	$\Gamma_2^{(1)}$	$\Gamma_2^{(V)}$	$\Gamma_2^{(1)}$	$\Gamma_2^{(V)}$	$\Gamma_2^{(1)}$	$\Gamma_2^{(V)}$	$\Gamma_2^{(1)}$	$\Gamma_2^{(V)}$	$\Gamma_2^{(1)}$	$\Gamma_2^{(V)}$
20	5.4	5.6	6.0	6.2	5.5	5.7	6.4	6.5	6.5	6.7	5.8	6.0
40	9.9	10.6	11.2	12.1	10.3	10.9	12.1	12.7	12.3	12.9	10.7	11.4
60	13.5	15.0	15.4	17.3	14.3	15.6	17.1	18.5	17.3	18.9	14.8	16.3
80	16.1	18.5	18.7	22.0	17.5	19.8	21.4	23.9	21.5	24.3	17.9	20.5
100	17.8	21.2	20.9	25.8	19.9	23.2	24.9	28.8	24.8	29.0	20.0	23.8
120	18.5	22.8	22.3	28.9	21.5	26.0	27.7	33.3	27.3	33.3	21.1	26.2

TABLE II

CALCULATED VALUES OF THE SURFACE THICKNESS, t, AT 100 ATM.[a]

	Equation 20	Equation 21
N_2–water	3.1 Å.	4.0 Å.
N_2–*n*-hexane	4.5	4.6
Ar–water	3.0	3.9
Ar–*n*-hexane	4.5	4.4
Ar–*n*-octane	4.5	4.3
Ar–methanol	3.8	4.2

[a] Areas of molecules (Å.)^2 were taken as follows: H_2O = 11, Ar = 15, N_2 = 16, CH_3OH = 20, *n*-C_6H_{14} = 55, $n-C_8H_{18}$ = 65.

the solubility of the gas, as reflected in C_2^{α}, is extremely small.

Plots (Fig. 3) of the fraction of the total surface area occupied by gas molecules

$$f = n_2 A_2 \qquad (22)$$

as a function of pressure show several interesting features. At the highest pressures reached, only about 25–40% of the surface is occupied by nitrogen or argon molecules, indicating that the monomolecular layer is only partially filled in each of the gas–liquid systems studied.

It is hardly surprising that at pressures up to 100 atm., f for the systems involving hydrocarbon solvents should be a nearly linear function of pressure. The displacement of a hydrocarbon molecule at the surface by a non-polar argon or nitrogen molecule should occur rather easily. One can speculate that at higher pressures where the monomolecular layer approaches completion the extent of adsorption in these systems would begin to level off.

In the two systems involving water as a solvent, deviations from the straight line relationship between f and p appear at pressures well below 100 atm. For example, in the argon–water system, the slope of the curve (Fig. 3) has decreased at 100 atm. to less than one-half of its initial value. Indeed, it would appear that the fraction of the surface occupied by argon molecules is approaching a limiting value corresponding roughly to 30% coverage. This could be interpreted to mean that at low pressures gas molecules enter the surface with relatively little distortion of the water structure, while further adsorption requires the rupture of hydrogen bonds holding water molecules together. A similar though less pronounced effect appears in the argon–methanol system.

THE CONDENSATION COEFFICIENT AND THE VAPORIZATION PROCESS

BY N. W. GREGORY

Department of Chemistry, University of Washington, Seattle, Washington

Received August 23, 1962

Values for the entropies and enthalpies of activation for condensation and vaporization processes and their relation to the condensation coefficient are discussed.

Information on the kinetics of the vaporization of solids may be obtained from steady state (near equilibrium) effusion data as well as from direct measurement of rates of vaporization. Although determination of the actual area of the vaporizing surface is difficult, if not impossible, reasonable values of the condensation coefficient, α_c, the fraction of molecules colliding with the surface which condense, appear to have been determined for a number of vaporization processes. α_c and its temperature dependence can be used to calculate activation enthalpies and entropies for the condensation process and, when used in conjunction with equilibrium vapor pressure data, similar activation values for the vaporization process. The significance of these values, based on a pseudo-equilibrium theory and suggestive of the molecular characteristics in the activated state, depends on the manner in which the activated state is defined and the concomitant method of calculation.

Consider a region on the crystal surface, essentially a monolayer, λ cm. thick. Molecules enter this region from the vapor at a frequency which may be calculated from kinetic gas theory; (the rate of striking is equal to

$$n_g v^* = P(2\pi MRT)^{-1/2} \text{ moles cm.}^{-2} \text{ sec.}^{-1} \qquad (1)$$

where n_g is the number of moles cm.$^{-3}$ of gas, corresponding to the pressure P at temperature T, and $v^* = (kT/2\pi m)^{1/2}$, the average one-dimensional velocity in the direction of surface) or from the solid through vibration of particles at the surface. Only a certain fraction have the necessary characteristics to undergo condensation or vaporization, respectively. For condensation, this fraction is α_c; hence the rate of condensation is equal to

$$\alpha_c P(2\pi MRT)^{-1/2} = \alpha_c n_g v^* \text{ moles cm.}^{-2} \text{ sec.}^{-1} \quad (2)$$

The time of transit through distance λ cm. is λ/v^* sec. Since the number of "activated" molecules ($n^* = \alpha_c n_g$) entering (or which become activated) from the gas is n^*v^* moles cm.$^{-2}$ sec.$^{-1}$, $n^*\lambda$ may be taken as the concentration of condensing molecules in the surface monolayer. Thus the activated state is visualized as a gas molecule, with certain special characteristics, found at a fixed "equilibrium" concentration at the surface monolayer of the crystal. α_c may be considered an "activation equilibrium constant" and used to define and assign values to the enthalpy and entropy of activation for condensation.

$$\alpha_c = K_c^* = \exp(-\Delta F_c^*/RT) = \exp(\Delta S_c^*/R - \Delta H_c^*/RT) \quad (3)$$

ΔS_c^* and ΔH_c^* are standard state values in the usual thermodynamic sense; since the process is unimolecular, however, they represent the difference in the corresponding properties of activated state and normal gas molecules if the two were at the same concentration (ideal gas basis). If α_c is unity at all temperatures, both ΔS_c^* and ΔH_c^* are zero.

α_c may be related to an Absolute Rate Theory type rate constant, k_c. Let rate of condensation = (frequency factor) (moles cm.$^{-2}$ activated molecules in surface monolayer) =

$$(v^*/\lambda)(n^*\lambda) = v^*n^* \text{ moles cm.}^{-2} \text{ sec.}^{-1} \quad (4)$$

$$= k_c n_g \lambda = k_c \frac{n^*}{\alpha_c} \lambda \quad (5)$$

From (4) and (5)

$$k_c = v^*\alpha_c/\lambda = v^*K_c^*/\lambda = (v^*/\lambda)(Z^*/Z_g)\exp(-\Delta E_c^*/RT) \text{ sec.}^{-1} \quad (6)$$

where Z^* and Z_g represent the total partition functions for the activated state and normal gas molecules, respectively, and ΔE_c^* the zero-point energy of activation. Z^* may be expected to correspond to a partition function for a loosely bound molecule on a surface with at least one of the free gas translational degrees of freedom changed to a contribution more nearly equivalent to a low frequency vibration. If α is unity at all temperatures, however, Z^* must be the same as Z_g.

In (6) we have

$$\alpha_c = (Z^*/Z_g)\exp(-\Delta E_c^*/RT) \quad (7)$$

(7) reduces to the same expression given for the transmission coefficient by Mortensen and Eyring[1] under special conditions. They begin with the usual ART form

$$k_c = \kappa(kT/h)(Z^{\ddagger}/Z_i)\exp(-\Delta E_c^*/RT) \quad (8)$$

where κ is the transmission coefficient; $Z^{\ddagger}$, the partition function for the activated state, is taken as that of a normal gas molecule but with only two translational degrees of freedom, and Z_i, the partition function for the initial state, *i.e.*, $Z_i = Z_g$ for the condensation case. Comparing (6) and (8) and recognizing that $kT/h = Z_t^1 v^*/\lambda$ (Z_t^1 is a one-dimensional translational partition function for distance λ) one concludes that

(1) E. M. Mortensen and H. Eyring, *J. Phys. Chem.*, **64**, 846 (1960).

$$\alpha_c = \kappa(Z_t^1 Z^{\ddagger}/Z_g)\exp(-\Delta E_c^*/RT) \quad (9)$$

In the special case where $Z_t^1 Z^{\ddagger} = Z_g$ and the activation energy for condensation is zero, $\alpha_c = \kappa$. α_c, or κ, as noted by Mortensen and Eyring and as seen from (7), then becomes equal to the true partition function of the activated state molecule over that of the normal gas molecule, which, they suggest, will be principally determined by the ratio of the rotational parts of the partition functions.

It should be emphasized that the frequently used alternate form of (8)

$$k_c = \kappa(kT/h)\exp(-\Delta F_c^*/RT) \quad (10)$$

or equivalent expressions in terms of ΔS_c^* and ΔH_c^*, will not give activation entropies and enthalpies equivalent to (3) because the transmission coefficient and kT/h contain some of the pertinent terms of the partition function for the activated state.

At the equilibrium vapor pressure the rate of condensation must equal the rate of vaporization. Equation 4 also may be written for the rate at which vaporizing molecules move through the surface monolayer to the gas phase (v^* is the one-dimensional velocity in the direction away from the surface in this case). An activation "equilibrium constant" for vaporization, K_v^*, which could be called the vaporization coefficient, may be defined as

$$K_v^* = n^*\lambda/n_s\lambda = n^*/n_s \quad (11)$$

where $n^*\lambda$ is again the concentration of molecules in the activated state in moles cm.$^{-2}$ of monolayer, the same as the term considered in the condensation case (rate of vaporization = rate of condensation), and $n_s\lambda$ the corresponding concentration term for the normal solid; n_s may be evaluated from the density of the crystal. Since $n^* = \alpha_c n_g$

$$K_v^* = P_e\alpha_c/n_s RT \quad (12)$$

Thus the rate of vaporization is equal to

$$(v^*/\lambda)(n^*\lambda) = v^*K_v^*n_s \text{ moles cm.}^{-2} \text{ sec.}^{-1} \quad (13)$$

or for the corresponding form of the rate constant

$$k_v = \text{rate vap.}/n_s\lambda = K_v^*v^*/\lambda = (v^*/\lambda)(Z^*/Z_s)\exp(-\Delta E_v^*/RT) \text{ sec.}^{-1} \quad (14)$$

The activation entropy ΔS_v^* and enthalpy ΔH_v^* may be defined by and evaluated from K_v^* and its temperature dependence in the usual fashion. Again these are standard state quantities; for the unimolecular model they relate properties of the activated state and the normal solid at equal concentrations.

The actual fraction of the vibrating particles in the solid surface which have the necessary free energy of activation cannot be determined without knowledge of the actual vibration frequency at the surface. If the ratio v^*/λ over the actual solid surface vibration frequency is x, the concentration of activated molecules in a solid surface monolayer then would be $xn^*\lambda$ moles cm.$^{-2}$, *i.e.*, just sufficient to maintain the concentration $n^*\lambda$ in the transition monolayer. $K_v^{*\prime}$ then might be defined as xn^*/n_s, or xK_v^*.

For an oscillating molecule in the solid with classical energy kT per vibrational degree of freedom, the ve-

locity (in the direction of the surface, one-half the time) ranges from zero to $(2kT/m)^{1/2}$ with a mean roughly equivalent to v^*. The distance to travel is λ cm.; hence the frequency term for such a simple model is virtually the same as for the gas (of the order of 10^{11} sec.$^{-1}$). Alternatively, since the Einstein and Debye models give reasonably similar results at temperatures well above the Debye temperature of the crystal, the mean Debye frequency, 10^{12}–10^{13} sec.$^{-1}$, would seem a reasonable value for the solid surface frequency factor. However, MacRae and Germer[2] have found evidence that the effective Debye temperature on the surface of nickel crystals is about 310°K. as compared with the bulk crystal value 390°K. Furthermore, probability factors also may reduce the effective value of the frequency factor, *i.e.*, if the crystal is not molecular, cooperative movement of the components of the vaporizing molecule is required to separate a molecular unit from the crystal.

It seems reasonable to suggest that the value of x is somewhere between unity and 0.1. If this ratio is not significantly dependent on temperature, the corresponding effect on ΔS_v^* would be *ca.* 0–4.6 e.u. For convenience (11) has been used to define K_v^* and ΔS_v^* and ΔH_v^* without attempting to guess at the magnitude of x.

To relate activation entropies and enthalpies to the usual standard quantities for complete vaporization, it is convenient to choose a standard state for n_g (and therefore n^* in the condensation process) which corresponds to $P = 1$ atm. (as an ideal gas) and for n_s (and therefore n^* for the vaporization process), the normal concentration of molecules in the crystal under 1 atm. external pressure. The following three processes serve to clarify the relationship and significance of these standard state quantities.

(1) Solid (normal) → activated state (an ideal gas surface state at the same concentration as the solid)

$$\Delta F_v^*;\ \Delta H_v^*;\ \Delta S_v^*$$

(2) Activated state (at solid concentration) → activated state (at an ideal gas pressure of 1 atm.)

$$\Delta H = 0;\ -\Delta F = T\Delta S = RT \ln n_s RT$$

(3) Activated state (1 atm.) → gas (normal, standard state, ideal gas, 1 atm.)

$$-\Delta F_c^*;\ -\Delta H_c^*;\ -\Delta S_c^*$$

The sum of the changes (1), (2), and (3) gives the usual standard thermodynamic quantities for the sublimation process as calculated from equilibrium vapor pressure data.

Some results for vaporization of iodine and iron(III) chloride may be considered. For the vaporization of crystalline iodine at 0°, assume $P_e = 4.35 \times 10^{-5}$ atm., $\Delta H_s^0 = 14{,}960$ cal. mole^{-1}, $\Delta S_s^0 = 34.8$ cal. deg.$^{-1}$ mole^{-1}, $\alpha_c = 0.01$, and d ln α_c/d$(1/T) = 1460$.[3] Hence for condensation

$$n^* = 1.94 \times 10^{-11} \text{ mole cm.}^{-3}$$

$$\Delta H_c^* = -2900 \text{ cal. mole}^{-1}$$

$$\Delta S_c^* = -20 \text{ cal. deg.}^{-1} \text{ mole}^{-1}$$

$$\Delta F_c^* = 2500 \text{ cal. mole}^{-1}$$

These numbers are for the reverse of reaction 3 for iodine. For vaporization

$K_v^* = 1 \times 10^{-9}$ from α_c and P_e and $n_s = 0.0194$ mole cm.$^{-3}$ (from the crystal density)

$n^*\lambda = 7.8 \times 10^{-19}$ mole cm.$^{-2}$ monolayer (λ taken as 4×10^{-8} cm.)

$\frac{v^*}{\lambda} = 10^{11}$ sec.$^{-1}$; average Debye frequency (θ_D = 106°) is 1.6×10^{12}

$$\Delta H_v^* = 12060 \text{ cal. mole}^{-1}$$

$$\Delta S_v^* = 3 \text{ cal. deg.}^{-1} \text{ mole}^{-1}$$

$$\Delta F_v^* = 11{,}250 \text{ cal. mole}^{-1}$$

The last three quantities correspond to reaction 1 for iodine. The changes in entropy and free energy for (2) are 12 e.u. and -3276 cal. mole^{-1}, respectively. Relative to the activated state as an ideal gas at 1 atm. pressure, the activation entropy would be 15 e.u. (this value and ΔH_v^* are not quite the same as reported previously,[2] where a slightly different definition of states was used).

Compared to the normal gas state at a comparable pressure, the activated state for iodine has lost nearly 60% of its condensation entropy and about 20% of the condensation enthalpy. If one thinks of a surface molecule with these properties, the energy term appears of the order of a van der Waals interaction; the entropy indicates considerable freedom on the surface but much less than in the gas. From the vaporization point of view, the activated molecules, at an equivalent concentration to the average for the crystal, gain only three entropy units but 80% of the necessary energy for vaporization. A larger increase in entropy is manifested by the change to the gas standard state, or, in the actual vaporization case, by the very low concentration of activated molecules on the surface.

The average Debye frequency, calculated from the ordinary Debye temperature without allowance for surface or for specific effects associated with vaporization from preferred faces or edges, is 16 times larger than v^*/λ.

The simultaneous vaporization reactions

$$2FeCl_3(s) \longrightarrow Fe_2Cl_6(g)$$

$$2FeCl_3(s) \longrightarrow 2FeCl_2(s) + Cl_2(g)$$

recently have been studied by effusion.[4] For the sublimation of Fe_2Cl_6 at 408°K., assume[5] $P_e = 5.5 \times 10^{-6}$ atm., $\Delta H_v^0 = 32{,}600$ cal. mole^{-1}, $\Delta S_v^0 = 56$ cal. deg.$^{-1}$ mole^{-1}, $\Delta F_v^0 = 9800$ cal. mole^{-1}; $\alpha = 7 \times 10^{-3}$ and d ln α/d$(1/T) = -3180$. Hence

$\Delta H_c^* = 6300$	$\Delta H(2) = 0$
$\Delta S_c^* = 5.6$	$\Delta S(2) = 11.2$
$\Delta F_c^* = 4010$	$\Delta F(2) = -4600$

$$\Delta H_v^* = 38900 \text{ cal. mole}^{-1}$$
$$\Delta S_v^* = 50.4 \text{ cal. mole deg.}$$
$$\Delta F_v^* = 18{,}400 \text{ cal. mole}$$

(2) A. U. MacRae and L. H. Germer, *Phys. Rev. Letters*, **8**, 489 (1962).
(3) J. H. Stern and N. W. Gregory, *J. Phys. Chem.*, **61**, 1226 (1957).
(4) R. R. Hammer and N. W. Gregory, *ibid.*, **66**, 1705 (1962).
(5) For a summary of equilibrium data of various workers, see L. E. Wilson and N. W. Gregory, *ibid.*, **62**, 433 (1958).

(if $n_s = 0.0086$ mole cm.$^{-3}$ for $(FeCl_3)_2$)

$$n^*\lambda = 6 \times 10^{-20} \text{ mole cm.}^{-2} \text{ (if } \lambda \cong 5 \times 10^{-6})$$

$$\frac{v^*}{\lambda} = 0.8 \times 10^{11} \text{ sec.}^{-1}$$

(the estimated Debye temperature ~480°K. gives a mean frequency of 0.8×10^{13} sec.$^{-1}$). Here ΔH_c^* and ΔS_c^* are both positive (rather than negative as found for iodine) and ΔH_v^* and ΔS_v^* are very large. The activated state for vaporization–condensation may be presumed to be $FeCl_3$ molecules or perhaps pairs of $FeCl_3$, *i.e.*, incipient Fe_2Cl_6 molecules. The normally large condensation entropy loss as gas molecules move to the activated state may be offset by virtual dissociation of Fe_2Cl_6 into $FeCl_3$ monomers. In the gas phase ΔS^0 for this dissociation is 29.3 e.u.[6] An entropy change approaching this magnitude plus the loss on moving to the surface then could give a net small positive ΔS_c^*. A similar qualitative argument may be presented for a positive ΔH_c^*.

On vaporization, the six iron–chlorine bonds formed by each iron atom in the semi-ionic sandwich layer type solid are replaced by four interactions per iron atom in the gas dimer, or three if the activated state is a monomer; one would expect a large enthalpy and entropy increase in such a process.

The estimated Debye frequency is about one hundred times larger than v^*/λ (using the molecular weight of Fe_2Cl_6). However, in addition to any surface reduction of the Debye temperature, one also would expect probability factors to lower the effective frequency. If the ions in the solid move more or less independently, a coöperative motion of the iron ion and its neighboring chloride ions is required for release of $FeCl_3$(g). If the iron ion and three chloride ions must move together toward the surface while the other three neighboring chloride ions move away, a probability factor between $(1/2)^7\ 20 \cong 1/6$, if any three Cl^-, and 1/128, if only specified ones, might be expected; direct release of Fe_2Cl_6 would be even less probable.

α_c for the process $2FeCl_3(s) \rightarrow 2\ FeCl_2(s) + Cl_2(g)$ is very small and could only be roughly estimated as 10^{-6} with no temperature dependence apparent. With equilibrium data,[7] $\Delta H^0 = 26{,}000$ cal., $\Delta S^0 = 39$ e.u., and $P_e = 4 \times 10^{-6}$ atm. at 408°K., one may tentatively suggest the following

$\Delta H_c^* = 0$	$\Delta H(2) = 0$
$\Delta S_c^* = -27.5$	$\Delta S(2) = 11.2$
$\Delta F_c^* = 11{,}200$	$\Delta F(2) = -4600$

$$\Delta H_v^* = 26{,}000 \text{ cal. mole}^{-1}$$
$$\Delta S_v^* = 0.3 \text{ cal. deg.}^{-1} \text{ mole}$$
$$\Delta F_v^* = 26{,}000 \text{ cal. mole}^{-1}$$
$$n^*\lambda = 3.2 \times 10^{-24} \text{ mole cm.}^{-2}$$
$$(\lambda \sim 3 \times 10^{-8} \text{ cm.})$$
$$v^*/\lambda \cong 1.6 \times 10^{11} \text{ sec.}$$

v^*/λ is somewhat closer to the Debye frequency than in the case of Fe_2Cl_6. The vibration probability factor should be larger here; only two chlorine atoms must move together, while the iron ion with which they are associated in the solid moves away.

ΔH_v^* appears to account for the full vaporization enthalpy and no appreciable change in standard entropy is associated with vaporization activation. The entire entropy of condensation is accounted for by ΔS_c^* together with the standard state change term. The activated state would appear to correspond to an energetically unchanged chlorine gas molecule which finds an appropriate site on the $FeCl_2$–$FeCl_3$ surface; however, the sites are few and far between and virtually no translational motion is permitted once the molecule enters the condensation site.

Acknowledgment.—This work was supported by the National Science Foundation.

(6) W. Kangro and H. Bernstorff, *Z. anorg. allgem. Chem.*, **263**, 316 (1950); H. Schäfer, *ibid.*, **259**, 53 (1949).

(7) H. Schafer and E. Oehler, *ibid.*, **271**, 205 (1953).

THE CONDUCTANCE OF SYMMETRICAL ELECTROLYTES. II. THE RELAXATION FIELD

BY RAYMOND M. FUOSS AND LARS ONSAGER

Contribution No. 1715 from the Sterling Chemistry Laboratory, Yale University, New Haven, Connecticut

Received August 27, 1962

The Poisson equation for the asymmetry potentials of a symmetrical electrolyte in the conductance process has been integrated by the use of the corresponding Green's function in order to obtain the purely electrostatic terms of the relaxation field. The Boltzmann factor in the distribution function was retained explicitly as an exponential throughout the calculation, instead of approximating it as a truncated series as has been customary in previous derivations. The consequence of this refinement in mathematical methods is the appearance in the relaxation field of a term which will lead to a decrease in conductance with increasing concentration or decreasing dielectric constant. The decrease is proportional to the product of concentration and the square of the mean activity coefficient. It depends on dielectric constant through a function which has as its asymptotic limit e^b/b^3 ($b = \epsilon^2/aDkT'$), which is the form of the theoretical association constant for contact pairs. This result means that the *ad hoc* hypothesis of ion pairing controlled by a mass action equilibrium is no longer needed to obtain a satisfactory conductance function; the former mass action term is derivable from the Poisson equation. It was missed in earlier theoretical work by too drastic approximation of the Boltzmann factor.

The relaxation field ΔX which retards the motion of ions moving in an external electrical field is given by the component in the field direction of the negative gradient of the potential ψ' which the asymmetry in the distribution of the other ions produces at the location of a given ion

$$\Delta X = -\nabla_x \psi'(a) = -\partial\psi'/\partial x \qquad (1)$$

The potential is obtained by solving the corresponding Poisson equation

$$n_j \Delta\psi'_j = -(4\pi/D)\Sigma_i f'_{ji}\epsilon_i \qquad (2)$$

but in order to solve (2), the perturbation f'_{ji} in the distribution must, of course, first be known. It can be obtained by solving the equation of continuity, which relates the distribution functions f_{ji} and the velocities of the ions. Previous solutions of the problem have always started with an additive separation

$$f_{ji}(\mathbf{r}) = f^0_{ji}(r) + f'_{ji}(\mathbf{r}) \qquad (3)$$

which eventually required approximating the Boltzmann factor in the distribution function

$$f^0_{ji} = n_j n_i \exp(-\epsilon_i\psi^0_j/kT) \qquad (4)$$

by the first few terms of its series. For low concentrations in solvents of high dielectric constants, this approximation is valid (as confirmed by the excellent agreement in those cases between theory and experiments, but when the dielectric constant becomes small, the exponent

$$\zeta = -\epsilon_i\psi_j/kT \qquad (5)$$

becomes significantly larger than unity, especially for ions in contact, and then the truncated series no longer leads to a conductance equation $\Lambda = \Lambda(c)$ of the correct functional form. (Theory, concave-up; observation concave-down or inflection range, on a $\Lambda - c^{1/2}$ scale.)

An equation which accurately reproduces the observed conductance in these cases can be obtained by postulating first, that ion pairs contribute nothing to conductance, and second, that their concentration can be calculated by a classical mass action equilibrium between free ions and pairs. The earlier forms of this theory encountered difficulties in the definition of ion pairs; these finally were resolved by defining pairs to mean pairs in contact[1] but even so, the *ad hoc* hypothesis of mass action equilibrium had to be retained. If the decrease of conductance ascribed to association were due solely to the effects of electrostatic forces between the ions, one should in principle be able to predict such a decrease from the solution of the Poisson equation, without recourse to an additional hypothesis. Since the theoretical association constant was found to be proportional to e^b, where

$$b = \epsilon^2/aDkT \qquad (6)$$

and since e^b is the value which e^ζ approaches at low concentrations for ions in contact, we began to suspect the series approximation of the Boltzmann factor in the equation of continuity as the source of the failure of the 1957 equation[2] for "associated" electrolytes.

In the previous paper[3] of this series. a new approach to the problem was made in which a multiplicative separation

$$f_{ji}(\mathbf{r}) = f^0_{ji}(r)[1 + \chi_{ji}(\mathbf{r})] \qquad (7)$$

of the distribution function permitted the explicit retention of the exponential function throughout the calculation. Introduction of a function $\theta(r,\vartheta)$ for the coördinate dependence of the asymmetry potentials for binary electrolytes

$$\theta(r,\vartheta) = \psi_1'(\mathbf{r})/\epsilon_1 = -\psi_2'(\mathbf{r})/\epsilon_2 \qquad (8)$$

simplified the Poisson equation to the form

$$\epsilon_1\epsilon_2\Delta\theta = \gamma^2 kTe^\zeta\chi_{21} \qquad (9)$$

where the coefficient

$$\gamma^2 = q^2\kappa^2 = (4\pi/DkT)(n_1\epsilon_1^2\omega_1 + n_2\epsilon_2^2\omega_2)/(\omega_1 + \omega_2) \qquad (10)$$

reduces to $\kappa^2/2$ for this case. where $n_1 = n_2$, $\epsilon_1 = -\epsilon_2$. Then the total electrochemical potential μ_{21} for an ion of species 1 in the vicinity of a reference ion of species 2

$$\mu_{21} = -\epsilon_1 Xx + kT\chi_{21} + \epsilon^2\theta \qquad (11)$$

reduced the equation of continuity to the elegant form

$$\nabla\cdot(e^\zeta\,\Delta\mu_{21}) = V(r) \qquad (12)$$

where $V(r)$ depends on the local velocity field. The latter is known[4] to give terms of order c log c and c in $\Lambda(c)$. In order to focus attention on purely electrostatic terms (rather than hydrodynamic), μ_{21} was separated into two terms

$$\mu_{21} = \mu'_{21} + \mu''_{21} \qquad (13)$$

where μ'_{21} was defined as the solution of the homogeneous equation

$$\nabla\cdot e^\zeta\nabla\mu'_{21} = 0 \qquad (14)$$

leaving μ''_{21}, the term of hydrodynamic origin, as the solution of

$$\nabla\cdot e^\zeta\nabla\mu''_{21} = V(r) \qquad (15)$$

Treatment of (15) will be given in a later paper. The solution of (14) was found to an approximation valid up to terms of order $c^{3/2}$ in $\Lambda(c)$

$$\mu'_{21} = -\epsilon_1 XR(r)\cos\vartheta \qquad (16)$$

where $R(r)$ is given explicitly by eq. (2.31) of part I.

If $\theta(r,\vartheta)$ is separated in a fashion analogous to that for the total potential

$$\theta = \theta' + \theta'' \qquad (17)$$

and likewise χ_{21}, the Poisson equation becomes

$$\Delta\theta' - \gamma^2 e^\zeta\theta' = (\gamma^2 Xe^\zeta/\epsilon_1)[R(r) - r]\cos\vartheta \qquad (18)$$

The purpose of the present paper is to present the solution of (18), which through (1) and (8) will give the electrostatic part ΔX_e of the relaxation field.

Before beginning the mathematical development, it will be convenient to define several new functions. Since $\theta'(r,\vartheta)$ is proportional to the asymmetry potentials ψ'_j, it must satisfy the boundary condition

$$[r(\partial\theta'/\partial r) - \theta']_a = 0 \qquad (19)$$

and since it necessarily is of the form

$$\theta'(r,\vartheta) = H(r)\cos\vartheta = xH/r \qquad (20)$$

(1) R. M. Fuoss, *J. Am. Chem. Soc.*, **80**, 5059 (1959).
(2) R. M. Fuoss and L. Onsager, *J. Phys. Chem.*, **61**, 668 (1957).
(3) R. M. Fuoss and L. Onsager, *ibid.*, **66**, 1722 (1962). Symbols defined in part I will be used in part II without redefinition.
(4) R. M. Fuoss, *ibid.*, **73**, 633 (1959).

the boundary condition simplifies to

$$[r(\mathrm{d}H/\mathrm{d}r) - H]_a = (rH' - H)_a = 0 \quad (21)$$

The part of the relaxation field ΔX_e corresponding to θ' is given by

$$\Delta X_e = -\epsilon_1(\partial\theta'/\partial x)_a \quad (22)$$

$$= -\epsilon_1[H/r - (x^2/r^3)(rH' - H)]_a \quad (23)$$

By virtue of (21), this reduces at once to

$$\Delta X_e = -\epsilon_1 H(a)/a \quad (24)$$

This means that we need only the value of $H(r)$ at $r = a$ in order to obtain ΔX_e. In order to simplify coefficients, we introduce $Q(r)$, defined by

$$Q(r) = -\epsilon_1 H(r)/Xa \quad (25)$$

which leads to the compact statement

$$\Delta X_e/X = Q(a) \quad (26)$$

Here, $Q(r)$ satisfies the differential equation

$$(r^2Q')' - (2 + \gamma^2r^2e^\zeta)Q(r) = -(\gamma^2r^2e^\zeta/a)[R(r) - r] \quad (27)$$

which results from substituting (25) in (20) and the result in (18) and then expanding the Laplacian operator and dividing out $\cos\vartheta$. In (27), primes denote differentiation with respect to r.

Now (27) obviously is a difficult equation to treat, on account of the appearance of e^ζ as a multiplier of the unknown function $Q(r)$ on the left. By expanding essentially in terms of $(e^\zeta - 1)$, however, an approximation to ΔX_e, valid through terms of order κ^2, can be obtained. Let

$$Q(r) = F(r) + g(r) \quad (28)$$

Substitute in (27) and define $F(r)$ as the solution of

$$(r^2F')' - (2 + \gamma^2r^2)F(r) = -(\gamma^2r^2e^\zeta/a)[R(r) - r] \quad (29)$$

whence $g(r)$ is the solution of

$$(r^2g')' - (2 + \gamma^2r^2)g(r) = \gamma^2r^2(e^\zeta - 1)F(r) + \gamma^2r^2(e^\zeta - 1)g(r) \quad (30)$$

It is clear that the first inhomogeneous term of (30) is of order κ^2F, and since F gives as its leading term in $\Lambda(c)$ the square root term ($\sim\kappa$), we conclude that g must give terms of higher order than κ^2. Investigation shows that the leading term of g is of the order $\kappa^3a^3 \ln \kappa a$. The second inhomogeneous term on the right side of (30) is clearly of still higher order. Therefore, in order to obtain $\Lambda(c)$ through terms of order c, we may neglect the contribution of $g(r)$ to (26) and need only the solution of (29) which will give the relaxation field

$$\Delta X_e/X = F(a) \quad (31)$$

to the desired order in concentration. In (31), $F(a)$ is the value at $r = a$ of the solution $F(r)$ of (29), which is subject to the boundary conditions

$$F(\infty) = 0 \quad (32)$$

$$(r\,\mathrm{d}F/\mathrm{d}r - F)_a = 0 \quad (33)$$

The differential equation which determines $F(r)$ can be written symbolically as

$$L(F) = -\phi(r) \quad (34)$$

where L represents the operator on the left in (29) and $-\phi(r)$ the inhomogeneous term on the right. The most direct method of evaluating $F(a)$ is by use of the Green's function[5] $G(r,z)$, by means of which the solution of a differential equation of the form of (29) can be expressed as a definite integral

$$F(r) = \int_a^\infty G(r,z)\phi(z)\,\mathrm{d}z \quad (35)$$

$$= \int_a^r G_{\mathrm{I}}(r,z)\phi(z)\,\mathrm{d}z + \int_r^\infty G_{\mathrm{II}}(r,z)\phi(z)\mathrm{d}z \quad (36)$$

where $G_{\mathrm{I}}(r,z)$ is the value of $G(r,z)$ for $r \geqslant z$ and G_{II} for $r \leqslant z$. The first derivative of $G(r,z)$ has a discontinuity at $r = z$; elsewhere G and its first two derivatives are continuous functions of r for a fixed value of z. Then

$$F(a) = \int_a^\infty G_{\mathrm{II}}(r,z)\phi(z)\,\mathrm{d}z \quad (37)$$

Green's function is constructed from the solutions of the homogeneous equation

$$L(F) = 0 \quad (38)$$

which are

$$f_1(r) = e^{-\gamma r}(1 + \gamma r)/\gamma^2r^2 \quad (39)$$

and

$$f_2(r) = e^{\gamma r}(1 - \gamma r)/\gamma^2r^2 \quad (40)$$

Green's function is defined as

$$G(r,z) = A(z)f_1(r) + B(z)f_2(r) \pm [f_1(z)f_2(r) - f_2(z)f_1(r)]/2p(z)W(z) \quad (41)$$

where $p(z)$ equals z^2 for our operator L and $W(z)$ is the Wronskian

$$W(z) = f_1f_2' - f_1'f_2 = -2/\gamma z^2 \quad (42)$$

In (41), the positive sign holds for $a \leqslant z \leqslant r$ and the negative for $r \leqslant z \leqslant \infty$. The functions $A(z)$ and $B(z)$ are determined by the condition that $G(r,z)$ must satisfy the boundary conditions (32) and (33). From the first

$$B(z) = \gamma f_1(z)/4 \quad (43)$$

Using this result, the second boundary condition then requires

$$[A(z) - f_2(z)]\{r(\mathrm{d}f_1/\mathrm{d}r) - f_1(r)\}_a + 2f_1(z)\{r(\mathrm{d}f_2/\mathrm{d}r) - f_2\}_a = 0 \quad (44)$$

Since the condition applies at $r = a$, the exponentials $e^{\pm\gamma a}$ may be expanded in series; it is found that the two factors in braces in (44) are *identical* through terms of order γ^4a^4. These two terms therefore may be divided out, within the limits of our present approximation, giving

(5) H. Margenau and G. M. Murphy, "The Mathematics of Physics and Chemistry," van Nostrand, New York, N. Y., 1951; pp. 516–519.

$$A(z) = (\gamma/4)[f_2(z) - 2f_1(z)] \quad (45)$$

Substitution of (43) and (45) in (41) and of the result in (37) leads to

$$F(a) = (\gamma/2)[f_1(a) - f_2(a)] \int_a^\infty f_1(r)\phi(r)\, dr \quad (46)$$

Finally, the functions in brackets in (46) are expanded in series; dropping terms of order $\kappa^3 a^3$ and higher, we find

$$F(a) = (\kappa^2/6) \int_a^\infty e^{-\gamma r}(1 + \gamma r)e^{\xi}[R(r) - r]dr \quad (47)$$

There remains the task of evaluating the definite integral in (47) in order to obtain ΔX_e. It is guaranteed convergent by the presence of the factor $e^{-\gamma r}$ in the integrand which, of course, dominates all powers of r. The integral cannot, however, be evaluated in closed form due to the simultaneous presence of $\exp(-\gamma r)$ and $e^{\xi} = \exp(\beta e^{-\kappa r}/r)$; their limits for $r = 0$ are, respectively, 1 and ∞ while for $r = \infty$, they approach 0 and 1. Consequently devices which handle the first function fail for the second and *vice versa*. Fortunately, the leading terms of the integral *qua* function of κ can be evaluated explicitly if all that is required is a conductance function valid through terms of order $c \sim \kappa^2$.

The principle of the method used is illustrated by the following example, which is typical of the terms which appear in (47) when the previously derived value of $R(r)$ is substituted. Consider

$$I(\kappa) = \int_a^\infty e^{-\gamma r} e^{\xi}\, dr \quad (48)$$

Note that the integral in (47) has a coefficient κ^2; hence for our goal, all we need is $I(0)$. But if $\gamma = q\kappa$ is set equal to zero in (48), the integral obviously diverges. Clearly, caution is indicated in the process of letting κ approach zero. The source of the apparent contradiction in convergence properties lies in the square root and transcendental terms of $\Lambda(c)$ which derive from integrals of the form (48). While $I(0)$ is indeed infinite, investigation shows that the limit of $\kappa^2 I(\kappa)$ as κ approaches zero must be of the form

$$\kappa^2 I(\kappa) = A\kappa + B\kappa^2 \ln \kappa a + C\kappa^2 + \ldots \quad (49)$$

We therefore add and subtract compensating terms at strategic points in (48) in such a way that the singularities become harmless, as shown below

$$I(\kappa) = \int_a^\infty e^{-\gamma r}(e^{\xi} - 1 - \xi)\, dr + \int_a^\infty e^{-\gamma r}\, dr + \beta \int_a^\infty e^{-p\kappa r}\, dr/r \quad (50)$$

$$= I_1 + I_2 + \beta I_3 \quad (51)$$

where $p = (1 + q)$. The last two integrals are elementary

$$I_3 = E_n(p\kappa a) \quad (52)$$

where E_n is the negative exponential integral

$$E_n(x) = \int_x^\infty e^{-u}\, du/u = -\Gamma - \ln x + x - \ldots \quad (53)$$

Here Γ is Euler's constant, 0.5772 . . . . .

$$I_2 = e^{-\gamma a}/\gamma = 1/q\kappa - a + \ldots \quad (54)$$

In I_1, we first approximate the exponential $e^{-\kappa r}$ in ξ by $(1 - \kappa r)$, and obtain

$$I_1(\kappa) \approx \int_a^\infty e^{-\gamma r}(e^{\beta/r}e^{-\beta\kappa} - 1 - \beta/r + \beta\kappa)\, dr \quad (55)$$

$$\approx e^{-\beta\kappa} \int_a^\infty e^{-\gamma r}(e^{\beta/r} - 1 - \beta/r)\, dr \quad (56)$$

The coefficient $e^{-\beta\kappa}$ is the limiting value of the square of the activity coefficient because

$$-\ln f_\pm = \epsilon^2\kappa/2DkT = \beta\kappa/2 \quad (57)$$

In the integrand of (56), we may now approximate $e^{-\gamma r}$ by unity because

$$I_1(0) = \int_a^\infty (e^{\beta/r} - 1 - \beta/r)\, dr \quad (58)$$

is convergent, as is readily seen by series expansion of $e^{\beta/r}$ and termwise integration. The first surviving term in the integrand of (58) is $\beta^2/2r^2$ which integrates to $\beta^2/2a^2 = b^2/2$. In the Appendix, it will be shown that

$$\beta I_1(0) = E_p(b) - \ln b - \Gamma - e^b/b + 1 + 1/b \quad (59)$$

where $E_p(b)$ is the positive exponential integral

$$E_p(b) = \int_{-\infty}^b e^u du/u \quad (60)$$

$$\sim (e^b/b)(1 + 1!/b + 2!/b^2 + \ldots) \quad (61)$$

Combining the results for the three terms of $I(\kappa)$, we finally have

$$\kappa^2 I(\kappa) = \beta\kappa^2 f_\pm^2 I_1(0) + \kappa e^{-q\kappa a}/q + \beta\kappa^2 E_n(p\kappa a) \quad (62)$$

By expanding $e^{-q\kappa a}$ and $E_n(p\kappa a)$ in series, it is seen that (62) is of the expected form (49). It is also clear that the integral (47) will lead to terms in $\Lambda(c)$ of the form

$$\Delta\Lambda = \alpha c^{1/2} + \beta c \ln c + \gamma c + \delta e^b f_\pm^2 c + O(c^{3/2}) \quad (63)$$

and we already see the pseudo-mass action term beginning to appear.

Details of the evaluation of the integral (47) are presented in the Appendix. Before stating the final result for ΔX_e, however, it is necessary to calculate the contribution ΔX_a to the relaxation field which was temporarily absorbed into the external field X without change of symbols.[6] This[7] is a term of order κ^2 and we therefore may use the limiting law in its calculation. Define θ_0 by the relation

$$\Psi_0 = \epsilon\theta_0 \quad (64)$$

where the leading term Ψ_0 of the asymmetry potential is known[8]; in our present notation

(6) Reference 3, following eq. 1.25.

(7) (a) R. M. Fuoss and F. Accascina, "Electrolytic Conductance, Interscience Publishers, New York, N. Y., 1959; eq. 14.77; (b) reference 2, eq. 6.22.

(8) Reference 7, eq. 11.29.

$$\theta_0 = (\beta X/\epsilon)(\partial/\partial x)[(e^{-\kappa r} - 1)/\kappa^2 r - (e^{-\gamma r} - 1)/\gamma^2 r] \quad (65)$$

On differentiating with respect to x, and then expanding the exponentials in series

$$\theta_0 = [\beta X \kappa(1 - q)/3\epsilon]r \cos\vartheta + O(\kappa^2) \quad (66)$$

whence

$$\epsilon^2 \nabla\theta_0(a) = \beta\kappa X\epsilon(1 - q)/3 \quad (67)$$

is the result for the correction to the external field due to the asymmetry of the atmosphere of the reference ion. The leading term[9] in ΔX_e is the square root term

$$\Delta X_0 = -\epsilon^2\kappa X/6DkT(1 + q) = -\beta\kappa X/6(1 + q) \quad (68)$$

If we replace X in (68) by $[X + \epsilon\nabla\theta(a)]$, we obtain

$$\Delta X_0/X = -\beta\kappa/6(1 + q) - \beta^2\kappa^2(1 - q)/18(1 + q) \quad (69)$$

and consequently

$$\Delta X_a/X = -\beta^2\kappa^2(1/6 - 2q/9) \quad (70)$$

which is in exact agreement with our 1957 result. Dropping terms of order κ^2 in (66) above is permitted because they would lead to terms of order κ^3 in (70). The value just found for ΔX_a will be combined with the terms obtained by evaluating the integral (47).

We introduce a new independent variable[10] τ at this point

$$\tau = \beta\kappa/2 = 4.2016 \times 10^6 c^{1/2}/(DT)^{3/2} \quad (71)$$

It is the ratio of the Bjerrum distance $\beta/2$, where ion pair probability functions usually have their minima,[11-13] to the distance κ^{-1}, where the maximum charge of the ion atmosphere is located. It varies as $c^{1/2}/(DT)^3$; two electrolytic solutions which have the same value of τ are in corresponding electrostatic states, regardless of concentration, dielectric constant, and temperature. It is shown in the Appendix that the electrostatic part of the relaxation field, obtained by evaluating the integral (47) and inserting the correction (70), is given by the equation

$$\Delta X_e/X = -\tau/3(1 + q) + (\tau^2/3)\ln\tau + \tau^2 N'(b) - \tau^2 e^{-2\tau} K(b) \quad (72)$$

where

$$N'(b) = 1.4985 + (0.2071 T_1 - 0.03066)/(1 - T_1) \quad (73)$$

$$T_1 = e^{-b}(1 + b + b^2/2) \quad (74)$$

and

$$K(b) = (1/3)[E_p(b) - (e^b/b)(1 + 1/b)] \quad (75)$$

Each of the four terms of (72) has a special significance. The first one, in conventional units, becomes

$$\tau/3(1 + q) = \epsilon^2\kappa/6DkT(1 + q) = \alpha c^{1/2} \quad (76)$$

and is seen to be the Onsager limiting value; we note that, in terms of τ as independent variable, the relaxation coefficient is the same for all symmetrical electrolytes. The second one is the former[14] $E_1 c \log c$ and part of the former Jc term; the transcendental term represents the second approximation to the long range shielding. The function $N'(b)$ is not very sensitive to the value of b in the practical working range of this parameter; numerical values are given in Table I. It can be closely approximated by the equation

$$N'(b) = 1.468 + 4.32\exp(-1.17b) \quad (77)$$

TABLE I

VALUES OF $N'(b)$

b	$N'(b)$	b	$N'(b)$
1.5	2.2144	6	1.4795
1.7	2.0181	8	1.4703
2.0	1.8371	10	1.4683
2.5	1.6782	12	1.4679
3.0	1.5973	14	1.4679
4.0	1.5230	∞	1.4678

The last term is the most interesting; the coefficient $e^{-2\tau}$ is recognized as the square of the (limiting) activity coefficient

$$e^{-2\tau} = \exp(-\epsilon^2\kappa/DkT) = f_\pm^2 \quad (78)$$

and using the asymptotic expansion of $K(b)$, we find

$$\tau^2 e^{-2\tau} K(b) \approx (4\pi N a^3 e^b/3000) f_\pm^2 c \quad (79)$$

where the coefficient of $f_\pm^2 c$ is identical with the value of the association constant calculated on the basis of the contact model.[1] Both the last two terms of (72) depend on b, but $K(b)$ increases rapidly with increasing b, as shown in Table II.

TABLE II

VALUES OF $K(b)$

b	$K(b)$	b	$K(b)$
1.5	−0.560	6	2.515
1.7	−0.398	8	7.06
2.0	−0.196	10	23.10
2.5	+0.084	12	88.8
3.0	0.336	14	385.6
4.0	0.856	15	831.0

It is clear that the rapid decrease of conductance at fixed concentration with decreasing dielectric constant finds its theoretical description in the fourth term of (72). Furthermore, the variation of a_J with solvent composition[15] probably is due to the fact that the coefficient J, besides containing $N'(b)$ as it should, also absorbed part of what is here called $K(b)$ as a consequence of the approximation of the Boltzmann factor by the leading terms of its series. In the present calculation, as has been emphasized, the Boltzmann factor is kept intact, and it cannot therefore contribute to the c-term but only to the $cf_\pm^2$ term in the conductance equation.

The last term of (72) will replace the former mass action term $K_A c f_\pm^2$, which in effect was obtained by

(9) Reference 7, eq. 11.40.

(10) R. M. Fuoss and L. Onsager, *Proc. Natl. Acad. Sci. U. S.*, **47**, 818 (1961).

(11) N. Bjerrum, *Kgl. Danske Videnskab Selskab, Mat.-Fys. Medd.*, **7**, 1 (1926).

(12) R. M. Fuoss, *Trans. Faraday Soc.*, **30**, 967 (1934).

(13) J. C. Poirier and J. H. de Lap, *J. Chem. Phys.*, **35**, 213 (1961).

(14) R. M. Fuoss, *J. Am. Chem. Soc.*, **81**, 2659 (1959).

(15) E. Hirsch and R. M. Fuoss, *ibid.*, **82**, 1018 (1960); D. S. Berns and R. M. Fuoss, *ibid.*, **83**, 1321 (1961); J. E. Lind, Jr., and R. M. Fuoss, *J. Phys. Chem.*, **65**, 999, 1414 (1961).

grafting the ion pair hypothesis onto the conductance function for "unassociated" electrolytes.[2] It is now clear that this *ad hoc* hypothesis is no longer necessary; retention of the Boltzmann factor explicit in the equation of continuity

$$\nabla \cdot e^{\zeta} \nabla \mu_{21}' = 0 \qquad (80)$$

automatically leads to the fourth term in (72). The physical meaning of the latter is simply that there will be a decrease in conductance due to pairs of ions in contact (recall that $K(b)$ appears in $F(a)$ as a consequence of setting $r = a$ in the lower limit of the Green integral); the concentration of such pairs is given by the fundamental distribution functions which were used in setting up the equation of continuity. When the part of the relaxation term arising from the velocity field, the osmotic term, and the electrophoresis also have been computed using the Boltzmann factor explicitly, we anticipate a conductance equation of the form

$$\Lambda = \Lambda_0 - Sc^{1/2} + Ec \log c + J'c - K(b)cf^2\Lambda_0 \qquad (81)$$

where S and E have their former values, and J' will have a functional dependence on $b = \beta/a$ which will be different from that of our former $J(a)$. Furthermore, (81) is the limiting form ($\gamma \approx 1$) for low concentrations of the equation

$$\Lambda = \Lambda_0 - Sc^{1/2}\gamma^{1/2} + Ec\gamma \log c\gamma + J'c\gamma - K(b)c\gamma f^2/\Lambda \qquad (82)$$

which has been shown to reproduce conductance data in dilute solutions over a wide range of dielectric constant.[16] Equation 82 is a semi-empirical equation which is obtained by assuming that paired ions do not contribute to transport conductance, and that the fraction $(1 - \gamma)$ of solute present as ion pairs is given by the mass action equation

$$1 - \gamma = K_A c\gamma^2 f_{\pm}^2 \qquad (83)$$

where the former K_A is now identified with the function $K(b)$. Equation 81 is simultaneously an approximate solution (to order $c^{3/2}$) of the fundamental differential equations and the limiting form of (82). We therefore advance the heuristic argument that a more exact theoretical treatment should lead to an equation which would agree with the full form of the empirical eq. 82. Finally, we note that (82) is a two parameter equation: it contains only two arbitrary constants, Λ_0 and b.

Appendix

First we consider the integral $I(\theta)$ which appeared in (58).

$$I(0) = \int_a^{\infty} (e^{\beta/r} - 1 - \beta/r)\, dr = \beta J(0) \qquad (A1)$$

Substitution of $u = \beta/r$ gives

$$I(0) = \beta \int_0^b (e^u - 1 - u)\, du/u^2 \qquad (A2)$$

Partial integration of the term in u^2 leads to

$$J(0) = \int_0^b (e^u - 1)\, du/u - (e^b - 1)/b + \lim (e^u - 1)/u$$

The limit of the last term for $u = 0$ is unity. The first term can be expanded as

$$j_p(b) = \int_0^b (e^u - 1)\, du/u = \int_0^1 (e^u - 1)\, du/u + E_p(b) - E_p(1) - \ln b$$

Series expansion and termwise integration gives the numerical value 1.31789 for the integral above; $E_p(1) = 1.8951$ and the difference is -0.5772, Euler's constant. Therefore

$$j_p(b) = E_p(b) - \ln b - \Gamma \qquad (A3)$$

Substituting in the expression for $J(0)$, we find

$$J(0) = j_p(b) - e^b b + 1/b + 1 \qquad (A4)$$

We now consider the integral (47)

$$F(a) = \frac{\kappa^2}{6} \int_a^{\infty} e^{-\gamma r} (1 + \gamma r) e^{\zeta} [R(r) - r]\, dr \qquad (A5)$$

Substituting the known value of $R(r)$, the bracketed part of the integrand gives

$$e^{\zeta}(1 - T_1)(R - r) = r - \kappa^{-2}(\beta r^{-2} + d\zeta/dr) + \beta e^{-\kappa r} + T_1\kappa^{-2}e^{\zeta}(\beta r^{-2} + d\zeta/dr) - re^{\zeta} \qquad (A6)$$

By the device illustrated by eq. 50, (A6) can be written as a sum of elementary integrals and integrals which converge for $\kappa = 0$, as

$$e^{\zeta}(1 - T_1)(R - r) = \kappa^{-2}(T_1 - 1)(\beta r^{-2} + d\zeta/dr) + \kappa^{-2}T_1(e^{\zeta} - 1)(\beta r^{-2} + d\zeta/dr) - \beta^2 e^{-2\kappa r}/2r - r(e^{\zeta} - 1 - \zeta - \zeta^2/2) \qquad (A7)$$

Then $F(a)$ becomes the sum of four integrals

$$F(a) = -I_1/6 + T_1 I_2/6(1 - T_1) - \beta^2\kappa^2 I_3/12(1 - T_1) - \kappa^2 I_4/6(1 - T_1) \qquad (A8)$$

where $I_1, \ldots, I_4$ correspond to the four terms on the right of (A7). Their evaluation follows.

The first and third are elementary integrals. First

$$I_1 = \int_a^{\infty} e^{-\gamma r} (1 + \gamma r)(\beta r^{-2} + d\zeta/dr)\, dr \qquad (A9)$$

where

$$d\zeta/dr = -\beta e^{-\kappa r}(1 + \kappa r)/r^2 \qquad (A10)$$

Substituting (A10) in (A9) and performing the indicated elementary operations

$$I_1 = (\beta e^{-\gamma a}/a)[1 - e^{-\kappa a} - q\kappa a e^{-\kappa a}/(1 + q)] = \beta\kappa/(1 + q) - \beta\kappa^2 a/2 + O(\kappa^3 a^3) \qquad (A11)$$

$$= 2\tau/(1 + q) - 2\tau^2/b + O(\tau^3) \qquad (A12)$$

The leading term is the limiting $c^{1/2}$ term in the relaxation. Next

(16) See references 7–22 of part I.

$$I_3 = \int_a^\infty e^{-s\kappa a}(1 + \gamma r)\, dr/r \qquad (A13)$$

where

$$s = 2 + q \qquad (A14)$$

$$I_3 = E_n(s\kappa a) + qe^{-s\kappa a}/(2 + q) \qquad (A15)$$

The fourth integral has a coefficient κ^2, and is seen to be convergent for $\kappa = 0$; hence we may set $\kappa = 0$ in the integrand, after factoring out $e^{-2\tau}$ as was done in eq. 56. The result is

$$I_4 = \beta^2 e^{-2\tau} \int_0^b (e^u - 1 - u - u^2/2)\, du/u^3 \qquad (A16)$$

after substituting $u = \beta/r$. By a procedure analogous to that used in evaluating $I(0)$ at the beginning of this section, we find

$$I_4 = (\beta^2 e^{-2\tau}/2)[J(0) - e^b/b^2 + 1/b + 1/b^2 + 1/2] \qquad (A17)$$

Rearrangement of the last four terms in the brackets converts I_4 to the convenient form

$$I_4 = (\beta^2 e^{-2\tau}/2)[J(0) - e^b(1 - T_1)/b^2] \qquad (A18)$$

where

$$T_1 = e^{-b}(1 + b + b^2/2) \qquad (A19)$$

The second integral in (A8) diverges for $\kappa = 0$ but again the device of adding and subtracting compensating terms in the integrand leads to a result which is valid through terms of order κ^2. We proceed as

$$I_2 = \beta \int_a^\infty e^{-\gamma r}(1 + \gamma r)(e^\xi - 1 - \zeta)[1 - e^{-\kappa r}(1 + \kappa r)]\, dr/r^2 + \beta^2 \int_a^\infty e^{-p\kappa r}(1 + \gamma r)[1 - e^{-\kappa r}(1 + \kappa r)]dr/r^3 \qquad (A20)$$

$$= \beta I_{21} + \beta^2 I_{22} \qquad (A21)$$

In I_{21}, the exponentials $e^{-\gamma r}$ and $e^{-\kappa r}$ are expanded in series, giving

$$I_{21} = (\kappa^2 e^{-2\tau}/2) \int_a^\infty (e^{\beta/r} - 1 - \beta/r)\, dr + O(\kappa^3) \qquad (A22)$$

$$= (\beta\kappa^2 e^{-2\tau}/2)[j_p(b) + 1 + 1/b - e^b/b] \qquad (A23)$$

where $j_p(b)$ is defined by (A3). The second integral, I_{22}, can be evaluated explicitly.

$$I_{22} = (e^{-p\kappa a}/2a^2)(1 - \kappa a + q\kappa a) - (e^{-s\kappa a}/2a^2)(1 + q\kappa a) + (\kappa^2/4)[E_n(p\kappa a) + E_n(s\kappa a)] \qquad (A24)$$

where $s = (q + 2)$ and $E_n(x)$ is the negative exponential integral. Expansion of the exponentials in the first two terms on the right of (A24) then gives

$$I_{22} = (\kappa^2/2)(q - 1/2) + (\kappa^2/4)[E_n(p\kappa a) + E_n(s\kappa a)] + O(\kappa^3) \qquad (A25)$$

Substitution of the values of I_{21} and I_{22} in (A21) then evaluates I_2

$$I_2 = (\beta^2\kappa^2 e^{-2\tau}/2)[j_p(b) + 1 + 1/b - e^b/b] + (\beta^2\kappa^2/2)(q - 1/2) + (\beta^2\kappa^2/4)[E_n(p\kappa a) + E_n(s\kappa a)] \qquad (A26)$$

Finally the values of the four integrals are substituted in (A8), giving after rearrangement

$$F(a) = -\tau/3(1 + q) - (\tau^2/3)E_n(s\kappa a) - \tau^2 e^{-2\tau}K(b) + (\tau^2/3)(\ln b + \Gamma - 1) + [\tau^2/3(1 - T_1)][(T_1/2)\{E_n(p\kappa a) - E_n(s\kappa a)\} - q/(2 + q) + T_1(q - 1/2)] \qquad (A27)$$

Further simplification is possible only by expansion of the exponential integrals, using (53). Noting that

$$\kappa a = 2\tau/b \qquad (A28)$$

(A27) becomes

$$F(a) = -\tau/3(1 + q) + (\tau^2/3) \ln \tau - \tau^2 e^{-2\tau}K(b) + N''(b)(\tau^2/3) \qquad (A29)$$

where

$$N''(b) = 2\Gamma - 1 + \ln 2 + \ln (2 + q) + (1 - T_1)^{-1}[T_1(q - 1/2) - q/(2 + q) + (T_1/2) \ln (2 + q)/(1 + q)] \qquad (A30)$$

In order to obtain the final value of ΔX_e, the correction ΔX_a given by (70) is added to (A29); it is a constant times τ^2 and merely changes $N''(b)$ above. On substituting numerical values of the constants, the coefficients shown in (73) result.

A general method for evaluating integrals of the type of I_2 termwise also has been worked out. For further reference, it is described below. Consider

$$I(\lambda\kappa) = \int_a^\infty e^\xi e^{-\lambda\kappa r}\, dr/r^2 \qquad (A31)$$

where λ is a numerical constant (q, $1 + q$, etc.). Assume that $I(\lambda\kappa)$ may be expanded as

$$I(\lambda\kappa) = A + B\kappa + C\kappa E_n(\lambda\kappa a) + D\kappa^2 + F\kappa^2 E_n(\lambda'\kappa a) + \ldots \qquad (A32)$$

where $\lambda' = (\lambda + 1)$ is an abbreviation which will keep the equations more compact. Assume that no higher terms are needed than those given. (The number of terms retained in such expansions depends of course on the power of κ in the coefficient of the integral being considered.) The integral (A32) converges for $\kappa = 0$ and therefore A is obtained simply by setting $\kappa = 0$ in the integrand

$$A = I(0) = \int_a^\infty e^{\beta/r}\, dr/r^2 = (e^b - 1)/\beta \qquad (A33)$$

Differentiating $I(\lambda\kappa)$ partially with respect to κ gives

$$-\beta \int_a^\infty e^\xi e^{-\lambda'\kappa r}\, dr/r^2 - \lambda \int_a^\infty e^\xi e^{-\lambda\kappa r}\, dr/r = B + CE_n(\lambda\kappa a) - Ce^{-\lambda\kappa a} + 2D\kappa + 2F\kappa E_n(\lambda'\kappa a) - F\kappa e^{-\lambda'\kappa a} \qquad (A34)$$

Now compensating terms are inserted in the second integral on the left, giving

$$LHS = -\beta \int_a^\infty e^\xi e^{-\lambda'\kappa r}\, dr/r^2 - \lambda \int_a^\infty e^{-\lambda\kappa r}(e^\xi - 1)\, dr/r - \lambda \int_a^\infty e^{-\lambda\kappa r}\, dr/r$$

The last integral is simply $E_n(\lambda\kappa r)$; therefore by setting

$$C = -\lambda \qquad \text{(A35)}$$

the logarithmic singularity is eliminated from both sides of (A34) and the constant C is determined. After cancelling these terms, κ may be set equal to zero in the result

$$-\beta \int_a^\infty e^{\beta/r}\, dr/r^2 - \lambda \int_a^\infty (e^{\beta/r} - 1)\, dr/r = B + \lambda$$

whence

$$B = -\lambda - \beta A - \lambda j_p(b) \qquad \text{(A36)}$$

where $j_p(b)$ is the integral defined by (A3). Then a second differentiation with respect to κ and a repetition of the compensating process shows that

$$F = \beta(\lambda + 1)^2/2 \qquad \text{(A37)}$$

Finally, letting κ go to zero again, after cancelling exponential integrals on the two sides of the equation, D is evaluated

$$D = \beta^2 A/2 + \beta(1 + 2\lambda) j_p(b)/2 + (\lambda^2/2)J(0) + \lambda^2 a/2 + 3\beta(1 + \lambda)^2/4 \qquad \text{(A38)}$$

where $J(0)$ is the integral defined by (A4).

THE CONDUCTANCE OF SYMMETRICAL ELECTROLYTES. III. ELECTROPHORESIS

BY RAYMOND M. FUOSS AND LARS ONSAGER

Contribution No. 1720 from the Sterling Chemistry Laboratory, Yale University, New Haven, Connecticut

Received October 18, 1962

The electrophoretic velocity in a dilute solution of a symmetrical electrolyte has been computed, with the following improvements over earlier treatments of the problem: (1) the volume force is calculated as the gradient of the potential of the total force acting on an ion instead of being approximated merely by the force due to the external field; (2) the Boltzmann factor is retained explicitly, instead of being approximated by a truncated series; and (3) the Oseen equations of motion (rather than the Stokes) are used. The result gives the Onsager 1926 limiting value ($-\epsilon_j \kappa X/6\pi\eta$) as the leading term; to next approximation, this is opposed by a term proportional to concentration, which depends on $b = \epsilon^2/aDkT$ in a non-exponential fashion. For example, for $b = 1.5 (D \approx 100)$, $F(b) = 2.31$ and for $b = 15$ ($D \approx 10$), $F(b) = -0.77$. The coefficient goes through zero near $b = 5$.

Forces acting on ions in solution are transmitted to the solvent through which they move; the resulting local hydrodynamic currents in the latter are the source of the electrophoretic correction to the mobility. For a solution containing n_i ions of species i per unit volume, the volume force acting on the ions is $\Sigma_i n_i \mathbf{k}_i$, where $\mathbf{k}_i$ is the force acting on one i-ion. In the steady state reached in the conductance process, the net force per unit volume of solution vanishes (there is no bulk flow); therefore

$$\Sigma_i n_i \mathbf{k}_i + n_0 \mathbf{k}_0 = 0 \qquad (1)$$

where $\mathbf{k}_0$ is the average force acting on one of the solvent molecules and n_0 is the number of the latter per unit volume. In the vicinity of a specified reference ion of species j, however, the concentration of i-ions is n_{ji} and the net force acting on an element of volume dV becomes

$$d\mathbf{F} = (\Sigma_i n_{ji} \mathbf{k}_{ji} + n_0 \mathbf{k}_0) dV \qquad (2)$$

where $\mathbf{k}_{ji}$ is the local force acting on an i-ion, given a j-ion at the origin of coördinates. Combining (1) and (2), the elementary volume force becomes

$$d\mathbf{F} = \Sigma_i (n_{ji} \mathbf{k}_{ji} - n_i \mathbf{k}_i) dV \qquad (3)$$

In previous calculations[1-3] of the electrophoretic velocity from (3), the force $\mathbf{k}_{ji}$ was approximated by its leading term $X\epsilon_i \mathbf{i}$, that due to the external field X. This approximation is sufficient to give the limiting square root term, but neglects contributions to the total force produced by the atmospheric fields. As will be shown here, these lead to terms of order c in the conductance function $\Lambda(c)$, and clearly should be considered in any attempt to deal consistently with terms of order c. Their previous neglect is undoubtedly part of the reason for the observed variation[4] of the size parameter a_J derived from J, the coefficient of the linear term in $\Lambda(c)$. The purpose of this paper is to present a higher approximation obtained by using the gradient of the potential of the total force[5] in the calculation of the velocity instead of merely the leading term $X\epsilon_i \mathbf{i}$. The Boltzmann function will be kept explicit.

In our recent computations of the local fields and charge distributions in the ionic atmospheres, we found it convenient to consider for some purposes not just the electrical forces (due to the external field and to local charges) $\mathbf{E}_{ji}\epsilon_i$ but rather the total potential ($\mathbf{E}_{ji} \cdot \epsilon_i - kT$ grad ln f_{ji}). According to the equations of motion for an incompressible fluid, the formal forces representing the concentration gradients will not affect the resulting velocity field; it is exactly compensated by a redefinition of the pressure to include the osmotic pressure. We retained the hypothesis that the atmospheric charge densities of neighboring ions may be superimposed. To that approximation (at least), the local electric field will be a gradient field (derivable from a potential), and the virtual osmotic force field ($-kT$ grad ln f) is inherently a gradient field.

In the first paper[5] of this series, it was shown that the total potentials are

(1) L. Onsager, *Physik. Z.*, **27**, 388 (1926).
(2) L. Onsager and R. M. Fuoss, *J. Phys. Chem.*, **36**, 2689 (1932).
(3) D. J. Karl and J. L. Dye, *ibid.*, **66**, 477 (1962).
(4) J. E. Lind, Jr., and R. M. Fuoss, *ibid.*, **65**, 999, 1414 (1961); **66**, 1727 (1962).
(5) R. M. Fuoss and L. Onsager, *ibid.*, **66**, 1722 (1962). Symbols defined in parts I and II will be used here without redefinition.

$$\mu_{ji} = -\epsilon_i X R(r) \cos\vartheta \quad (4)$$

$$\mu_{ii} = -\epsilon_i X P(r) \cos\vartheta \quad (5)$$

depending on whether the reference ion has a different charge or a like charge with respect to the i-ion located by coördinates r, ϑ. The functions $R(r)$ and $P(r)$ are given by eq. 2.31 and 2.37 of ref. 5. Since the potential depends on both r and ϑ (*i.e.*, on x, y, and z), the simple Stokes equation

$$\mathrm{d}\mathbf{v} = \mathrm{d}\mathbf{F}/6\pi\eta r \quad (6)$$

which is valid when the force $\mathrm{d}\mathbf{F}$ has only an x-component, may no longer be used to calculate the component of local velocity in the field direction. Instead, we must use the more general Oseen equation[6]

$$\mathrm{d}\mathbf{v} = [\mathrm{d}\mathbf{F} + (\mathrm{d}\mathbf{F}\cdot\mathbf{r})\mathbf{r}/r^2]/8\pi\eta r \quad (7)$$

which gives the velocity $\mathrm{d}\mathbf{v}$ produced by a volume force $\mathrm{d}\mathbf{F}$, acting at the origin, at a point located by the vector $\mathbf{r}$ in a medium whose viscosity is η. We are interested only in the component v_{jz} of velocity in the field direction produced by the force; it is obtained by projecting $\mathbf{v}_j$ in the field direction, *i.e.*, by forming the scalar product of $\mathbf{v}_j$ and $\mathbf{i}$, the unit vector in the field direction

$$\mathrm{d}v_{jz} = [\mathbf{i}\cdot\mathrm{d}\mathbf{F}_j + (\mathbf{r}_1\cdot\mathrm{d}\mathbf{F}_j)\cos\vartheta]/8\pi\eta r \quad (8)$$

where $\mathbf{r}_1$ is the unit vector in the radial direction. Let $\mathrm{d}V = 2\pi r^2 \sin\vartheta\ \mathrm{d}\vartheta\ \mathrm{d}r$ be an annular element of volume located by r, ϑ. Then from (3)

$$\mathrm{d}\mathbf{F}_j/\mathrm{d}V = -\Sigma_i n_{ji}\nabla\mu_{ji} \quad (9)$$

where $\mathbf{k}_{ji}$ is replaced by $\nabla\mu_{ji}$ and $\Sigma_i m_i\mathbf{k}_i$ in (3) vanishes by the condition of electroneutrality since $\mathbf{k}_i = X\epsilon_i\mathbf{i}$. For a binary electrolyte, $n_1 = n_2 = n$ and

$$n_{11} = ne^{-\zeta},\ n_{12} = ne^{\zeta} \quad (10)$$

where

$$\zeta = |\epsilon\psi|/kT \quad (11)$$

and ψ is of course the electrostatic potential. Substituting (10) in (9), and recalling that $\epsilon_1 = -\epsilon_2 = \epsilon$, we obtain

$$\mathrm{d}\mathbf{F}_1/\mathrm{d}V = -n_{11}\nabla\mu_{11} - n_{12}\nabla\mu_{12} = \quad (12)$$

$$n\epsilon X[e^{-\zeta}\nabla(P\cos\vartheta) + e^{\zeta}\nabla(R\cos\vartheta)] \quad (13)$$

where

$$\nabla(R\cos\vartheta) = \mathbf{i}(R/r) + \mathbf{r}_1(\mathrm{d}R/\mathrm{d}r - R/r)\cos\vartheta \quad (14)$$

and similarly for $\nabla(P\cos\vartheta)$.

In order to obtain the electrophoretic velocity, the scalar products $\mathbf{i}\cdot\mathrm{d}\mathbf{F}_1$ and $\mathbf{r}_1\cdot\mathrm{d}\mathbf{F}_1$ are formed, using (13) and (14), where $\mathbf{i}\cdot\mathbf{r}_1 = \cos\vartheta$. The results are substituted in (8) and the integrations over ϑ ($0 \leq \vartheta \leq \pi$) and r are performed. The result, after collecting terms and rearranging, is

$$v_{jz} = -(n\epsilon_j X/3\eta)\int_a^\infty [e^{\zeta}\,\mathrm{d}(rR)/\mathrm{d}r - e^{-\zeta}\,\mathrm{d}(rP)/\mathrm{d}r]\,\mathrm{d}r \quad (15)$$

The form of (15) suggests a partial integration. In the exponent ζ, we use the Debye–Hückel first approximation for ψ, giving

$$\xi = \epsilon^2 e^{-\kappa r}/rDkT = \beta e^{-\kappa r}/r \quad (16)$$

where β is a constant defined in (16).

The partial integration leads to the result

$$v_{jz} = -(n\epsilon_j X\beta/3\eta)\int_a^\infty e^{-\kappa r}(1+\kappa r)[e^{\zeta}R(r) + e^{-\zeta}P(r)]\,\mathrm{d}r/r + (n\epsilon_j Xa/3\eta)[e^{b}R(a) - e^{-b}P(a)] \quad (17)$$

where

$$b = \epsilon^2/aDkT \quad (18)$$

The result (17) follows from (15) by inspection: the limits of e^{ζ} and $e^{-\zeta}$ for $r = \infty$ are unity and the limits of both $P(r)$ and $R(r)$ for large r are simply r; hence the integrated term vanishes at the upper limit. At the lower limit, where $r = a$, $e^{\pm\zeta}$ becomes $e^{\pm b}$ plus terms of order κa; since the P-term has a coefficient $(-e^{-\zeta})$, differentiation gives it the same sign as the R-term. There now remains the explicit evaluation of the integral in (17) and the function in brackets.

The functions $P(r)$ and $R(r)$ are given explicitly by the equations[5]

$$P(r) = MP_1(r) + Ne^{\zeta}P_2(r) \quad (19)$$

$$P_1(r) = r + (\beta/\kappa^2 r^2)g_1(r) \quad (20)$$

$$P_2(r) = r + (\beta/\kappa^2 r^2)g_2(r) \quad (21)$$

$$M = T_2/(T_2 - 1) \quad (22)$$

$$N = -1/(T_2 - 1) \quad (23)$$

$$T_2(b) = e^{b}(1 - b + b^2/2) \quad (24)$$

$$g_1(r) = 1 - e^{-\kappa r}(1 + \kappa r) \quad (25)$$

$$g_2(r) = 1 - e^{-\kappa r}(1 + \kappa r + \kappa^2 r^2) \quad (26)$$

$$R(r) = AR_1(r) + Be^{-\zeta}R_2(r) \quad (27)$$

$$R_1(r) = r - (\beta/\kappa^2 r^2)g_1(r) \quad (28)$$

$$R_2(r) = r - (\beta/\kappa^2 r^2)g_2(r) \quad (29)$$

$$A = -T_1/(1 - T_1) \quad (30)$$

$$B = 1/(1 - T_1) \quad (31)$$

$$T_1(b) = e^{-b}(1 + b + b^2/2) \quad (32)$$

Since the operations at this stage of the derivation involve r as the independent variable, the functions P and R above are written as $P(r)$ and $R(r)$ for compactness. We must, however, bear in mind that both functions also depend on concentration *via* κ^2 and on the contact distance $a = \beta/b$.

The integrated term of (17) is easily evaluated, because at $r = a$, the exponential functions in $g_1(a)$ and $g_2(a)$ may be expanded as series, giving

$$g_1(a) = \kappa^2 a^2/2 + O(\kappa^3 a^3) \quad (33)$$

$$g_2(a) = -\kappa^2 a^2/2 + O(\kappa^3 a^3) \quad (34)$$

Higher terms than the one of order $\kappa^2 a^2$ are not needed explicitly here, because the coefficient $(n\epsilon_i Xa/3\eta)$ is already proportional to concentration and terms of order $\kappa^3 a^3$ in $g_1(a)$ and $g_2(a)$ would therefore give

(6) C. W. Oseen, "Hydrodynamik," Akademische Verlagsgesellschaft, Leipzig, 1927.

terms of order κa in $R(a)$ and $P(a)$, whence terms of order $c^{3/2}$ in $\Lambda(c)$. To our present approximation, we may neglect them. The integrated term then becomes

$$(\epsilon_j X\tau^2/6\pi\eta\beta)(b/4)[(1 - T_1)^{-1} - (T_2 - 1)^{-1}] = (\epsilon_j X\tau^2/6\pi\eta\beta)F_2(b) \quad (35)$$

where we have substituted

$$n = \kappa^2/8\pi\beta \quad (36)$$

in the coefficient of the integral of (17), and made use of the abbreviation[5]

$$\tau = \beta\kappa/2 \quad (37)$$

Next we consider the integrals in (17). These are similar to the integrals which appeared in the calculation of the relaxation field[7] and will be evaluated by the methods described in the Appendix of part II of this series. Let I_1 represent one of the integrals in (17)

$$I_1 = \int_a^\infty e^{-\zeta} P(r) e^{-\kappa r}(1 + \kappa r)\, dr/r \quad (38)$$

It diverges for $\kappa = 0$; as we shall see shortly, it is of the form

$$I_1 = A/\kappa + B_1 + CE_n(2\kappa a) + O(\kappa) \quad (39)$$

Since I_1 has a coefficient $n \sim \kappa^2$ in the electrophoretic velocity, it is clear that part of the square root term comes from A/κ, while B_1 contributes to linear terms in Λ(c). The transcendental term in (39) does not, however, lead to an additional c log c term in Λ(c), because it will be found that

$$I_2 = A/\kappa + B_2 - CE_n(2\kappa a) \quad (40)$$

and the exponential integrals therefore cancel in the sum $(I_1 + I_2)$.

On substituting the explicit value of $P(r)$, given by (19)–(26), the following integral appears as one of the terms of I_1

$$I(\kappa) = \int_a^\infty e^{-\zeta} e^{-\kappa r}(1 + \kappa r)\, dr \quad (41)$$

It clearly diverges for $\kappa = 0$, but by adding and subtracting compensating terms in the integrand, we shall see that $I(\kappa)$ can be put into the form

$$I(\kappa) = a_1/\kappa + a_2 + a_3 \ln \kappa a + a_4\kappa \ln \kappa a \quad (42)$$

When inserted in (17) to give the velocity, the coefficient n reduces the a_1/κ term above to the leading square root term in $\Lambda(c)$; the a_3 ln κa term is, as already mentioned, cancelled by an opposing term from I_2; and the a_4 term is of higher order than $\kappa^2 \sim c$ and is therefore dropped.

First, write $I(\kappa)$ as

$$I(\kappa) = \int_a^\infty (e^{-\zeta} - 1 + \zeta)e^{-\kappa r}(1 + \kappa r)\, dr + \int_a^\infty e^{-\kappa r}(1 + \kappa r)\, dr - \beta\int_a^\infty e^{-2\kappa r}(1 + \kappa r)\, dr/r = J_1(\kappa) + J_2(\kappa) - \beta J_3(\kappa) \quad (43)$$

If the exponential $e^{-\zeta}$ in $J_1(\kappa)$ is expanded, the leading term is seen to give

$$J_{11}(\kappa) = (\beta^2/2)\int_a^\infty e^{-3\kappa r}(1 + \kappa r)\, dr/r^2 \quad (44)$$

which clearly converges to $J_{11}(0) = \beta^2/2\ a$ in the limit $\kappa = 0$. The higher terms likewise are well behaved. Hence we need only $J_1(0)$ in order to obtain the desired conductance function

$$J_1(0) = \int_a^\infty (e^{-\beta/r} - 1 + \beta/r)\, dr \quad (45)$$

(A more rigorous argument which justifies replacing $J_1(\kappa)$ by $J_1(0)$ here is given in the Appendix.) By the methods used in part II, $J_1(0)$ is found to have the value

$$J_1(0) = \beta J_n(b) = \beta[j_n(b) - 1 + (1 - e^{-b})/b] \quad (46)$$

where

$$j_n(b) = E_n(b) + \ln b + \Gamma \quad (47)$$

$E_n(b)$ is the negative exponential integral and Γ is Euler's constant, 0.5772157 . . . .

The other two terms of $I(\kappa)$ are familiar integrals

$$J_2(\kappa) = 2e^{-\kappa a}/\kappa + \beta e^{-\kappa a}/b \quad (48)$$

$$J_3(\kappa) = E_n(2\kappa a) + e^{-2\kappa a}/2 \quad (49)$$

We now return to the calculation of I_1. After using the device of compensating terms just described, and using the condition that the sum of M and N must be unity, I_1 can be put into the form

$$I_1 = I_2(\kappa) - \beta I_3(\kappa) + M\beta J_n(b) + (N\beta/\kappa^2)I_4(\kappa) + (M\beta/\kappa^2)I_5(\kappa) \quad (50)$$

The integral $I_4(\kappa)$, given by

$$I_4(\kappa) = \int_a^\infty e^{-\kappa r}(1 + \kappa r)[1 - e^{-\kappa r}(1 + \kappa r)]\, dr/r^3 \quad (51)$$

$$= \int_a^\infty f_4(\kappa r)\, dr \quad (52)$$

is an elementary integral, and is found to have the explicit value

$$I_4(\kappa) = (e^{-\kappa a}/2a^2)(1 - e^{-\kappa a}) + (\kappa e^{-\kappa a}/a) \times (1/2 - e^{-\kappa a}) + \kappa^2 E_n(2\kappa a) - (\kappa^2/2)E_n(\kappa a) \quad (53)$$

On approximating the exponential $e^{-\kappa a}$ by the first few terms of its series, we obtain

$$I_4(\kappa) = 3\kappa^2/4 + \kappa^2 E_n(2\kappa a) - (\kappa^2/2)E_n(\kappa a) + O(\kappa^3 a) \quad (54)$$

The integral $I_5(\kappa)$ is explicitly

$$I_5(\kappa) = \int_a^\infty e^{-\zeta} f_4(\kappa r)\, dr \quad (55)$$

where $f_4(\kappa\pi)$ is the same screening function which appeared in $I_4(\kappa)$. Using the methods described in the Appendix of part II, we find

$$I_5(\kappa) = \kappa^2[3/4 - (1/2)j_n(b) - (1/2)E_n(\kappa a) + E_n(2\kappa a)] \quad (56)$$

Combining the five terms which make up I_1, we obtain the sum

(7) R. M. Fuoss and L. Onsager, *J. Phys. Chem.*, **67**, 621 (1963).

$$I_1 = 2e^{-\kappa a}/\kappa + \beta e^{-\kappa a}/b - \beta e^{-2\kappa a}/2 + 3\beta/4 - (\beta/2)E_n(\kappa a) + \beta M[(1/2)j_n(b) - 1 + (1 - e^{-b})/b] \quad (57)$$

In a similar fashion, the integral I_2 (the term for unlike ions at origin and in dV) can be evaluated; the result is

$$I_2 = 2e^{-\kappa a}/\kappa + \beta e^{-\kappa a}/b + \beta e^{-2\kappa a}/2 - 3\beta/4 + (\beta/2)E_n(\kappa a) + \beta A[(1/2)j_p(b) + 1 - (e^{b} - 1)/b] \quad (58)$$

On adding, considerable simplification by cancellation appears

$$(I_1 + I_2)/\beta = (4e^{-\kappa a}/\beta\kappa)(1 + \kappa a/2) + MF_n(b) + AF_p(b) \quad (59)$$

where $F_n(b)$ and $F_p(b)$ are abbreviations for the bracketed quantities in the preceding two equations. Again expanding $e^{-\kappa a}$ and retaining only terms of order $\kappa^2 a^2$, and abbreviating the last two terms of (59) which depend on b by $F_1(b)$, the integrated terms reduce to

$$(I_1 + I_2)/\beta = 4/\beta\kappa - 2/b + F_1(b) + O(\kappa a) \quad (60)$$

The results (35) and (60) are now substituted in the expression (17) for the component v_{jx} of electrophoretic velocity in the field direction, giving

$$v_{jx} = -\epsilon_j \kappa X/6\pi\eta + (\epsilon_j X\tau^2/6\pi\eta\beta)F(b) \quad (61)$$

where $\tau = \beta\kappa/2$ and $F(b)$ is given by

$$F(b) = 2/b + (b/4)[(1 - T_1)^{-1} - (T_2 - 1)^{-1}] - F_1(b) \quad (62)$$

In turn $F_1(b)$ is given by inspection of (57) and (58); the functions $j_n(b)$ and $j_p(b)$ are defined as

$$j_n(b) = E_n(b) + \ln b + \Gamma \quad (63)$$

$$j_p(b) = E_p(b) - \ln b - \Gamma \quad (64)$$

The "constants" M and A (actually functions of b) are defined by (22) and (30); the corresponding functions $T_2(b)$ and $T_1(b)$ are given explicitly by (24) and (32). As will be shown in the Appendix, for very large values of b, $F(b)$ asymptotically decreases as the logarithm of b

$$F(b) \sim 3/4 - \Gamma/2 - 1/2b - (1/2)\ln b \quad (65)$$

The first term of (61) will be recognized immediately as Onsager's 1926 value for the electrophoretic term of the limiting tangent. The second term of (61) is proportional to the concentration through τ^2 and will contribute a linear term in $\Lambda(c)$ in addition to the $J_1 c$ term of the 1957 equation.[8] It will be noted that the function $F(b)$, for which numerical values are given in Table I,[9] is not a sensitive function and involves no exponential dependence on $b = \epsilon^2/aDkT$, despite the fact that the explicit Boltzmann functions $e^{\pm\zeta}$ were used in the derivation. (We recall that $\zeta(a) = b - \beta\kappa + \ldots$.)

(8) R. M. Fuoss and L. Onsager, *J. Phys. Chem.*, **61**, 668 (1957).

(9) We are grateful to Mr. James F. Skinner of this Laboratory, who programmed the function for computation on the IBM 709.

TABLE I

FUNCTION $F(b)$ OF $b = \epsilon^2/aDkT = 560/\mathring{a}D_{25}$

b	$F(b)$	b	$-F(b)$	b	$-F(b)$
1.5	2.3100	3.0	0.8827	6.0	0.0217
1.6	2.1413	3.2	.7825	6.5	.1054
1.7	1.9912	3.4	.6920	7.0	.1793
1.8	1.8564	3.6	.6095	7.5	.2451
1.9	1.7346	3.8	.5340	8.0	.3043
2.0	1.6239	4.0	.4645	8.5	.3579
2.1	1.5225	4.2	.4001	9.0	.4069
2.2	1.4294	4.4	.3404	9.5	.4524
2.3	1.3434	4.6	.2847	10	.4954
2.4	1.2638	4.8	.2325	11	.5785
2.5	1.1896	5.0	.1837	12	.6454
2.6	1.1203	5.2	.1377	13	.6965
2.7	1.0554	5.4	.0944	14	.7430
2.8	0.9944	5.6	.0536	15	.7857
2.9	0.9370	5.8	.0149		

If one back-tracks through the equations, he finds that $R(r)$, for example, has one term depending on $e^{-\zeta}$. Now $R(r)$ has a multiplier e^{ζ} in the electrophoresis integral—the product e^{ζ}. $e^{-\zeta}$ is of course unity. The other term in $e^{\zeta}R(r)$, which does *not* contain the factor $e^{-\zeta}$, is multiplied by the constant A and the latter contains a factor e^{-b}; again the exponential behavior is suppressed.[10]

Appendix

We now re-examine the integral[11]

$$J_1(\kappa) = \int_a^\infty (e^{-\zeta} - 1 + \zeta)e^{-\kappa r}(1 + \kappa r)\, dr$$

which appeared in the previous discussion. First

$$J_1(\kappa) \leq H(\kappa) = \int_a^\infty (e^{-\zeta} - 1 + \zeta)\, dr \quad (A1)$$

because the screening function $e^{-\kappa r}(1 + \kappa r)$ is always less than unity for $\kappa \neq 0$ and equals unity for $\kappa = 0$. To find the order of the error made in approximating $J_1(\kappa)$ by the constant $H(0)$, consider

$$-\partial H/\partial\kappa = \int_a^\infty (1 - e^{-\zeta})(-\partial\zeta/\partial\kappa)\, dr \quad (A2)$$

Then we see that

$$0 \leq (-\partial H/\partial\kappa) < \int_a^\infty \zeta(-\partial\zeta/\partial\kappa)\, dr \quad (A3)$$

because

$$1 - e^{-\zeta} < \zeta \quad (A4)$$

for all positive values of ζ. Substituting for ζ explicitly

$$0 < (-\partial H/\partial\kappa) < \beta^2 \int_a^\infty e^{-2\kappa r} dr/r = \beta^2 E_n(2\kappa a) \quad (A5)$$

Integrating

$$H(\kappa) < \beta^2 \kappa E_n(2\kappa a) - e^{2\kappa a}/2a \quad (A6)$$

(10) A recent computation[3] of the electrophoresis by electronic computer, starting with the Onsager–Stokes integral and with the Boltzmann factor explicit, leads to an exponential behavior at $r = a$. This result is the consequence of approximating the total force ($-\nabla\mu_{ii}$) by its leading term $X\epsilon_i\mathbf{i}$. The latter gives the correct behavior for large distances, of course, but disregards short range effects. It is the latter which decide the presence or absence of $e^{\pm b}$; as just explained, our formulation *via* explicit Boltzmann function and *total* force (both long and short range) leads to a cancellation of exponential functions in the final result. As shown in part II of this series, the observed e^{b} term in $\Lambda(c)$ has its origin in the relaxation field.

(11) Several related integrals also have been investigated; see L. Onsager and N. N. T. Samaras, *J. Chem. Phys.*, **2**, 528 (1934).

and since $E_n(2\kappa a)$ is of order $\ln 2\kappa a$

$$H(\kappa) = O(\kappa \ln \kappa a) + \text{const.} \quad \text{(A7)}$$

Since $J_1(\kappa)$ has a coefficient of order κ^2, we see that the error in $\Lambda(c)$ resulting from the replacement of $J_1(\kappa)$ by $J_1(0)$ is of order $\kappa^3 \ln \kappa a \sim c^3/2 \ln c$ and hence permissible within our desired order of approximation.

Finally, we consider the asymptotic expansion of the function $F(b)$ which appears in (61); it may be written

$$F(b) = 2/b + (b/4)F_2(b) - MF_n(b) - AF_p(b) \quad \text{(A8)}$$

where $F_2(b)$ is the bracketed quantity in (62), $F_n(b)$ and $F_p(b)$ are the bracketed quantities in (57) and (58), and M and A are given by (22), (24), (30), and (32). Since $T_1 \sim b^2e^{-b}/2$ and $T_2 \sim b^2e^b/2$, it is easy to see that $F_2(b)$ approaches unity for large values of b. The coefficient M also approaches unity. In $F_n(b)$, the function $j_n(b)$ asymptotically behaves like e^{-b}/b and hence becomes negligible compared to $\ln b$; hence

$$F_n(b) \sim 1/b - 1 + \Gamma/2 + (\ln b)/2 \quad \text{(A9)}$$

The last term of (A8) is most readily estimated by carrying the e^{-b} of T_1 inside; $(1 - T_1)$ in the denominator can safely be approximated by unity for large b. Then

$$AF_p(b) \sim (1 + b + b^2/2)[(1/2b)(1 + 1/b + 2!/b^2 + \ldots) - (1 - e^{-b})/b + e^{-b}]$$
$$\sim -b/4 - 1/4 + 1/2b + O(b^{-2}) \quad \text{(A10)}$$

Combining the asymptotic values of the three functions, the final result is

$$F(b) \sim 3/4 - \Gamma/2 - (\ln b)/2 - 1/2b \quad \text{(A11)}$$

For very large values of b

$$F(b) \sim -(\ln b)/2 \quad \text{(A12)}$$

as announced earlier.

KINETICS OF THE ACID-CATALYZED HYDROLYSIS OF ACETAL IN WATER–ACETONE SOLVENTS AT 15, 25, AND 35°

BY RICHARD K. WOLFORD

Solution Chemistry Section, National Bureau of Standards, Washington 25, D. C.

Received August 30, 1962

Rate constants for the acid-catalyzed hydrolysis of acetal in water–acetone mixtures have been obtained as a function of solvent composition and temperature. The reaction rate passes through a minimum at an approximately equimolar mixture of water and acetone. The activation energy determined for solutions of the same composition tends to increase as acetone content increases while the activation energy determined for solutions of the same dielectric constant increases as the dielectric constant of the solvent increases.

Introduction

There are many examples in the literature of the effect of solvent change on acid-catalyzed hydrolysis reactions of esters,[1,2] but the number of such studies dealing with the effect of solvent on acid-catalyzed hydrolysis reactions of acetals has been small.[3] The purpose of this investigation, therefore, was to study the effects of solvent change and temperature on the hydrolysis of acetal, $CH_3CH(OC_2H_5)_2$, in water–acetone mixtures and to compare these results with those obtained for ester hydrolyses by other workers. In addition, a correlation of the kinetic behavior with other measures of acidity in these mixed solvents has been attempted. The relation between the activation energy at constant composition and the activation energy at constant dielectric constant was examined to understand better specific solvation and electrostatic effects.

Acetal hydrolysis in aqueous solution is extremely sensitive to hydrogen ion and undergoes specific hydrogen ion catalysis.[4] The reaction has been studied in amide–water mixtures as a function of temperature and solvent composition.[5] An explanation of the rate behavior in the amide–water system is difficult, due to the complex nature of the solvent. It is to be expected that a better understanding of the hydrolysis of acetal in mixed solvents can be attained by use of the water–acetone solvent system.

Experimental

The rate of reaction was followed by observing the change in density of the reaction mixture using a dilatometric procedure. The apparatus and the method of purifying the acetal already have been described.[5] The rate of the reaction

$$CH_3CH(OC_2H_5)_2 + H_2O \longrightarrow CH_3CHO + 2C_2H_5OH$$

is given by $v = k_1C_A = k_2C_AC_{H^+}$ where k_1 is the first-order rate constant in sec.^{-1}, C_A the molar concentration of acetal, C_{H^+} the stoichiometric molar concentration of hydrochloric acid, and k_2 the second-order rate constant in $\text{sec.}^{-1}\ M^{-1}$. The procedure used to obtain k_1 from dilatometer readings taken at time t is similar to that used by Swinbourne.[6]

Spectral Grade acetone (Eastman White Label) was used without further purification.

All solutions were made up by weight with the appropriate vacuum correction applied. The concentration of each component was based on the total weight of all components. Density measurements at the temperature of the experiment permitted the calculation of molar concentrations.

The rate constants are considered to be accurate to within ± 2%. The reproducibility of a given run is not good for solvent mixtures containing 89 mole % acetone. The reason is that as the acetone content increases, the water content decreases, and since one mole of water reacts per mole of acetal, the initial acetal concentration had to be maintained at a value such that the

(1) E. Tommila and A. Hella, *Ann. Acad. Sci. Fennicae, Ser. A*, **II**, No. 53, 3 (1954).

(2) H. S. Harned and A. M. Ross, *J. Am. Chem. Soc.*, **63**, 1993 (1941).

(3) P. Salomaa, *Acta Chem. Scand.*, **11**, 461 (1957).

(4) J. N. Bronsted and W. F. K. Wynne-Jones, *Trans. Faraday Soc.*, **25**, 59 (1929).

(5) R. K. Wolford and R. G. Bates, *J. Phys. Chem.*, **66**, 1496 (1962).

(6) E. S. Swinbourne, *J. Chem. Soc.*, 2371 (1960).

change in water content was negligible. Thus the requirement that the water content remain constant forces one to decrease the initial acetal concentration and this manifests itself in a decrease in the over-all volume change from which the rate data are obtained.

Results

Pertinent data for the hydrolysis rates of acetal in aqueous hydrochloric acid–acetone solutions at various temperatures are presented in Table I. A close examination of Table I will verify the constancy of k_2 at more than one acid concentration for a given solvent composition.

TABLE I

HYDROLYSIS RATES FOR ACETAL IN HYDROCHLORIC ACID–WATER–ACETONE MIXTURES AT VARIOUS TEMPERATURES

Mole % acetone	$10^3 c_{HCl}$ moles l.$^{-1}$	$10^3 k_1$, sec.$^{-1}$	k_2, l. mole^{-1} sec.$^{-1}$	c (Acetal), mole l.$^{-1}$	Density, g. ml.$^{-1}$	c_{KCl}, moles l.$^{-1}$
			$t = 15°$			
0	2.126	0.825	0.388	0.068	0.9981	....
0	2.126	.838	.394	.068	.9981	....
9.93	2.127	.341	.1601	.068	.9965	....
20.1[a]	5.113	.356	.0696	.065	.9340	....
20.1[a]	5.100	.390	.0764	.065	.9368	.0402
29.9[b]	9.896	.431	.0436	.063	.9094	.0389
29.8[b]	9.923	.420	.0423	.064	.9091	.0234
29.9[b]	9.908	.399	.0403	.063	.9098	....
39.8[c]	19.31	.552	.0286	.062	.8845	....
40.1[c]	19.31	.587	.0304	.062	.8855	.0379
49.9[d]	14.91	.347	.0233	.063	.8642	....
50.0[d]	14.89	.401	.0270	.064	.8658	.0390
49.9[d]	14.91	.364	.0244	.064	.8646	.0156
70.9	10.20	.272	.0267	.033	.8300	....
70.9	10.20	.270	.0265	.033	.8300	....
89.0	5.717	.468	.0819	.021	.8078	....
89.0	5.717	.498	.0871	.021	.8078	....
89.0	5.708	.481	.0842	.020	.8079	....
			$t = 25°$			
9.68	1.049	0.611	0.582	0.067	0.9603	....
19.4	1.114	.300	.269	.072	.9284	....
29.4	1.955	.290	.1483	.063	.8992	....
38.0	1.945	.216	.1108	.062	.8778	....
49.4[e]	8.982	.816	.0909	.057	.8542	....
49.4[e]	4.488	.424	.0945	.057	.8542	....
49.6[e]	8.970	1.040	.1159	.057	.8581	.1055
49.5[e]	8.964	0.949	.1058	.057	.8562	.0493
70.9	5.043	0.561	.1112	.032	.8191	....
70.9	10.07	1.113	.1105	.032	.8192	....
89.0	5.615	1.901	.3386	.020	.7964	....
89.0	3.192	1.102	.3451	.020	.7964	....
			$t = 35°$			
9.69	0.538	1.056	1.964	0.068	0.9538	....
20.0	.515	0.474	0.921	.065	.9181	....
29.8	.981	.512	.522	.063	.8895	....
39.8	.986	.365	.370	.063	.8639	....
47.8	1.424	.486	.341	.061	.8469	....
70.9	1.753	.698	.398	.032	.8076	....
70.9	0.985	.385	.391	.032	.8076	....
89.0	1.043	1.37	1.32	.020	.7849	....
89.0	1.043	1.47	1.41	.020	.7852	....
89.0	1.037	1.44	1.39	.020	.7851	....

Intercepts and positive slopes of plots of log k_2 against the ionic strength.

a	−1.163	0.98
b	−1.402	0.84
c	−1.559	0.74
d	−1.662	1.66
e	−1.041	1.10

The primary salt effect was studied by adding potassium chloride. This was done because acetal hydrolysis in aqueous solution shows an appreciable salt effect.[7] Although there may be some question concerning the proper relations between k_2 and ionic strength, the present results show that a plot of log k_2 against the ionic strength is linear in the range of ionic strength considered (<0.1 M). A theory of ion–neutral molecule reactions predicts such a plot for solutions of constant dielectric constant.[8] From a consideration of the slopes of the plots of log k_2 against the ionic strength listed at the bottom of Table I, it is apparent that values of k_2 for concentrations of hydrochloric acid of the order 1×10^{-2} M or less can be considered as the values at infinite dilution.

Table II was constructed in the following manner. Values of log k_2 were corrected for expansion of the solvent due to temperature change (by using 25° as reference, this correction amounts to about 0.5 to 1.5% in k_2) and then plotted against mole % acetone for the three temperatures (see, for example, Fig. 1, curve A). Values at 10, 20, 30, 40, and 47.5 mole % acetone were interpolated from this graph and are given in Table II. It can be seen from Fig. 1 that the rate passes through a minimum at about an equimolar mixture of acetone and water. This is the same region of solvent composition at which Hammett's acidity function, H_0, for aqueous acetone solutions 0.1 M in hydrochloric acid passes through a maximum.[9] The Hammett acidity function measures the tendency of a solution to transfer a proton to a neutral base.[10]

Activation Energy at Constant Composition.—In order to obtain this quantity, the values of log k_2 (Table II) were plotted against $1/T$. The constants of the Arrhenius equation, $\log k_2 = \log A - \Delta E/(2.3RT)$, were obtained by the least squares treatment, and values of log k_2 calculated from them are given in Table II in parentheses. The uncertainty in the values of the rate constants is such that the error in the activation energies is ±0.4 kcal. mole^{-1}.

Activation Energy at Constant Dielectric Constant.—From the data of Åkerlöf,[11] one can obtain values of the dielectric constant of each of the eight solvent mixtures listed in Table II at each of the three temperatures, in order to examine the variation of log k_2 as a function of dielectric constant. It is remarkable that, at each temperature, log k_2 is a linear function of the dielectric constant over a considerable range of solvent compositions (see, for example, Fig. 1, curve C). There is no difficulty in interpolating values of log k_2 at each of the three temperatures for D_0 = 80, 70, 60, 50, 40, and 35. For a given D_0, log k_2 is found to be linear in $1/T$ and values of ΔE_D, the activation energy at constant dielectric constant, can be calculated as 26.8, 26.5, 26.0, 25.6, 25.0, and 24.2 kcal. mole^{-1}, respectively. A similar interpolation at round values of D_0 is not possible for $D_0 < 35$, but a plot of log k_2 against D_0^{-1} gives the desired information (see, for example, Fig. 1, curve B). The values of ΔE_D obtained with the aid of the latter plot were 25.9, 25.9, 25.1, 24.7, 24.4, 24.5, 23.8, and 21.4 kcal. mole^{-1} at values of D_0 = 58.8, 52.6, 43.5, 40.0, 34.5, 33.3, 26.3, and 24.4, respectively. The

(7) M. Kilpatrick and E. F. Chase, *J. Am. Chem. Soc.*, **53**, 1752 (1931).

(8) S. Glasstone, K. J. Laidler, and H. Eyring, "The Theory of Rate Processes," McGraw-Hill Book Co., Inc., New York, N. Y., 1941, p. 441.

(9) E. A. Braude and E. S. Stern, *J. Chem. Soc.*, 1976 (1948).

(10) L. P. Hammett, "Physical Organic Chemistry," McGraw-Hill Book Co., Inc., New York, N. Y., 1940, p. 267.

(11) G. Åkerlöf, *J. Am. Chem. Soc.*, **54**, 4125 (1932).

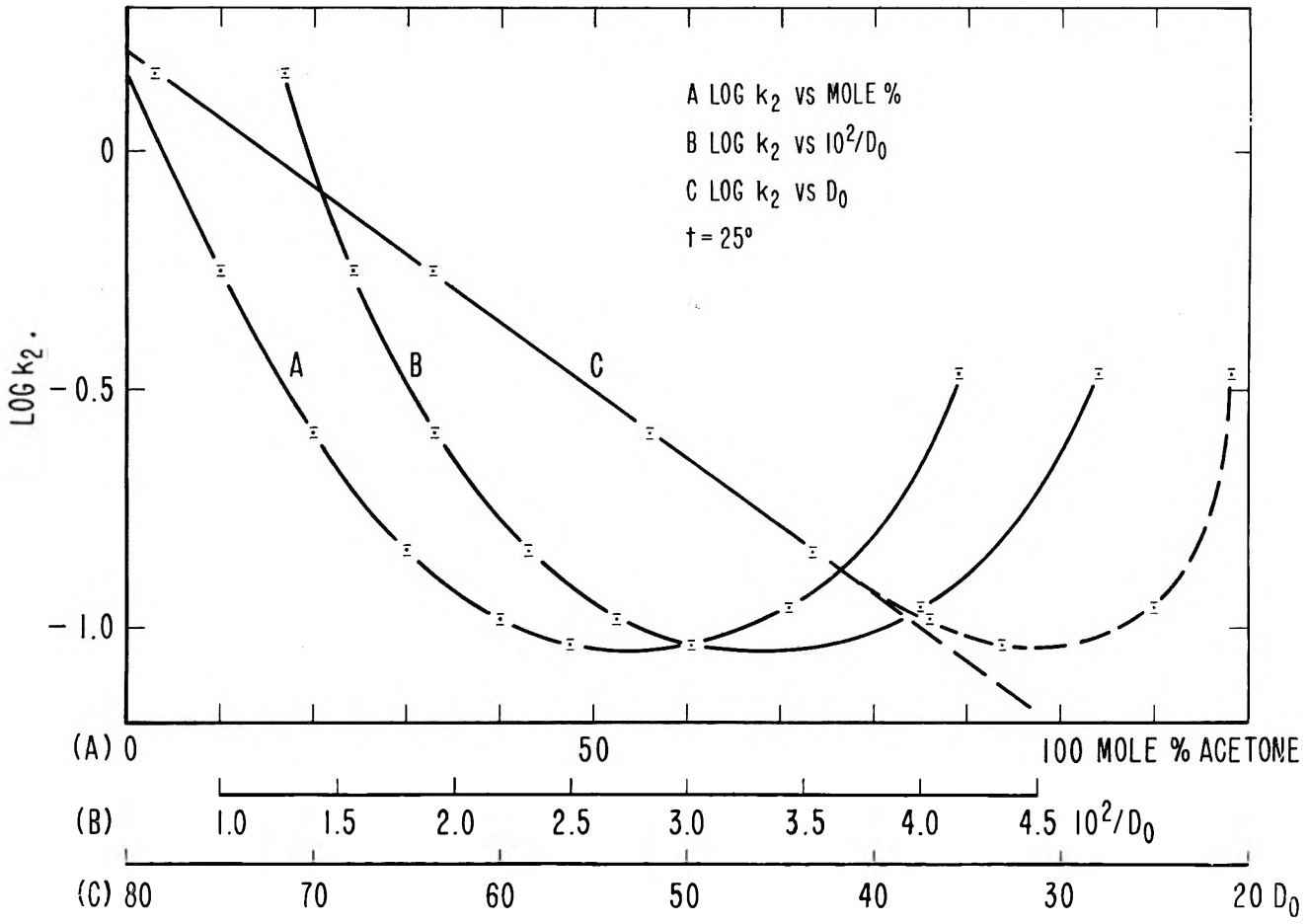

Fig. 1.—Log k_2 (corrected for expansion of the solvent) for the hydrolysis of acetal as a function of mole % acetone (curve A), the reciprocal of the dielectric constant of the solvent (curve B), and the dielectric constant of the solvent (curve C) for aqueous hydrochloric acid–acetone mixtures at 25°.

TABLE II

A COMPARISON OF THE VALUES FOR LOG k_2 AT VARIOUS TEMPERATURES AND SOLVENT COMPOSITIONS WITH THOSE CALCULATED FROM THE ARRHENIUS EQUATION (IN PARENTHESES)

Mole % acetone	15°	20°	25°	30°	35°	log A	ΔE
0	− 0.407	−0.105[a]	+0.165[a]	+0.432[a]	.....	16.6	22.4
	(− .402)	(−0.113)	(+ .166)	(+0.435)			
10	− .793		− .250		+0.282	15.8	21.9
	(− .797)		(− .243)		(+ .278)		
20	− 1.159		− .590		− .040	15.9	22.6
	(− 1.157)		(− .585)		(− .048)		
30	− 1.405		− .837		− .285	15.9	22.8
	(− 1.409)		(− .831)		(− .288)		
40	− 1.560		− .980		− .440	15.7	22.8
	(− 1.560)		(− .982)		(− .439)		
47.5	− 1.635		−1.035		− .470	16.3	23.7
	(− 1.636)		(−1.035)		(− .471)		
70.9	− 1.569		−0.955		− .410	16.3	23.6
	(− 1.564)		(− .966)		(− .404)		
89.0	− 1.069		− .466		+ .131	17.4	24.2
	(− 1.075)		(− .456)		(+ .126)		

[a] R. K. Wolford and R. G. Bates, *J. Phys. Chem.*, 66, 1496 (1962).

results obtained using both procedures appear to agree (Fig. 2).

Discussion

Comparison of Acetal Hydrolysis Rates with Other Acid-Catalyzed Hydrolysis Rates.—The rates[1] for the hydrochloric acid-catalyzed hydrolysis of ethyl formate, ethyl acetate, ethyl propionate, ethyl butyrate, methyl acetate, and propyl acetate all pass through a minimum at about 50 mole % acetone in water–acetone solvents. The Arrhenius parameters ΔE and log A pass through a minimum at about 12 mole % acetone and increase thereafter up to a solvent composition of about 75 mole % acetone. This is very similar to the behavior exhibited by acetal hydrolysis in the same solvent (Fig. 1, Table II), *i.e.*, ΔE and log A pass through a minimum at about 10 mole % acetone and increase thereafter, while at the same time the reaction rate passes through

a minimum at about 50 mole % acetone. It is tempting to conclude that the reaction mechanism is the same for both ester hydrolysis and acetal hydrolysis in these mixed solvents.

Relation between ΔE and ΔE_D.—The relation between the activation energy determined for solutions of the same composition, ΔE, and the activation energy determined for solutions of the same dielectric constant, ΔE_D, is shown in Fig. 2. As the acetone content increases, ΔE_D decreases and ΔE increases. If the present reaction is considered from the point of view of an ion–dipole reaction (solvated proton as ion, neutral acetal molecule as dipole or protonated acetal as ion, and water molecule as dipole), then ΔE_D would be expected to decrease as the acetone content decreases because the attractive force between an ion and a dipole (assuming correct orientation for the dipole) becomes greater as the dielectric constant decreases.

The mechanism of the reaction in the mixed solvents, differences in solvation of the ground state with respect to the transition state as a function of solvent composition, and the interaction between the solvent components (*i.e.*, the structure of the water–acetone solvent) should all manifest themselves in the behavior of ΔE. The generally accepted mechanism for the acid-catalyzed hydrolysis of acetals in aqueous solution[12] consists of a fast pre-equilibrium between solvated proton, acetal, and the protonated form of acetal, followed by the rate-determining unimolecular formation of a carbonium ion from the protonated form of acetal. It has not been established clearly that this mechanism governs the rate when acetone is added.

Some idea of the structure of aqueous acetone solvents may be gained from the fact that measurements of the OH proton resonance shift in water–acetone solvents indicate that hydrogen bonding of water in the mixture is less than that in pure water,[13] that the viscosity passes through a maximum at about 10–12 mole % acetone for water–acetone mixtures,[14] and that the partial molal enthalpy of mixing of acetone passes through a minimum and that for water a maximum at 50 mole % acetone.[15] It is not clear what is the predominant factor that requires ΔE to increase with acetone content. Winstein and Fainberg have separated the effects of solvent on the ground state and transition states of alkyl halide ionization reactions in mixed solvents.[16] It is possible that a similar procedure would be useful here.

The relation between ΔE and ΔE_D can be explained in the following manner. With salt effects eliminated, one may write $\log k_2 = f(T, D_0)$.[17,18]

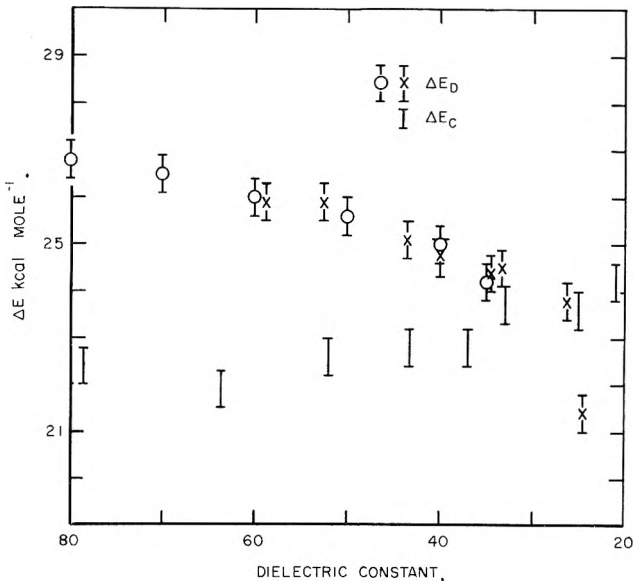

Fig. 2.—The activation energies, ΔE_D and ΔE, for the hydrolysis of acetal in aqueous hydrochloric acid–acetone mixtures as a function of the dielectric constant of the solvent, D_0. The values of D_0 used for ΔE are those at 25°.

Thus

$$\frac{d \log k_2}{dT} = \left(\frac{\partial \log k_2}{\partial T}\right)_{D_0} + \left(\frac{\partial \log k_2}{\partial D_0}\right)_T \frac{dD_0}{dT} \quad (1)$$

and

$$\Delta E = \Delta E_D + 2.3RT^2 \left(\frac{\partial \log k_2}{\partial D_0}\right)_T \frac{dD_0}{dT} \quad (2)$$

It can be shown that

$$\Delta E = \Delta E_D - (2.3)bD_0RT^2 \left(\frac{\partial \log k_2}{\partial D_0}\right)_T \quad (3)$$

where b is the slope of a plot of log D_0 against T.[19] The slope b from our plots of Åkerlöf's data is about 4.97×10^{-3} deg.$^{-1}$. The slope of the plot of log k_2 as a function of D_0 is positive and has the value 0.0285 for the first four points of the curve for 25° (Fig. 1, curve C). The approximate values for the next two points before the slope changes sign are approximately +0.018 and +0.01. Similar orders of magnitude are observed for the slopes of a log k_2–D_0 plot at 15 and 35°. Enough information has been provided so that it can be seen that the difference $\Delta E - \Delta E_D$ has the correct sign and the right order of magnitude over the whole range of solvent compositions. In other words, ΔE_D and ΔE should approach each other in the region where the slope of a log k_2–D_0 plot changes sign (D_0 30–35). It can be seen that this is true by referring to Fig. 1 and Fig. 2. On one side of the minimum $\Delta E_D > \Delta E$ and on the other side the reverse is true.

Correlations with H_0.—Braude and Stern[9] interpreted their results as indicating that the proton affinity of water is greater in aqueous acetone solvents than in pure water and base their arguments on the fact that the quasi-crystalline structure of water is broken down as acetone is added. We have interpolated values of log k_2 from our data at the compositions at which Braude

(12) F. A. Long and M. A. Paul, *Chem. Rev.*, **57**, 935 (1957).
(13) W. Drinkard and D. Kivelson, *J. Phys. Chem.*, **62**, 1494 (1958).
(14) "International Critical Tables," Vol. 5, McGraw-Hill Book Co., New York, N. Y., 1929, p. 22.
(15) H. E. Eduljee, V. N. Kumarkrishnarao, and M. Narasinga Rao, *Chem. Eng. Data Ser.*, **3**, 44 (1958).
(16) S. Winstein and A. H. Fainberg, *J. Am. Chem. Soc.*, **79**, 5937 (1957).
(17) W. J. Svirbely and J. C. Warner, *ibid.*, **57**, 1883 (1935).
(18) The fact that log k_2 (which is a measure of the free energy of activation) appears to be a function only of T and D_0 can be misleading. The behavior of the free energy of activation as solvent composition changes is very different from that of ΔE (which is a measure of the enthalpy of activation) and log A (which is a measure of the entropy of activation). The latter quantities, which determine the free energy of activation and which depend on factors mentioned above (solvation effects, solvent structure, etc.), change in the same manner as solvent composition is varied. This compensatory effect may make it appear that the free energy of activation is determined only by T and D_0. As a consequence of this, the fact that ΔE and ΔE_D follow eq. 3 may be fortuitous.

(19) Equation 3 is obtained as follows: Åkerlöf's data may be expressed as $D_0 = a \exp(-bt)$ for each solvent mixture, where a and b are constants independent of temperature. Differentiation of this equation and substitution into (2) gives (3).

and Stern determined H_0 for aqueous acetone solutions that were 0.1 M in hydrochloric acid. A plot of log k_2 against H_0 gives a good straight line of slope 0.83. A linear plot of the logarithm of the rate constant against H_0 with unit slope has been used for many years as a criterion for an A-1 mechanism in concentrated aqueous solutions of mineral acids.[12,20] The usefulness of this criterion has been questioned for the past several years, and other proposals have been advanced to take its place.[21,22] It has been pointed out that the H_0 concept loses some of its generality as one goes from aqueous solution to media of lower dielectric constant.[23] This has been demonstrated many times. It appears then that one cannot assign a mechanism to a reaction occurring in mixed solvents on the basis of a rate–H_0 correlation.

Although the H_0 scale has not been established on an absolute basis in aqueous binary solvents or nonaqueous solvents, there are many instances[24] of good correlations of rates with indicator acidities to which the results of this work may be added.

(20) Reference 10, p. 273.
(21) J. F. Bunnett, *J. Am. Chem. Soc.*, **83**, 4968 (1961).
(22) E. Whalley, *Trans. Faraday Soc.*, **55**, 798 (1959).
(23) B. Gutbezahl and E. Grunwald, *J. Am. Chem. Soc.*, **75**, 559 (1953).
(24) See, for example, ref. 3 and C. A. Bunton, J. B. Ley, A. J. Rhind-Tutt, and C. A. Vernon, *J. Chem. Soc.*, 2327 (1957); E. A. Braude and E. S. Stern, *ibid.*, 1982 (1948).

MICROCATALYTIC STUDIES OF THE HYDROGENATION OF ETHYLENE. I. THE PROMOTING EFFECT OF ADSORBED HYDROGEN ON THE CATALYTIC ACTIVITY OF METAL SURFACES

BY W. KEITH HALL AND J. A. HASSELL

Mellon Institute, Pittsburgh, Pa.

Received August 30, 1962

The enhanced activity of copper–nickel alloy catalysts, brought about by pretreatment with hydrogen, is shown to result from alteration of a surface property; it is not a bulk effect as previously supposed. The activity difference is maintained at sub-zero reaction temperatures, even in a flowing stream of hydrogen. The metals of the first transition series have been surveyed, and it has been found that iron, cobalt, and nickel are poisoned by activated hydrogen chemisorption, while copper and copper–nickel alloys are promoted. Small amounts of oxygen left within the catalysts following reduction do not alter their activities substantially. When hydrogen was substituted for helium as carrying gas, the ortho–para hydrogen conversion could be measured concomitantly and was affected by pretreatment in the same way as the ethylene hydrogenation. The rates of these two reactions were generally correlative, but it was also observed that the o–p conversion was catalyzed, rather than poisoned, by the carbonaceous residues left from the hydrogenation. Similar behavior was observed for the H_2–D_2 exchange. It was concluded, therefore, that the activity variations result from alteration of the ability of the catalyst to activate hydrogen. Studies of the interaction of C_2H_4 with the surfaces did not show a correlation with pretreatment, as C_2H_6 was produced only on hydrogen treated surfaces, regardless of the catalyst composition. These results, nevertheless, provide some insight into the situation on the surface during hydrogenation.

Introduction

In earlier work[1] with a series of copper–nickel alloy catalysts, it was observed that cooling from the reduction temperature (250 or 350°) to the reaction temperature ($\sim -80°$) in the presence of hydrogen resulted in catalysts from two- to tenfold more active for the hydrogenation of ethylene than were produced when the alloys were outgassed at the reduction temperature and cooled *in vacuo* or in flowing helium. Further experiments[2] showed that the amounts of hydrogen reversibly sorbed (corresponding to the difference in pretreatment) varied somewhat with pretreatment conditions but were many times their BET monolayer equivalents. This work also revealed that the hydrogen, in excess of that adsorbed on the catalyst surface, was in some way associated with small amounts of oxygen (less than 5 atom %) left trapped within the matrix of the metal following the reduction of the mixed oxides. This knowledge led to the supposition that the oxygen, and/or the hydrogen associated with it, had a controlling influence on the catalytic activity.

In discussing this paper[2] at the Second International Congress on Catalysis, H. S. Taylor suggested that our observations offered an explanation for the well known difference in the behavior of evaporated copper films and bulk copper catalysts. His idea was that the small amount of oxide dissolved in the metal provided the vacant d-orbitals required for the adsorption of hydrogen. The need for further work to ascertain the relationship of our observations to the basic theory of catalysis was pointed out.[3] The present work was undertaken with this view and it has been found that the catalytic activity does not depend upon either the small amount of encapsulated oxide or on the rather large portion of hydrogen associated with it, but only upon that relatively small portion held on the catalyst surface or in solution in the metal. This finding is in accord with our earlier results[1] for a pure nickel catalyst, which was poisoned by cooling in hydrogen but which had sufficient hydrogen associated with it to cover only about 80% of its surface. It is also in accord with the recent findings of Gharpurey and Emmett[4] that the activity pattern obtained from evaporated copper–nickel alloy films, which were presumably free from oxygen, was substantially the same as that observed for our reduced oxide alloys.[1]

The phenomenon of chemical promotion has long been known, *e.g.*, the effect of 0.5% K_2O added to iron catalysts used for the ammonia synthesis, but it still is

(1) W. K. Hall and P. H. Emmett, *J. Phys. Chem.*, **63**, 1102 (1959).
(2) W. K. Hall, F. J. Cheselske, and F. E. Lutinski, "Congres International de Catalyse," 2ieme, Paris, 1960. Actes. Paris, Editions Technip, Vol. 2, 1961, p. 2199.
(3) P. H. Emmett, ref. 2, Vol. 2, p. 2218.
(4) M. K. Gharpurey and P. H. Emmett, *J. Phys. Chem.*, **65**, 1182 (1961).

little understood. The effects of a high temperature form of chemisorbed hydrogen on catalytic behavior have been known for many years[1,5-10] but so far have not been studied systematically. The present paper is a step in this direction.

Experimental

Catalysts.—The principal part of the present work was carried out using fresh samples of the same unpromoted copper–nickel alloy catalysts reported previously.[1] Notes on their preparation and purity are given elsewhere.[11] It will suffice to say here that the coprecipitated oxides were reduced with hydrogen according to Best and Russell's modification[12] of the method of Long, Fraser, and Ott.[13] A separate study[14] showed that alloying was substantially complete; this was re-checked in the present work with the catalysts reduced by method B (see later). The designations and compositions of the reduced binary alloys in order of decreasing *atom* % nickel are[11]: VIII = 100%; V = 84.8%; VI = 72.4%; VII = 53.8%; IV = 20.6%; XI = 14.7%; I = II = 0%. Also, a catalyst having an over-all composition of 95.0% was made by grinding together aliquots of catalysts VIII and V. That complete alloying took place during reduction was checked by X-ray measurements.[14]

A number of other transition metals and several commercial catalysts were tested to ascertain the generality of the promoting effect of preadsorbed hydrogen. These materials, their sources, and information concerning their purity follow. Catalysts G-Fe-51 and G-Co-51 were spectroscopically pure iron and cobalt oxide catalysts purchased from the M. K. Research & Development Co., Pittsburgh, Pa. Spark spectra analysis indicated that their total metallic impurity contents were less than 50 p.p.m. and made up principally of Ca and Na. Catalysts P-2007 and 89EE were furnished by the Bureau of Mines. The former was a 3% Al_2O_3 singly promoted iron–synthetic ammonia catalyst made from pure Allen Wood magnetite, while the latter was a cobalt–thoria–magnesia–kieselguhr catalyst having a composition ratio of 100:6:12:200. The method of its preparation[15] and its physical properties[16] are described elsewhere. Catalyst Ni (0104), a commercial nickel–kieselguhr catalyst, was a gift of the Harshaw Chemical Co.; it had a nominal composition of 59% Ni.

Gases Used.—The hydrogen and helium were obtained from the Air Reduction Sales Co. and had nominal purities of 99.8 and 99.95%, respectively. The ultimate practical limit of purification was used for all of the gases. The train for hydrogen consisted of a Deoxo purifier, anhydrous magnesium perchlorate, platinized asbestos at 375°, more anhydrous magnesium perchlorate, and a trap containing approximately 25 g. of high area charcoal thermostated at −195°; this trap was evacuated at 375° at weekly intervals, *i.e.*, between every one or two experiments.

The helium carrying gas flowed continuously over the catalysts at a rate of 50 cc./min. for intervals of over 24 hr. In order to remove the last vestiges of poisoning of our most sensitive catalysts from this source, a series of traps was required. The system devised included a multistage Dry Ice trap followed by two liquid nitrogen traps, filled with high area charcoal. Water appeared to be the chief impurity removed in the first trap.

The ethylene used was C.P. grade obtained from the Matheson Co. It had a nominal purity of 99.7%, the chief impurities being ethane, propane, and propylene to the extent of about 0.1% each. After drying by passing through a two-stage Dry Ice trap (−80°), it was further purified by passing over a large amount (approximately 600 g.) of the commercial nickel–kieselguhr catalyst (Ni 0104). This was treated with pure hydrogen at 375° between runs and brought to the temperature of Dry Ice before diverting the ethylene stream over it. Since severe poisoning was observed in only a few cases, *e.g.*, with pure Ni and Co, and generally not at all, it could be attributed to carbonaceous residues resulting from the reaction.

For some experiments, blends of hydrogen and ethylene, separately purified as above, were made and stored at above atmospheric pressure in glass bulbs attached to an all-glass vacuum system. The use of blends freed the hydrogen train for use as carrying gas. The ortho-para ratio of this hydrogen corresponded to equilibrium at the temperature of liquid nitrogen.

Equipment and Procedure.—The equipment used in this work has been described in detail elsewhere.[1,17,18] It consisted of an all-glass vacuum system and auxiliary microcatalytic equipment. The catalyst was contained in the approximately 2 mm. annular space between the thermocouple well and the outside wall of the all-glass reactor. The catalyst volume was usually about 5 cc. The reactor was connected to the dosing device which could be filled with the blend of reactant gases (60% H_2, 40% C_2H_4) either from the storage bulb or by flushing with a blend of the same composition prepared by mixing metered flows of the pure reactants. The flow meters used for this purpose were of an all-glass, vacuum tight design. This procedure was used for the evaluations of catalyst activity, as in the earlier work.[1,17] Also, when the flow technique was used, the all-glass dosing device could be replaced by a semi-automatic dosing system described previously.[18] It was found that these techniques all yielded the same results within the limits of reproducibility. The slug size was approximately 16 cc. (NTP) and the blends were carried over the catalyst by helium at a flow rate of 50 ± 1 cc./min.

The evacuated glass doser was filled from the storage bulb, *via* a BET system, in a number of special experiments. These included tests made with hydrogen carrying gas and studies of the self-hydrogenation of ethylene using blends of C_2H_4 and He.

The catalysts were heated by surrounding the all-glass reactor with a resistance-wound furnace controlled by a thyratron circuit. For studies carried out below room temperature, the furnace was replaced by the thyratron-controlled cryostat described earlier.[1] The temperature of this could be set manually or programmed to change automatically in synchronism with the dosing device[18]; in the latter case, it was provided with a liquid nitrogen leveling device and could be operated continuously for several days without difficulty; the temperature could be controlled reproducibly to ±0.2°.

The catalysts were reduced by two methods. In *method A*, the reduction was started in a high flow of H_2 at 170°. The onset of the reduction was indicated by the appearance of water vapor in the cool portion of the out-gas tube, and at this point it was customary to drop the furnace to slow down the reaction. Despite this precaution, the catalyst frequently was observed to glow briefly. This tendency was more pronounced the higher the copper content; with the pure nickel catalyst, the phenomenon was never observed. When the last vestiges of water had disappeared, the furnace was replaced and the temperature raised to, and maintained at, 350° overnight. All subsequent reductions were carried out at lower temperatures except where otherwise noted. At first it was thought that the "glow phenomenon" corresponded to a rapid loss in surface area as the physical structure of the high area oxide was broken down[1,2] and it was supposed that the catalyst was still largely in the form of oxide until the furnace was replaced and the reduction continued at higher temperature. More recent measurements have shown that such is not the case; actually, it was found that over 95% of the reduction takes place during the first few minutes at 150°.

In reduction *method B*, the reduction was started with a slow flow of a 50–50 blend of H_2 and He. In this method, no glow was observed in any case. After 1 hr. at 150°, the temperature was raised to 350° and the reduction continued overnight in pure H_2. Subsequent reductions were carried out at 250°.

Catalytic hydrogenation was tested after two different pretreatment procedures. In one of these, the hydrogen reduction stream was replaced with the purified helium carrying gas at 250°; the helium flow was maintained for 1 hr. at this temperature and then the catalyst was cooled rapidly to the sub-zero reaction temperature. Hereinafter, in this condition, catalysts are said to be in the *helium-treated state*. The other method of pretreatment involved cooling the catalyst from 250 to 50° in H_2

(5) P. H. Emmett and R. W. Harkness, *J. Am. Chem. Soc.*, **57**, 1628 (1935).
(6) J. T. Kummer and P. H. Emmett, *J. Phys. Chem.*, **56**, 258 (1952).
(7) C. L. McCabe and G. D. Halsey, *J. Am. Chem. Soc.*, **74**, 2732 (1952).
(8) A. Amano and G. Parravano, *Advan. Catalysis*, **9**, 716 (1957).
(9) R. E. Cunningham and A. T. Gwathmey, *ibid.*, **9**, 25 (1957).
(10) P. B. Shallcross and W. W. Russell, *J. Am. Chem. Soc.*, **81**, 4132 (1959).
(11) W. K. Hall and P. H. Emmett, *J. Phys. Chem.*, **62**, 816 (1958).
(12) R. J. Best and W. W. Russell, *J. Am. Chem. Soc.*, **76**, 838 (1954).
(13) J. H. Long, J. C. W. Fraser, and E. Ott, *ibid.*, **56**, 1101 (1934).
(14) W. K. Hall and L. Alexander, *J. Phys. Chem.*, **61**, 242 (1957).
(15) R. B. Anderson, A. Krieg, B. Seligman, and W. E. O'Neill, *Ind. Eng. Chem.*, **39**, 1548 (1947).
(16) R. B. Anderson, W. K. Hall, H. Hewlett, and B. Seligman, *J. Am. Chem. Soc.*, **69**, 3114 (1947).
(17) W. K. Hall and P. H. Emmett, *ibid.*, **79**, 2091 (1957).
(18) W. K. Hall, D. S. MacIver, and H. P. Weber, *Ind. Eng. Chem.*, **52**, 421 (1960).

at the normal cooling rate of the furnace. At this point, the furnace was removed and was replaced by a cryostat, which was cooled at the rate of about 1°/min. from room temperature to the sub-zero reaction temperature. Then, the helium carrying gas was turned over the catalyst. Hereinafter, the catalyst in this condition is said to be *promoted* by hydrogen or to be in the *hydrogen-treated state*. Differences in catalytic behavior obtained from catalysts following these two conditions of pretreatment provide the basis for the *promoting effect* discussed in the next section.

The capacity of a catalyst to sorb hydrogen was measured by attaching the tubes to a conventional BET system. The catalyst was then brought again to 250° in H_2 and evacuated at this temperature for about 2 hr. The reversible hydrogen sorption was determined at 700 mm. pressure and 250°. Under these conditions, the sorption isotherm is at its maximum. For measurement of the total hydrogen held by the catalyst, the method of deuterium exchange used earlier[2] was employed. The same samples of catalyst then were used for activity measurements.

Results

Stability of the Hydrogen Promoter.—Some exploratory experiments, using hydrogen as a carrying gas, were made for several reasons. The first of these was to prove that different activity levels, corresponding to the hydrogen-treated and the helium-treated states, could be maintained for long periods of time, even in a flowing stream of hydrogen. It had been shown previously[1] that when a catalyst was in the helium-treated state, its activity could be altered appreciably by treating it with hydrogen for 30 min. at −42°. However, the change was much smaller than that obtained when the catalyst was cooled in hydrogen from the reduction temperature. Moreover, it was observed that all of the alloy catalysts, when in the helium-treated state, increased in activity with slug number, whereas the same catalysts in the hydrogen-treated state did not. The use of hydrogen carrying gas afforded the opportunity to evaluate the degree of interconversion achievable at low temperature.

A second reason for the use of hydrogen carrying gas stemmed from the recent kinetic treatment of microcatalytic reactors by Bassett and Habgood.[19] These workers pointed out that the catalyst itself may act as a chromatographic column and actually cause separation of reactants. The obvious way to circumvent this difficulty was to use hydrogen as a carrying gas. Such data were needed to evaluate properly our earlier work.[1]

Table I provides a comparison of the results obtained from two catalysts. Two facts emerge from these experiments: (a) the effect of the pretreatment procedure persists even when hydrogen is used as the carrying gas, *i.e.*, catalyst VIII is poisoned while catalyst VI is promoted by hydrogen treatment; and (b) higher conversions are obtained at the same temperature with hydrogen carrying gas regardless of the nature of the pretreatment, even with catalyst VIII, which is poisoned by hydrogen treatment at higher temperature. An auxiliary observation was that catalyst VIII did not poison noticeably with slug number when hydrogen was the carrying gas, in contrast to its behavior when helium was used.

The higher activities observed with hydrogen carrying gas are due, at least in part, to a clean-up of the surface during the 30-min. periods between test slugs. However, several other factors are also involved. The reaction is first order in hydrogen pressure and the average hydrogen pressure is higher with hydrogen carrying gas.

(19) D. W. Bassett and H. W. Habgood, *J. Phys. Chem.*, **64**, 769 (1960).

TABLE I

EFFECT OF CARRYING GAS ON HYDROGENATION OF ETHYLENE IN MICROCATALYTIC REACTOR

Catalyst[a] no.	Temp., °C.	Carrying[b] gas	Conversion at T°, % He treated	% H_2 treated
VIII	−94	He	88	18
VIII	−94	H_2	99	32
VIII	−95.5	H_2	95	..
VI	−87	He	9	24
VI	−87	H_2	31	57

[a] Catalyst VIII is pure nickel; catalyst VI is a copper–nickel alloy containing 72.4 % Ni. [b] Flow rate = 50 cc. (NTP)/min.

Moreover, the ethylene conversion is raised when the surface is saturated with preadsorbed hydrogen; when helium is used, the chromatographic effect, noted above, causes the more strongly adsorbed ethylene to trail the hydrogen as the slug leaves the bed. When these factors are taken into account, the several-fold higher conversions seem quite reasonable and it can be seen that the chromatographic separation of reactants could not have been sufficiently complete to vitiate any of our earlier conclusions.[1] Finally, the fact that two different activity levels can be maintained even in the presence of hydrogen carrying gas demonstrates that the processes of sorption and desorption of the hydrogen promoter have activation energies associated with them.

TABLE II

EFFECT OF REDUCTION METHOD ON CAPACITY OF Cu–Ni CATALYSTS TO HOLD HYDROGEN

Compn., atom % Ni	Reduction method[a]	Max. red. temp., °C.	Total H_2 content,[b] cc./g.	Reversible hydrogen sorption at 250°,[b] cc./g.	V_m (H_2),[c] cc./g.
72.4	A	350	8.0	7.8	0.67
72.4	A	550	1.1	..	.29
53.8	A	350	4.5	4.1	.75
53.8	A	550	..	0.4	.45
53.8	B	350	0.25	0.24	.81
20.7	A	350	6.6	2.6	.23
20.7	B	350	0.39	..	.41
14.7	A	350	8.8	1.5	.16
14.7	A	550	0.46	..	.13
14.7	B	350	..	0.31	.23
14.7	B	550	0.09	0.04	.14

[a] In method B, the reduction is started with a 50/50 mixture of H_2 and He; with method A, pure H_2 is used; in the latter case, the catalysts glowed briefly during the initial stage of the reduction. [b] With nickel-rich alloys, the reversible hydrogen sorption is about equal to the total present; with copper-rich alloys, only a portion is reversible; see ref. 2. [c] BET V_m corrected by multiplying by ratio of cross sectional areas, assuming 6.17 Å.²/H site.

Catalyst Activity and Hydrogen Sorption Capacity.—Earlier work[2] revealed that an amount of hydrogen, equivalent to many monolayers, can be reversibly sorbed and desorbed by the alloys and that this gas is intimately associated with small amounts of oxygen left trapped within the matrix of the metal during the reduction process. The elimination of oxygen can be rendered more complete by increasing the reduction temperature to above 500°, thus affording a way of altering the ability of the alloy to hold hydrogen. When reduction method B was devised, it was found to be even more effective in this regard. The data collected in Table II show that the capacity to hold hydrogen is lower when the catalyst is reduced by method B at only

350° than by method A at 550°. These data strongly support the view that oxide is trapped during the initial stages of the reduction, in an amount which is dependent upon the rapidity of the reduction.

Superficially, the alloys prepared by the two reduction methods appeared different, the colors being darker when method B was used. Nevertheless, X-ray patterns of the alloys showed no twinning of lines, even when method B was used, demonstrating that the alloying was complete at 350°. This substantiates the conclusion reached earlier.[14]

The data of Table III demonstrate that the specific activity of a given catalyst is virtually independent of its capacity to hold hydrogen and therefore of its residual oxygen content.[2] The same data, however, demonstrate that the activity is strongly dependent upon the same pretreatment which causes the reversible hydrogen sorption shown in Table II. It is concluded, therefore, that the activity is controlled, not by the large portion of hydrogen which is associated with residual oxygen, but rather upon that small portion which is adsorbed on the catalyst surface or is in solution in the metallic lattice. Since the solubility of hydrogen in nickel does not exceed 100 p.p.m. (0.025 cc. (NTP)/g. at 300° and 1 atm., *i.e.*, *ca.* 10% or less of the monolayer capacities shown in Table II) in the temperature region of our treatments[20a] and since the solubility of copper is considerably less,[20b] it is very probable that the promoting effect results from alteration of a surface property rather than from a bulk effect. In this connection, it may be noted that the activity changes brought about by pretreatment are as large as those corresponding to much larger changes in alloy composition, *e.g.*, 5 atom % Cu into Ni.

TABLE III

INDEPENDENCE OF CATALYST ACTIVITY ON SORBED HYDROGEN CONTENT[a]

Catalyst compn., atom % Ni	Reduction method	Max. red. temp., °C.	H_2 content, cc./g.	Specific activity % Conv. (at 200°K.) per M^2 H_2 treated	Specific activity % Conv. (at 200°K.) per M^2 He treated	Activity ratio H_2/He treated
72.4	A[b]	350	8.0	30.4	13.7	2.2
72.4	A	350	8.9	34.3	12.9	2.7
72.4	A	550	0.16	25.3	8.6	2.9
53.8	A[b]	350	4.0	13.2	6.8	1.9
53.8	A	350	4.1	9.6	2.9	3.3
53.8	A	550	0.4	7.1	2.1	3.3
14.7	A[b]	350	8.8	14.8	1.2	12.3
14.7	B	350	0.5	11.8	3.1	3.8
14.7	B	550	0.4	13.3	1.5	8.9

[a] Helium carrying gas was used for the experiments at flow rate of 50 cc. (NTP)/min. [b] This row of data was taken from *J. Phys. Chem.*, **63**, 1102 (1959).

Generality of Hydrogen Promotion or Poisoning.—The data of Table I confirm[1] that the activities of nickel and copper–nickel alloys are decreased and increased, respectively, for the low temperature hydrogenation of ethylene by the activated chemisorption of hydrogen. Two stable activity levels are produced; these can be defined when the data for a given catalyst are expressed in the form of Arrhenius plots. The data obtained from iron, cobalt, nickel, and copper catalysts, collected in Table IV, were obtained in this way. Columns 5 and 6 list the activities derived from the same sample of catalyst in successive experiments. Column 7 gives the ratio of these activities, the ratio exceeding unity when the catalyst is promoted. With the possible exception of cobalt Fischer–Tropsch catalyst 89EE, only pure copper is more active when cooled in hydrogen. The data for Cu are in fair agreement with earlier work[1,7]; the large sample of catalyst was required to allow measurements to be made in a temperature range where the hydrogen promoter would not evaporate into the helium carrying gas.

Catalysts 89EE and Ni(0104) did not give interpretable data. At the higher temperatures, their abilities to hydrogenate did not appear to change with temperature nor did they poison rapidly. When the temperature was reduced below a critical point, however, the conversions obtained depended critically upon both temperature and slug number. Therefore, the simple numerical nefinition used for the remaining catalysts could not be evaluated for these catalysts. However, the behavior just described took place at slightly higher temperatures when the nickel was hydrogen-cooled and the cobalt was helium-cooled, allowing the inference to be drawn that the former is poisoned and the latter is promoted by chemisorbed hydrogen. It is of interest to note that the iron synthetic ammonia-type catalyst (P-2007) did not behave in this abnormal fashion.

Effect of Pretreatment on the Interaction of C_2H_4 with the Surface.—A number of experiments were carried out in which helium was substituted for the hydrogen ordinarily contained in the standard slugs of hydrogen–ethylene blends. In this way, pure ethylene could be passed over the catalyst under conditions strictly comparable with those used in the hydrogenation experiments. As the results from pure nickel and from the alloys were quite similar, the data of Table V may be taken as representative.

The sample of catalyst VIII was found to convert about 40% of the ethylene from a standard hydrogen–ethylene blend at −93.1° when in the helium-treated state; in the hydrogen-treated state, a temperature of −70.5° was required to give approximately the same result. Hence, two comparisons are made in Table V, *i.e.*, the results obtained when ethylene is passed over the hydrogen-treated and helium-treated surface at the same activity level for the hydrogenation of ethylene, or at the same temperature.

When three successive slugs of ethylene were passed over a catalyst at approximately 0.5-hr. intervals, absolutely no ethane was detected from any helium-treated catalyst (the detectability limit for ethane is approximately 0.02 cc. (NTP)). However, always a fairly large amount was formed on hydrogen-treated surfaces, particularly with the first slug. On the other hand, in all instances, the carbon balance indicated that an amount of ethylene equivalent to a large fraction of a monolayer was unaccounted for. Presumably, this remained adsorbed on the catalyst surface in the form of carbonaceous residues. For the data shown, this amounted to coverage of over half the available surface area. Similar results have been noted by others on evaporated nickel films,[21-23] on reduced nickel

(20) M. Hansen, "Constitution of Binary Alloys," McGraw-Hill Book Co., New York, N. Y., 1958; (a) p. 788; (b) p. 587.

(21) O. Beeck and A. W. Ritchie, *Discussions Faraday Soc.*, **8**, 159 (1950).
(22) G. I. Jenkins and E. Rideal, *J. Chem. Soc.*, 2490, 2496 (1955).
(23) O. Beeck, *Rev. Mod. Phys.*, **17**, 61 (1945), and related work.

TABLE IV

GENERALITY OF HYDROGEN PROMOTION OR POISONING AMONG THE TRANSITION METALS[a]

Catalyst	Reduced wt., g.	Total surface, m.²	Exptl. temp. range, °K.	Conversion at 200°K., % He treated	H_2 treated	Activity ratio H_2/He treated	Degree of poisoning by reactants.[b] Ratio of slugs 3 and 30
G-Fe-54	6.34	2.4	175 to 216	150	14	0.1	15
P-2007	0.80	20.0	191 to 215	34	14	0.4	4
G-Co-51	.657	1.0	172 to 199	216	76	0.4	5
89EE	.019	0.9	186 to 216	...[c]	...[c]	Promoted[c]	Severe[c]
VIII	3.61	4.0	179 to 211	150	38	0.3	3
Ni (0104)	0.115	19.8	157 to 176	...[d]	...[d]	Poisoned[d]	Severe[d]
I (Cu)	27.22	9.3	300 to 323	0.0023	0.027	12[e]	~1

[a] Helium carrying gas was used in these experiments at flow rate of 50 cc. (NTP)/min. [b] The rate at which the catalysts are poisoned by carbonaceous residues, formed from the reactants, may be judged by how much more reactive they were initially than after a large number of slugs were passed; since in some cases, large portions of the first several slugs were held up to form these residues, the rate was calculated from the third and thirtieth slugs. The results listed are averages of the ratios for the hydrogen promoted and unpromoted states; in all cases, these values agreed within a few per cent. [c] The catalytic behavior of this catalyst was abnormal (see text) so that satisfactory numerical data cannot be provided. However, if anything, this catalyst was slightly promoted by hydrogen. [d] Same as *b*, except this catalyst appeared to be poisoned by hydrogen. [e] This value was only 4 in the temperature range of the experiment; the larger value quoted was obtained by extrapolation of divergent Arrhenius plots.

TABLE V

MICROCATALYTIC STUDIES OF THE REACTION OF C_2H_4 WITH THE SURFACE OF CATALYST VIII[a]

Total BET surface area = 5.5 m.²; equivalent monolayer capacity[b] for H_2 is 1.67 cc. and for C_2H_4 is ~0.8 cc.

	Reactant slug		Carbon balance, cc. (NTP) — He-treated state at −93.1°			H_2-treated state at −70.5°			H_2-treated state at −93.1°		
Step no.	Gas	Amount cc. (NTP)	C_2H_6 evolved	C_2H_4 adsorbed	Cumulative C_2H_4 adsorbed	C_2H_6 evolved	C_2H_4 adsorbed	Cumulative C_2H_4 adsorbed	C_2H_6 evolved	C_2H_4 adsorbed	Cumulative C_2H_4 adsorbed
1	C_2H_4	2.9	nil	0.7	0.7	0.73	0.4	0.4	0.27	0.4	0.4
2	C_2H_4	2.9	nil	.1	.8	.11	.2	.6	.03	.1	.5
3	C_2H_4	2.9	nil	.1	.9	.04	.1	.7	nil	.1	.6
4	H_2	7.3	0.29	−0.3	.6	.07	−0.1	.6	0.03	..	.6

[a] Reduced weight of catalyst = 3.56 g.; He carrying gas was used at 50 cc. (NTP)/min. [b] Beeck's[21] experimental value for H_2 (12.3 Å.²/H_2 molecule) is adopted here; the value for C_2H_4 assumes four crystallographic sites for this molecule. Although Jenkins and Rideal[22] contend the C_2H_4 monolayer equivalent should be somewhat larger, further refinement is not warranted here.

powder,[24] on palladium films,[25] and on nickel–silica catalysts.[26]

The present data do not define the source of the hydrogen used for the production of ethane. Since the latter forms only on surfaces in the hydrogen-treated state, even in the case of nickel which is poisoned by hydrogen, it may be supposed that some of the presorbed hydrogen has reacted. Certainly the simplest interpretation is that the more loosely held portion of chemisorbed hydrogen (perhaps that portion taken up at low temperatures as the catalyst is cooled in hydrogen) reacts from the catalyst. On the other hand, the requirement amounts to from 20 to 50% of a monolayer and, yet, it has been shown[1] that much larger amounts of gaseous ethylene may be passed without diminishing the promoting action of chemisorbed hydrogen. Moreover, in all instances, the adsorbed ethylene is ample to supply the hydrogen requirement. Tracer work might settle this point.

In all cases studied, it was observed that more ethylene was adsorbed on catalysts when in their more active condition of pretreatment. This is a little surprising in view of the fact that the greater tendency to form residues might be expected to reduce hydrogenation activity by lowering the extent of the available surface.

When a slug of hydrogen was passed over the catalysts (step 4), a portion of the carbonaceous residue was removed as ethane. The amount of ethane generated in this step was always somewhat greater for a catalyst in its more active condition of pretreatment. This suggests that a portion of the residue is in the form of active intermediate and that this portion was larger in the more active pretreatment condition. It is of interest to note that the cumulative carbon balance is now nearly the same for all three experiments shown in Table V. For all catalysts, it was found that further slugs of hydrogen, when passed at the same temperature, produced no further trace of ethane.

According to McKee,[24] when ethylene is admitted to out-gassed nickel in the temperature range of these experiments, ethane is not generated at a detectable rate until a critical volume of ethylene has been adsorbed. This amount increases with decrease in temperature by an amount (normalized to our surface area) from 0.06 cc. at −31° to about 0.2 cc. at −78°. Once this critical amount has been adsorbed, ethane is produced at a rate which is dependent upon the excess amount of ethylene added. Extrapolation of these data to −93° indicates that the rate of self-hydrogenation for our comparable helium-treated catalyst would be below our detectability limit (0.05 cc./min.). Moreover, even the most pessimistic estimates show that the rate would be so slow that a measurable decrease in the carbon balance should not occur in the 30-min. periods between the steps of the experiment.

Relationship of Ethylene Hydrogenation and Ortho–Para-Hydrogen Conversion.—The use of hydrogen as a carrying gas afforded the opportunity of simultaneously observing the ortho–para-hydrogen conversion and the ethylene hydrogenation reaction. Some results obtained for copper–nickel alloy catalyst VI in the hydrogen-treated and helium-treated states are shown in Fig.

(24) D. W. McKee, *J. Am. Chem. Soc.*, **84**, 1109 (1962).
(25) S. J. Stephens, *J. Phys. Chem.*, **62**, 714 (1958).
(26) R. P. Eischens and W. A. Pliskin, *Advan. Catalysis*, **10**, 4 (1958).

1 and 2, respectively. The experiments start at the right of the figures and progress to the left. In Fig. 1, A corresponds to the base line of the by-passed hydrogen carrying gas. This contained the equilibrium o–p ratio at the temperature of liquid nitrogen and served as a reference standard throughout the experiment. The response obtained when the gas was turned over the catalyst is shown by B. Hydrogen that had been trapped in the tube in contact with the catalyst for 5 min. or more was swept out and, as indicated by the horizontal marks at the edge of the figure, was found to have approximately the equilibrium ratio at the catalyst temperature (−87°). As shown by C, the clean (freshly reduced) catalyst was capable of maintaining a ratio intermediate between the equilibrium values at the catalyst temperature and at liquid nitrogen temperature. When a slug containing the standard ethylene–hydrogen blend was passed over the catalyst, the o–p ratio of the unreacted hydrogen was unaltered. Thus, as shown by D, the conversion was blocked while the ethylene hydrogenation took place. This confirms the similar earlier finding by Twigg[27] and implies that hydrogen, which is adsorbed in the presence of gaseous ethylene, does not escape the catalyst as hydrogen gas but is consumed to form ethane. It is interesting to note, however, that once the blend has passed the catalyst, its activity for the o–p conversion, E, has been enhanced almost to equilibrium. This would not have been expected from the simple consideration that the rate varies as the extent of metal surface available for reaction. Note that E designates the position of the chromatographic base-line (o–p ratio) when the hydrogen carrying gas is passing over the *contaminated* (with carbonaceous residues) surface.

The results of a companion experiment, carried out at the same temperature over the same catalyst but in the helium-treated state, are presented in Fig. 2. The catalyst was now much less active for the ortho–para conversion. Thus, the base line shifted very little when the carrying gas was turned over the catalyst (compare C with A). When the first slug was admitted, the conversion was blocked as before, until the hydrogenation was complete; the rate of the o–p conversion increased after the slug had passed. However, unlike the hydrogen-treated catalyst, equilibrium was not achieved. The activity for ethylene hydrogenation, as indicated by F and G, also was much lower and, in agreement with earlier work,[1] increased with slug number. When the catalyst was by-passed, the original base line, A, was reproduced and on turning the flow back over the catalyst, the conversion returned to its original level, E. On admitting more slugs, this behavior was reproduced, but each time the activity of the catalyst for hydrogenation of ethylene and for o–p conversion increased together. The situation after four slugs is depicted on the left hand part of Fig. 2. The ethane and ethylene peaks have increased and decreased, respectively, and the o–p conversion, E, has moved closer to the equilibrium value, but is still a considerable distance away. With the passage of six slugs, the ethylene conversion (to ethane) increased monatonically from about 24 to 29% while the o–p conversion increased from about 10 to 47% of the distance to equilibrium.

The effect of pretreatment and of temperature on the

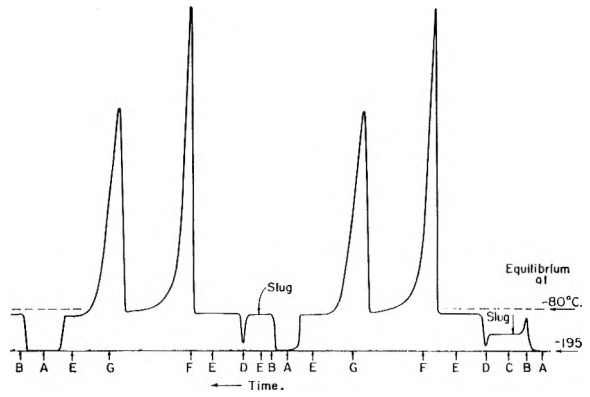

Fig. 1.—Results of microcatalytic experiments over Cu–Ni catalyst VI (contains 72.4 atom % Ni) in hydrogen-treated state.

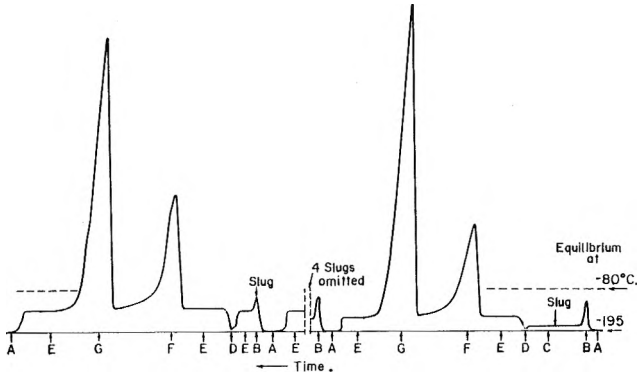

Fig. 2.—Results of microcatalytic experiments over Cu–Ni catalyst VI (contains 72.4 atom % Ni) in helium-treated state.

relative behavior of the two reactions was tested with several more catalysts. It was found that the rates of the two reactions increased and decreased together, *i.e.*, the rates of both reactions were slower on pure nickel catalyst VIII in its hydrogen-treated state than in its helium-treated state, whereas the reverse was true with the copper–nickel alloys; both rates increased with temperature in all cases. Exactly analogous results were obtained for the H_2–D_2 exchange over these catalysts; these data will be reported elsewhere. It was of particular interest that the rates increased markedly after the first slug had passed over He-treated catalyst VIII, which is poisoned by hydrogen, as with the alloys. Thus, two factors seem to influence the rate of hydrogen activation. These are the intrinsic activity level of the catalyst and the carbonaceous residues deposited during the ethylene hydrogenation reaction. Our results are in agreement with those of Kokes and Emmett,[28] who observed that the rates of these reactions correlated on Raney nickel catalysts, and of Shallcross and Russell,[10] who noted that the rate of the o–p conversion was higher for hydrogen-treated copper–nickel alloy catalysts (and lower for pure nickel) at −20° than the corresponding helium-treated catalysts.

Discussion

The present work has confirmed our earlier view[1] that the promoting effect of hydrogen stems from a stable chemisorbed species which is reversibly adsorbed above 100°, but which becomes irreversible at sub-zero reaction temperatures. This conclusion is in agreement with that of McCabe and Halsey[7] and it corrects the errone-

(27) G. H. Twigg, *Discussions Faraday Soc.*, **8**, 152 (1950).

(28) R. J. Kokes and P. H. Emmett, *J. Am. Chem. Soc.*, **82**, 4497 (1960).

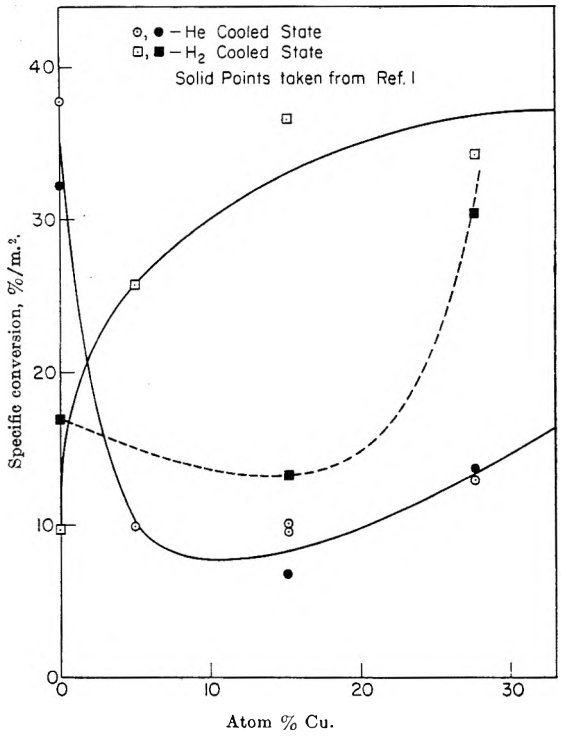

Fig. 3.—Effect of composition and pretreatment on activity of copper–nickel alloys at 200°K.

ous inference derived from the observation[2] of a much larger amount of hydrogen which concomitantly sorbs or desorbs and which is associated with the oxygen impurity left when the catalyst was reduced. This is now understood as it has been shown recently[29] that this hydrogen is held in the form of liquid water, in microvoids within the metal.

The data provide no insight into the mechanism of the promoting action, but they are sufficient to indicate certain generalities. The d-metals of the first transition series are poisoned by hydrogen for the ethylene hydrogenation, for the ortho–para conversion, and H_2–D_2 exchange. Copper and its alloys are promoted by the same treatment for these reactions at temperatures down to −100°. At liquid nitrogen temperature, it has been observed that nickel, copper–nickel alloys,[10] and doubly promoted synthetic ammonia catalysts[5,6] all are poisoned by hydrogen for the o–p conversion, but here the magnetic mechanism may be rate controlling. Kowaka[30] found an analogous situation with Pd and Pd–Ag alloys, *i.e.*, hydrogen poisoned pure Pd but acted as a promoter for ethylene hydrogenation over the alloys. Since Pd and its Ag alloys absorb hydrogen, these observations may correspond to a bulk effect. Nevertheless, the analogy with the closely related copper–nickel system suggests that a common surface effect cannot be excluded.

The hydrogenation proceeds on surfaces that are largely covered with carbonaceous residues. These residues have been studied on nickel by Beeck,[23] McKee,[24] Jenkins and Rideal,[31] and Eischens[26] and on Pd by Stephens,[25] and it is known that hydrogen can be added to and abstracted from these residues. Eischens concluded that the adsorption of ethylene on nickel surfaces on which hydrogen has been preadsorbed is largely associative. When such a system was treated with 4 mm. of hydrogen at 35°, adsorbed ethyl radicals were observed. When ethylene was admitted to an outgassed surface, it was chemisorbed dissociatively, but on addition of hydrogen to the system, ethyl radicals again appeared. It seemed likely, therefore, that the final distribution of surface species was different on outgassed surfaces than on those covered with preadsorbed hydrogen. This, in turn, could alter the overall mechanisms. Laidler and Townsend[32] suggested that two mechanisms take place simultaneously on metal surfaces, *i.e.*, a Langmuir–Hinshelwood reaction between adsorbed hydrogen and ethylene and a Rideal-type reaction between adsorbed hydrogen and gaseous ethylene, the latter being favored by admitting hydrogen first to the system. Evidence that the activity differences due to hydrogen promotion might result from such mechanistic changes was sought, but not obtained, in the experiments corresponding to the data of Table V. To the contrary, these results indicate that the activity differences correspond to changes in the intrinsic properties of the catalyst, *i.e.*, larger quantities of ethylene are held less tenaciously by the more active surfaces. This view is confirmed by the fact that the rates of both the o–p hydrogen conversion and the H_2–D_2 exchange reaction vary in the same way with pretreatment as the ethylene hydrogenation reaction. This correlation in rates implies that all these reactions have a common rate determining step, *i.e.*, the activation of hydrogen.[28] Finally, it should be noted that hydrogen activation is greatly accelerated on surfaces which are extensively covered with carbonaceous residues for reasons which are presently not understood.

The alteration of catalyst activity by chemisorbed hydrogen could be caused by either a geometric or an electronic factor. Infrared data suggest the latter. In the cases so far studied,[26] the carbon–oxygen stretching frequency from CO adsorbed on metals is reduced by preadsorbed hydrogen, an effect associated with the transfer of electrons from the metal to the adsorbate.

Kokes and Emmett[28] correlated the activities of a series of Raney nickel catalysts for the ethylene hydrogenation reaction with the electron concentration in the metal. The latter was varied by removing hydrogen from a parent catalyst by evacuating it to successively higher temperatures. The activity fell to a minimum as the electron concentration was lowered and then increased strongly again as the last of the hydrogen was removed. They were able to correlate the earlier data of Hall and Emmett[1] on the same curve. Catalysts VIII, V, and VI were used for this purpose, as they spanned the range of electron concentration found for the Raney nickel. The point of interest is that catalyst V (the alloy containing the least copper), fell at the minimum of the curve. Thus, if it is assumed that hydrogen treatment increases the electron concentration, both of these alloys would be promoted by hydrogen treatment while nickel would be poisoned, as observed. To test this hypothesis, a new catalyst containing 95 atom % Ni was prepared and tested. Rather than being poisoned by hydrogen as required, it was promoted. Hence, the effect of chemisorbed hydrogen apparently cannot be correlated in this simple way.

Our new data, relating specific catalytic activity for

(29) N. A. Scholtus and W. K. Hall, *Trans. Faraday Soc.*, in press.
(30) M. Kowaka, *J. Japan Inst. Met.*, **23**, 655 (1959).
(31) G. J. Jenkins and E. Rideal, *J. Chem. Soc.*, 2490 (1955).
(32) K. J. Laidler and R. E. Townsend, *Trans. Faraday Soc.*, **57**, 1590 (1961).

ethylene hydrogenation with alloy composition in the nickel-rich region, are plotted together with those taken from our earlier work in Fig. 3. For the helium-treated state, the rapid decline in activity from pure Ni to a shallow minimum near 10% Cu appears to be established; this conclusion is supported by the data of Emmett and Pass[33] and by the fact that Kowaka[30] found a similar minimum in the same region of composition with the Pd–Ag system. The new data for the hydrogen-treated catalysts do not show the minimum; the point at 15.2% Cu for catalyst V, taken from the earlier work (solid square), is therefore suspect. The dashed line indicates the old curve for the hydrogen-treated state. It should be noted that Kokes and Emmett used the well defined data for the helium-treated state in their correlation.

The possibility that the promoting effect results from geometric factors cannot be ignored. Germer and MacRae[34] recently have demonstrated that the surfaces of single crystals of nickel rearrange on the adsorption of hydrogen; with copper alloys, this may not occur or the behavior may be different. With nickel, they observe that 110 faces are rearranged while 100 and 111 faces are not. It is of interest to note that the findings of Beeck, *et al.*,[35] led to the suggestion[36] that the 110 planes are much more active for ethylene hydrogenation than any other simple plane of metallic nickel.

The sp metal, Cu, is promoted by hydrogen; the d metals Fe, Co, and Ni are poisoned. The alloys all are promoted, suggesting that they may be copper-rich on the surface. Whatever the cause, it seems certain that the final solution of the problem lies in studies of the interaction of hydrogen with these surfaces.

Acknowledgment.—This work was sponsored by the Gulf Research & Development Company as part of the research program of the Multiple Fellowship on Petroleum.

(33) See footnote 22 of ref. 28.
(34) L. H. Germer and A. U. MacRae, *J. Chem. Phys.*, **37**, 1382 (1962).
(35) O. Beeck, A. E. Smith, and A. Wheeler, *Proc. Roy. Soc.* (London), **A177**, 62 (1940).
(36) O. Beeck, *Discussions Faraday Soc.*, **8**, 118 (1950).

AN INTERFEROMETRIC DETERMINATION OF DIFFUSION CONSTANTS OF COPPER(II) ION IN COPPER(II) SULFATE SOLUTIONS

BY ROBERT N. O'BRIEN AND CHRISTINE ROSENFIELD

Department of Chemistry, University of Alberta, Edmonton, Canada

Received August 31, 1961

An expression for single ion diffusion constants is derived from an equation due to Levich and developed by Tobias and Keulegan, which treats diffusion of an electrolyte during electrodeposition as two parts, normal and forced diffusion. Diffusion gradients obtained interferometrically are used to find the temperature dependence of the diffusion constant of cupric ions in copper sulfate solutions. Agreement with published values is interpreted as support for the theory.

The traditional methods of obtaining diffusion constants in aqueous solution yield data which pertain to the solvated molecular species. In the case of an electrolyte, a function of the mobilities of all ions present, known as the Nernst–Hartley relationships, must be used unless it can be shown that the motion of only one ion is important. It is the intention to show later that in the cell Cu–$CuSO_4$–Cu, when stable concentration gradients have been established across the cell, only the motion of the cupric ions need be considered since the motions of the sulfate ions need only be local and the net time average migration of the anion is zero. This work concerns the application of interferometry to the problem since interference fringes are a good approximation of concentration gradients.

Samarcev[1] has shown that it is possible to calculate diffusion constants on the basis of concentration polarization, where the diffusion gradient is found by interferometry. That is, the perturbations to the interference fringe system are interpreted as concentration changes from a knowledge of the effect of concentration on refractive index of the electrolyte. The authors believe they have advanced the technique in speed and accuracy.

Experimental

The principal piece of apparatus used was a multiple-beam interferometer.[2] Auxiliary apparatus was a microscope with a camera attachment for taking photomicrographs, or interferograms, and a sodium vapor lamp to supply monochromatic light from a pinhole source. The microscope was an Ernst-Leitz-GMBH-Wetzlar with Makam Leica camera attachment.

The light path is shown in Fig. 1 together with a scale schematic diagram of the interferometer, which is also the electrodeposition cell, and Fig. 2 is a cut-away drawing of a typical cell. Figure 3 shows a much enlarged section of the wedge of electrolyte between the working electrodes; the wedge, whose angle is too small to show to scale, is increasing in thickness into the paper. The coated flats were horizontal in all reported experiments.

To consider the parts of the apparatus whose functions are not obvious in their consecutive order of encounter by the collimated monochromatic beam of light; the 45° first surface mirror merely changes the direction of the light and allows the use of an optical bench and the convenience of clamping all parts firmly relative to each other.

From the mirror, the light enters the cell and the amplitude is split by the coating on the bottom glass flat. At the coating–solution interface, 90% of the light was reflected out of the cell and about 10% passed through the solution. At the solution–coating interface of the top flat, the 10% was further split. About 60% passed through and into the microscope. The remaining 40% is reflected back to the solution–coating interface of the bottom flat where 90% of the incident light is reflected back to the top flat coating–solution interface. The 60% of the light which is passed by the top flat coating becomes the second and contiguous beam to form interference fringes localized in the interference wedge.

The electrodes were made by turning a 2 mm. thick disk from a 1.5 in. bar of fully annealed copper, then cutting a 3 mm. slice out of the center to give two nearly semicircular electrodes. A

(1) A. G. Samarcev, *Z. physik. Chem.*, **A168**, 45 (1934).
(2) S. Tolansky, "Multiple Beam Interferometry," Oxford University Press, 1948, p. 1.

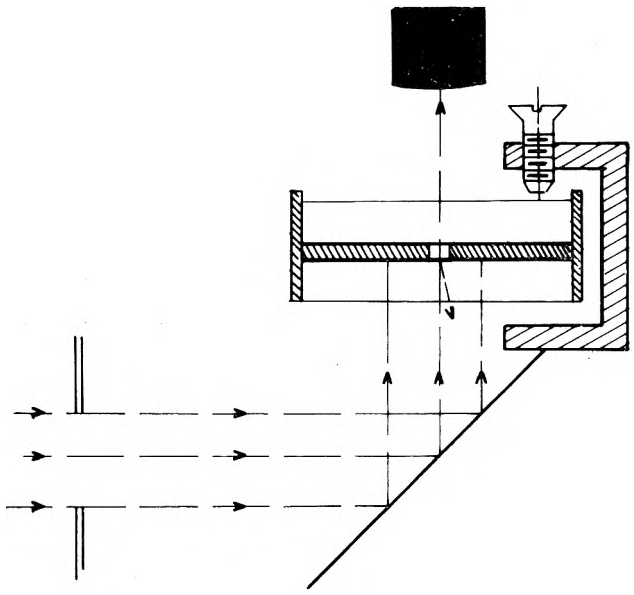

Fig. 1.—Schematic diagram showing the light path of the collimated monochromatic light (sodium vapor) through the electrodeposition cell, which is also an interferometer, into the microscope.

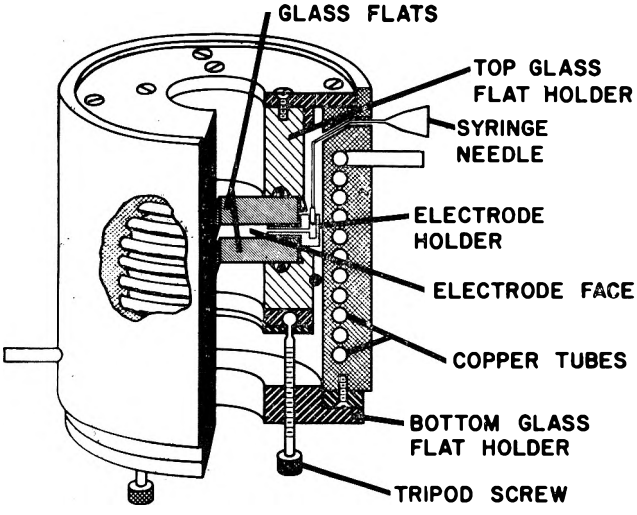

Fig. 2.—A cutaway drawing to scale of a typical electrodeposition cell.

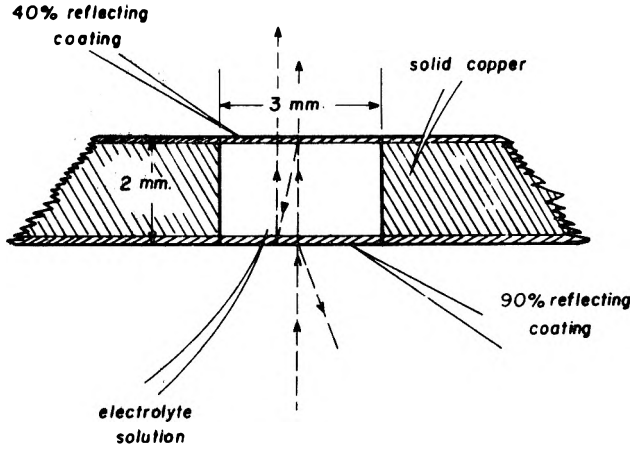

Fig. 3.—The electrolyte and electrodes of the electrodeposition cell shown much enlarged. The wedge angle is 1.7 minutes of arc. The wedge of electrolyte may be visualized as increasing in depth into the paper.

wedge angle of about 1.7 minutes of arc was polished into the electrodes and the glass flats were clamped onto these surfaces. The electrodes were held apart by Lucite[3] spacers. The coated glass flats were supplied by the Liberty Mirror Division of the Libbey-Owens-Ford Glass Co. The uncoated faces had a 1° wedge so that any reflections from them would not enter the microscope. The cell itself was cast from an epoxy resin (Araldite,[4] manufactured by Ciba) around a coil of copper tubing so that a constant temperature could be maintained by pumping water through the coil. The water was supplied from a 15-l. reservoir maintained to within ±0.02° of the desired temperature. The temperature of the solution in the cell was found for a series of temperatures of circulating water with a copper–constantan thermocouple.

The electrolyte solution was $CuSO_4$ and was made up from triply distilled water which then was boiled and added to solid analytical grade $CuSO_4 \cdot 5H_2O$. It was found that while triply distilled water gave near "conductivity water" values of conductivity that electrolyzing this water in the interferometer showed that some ions were present, probably carbonate, since concentration gradients were formed. This did not occur with the freshly boiled water. Wide ranges of concentrations were used but only the temperature variation of the diffusion constant at 10 g./l. $CuSO_4$ is reported here.

Previous to an experimental run, the bottom flat was sealed into the cell with melted paraffin and electrodes were laid in on top of it, the working faces having been mechanically polished and etched in dilute HNO_3, then washed in distilled water and dried. Lucite spacers then were placed between the electrodes and the top flat clamped down in such a way as to give fringes formed by the path difference in air between the reflecting coatings on the two flats. The solution then was injected and the whole allowed to come to thermal equilibrium. The volume of electrolyte was about 25 × 2 × 3 mm., or 0.15 ml.

During this period, the fringe system was manipulated by adjusting the clamping screws to give the most easily photographed pattern. The fringe separation could be varied and also the orientation, since the wedge angle polished into the electrodes was uneven and the flats could be rocked on high spots to some extent. It usually was convenient to have the fringes inclined at 90° to the working surfaces of the electrodes and to have about 15 to 20 fringes per mm.

When thermal equilibrium was attained, a desired potential was impressed across the cell. This potential was supplied by a lead–acid storage cell and measured with a potentiometer. The current was measured by the potential drop across a known resistance or in some cases by an ammeter. The current densities used were adjusted to give easily measured concentrations. They therefore varied widely even beyond the range of 1–10 ma./cm.^{2}, which for this system give times of residence for cupric ions from 90 sec. to 15 min.

A series of perturbations appeared on the usually straight, parallel fringe pattern. The perturbed pattern became stable in about 1 min. and remained so for several hours or at high current densities until irregular deposits on the cathode began to cause local perturbations. Soon after stability was achieved, a photomicrograph (Fig. 4) was taken using exposures which varied from 10 sec. to several minutes. The photomicrographs then were enlarged and the amplitude of the perturbations was measured with a millimeter grid.

The optical path length traveled by beams which interfere in these experiments differ by $2aN$, where a is the optical path distance through the solution and N may be any positive integer but in practice does not become larger than about 5. Displacements of the fringe pattern were related to concentration changes through the equation $m\lambda = \Delta n d \cos\varphi$, in which d is the difference in the distance traveled by the two interfering beams, λ the wave length, in this case 5893 Å., Δn the change in the refractive index of the solution, m the displacement of the interference fringes in units of the distance between consecutive fringes, and φ the angle between the reflected beam and the perpendicular to the surface of the flats.

The effect of having a concentration gradient near the electrode is to cause displacement of the beam, inward at the cathode and outward at the anode since the gradient constitutes an optical wedge inclined to the main portion of the interferometer. At the cathode each succeeding passage of light through the solution results in further displacement. At high concentration gradients and high orders of interference, the discreteness of the fringe system is destroyed. This system therefore is limited to a small

(3) Registered trade mark of E. I. du Pont de Nemours and Co., Inc.

(4) Registered trade mark of the Ciba Co., Inc.

number of reflections (~10) and concentration gradients of about 10 g./l./mm.

Results

A series of experiments in which interferograms were taken and measured was performed on a 10 g./l. solution of $CuSO_4$ at temperatures ranging from 6 to 50°. The results are shown in Table I. The diffusion coefficients have been calculated using the formula

$$\left(\frac{\partial C_{Cu^{2+}}}{\partial y}\right)_{y=0} = \frac{1}{4}\frac{I}{AFD_{Cu^{2+}}} \qquad (I)$$

(which is derived in Appendix I) where C is concentration in moles/l., y is the perpendicular distance from the electrode, I is the total current in amperes, A is the area of the diffusion reference frame, F is the faraday, and D is the diffusion coefficient.

The best values obtained from the literature are included for comparison. These are values for $CuSO_4$ rather than Cu^{2+} and are quoted as having a probability error of $\mp 10\%$ or more. We believe our values to be accurate to $\mp 2\%$ from the experienced uncertainty in measurements.

Figure 5 is an Arrhenius plot of the raw diffusion coefficients found and one in which the diffusion coefficient has been divided by the viscosity of water in centipoises at that temperature. It is realized that the viscosity of a 10 g./l. solution of $CuSO_4$ will be different from that of water, but because the difference would be expected to be small (about a 1% increase for molar solutions[5]) and no experimental values could be found, the accepted values for water were used.

The raw values did not give a convincing straight line but a tentative one was drawn through the points at high temperatures giving an activation energy of 1.3 kcal. Removal of the effect of the change in the viscosity of the water gave an increase in the activation energy to 2.1 ± 0.1 kcal., showing that the change in the viscosity cannot account for the change in diffusion constants.

TABLE I

DIFFUSION CONSTANTS OF Cu^{2+} IN $CuSO_4$ AT VARIOUS TEMPERATURES (CM.²/SEC.) AT A CONCENTRATION 10 G./L.

Temp., °C.	$D_{Cu^{2+}}$	D_{CuSO_4} ICT	Temp., °C.	$D_{Cu^{2+}}$
6	0.47×10^{-5}		30	0.62×10^{-5}
7.5	$.49 \times 10^{-5}$		35	$.66 \times 10^{-5}$
8.7	$.42 \times 10^{-5}$		39	$.68 \times 10^{-5}$
10.0		0.40×10^{-5}		
13.5	$.43 \times 10^{-5}$		42	$.79 \times 10^{-5}$
15	$.44 \times 10^{-5}$		46	$.93 \times 10^{-5}$
17		$.45 \times 10^{-5}$		
20		$.50 \times 10^{-5}$		
27.7	$.54 \times 10^{-5}$		50	1.17×10^{-5}

The anomalous increase in the diffusion constant at the lower temperatures can, at the moment, be only tentatively assigned to change of short range crystal structure in water near its maximum density temperature of about 4°.

Theory

The electrodeposition cell used contained about 0.15 ml. of $M/16$ $CuSO_4$ solution. The anode reaction was $Cu \rightarrow Cu^{2+} + 2e$ and the cathode reaction the exact reverse $Cu^{2+} + 2e \rightarrow Cu$, or no net chemical reaction occurred. The only change during electrolysis was the transport of Cu^{2+} ion from the anode to the cathode resulting in a decrease in the weight of the anode, an increase in the weight of the cathode, and a slight spatial shift of the electrode faces in the cell.

Since, for electrical neutrality, the concentration of sulfate ions must equal the concentration of cupric ions, then if the only mode of transport of charged particles is by diffusion and electromigration there is no reason for the sulfate ions to move (except for their normal thermal motion and that connected with electrophoretic and relaxation effects) once the stable concentration gradients are set up or it is suggested that a stream of migrating Cu^{2+} ions merely penetrates and locally perturbs an essentially stationary array of SO_4^{2-} ions.

Convection is, however, known to occur[6] at current densities over 3 ma./cm.² in solutions in the range of concentration used. The convection is "natural" or is a laminar flow and does not destroy the "diffusion layer" concentration gradient (except in the anode over cathode position where turbulent flow occurs).[7]

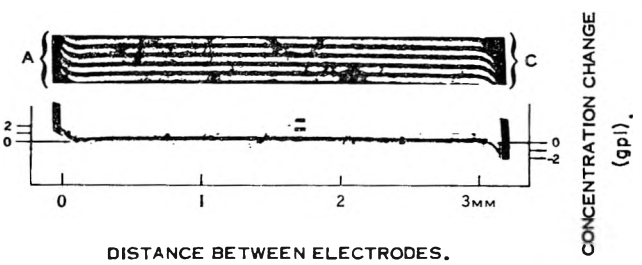

Fig. 4.—A typical interferogram. A mask has been placed over the lower portion to outline one fringe and show a concentration scale. The dark side pieces are copper electrodes. A 30 g./l. solution is being electrolyzed at 400 μamperes at 10°.

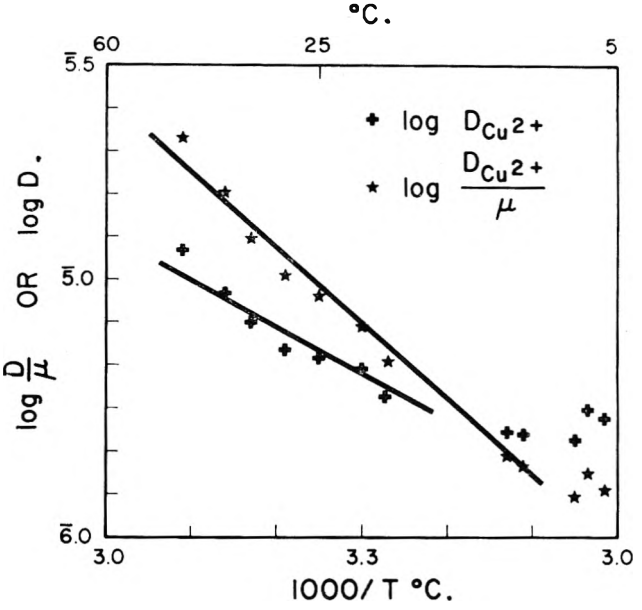

Fig. 5.—An Arrhenius plot of the change in the diffusion coefficient of Cu^{2+} with temperature showing an activation energy of 1.2 kcal./mole for the higher temperature range. The upper curve shows that subtracting the effect of the change of the viscosity of water cannot account for the temperature coefficient of diffusion.

(5) R. A. Robinson and R. H. Stokes, "Electrolyte Solutions," Second Ed., Butterworths Scientific Publications, London, 1959, p. 304.

(6) N. Ibl and R. Muller, *Z. Elektrochem.*, **59**, 671 (1955); *J. Electrochem. Soc.*, **105**, 346 (1958); C. W. Tobias, M. Eisenberg, and C. R. Wilke, *ibid.*, **99**, 12 (1952).

(7) Unpublished data given in part at the 121st Meeting of the Electrochemical Society by R. N. O'Brien.

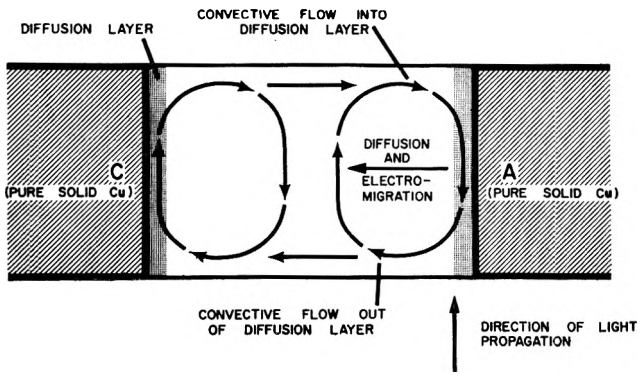

Fig. 6.—A schematic drawing of the type of natural convection found at current densities of more than 3 ma./cm.^{2} found in the cell with the electrodes in the shallow vertical position. The height of the electrodes is 2 mm. and the separation 3 mm.

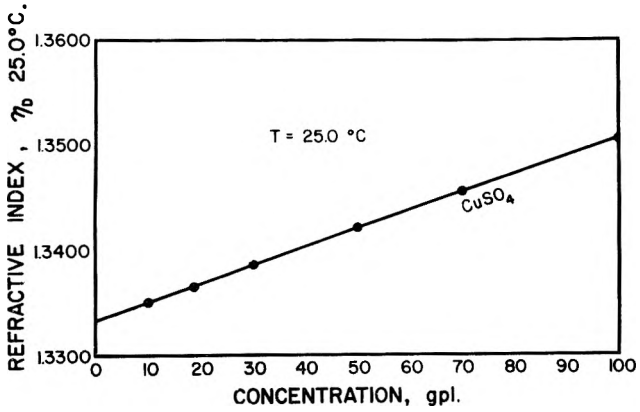

Fig. 7.—The dependence of refractive index on concentration of $CuSO_4$, at 25° using the sodium-D line.

Figure 6 was drawn to show the effect of superimposing a third transport mode, convection, on the concentration gradients of the cell. From observations made in this Laboratory of insoluble, suspended material purposely introduced during electrolysis the pattern shown was drawn. It is characteristic of the geometry of the cell used in this investigation.

We must first consider the case of gently stirring (so that no turbulence results) a liquid in an interferometric electrodeposition cell when no current is flowing. The motion of the electrolyte could not be detected by interferometry, only by the motion of suspended particles. If we now cease stirring and begin electrolysis, at a certain current density, the difference in density of the electrolyte close to the electrodes will be enough to overcome the frictional forces and convection will begin. This point appears to be about 3 ma./cm.^{2} for most electrolytes. In a cell of a certain geometry, it will be possible to detect this interferometrically since a pattern of convective flows such as that shown in Fig. 6 results. The convective flow penetrates the "diffusion layer," but because of the direction of the propagation of light, the fringe perturbation taken as the concentration gradient is an integral value given at the cathode by

$$\text{convection in} - \text{convection out} = \text{ions deposited}$$

The ions are deposited at a given rate and must be supplied at this rate by all three transport mechanisms; convection, diffusion, and electrical migration. The effects of convection on the concentration gradient in the diffusion layer have been seen to cancel out. This does not mean, of course, that convection does not contribute to transport of charge in a cell; it has the effect of lowering the ohmic resistance or shortening the diffusion and electromigration path, as does turbulent and forced convection. The calculated speed of convective motion (using Ibl's formula) in a 2-mm. deep cell is about two orders of magnitude greater than the mobility of the ions under the conditions used.

An expression (eq. I) has been developed which takes into account electromigration so that a pure diffusion constant can be found electrochemically. The left-hand term was found experimentally by taking a tangent to the bend of the fringes at $y = 0$, that is at the anode. In most cases, the fringes in the diffusion layer approximated a straight line to within the experimental error and so the diffusion coefficient is given as an average value between 0 and 10 g./l. since, depending on the current density, the concentration at the electrode varied from nearly zero to almost 10 g./l.

A sample calculation is shown below in which a 10 g./l. $CuSO_4$ solution was electrolyzed at 500 μa. between electrodes with an area of 0.48 cm.^{2} and showed a fringe shift of one fringe at 15°. The fringes in the region of the first wave or diffusion layer were very nearly straight, showing small dependence of $D_{Cu^{2+}}$ on concentration, and the measured width of the diffusion layer was 0.110 mm.

One fringe shift in the system was produced by a change in refractive index of 0.000137, or, knowing that the thickness of cell and electrodes was 1.92 mm. and hence the optical path length difference for the two interfering beams was 6.52×10^3 wave lengths of Na_D line light, we get one fringe = 1.12 g./l. of $CuSO_4$. Figure 7 gives the dependence of refractive index of cupric sulfate solutions on concentration at 25°. The relationship between refractive index (for a given concentration) and temperature also was an essentially straight line so that the above computation also should hold good for 15°. Any error introduced would be smaller in any event than that involved in measuring the fringe shift which, by using the fringe splitting resulting from the Na_D doublet, gave a maximum error of $\pm 1/20$th of a fringe. For this reason, most of the diffusion constants were calculated from interferograms taken at high current density where the fringe shift was 4–5.

Now substituting in eq. I the molar values of concentration and expressing all quantities in the c.g.s. system

$$\frac{0.00112 \text{ g./cc./160 g.}}{0.0110 \text{ cm.}} = \frac{5 \times 10^{-4} \text{ amp.}}{4 \times 0.48 \text{ cm.}^2 \times 96{,}489.9 D_{Cu^{2+}}}$$

then

$$D_{Cu^{2+}}(15°, 0.0625\ M) = 4.4 \times 10^{-6} \text{ cm./sec.}$$

Which compares to $4.5 \times 10^{-6} \pm 0.5$ for 0.1 N $CuSO_4$ at 17° from the International Critical Tables.

Discussion of Results

The results obtained using the derived expression and the observed concentration gradients have been compared with the best values found in the literature

The literature values are of the diffusion constant for $CuSO_4$ and were found by various methods including conductivity. They are all rather old and the precision claimed is not high.

It is realized that direct comparison of single ion diffusion constants with that of the parent electrolyte is not valid. Consideration of the Nernst–Hartley relationships suggests that the Cu^{2+} diffusion constant should be about 85% of that for $CuSO_4$. Inspection of the data, remembering the precision claimed, shows that they are in the right range.

It also is realized that except at infinite dilution, the presence of oppositely charged ions will affect the diffusivity. Our values are integral values and hence apply to finite concentrations. They should, however, be independent of the specific anion present provided it has the same over-all charge and similar solubility characteristics.

Appendix I

Derivation of Diffusion Equation.—According to Levich[8] and Keulegan,[9] we may represent the total ion flux which is related to the concentration gradient developed in a solution in the presence of an applied potential by the expression

$$-\frac{\partial n_j}{\partial t} = AD_j\frac{\partial C_j}{\partial y} + AU_jC_jZ_je\frac{\partial V}{\partial y} \qquad (1)$$

in which $\partial n_j/\partial t$ represents the number of ions of the jth kind passing per unit time; A is the cross-sectional area; D_j is the Fick diffusion constant of the jth ion; U_j is the mobility of the jth ion; Z_j is its valence; C_j is its concentration; e is the charge on an electron; V is the electrical applied potential; and y is the distance perpendicular to the electrode.

Since for an ideal solution $D_j = U_jkT$, in which k is the Boltzmann constant and T is the absolute temperature[10]

$$-\frac{\partial n_j}{\partial t} = AD_j\frac{\partial C_j}{\partial y} + \frac{AC_jD_jZ_je}{kT}\frac{\partial V}{\partial y} \qquad (2)$$

If we let f_j be the number of ions reacting per faraday of current passing, then at the electrode–electrolyte interface ($y = 0$)

$$-\frac{\partial n_j}{\partial t} = \frac{f_jI}{F}$$

Thus

$$\frac{f_jI}{F} = AD_j\left(\frac{\partial C_j}{\partial y}\right)_{y=0} + \frac{AC_jD_jZ_je}{kT}\left(\frac{\partial V}{\partial y}\right)_{y=0} \qquad (3)$$

Multiplying (3) through by the factor Z_j/D_j, we obtain

$$\frac{f_jIZ_j}{FD_j} = AZ_j\left(\frac{\partial C_j}{\partial y}\right)_{y=0} + \frac{AC_j}{kT}Z_j^2e\left(\frac{\partial V}{\partial y}\right)_{y=0} \qquad (4)$$

for the jth ions. If there are i ions in the solution, a similar equation may be written for each of them. Summing all such equations, we obtain

$$\frac{I}{F}\sum\frac{f_iZ_i}{D_i} = A\sum Z_i\left(\frac{\partial C_i}{\partial y}\right)_{y=0} + \frac{Ae}{kT}\left(\frac{\partial V}{\partial y}\right)_{y=0}\sum Z_i^2C_i \qquad (5)$$

Since there can be no macroscopic separation of charges in the solution, the sum for all ions, $Z_iC_i = 0$, and the first term on the right-hand side of (5) must vanish. Solving the remaining expression for $(\partial V/\partial y)_{y=0}$ the result is

$$\frac{IkT}{AFe}\frac{\sum Z_if_i/D_i}{\sum Z_i^2C_i} = \left(\frac{\partial V}{\partial y}\right)_{y=0} \qquad (6)$$

Substituting (6) into (3) gives

$$\left(\frac{\partial C_j}{\partial y}\right)_{y=0} = \frac{I}{AF}\left[\frac{f_j}{D_j} - \sum C_jZ_j\frac{\sum f_iZ_i/D_i}{\sum Z_i^2C_i}\right]_{y=0} \qquad (7)$$

Now let us consider a solution of $CuSO_4$. The only ions present in appreciable quantities will be Cu^{2+} and SO_4^{2-}. In a solution of concentration a, these relations will hold

For Cu^{2+}:

$$\left(\frac{\partial C_{Cu^{2+}}}{\partial y}\right)_{y=0} = \frac{I}{AF}\left[\frac{1/2}{D_{Cu^{2+}}} - 2a\frac{\left(1/2\cdot 2/D_{Cu^{2+}} + \dfrac{O(-2)}{D_{SO_4^{2-}}}\right)}{4a + 4a}\right] = \frac{1}{4}\frac{I}{AFD_{Cu^{2+}}}$$

For SO_4^{2-}:

$$\left(\frac{\partial C_{SO_4^{2-}}}{\partial y}\right)_{y=0} = \frac{I}{AF}\times$$

$$\left[\frac{O}{D_{SO_4^{2-}}} + \frac{2a\left(1/2\cdot 2D_{Cu^{2+}}\dfrac{O(-2)}{D_{SO_4^{2-}}}\right)}{4a + 4a}\right] = \frac{1}{4}\frac{I}{AFD_{Cu^{2+}}} \qquad (8)$$

Applying eq. 8 to the case of a solution of pure $CuSO_4$ in which the only two ions present in appreciable quantity are Cu^{2+} and SO_4^{2-}, and the reaction at either electrode is the dissolution or deposition of Cu, the experimental data may be used to calculate the diffusion coefficient for Cu^{2+}. That is, the slope of the interference fringe in the diffusion layer is used for $\partial C_{Cu^{2+}}/\partial y$ in our final eq. 8 above.

(8) B. Levich, *Acta Physicochim. URSS*, **17**, 257 (1942).
(9) G. H. Keulegan, *J. Res. Natl. Bur. Std.*, **47**, 156 (1951).
(10) H. S. Harned and B. B. Owen, "The Physical Chemistry of Electrolytic Solutions," 3rd Ed., Reinhold Publ. Corp., New York, N. Y., 1958, p. 118.

ELECTRON IMPACT INVESTIGATIONS OF SULFUR COMPOUNDS. II. 3-METHYL-2-THIABUTANE, 4-THIA-1-PENTENE, AND 3,4-DITHIAHEXANE[1]

BY BRICE G. HOBROCK AND ROBERT W. KISER

Department of Chemistry, Kansas State University, Manhattan, Kansas

Received August 31, 1962

Appearance potentials and relative abundances of the principal positive ions from 3-methyl-2-thiabutane, 4-thia-1-pentene, and 3,4-dithiahexane are reported. Probable ionization and dissociation processes are postulated in agreement with the computed energetics. Heats of formation, consistent with the proposed processes, are given. From appearance potential data, the ionization potential of C_2H_5SSH is derived to be 9.4 ± 0.3 e.v., in agreement with the group orbital calculations. More accurate values for the proton affinities of hydrogen sulfide and methanethiol are found to be −197 ± 7 and −199 ± 10 kcal./mole, respectively.

Introduction

In the first of a series of papers concerning the electron impact spectroscopy of sulfur compounds, we reported electron impact data for 2-thiabutane, 2-thiapentane, and 2,3-dithiabutane.[2] In the course of our further investigation of sulfides and disulfides, we have completed studies of 3-methyl-2-thiabutane, 4-thia-1-pentene, and 3,4-dithiahexane and report the results in this article. Mass spectral cracking patterns as well as ionization and appearance potentials for the principal positive ions have been determined experimentally for these compounds. From the measured appearance potentials, probable processes for the formation of the various positive ions are postulated. Some of the interesting species (H_3S^+, CH_5S^+) observed in the mass spectra of the compounds in a previous paper[2] also were studied from the mass spectra of the compounds reported in this investigation; therefore, slightly revised values for the proton affinities of hydrogen sulfide and methanethiol are reported based on our additional experimental results. As was reported recently,[3] the very interesting species, $H_2S_2^+$, is observed in the mass spectrum of 3,4-dithiahexane.

Experimental

The experimental data were obtained using a time-of-flight mass spectrometer. A previous description of the instrumentation has been given.[4] The mass spectra which we report were obtained at nominal electron energies of 70 e.v. Calibration of the voltage scale in the determination of ionization and appearance potentials was accomplished by intimately mixing xenon with the compound being investigated. Appearance potentials were determined primarily by the extrapolated voltage difference method.[5] The technique of Lossing, Tickner, and Bryce[6] and the energy compensation technique[7] also was used and appeared to give somewhat better values for the ionization potentials of these sulfur compounds than did the extrapolated voltage difference method.

In early experiments we noted some difficulty in obtaining accurate values for the ionization potentials of the organic disulfides. We found that this problem could be resolved by removing any accumulated heavy deposits of electronic "dirt" from the source components. This was accomplished by treating the ion source components with 12% HF in a Sonblaster ultrasonic sound generator[8] for 2 min. or less. Longer treatment to the 12% HF in the ultrasonic cleaner was found to cause some coloration of the metallic components.

The samples of 3,4-dithiahexane, 3-methyl-2-thiabutane, and 4-thia-1-pentene were obtained from commercial sources. The purity of each of the compounds was checked by gas–liquid partition chromatography. The 3,4-dithiahexane showed no impurities. Both 4-thia-1-pentene and 3-methyl-2-thiabutane were found to contain small impurities of lower molecular weight, present in quantities less than 3 mole %. The mass spectrum of 3-methyl-2-thiabutane shows no significant differences with serial no. 589 and 912 in the API tables[9] so no interference was expected. The impurity in 4-thia-1-pentene appeared to be methyl sulfide, since a peak of variable size appeared at *m/e* 62 in the mass spectrum. Appearance potential measurements on the ion at *m/e* 62 indicated that it was a parent molecule-ion and subsequently the impurity was identified as methyl sulfide by comparison with its reported mass spectrum.[9]

Results

Experimentally determined mass spectra and appearance potentials for the principal ions formed from the three compounds being investigated are given in columns two and three of Tables I–III. The probable processes for the formation of the various ions are given in column four and the heats of formation consistent with the proposed processes are presented in the last column.

The heat of formation of 4-thia-1-pentene was not available and we therefore estimated it to be 10 kcal./mole, using the method of Franklin.[10] The heats of formation for 3-methyl-2-thiabutane and 3,4-dithiahexane are −21.43[11] and −17.42,[12] respectively. Other heats of formation employed in our calculations were those tabulated by Gallegos.[13]

Discussion

Ionization Potentials.—Ionization potentials were calculated for the complete series of disulfides, $C_2H_6S_2$ to $C_6H_{14}S_2$ (symmetrical and unsymmetrical) using a group orbital treatment[14] and the ionization potential of H_2S_2 (10.2 e.v.)[3] determined in this study. A C–SS interaction parameter of 2.06 is calculated using the ionization potential of 8.46 e.v. reported for 2,3-dithia-

(1) This work was supported by the U. S. Atomic Energy Commission under contract no. AT(11-1)-751 with Kansas State University. This is a portion of a dissertation to be presented by B. G. Hobrock to the Graduate School of Kansas State University in partial fulfillment of the requirements for the degree of Doctor of Philosophy.

(2) B. G. Hobrock and R. W. Kiser, *J. Phys. Chem.*, **66**, 1648 (1962); note that a minor change has been made in the title of this series of papers to avoid any confusion over the term *electron impact spectroscopy*. This change was made at the suggestion of S. Meyerson, and we wish to thank him for his comments.

(3) R. W. Kiser and B. G. Hobrock, *ibid.*, **66**, 1214 (1962).

(4) E. J. Gallegos and R. W. Kiser, *J. Am. Chem. Soc.*, **83**, 773 (1961).

(5) J. W. Warren, *Nature*, **165**, 811 (1950).

(6) F. P. Lossing, A. W. Tickner, and W. A. Bryce, *J. Chem. Phys.*, **19**, 1254 (1951).

(7) R. W. Kiser and E. J. Gallegos, *J. Phys. Chem.*, **66**, 947 (1962).

(8) "Sonblaster" Ultrasonic Generator, Series 600; The Narda Ultrasonics Corp., Westbury, L. I., New York.

(9) "Mass Spectral Data," American Petroleum Institute Research Project 44, National Bureau of Standards, Washington, D. C.

(10) J. L. Franklin, *Ind. Eng. Chem.*, **41**, 1070 (1949).

(11) W. N. Hubbard, W. D. Good, and G. Waddington, *J. Phys. Chem.*, **62**, 614 (1958).

(12) W. N. Hubbard, D. R. Douslin, J. P. McCullough, D. W. Scott, S. S. Todd, J. F. Messerly, I. A. Hossenlopp, and G. Waddington, *J. Am. Chem. Soc.*, **80**, 3547 (1958).

(13) E. J. Gallegos, "Mass Spectrometric Investigation of Saturated Hetero-cyclics," Doctoral Dissertation, Kansas State University, Manhattan, Kansas, January, 1962.

(14) J. L. Franklin, *J. Chem. Phys.*, **22**, 1304 (1954).

TABLE I

APPEARANCE POTENTIALS AND HEATS OF FORMATION OF THE PRINCIPAL IONS FROM 3-METHYL-2-THIABUTANE

m/e	Relative abundance	Appearance potentials, e.v.	Process	ΔH_f^+, kcal./mole
15	11.5	19.4 ± 0.5	$C_4H_{10}S \rightarrow CH_3^+ + (?)$	
27	52.4	16.5 ± .5	$\rightarrow C_2H_3^+ + CH_3 + S + CH_4$ (?)	292
39	35.8	21.0 ± .5	$\rightarrow C_3H_3^+ + CH_3 + S + 2H + H_2$	274
41	89.5	15.2 ± .2	$\rightarrow C_3H_5^+ + CH_3 + SH + H$	214
42	22.8	13.5 ± .2	$\rightarrow C_3H_6^+ + CH_2 + H_2S$	226
			$\rightarrow C_3H_6^+ + CH + SH$	227
43	100.0	12.7 ± .2	$\rightarrow C_3H_7^+ + CH_3 + S$	186
45	21.2	16.4 ± .4	$\rightarrow CHS^+ + C_3H_6 + H + H_2$	300
			$\rightarrow CHS^+ + C_2H_5 + CH_2 + H_2$	267
46	6.2	15.5 ± .4	$\rightarrow CH_3S^+ + C_2H_4 + CH_3 + H$	240
			$\rightarrow CH_3S^+ + C_3H_6 + 2H$	227
47	28.1	15.3 ± .2	$\rightarrow CH_3S^+ + C_2H_5 + CH_2$	242
48	62.9	12.0 ± .2	$\rightarrow CH_4S^+ + C_2H_2 + CH_4$	219
49	34.3	12.1 ± .2	$\rightarrow CH_5S^+ + C_2H_2 + CH_3$	172
59	8.6	16.1 ± .3	$\rightarrow C_2H_3S^+ + 2CH_3 + H$	234
61	6.2	13.5 ± .3	$\rightarrow C_2H_5S^+ + C_2H_3 + H_2$	226
			$\rightarrow C_2H_5S^+ + C_2H_4 + H$	225
75	83.1	11.7 ± .2	$\rightarrow C_3H_7S^+ + CH_3$	217
77	3.9			
90	58.9	8.7 ± .2	$\rightarrow C_4H_{10}S^+$	179
92	2.5			

TABLE II

APPEARANCE POTENTIALS AND HEATS OF FORMATION OF THE PRINCIPAL IONS FROM 4-THIA-1-PENTENE

m/e	Relative abundance	Appearance potential, e.v.	Process	ΔH_f^+, kcal./mole
15	15.8	17.7 ± 0.5	$C_4H_8S \rightarrow CH_3^+ + (?)$	
27	26.9	16.5 ± .4	$\rightarrow C_2H_3^+ + CH_3S + CH_2$	285
			$\rightarrow C_2H_3^+ + CH_2S + CH_3$	283
35	18.1	14.8 ± .2	$\rightarrow H_3S^+ + CH + C_2H_4$	163
37	6.3	16.6 ± .5	$\rightarrow C_3H^+ + CH_3 + S + 2H_2$	308
38	12.4	20.3 ± .5	$\rightarrow C_3H_2^+ + CH_3S + H + H_2$	388
39	73.6	16.5 ± .4	$\rightarrow C_3H_3^+ + CH_3 + SH + H$	275
			$\rightarrow C_3H_3^+ + CH_2 + H_2S + H$	275
40	8.4			
41	82.9	12.7 ± .3	$\rightarrow C_3H_5^+ + CH_3 + S$	218
42	6.9			
45	92.6	13.8 ± .3	$\rightarrow CHS^+ + C_3H_6 + H_2$	296
			$\rightarrow CHS^+ + CH_3 + C_2H_4$	284
46	44.0	11.4 ± .3	$\rightarrow CH_2S^+ + C_2H_4 + H_2$	227
47	67.3	11.9 ± .2	$\rightarrow CH_3S^+ + C_2H_5$	252
48	11.2	11.5 ± .2	$\rightarrow CH_4S^+ + C_3H_4$	229
49	5.1	11.7 ± .4	$\rightarrow (CH_3S^{34})^+ + C_3H_5$	248
61	33.8	12.0 ± .2	$\rightarrow C_2H_5S^+ + C_2H_3$	223
73	72.5	11.0 ± .2	$\rightarrow C_3H_5S^+ + CH_3$	232
87	6.2			
88	100.0	8.70 ± 0.2	$\rightarrow C_4H_8S^+$	211
89	6.0			
90	5.2			

butane.[15] A value of 8.25 e.v. was calculated for 3,4-dithiahexane and is in very good agreement with our experimental value of 8.30 e.v., a previously calculated value of 8.36 e.v.,[2] and a literature value of 8.27 e.v.[15] The ionization potentials of the other disulfides were calculated to fall in the range of 8.2–8.4 e.v.

Heats of Formation of Ions.—In general, the ΔH_f^+ of the various ions, as summarized in Tables I–III, are in agreement with literature values. A few specific cases are discussed in the following paragraphs.

m/e = **35.**—The formation of H_3S^+ is noted in the study of two of these molecules. From 4-thia-1-pentene the formation of H_3S^+ appears to be accompanied by the neutral fragments CH + C_3H_4. $\Delta H_f^+(H_3S)$ = 163 kcal./mole is calculated, which agrees well with previously determined values.[2]

(15) K. Watanabe, T. Nakayama, and J. Mottl, "Final Report on Ionization Potentials of Molecules by a Photoionization Method," December, 1959. Department of Army 5B99-01-004 ORD-TB2-001-OOR-1624. Contract No. DA-04-200 ORD 480 and 737.

TABLE III

APPEARANCE POTENTIALS AND HEATS OF FORMATION OF THE PRINCIPAL IONS FROM 3,4-DITHIAHEXANE

m/e	Relative abundance	Appearance potential, e.v.	Process	ΔH_f^+, kcal./mole
26	8.6	19.5 ± 0.5	$C_4H_{10}S_2 \rightarrow C_2H_2^+ + (?)$	
27	65.0	17.2 ± .4	$\rightarrow C_2H_3^+ + C_2H_5S + S + H_2$	287
29	100.0	14.2 ± .2	$\rightarrow C_2H_5^+ + C_2H_5S + S$	218
35	7.4	15.3 ± .2	$\rightarrow H_3S^+ + 2C_2H_3 + SH$	177
			$\rightarrow H_3S^+ + C_2H_2 + H + C_2H_4S$	154
45	13.5	17.8 ± .5	$\rightarrow CHS^+ + CH_3 + C_2H_4S + H$	270
46	4.5			
58	5.4	18.6 ± .5	$\rightarrow C_2H_2S^+ + C_2H_5 + S + H + H_2$	284
59	10.6	16.2 ± .3	$\rightarrow C_2H_3S^+ + CH_3 + CH_3S + H$	234
			$\rightarrow C_2H_3S^+ + CH_3 + CH_2S + H_2$	248
60	10.6	12.3 ± .3	$\rightarrow C_2H_5S^+ + C_2H_5 + SH$	213
61	7.8	12.5 ± .3	$\rightarrow C_2H_5S^+ + C_2H_5S$	232
64	7.3	14.9 ± .4	$\rightarrow S_2^+ + 2C_2H_6$	282
66	66.7	12.2 ± .2	$\rightarrow H_2S_2^+ + 2C_2H_5$	239
68	5.8	12.2 ± .2	$\rightarrow (H_2SS^{34})^+ + 2C_2H_4$	239
70	0.2			
79	5.5	14.6 ± .2	$\rightarrow CH_3S_2^+ + CH_2 + C_2H_5$	229
			$\rightarrow CH_3S_2^+ + CH_3 + C_2H_2 + H_2$	233
94	50.2	10.8 ± .3	$\rightarrow C_2H_6S_2^+ + C_2H_4$	219
95	4.3			
96	4.8			
122	51.9	8.30 ± 0.15	$\rightarrow C_4H_{10}S_2^+$	174
123	5.8			
124	5.4			

Two processes are believed to contribute to the formation of H_3S^+ from 2,3-dithiahexane. These processes appear to involve the presence of C_2H_2 + H + C_2H_4S and $2C_2H_3$ + SH as neutral fragments. $\Delta H_f^+(H_3S)$ which results from this study and those values obtained in the previous investigation[2] is 165 ± 6 kcal./mole. A proton affinity of −197 ± 7 kcal./mole is obtained, which is not greatly different from that reported previously.[2]

m/e = **49.**—The interesting species at *m/e* = 49 appears in two of the compounds investigated here, 3-methyl-2-thiabutane and 4-thia-1-pentene. For 3-methyl-2-thiabutane, if the neutral fragments are assumed to be C_2H_2 + CH_3, $\Delta H_f^+(CH_5S)$ = 172 kcal./mole. It is believed that the major portion of the ion at *m/e* = 49 from 4-thia-1-pentene is due to the natural abundance of S^{34} and that the ion is $(CH_3S^{34})^+$. From the appearance potential, 11.7 e.v., which is nearly the same as 11.9 e.v. for *m/e* = 47, $\Delta H_f^+(CH_3S^{34})$ = 248 kcal./mole.

An average value for $\Delta H_f^+(CH_5S)$ from previous study[2] and the value of 172 kcal./mole obtained in this work is 163 ± 10 kcal./mole. From this value and using $\Delta H_f^+(H)$ = 367 kcal./mole and $\Delta H_f(CH_3SH)$ = −5.46 kcal./mole,[16] the proton affinity of methanethiol is calculated to be −199 ± 10 kcal./mole.

m/e = **61.**—The ion at *m/e* = 61 is $C_2H_5S^+$ and appears in significant quantities in each of the investigated compounds. From 3-methyl-2-thiabutane, two processes are thought to be of about equal probability and lead to $\Delta H_f^+(C_2H_5S)$ = 226 and 225 kcal./mole. (See Table I for the processes involved.) Good internal agreement is noted as $\Delta H_f^+(C_2H_5S)$ = 223 kcal./mole in the 4-thia-1-pentene study. The neutral fragment in this case is ethylene.

For the appearance potential of the *m/e* = 61 ion from 3,4-dithiahexane and for the subsequent heat of

(16) W. D. Good, J. L. Lacina, and J. P. McCullough, *J. Phys. Chem.*, **65**, 2229 (1961).

formation of $C_2H_5S^-$ we obtain 12.5 ± 0.3 e.v. and 232 kcal./mole, respectively. Our appearance potential is 1.3 e.v. higher than that reported by Franklin and Lumpkin.[17] It was feared that any possible dirty conditions in the source of the mass spectrometer (see Experimental) might prevent our obtaining accurate values as in the case of the ionization potentials of the disulfides. This was not the case, however; we found that an appearance potential of 11.2 e.v. could not be obtained under any experimental conditions in our instrument.

In addition, the value of $\Delta H_f^+(C_2H_5S)$ = 232 kcal./mole, subject to some uncertainty in our use of $\Delta H_f(C_2H_5S)$ = 39 kcal./mole, agrees well with the values of 223 and 225 or 226 kcal./mole reported above and with values of 225, 213, and 233 kcal./mole reported in our earlier study.[2] We conclude that $\Delta H_f^+(C_2H_5S)$ = 225 ± 5 kcal./mole, and by using our determined appearance potential of 12.5 e.v., that $\Delta H_f(C_2H_5S)$ = 40 ± 4 kcal./mole. These values are somewhat different from those reported by Franklin and Lumpkin.[17]

m/e = **64.**—The presence of S_2^+ is observed in the mass spectrum of 3,4-dithiahexane. From the measured appearance potential, $\Delta H_f^+(S_2)$ = 282 kcal./mole, which is in excellent agreement with that calculated from the 2,3-dithiabutane case.[2] The derived ionization potential for S_2 is unchanged from that obtained previously, 11.0 ± 0.2 e.v.[2]

m/e = **66 and 68.**—The ion at *m/e* = 66 is quite intense in the mass spectrum of 3,4-dithiahexane and is the very interesting specie, $H_2S_2^+$. The natural abundance of S^{34} and the abundances of ions at *m/e* = 68 to 70 indicate that the ion must contain two sulfur atoms. Measurements on both *m/e* = 66 and 68 give an appearance potential of 12.2 e.v. for $H_2S_2^+$. The low value of the appearance potential indicates that the ionization and dissociation process leading to $H_2S_2^+$ should be relatively simple. The formation of two molecules of ethylene as neutral fragments is such a process and leads to $\Delta H_f^+(H_2S_2)$ = 239 kcal./mole.[16] Kiser and Hobrock[3] have reported that from these data $I(H_2S_2)$ = 10.2 e.v. and have concluded that D(HS–SH) = 59 ± 3 kcal./mole.

m/e = **79.**—$CH_3S_2^+$ appears in the mass spectrum of 3,4-dithiahexane, even as it did in the mass spectrum of 2,3-dithiabutane. The structure may be CH_2SSH^+, however, as we note the ease with which hydrogen and sulfur form bonds (H_3S^+, CH_5S^+, $H_2S_2^+$). Either or both of two processes may be responsible for the formation of $CH_3S_2^+$ and are shown in Table III. $\Delta H_f^+(CH_3S_2)$ = 240 kcal./mole.[2] An average value of 234 kcal./mole together with the estimated value of $\Delta H_f^+(CH_3S_2)$ = 21 kcal./mole leads to $I(CH_3S_2)$ = 9.3 ± 0.3 e.v.

m/e = **88.**—This is the parent molecule-ion from 4-thia-1-pentene. The measured ionization potential of 8.70 e.v. results in $\Delta H_f^+(C_4H_8S)$ = 211 kcal./mole, which is somewhat higher than $\Delta H_f^+(C_4H_8S)$ = 190 kcal./mole from tetrahydrothiophene.[18] Assuming that the tetrahydrothiophene ion retains its cyclic structure, this difference is probably not too surprising.

m/e = **90.**—This ion appears to a significant extent only in the mass spectrum of 3-methyl-2-thiabutane and is the parent molecule-ion of this compound. $\Delta H_f^+(C_4H_{10}S)$ = 179 kcal./mole.

m/e = **94.**—Instead of simple cleavage of a C_2H_5 group to give an ion at *m/e* = 93, a hydrogen atom apparently rearranges to give the ion at *m/e* = 94, $C_2H_6S_2^+$. Assuming that the neutral fragment is C_2H_4, $\Delta H_f^+(C_2H_6S_2)$ = 219 kcal./mole. Now, if we assume that the structure is C_2H_5SSH, and estimating $\Delta H_f(C_2H_5SSH)$ = 2 kcal./mole, we may calculate the ionization potential of C_2H_5SSH to be 9.4 ± 0.3 e.v. By use of the group orbital method[14] and parameters by Gallegos and Kiser,[19] the ionization potential of C_2H_5SSH is calculated to be 8.95 e.v. Alternatively, using the parameters associated with the treatment of –SS– as a group, $I(C_2H_5SSH)$ is calculated to be 9.05 e.v. The agreement suggests that the structure of $C_2H_6S_2^+$ is $C_2H_5SSH^+$, rather than the ion which might be formed by rearrangement, $CH_3SSCH_5^+$.

m/e = **122.**—The value determined for the ionization potential of 3,4-dithiahexane is 8.30 e.v. and agrees well with literature values.[15] $\Delta H_f^+(C_4H_{10}S_2)$ = 174 kcal./mole, as calculated from the measured ionization potential and $\Delta H_f(C_4H_{10}S_2)$.

Acknowledgments.—We wish to express our indebtedness to Drs. H. C. Moser and A. A. Sandoval for their suggestion to use the 12% HF solution in the ultrasonic cleaner and for their aid in those operations.

(17) J. L. Franklin and H. C. Lumpkin, *J. Am. Chem. Soc.*, **74**, 1023 (1952).

(18) E. J. Gallegos and R. W. Kiser, *J. Phys. Chem.*, **66**, 136 (1962).

(19) E. J. Gallegos and R. W. Kiser, *ibid.*, **65**, 1177 (1961).

ON THERMODYNAMIC COUPLING OF CHEMICAL REACTIONS CLOSE TO EQUILIBRIUM

BY MILTON MANES

Pittsburgh Chemical Company, Pittsburgh 25, Pa.

Received September 4, 1962

In a two-reaction system close to equilibrium wherein each rate is completely determined by the corresponding affinity (*i.e.*, where the rates are diagonal in the affinities), the contribution of each reaction to the entropy production must always be positive. However, if such a system is described in terms of equations that do not represent the individual reactions, the rates become non-diagonal in the affinities. In this new language one can confer or revoke thermodynamic coupling (the apparent existence of an entropy-reducing reaction) by appropriate modifications of the manner in which one chooses to perturb the system from equilibrium. Caution is therefore suggested in ascribing physical significance to thermodynamic coupling in the absence of a reaction mechanism.

Koenig, Horne, and Mohilner[1] have recently cast doubt on the physical significance of "thermodynamic coupling" (the existence of some entropy-reducing reactions in a multi-reaction system) by demonstrating that any set of net chemical reactions in which coupling does not occur can be transformed by linear combination into a set in which it does occur, and conversely. van Rysselberghe,[2] however, has objected to the use by Koenig, *et al.*,[1] of sets of equations that are not written in an "intrinsic" manner, citing De Donder's requirement that only such "intrinsic" sets may be properly used in ascertaining the occurrence of thermodynamic coupling. Hooyman[3] has shown how to write such a set (the criteria for which are stoichiometric in nature) and concludes that the division into reactions with positive or with negative entropy production is then uniquely determined.

This article is to draw attention to the fact that at least in systems close to equilibrium one can in general confer and revoke coupling by modifying the affinities (*e.g.*, by perturbations of the composition), *without making any changes in the equations*. The only set of equations within which coupling cannot be conferred or revoked in this manner turns out to be the set of equations (if such exist) in which each rate depends only on the corresponding affinity. If such a set does exist, *i.e.*, if the real reactions in the system are in fact uncoupled, we can always transform this set into one in which we can confer or revoke coupling. In such cases at least, the coupling cannot be more than an artifact of the mathematics. Although this does not prove that thermodynamic coupling cannot exist, it does suggest caution in ascribing physical significance to it in the absence of a reaction mechanism.

The point can be illustrated by an assumed two-reaction system, which can be readily generalized. Following Verschaffelt,[4] we assume the existence of a pair of reactions in which the rates are diagonal in the affinities and transform it to a set in which the rates are not diagonal in the affinities. It is then a simple matter to show how the non-diagonal pair (or any non-diagonal pair) can be coupled or uncoupled.[5]

In the assumed two-reaction case close to equilibrium the observable rates, v_1 and v_2, are related to the affinities, A_1 and A_2, by the equations

$$v_1 = r_1 A_1$$
$$v_2 = r_2 A_2 \qquad (1)$$

where the proportionality constants r_1 and r_2 are proportional to the equilibration velocities, or "gross reaction rates."[6] They are always positive and represent the assumed real rates in the system.

We now define a new set of affinities, A_1' and A_2' (by assuming a new set of equations), for example

$$A_1' = A_1$$
$$A_2' = A_1 + A_2 \qquad (2)$$

in which case the new rates v_1' and v_2' become

$$v_1' = v_1 - v_2$$
$$v_2' = v_2 \qquad (3)$$

Substitution of the v's from equation 1 and the A's from equation 2 gives the new velocities in terms of the new affinities as

$$v_1' = (r_1 + r_2)A_1' - r_2 A_2'$$
$$v_2' = -r_2 A_1' + r_2 A_2' \qquad (4)$$

In the transformed set the velocities are no longer diagonal in the affinities and we can therefore couple or uncouple the equations by our choice of the A'. For example, v_1' is negative for positive A_1' when $A_2' > A_1'(r_1 + r_2)/r_2$ (in which case v_2' must be positive for positive A_2') and v_2' is negative for positive A_2' if $A_1' > A_2'$ (in which case v_1' must be positive for positive A_1'). Since it is the non-diagonality of the rates in the affinities that makes this kind of manipulation possible, one cannot avoid it by choosing equations on the basis of *any* stoichiometric criteria, except in the trivial case where the assumed set of equations represents the actual uncoupled reactions in the system.

As an example, if we assume as our uncoupled reactions the pair

$$CO + H_2O \rightleftarrows CO_2 + H_2 \qquad (I)$$
$$CH_4 + H_2O \rightleftarrows CO + 3H_2 \qquad (II)$$

the set resulting from the transformation of equation 2 can be written

$$CO = CO_2 + H_2 - H_2O \qquad (I')$$

(1) F. O. Koenig, F. H. Horne, and D. M. Mohilner, *J. Am. Chem. Soc.*, **83**, 1029 (1961). See this article for detailed references and definitions.

(2) P. van Rysselberghe, *Bull. soc. chim. Belg.*, **70**, 592 (1961). This article cites De Donder, *Bull. Classe Sci. Acad. Roy. Belg.*, **23**, 770 (1937).

(3) G. J. Hooyman, *Proc. Natl. Acad. Sci. U. S.*, **47**, 1169 (1961).

(4) J. E. Verschaffelt, *Bull. Classe Sci. Acad. Roy. Belg.*, **41**, 316 (1955).

(5) This was not considered in Verschaffelt's article.

(6) M. Manes, L. J. E. Hofer, and S. Weller, *J. Chem. Phys.*, **18**, 1355 (1950).

$$CH_4 = CO_2 + 4H_2 - 2H_2O \qquad (II')$$

This set conforms to Hooyman's[3] criteria, since CO appears only in equation I′ and CH_4 only in equation II′. As we have seen, however, the number of "positive" and "negative" equations is in fact not invariant, except in the trivial case where we fix both the equations *and* the composition.

Although the foregoing discussion does not prove the non-existence of thermodynamic coupling, we see that it can appear as a consequence of ascribing physical significance to arbitrary equations.

THE SECOND DISSOCIATION CONSTANT OF DEUTERIOSULFURIC ACID FROM 25 TO 225°

BY M. H. LIETZKE AND R. W. STOUGHTON

Chemistry Division, Oak Ridge National Laboratory,[1] Oak Ridge, Tennessee

Received September 6, 1962

The second dissociation constant of deuteriosulfuric acid has been computed from 25 to 225° from data on the solubility of Ag_2SO_4 in D_2SO_4 solutions. In addition, the thermodynamic constants for the reaction $DSO_4^- = D^+ + SO_4^{-2}$ are presented. A comparison with the corresponding values for the H_2SO_4 system is given.

In a previous paper[2] the calculation of the bisulfate acid constant from 25 to 225° was reported. In the present work the second dissociation constant of deuteriosulfuric acid has been computed from data on the solubility of Ag_2SO_4 in D_2SO_4 solutions over the same temperature range. In addition the thermodynamic constants ΔF^0, ΔH^0, and ΔS^0 for the reaction

$$DSO_4^- = D^+ + SO_4^{-2} \qquad (1)$$

are presented.

Experimental

The D_2SO_4 solutions were prepared by diluting a 1 *m* stock solution of D_2SO_4 with D_2O where *m* represents moles per 1000 g. of solvent. The D_2SO_4 stock solution was prepared according to the method given by Shudde,[3] which consists essentially of bubbling SO_3 vapor through D_2O. The SO_3 vapor (obtained by heating Sulfan B (γ-SO_3) from the Allied Chemical Co.) was conveyed with a stream of dry helium through the all-glass system. The D_2O was prepared by twice distilling 99.7% D_2O under an atmosphere of nitrogen that had been dried over $Mg(ClO_4)_2$: the first distillation was made from a 1 *m* D_2SO_4 and 0.5 *m* $K_2Cr_2O_7$ solution and the second from 2% $KMnO_4$ and 0.04 *m* NaOD. Extreme precautions were taken at all times to exclude any contamination by H_2O.

The Ag_2SO_4 was prepared according to the method described by Archibald.[4] The solubility measurements were carried out using the synthetic method described previously.[5]

Results and Discussion

The solubility of Ag_2SO_4 was measured in D_2O and in 0.1, 0.25, 0.5, 0.75, and 1.0 *m* D_2SO_4 from 25 to at least 225°. The experimental solubility values in each solution then were fitted by the method of least squares to a cubic equation in the temperature.

In Table I is shown a comparison between the experimental solubility points and the values calculated using the equations whose coefficients are given in Table II. At any temperature the solubility of Ag_2SO_4 is lower in D_2O than in H_2O (0.019 *m* in D_2O at 25° compared to 0.027 *m* in H_2O). In 0.1 *m* D_2SO_4 the solubility of Ag_2SO_4 is lower than in H_2SO_4, in 0.25 and 0.5 *m* D_2SO_4 the solubility is about the same as in H_2SO_4, while in 0.75 and 1.0 *m* D_2SO_4 the solubility is higher than in the corresponding protonated systems. Thus the ionic strength effect is greater in the deuterated media.

Method of Calculation.—In carrying out the calculations it was assumed that only the species Ag^+, D^+, SO_4^{-2}, and DSO_4^- existed in a solution of Ag_2SO_4 dissolved in D_2SO_4. As in previous work[6] it was also assumed that

$$\ln Q_2 = \ln K_2 + 4S_T\left[\frac{\sqrt{I}}{1 + A\sqrt{I}}\right] \qquad (2)$$

and

$$\ln S = \ln 4\, s_0^3 + 6S_T\left[\frac{\sqrt{I}}{1 + P\sqrt{I}} - \frac{\sqrt{3s_0}}{1 + P\sqrt{3s_0}}\right] \qquad (3)$$

where K_2 is the DSO_4^- acid constant, S_T is the Debye–Hückel limiting slope at temperature *T* for a singly charged ion, s_0 is the solubility of Ag_2SO_4 in D_2O at temperature *T*, *P* and *A* are adjustable parameters, and *I* is the ionic strength of the solution, given by

$$I = m + s + 2[SO_4^{-2}] \qquad (4)$$

where *s* is the molal solubility of Ag_2SO_4 in D_2SO_4 of molality *m*.

Hence the over-all problem involves the evaluation of $\ln K_2$, *A*, and *P* by a non-linear least squares procedure subject to the restrictions represented by the equation for conservation of total sulfate, and those expressing the (molality) solubility product of Ag_2SO_4 and the acid dissociation quotient in terms of the concentrations of the ionic species. Details of the calculation are very similar to those in the bisulfate acid constant calculation[2] and will not be repeated here. One difference, however, should be emphasized: measurement of Ag_2SO_4 in five different concentrations of D_2SO_4 permitted the direct evaluation of all three parameters. It was not necessary, as in the HSO_4^- calculation (where the solubility of Ag_2SO_4 was studied in only three different concentrations of H_2SO_4), to permute

(1) Work performed for the U. S. Atomic Energy Commission and for the Office of Saline Water, U. S. Department of the Interior, at the Oak Ridge National Laboratory, operated by Union Carbide Corporation for the U. S. Atomic Energy Commission.

(2) M. H. Lietzke and R. W. Stoughton, *J. Phys. Chem.*, **65**, 2247 (1961).

(3) R. H. Shudde, North American Aviation Document NAA-SR-2158.

(4) E. H. Archibald, "The Preparation of Pure Inorganic Substances," John Wiley and Sons, Inc., New York, N. Y., 1932.

(5) M. H. Lietzke and R. W. Stoughton, *J. Am. Chem. Soc.*, **78**, 3023 (1956).

(6) M. H. Lietzke and R. W. Stoughton, *J. Phys. Chem.*, **63**, 1183, 1186, 1188, 1190, 1984 (1959); **64**, 816 (1960).

TABLE I

SOLUBILITY OF Ag_2SO_4 IN D_2O AND D_2SO_4 SOLUTIONS AS A FUNCTION OF TEMPERATURE

D_2O			0.1 m D_2SO_4			0.25 m D_2SO_4		
	$m_{Ag_2SO_4}$			$m_{Ag_2SO_4}$			$m_{Ag_2SO_4}$	
t, °C.	(Obsd.)	(Calcd., eq. 3)	t, °C.	(Obsd.)	(Calcd., eq. 3)	t, °C.	(Obsd.)	(Calcd., eq. 3)
25.0	0.0193	0.0194	25.0	0.0248	0.0247	25.0	0.0272	0.0275
57.0	.0257	.0259	95.3	.0618	.0632	93.0	.0928	.0912
64.1	.0279	.0270	110.0	.0717	.0704	98.0	.0983	.0968
74.0	.0289	.0284	147.0	.0867	.0859	112.0	.1113	.1127
75.6	.0277	.0286	170.0	.0920	.0929	129.0	.1310	.1322
81.0	.0293	.0293	234.0	.0984	.0983	132.0	.1362	.1356
102.5	.0309	.0312				143.0	.1451	.1480
180.0	.0309	.0304				175.0	.1834	.1818
190.0	.0293	.0295				179.0	.1868	.1856
195.0	.0289	.0290				232.0	.2238	.2243
0.5 m D_2SO_4			0.75 m D_2SO_4			1.0 m D_2SO_4		
t, °C.	(Obsd.)	(Calcd., eq. 3)	t, °C.	(Obsd.)	(Calcd., eq. 3)	t, °C.	(Obsd.)	(Calcd., eq. 3)
25.0	0.0303	0.0301	25.0	0.0292	0.0292	25.0	0.0288	0.0296
91.0	.1013	.1036	100.0	.1500	.1497	91.0	.1333	.1287
115.0	.1524	.1485	122.0	.2030	.2024	100.0	.1529	.1523
139.0	.1970	.1984	160.0	.3052	.3071	117.0	.2014	.2026
158.0	.2391	.2396	180.0	.3664	.3678	129.0	.2385	.2420
164.0	.2526	.2526	195.0	.4187	.4153	144.0	.2942	.2955
217.0	.3605	.3603	225.0	.5129	.5138	159.0	.3500	.3530
						169.0	.3926	.3934
						189.0	.4852	.4781
						232.0	.6712	.6731

TABLE II

COEFFICIENTS[a] OF CUBIC EQUATIONS DESCRIBING THE SOLUBILITY OF Ag_2SO_4 IN D_2O AND IN D_2SO_4 SOLUTIONS

	a_0	$a_1 \times 10^4$	$a_2 \times 10^6$	$a_3 \times 10^{10}$	σ_{fit}[b]
D_2O	0.0125795	3.04525	− 1.27999	7.74237	6.14×10^{-4}
0.1 m D_2SO_4	.0109412	5.36589	0.687999	− 59.2311	1.62×10^{-3}
0.25 m D_2SO_4	.0138302	3.98960	6.31358	−177.706	1.89×10^{-3}
0.5 m D_2SO_4	.0305152	−4.06263	16.4867	−350.694	2.77×10^{-3}
0.75 m D_2SO_4	.0140920	3.17410	11.9268	−154.042	2.50×10^{-3}
1.0 m D_2SO_4	.0325238	−6.26753	21.0097	−276.151	4.12×10^{-3}

[a] $s = a_0 + a_1 t + a_2 t^2 + a_3 t^3$ (1). [b] Standard error of fit.

over a range of set values of one of the parameters. Also, the least squares matrix (X^TX) was inverted permitting a calculation of the standard error in ln K_2 at each temperature.

In order to compute the value of S_T, the Debye–Hückel limiting slope at temperature T, it is necessary to know the density and dielectric constant of D_2O as a function of temperature. Values of the density of D_2O from 30 to 250° are given by Heiks, *et al.*,[7] while the dielectric constant from 4 to 100° has been measured by Malmberg.[8] Above 100° the dielectric constant of H_2O was used in preference to extrapolating the D_2O values, since the experimental values for the two solvents tended to merge at 100° and since different expressions for D_2O gave widely different values on extrapolating to higher temperatures (some higher and some lower than the H_2O values). The H_2O values used were computed at each temperature using the equation given by Åkerlof and Oshry.[9]

The values of log K_2 obtained as a function of temperature were fitted by the method of least squares (eq. 5)

$$\log K_2 = \frac{22.86565}{T} + 1.253986 - 0.01231753T \quad (5)$$

where T is the absolute temperature.

(7) J. R. Heiks, M. K. Barnett, L. V. Jones, and E. Orban, *J. Phys. Chem.*, **58**, 488 (1954).
(8) C. G. Malmberg, *J. Research Natl. Bur. Std.*, **60**, 609 (1958).
(9) G. C. Åkerlof and H. J. Oshry, *J. Am. Chem. Soc.*, **72**, 2844 (1950).

In Table III are summarized the values of P, A, and log K_2 computed at each 25° interval from 25 to 225° along with the standard error in log K_2; in the last column are shown the values of log K_2 for H_2SO_4[2] for comparison. It can be seen that the value of K_2 for D_2SO_4 is a factor of about 2.3 lower than the corresponding value for H_2SO_4 at 25°, while the values are about equal at 200°. Above 200° the value of K_2 for D_2SO_4 is larger than the value for H_2SO_4. At 225° the ratio $K_{HSO_4^-}/K_{DSO_4^-}$ is about 0.87.

TABLE III

VALUES OF LOG K_2 FOR D_2SO_4 AS A FUNCTION OF TEMPERATURE

t	P	A	$-\log K_2$ (DSO_4^-) (eq. 2 and 3)	$\sigma_{\log K_2}$[a]	$-\log K_2$ (DSO_4^-) (eq. 5)	$-\log K_2$ (HSO_4^-)[b]
25	0.635	0.234	2.326	0.043	2.342	1.987
50	.576	.216	2.668	.13	2.656	2.301
75	.461	.210	2.976	.13	2.969	2.636
100	.400	.224	3.287	.095	3.281	2.987
125	.417	.307	3.591	.061	3.593	3.352
150	.451	.391	3.906	.034	3.904	3.728
175	.481	.456	4.208	.024	4.215	4.113
200	.504	.505	4.524	.036	4.526	4.506
225	.515	.539	4.842	.042	4.836	4.905

[a] Standard error in log K_2. [b] Reference 2.

In Table IV is given a comparison of the solubility of Ag_2SO_4 in D_2SO_4 solutions as calculated using eq. 1 and using eq. 2–5. In all cases the agreement is very good.

TABLE IV

COMPARISON OF THE SOLUBILITY OF Ag_2SO_4 IN D_2SO_4 SOLUTIONS AS CALCULATED USING EQ. 1 AND USING EQ. 2–5

$m_{D_2SO_4}$	$s_{calc.}$ (eq. 1)	$s_{calc.}$ (eq. 2, 3, 4, 5)	$s_{calc.}$ (eq. 1)	$s_{calc.}$ (eq. 2, 3, 4, 5)
	t = 25°		t = 50°	
0.1	0.0252	0.0247	0.0392	0.0388
0.25	.0276	.0275	.0464	.0473
0.5	.0290	.0301	.0506	.0470
0.75	.0296	.0292	.0523	.0579
1.0	.0299	.0296	.0531	.0503
	t = 75°		t = 100°	
0.1	0.0537	.0526	.0676	.0656
0.25	.0703	.0718	.0975	.0991
0.5	.0831	.0780	.1244	.1197
0.75	.0905	.0985	.1420	.1497
1.0	.0959	.0920	.1560	.1523
	t = 125°		t = 150°	
0.1	.0794	.0772	.0887	.0869
0.25	.1261	.1276	.1540	.1558
0.5	.1723	.1688	.2244	.2222
0.75	.2047	.2100	.2760	.2781
1.0	.2308	.2285	.3187	.3180
	t = 175°		t = 200°	
0.1	0.0952	0.0942	0.0992	0.0984
0.25	.1792	.1818	.2003	.2040
0.5	.2776	.2764	.3291	.3282
0.75	.3533	.3523	.4337	.4314
1.0	.4174	.4183	.5251	.5266
	t = 225°			
0.1	0.1014	0.0990		
0.25	.2167	.2208		
0.5	.3762	.3743		
0.75	.5143	.5138		
1.0	.6400	.6406		

In Table V are summarized the thermodynamic constants for the reaction

$$DSO_4^- = D^+ + SO_4^{-2}$$

from 25 to 225° as computed by using equation 5.

TABLE V

THERMODYNAMIC CONSTANTS FOR THE REACTION $DSO_4^- = D^+ + SO_4^{-2}$

t	ΔF^0, kcal.	ΔH^0, kcal.	ΔS^0, e.u.
25	3.196	− 5.116	−27.88
50	3.928	− 5.992	−30.70
75	4.731	− 6.938	−33.52
100	5.604	− 7.955	−36.33
125	6.547	− 9.042	−39.15
150	7.561	−10.200	−41.97
175	8.646	−11.428	−44.79
200	9.801	−12.726	−47.61
225	11.026	−14.095	−50.53

As in the previous work on the bisulfate acid constant[2] the entropy of dissociation is negative and attains a higher negative value the higher the temperature (although the temperature variation is smaller in the deuterated system). A similar effect was also observed[6] for the dissociation of UO_2SO_4 into UO_2^{+2} and SO_4^{-2}, and for the dissolution of Ag_2SO_4 in H_2O media. The isotope effect, which results in a value of K_2 for D_2SO_4 a factor of 2.3 lower than the value for H_2SO_4 at 25°, decreases as the temperature increases and reverses above 200°.

Acknowledgments.—The authors wish to express their appreciation to Miss Sarah Ledford and Mr. Ralph Whitfield who performed the experimental measurements, and to Miss Lucy Scroggie of the Ionic Analysis Group, who performed the necessary analytical work.

THERMOELASTICITY AND TEMPERATURE VARIATION OF UNPERTURBED CHAIN DIMENSION OF POLYVINYL ALCOHOL[1]

BY AKIO NAKAJIMA AND HIROO YANAGAWA

Department of Polymer Chemistry, Kyoto University, Kyoto, Japan

Received September 10, 1962

Force–elongation measurements have been carried out on amorphous polyvinyl alcohol networks cross-linked by γ-radiation, at different temperatures between 20 and 80° and in diluents. Water and 18% glycol–water mixture were used as the diluents. In the latter diluent, the length of sample extrapolated to zero force is independent of temperature. From these thermoelastic measurements, the relative values of the unperturbed mean square end-to-end distance of the chain have been calculated as a function of temperature. It was found that the unperturbed chain dimension obtained from the experiments both in water and in 18% glycol–water mixture is independent of temperature. Thus we conclude that the conformations of the polyvinyl alcohol chain are energetically equivalent.

Introduction

Very little is known about direct estimation of the average chain dimension of polyvinyl alcohol in solution. The light scattering measurements of this material, for instance in water, may be affected by factors arising from the short range interactions among the hydroxyl groups of the polymer and solvent: the Zimm plot of this system was pointed out[2] to give abnormal forms unless conditions of the solution preparation and of the measurements are particularly taken into consideration.

To discern the state of polymer chains in solution, primarily one may be interested in the temperature variation of the unperturbed mean square end-to-end distance of a chain, which directly relates to the configurations and dimensions of basic chain elements. The real polymer chain dimensions in usual solutions may be understood by integrating the effects of polymer–solvent interactions to the unperturbed dimension. However, in the polyvinyl alcohol–water system, such interactions as leading to the formation of hydro-

(1) Results of this investigation were reported at the 11th Annual Meeting of the Society of Polymer Science Japan, Nagoya, May 27, 1962.

(2) T. Matsuo and H. Inagaki, *Makromol. Chem.*, **53**, 130 (1962).

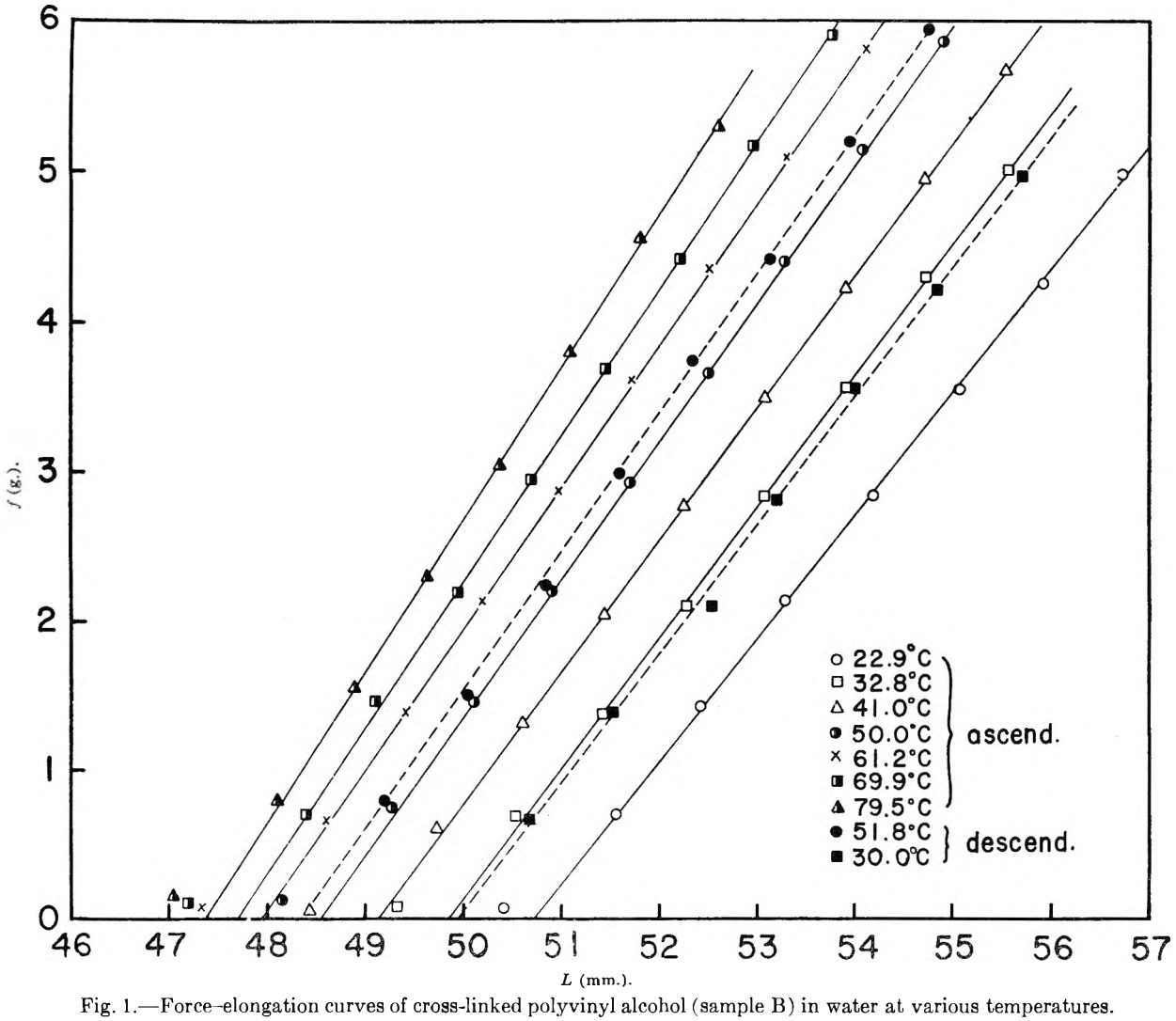

Fig. 1.—Force–elongation curves of cross-linked polyvinyl alcohol (sample B) in water at various temperatures.

gen bonds may be included; thus the situation of this system may be somewhat different from one that does not include such short range interactions.

In this paper, we are concerned primarily with the currently developed[3-7] force–temperature measurements to investigate the variation of the unperturbed dimension with temperature, instead of using the approach to obtain directly the unperturbed dimension by measuring the properties of the polymer molecule in dilute solutions.

Elasticity of Amorphous Polymer Networks in Diluent.—Theoretical and experimental treatments[5-7] to estimate the temperature dependence of the unperturbed mean square end-to-end distance $<R_0^2>$ from the force–temperature relationships are mainly concerned with amorphous polymer networks in the absence of diluent. However, in an open system in which polymer network is in equilibrium with diluent, the quantity of diluent in the gel phase will be a function of temperature and of length of the sample. For such an open system, Hoeve and Flory[4] obtained the temperature dependence of unperturbed mean square end-to-end distance by carrying out the force–elongation measurements at different temperatures in a diluent in which the volume of the swollen undeformed polymer network is independent of temperature at constant pressure and length, *i.e.*, $(\partial V/\partial T)_{P,L} = 0$.

In the present paper, we will deal with not only the case in which the volume of the gel phase V is independent of temperature but also the case in which V is temperature-dependent.

The change of Helmholtz free energy, dF, of a gel phase containing a diluent is related to the force f for simple elongation by the equation

$$dF = -S\,dT - P\,dV + f\,dL + \mu_1\,dN_1 \quad (1)$$

S being the entropy, T the absolute temperature, P the pressure, V the volume of the gel phase, L the length of the elongated gel, μ_1 the chemical potential of the diluent, and N_1 the number of the diluent molecules in the gel phase.

The volume of the gel phase may be given by

$$V = N_1V_1 + N_2V_2 \quad (2)$$

where V_1 and V_2 are the molecular volumes of the solvent and polymer (unit chain), respectively, and N_2 is the number of unit chains and is constant in this case. Accordingly, it follows from eq. 1 that

$$f = \left(\frac{\partial F}{\partial L}\right)_{T,V,N_1} \quad (3)$$

The free energy change involved in deformation of a

(3) P. J. Flory, *J. Am. Chem. Soc.*, **78**, 5222 (1956).
(4) C. A. J. Hoeve and P. J. Flory, *ibid.*, **80**, 6523 (1958).
(5) P. J. Flory, C. A. J. Hoeve, and A. Ciferri, *J. Polymer Sci.*, **34**, 337 (1959).
(6) P. J. Flory, *Trans. Faraday Soc.*, **57**, 829 (1961).
(7) A. Ciferri, *ibid.*, **57**, 846 (1961).

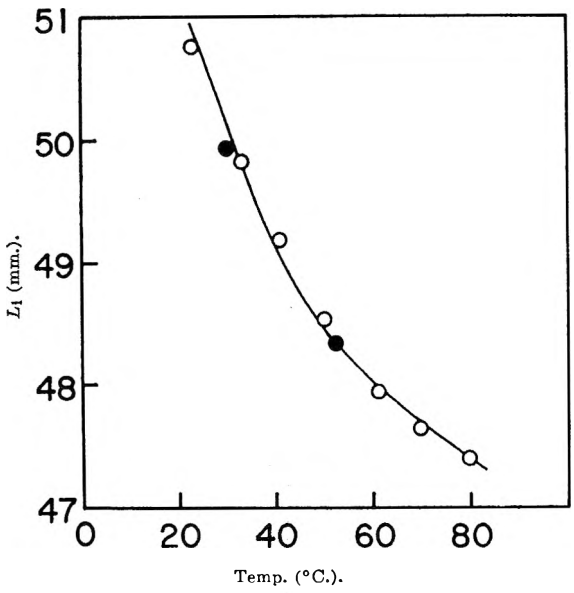

Fig. 2.—L_i plotted against temperature for sample B in water: O, ascending temperature; ●, descending temperature.

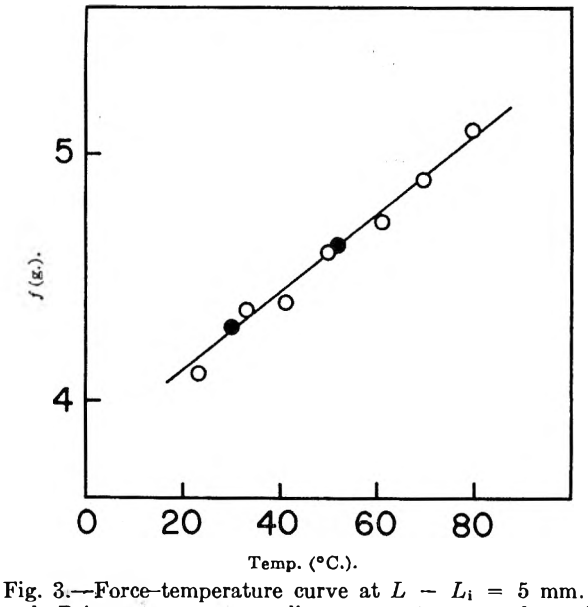

Fig. 3.—Force–temperature curve at $L - L_i = 5$ mm. for sample B in water: O, ascending temperature; ●, descending temperature.

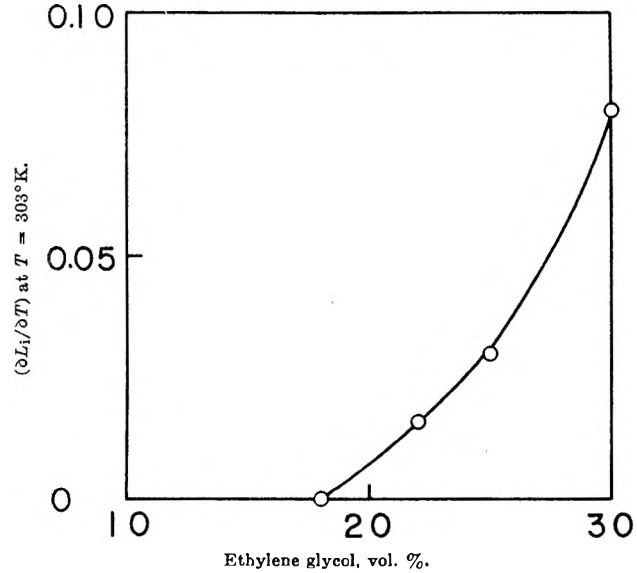

Fig. 4.—Temperature coefficient of L_i as a function of glycol content in glycol–water mixture.

network in solvent, ΔF, may be given by the sum of the free energy of mixing the unit chain and solvent, ΔF_{mix}, and the elastic free energy change of the network, ΔF_{el}: these are given by the equations[8]

$$\Delta F_{mix} = kT[N_1 \ln v_1 + N_2 \ln v_2 + \chi_1 N_1 v_2] \quad (4)$$

$$\Delta F_{el} = (\nu kT/2)[(\lambda_1^2 + \lambda_2^2 + \lambda_3^2 - 3) - \ln (\lambda_1\lambda_2\lambda_3)] \quad (5)$$

where k is the Boltzmann constant, v_1 and v_2 are, respectively, the volume fractions of solvent and unit chain, χ_1 is the interaction parameter for solvent–polymer interaction, ν is the total number of unit chains in the network structure, and λ_i denotes the principal deformation ratio in the i-direction referred to the unstrained and unswollen state. The principal deformation ratio may be given by the product of two terms: the dilatation term, $(V/V_0)^{1/3}$, and the distortion at constant volume, α_i, *i.e.*, the ratio of the strained length L to the length at zero force, L_i

$$\lambda_i = (V/V_0)^{1/3}\,\alpha_i \quad (6)$$

Further, for distortions at constant volume $\alpha_1\alpha_2\alpha_3 = 1$. In eq. 6, V and V_0 are, respectively, the volumes of the swollen network and of the unswollen unconstrained polymer. For simple elongation $\alpha_1 = \alpha$, $\alpha_2 = \alpha_3 = \alpha^{-1/2}$, where α is the elongation ratio in the direction of elongation. Therefore, eq. 5 is written as

$$\Delta F_{el} = (\nu kT/2)[(V/V_0)^{2/3}(\alpha^2 + 2\alpha^{-1} - 3) - \ln (V/V_0)] \quad (7)$$

The reference state for eq. 5 is defined in such a way that, at V_0, the mean square end-to-end distance for the unit chains equals the unperturbed mean square end-to-end distance $\langle R_0^2\rangle$ for a free chain. Accordingly

$$V_0^{2/3} = a\langle R_0^2\rangle \quad (8)$$

where a is a constant. As V is necessarily proportional to L_i^3, we have

$$V^{1/3} = bL_i \quad (9)$$

where b is a constant.

Inserting eq. 4 and 7 in eq. 3, we have the elastic equation of state for a deformed swollen network in a diluent. If we assume that χ_1 is independent of L, we obtain

$$f = \left(\frac{\partial \Delta F}{\partial L}\right)_{T,V,N_1} = \frac{b^2k}{a}\,\frac{\nu T}{\langle R_0^2\rangle}\,L_i(\alpha - \alpha^{-2}) \quad (10)$$

If we put $\alpha = 1 + \gamma$, expand eq. 10 in powers of γ for $\gamma < 1$ and neglect all but the first term, we obtain

$$= \frac{3b^2k}{a}\,\frac{\nu T}{\langle R_0^2\rangle}\,L_i\gamma = A\,\frac{\nu T}{\langle R_0^2\rangle}(L - L_i) \quad (11)$$

where A is a constant.

During the elongation process of a cross-linked polyvinyl alcohol in a diluent, some secondary linkages

(8) P. J. Flory, "Principles of Polymer Chemistry," Cornell Univ. Press, Ithaca, N. Y., 1953, pp. 468, 492, 509.

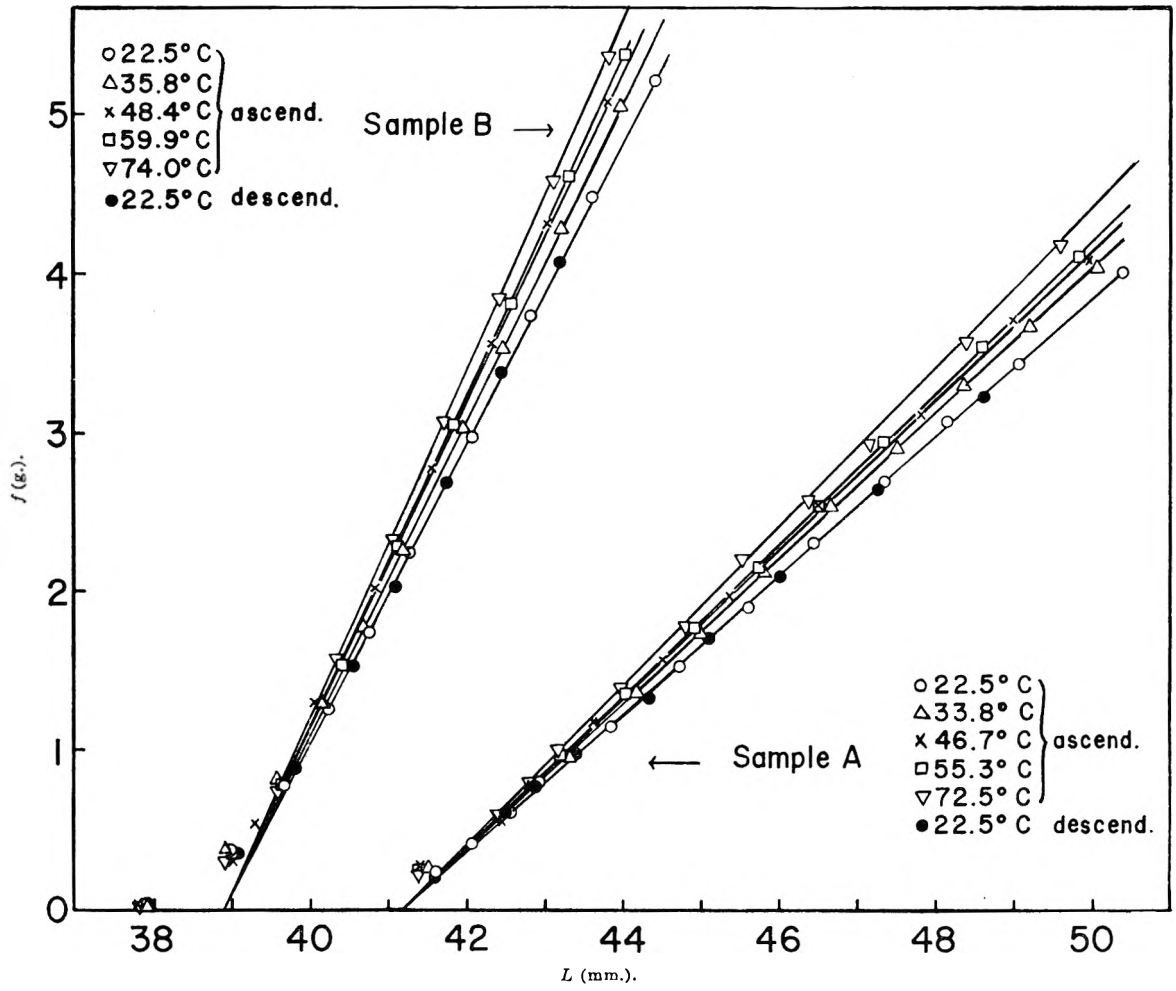

Fig. 5.—Force–elongation curves of cross-linked polyvinyl alcohol, sample A and sample B, in 18% glycol–water mixture at various temperatures.

may contribute to the stress in addition to the permanent cross-linkages introduced by γ-radiation; thus ν may change with L particularly in the range of very small values of γ. Further, it was experimentally recognized that the change of ν is almost reversible. Thus the change of f with L at equilibrium may be given by the equation

$$\left(\frac{\partial f}{\partial L}\right)_{T,P,e} = \frac{A\nu T}{\langle R_0^2\rangle}\left[1 - \left(\frac{\partial L_i}{\partial L}\right)_{T,P,e}\right] + \frac{AT}{\langle R_0^2\rangle}(L - L_i)\left(\frac{\partial \nu}{\partial L}\right)_{T,P,e} \quad (12)$$

As mentioned above it is assumed that $(\partial V/\partial L)_{T,P,e} = 0$ for small elongations, so $(\partial L_i/\partial L)_{T,P,e} = 0$. Accordingly, under the condition of $(\partial \nu/\partial L)_{T,P,e} = 0$, it follows from eq. 11 and 12 that, provided $L - L_i$ = constant, the unperturbed mean square end-to-end distance $\langle R_0^2\rangle$ is given by the equation

$$\langle R_0^2\rangle = B(T/f)_{L\text{-}L_i} \quad (13)$$

where B is a constant, *i.e.*, $B = A\nu(L - L_i)$.

Thus we can estimate the relative values of $\langle R_0^2\rangle$ from the force–temperature relationship under the condition of $L - L_i$ = constant. Furthermore, if we use a diluent in which L_i is independent of T, then we can estimate $\langle R_0^2\rangle$ from the temperature–force coefficient at constant L.

$$\langle R_0^2\rangle = B(T/f)_L \quad (14)$$

Experimental

Preparation of Films.—Conventional polyvinyl alcohol was resaponified, and fractionated from aqueous solution with *n*-propyl alcohol as a precipitant. A fraction with a viscosity-average degree of polymerization of 2300 was used for preparing films. Polyvinyl alcohol films of 0.085 mm. thickness (dry) were obtained by casting a 6% aqueous solution onto glass plate. The films were cut into strips of 5 mm. width and 12 mm. length, and stored in water at room temperature. The water-swollen films were then cross-linked by γ-irradiation in the presence of air with a cobalt-60 source at doses of 5×10^6 r. (sample A) and 1×10^7 r. (sample B). The irradiated films were then washed in hot and cold water alternately to eliminate the soluble parts (linear polymers) and to loosen crystalline parts, if any, and stored in water without drying. The degrees of swelling (by weight) in water at 30° were 8.74 (sample A) and 6.85 (sample B). The samples thus prepared are regarded as fully isotropic and amorphous networks. Detailed information of the irradiation process and on the swelling behaviors of such samples was reported elsewhere.[9,10]

Force Measurements.—The dynamometer used for the force measurements[11] is attributed to that used in the previous paper.[12] The sample length was about 4–5 cm. The force measurements were carried out by measuring the deformation of a calibrated spring by means of a cathetometer with the scale divisions 0.01 mm. The calibrated stress–strain curve for this spring was almost linear within the experimental range. The sensitivity of the spring was *ca.* 3 mm./g. The lengths of the samples were measured simultaneously with the force by the cathetometer.

(9) I. Sakurada, A. Nakajima, and H. Aoki, *Mem. Faculty Eng., Kyoto Univ.*, **21**, 94 (1959).

(10) I. Sakurada, O. Yoshizaki, and H. Yanagawa, Report of Poval Committee Japan, No. 37, 129, July 18, 1960.

(11) We are much obliged to Professor H. A. Scheraga of the Department of Chemistry, Cornell University, Ithaca, N. Y., for the apparatus.

(12) A. Nakajima and H. A. Scheraga, *J. Am. Chem. Soc.*, **83**, 1575 (1961).

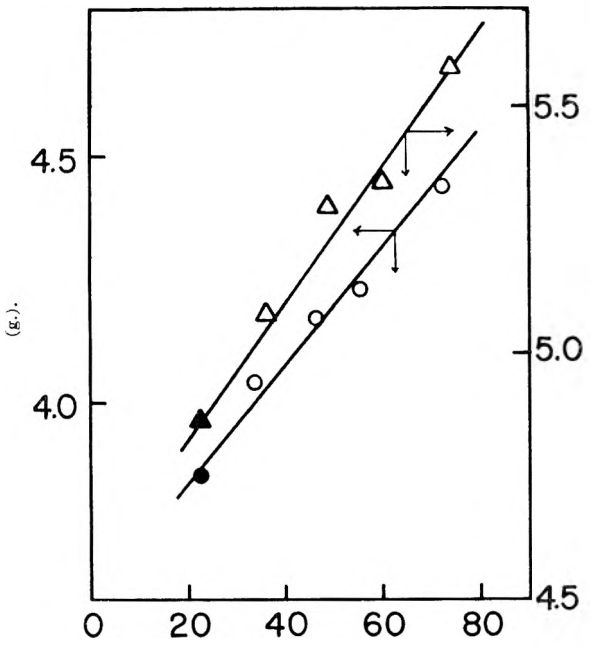

Fig. 6.—Force at constant length *vs.* temperature in 18% glycol–water mixture: L = 50 mm., sample A: ○, ascending temperature; ●, descending temperature. L = 44 mm., sample B: △, ascending temperature; ▲, descending temperature.

The force–elongation measurements were carried out in water and in 18% ethylene glycol–water mixture at various temperatures. In the latter system the extrapolated length at zero force, L_i, is constant, independent of the temperature.

The sample, after conditioning in the solvent to be used, was mounted between two clamps in the solvent, then stretched and relaxed repeatedly at the highest experimental temperature to eliminate plastic contributions. Then the temperature was brought down to a lower temperature of about 20° at which the force–elongation measurements were carried out at constant temperature. Successive force–elongation measurements were done at the constant temperatures at intervals of about 10° up to *ca.* 80°. After the experiments at the highest temperature were over, the same experiments were done also for descending temperature run at several temperatures. As is obvious from Fig. 2, 3, and 6, no hysteresis was found for the present system. Thus the establishment of reversibility provides the theoretical treatments of the results.

Results and Discussion

Experiments in Water.—The results of the force–elongation measurements for sample B at different temperatures in water are given in Fig. 1. As are shown in the figure, the experimental points for very small values of f deviate from the straight lines: the curves are concave above in the range of very small values of f, then become thoroughly linear at higher values of f. These behaviors may be explained according to eq. 12: in the range of very small values of f, the second term of eq. 12 may contribute, that is, $(\partial\nu/\partial L)_{T,P,e} < 0$ and $(\partial^2\nu/\partial L^2)_{T,P,e} > 0$. This means that, in this region, some weak bonds such as secondary linkages may be broken by elongation and that the rate of rupture may decrease with increasing elongation. However, at higher elongations where the condition of $(\partial\nu/\partial L)_{T,P,e} = 0$ is satisfied, the change of f with L is explained only by the first term of eq. 12: presumably, in such a region, the permanent cross-linkages introduced by γ-radiation relate exclusively to the stress.

Accordingly, L_i, the isotropic length at zero force, as is shown in Fig. 1, was obtained in the present experiments by extrapolating the straight lines to zero force. The variation of L_i with temperature was illustrated in Fig. 2, in which the points for both ascending and descending temperature runs fell on a single curve, in conformity with the conclusion that reversibility holds for the present system.

Figure 3 shows the relation between the force and temperature at $L - L_i = 5$ mm., replotted from Fig. 1. The curve obtained is a straight line within the experimental error and here also the reversibility of the process is confirmed. The linear relationship in Fig. 3 is in accord with the theoretical relation given by eq. 11 for constant ν and for small values of γ.

Finally, the unperturbed mean square end-to-end distance $\langle R_0^2 \rangle$ relative to that at reference temperature (22.9°) was calculated by means of eq. 13. The result obtained is that $\langle R_0^2 \rangle$ was almost constant within ±2% in the temperature range of 20 to 80°. This conclusion will be compared later with that obtained from the experiments in 18% glycol–water mixture.

Experiments in 18% Glycol–Water Mixture.—The volume of the swollen polymer at zero force (proportional to L_i^3) depends on the temperature coefficients of $\langle R_0^2 \rangle$ and of χ_1, *i.e.*, the normal thermal expansion of the swollen material may be regarded as being counterbalanced with deswelling owing to the temperature variations of both $\langle R_0^2 \rangle$ and χ_1. Therefore, if we choose a diluent in which L_i remains constant with temperature and estimate the temperature variation of $\langle R_0^2 \rangle$ by eq. 14 from the force–temperature data at constant length, we can have information about the temperature variation of χ_1.

The temperature dependence of L_i was examined using glycol–water mixtures of different glycol contents, and it was found that L_i in 18% glycol–water mixture (by volume) is constant within experimental error in the range of 20 to 80°. The temperature coefficients of L_i, for example at 30°, are given in Fig. 4 as a function of glycol content.

The same kind of experiments as those in the water system were carried out for the 18% glycol–water system. The force–elongation curves for sample A and sample B were given in Fig. 5. Also in this system, deviations from the linear curves were observed at very small values of f. This shows that even in such a mixed solvent as glycol–water the secondary weak bonds are contributing to the stress at very small f. The data obtained in Fig. 5 were treated with eq. 14 to estimate temperature variation of the unperturbed chain dimensions. Figure 6 shows the relations between the force and temperature at L = 50 mm. for sample A and at L = 44 mm. for sample B.

The unperturbed mean square end-to-end distances $\langle R_0^2 \rangle$ referred to that at 22.5°, obtained from the data both for sample A and B, were calculated according to eq. 14. It is concluded that the unperturbed chain dimension is independent of temperature within ±2% deviation. This result satisfactorily agrees with the result obtained from the measurements in the water system.

The experimental results obtained indicate that the internal energy of the polyvinyl alcohol chain is independent of conformation, *i.e.*, all the conformations of

the chain are energetically equivalent under the condition whereby the short range interactions are suppressed. Presumably, for the conventional polyvinyl alcohol used here, the random occurrence of *d*- and *l*-configurations of the asymmetric carbon atoms along the chain together with the smallness in size of the side residue may contribute, on the average, to reduce the change of energy with chain conformation. Combining $\partial\langle R_0^2\rangle/\partial T = 0$ and $\partial L_i/\partial T = 0$, it follows that $\partial\chi_1/\partial T = 0$ for polyvinyl alcohol in 18% glycol–water mixture: in other words, polyvinyl alcohol forms an athermal solution in 18% glycol–water mixture. A similar result that the unperturbed chain dimension is independent of temperature was obtained by Hoeve and Flory[3] on elastin from the force–temperature measurements in 30% glycol–water mixture. Further investigations with stereospecific polyvinyl alcohol are now under contemplation.

Acknowledgment.—The authors wish to thank Professor Ichiro Sakurada, Kyoto University, for his valuable suggestions. They also are grateful to Professor Leo Mandelkern, the Florida State University, for reading the manuscript and for his interest in this work. This work was partially supported by Scientific Research Funds provided by the Education Ministry of Japan.

THERMOPHYSICAL PROPERTIES OF THE LANTHANIDE OXIDES. III. HEAT CAPACITIES, THERMODYNAMIC PROPERTIES, AND SOME ENERGY LEVELS OF DYSPROSIUM(III), HOLMIUM(III), AND ERBIUM(III) OXIDES[1]

BY EDGAR F. WESTRUM, JR., AND BRUCE H. JUSTICE

Department of Chemistry, University of Michigan, Ann Arbor, Michigan

Received September 11, 1962

Heat capacities of three C-type lanthanide oxides have been resolved into lattice contributions and electronic Schottky-type anomalies; low-lying crystalline field levels have been delineated from these data. The lattice contributions were evaluated from the ytterbium(III) oxide and gadolinium(III) oxide heat capacities. Enthalpy increments ($H^0 - H^0_{10}$) at 298.15°K. have been evaluated from the measurements as 5025, 5009, and 4779 cal. (g.f.w.)$^{-1}$ for Dy_2O_3, Ho_2O_3, and Er_2O_3. By estimation of the remaining electronic entropy and the extrapolated lattice contribution below 10°K., practical entropies (S^0) at 298.15°K. have been evaluated as 35.8, 37.8, and 36.6 cal. (g.f.w. °K.)$^{-1}$.

Introduction

This paper describes the third of a series[2,3] of endeavors concerned with the evaluation of crystalline field states of the ground terms in the lanthanide(III) oxides from heat capacity measurements. The resolution of the electronic heat capacities of dysprosium, holmium, and erbium cubic (C-type) oxides[4] into magnetic and lattice components was effected by using the previously-described[3] lattice heat capacity for the C-type structure. Large degeneracies of the ground terms of Dy^{+3} ($4f^9$ — $^6H_{15/2}$), Ho^{+3} ($4f^{10}$ — $^5I_8$), and Er^{+3} ($4f^{11}$ — $^4I_{15/2}$) suggest that the electronic heat capacities might be very large over the temperature range of this study and thus provide unusually good data for the accurate evaluation of the crystal field levels. Spectrographic investigations[5-9] on the lanthanide octahydrated sulfates suggested that erbium has an essentially cubic crystal field symmetry, whereas holmium and dysprosium ions have important noncubic contributions to their fields. Theoretical calculations by Kynch[10] served as a model for these studies. The essentially cubic oxygen ligand field surrounding these ions in the oxides makes it especially desirable to test the earlier hypotheses on these magnetically concentrated substances. Recent neutron scattering data[11] giving independent estimates of energy levels in the holmium and erbium oxides provide further motivation for extending this study.

Experimental

Dysprosium(III), Holmium(III), and Erbium(III) Oxide Samples.—The 320 mesh oxide samples from Michigan Chemical Company were claimed to have a purity in excess of 99.9% with certified analyses for impurities summarized in Table I. All of the finely-divided samples were run as powders after muffle-furnace firing to constant weight at 1170°K. in the ambient atmosphere. Holmium and erbium oxides were fired in a platinum dish previously cleaned in nitric acid and heated to constant weight, while the dysprosium oxide heat treatment was done in a pre-ignited Alundum crucible. The cooling and loading of the samples were done in a nitrogen-filled drybox. The calorimeter subsequently was sealed off in a high vacuum line with a pressure of about 10 cm. of helium for thermal conduction. X-Ray powder diffraction patterns of the fired materials revealed a typical C-type oxide structure exclusively.

TABLE I

DETAILS CONCERNING THE CALORIMETRIC SAMPLES

Sample	Impurities (p.p.m.)	Mass of sample (g. *vacuo*)	Gram formula weight	Densities (g. cm.$^{-3}$)
Dy_2O_3	Y-150, Si-100, Ca-100	146.8071	373.02	8.23
Ho_2O_3	Er-100, Si-100, Ca-100	184.5233	377.88	8.40
Er_2O_3	Tm-350, Ho-50, Dy-100, Si-100, Ca-100	151.8315	382.54	8.64

Cryostat and Calorimeter.—Measurements were made in the Mark I calorimetric cryostat employing the adiabatic technique. Both cryostat and technique are similar in most respects to those previously described.[12] A capsule-type, platinum resistance

(1) This investigation is a part of a doctoral thesis submitted by BHJ to the Horace H. Rackham School of Graduate Studies of the University of Michigan. This work was supported in part by the Division of Research of the United States Atomic Energy Commission and was presented at the Second Conference on Rare Earth Research at Glenwood Springs, Colorado, October, 1961.

(2) B. H. Justice and E. F. Westrum, Jr., *J. Phys. Chem.*, **67**, 339 (1963).

(3) B. H. Justice and E. F. Westrum, Jr., *ibid.*, **67**, 345 (1963).

(4) L. Pauling, *Z. Krist.*, **69**, 415 (1929).

(5) E. J. Meehan and G. C. Nutting, *J. Chem. Phys.*, **7**, 1002 (1939).

(6) H. Severin, *Ann. Physik*, [6] **1**, 41 (1947).

(7) A. M. Rosa, *ibid.*, [5] **43**, 161 (1943).

(8) S. Singh, *Optik*, **2**, 133 (1947).

(9) H. Severin, *Z. Physik*, **125**, 455 (1949).

(10) G. J. Kynch, *Trans. Faraday Soc.*, **33**, 1402 (1937).

(11) D. Cribier and B. Jacrot, *Compt. rend.*, **250**, 2871 (1960).

TABLE II

HEAT CAPACITIES OF DYSPROSIUM(III), HOLMIUM(III), AND ERBIUM(III) OXIDES

[In cal. (g.f.w. °K.)$^{-1}$]

T, °K.	C_p	T, °K.	C_p	T, °K.	C_p
Dysprosium oxide (Dy_2O_3)					
Series I		40.66	4.878	165.06	20.52
		44.92	5.532	174.35	21.36
6.36	0.187	49.57	6.220		
7.24	0.266			Series VI	
8.16	0.265	Series III			
9.31	0.319			177.48	21.60
10.35	0.365	53.15	6.726	186.19	22.30
11.42	0.420	58.44	7.458	194.78	22.95
12.49	0.505	64.37	8.286	203.32	23.54
13.64	0.615	70.77	9.125	212.31	24.12
14.90	0.744	77.39	10.011	221.54	24.66
16.27	0.903	84.82	11.062	230.64	25.14
17.79	1.100				
19.52	1.344	Series IV		Series VII	
21.50	1.651				
		84.33	10.996	239.84	25.65
Series II		91.92	12.000	245.45	25.87
		99.39	12.961	254.80	26.28
15.54	0.817	107.09	13.958	263.29	26.63
16.87	0.980	115.16	14.993	272.50	27.00
18.42	1.184	122.74	15.94	281.86	27.30
20.17	1.442			291.18	27.59
22.23	1.766	Series V		300.40	27.84
24.72	2.185			309.76	28.10
27.55	2.674	130.43	16.87	319.15	28.31
30.52	3.191	138.70	17.81	328.56	28.50
33.55	3.716	147.25	18.76	337.99	28.72
36.89	4.275	155.99	19.65	346.58	28.85
Holmium oxide (Ho_2O_3)					
Series I		247.41	26.02	18.81	1.342
		256.66	26.35	20.58	1.393
70.63	8.159	265.87	26.65	22.39	1.497
77.08	9.183	275.00	26.91	24.35	1.626
83.72	10.287	284.06	27.15	26.58	1.818
90.54	11.391	293.10	27.37	29.09	2.073
97.87	12.524	302.21	27.57	31.85	2.395
105.81	13.744	311.55	27.75		
113.89	14.962	320.91	27.96	Series IV	
121.35	16.05	329.92	28.11		
129.99	17.23	338.42	28.23	10.20	1.585
138.60	18.31	346.71	28.35	11.26	1.456
147.16	19.32			12.49	1.397
155.96	20.26	Series III		13.86	1.367
165.02	21.14			15.35	1.334
174.24	21.95	5.75	0.306	ΔH Run	
183.42	22.67	6.11	0.402	33.61	2.611
192.85	23.34	6.64	0.670	37.25	3.107
202.33	23.92	7.32	1.193	41.08	3.644
211.49	24.43	8.49	1.581	45.31	4.244
220.62	24.90	9.61	1.605	50.10	4.984
		10.84	1.519	55.32	5.775
Series II		12.36	1.403	60.63	6.601
		14.00	1.363	66.18	7.470
229.08	25.30	15.62	1.331	72.31	8.415
238.25	25.68	17.20	1.323	79.44	9.570
Erbium oxide (Er_2O_3)					
Series I		19.07	2.674	54.76	7.863
				60.14	8.442
80.89	10.620	Series III		65.47	9.007
87.29	11.317			71.16	9.570
94.21	12.030	8.33	0.838	77.79	10.251
101.76	12.808	9.57	1.027	84.94	11.065
109.79	13.659	11.00	1.222	ΔH Run	
117.87	14.501	12.41	1.426	179.34	20.08
126.06	15.35	13.76	1.673	188.44	20.74
134.50	16.20	15.19	1.931	197.78	21.36
143.25	17.04	16.76	2.234	207.09	21.94
151.94	17.84	18.38	2.534		
160.54	18.58	20.02	2.863	Series V	
169.21	19.30	21.67	3.180		
178.22	19.99	23.31	3.502	208.99	22.05
		24.96	3.814	217.95	22.57
Series II		26.64	4.117	227.01	23.05
		28.39	4.416	236.11	23.50
5.26	0.149	30.23	4.730	244.97	23.96
5.78	0.327	32.51	5.094	253.90	24.33
6.46	0.579			262.98	24.70
7.28	0.669	Series IV		272.02	25.06
8.06	0.817			281.19	25.39
9.12	0.957	28.46	4.426	290.33	25.69
10.53	1.160	31.50	4.936	299.53	25.97
11.98	1.355	34.66	5.421	308.44	26.22
13.32	1.588	38.06	5.897	317.78	26.47
14.58	1.823	41.65	6.353	327.16	26.70
15.89	2.065	45.47	6.819	336.58	26.92
17.43	2.358	49.75	7.314	345.64	27.10

thermometer (laboratory designation A-3), calibrated at the National Bureau of Standards on the international temperature scale above 90°K. and against the Bureau's scale[13] from 10 to 90°K., was employed. This scale is considered to be reliable to within 0.03°K. from 4 to 90°K. and to within 0.04°K. at higher temperatures. All measurements of mass, potential, resistance, and time were referred to devices certified by the National Bureau of Standards. A previously described[2] copper calorimeter (laboratory designation W-16) was employed for measurements on all three samples. The heat capacity of the thermometer–heater–calorimeter assembly was determined in a separate experiment and represented between 10 and 40% of the total heat capacity over most of the temperature range. Where necessary, small adjustments were applied for the small measured differences of helium, solder, and grease employed, and buoyancy corrections were made on the basis of the calculated densities indicated in Table I.

Results and Discussion

Heat Capacities for Dysprosium(III), Holmium(III), and Erbium(III) Oxides.—The experimental data on the heat capacities of these three oxides are presented in Table II in chronological order so that the approximate temperature increments usually may be estimated by differencing the adjacent mean temperatures. These data also have been plotted in Fig. 1. A small adjustment for curvature has been applied to correct for the finite temperature increments used in the measurements. These data are based on the formula weights indicated in Table I, the defined thermochemical calorie of 4.1840 abs. j., and an ice point of 273.15°K. The values of the heat capacity at selected temperatures derived from a smoothed curve through the experimental data points are presented in Table III. Quadrature of the data to yield the thermodynamic functions also presented in Table III was performed by exact integration of an analytical expression through the experimental points by means of an IBM digital computer program.[14] These thermodynamic

(12) E. F. Westrum, Jr., J. B. Hatcher, and D. W. Osborne, *J. Chem. Phys.*, **21**, 419 (1953).

(13) H. J. Hoge and F. G. Brickwedde, *J. Res. Natl. Bur. Std.*, **22**, 351 (1939).

(14) B. H. Justice, "Calculation of Heat Capacities and Derived Thermodynamic Functions from Thermal Data with a Digital Computer," Appendix to Ph.D. Dissertation, University of Michigan; United States Atomic Energy Commission Report TID-12722, 1961.

TABLE III

THERMODYNAMIC FUNCTIONS OF DYSPROSIUM(III), HOLMIUM(III), AND ERBIUM(III) OXIDES

[In cal., g.f.w., °K.]

	Dysprosium oxide (Dy_2O_3)			Holmium oxide (Ho_2O_3)			Erbium oxide (Er_2O_3)		
T	C_p	$S^0 - S_{10}^0$	$H^0 - H_{10}^0$	C_p	$S^0 - S_{10}^0$	$H^0 - H_{10}^0$	C_p	$S^0 - S_{10}^0$	$H^0 - H_{10}^0$
10	0.345	...	...	1.575	...	...	1.088	...	...
15	0.754	0.206	2.60	1.334	0.580	7.11	1.898	0.582	7.31
20	1.416	0.509	7.95	1.379	0.965	13.81	2.852	1.258	19.18
25	2.234	0.910	17.03	1.678	1.300	21.33	3.820	2.000	35.90
30	3.103	1.394	30.37	2.179	1.648	30.91	4.690	2.775	57.21
35	3.959	1.937	48.04	2.797	2.029	43.31	5.464	3.557	82.63
40	4.774	2.520	69.89	3.484	2.447	59.00	6.151	4.332	111.70
45	5.544	3.127	95.70	4.210	2.899	78.22	6.771	5.093	144.03
50	6.278	3.749	125.27	4.958	3.381	101.13	7.344	5.837	179.33
60	7.677	5.019	195.10	6.495	4.420	158.36	8.418	7.272	258.20
70	9.038	6.304	278.69	8.069	5.539	231.16	9.465	8.648	347.62
80	10.390	7.600	375.84	9.667	6.720	319.82	10.519	9.980	447.52
90	11.733	8.901	486.46	11.272	7.952	424.52	11.581	11.281	558.0
100	13.055	10.206	610.4	12.857	9.222	545.2	12.642	12.556	679.1
110	14.348	11.511	747.5	14.393	10.520	681.5	13.694	13.810	810.8
120	15.60	12.814	897.2	15.86	11.836	832.8	14.729	15.046	953.0
130	16.81	14.110	1059.3	17.22	13.159	998.3	15.74	16.265	1105.3
140	17.96	15.398	1233.2	18.48	14.482	1176.9	16.72	17.468	1267.7
150	19.04	16.674	1418.2	19.63	15.798	1367.6	17.66	19.654	1439.6
160	20.05	17.936	1613.7	20.67	17.098	1569.2	18.54	19.822	1620.6
170	20.98	19.180	1818.9	21.59	18.380	1780.6	19.37	20.971	1810.2
180	21.82	20.403	2033.0	22.41	19.637	2000.7	20.13	22.100	2007.8
190	22.60	21.604	2255.2	23.14	20.869	2228.5	20.84	23.208	2212.7
200	23.31	22.781	2484.8	23.78	22.073	2463.2	21.50	24.294	2424.4
210	23.96	23.935	2721.2	24.36	23.247	2704.0	22.11	25.357	2642.5
220	24.57	25.064	2963.9	24.87	24.392	2950.2	22.68	26.399	2866.4
230	25.12	26.168	3212.4	25.33	25.508	3201.2	23.21	27.419	3095.9
240	25.63	27.248	3466.2	25.74	26.595	3456.6	23.71	28.417	3330.5
250	26.09	28.304	3724.8	26.12	27.654	3715.9	24.17	29.394	3569.9
260	26.51	29.336	3987.8	26.46	28.685	3978.9	24.59	30.351	3813.7
270	26.89	30.343	4254.8	26.77	29.690	4245.1	24.98	31.286	4061.6
280	27.24	31.327	4525.5	27.05	30.668	4514.2	25.34	32.201	4313.2
290	27.56	32.289	4799.4	27.29	31.622	4785.9	25.67	33.096	4568.3
300	27.84	33.228	5076.5	27.52	32.551	5060.0	25.98	33.972	4826.6
350	28.94	37.61	6498	28.40	36.86	6460	27.19	38.08	6158
273.15	27.00	30.66	4340	26.86	30.00	4330	25.10	31.58	4140
298.15	27.79	33.06	5025	27.48	32.38	5009	25.93	33.81	4779

functions are considered to have a probable error of less than 0.1% above 100°K. An additional digit beyond those significant often is included in order to provide internal consistency and permit interpolation. It will be noted that these values are referred to 10°K. (near the lowest temperature of measurement) rather than 0°K. because of the uncertainty, to be discussed subsequently, in the true heat capacity curve below this temperature.

As a further test of the experimental accuracy and precision, enthalpy-type runs were made over relatively large temperature increments and the results of the enthalpy input compared with the integral under the smoothed heat capacity *vs.* temperature curve. For example, such a run on holmium between 16.12 and 31.25°K. required 25.10 cal. (g.f.w.)$^{-1}$, which accords well with the value of 25.12 cal. (g.f.w.)$^{-1}$ obtained from the integral of the heat capacity (for holmium oxide). Similarly, for erbium oxide the enthalpy increment required to change the temperature from 88.42 to 174.87°K. was 1364.3 cal. (g.f.w.)$^{-1}$, which compares with 1365.0 obtained from the integral of the heat capacity.

Experimental Electronic Heat Capacities.—For the three trivalent ions, electronic heat capacities have been computed by deducting the lattice contribution estimates based on gadolinium and ytterbium oxide data by the procedure discussed previously.[3] These values have been plotted in Fig. 2 as open circles, and it is evident that the heat capacity anomalies are Schottky effects.[15] In terms of the partition function, Q, the electronic heat capacity, C_{el}, may be written

$$C_{el} = (dE/dT) = \frac{d}{dT}\left(RT^2 \frac{d \ln Q}{dT}\right) = Q^{-2}R^{-1}T^{-2}\left\{Q \sum_{i=1}^{n} g_i E_i^2 \exp(-E_i/RT) - \left[\sum_{i=1}^{n} g_i E_i \exp(-E_i/RT)\right]^2\right\} \quad (1)$$

in which g_i and E_i are the respective degeneracies and energies of the ith level. The electronic entropy is then by definition $\Delta S_{el} = d/dt\,(RT \ln Q) = R \ln Q + \bar{E}/T$, in which $\bar{E}$ is the mean energy derived from the partition function by standard procedures. The degeneracies and energy levels found by successive approximation on

(15) W. Schottky, *Physik. Z.*, **23**, 448 (1922).

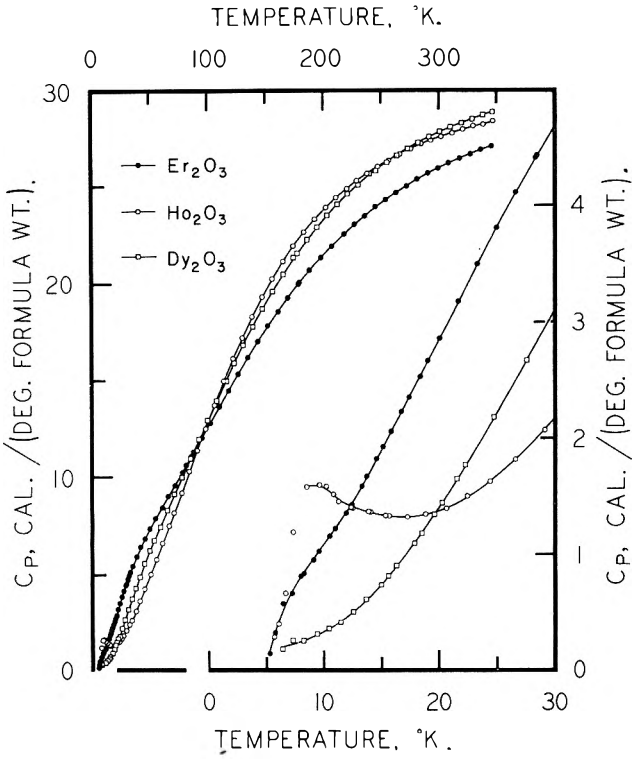

Fig. 1.—Heat capacities of Dy_2O_3, Ho_2O_3, and Er_2O_3.

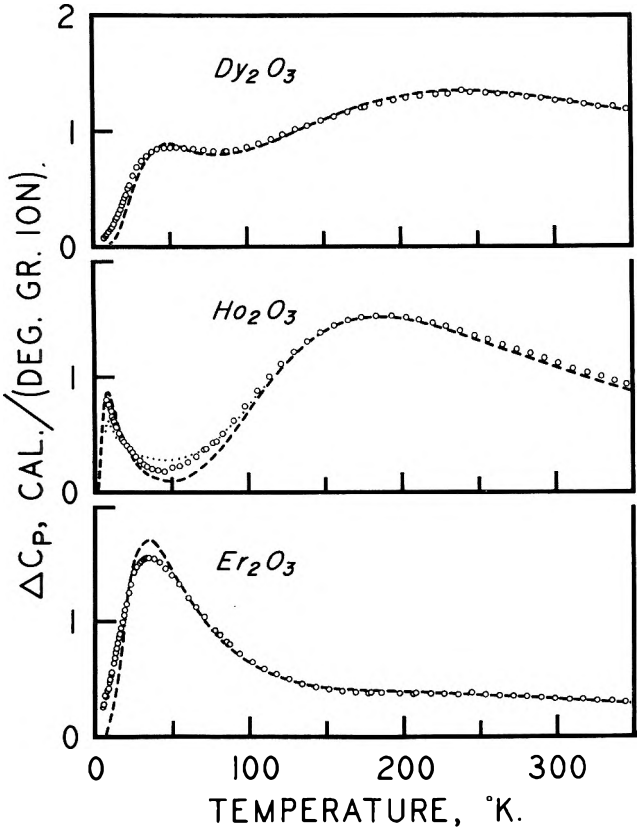

Fig. 2.—Electronic heat capacities of Dy_2O_3, Ho_2O_3, and Er_2O_3 on a gram ion basis. The circles represent the experimental values and the dashed curves indicate the Schottky effects calculated from the proposed energy level schemes.

a high-speed digital computer to best fit the experimental electronic heat capacities are presented in Table IV. The dashed lines in Fig. 2 are the theoretical curves derived from eq. 1 and the three energy level schemes noted in Table IV.

TABLE IV

SOME ENERGY LEVELS OF THE LANTHANIDE(III) OXIDES

Ion	Degeneracy This research	Energy (cm.$^{-1}$) This research	Energy (cm.$^{-1}$) Cribier and Jacrot[11]	Energy (cm.$^{-1}$) Rosenberger[18]
Dy	2	0		
	2	75		
	4	365		
	4	720		
	(4)	...		
Ho	3	0	0	
	2	14	...	
	1	75	75	
	11	365	365	
Er	2	0	0	0
			41	38.9
	4	58		76.5
			81	
	2	120		89.3
	2	490	421	
	(6)	...		

Crystal Field Levels of Dysprosium(III) Ion.—Pauling and Shappell[16] have shown that cubic (C-type) lanthanide(III) oxide cations are surrounded by six oxide ions at the corners of a cube with the two missing oxide ions located at the ends of a body or face diagonal of this cube. The crystal field calculations[10,17] show that the spin orbit state is split by an eightfold cubic coördination in such a manner as to have the relative spacings and degeneracies of the energy levels inverted with respect to the splittings of a sixfold octahedral coördination. Lower components of symmetry tend to remove higher degeneracies of these states (except Kramers degeneracies) by splitting these levels further.

The theoretical curve in Fig. 2 accounts for only 12 of the 16 degeneracies of the ground state ($^6H_{15/2}$). Adjustments, especially to the higher temperature end of the lattice heat capacity as discussed previously,[3] might permit better correlation of the present energy scheme using corrected statistical weights. However, if two more doublets (or one quartet) exist, it can be inferred that they lie above the level at 720 cm.$^{-1}$. For instance, if there were another doublet between the ground state and the first observed excited state, only one of less than 10 cm.$^{-1}$ splitting would have occurred at a sufficiently low temperature to escape detection. The ground state then would be an effective quartet level at the temperature of the first observed Schottky anomaly in this investigation, and it would be necessary to double the statistical weights of the excited levels observed to accord with the experimental electronic heat capacity. This would lead to a degeneracy of 24 for the term, which is not possible under the assumption of Russell–Saunders coupling. The first excited level is easily observed from the plot of Fig. 2, but the subsequent two quartets are not discernible as separate peaks. The only dysprosium compound for which all of the Stark levels of the ground state have been observed is $DyCl_3 \cdot 6H_2O$, on which Dieke and Singh[19] made optical absorption and fluorescence observations and reported eight doublets at 0, 33, 62, 77, 92, 111, 154, and 494 cm.$^{-1}$. Since this

(16) L. Pauling and M. D. Shappell, *Z. Krist.*, **75**, 128 (1930).
(17) F. H. Spedding, *J. Chem. Phys.*, **5**, 316 (1937).
(18) D. Rosenberger, *Z. Physik.*, **167**, 349, 360 (1962).
(19) G. H. Dieke and S. Singh, *J. Opt. Soc. Am.*, **45**, 495 (1956).

compound has only axial symmetry, the complex spectrum is to be expected. The optical absorption spectrum of $Dy_2(SO_4)_3 \cdot 8H_2O$[5,7,8] reveals that cubic symmetry with sixfold octahedral coördination to oxygen anions is not the dominant characteristic of the effective crystalline field. Hence it is not surprising that the C-type dysprosium oxide fails to show the inverse relative spacing of the energy levels calculated for the octahydrated sulfate.[10] The observed electronic heat capacity can be reproduced equally well by six doublets at 0, 75, 310, 450, 600, and 800 cm.$^{-1}$ as by the assignment in Table IV. In this instance heat capacity measurements do not permit the resolution of a set of closely-spaced levels. The possibility (discussed more in detail under erbium oxide) that crystallographically non-identical atoms may have different energy level schemes also obtains here. A more sensitive measurement, such as optical absorption or paramagnetic resonance, possibly could delineate the energy level diagram.

The entropy calculated between 10 and 298.15°K. from eq. 1 involving the partition function for the energy assignment in Table IV is 5.0 cal. (g.f.w. °K.)$^{-1}$, in good accord with the observed figure of 5.3 cal. (g.f.w. °K.)$^{-1}$. As yet no experimental evidence for the onset of antiferromagnetism or other enhanced ordering of the magnetic moments has been reported at low temperatures, but the double degeneracy of the lowest Stark level certainly is removed before absolute zero is attained. In this case the entropy of the cubic form of dysprosium(III) oxide at 298.15°K. is 35.8 cal. (g.f.w. °K.)$^{-1}$. This estimate is a practical entropy which neglects nuclear spin and isotope mixing effects and is consequently a suitable value for use in chemical thermodynamic calculations.

Crystalline Field Levels of Holmium(III) Oxide.—The only oxide possessing an even number of 4f electrons ($4f^{10}$) per ion on which heat capacity determinations were made in this investigation was that of holmium. The fact that the Stark levels no longer possess Kramers degeneracies tends to make the interpretation of the observed heat capacity more difficult. The ground term of trivalent holmium has a degeneracy of 17 ($^5I_8$), which is the largest value among lanthanide ions. The dotted curve in Fig. 2 is calculated from the experimental energy levels presented in Table IV using eq. 1. There is an obvious Schottky anomaly with a peak near 8°K. Since the lattice heat capacity is considerably less than 0.1 cal. (g.f.w. °K.)$^{-1}$ at these temperatures, there is no difficulty in discerning the effect directly from the heat capacity curve. Another large contribution to the electronic heat capacity with a maximum at 190°K. is noticeable only in the C_{el} plot. The largest heat capacity measured below 10°K. was 1.60 cal. (g.f.w. °K.)$^{-1}$ at 9.61°K., giving an electronic contribution of 1.54 cal. (g.f.w. °K.)$^{-1}$ for holmium oxide. Because of the absorption of helium gas, extending the measurements to lower temperatures was not possible. The energy level at 365 cm.$^{-1}$ has an observed maximum of 1.52 cal. (g. ion °K.)$^{-1}$, so it must have a degeneracy of about twice the sum of the degeneracies of the energy levels below it. This presumably complex level is probably the statistically weighted average of several levels close to 365 cm.$^{-1}$ and might have a splitting of about 75 cm.$^{-1}$.

The spectra of holmium compounds[9,20] are incompletely resolved. The holmium ion in the octahydrated sulfate is apparently under the influence of a potential field of other than simple cubic symmetry, and the energy levels in holmium oxide are not entirely explained by Kynch's calculations[10] for fields of cubic symmetry.

By a neutron scattering experiment Cribier and Jacrot[11] found a holmium oxide Stark level at 365 cm.$^{-1}$, which accords with that found in this investigation. If a level exists at 75 cm.$^{-1}$, it is a singlet by these measurements and requires the ground state to be a triplet and the level at 14 cm.$^{-1}$ to be doubly degenerate to give the best agreement with the electronic heat capacity data. With this energy level diagram the peak in the electronic heat capacity curve due to the first excited level should occur at 9.1°K. with a value of 0.62 cal. (g. ion °K.)$^{-1}$, as compared to the observed value of 0.77 cal. (g. ion °K.)$^{-1}$. The level at 365 cm.$^{-1}$ can have a degeneracy of 11 because six of the 17 degeneracies have been used for the first three Stark levels. Kynch's calculations[10] indicating that the lowest level in a cubic field (eightfold cubic coördination) should be a triplet and the next level a doublet tend to support the proposed assignment of levels. However, the electronic heat capacity can be expressed almost equally as well by energy levels at 0, 14, and 350 cm.$^{-1}$ with (relative) degeneracies of 1, 1, and 4. The dashed curve lying below the points in Fig. 2 is the result of the calculation of the heat capacity from this energy level diagram. If this were the correct interpretation of the data, the first excited level would have a peak of 0.87 cal. (g. ion °K.)$^{-1}$ at 8.1°K. The level detected by neutron scattering[11] at 75 cm.$^{-1}$ might involve the observation of a transition between two excited levels. The previous observation that the level at 365 cm.$^{-1}$ is probably the statistical mean of several levels would allow this interpretation. Spectral data would assist in resolving the interpretation of the energy level scheme. The preceding discussion shows the difficulty in delineating levels with small degeneracies compared to the sum of the degeneracies of the lower-lying Stark levels. Here too, the possibility of separate level schemes for crystallographically distinct cations exists. The maximum contribution of a level at 75 cm.$^{-1}$ is about 0.16 cal. (g. ion °K.)$^{-1}$ from a consideration of the statistical weights involved (~1/5 of 0.87).

Removal of the ground state degeneracy (whenever it exists) for "even-electron" ions may occur by Jahn–Teller[21] distortions of the crystal which can split the ground state, but the splittings are expected to be of the order of 10^{-2} cm.$^{-1}$ for the rare earth ions.[22] Heat capacity determinations at temperatures of 10^{-3}°K. would be necessary to observe the Schottky anomaly associated with such small energy differences. Paramagnetic resonance data could resolve this problem if the degeneracy of the ground state were removed by this effect. Alternatively, a coöperative effect may

(20) I. Grohmann, K. H. Hellwege, and H. G. Kahle, *Naturwissenschaften*, **47**, 277 (1960).

(21) H. A. Jahn and E. Teller, *Proc. Roy. Soc.* (London), **A161**, 220 (1937).

(22) J. H. Van Vleck, *J. Chem. Phys.*, **7**, 61 (1939).

take place as it does in holmium oxide as a result of antiferromagnetic coupling at 6.5°K.,[23] and this might remove the proposed degeneracy of the ground state. Accurate measurements of the heat capacity in the range 1 to 10°K. would allow the resolution of that connected with the Schottky anomaly from that due to the antiferromagnetic transition. If the antiferromagnetic contributions to the heat capacity are still large near 8°K., the fact that the magnetic heat capacity is high in comparison to the expected Schottky heat capacity from the proposed energy level diagram might be explained.

The electronic entropy of the trivalent holmium ion in cubic holmium oxide is calculated to be 4.6 cal. (g.f.w. °K.)$^{-1}$ in the range 10 to 298.15°K. from the levels in Table IV and eq. 1. The experimental value is 4.7 cal. (g.f.w. °K.)$^{-1}$. The alternative energy levels give a calculated entropy from 10 to 298.15°K. of 4.4 cal. (g.f.w. °K.)$^{-1}$. The entropy at 298.15°K. may be estimated on the basis of the proposed energy levels by eq. 1, including the ground state degeneracy of $2R$ ln 3. This estimate of 37.8 cal. (g.f.w. °K.)$^{-1}$ does not include a correction for the effects of nuclear spin and isotope mixing.

Schottky Energy Levels of Erbium(III) Oxide.—With respect to unpaired electrons, erbium and neodymium ions are isoelectronic structures (Nd^{+3} has a $4f^3$ structure and Er^{+3} a $4f^{14-11}$ structure). Because of the inversion of the ground multiplet, the lowest term ($^4I_{15/2}$) of the erbium ion has a degeneracy of 16. The electronic heat capacity shown in Fig. 2 has a maximum at 35°K. so the anomaly is barely perceptible in the heat capacity curve. A slight peak also appears to exist in the C_{el} curve at 250°K., suggesting the existence of the level at 490 cm.$^{-1}$. Table IV contains the levels and degeneracies used in the computation of the dashed curve in Fig. 2. By an argument similar to that used with the dysprosium ion, one can ascertain that no other Stark components occur between the ground state and the first observed level.

The observations[5,6] and calculations[10,17] for the octahydrated erbium sulfate indicate that to a good approximation the crystalline electric field has cubic symmetry. If the same symmetry exists for C-type erbium oxide, the Stark levels will be inverted with respect to those in the octahydrated sulfate (*cf.* Low[24]). The possibility of the existence of two sets of energy levels in the cubic oxides as a consequence of the two types of non-equivalent cations in the lattice also is relevant. The six oxide ions are coördinated to cations at the corners of a cube, with the two missing anions located either on the ends of a body-diagonal[4] (such a cation is designated as M-I and possesses trigonal axial symmetry) or on a face-diagonal for the other type of metal ion (M-II, digonal axial symmetry) in the ratio of 1:3, respectively. Since the symmetry of the ligand field profoundly affects the splitting of the free-ion state, it is to be anticipated that the different metal ions will have differing energy levels. By spectrographic analysis Rosenberger[18] found four levels for Er^{+3} in C-type Yb_2O_3 which were attributed to the digonal symmetry group. Although the other cations (M-I) are not likely to be highly different energetically complete analysis requires further information in this matter.

The selected levels are shown in Table IV and comparison with Fig. 2 indicates a generally excellent fit (except at very low temperatures where other electronic contributions occur). Admittedly, the fourfold degenerate level at 58 cm.$^{-1}$ may be complex. The level Cribier and Jacrot[11] found by neutron scattering at 41 cm.$^{-1}$ probably is identical with that found by Rosenberger[18] at 38.9 cm.$^{-1}$. The level found by the former investigators at 81 cm.$^{-1}$ may be a combination of the levels at 76.5 and 89.3 cm.$^{-1}$ observed by Rosenberger. The level of Jacrot and Cribier at 421 cm.$^{-1}$ accords well with the electronic heat capacities. Since the levels of Rosenberger also fit the data reasonably well, the other set of levels may be assumed to make nearly the same net contributions to the electronic heat capacity. The spacing of the levels and their double degeneracies indicate that the crystalline fields surrounding the Er^{+3} ions are not largely cubic, as the levels calculated by Kynch[10] have degeneracies of 4, 4, 2, 4, and 2, with relative spacings of 4:4:10:1.

The magnetic entropy calculated for erbium(III) oxide between 10 and 298.15°K. is 5.78 cal. (g.f.w. °K.)$^{-1}$ in comparison to the observed value of 6.08 cal. (g.f.w. °K.)$^{-1}$. As in the case of dysprosium oxide, the discrepancy arises in the difference between the observed and calculated magnetic heat capacities from 10 to 25°K. The absorption of the conduction helium gas prevented measurements of the coöperative anomaly corresponding to the antiferromagnetic ordering in erbium oxide reported by Wilkinson, *et al.*,[23] at lower temperatures. It is probable, however, that this ordering removes the degeneracy of the ground state, so that an estimate of the entropy at 298.15°K. can be made by adding the value of the entropy at 10°K. (calculated from the partition function) and a small correction for the lattice entropy to the tabulated value. The entropy for the cubic phase of erbium oxide at 298.15°K. is estimated to be 36.6 cal. (g.f.w. °K.)$^{-1}$ exclusive of nuclear spin and isotope mixing effects. Final correlation of theory and experiment can be made upon resolution of the uncertainties in the lattice heat capacity and elucidation concerning the nature of the thermal anomaly in erbium oxide at 4°K. by further measurements of the heat capacity at lower temperatures.

TABLE V

FORMATION VALUES FOR THREE LANTHANIDE OXIDES AT 298.15°K.

[In cal., g.f.w., °K.]

Oxide	S^0_{metal}	S^0_{oxide}	$-\Delta S_f^0$	$-\Delta H_f^0 \times 10^{-3}$	$-G_f^0 \times 10^{-3}$
Dy_2O_3	17.87	35.8	73.4	445.84	424.0
Ho_2O_3	18.0	37.8	71.7	449.55	428.2
Er_2O_3	17.52	36.6	71.9	453.60	432.2

Thermochemical Functions of Formation for the Oxides.—The Gibbs energies of formation for these substances can now be derived from available thermodynamic data. Using the enthalpies of formation from Huber, *et al.*,[25] entropies of the metals from Wes-

(23) M. K. Wilkinson, W. C. Koehler, E. O. Wollan, and J. W. Cable, *Bull. Am. Phys. Soc.*, [2] 2, 127 (1956).

(24) W. Low, "Paramagnetic Resonance in Solids," Academic Press, New York, N. Y., 1960.

(25) E. J. Huber, Jr., E. L. Head, and C. E. Holley, Jr. *J. Phys. Chem.*, **60**, 1457 (1956) [Dy_2O_3]; **61**, 1021 (1957) [Ho_2O_3]; **60**, 1582 (1956) [Er_2O_3].

trum and Grønvold[26] based on the heat capacities by various authors[27] and that of O_2 by Kelley,[28] the values given in Table V result.

(26) E. F. Westrum, Jr., and F. Grønvold, "Proceedings of the IAEA Symposium on Thermodynamics of Nuclear Materials," Vienna, Austria, 1962, p. 3.

(27) M. Griffel, R. E. Skochdopole, and F. H. Spedding, *J. Chem. Phys.*, **25**, 75(1956) [Dy]; B. C. Gerstein, M. Griffel, L. D. Jennings, R. E. Miller, R. E. Skochdopole, and F. H. Spedding, *ibid.*, **27**, 394 (1957) [Ho]; R. E. Skochdopole, M. Griffel, and F. H. Spedding, *ibid.*, **23**, 2258 (1955) [Er].

(28) K. K. Kelley and E. G. King, "Contributions to the Data on Theoretical Metallurgy. XIV. Entropies of the Elements and Inorganic Compounds," Bureau of Mines Bulletin 592, 1961.

Acknowledgment.—The authors acknowledge with gratitude the assistance of Norman Levitin in certain of the measurements and the partial financial support of the United States Atomic Energy Commission.

FURTHER SHOCK-TUBE STUDIES BY INFRARED EMISSION OF THE DECOMPOSITION OF AMMONIA

BY T. A. JACOBS[1]

California Institute of Technology, Pasadena, California

Received September 12, 1962

The decomposition of shock heated NH_3 has been studied by monitoring the infrared emission of the 2.7–3.2 μ fundamental region. It appears that the decomposition follows a kinetic law given by $d(NH_3)/dt = k(NH_3)^{3/2}(Ar)^{1/2}$, with $k = (2.5 \times 10^{13})e^{-77,700/RT}$ l./mole-sec.

Introduction

Some time ago this Laboratory initiated a program to study decomposition kinetics in a shock tube employing infrared emission techniques. The choice to make shock tube measurements in the infrared region of the spectrum was made possible by the appearance on the commercial market of infrared detectors of rapid response (time constants < 1 μsec.). Although Windsor, Davidson, and Taylor[2] preceded us in their study of CO vibrational relaxation in a shock tube, we believe this Laboratory was the first to report kinetic rate data obtained from infrared emission.

In previous publications,[3] we reported on our preliminary study of the homogeneous rate of decomposition of NH_3 in a shock tube. We have subsequently improved our experimental procedures and in this paper we present the results of a new series of measurements which we believe gives more insight into the nature of the NH_3 decomposition processes.

Our basic technique of measurement remained as before, *i.e.*, the infrared emission intensity of the 3 μ band of NH_3 was recorded as a function of time. For judiciously chosen optical depths, the gas may be shown to be transparent, to a reasonable approximation, so that the emission intensity is proportional to the NH_3 concentration. We abandoned, however, our earlier attempts to measure initial reaction rates by extrapolation to zero time. Instead we measured the NH_3 concentration for a period of time behind the shock wave and then, by using the conventional integration methods, determined an apparent order of reaction. The difference in these measuring techniques may be inferred by reference to Fig. 1 which is reproduced from an actual experimental record. From the figure it can be seen that, due to the response time of the detector and associated electronics, linear extrapolation of the trace is likely to yield a considerable error in the initial slope; however, only a relatively small error is expected in the initial trace height. Therefore, we have used linear extrapolation to determine only the proportionality constant relating oscilloscope voltage to NH_3 concentration (since the gas composition is known immediately behind the shock wave). Data then were taken from the trace only for times greater than those indicated by point A in Fig. 1. Radiation of reaction intermediates in the wave length region of measurement was assumed to be negligible.

(1) Aerospace Corp., El Segundo, California.

(2) M. Windsor, N. Davidson, and R. Taylor, "Seventh Symposium on Combustion," Butterworths Scientific Publications, London, 1959.

(3) (a) T. A. Jacobs, Calif. Inst. of Tech. Technical Note 12, AF 18(603)-2 (1960); (b) Ph.D. Thesis, Calif. Inst. of Tech., 1960; (c) "Eighth Symposium on Combustion," Butterworths Scientific Publications, London, 1962.

Experimental Studies

A. The Shock Tube and Associated Measuring Equipment.—The shock tube and associated equipment are of conventional design and remain essentially as described earlier.[3] Improvements incorporated in the gas handling and pumping systems have reduced the ultimate pressure achieved in the tube from 0.1 to 0.05 μ. The leak rate has been reduced from 0.1 to about 0.02 μ/min.

Radiant emission from the shock tube passed through sapphire observation windows and was focused in the slits of a monochromater by means of a LiF lens. A NaCl prism allowed a spectral bandpass of 2.7 to 3.2 μ to be covered with about 1 mm. of slit width.

Detection was provided by a Westinghouse Type 812 gold-doped germanium cell. Using a carefully constructed cathode follower and a cell load resistance of 10^5 ohms, the measured time constant of the detector was found to be approximately 0.7 μsec. The output of the dectector was fed to a Tektronix Type 535 oscilloscope. Shock velocity measurements were made using thin film resistance gages and a Berkeley counter.

B. Test Gas Mixtures.—Test gas mixtures of 1 and 8% (nominal) NH_3 in Ar at a total pressure of 1000 p.s.i. were prepared by the Matheson Company. Chemical analysis provided by Matheson gave the NH_3 concentration with an accuracy of about 1%. In our previous studies, we prepared our mixtures of NH_3 and Ar in a low-pressure mixing system with the total gas pressure never exceeding 15 p.s.i.; a chemical analysis (3% precision) of the gas introduced into the tube was performed for each shock tube run to determine the gas composition.

Unfortunately, our chemical analysis was designed to measure the fraction of NH_3 in Ar only, rather than to determine the total composition including impurities. As we shall discuss later, we now suspect that the NH_3 in our original study was contaminated with oxygen.

C. Calculation of Thermodynamic Properties behind the Shock.—The labor of calculating the thermodynamic parameters after passage of a shock wave in a non-dilute gas mixture was greatly reduced in the present investigation by the use of a digital computer program. We are indebted to Dr. James Lloyed of the California Institute of Technology for this program and

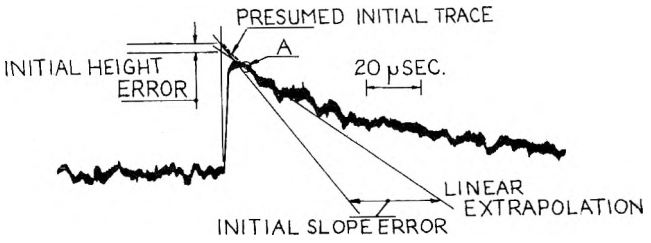

Fig. 1.—Typical experimental record, with indication of errors incurred in extrapolation of experimental trace to the initial time of reaction: T = 2480°K., P = 1.21 atm., 7.9% NH_3, balance Ar.

we then determined an apparent reaction order that yielded the best fit to the concentration–time records. Running the gamut of integral and half integral orders, we found that the 3/2 order with respect to NH_3 yielded the best fit for all our experimental data. Four records, shown in Fig. 2, indicate the closeness of the 3/2 order fit. Thus in determining rate constants, 3/2 order in NH_3 was assumed; least square straight line correlation then yielded the rate constant k' from the integrated form of the rate equation

$$\left[\frac{(NH_3)_0}{(NH_3)}\right]^{-1/2} = 1 + {}^1/_2 k'(NH_3)_0^{1/2} t \qquad (2)$$

where t is the particle time, obtained from oscilloscope time by

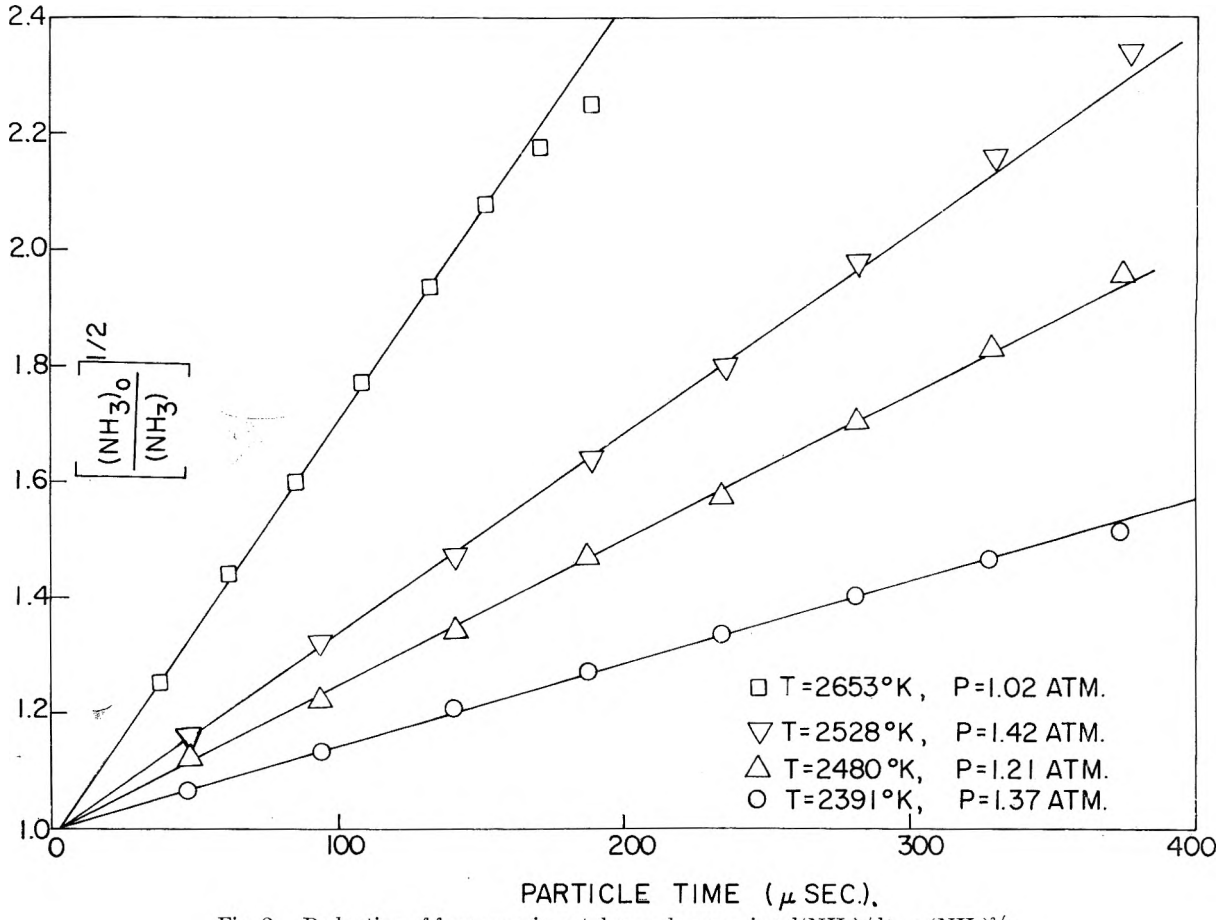

Fig. 2.—Reduction of four experimental records assuming $d(NH_3)/dt \propto (NH_3)^{3/2}$.

to the Western Data Processing Center, U.C.L.A., for the use of an IBM 709 computer.

D. Experimental Results.—The rate of decomposition of NH_3 in Ar has been measured between 2000 and 3000° K. by following the rate of decrease of NH_3 emission intensity in the 2.7 to 3.2 μ wave length region. Figure 1 illustrates a typical experimental record.

Assuming transparent gas radiation, the oscillocope voltage, V, registered by the detector is directly proportional to the ammonia concentration. Thus

$$\frac{V}{V_0} = \frac{(NH_3)}{(NH_3)_0} \qquad (1)$$

where the subscript 0 refers to conditions immediately behind the shock wave.

By using eq. 1 and the calculated thermodynamic parameters, each experimental record yielded (NH_3) as a function of time at a particular temperature. We took the temperature to be the temperature of the gas immediately after passage of the shock wave. Because the heat of formation of NH_3 is −11.04 kcal., the calculated difference in the frozen and equilibrium temperatures behind the shock wave is only about 150° for an 8% mixture of NH_3 in Ar. We determined, however, that this temperature decrease was largely compensated for by shock wave attenuation in our tube. Using conventional integral methods, use of the appropriate density ratio. In eq. 2, the rate constant includes the (Ar) dependence. It should be noted from the figure that the extrapolation to zero time did not quite yield the correct initial concentration.

We are unable to determine unequivocally the Ar reaction order by changing concentration because of limitations of detector sensitivity, gas transparency requirements, and shock testing time, which restricted us to a narrow range of concentrations. However, by taking

$$k' = (\mathrm{Ar})^n k \qquad (3)$$

the least scatter of the data points on an Arrhenius type plot of rate constant *vs.* reciprocal temperature was obtained for n = ${}^1/_2$. Figure 3 shows the Arrhenius plot. The apparent activation energy determined on this basis was found to be 77.7 kcal./mole, with a pre-exponential factor of 2.5×10^{13} l./mole-sec.

Conclusion

Our investigation supports the tentative conclusion that the thermal decomposition of ammonia follows a kinetic law given by

$$\frac{d(NH_3)}{dt} = k(NH_3)^{3/2}(\mathrm{Ar})^{1/2} \qquad (4)$$

with $k = (2.5 \times 10^{13}) e^{-77{,}700/RT}$ l./mole-sec.

Mathews, Gibbs, and Holsen[4] in a recent report have studied the NH_3 decomposition using a single pulse shock tube. They determined an activation energy of about 80 kcal./mole based on unimolecular decomposition. Since the activation energy would not be very sensitive to the assumed order of reaction, it appears that our experimental data are in agreement with the results obtained in ref. 4.

In our earlier work we reported an activation energy of about 52 kcal. for the homogeneous NH_3 decomposition. The scant data available in the literature, however, indicated that a value in the neighborhood of 80 kcal. would be more likely. Hinshelwood and Burk's study of the homogeneous decomposition[5] yielded the qualitative facts that the decomposition could not be detected below temperatures of about 1500°K., whereas above this temperature it was too fast to be measured with the equipment available to them at the time. (More recently, Sage, using a ballistic piston, found similarly that there was practically no conversion of NH_3 below 1500°.[6]) Hinshelwood inferred from his study that an activation energy of at least 80 kcal. was called for in order to explain the observations.[7] If we couple this estimate with the reported activation energies[8] of 45–49.5 kcal. for the oxidation of NH_3, the low value of activation energy obtained in our original measurements certainly suggests oxygen contamination. One would, of course, suspect air leakage, since the manufacturers' minimum purity specifications (anhydrous grade NH_3, 99.99%; standard grade Ar, 99.998%) indicate negligible contaminants. We therefore set about to improve our vacuum system as was discussed earlier. Also, as discussed before, we replaced the low pressure mixing system with high pressure premixed gases, prepared by the Matheson Co.

It recently has come to our attention that many liquefied gases purchased on the West Coast of the United States are shipped *via* tank cars with small cylinders being filled at railroad sites. Only minimum precautions are taken (from a laboratory, not commercial, viewpoint) to remove entrapped air in the cylinders. Apparently, the cylinders are not pumped before filling; rather, the liquefied gas itself is used to expel air. The premixed gases used in the present study were prepared by Matheson at their East Rutherford plant and were not subject to this air contamination. We believe that objectionable contamination has been eliminated in our present experiments and the data obtained are representative of the homogeneous thermal decomposition of NH_3.

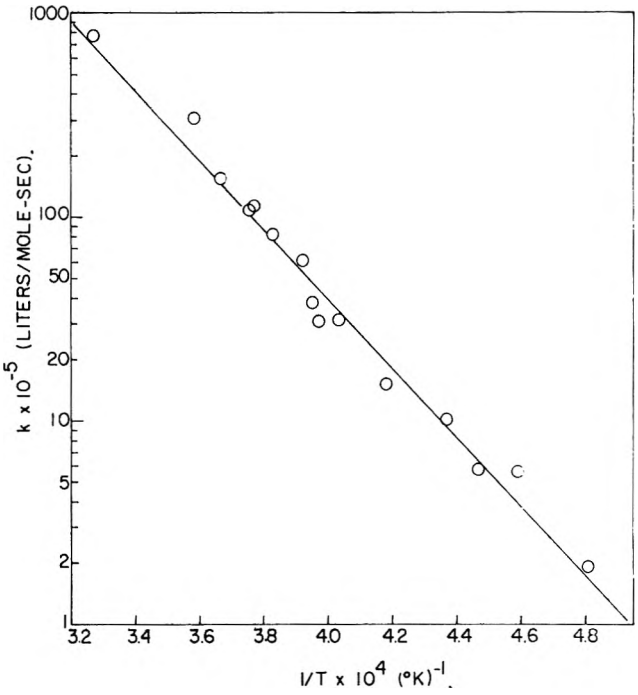

Fig. 3.—Determination of apparent activation energy assuming that $d(NH_3)/dt = k(NH_3)^{3/2}(Ar)^{1/2}$.

The suggestion of a mechanism for the decomposition presents a problem which we prefer to defer until further experimental study is accomplished.

Acknowledgment.—The author wishes to thank Professor S. S. Penner for his stimulating interest during the course of this work. This work was supported by the Air Force Office of Scientific Research under Contract AF 49(638)-984.

(4) J. C. Mathews, M. E. Gibbs, and J. N. Holsen, "A Shock Tube Study of the Ammonia Decomposition Reaction," presented at the 139th National Meeting, American Chemical Society, St. Louis, Mo. 1961.

(5) C. N. Hinshelwood and R. T. Burk, *J. Chem. Soc.* (London), **127**, 1105 (1925).

(6) B. H. Sage, private communication.

(7) C. N. Hinshelwood, "The Kinetics of Chemical Change," Oxford Univ. Press, London, 1940.

(8) E. R. Stephens and R. N. Pease, *J. Am. Chem. Soc.*, **72**, 1188 (1950); **74**, 3480 (1952); J. Verwimp and A. van Tiggelen, *Bull. soc. chim. Belges*, **62**, 205 (1953).

THERMOCHEMISTRY OF ANION MIXTURES IN SIMPLE FUSED SALT SYSTEMS. I. SOLUTIONS OF MONOVALENT CHLORIDES AND BROMIDES IN THE CORRESPONDING NITRATES

BY O. J. KLEPPA AND S. V. MESCHEL

Institute for the Study of Metals and Department of Chemistry, University of Chicago, Chicago 37, Illinois

Received September 15, 1962

Calorimetric measurements have been performed on the heats of solution and of dilution for monovalent chlorides and bromides dissolved in the corresponding liquid nitrates. It is found that all the studied alkali halide–alkali nitrate systems exhibit small positive enthalpies of mixing, with the largest effects observed for the sodium systems. It is suggested that these results may be explained in terms of a packing effect which is due to the repulsion between the second nearest neighbor anion cores. Corresponding data for the silver and thallium salts are more complex. They cannot be explained in terms of the second nearest neighbor interactions.

Introduction

Recent unpublished equilibrium work by Toguri, *et al.*,[1] indicates that simple MCl–MBr melts tend to exhibit *positive* deviations from ideality, the deviation increasing in the sequence Li < Na < K. This suggests that the anion mixtures differ in a marked way from the analogous cation mixtures. Thus, one of the authors found in a recent calorimetric study that all the binary alkali nitrate systems exhibit *negative* enthalpies of mixing, the magnitude of the enthalpy increasing in a regular manner with increasing differences in size between the component cations.[2]

The present investigation was initiated in order to explore by calorimetry the general problem of anion mixtures in fused salt systems. When our work started, the only calorimetric equipment available was the previously described twin reaction calorimeter suitable for work up to 500°.[3] This experimental restriction ruled out a study of the mentioned chloride–bromide systems, which melt at higher temperatures. These are now being investigated by means of a new calorimeter which can be operated at temperatures up to 800°, and will be the subject of later communications.

In the present work we discuss solutions of monovalent chlorides and bromides in the corresponding liquid nitrates. All experiments were carried out at or below about 450°. Due to the limitations imposed by temperature and by the thermal instability of the nitrates, our information covers only the nitrate-rich end of the considered binary systems.

Experimental and Materials

In the course of the present investigation the previously described calorimeter was modified slightly by inserting a close-fitting Pyrex liner (18-mm. diameter) in the stainless steel "protection" tube of the original calorimeter. This served to prevent attack on the stainless steel by the somewhat corrosive melts. The presence of this liner reduced the space available for experiments, but did not impair appreciably either the sensitivity or the accuracy of the apparatus.

The nitrates used in the present study were obtained from the same sources, and were treated in the same manner, as the nitrates used in our earlier work.[2] The lithium, potassium, and sodium halides were Mallinckrodt Analytical Reagents. The cesium, rubidium, and thallium halides were purchased from Millmaster Chemical Corporation and were stated by the manufacturer to be of 99.9% purity. This was checked by semiquantitative spectrochemical analysis. The silver halides were of analytical grade, obtained from Goldsmith Bros. All halides were used without further purification. The data reported below are based on calibration by the "gold drop method,"[2] *i.e.*, on the heat content equation for pure gold as calculated from the equation quoted by Kelley.[4]

The present investigation was conducted in a manner entirely analogous to that adopted in our earlier study of the solutions of the alkaline earth nitrates in the alkali nitrates.[5,6] Thus we carried out two different types of calorimetric experiments.

(a) **Solid–Liquid Mixing Experiments and (b) Dilution Experiments.**—In the solid–liquid experiments, the solid halides were dissolved in the corresponding nitrate melts. These measurements involved quite large endothermic heat effects, and presented no particular experimental problems. However, the heat effects associated with the dilution experiments were quite small, often of the order of 0.1 cal. or less. For these measurements, the uncertainties associated with heat generated in the breaking of the ampoule and in stirring became quite important. As a result, some of our dilution data are associated with quite large *relative* errors.

Results

All experimental results obtained in the course of the present work are shown in graphical form in Fig. 1. In the left-hand part of this figure we have plotted the mole fraction of halide along the abscissa, and the quantity $\Delta H^M/X$ along the ordinate axis. ΔH^M is the molar change in enthalpy associated with formation of a liquid solution of mole fraction X (of halide) from pure solid halide plus liquid nitrate. We have demonstrated elsewhere that the quantity $\Delta H^M/X$, and its derivative, are particularly useful for calculating partial molal heat quantities.[5] Direct experimental information on the derivative of $\Delta H^M/X$ with respect to X [actually on $\Delta(\Delta H^M/X)/\Delta X$] is provided by the dilution experiments, the results of which are presented in the right-hand part of Fig. 1.

The limiting value of $\Delta H^M/X$ at $X = 0$ is of special interest. This quantity represents the partial molal enthalpy associated with the transfer of one mole of halide from the pure crystalline state into "pure" liquid nitrate at the considered temperature. Formally this number may be considered to represent a sum of two terms: (a) the enthalpy change, $\Delta H^f(t)$, associated with the fusion of the pure halide at temperature t; (b) the enthalpy change associated with the solution of this undercooled liquid halide into the pure nitrate.

Although our experiments cover a limited range of halide concentrations only, the data contained in Fig. 1 permit an approximate separation of these quantities. This separation is based on the assumption that the various halide–nitrate mixtures have enthalpies of mix-

(1) J. Toguri, H. Flood, and T. Forland, unpublished results; quoted by H. Flood, *Discussions Faraday Soc.*, **32**, 168 (1961).

(2) O. J. Kleppa and L. S. Hersh, *J. Chem. Phys.*, **34**, 351 (1961).

(3) O. J. Kleppa, *J. Phys. Chem.*, **64**, 1937 (1960).

(4) K. K. Kelley, "Contributions to the Data on Theoretical Metallurgy," Bureau of Mines Bulletin Number 584, 1960.

(5) O. J. Kleppa and L. S. Hersh, *Discussions Faraday Soc.*, **32**, 99 (1961).

(6) O. J. Kleppa, *J. Phys. Chem.*, **66**, 1668 (1962).

TABLE I

SUMMARY OF THERMOCHEMICAL DATA FOR HALIDE–NITRATE SYSTEMS

System	t, °C.	$\Delta H^f(t) + a$, kcal.	a, kcal.	$\Delta H^f(t)$, kcal.	$\Delta H^f(t_m$, °C.), kcal.	ΔC_p^f, cal./deg.
Li(NO_3–Cl)	349	4.45	+0.21	4.24	4.77 (613)	2.0
Na(NO_3–Cl)	454	6.40	+0.40	6.00	6.77 (801)	2.2
Na(NO_3–Br)	454	6.10	+0.36	5.74	6.24 (755)	1.7
K(NO_3–Cl)	454	5.43	+0.21	5.22	6.24 (776)	3.2
K(NO_3–Br)	454	5.42	+0.12	5.30	6.10 (730)	2.9
Rb(NO_3–Cl)	452	5.05	+0.12	4.93	5.67 (715)	2.8
Rb(NO_3–Br)	452	5.00	+0.08	4.92	5.57 (682)	2.8
Cs(NO_3–Cl)[a]	454	5.12	+0.17	4.95	4.90 (646)	3.3
Cs(NO_3–Br)	454	5.25	+0.08	5.17	5.64 (636)	2.6
Tl(NO_3–Cl)	349	4.22	+0.74	3.48	3.95 (430)	5.8
Tl(NO_3–Br)	349	4.75	+1.12	3.63	4.12 (460)	4.4
Ag(NO_3–Cl)	234	2.32	−1.13	3.45	3.08 (455)	−1.7
Ag(NO_3–Br)	234	1.35	−2.17	3.52	2.19 (434)	−6.4

[a] For this system no direct comparison can be made between $\Delta H^f(454)$ and $\Delta H^f(646)$ unless heat of transformation of CsCl at about 470° is taken into account. In order to obtain quoted value of ΔC_p^f we have corrected for heat of transformation, which is 0.58 kcal./mole (C. E. Kaylor, G. E. Walden, and D. F. Smith, *J. Phys. Chem.*, **64**, 276 (1960)).

ing which, to a good approximation, may be represented by simple parabolic expressions of the type $aX(1 - X)$, where *the interaction parameter*, a, is a constant.

Under this assumption we have

$$\Delta H^M/X = \Delta H^f(t) + a(1 - X) \qquad (1)$$

Thus the slope of $\Delta H^M/X$ *vs.* X is simply equal to $-a$. The slopes drawn in the left-hand part of Fig. 1 are based on the average of the dilution data given in the right-hand part.

From the experimental results given in Fig. 1 we have in this manner obtained the thermochemical information which is summarized in Table I. In this table our own values of $\Delta H^f(t)$ are compared with the corresponding heats of fusion valid at the melting point, $\Delta H^f(t_m)$. For the alkali halides we have used the heats of fusion reported recently by Dworkin and Bredig,[7] for the silver and thallium halides our values are taken from Kelley.[4]

From the two heats of fusion values we have calculated the average ΔC_p^f between the temperature of our measurements and the melting point. This quantity is of considerable interest in evaluations of thermodynamic data from equilibrium phase diagrams. It will be noted that for most halides studied in the present work ΔC_p^f is positive, and falls in the range 2–3 cal./degree mole. On a molar, although not on a particle basis, the values are comparable to those for the rare gases.[8]

We are particularly interested in the new interaction parameters for the various halide–nitrate systems given in Table I. We note that while the two silver systems both exhibit fairly large negative interaction parameters, the thallium systems show positive values of comparable magnitude. However, the explored alkali halide–alkali nitrate mixtures all have relatively small positive interaction parameters. This is consistent with the results obtained in the mentioned work of Toguri, *et al.*[1]

Discussion

In earlier discussions of the solution chemistry of fused salt systems where the two components have a common ion, it has proved useful to emphasize the

(7) A. S. Dworkin and M. A. Bredig, *J. Phys. Chem.*, **64**, 269(1960).

(8) A. C. Hollis Hallett in "Argon, Helium and the Rare Gases," Vol. 1, Interscience Publishers, Inc., New York, London, 1961.

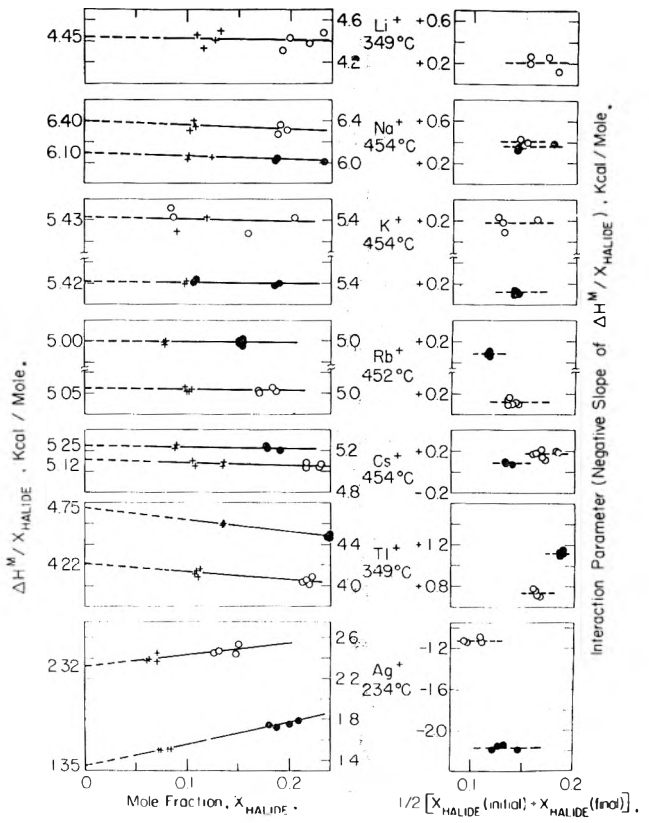

Fig. 1.—Heat data for solutions of chlorides (○) and bromides (●) in corresponding nitrates. Left part: $\Delta H^M/X_{halide}$ from direct experiments (○ and ●), and from direct experiments plus dilutions (+). Right part: interaction parameters from dilution experiments.

changes in the energy of interaction between second nearest neighbors associated with the mixing process. Thus we neglect, in this first approximation, changes in interaction both between nearest neighbors and between more distant neighbors.

On the basis of this simplification, it has been possible to show that the magnitude of the negative enthalpies of mixing found in the binary alkali nitrates is consistent with the reduction in second nearest neighbor Coulomb repulsion between the cations.[2] Similarly, it has been shown that the enthalpies of mixing of silver nitrate—alkali nitrate and thallium nitrate–alkali nitrate solutions may be explained by taking into account, in addition to the mentioned Coulomb terms, the change in van der Waals interaction between second

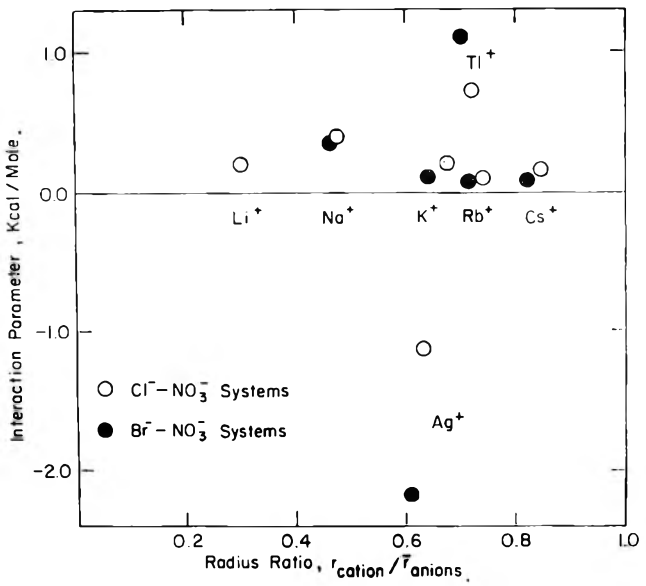

Fig. 2.—Interaction parameters *vs.* radius ratio for halide–nitrate mixtures.

nearest neighbor cations.[9] These van der Waals terms are *positive*, and are for some of the mentioned silver and thallium nitrate systems so large that they overshadow the negative Coulomb terms.

As we now go on to consider simple anion–anion mixtures, it seems appropriate to inquire whether the observed solution behavior of the alkali halide–alkali nitrate systems may possibly also be accounted for by a combination of the two above-mentioned factors. In order to answer this question we have made crude, order of magnitude estimates of the electrostatic and van der Waals contributions to the mixing enthalpies. These estimates suggest that the positive van der Waals terms arising from the interaction between the halide and nitrate ions are much too small to account for the observed positive mixing enthalpies.

We propose that it may be possible to explain our esults for the alkali halide–nitrate systems by taking into account, in addition to the electrostatic and van der Waals forces, the short range, repulsive potential between the ion cores. In particular we believe that anion–anion (*i.e.*, second nearest neighbor) core repulsion may be significant. This interpretation is essentially equivalent to the "packing effect" interpretation already advanced by Flood in his discussion of the mentioned bromide–chloride melts.[1] It can be justified by the fact that in all the considered anion mixtures, the size relations between anions and cations are such that the anions are not well separated.

If this interpretation is correct, we clearly might expect the mixing process to be associated with an appreciable volume expansion. While, unfortunately, no reliable volume data are available for anion–anion mixtures, the binary alkali nitrates are known to show small positive excess volumes.[10] These excess volumes increase sharply with increasing difference in size between the cations. Thus it is possible that a small positive packing effect may be present even in simple cation–cation mixtures.

In further support of the packing effect interpretation, we present in Fig. 2 a graph of our experimental interaction parameters (a) plotted *vs.* the radius ratio, $r_{\text{cation}}/\bar{r}_{\text{anion}}$; $\bar{r}_{\text{anion}}$ is the mean value of the two anion radii. For the radius of the nitrate ion we have adopted the value 2.19 Å.[2], while for the other ions we have used the Pauling radii.

This figure shows that for all the alkali metal cations, the interaction parameters fall on or near a general curve. This curve starts out with a positive value for the lithium nitrate–chloride system, rises to a maximum near the sodium systems, and decreases to quite small positive values for the potassium, rubidium, and cesium systems. We consider the decrease in interaction parameter with increasing radius ratio from sodium and up, and the extensive similarity between the values for the chloride–nitrate and bromide–nitrate systems, to offer strong support for the packing effect interpretation. In fact, as far as they go, our alkali halide–nitrate data confirm Flood's conjecture that positive deviations from ideality "are a quite general behavior of binary ionic systems when the common ion is the smaller."[1]

On the other hand, the decrease in interaction parameter from sodium to lithium at first seems inconsistent with the packing effect interpretation. There may be, of course, several reasons for this decrease. However, it should be noted that the lithium salts are the only ones covered in the present study for which a sodium-chloride-like, six-coördinated arrangement of the anions around the cations would result in direct anion–anion contact. Therefore, it seems probable that the liquid lithium salts may assume structures with a lower effective coördination number than the other alkali salts. This might in turn reduce the packing effect somewhat through two related mechanisms: on the one hand by increasing the anion–anion separations even in the pure salts, and on the other, by providing a somewhat larger amount of "unfilled volume" due to the looser packing.

While, as we have attempted to do above, it is possible to arrive at a rationalization of our experimental results for the alkali halide–nitrate systems on the basis of the second nearest neighbor interaction concepts, we consider these concepts to be entirely inadequate for the silver halide–nitrate and thallium halide–nitrate systems. We refer here in particular to the large negative departures for silver, the comparable positive departures for thallium, and the significant differences in interaction parameter for bromide–nitrate and chloride–nitrate.

It is possible that a part of these anomalies may be related to basic structural differences between the liquid silver and thallium salts. Thus it is reasonable to assume that the tendency of the silver ion to surround itself with a *small* number of nearest neighbors, and the analogous tendency of the thallium ion toward *high* coordination numbers, may cause departures in the right direction from the general curve in Fig. 2.

However, it seems unlikely that these structural differences alone could account for more than a fraction of the observed deviations. In particular, it is suggested that the large negative interaction parameters for the silver salts must be considered as evidence for a certain degree of chemical interaction in the mixture. Although we are unable to explain the nature of this bonding in any detail, it is suggested that the presence of a dissimilar anion neighbor may somehow strengthen

(9) M. Blander, *J. Chem. Phys.*, **36**, 1092 (1962).

(10) B. F. Powers, J. L. Katz, and O. J. Kleppa, *J. Phys. Chem.*, **66**, 103 (1962).

the slightly covalent character[11] of the silver halide bonds. Thus we conclude that the large departures from ideality of the silver and thallium systems in effect reflect the breakdown of the second nearest neighbor approximation.

Acknowledgments.—The authors are indebted to Miss M. C. Bachelder for performing the spectrochemical analyses. This work has been supported by the National Science Foundation (Grant G 19513) and by the Office of Naval Research under Contract Number Norr 2121(11) with the University of Chicago. The authors also wish to acknowledge the general support of the Institute for the Study of Metals by the A.E.C. and by the A.R.P.A.

(11) J. E. Mayer, *J. Chem. Phys.*, **1**, 270 (1933).

DIFFUSION OF IONS IN AN ELECTRIC FIELD[1]

By Richard W. Laity

Frick Chemical Laboratory, Princeton University, Princeton, N. J.

Received September 19, 1962

Rigorous mathematical treatment of ionic transport in a polarized diffusion layer requires the use of electrochemical potential gradients as the "thermodynamic forces" on charged species. This can be done in a particularly simple and useful manner by replacing the usual rate constants for the description of ionic transport in electrolytic systems (equivalent conductance, transference numbers, and diffusion coefficients) with an alternative set of quantities known as "friction coefficients." Phenomenological relations between current density and gradients of electrochemical potential of individual species in various types of electrolytic systems then can be integrated to give a complete description of steady-state polarization in terms of known properties of the system. The approach lends itself to quasi-thermodynamic interpretation, thereby giving useful physical insight. The necessity of limiting "diffusion currents" as well as the effects of supporting electrolytes are made apparent in terms of the three forces (diffusional, electrical, and frictional) that must be balanced in the steady state. Application of these concepts to diffusion-controlled oxidation–reduction reactions, *e.g.*, magnesium dissolution in acids, permits *a priori* calculation of reaction rate, and shows that even when no external circuit is present a gradient of electrical potential can be present in the diffusion layer and play a major role in fixing ionic velocities.

In experiments involving the removal of a single ionic species from solution, such as polarographic and related electrochemical separations, ionic transport very close to the electrode surface usually is described in terms of two concepts: migration and diffusion. Neither of these terms is strictly applicable, however, to a process in which gradients of both electrical potential and concentration are acting simultaneously. For even though the net flux J_i of a given ion can be determined unambiguously, it is not possible to specify an electric field strength $\nabla\varphi$ in a system of varying composition.[2] The thermodynamically defined "force" on the ion in such cases is the gradient of electrochemical potential $\nabla\bar{\mu}_i$. By employing this quantity, a rigorous treatment of "polarized diffusion" in any type of electrolytic system is possible. It will be shown here that a particularly simple set of equations for this purpose is provided by the "friction-coefficient" formalism.[3] In the specific applications to be considered it will be seen that the use of friction coefficients has the additional merit of lending itself to a simpler quasi-thermodynamic interpretation than that presently employed for intuitive understanding of such problems.

The equations used in applying this approach to a system composed of N ionic and/or neutral species are the phenomenological relations which define the friction coefficients r_{ik}

$$-\nabla\bar{\mu}_i = \sum_{k=1}^{N} r_{ik}X_k(v_i - v_k) \quad (i,k = 1,2,\ldots,N) \qquad (1a)$$

$$r_{ik} = r_{ki} \qquad (1b)$$

Here $\nabla\bar{\mu}_i$ is the gradient of electrochemical potential of the ith species, X_k is the concentration (mole fraction) of species k, and v_i and v_k are the velocities of the indicated species in a region sufficiently small for these quantities to be defined. Application of eq. 1 to the problems of interest here is simplified by choosing a planar electrode surface as reference for the velocities and considering only steady-state conditions. If species 1 is the only one involved in the electrode reaction, the net velocity of each other species in the "diffusion layer" must be zero. Hence

$$-\frac{d\bar{\mu}_1}{dx} = v_1 \sum_{k=2}^{N} X_k r_{1k} \qquad (2a)$$

and

$$-\frac{d\bar{\mu}_i}{dx} = -r_{1i}X_1v_1 \ (i = 2,\ldots,N) \qquad (2b)$$

Some simple examples will illustrate the application of equations of this type.

Case I. Aqueous Binary Electrolyte, Species 1 Being Removed at Electrode.—If species 1 is a cation, the current density i is given by

$$i = C_+v_+z_+F$$

where z_+F is the charge on one mole of cations and C_+ is the concentration per unit volume. Although three equations of the form (2) can be written, any two are sufficient.[3] Thus, noting that $C_i = X_i/V$ where V is the volume occupied by one mole of ions plus solvent molecules, the current density in the steady state determines the gradients at any point in the diffusion layer as

$$-\frac{d\bar{\mu}_+}{dx} = \frac{i}{C_+z_+F}(X_-r_{+-} + X_sr_{+s}) \qquad (3a)$$

$$\frac{d\mu_s}{dx} = \frac{i}{z_+F}Vr_{+s} \qquad (3b)$$

(1) Presented at the 138th National Meeting of the American Chemical Society, New York, N. Y. 1960, under the title "The Diffusion Layer at a Polarized Electrode."

(2) E. A. Guggenheim, *J. Phys. Chem.*, **33**, 842 (1929).

(3) R. W. Laity, *J. Chem. Phys.*, **30**, 682 (1959).

(3a) may be regarded as a current–potential relationship, while (3b) is used to relate current density and concentration gradients. The significance of the latter will be considered first.

To apply eq. 3b to a particular electrolytic system, it is necessary to know the concentration dependence of both μ_s and r_{+s}. Rather than choose a specific electrolyte here, we will make use of approximations that give a more general picture. Thus, the thermodynamic behavior of the solvent is assumed to be "ideal"

$$d\mu_s \approx \frac{RT\, dX_s}{X_s}$$

In strong electrolytes

$$dX_s = -dX_+ - dX_-$$
$$\approx -V\left(1 + \frac{\nu_-}{\nu_+}\right) dC_+$$

where ν_+ and ν_- are the numbers of moles of cations and anions, respectively, resulting from complete dissociation of one mole of electrolyte. Since $\nu_+ z_+ = \nu_- z_-$, eq. 3b can be written

$$-\frac{dC_+}{dx} \approx \frac{z_-}{z_+ + z_-} \cdot \frac{X_s r_{+s} i}{RTz_+F} \qquad (4)$$

As for r_{+s}, it is worthwhile to examine at this point the typical behavior of friction coefficients in aqueous solutions of strong electrolytes. They are calculated from conventional transport parameters by means of the equations

$$r_{+s} = \frac{t_-RT[X_e(\nu_+ + \nu_-) + X_s']}{\nu_+ D_{es}'} \qquad (5a)$$

$$r_{-s} = \frac{z_- t_+}{z_+ t_-} r_{+s} \qquad (5b)$$

$$r_{+-} = \frac{F^2}{\Lambda} \frac{X_e(\nu_+ + \nu_-) + X_s'}{X_e} - \frac{X_s' r_{+s} r_{-s}}{X_e(z_- r_{+s} + z_+ r_{-s})} \qquad (5c)$$

Here X_e and X_s' are the mole fractions of electrolyte and solvent, respectively, used in making up the solution. t_i and Λ have their usual significance, while D_{es}' is the thermodynamic mutual diffusion coefficient.[4] Applying these transformations to available data for aqueous NaCl at 25° gives the figures listed in Table I. It is seen that the ion–solvent friction coefficients are essentially independent of concentration over the range indicated (infinite dilution to 0.2 M), while the interionic friction coefficient varies approximately as $X_e^{-1/2}$.

(4) This term is related to the ordinary diffusion coefficient D_{es} by[1]

$$D'_{es} = D_{es} \Big/ \left(1 + \frac{d \ln f_e}{d \ln X_e}\right)$$

where f_e is the activity coefficient of the electrolyte taken as a whole. For purposes of calculation the following relation is useful

$$1 + \frac{d \ln f_e}{d \ln X_e} = (\nu_+ + \nu_-)\left(1 + \frac{d \log \gamma_\pm}{d \log m_e}\right)\left(1 + \frac{m_e M_s}{1000}\right)$$

Here m_e is the molality of electrolyte, M_s the molecular weight of solvent, and $\gamma_\pm$ the "mean molal ionic activity coefficient."

TABLE I

FRICTION COEFFICIENTS IN AQUEOUS NaCl AT 25°

Concn., M	Friction coefficients (joule sec. cm.$^{-2}$ mole^{-1} × 10^{-8}) r_{+s}	r_{-s}	r_{+-}	$X_e^{1/2} r_{+-}$
0.00	1.86	1.22	∞	..
.01	1.86	1.20	316	4.3
.02	1.86	1.19	220	4.2
.05	1.87	1.19	126	3.8
.10	1.89	1.19	82	3.5
.20	1.91	1.18	53	3.2

Employing the first of the above observations, we conclude from eq. 4 that in dilute solutions ($X_s \approx 1$) of an electrolyte of this type the gradient of concentration within the diffusion layer is constant. Furthermore, we can without loss of generality replace r_{+s} by its infinite-dilution value, as calculated from either of the equations[3]

$$\frac{z_+}{r_{+s}^0} = \frac{\lambda_+^0}{F^2}$$

or

$$\frac{1}{r_{+s}^0} = \frac{D_+^0}{RT}$$

where D_+^0 is the infinite-dilution value of the self-diffusion coefficient. The second of these relations makes it possible to write (4) in the form of a diffusion equation. Taking $X_s \approx 1$

$$J_+ \approx -\frac{z_+ + z_-}{z_-} D_+^0 \frac{dC_+}{dx} \qquad (6)$$

The factor $(z_+ + z_-)/z_-$ appears to represent the effect of the electric field superimposed on ordinary diffusion. Although this viewpoint is useful for intuitive purposes, it does not take into account the concentration dependence to be expected of a process in which cations diffuse past stationary anions. Subsequent discussion herein will elaborate this point.

If the diffusion layer is regarded as a region bounded on one side by the concentration present in the bulk and on the other by that at the electrode surface, eq. 4 (with X_s taken as unity) can be integrated to obtain the current density in terms of these concentration limits

$$i = \frac{z_+ + z_-}{z_-} \frac{RTz_+F}{r_{+s}} \frac{C_+^b - C_+^s}{\delta} \qquad (7)$$

Here δ is the "thickness" of the diffusion layer, a quantity that depends on stirring and geometric factors and is independent of current density. Thus i is linear in C_+^s; in a given experiment any increase in i must be accompanied by a corresponding decrease in the latter quantity. As this becomes negligibly small compared to the bulk concentration C_+^b, i approaches the limiting value given by[5]

(5) If instead of replacing r_{+s} in eq. 8a by z_+F^2/λ^0 we substitute the value given by eq. 5a, a relation essentially equivalent to the often-cited formula

$$i_{max} = \frac{Dz_+FC_+^b}{(1 - t_+)\delta}$$

is obtained. A significant revelation, however, is that D, which generally is referred to as the "ionic diffusion coefficient," turns out to be identical with D_{es}, the ordinary diffusion coefficient of the electrolyte taken as a whole, rather than a single-ion parameter like the self-diffusion coefficient D_+.

$$i_{max} = \frac{z_+ + z_-}{z_-} \frac{RTz_+FC_+^b}{r_{+s}\delta} \quad (8a)$$

or

$$i_{max} = \frac{z_+ + z_-}{z_-} \frac{RT\lambda_+^0 C_+^b}{F\delta} \quad (8b)$$

These equations demonstrate the linear dependence of i_{max} on bulk concentration of the discharging cation, and also provide a simple formula for assigning a value of δ from experimental data.

An interesting conclusion to be drawn from eq. 8b is that the only way in which the nature of the anion influences the limiting cationic current is through the magnitude of its charge. Changing from a salt like $CuSO_4$ to one like $Cu(NO_3)_2$ will increase the value of i_{max} by a factor of 3/2. (This approximation is subject to our assumption about ideal behavior. Activity coefficients in electrolytic solutions are, of course, particularly sensitive to a change of charge type.)

The significance of eq. 3a is best seen by integrating across the diffusion layer. To do this we first make use of eq. 4 to obtain dx in terms of dC_+. Substituting the result into (3a) gives

$$d\bar{\mu}_+ = \frac{(z_+ + z_-)RT(X_-r_{+-} + X_sr_{+s})}{z_-X_sr_{+s}} \frac{dC_+}{C_+} \quad (9)$$

The term containing r_{+-} can be ignored in dilute solutions (Table I). Integration then gives

$$\Delta\bar{\mu}_+ \approx \frac{z_+ + z_-}{z_-} RT \ln \frac{C_+^s}{C_+^b} \quad (10)$$

Now $\Delta\bar{\mu}_+$, the change across the diffusion layer in the electrochemical potential of the discharging ion, is equivalent to z_+F times the potential difference between electrodes reversible to that ion. Thus eq. 10 provides a basis for calculating that part of the observed electrode potential (potential difference measured between the electrode and a suitable reference placed just outside the diffusion layer) which is not due to irreversibility of the electrode process itself. The value of C_+^s to be used in eq. 10 can be obtained from eq. 7, provided δ has been determined (*e.g.*, *via* eq. 8b).

By employing quasi-thermodynamic concepts a useful physical picture emerges from the approach under consideration. If we first break up $\nabla\bar{\mu}_i$ into the sum $\nabla\mu_i \pm z_iF\nabla\varphi$ (positive sign for cations, negative for anions) three types of forces that can act on each species are distinguishable: diffusional (D), electrical (E), and frictional (F). Equations 1 express the fact that these forces must in steady state be balanced; *i.e.*, the net force on any species is zero. The balance of forces in the example under discussion is represented schematically in Fig. 1. Consider first the solvent species. Since it is uncharged ($z_s = 0$), only diffusional and frictional forces are significant here. In the steady state F_{s+} arises from the ion moving toward the electrode and must be countered by a gradient of solvent concentration (eq. 3b). It follows that the electrolyte becomes more dilute as the electrode surface is approached (eq. 4). This in itself is enough to explain the existence of a limiting current. As the electrolyte concentration at the surface approaches zero, D_s cannot be increased further, thereby putting an upper limit

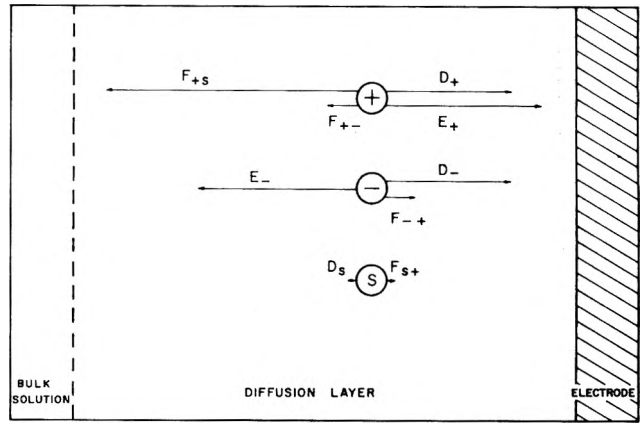

Fig. 1.—Balance of forces in a polarized diffusion layer. Case I. D = diffusional, E = electrical, F = frictional.

on F_{s+} and hence on the flux of the discharging ion (eq. 8).

The effect of the electrical potential gradient on the magnitude of the diffusion current is obtained by considering the balance of forces on the anion. Due to electroneutrality, the anion feels a diffusional force of the same magnitude as D_+ in the direction of the electrode surface. Neglecting the interionic frictional force (which is similarly oriented), a potential gradient sufficient to produce E_- equal and opposite to D_- is required. The effect of this potential gradient on the cation is, of course, an electrical force equal to $-(z_+/z_-)E_-$. Thus the total force driving the cation toward the electrode surface is increased by the factor $(1 + z_+/z_-)$ over that due to the concentration gradient alone (eq. 6). Taking interionic friction into account simply increases both the frictional and electrical forces on the cation by equal amounts, thus leaving the net effect unchanged.

The preceding deductions are borne out by quasi-thermodynamic interpretation of eq. 9, which permits evaluation of the variation of "potential" with concentration in the diffusion layer. Neglecting the term containing r_{+-}, eq. 9 can be written

$$d\mu_+ + z_+Fd\varphi \approx (1 + z_+/z_-)RT\ d\ln C_+$$
$$= (1 + z_+/z_-)d\mu_+$$

again showing that the contribution of potential gradient

$$\frac{d\varphi}{dx} = \frac{RT}{z_-F} \frac{d\ln C_+}{dx}$$

enhances the diffusion force $d\mu_+/dx$ by the factor $(1 + z_+/z_-)$.

Case II. Fused Mixture of 2 Binary Salts with Common Anion, Cation 1 Being Removed at Electrode. —The phenomenological equations

$$\frac{d\bar{\mu}_1}{dx} = \frac{i}{C_1z_1F}(X_2r_{12} + X_-r_{1-}) \quad (11a)$$

and

$$-\frac{d\bar{\mu}_-}{dx} = \frac{iX_1r_{1-}}{C_1z_1F} \quad (11b)$$

are sufficient here. If we use the convention[3] that the formula of a salt consisting of cations A and anions B

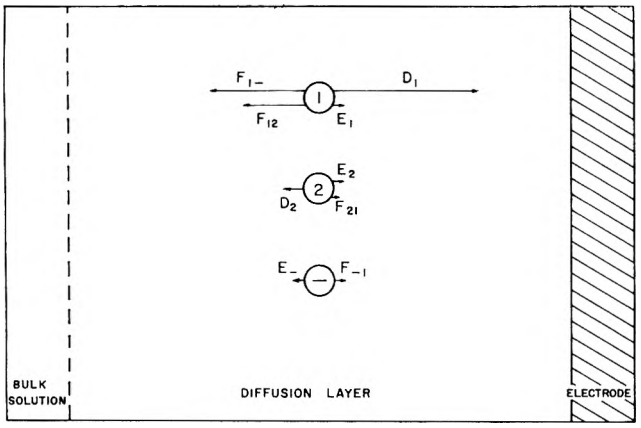

Fig. 2.—Balance of forces in a fused salt diffusion layer (Case II).

is written $A_{z_-}B_{z_+}$ (rather than the usual $A_{\gamma_+}B_{\gamma_-}$) the gradient of *chemical* potential of the salt containing cation 1 is given by

$$d\mu_{1-} = z_- d\bar{\mu}_1 + z_1 d\bar{\mu}_-$$

Combination of eq. 11 with the electroneutrality condition $z_1X_1 + z_2X_2 = z_-X_-$ then gives

$$\frac{-d\mu_{1-}}{dx} = \frac{(z_-r_{12} + z_2r_{1-})X_2 i}{C_1 z_1 F} \qquad (12)$$

Now eq. 11a can be regarded as a current–potential relation, while (12) gives the dependence of current density on concentration gradient. For the case where X_2 is very small, (11a) is a statement of Ohm's law and (12) is trivial. The case where X_1 is small is of greater interest and will be considered further here.

Assuming ideal behavior

$$d\mu_{1-} = RT(z_- d \ln C_1 + z_1 d \ln C_-)$$

When X_1 is small the second term on the right is negligible. Furthermore, $X_2 \approx z_-/(z_2 + z_-)$. Substitution into (12) gives

$$-\frac{dC_1}{dx} \approx \frac{(z_-r_{12} + z_2r_{1-})i}{(z_2 + z_-)z_1 FRT} \qquad (13)$$

Although the friction coefficients r_{12} and r_{1-} are not independent of concentration in most fused salt mixtures,[6] they are nearly so in dilute solution. Equation 13 thus shows that under these conditions the concentration gradient is essentially constant throughout the diffusion layer.

If we express (13) in the form of a diffusion law

$$J_1 = -\frac{(z_2 + z_-)RT}{z_-r_{12} + z_2r_{1-}} \frac{dC_1}{dx} \qquad (14)$$

the coefficient of the concentration gradient here can be compared with the ordinary diffusion coefficient. In ideal dilute solutions the latter is given by[7]

$$D_{12} = \frac{(z_2 + z_-)RT}{z_-r_{12} + z_2r_{1-}} \qquad (15)$$

showing that under these conditions the two are identical. Indeed, in contrast with case I, the "ionic diffusion coefficient" defined by eq. 14 is also identical in very dilute solutions with the self-diffusion coefficient of species 1, as can be seen from eq. 18a of ref. 3. Apparently any superimposed effect from the electric field is negligible here.

As in the preceding section, eq. 13 can be integrated by assuming $(z_-r_{12} + z_2r_{1-})$ independent of concentration

$$i = \frac{z_2 FD(C_1^{\,b} - C_1^{\,s})}{\delta} \qquad (16)$$

and hence

$$i_{max} = \frac{z_1 FDC_1^{\,b}}{\delta} \qquad (17)$$

Here D can be identified with any of the three diffusion coefficients mentioned above.

Returning to eq. 11a, we now compute the dependence of electrochemical potential on concentration in dilute ideal solutions. Taking $X_2 = z_-/(z_2 + z_-)$ and $X_- = z_2/(z_2 + z_-)$, and substituting eq. 13 gives

$$d\bar{\mu}_1 = RT \, d \ln C_1 \qquad (18)$$

and hence

$$\Delta\bar{\mu}_1 = RT \ln \frac{C_1^{\,s}}{C_1^{\,b}} \qquad (19)$$

As in case I, $C_1^{\,s}$ can be calculated from (16) after first determining δ by means of (17), so that eq. 19 permits calculation of the reversible part of the observed electrode potential.

A quasi-thermodynamic interpretation of these results gives further insight. The balance of forces in this system is represented in Fig. 2. If species 1 and 2 are of the same valence type there can be no concentration gradient of the anion. It follows that E_- must be equal and opposite to F_{-1}. The latter is small compared to F_{1-} due to the low concentration of species 1 (eq. 11). Thus, the gradient of electrical potential must be small, and the primary driving force on species 1 is D_1 (eq. 18). Even when cations of different valence types are involved the diffusional forces on both cation 2 and the anion are very small in dilute solutions of species 1 due to the negligible change in per cent concentration of these species, leaving the above conclusions unaltered.

Case III. Aqueous Solution Containing Excess Supporting Electrolyte, Cation 1 Being Removed at Electrode.—This case is perhaps the most familiar experimentally. A sufficient set of phenomenological equations is

$$-\frac{d\bar{\mu}_1}{dx} = \frac{i}{C_1 z_1 F}(X_2r_{12} + X_-r_{1-} + X_sr_{1s}) \qquad (20a)$$

$$\frac{d\bar{\mu}_-}{dx} = \frac{i}{C_1 z_1 F} X_1 r_{1-} \qquad (20b)$$

$$\frac{d\mu_s}{dx} = \frac{i}{C_1 z_1 F} X_1 r_{1s} \qquad (20c)$$

(6) R. W. Laity, *Ann. N. Y. Acad. Sci.*, **79**, 997 (1960).

(7) The full expression for the "thermodynamic mutual diffusion coefficient" in molten electrolytes of this type was given incorrectly in reference 3, due to an error in the statement of the condition of zero current (should be $X_{13}v_1 + X_{23}v_2 - v_3 = 0$). The correct relation is

$$\frac{D_{12}'}{RT} = \frac{z_1z_2 + X_{13}z_2z_3 + X_3z_1z_3}{z_3(z_2X_{13} + z_1X_{23})(z_3r_{12} + z_2X_{23}r_{13} + z_1X_{13}r_{23})}$$

Here subscript 3 refers to the anion. In ideal solutions $D_{12} = z_3D_{12}'$. In dilute solutions the equivalent fraction X_{23} approaches unity as X_{13} goes to 0, giving eq. 15 above.

Following the same approach as in the preceding section, we conclude from (20a) and (20b) that

$$-\frac{dC_1}{dx} \approx \frac{(X_2 r_{12} + X_- r_{1-} + X_s r_{1s})i}{z_1 FRT} \quad (21)$$

Equation 21 can be written

$$J_1 = -\frac{RT}{X_2 r_{12} + X_- r_{1-} + X_s r_{1s}} \frac{dC_1}{dx} \quad (22)$$

which defines an aqueous "ionic diffusion coefficient." It is readily shown that when X_1 is small compared with X_2 and X_s, this is identical with the self-diffusion coefficient of ion 1.

The limiting current for this case is found to be that given by eq. 17, while (19) again permits calculation of the reversible electrode potential.

Figure 3 shows the balance of forces in this system. The frictional force on the solvent requires that D_s be directed away from the surface. The concentration of electrolyte therefore decreases as the surface is approached. When both cations are of the same valence type, the anion concentration at any point is a measure of the total electrolyte concentration. Thus D_- points toward the surface. Since F_{-1} is similarly oriented, E_- must be in the opposite direction, and since the potential gradient responsible for E_- points E_2 in the same direction as F_{21}, cation 2 must experience a diffusional force away from the surface. Now we see that the diffusional forces on the two ions that comprise the supporting electrolyte are in opposite directions. In view of electroneutrality we conclude that both D_2 and D_- must be small. Due to the small concentration of species 1, F_{21} and F_{-1} must also be small compared with F_{12} and F_{1-} (eq. 20). It follows that E_2 and E_- and hence E_1 must be small, which accounts for the predominance of the diffusional force on species 1 (eq. 22).

Case IV. "Diffusion-Controlled" Oxidation–Reduction Reactions. Metal Corrosion.—This final section will show how the friction-coefficient approach can be extended to ionic reactions occurring at an interface even when no external circuit is involved. As an example, consider the dissolution of a metal like zinc or magnesium in acid solution. Although such reactions have been called "diffusion-controlled," it is evident that the ionic transport occurring in the steady-state diffusion layer consists entirely of cation fluxes: hydrogen ions move toward the surface while metal ions move away. The ordinary diffusion coefficient of the acid (hydrogen ion plus anion) in water is therefore inadequate to characterize the rate of the process.

We first seek to obtain an expression for the velocity of the reaction (as measured by J_H) in terms of the bulk concentration of H^+. If there are no metal ions present in solution initially, and if we assume that C_{H^+} becomes negligibly small at the surface, it is apparent that the concentration gradients of all three ionic species in the diffusion layer may be substantial. Thus, it is not helpful to obtain chemical potential gradients of neutral electrolytes, and we go immediately to the quasi-thermodynamic approach.

Although any three are sufficient, it is convenient this time to write all four phenomenological equations

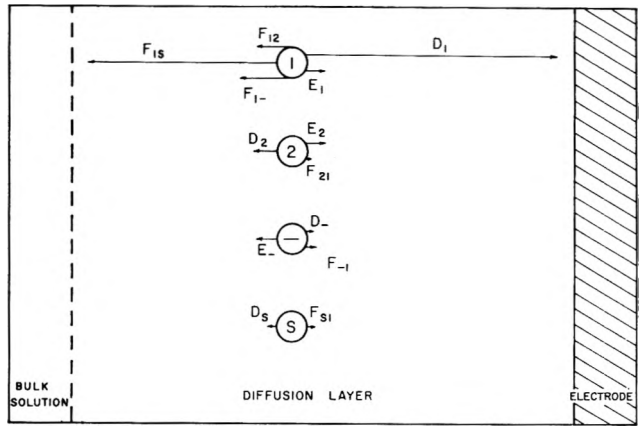

Fig. 3.—Balance of forces in presence of supporting electrolyte (Case III).

$$-\frac{d\mu_H}{dx} - F\frac{d\varphi}{dx} = X_M r_{HM}(v_H - v_M) + (X_- r_{H-} + X_s r_{Hs})v_H \quad (23a)$$

$$-\frac{d\mu_M}{dx} - 2F\frac{d\varphi}{dx} = X_H r_{HM}(v_M - v_H) + (X_- r_{M-} + X_s r_{Ms})v_M \quad (23b)$$

$$-\frac{d\mu_-}{dx} + z_- F\frac{d\varphi}{dx} = -X_H r_{H-} v_H - X_M r_{M-} v_M \quad (23c)$$

$$-\frac{d\mu_s}{dx} = -X_H r_{Hs} v_H - X_M r_{Ms} v_M \quad (23d)$$

Using the approximation of ideal behavior together with the electroneutrality condition $C_H + 2C_M = z_- C_-$, eq. 23a, b, and c can be solved simultaneously to give an expression for dC_H/dx. Putting in the condition of zero net current flux ($J_H + 2J_M = 0$) and rearranging yields a complicated expression of the form

$$-\frac{dC_H}{dx} = f(C_H, C_M, r_{HM}, r_{Hs}, r_{Ms}, r_{M-}, r_{H-})J_H \quad (24)$$

In order to integrate it is necessary not only to know the concentration dependences of all friction coefficients, but to have an expression for C_M in terms of C_H and x. The latter can be obtained by taking

$$\frac{d\mu_s}{dx} \approx \frac{RT}{X_s}\frac{dX_s}{dx} = -\frac{RT}{X_s}\left(\frac{dX_H}{dx} + \frac{dX_M}{dx} + \frac{dX_-}{dx}\right) = -\frac{RT}{X_s}\left[\left(1 + \frac{1}{z_-}\right)\frac{dX_H}{dx} + \left(1 + \frac{2}{z_-}\right)\frac{dX_M}{dx}\right]$$

substituting in eq. 23d and dividing through by V to give

$$\left(1 + \frac{1}{z_-}\right)dC_H + \left(1 + \frac{2}{z_-}\right)dC_M \approx \frac{X_s(1/2 r_{Ms} - r_{Hs})J_H}{RT}dx \quad (25)$$

Taking $X_s \approx 1$ and assuming that the constancy of ion–solvent friction coefficients found in solutions of

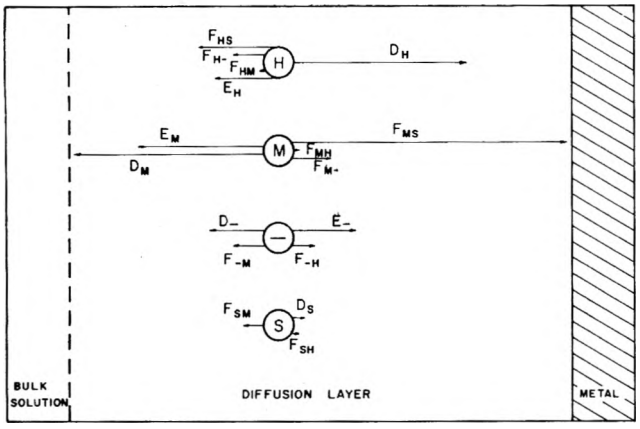

Fig. 4.—Balance of forces in diffusion controlled acidic corrosion of metals (Case IV).

separate binary electrolytes holds in the mixed system, eq. 25 can be integrated from the bulk solution to an arbitrary point x in the diffusion layer

$$\left(1 + \frac{1}{z_-}\right)(C_H - C_H^b) + \left(1 + \frac{2}{z_-}\right)(C_M - C_M^b) \approx \frac{(1/2 r_{Ms} - r_{Hs}) J_H x}{RT} \quad (26)$$

Now the value of C_M in (24) can be replaced by its equivalent from eq. 26. Putting some typical figures into the resulting expression and assuming that in the steady state C_H becomes negligibly small at the metal surface reveals that f has a substantial dependence on x. In sufficiently dilute solutions only ion–solvent friction coefficients are important, however, and with this approximation a differential equation is obtained which can be solved by straightforward methods. Since the result is rather involved, it will not be reproduced here. We have simply tried to demonstrate that the rate of this reaction can be calculated *a priori* from experimentally accessible transport parameters.[8]

In cases as mathematically complex as this one a qualitative viewpoint is particularly valuable. The balance of forces depicted in Fig. 4 can be rationalized as follows. The fact that hydrogen ions in aqueous solution are about ten times more mobile than doubly-charged metal ions implies that in spite of the hydrogen ion flux being twice that of the metal ion the net frictional force on the solvent is directed away from the interface. This must be counterbalanced by diffusional force (eq. 25d), so that the solvent becomes more dilute as the metal surface is approached. Hence the total electrolyte concentration must be greatest at the metal surface, implying that D_- is directed outward. The net frictional force on the anion also depends on the relative magnitudes of two opposing quantities, and again that due to the metal ion flux is greater. (This may be inferred from the markedly greater rate at which the conductances of electrolytes containing doubly-charged cations decrease with increasing concentration.) It follows that there must be a significant electrical force on the anion pointing toward the metal surface. This potential gradient, acting outward on the two cations, plays an important part in determining the over-all rate of the reaction. It accelerates the departure of metal ions, while retarding the influx of hydrogen ions. It is interesting to note that the existence of a substantial potential drop across the diffusion layer has been observed experimentally by a number of workers, but its effect on the rate of dissolution was apparently not realized.

A subsequent communication will elaborate the application of this approach to a time-dependent process (chronopotentiometry).

Acknowledgment.—This work is part of a program supported by the United States Atomic Energy Commission.

(8) A knowledge of δ also is required. Experiments have indicated that this quantity depends on the hydrogen evolution rate when the solution is not agitated mechanically. In any case, one could determine in advance an effective δ and its dependence on J_H by measuring the limiting hydrogen-discharge current density at various acid concentrations on a platinum electrode of similar size and shape.

TRIMETHYLALUMINUM: THERMODYNAMIC FUNCTIONS IN THE SOLID AND LIQUID STATES, 0–380°K.; VAPOR PRESSURE, HEAT OF VAPORIZATION, AND ENTROPY IN THE IDEAL GAS STATE[1]

BY J. P. MCCULLOUGH, J. F. MESSERLY, R. T. MOORE, AND S. S. TODD

Contribution No. 123 from the Thermodynamics Laboratory of the Bartlesville Petroleum Research Center, Bureau of Mines, U. S. Department of the Interior, Bartlesville, Okla.

Received September 19, 1962

This paper describes thermodynamic investigations of trimethylaluminum which were made by the Bureau of Mines as part of a program of studies of selected organic derivatives of elements in the second and third periods. From experimental measurements by low temperature calorimetry and comparative ebulliometry, the following properties of trimethylaluminum were determined: thermodynamic functions in the solid and liquid states (10–380°K.); vapor pressure (336–400°K.); heat of vaporization (298.15°K.); and entropy in the ideal gas state (298.15°K.).

The Bureau of Mines is studying the thermodynamic properties of selected organic derivatives of elements in the second and third periods. The experimental parts of these investigations include determination of accurate values of heat of formation, entropy, vapor pressure, vapor heat capacity, heat of vaporization, and related thermodynamic properties. If feasible, these results are used with spectroscopic and molecular-structure information in calculating chemical thermodynamic functions in the ideal gas state in the range 0–1500°K. and in evaluating thermochemical bond energies.

Studies of aluminum alkyls and their derivatives are in progress or planned. Results for trimethylaluminum reported in this paper include values of the thermodynamic functions in the solid and liquid states (0–380°K.), vapor pressure, heat of vaporization, and entropy in the ideal gas state at 298.15°K.

Experimental

Material.—A sample of trimethylaluminum was obtained from Ethyl Corporation, Baton Rouge, La., through the courtesy of J. R. Zietz, Jr. It was distilled in an efficient column at 65 mm. pressure; a center cut of 150 ml. was taken for thermodynamic studies. A calorimetric study of the melting point as a function of fraction of sample melted showed that the purified sample contained 0.19 mole % impurity (based on trimethylaluminum as a monomer). After the sample had been in the calorimeter at or below room temperature for about 3 months, a second determination also showed 0.19 mole % impurity. However, after the sample had been heated once to 350°K. and once to 383°K. (in the course of heat capacity measurements in a 3-day period) the impurity increased significantly to 0.25 mole %. All of the measurements below room temperature were made before the sample was heated above that temperature.

Physical Constants.—The reported values are based on the 1951 International Atomic Weights,[2] 1951 values of fundamental physical constants,[3] and the relations: 0°C. = 273.15°K. and 1 cal. = 4.184 joules (exactly). Temperature was measured with platinum resistance thermometers calibrated in terms of the International Temperature Scale[4] between 90 and 500°K. and the provisional scale[5] of the National Bureau of Standards between 11 and 90°K. All electrical and mass measurements were referred to standard devices calibrated at the National Bureau of Standards.

The calorimetric data for the solid and liquid states are based on the trimethylaluminum *monomer*, although the compound actually is almost completely *dimeric* below about 70°.[6,7] Values of thermodynamic properties for the gas state at 298.15°K. are given for the *dimer*.

Procedures.—The apparatus and techniques used for low temperature calorimetry were as previously described,[8] except that the temperature of the adiabatic shield was controlled automatically by an electronic device. A sample of 38.226 g. was sealed in a platinum calorimeter with helium (32 mm. pressure at room temperature) added to promote thermal equilibration. Measurements were made of heat capacity at saturation pressure, C_s, between 12 and 383°K., heat of fusion, ΔHm, and triple-point temperature, T_{tp}.

The vapor pressure of trimethylaluminum was measured in an ebulliometer system similar to that previously described,[9] except that a second comparison ebulliometer containing benzene was added to extend the range of measurements down to 82 mm.

Results

Low-Temperature Calorimetry.—The experimental values of heat capacity are listed in Table I. Corrections for premelting caused by impurity in the sample have not been applied to the results for the solid, but corrections for vaporization have been applied to some of the results for the liquid. The temperature increments used in the measurements were small enough to obviate curvature corrections: 10% of the absolute temperature below 50°K., 5 to 8° for the solid above 53°K., and 10° for the liquid. Above 30°K., the accuracy uncertainty generally is less than 0.2% of C_s,[10] but the accuracy at the highest temperatures may have been affected slightly by decomposition of the sample. The heat capacity of the liquid between 290 and 380°K. is represented within 0.04% by the empirical equation

$$C_s(\text{liq.}) = 23.723 + 4.6369 \times 10^{-2}T - 4.0739 \times 10^{-5}T^2 + 1.2346 \times 10^{-7}T^3, \text{ cal. deg.}^{-1}\text{ mole}^{-1} \quad (\textit{monomer}) \quad (1)$$

From four determinations, the heat of fusion was

(1) The research reported in this article was supported by the United States Air Force and the Advanced Research Projects Agency of the U. S. Department of Defense through the Air Force Office of Scientific Research of the Air Research and Development Command under Contract No. CSO-59-9, ARPA Order No. 24-59, Task 3. Reproduction in whole or in part is permitted for any purpose of the United States Government.

(2) E. Wichers, *J. Am. Chem. Soc.*, **74**, 2447 (1952). Use of the unified atomic weight scale of 1962 [*Chem. Eng. News*, Nov. 20, 1961, p. 43] would increase all molal values reported herein by 0.007%.

(3) F. D. Rossini, F. T. Gucker, Jr., H. L. Johnston, L. Pauling, and G. W. Vinal, *J. Am. Chem. Soc.*, **74**, 2699 (1952).

(4) H. F. Stimson, *J. Res. Natl. Bur. Std.*, **42**, 209 (1949).

(5) H. J. Hoge and F. G. Brickwedde, *ibid.*, **22**, 351 (1939).

(6) A. W. Laubengayer and W. F. Gilliam, *J. Am. Chem. Soc.*, **63**, 477 (1941).

(7) K. S. Pitzer and H. S. Gutowski, *ibid.*, **68**, 2204 (1946).

(8) H. M. Huffman, *Chem. Rev.*, **40**, 1 (1947); H. M. Huffman, S. S. Todd, and G. D. Oliver, *J. Am. Chem. Soc.*, **71**, 584 (1949); and D. W. Scott, D. R. Douslin, M. E. Gross, G. D. Oliver, and H. M. Huffman *ibid.*, **74**, 883 (1952).

(9) G. Waddington, J. W. Knowlton, D. W. Scott, G. D. Oliver, S. S. Todd, W. N. Hubbard, J. C. Smith, and H. M. Huffman, *ibid.*, **71**, 797 (1949).

(10) J. P. McCullough and J. F. Messerly, U. S. Bur. Mines Bull. 596 (1961).

Table I

Molal Heat Capacity of Trimethylaluminum in Cal. Deg.$^{-1}$ (Monomer)

T, °K.[a]	C_s[b]	T, °K.[a]	C_s[b]	T, °K.[a]	C_s[b]
Crystal		71.89	13.795	228.65	28.099
12.82	0.835	74.43	14.078	233.39	28.550
14.14	1.119	80.33	14.796	235.46	28.866
15.53	1.436	86.24	15.505	237.62	28.773
17.08	1.824	92.44	16.145	242.25	29.160
18.95	2.328	98.81	16.766	243.01	29.297
20.92	2.902	101.85	17.053	247.27	29.614
23.11	3.577	107.28	17.583	249.26	29.782
25.43	4.328	113.28	18.151	256.53	30.484[d]
27.65	5.050	119.59	18.742	263.64	31.272[d]
30.26	5.917	126.05	19.334	270.59	32.332[d]
33.58	6.985	132.67	19.923	277.33	34.553[d]
37.33	8.071	139.43	20.535	277.57	34.526[d]
41.58	9.118	146.28	21.133	280.57	37.321[c,d]
46.23	10.065	153.38	21.763	Liquid	
50.23	10.778	160.71	22.370	286.03	36.542[e]
50.45	10.776	167.87	22.980	295.14	37.033
51.07	10.924	175.24	23.601	300.45	37.318
53.66	11.332	182.84	24.231	305.17	37.576
54.00	11.390	190.27	24.850	314.36	38.096
58.22	12.017	197.70	25.465	318.29	38.341
59.00	12.115	205.01	26.069	331.94	39.153
63.20	12.685	212.30	26.719	342.88	39.811
64.05	12.811	219.90	27.353	354.66	40.556
67.56	13.265	223.38	27.603	366.23	41.302
68.87	13.418	227.77	28.034	377.56	42.071

[a] T is the mean temperature of each heat capacity measurement. [b] C_s is the heat capacity of the condensed phase at saturation pressure. [c] Values of C_s for crystals are *not* corrected for the effects of premelting caused by impurities. [d] The temperature increments of these measurements are in order of increasing T, °K.: 7.207, 7.053, 6.887, 6.643, 2.830, and 3.197. [e] Measured for undercooled liquid.

found to be 2101.0 ± 0.6 cal. mole^{-1} (monomer), the indicated uncertainty being the maximum deviation from the mean. Corrections for premelting due to impurity were applied in calculating this value.

The results of the first study of melting temperature, T_F, as a function of the fraction of total sample melted, F, are given in Table II. Also listed in this table are values for the triple point temperature, T_{tp}, the mole fraction of impurity in the sample, N_2*, and the cryoscopic constants,[11] A = $\Delta Hm/RT_{tp}^2$ and B = $1/T_{tp} - \Delta Cm/2\Delta Hm$, calculated from the observed results.

Table II

Trimethylaluminum: Melting Point Summary (Monomer)

T_{tp} = 288.43 ± 0.02°K.; N_2* = AF($T_{tp} - T_F$) = 0.0019; A = 0.01271 deg.$^{-1}$; B = 0.00256 deg.$^{-1}$

F	1/F	T_F, °K.	$T_{calcd.}$, °K.
0.1058	9.452	287.031	287.003
.3803	2.630[a]	288.032[a]	288.032
.5743	1.741	288.167	288.166
.8678	1.152[a]	288.255[a]	288.255
1.0000	1.000		288.278
Pure	0		288.429

[a] A straight line through these points was used to determine $T_{calcd.}$

The observed results were corrected and reduced to the molal basis, the heat capacity–temperature values were smoothed analytically, and a table of thermodynamic functions in the solid and liquid states was prepared by digital computer at the University of Oklahoma Computer Laboratory. Table III lists smoothed values of the thermodynamic properties at selected temperatures between 10 and 380°K. The values at 10°K. were computed from a Debye function for 6 degress of freedom with θ_D = 131.2°, which represents the experimental values between 14 and 21°K. Premelting corrections were applied in calculating the results in Table III.

(11) A. R. Glasgow, A. J. Streiff, and F. D. Rossini, *J. Res. Natl. Bur. Std.*, **35**, 355 (1945).

Table III

Molal Thermodynamic Properties of Trimethylaluminum (Monomer)[a]

T, °K.	$-(F_s - H°_0)/T$, cal. deg.$^{-1}$	$(H_s - H°_0)/T$, cal. deg.$^{-1}$	$H_s - H°_0$, cal.	S_s, cal. deg.$^{-1}$	C_s, cal. deg.$^{-1}$
		Crystal			
10	0.034	0.103	1.03	0.137	0.410
12	.059	.177	2.12	.236	.701
14	.094	.278	3.89	.372	1.084
16	.140	.407	6.52	.547	1.549
18	.195	.563	10.13	.758	2.066
20	.264	.741	14.82	1.005	2.629
25	.483	1.272	31.79	1.755	4.186
30	.769	1.893	56.80	2.662	5.828
35	1.111	2.571	89.97	3.682	7.411
40	1.498	3.263	130.48	4.761	8.749
45	1.923	3.933	177.00	5.856	9.829
50	2.370	4.569	228.46	6.939	10.739
60	3.307	5.729	343.7	9.036	12.255
70	4.271	6.755	472.9	11.026	13.561
80	5.233	7.681	614.5	12.914	14.757
90	6.188	8.533	768.0	14.721	15.901
100	7.128	9.319	931.9	16.447	16.878
110	8.051	10.050	1105.5	18.101	17.841
120	8.955	10.739	1288.6	19.694	18.779
130	9.840	11.393	1481.0	21.233	19.685
140	10.708	12.017	1682.3	22.725	20.584
150	11.557	12.618	1892.6	24.175	21.464
160	12.390	13.197	2111.5	25.587	22.312
170	13.208	13.758	2338.8	26.966	23.160
180	14.009	14.304	2574.6	28.313	23.996
190	14.797	14.836	2818.7	29.633	24.827
200	15.572	15.355	3071	30.93	25.655
210	16.332	15.867	3332	32.20	26.479
220	17.082	16.368	3601	33.45	27.293
230	17.822	16.857	3877	34.68	28.040
240	18.547	17.342	4162	35.89	28.840
250	19.267	17.816	4454	37.08	29.643
260	19.973	18.288	4755	38.26	30.47
270	20.675	18.752	5063	39.43	31.29
273.15	20.893	18.898	5162	39.79	31.55
280	21.366	19.214	5380	40.58	32.13
288.43	21.941	19.603	5654	41.54	32.87
		Liquid			
288.43	21.941	26.887	7755	48.83	36.68
290	22.086	26.941	7813	49.03	36.76
298.15	22.838	27.214	8114	50.05	37.19
300	23.006	27.277	8183	50.28	37.29
310	23.904	27.610	8559	51.51	37.84
320	24.787	27.938	8940	52.72	38.44
330	25.650	28.267	9328	53.92	39.04
340	26.501	28.591	9721	55.09	39.64
350	27.332	28.917	10121	56.25	40.26
360	28.153	29.239	10526	57.39	40.90
370	28.957	29.565	10939	58.52	41.55
380	29.752	29.887	11357	59.64	42.24

[a] The values tabulated are the free energy function, enthalpy function, enthalpy, entropy, and heat capacity of the condensed phases at saturation pressure.

Vapor Pressure.—The observed vapor pressure data are given in Table IV. At one atmosphere pressure

TABLE IV

THE VAPOR PRESSURE OF TRIMETHYLALUMINUM

Boiling point, °C.			p(obsd.) − p(calcd.), mm.	
Ref. compd.[a]	Trimethyl-aluminum	p(obsd.),[b] mm.	Antoine eq. 2	Cox eq. 3
21.720	63.818	81.64	−0.02	0.00
24.388	66.779	92.52	.00	.00
27.068	69.750	104.63	+ .01	.00
29.757	72.722	118.06	.03	.01
32.460	75.707	132.95	.03	.01
35.174 } 60.000 }	78.701	149.41	− .01	− .02
65	84.696	187.57	− .04	− .02
70	90.712	233.72	− .09	.00
75	96.748	289.13	− .16	+ .02
80	102.802	355.22	− .24	.02
85	108.869	433.56	− .27	.04
90	114.949	525.86	− .28	.01
95	121.039	633.99	.00	− .09
100	127.122	760.00	+ .84	.00

[a] The reference compound from 81.64 to 149.41 mm. was benzene; that from 149.41 to 2026.0 mm. was water. [b] From vapor pressure data for benzene ["Selected Values of Physical and Thermodynamic Data for Hydrocarbons and Related Substances," American Petroleum Institute Research Project 44, Carnegie Press, Pittsburgh, Pa., 1953] and for water [N. S. Osborne, H. F. Stimson, and D. C. Ginnings, *J. Res. Natl. Bur. Std.*, **23**, 261 (1939)].

the ebullition temperature of the trimethylaluminum sample was 0.026° greater than the condensation temperature, and the difference increased slowly with time. This observation and the calorimetric studies of sample purity show that trimethylaluminum decomposes slowly at temperatures above 100°, but it appears to be stable at room temperature. To avoid significant decomposition, vapor pressure measurements were not made above the normal boiling point.

The vapor pressure data were correlated by the following Antoine and Cox equations

$$\log p = 7.50746 - 1692.619/(238.681 + t) \quad (2)$$

and

$$\log (p/760) = A(1 - 400.272/T) \quad (3)$$

where

$$\log A = 0.901408 - 0.964561 \times 10^{-3} T + 1.19824 \times 10^{-6} T^2$$

In these equations, p is in mm., t is in °C., and T is in °K. As shown by the deviations between observed and calculated results (columns 4 and 5), the Antoine equation gives a poor fit to the experimental data above 90°. Laubengayer and Gilliam[6] have shown that trimethylaluminum vapor, dimeric at 70°, begins to dissociate appreciably at 100°. Apparently, the four-constant Cox equation represents results when dissociation occurs better than does the three-constant Antoine equation.

Heat of Vaporization and Entropy in the Ideal Gas State at 298.15°K.—As trimethylaluminum actually is dimeric at room temperature,[6] it is necessary to use the dimer as the basis for calculating the heat of vaporization, ΔHv, from vapor pressure data. The Cox equation in Table IV, an estimate of the second virial coefficient, $B = V(PV/RT - 1) = -4.9$ liter mole^{-1} (dimer), the density of the liquid, 0.75 g. ml.$^{-1}$,[7] and the Clapeyron equation were used to calculate $\Delta Hv_{298.15} = 10{,}010 \pm 50$ cal. mole^{-1} (dimer). This value and the value of S_s from Table III, converted to the dimer basis, were used to calculate $S°_{298.15}$ (dimer) as shown in Table V.

TABLE V

ENTROPY OF TRIMETHYLALUMINUM DIMER

S_s(liq.)	100.10
$\Delta Hv/T$	33.57
$R \ln (p/760)$	−8.23
$S_{ideal} - S_{real}$[a]	+0.01
$S_{298.15}$	125.45 ± 0.25, cal. deg.$^{-1}$ mole^{-1} (dimer)

[a] Estimated from an unpublished correlation.

Comparison with Previous Results.—No measurements of heat capacity have been reported for trimethylaluminum. Previous measurements of melting point[6,7,12] and vapor pressure[6,12,13] were made by techniques less accurate than those of the present study.

Acknowledgments.—Purification of the trimethylaluminum sample was done by C. J. Thompson and H. J. Coleman of this Center. D. R. Douslin and G. B. Guthrie assisted in some of the studies described.

(12) C. H. Bamford, D. L. Levi, and D. M. Newitt, *J. Chem. Soc.*, 468 (1946).

(13) T. Wartik and H. I. Schlesinger, *J. Am. Chem. Soc.*, **75**, 835 (1953).

CHEMICAL THERMODYNAMIC PROPERTIES AND INTERNAL ROTATION OF METHYLPYRIDINES. I. 2-METHYLPYRIDINE[1]

BY D. W. SCOTT, W. N. HUBBARD, J. F. MESSERLY, S. S. TODD, I. A. HOSSENLOPP, W. D. GOOD, D. R. DOUSLIN, AND J. P. MCCULLOUGH

Contribution No. 121 from the Thermodynamics Laboratory of the Bartlesville Petroleum Research Center, Bureau of Mines, U. S. Department of the Interior, Bartlesville, Okla.

Received September 19, 1962

Thermodynamic properties of 2-methylpyridine were measured, and the results were correlated by use of spectral and molecular-structure data to obtain values of the chemical thermodynamic properties in the ideal gas state (0 to 1500°K.). Internal rotation of the methyl group was found to be free or nearly so. Experimental studies provided the following information: values of heat capacity for the solid (12°K. to the triple point), liquid (triple point to 370°K.), and the vapor (388 to 500°K.); the triple-point temperature; the heat of fusion; thermodynamic functions for the solid and liquid (0 to 370°K.); heat of vaporization (359 to 403°K.); parameters of the equation of state; vapor pressure (353 to 442°K.); and the standard heat of formation at 298.15°K.

Thermodynamic studies of methylpyridines are being made by the Bureau of Mines as part of continuing research on organic nitrogen compounds. Results for 2-methylpyridine (α-picoline) are reported in this paper; results for 3-methylpyridine (β-picoline) are reported in the accompanying paper[2] hereafter referred to as **II**. The experimental work with 2-methylpyridine consisted of low temperature calorimetry, vapor flow calorimetry, combustion calorimetry, and comparative ebulliometry; the detailed results of this work are reported in the Experimental section. The experimental results were correlated by using spectral and molecular structure information and were used in calculating tables of chemical thermodynamic properties for the crystal, liquid, and ideal gas states. Two significant results were obtained in correlating the calorimetric data with spectral and molecular structure information. The first was an assignment of the fundamental vibrational frequencies of the 2-methylpyridine molecule, supported by accurate experimental values of the vapor heat capacity. The second was the observation that internal rotation of the methyl group is free or very nearly so. The calculations by methods of statistical mechanics will be discussed in the next section; for convenience, the calorimetric data that were used are collected in Table I.

TABLE I

OBSERVED AND CALCULATED THERMODYNAMIC PROPERTIES OF 2-METHYLPYRIDINE

	Entropy, $S°$, cal. deg.$^{-1}$ mole^{-1}			Heat capacity, $C_p°$, cal. deg.$^{-1}$ mole^{-1}	
T,° K.	Obsd.	Calcd.	T,° K.	Obsd.	Calcd.
359.35	82.66	82.60	388.25	31.02	31.03
379.48	84.28	84.20	413.20	32.91	32.90
402.54	86.10	86.05	438.20	34.72	34.70
			468.20	36.76	36.76
			500.20	38.84	38.83

$\Delta Hf°_{298.15}(\text{gas}) = 23.65 \pm 0.21$ kcal. mole^{-1}

Calculations by Methods of Statistical Mechanics

Vibrational Assignment.—An essential aspect of correlating calorimetric data by using spectral and molecular structure information is the assignment of the fundamental vibrational frequencies of the molecule. Therefore, the interpretation of the molecular spectra of 2-methylpyridine will be considered first. Bands observed in the Raman[3] and infrared[4] spectra are listed in Table II. Raman polarization data[3e] are included. The few reported Raman bands that seem to have arisen from pyridine or 2,6-dimethylpyridine impurity were ignored. Included in Table II are unpublished results for the far-infrared (grating) spectra obtained at the authors' request by Drs. F. A. Miller and W. G. Fateley of the Mellon Institute.

Rough correspondence is expected between the fundamental frequencies of the methylpyridines and of toluene, the former differing from the latter by replacement of a C—H group with a nitrogen atom. However, three frequencies that involve the replaced C—H group of toluene, a stretch, an in-plane bend, and an out-of-plane bend, can have no counterpart in each methylpyridine, and the particular C—H frequencies that have no counterpart may be different depending on which C—H group is replaced. These expectations are fulfilled, as demonstrated in Table III, in which the frequencies of toluene[5] are compared with the ones of 2-methylpyridine assigned here and the ones for 3-methylpyridine assigned in **II**. Note that the toluene frequencies 966 and 1155 cm.$^{-1}$ have no counterpart in 2-methylpyridine, whereas 842 and 1278 cm.$^{-1}$ have no counterpart in 3-methylpyridine.

The molecular spectra of 2-methylpyridine are particularly complex in three ranges of frequencies. Between 1030 and 1060 cm.$^{-1}$ occur the pyridyl group frequency at 1052 cm.$^{-1}$ and the two methyl rocking frequencies, which coincide at 1042 cm.$^{-1}$ as in isolated methyl groups on a benzene ring.[6] Between 1400 and 1500 cm.$^{-1}$ occur two pyridyl group frequencies

(1) This investigation was performed as part of American Petroleum Institute Research Project 52 on "Nitrogen Constituents of Petroleum," which is conducted at the University of Kansas in Lawrence, Kansas, and at the Bureau of Mines Petroleum Research Centers in Laramie, Wyoming, and Bartlesville, Oklahoma.

(2) D. W. Scott, W. D. Good, G. B. Guthrie, S. S. Todd, I. A. Hossenlopp, A. G. Osborn, and J. P. McCullough, *J. Phys. Chem.*, **67**, 685 (1963).

(3) (a) G. B. Bonino and R. Manzoni-Ansidei, *Mem. accad. sci. ist. Bologna, Classe sci. fis.*, [9] **1**, Sep. 7 pp. (Feb. 18, 1934); (b) S. K. K. Jatkar, *Indian J. Phys.*, **10**, 23 (1936); (c) K. W. F. Kohlrausch, A. Pongratz, and R. Seka, *Monatsh.*, **70**, 213 (1937); (d) R. Manzoni-Ansidei, *Boll. sci. fac. chim. ind. univ. Bologna*, 137 (1940); (e) E. Herz. L. Kahovec, and K. W. F. Kohlrausch, *Z. physik. Chem.*, **B53**, 124 (1943); (f) D. A. Long, F. S. Murfin, J. L. Hales, and W. Kynaston, *Trans. Faraday Soc.*, **53**, 1171 (1957); (g) American Petroleum Institute Research Project 44 at the Carnegie Institute of Technology, Catalog of Raman Spectal Data, Serial No. 252.

(4) (a) W. W. Coblentz, "Investigations of Infra-Red Spectra," Carnegie Institution of Washington, Washington, D. C., 1905; (b) J. Lecomte, *Compt. rend.*, **207**, 395 (1938); (c) H. Freiser and W. L. Glowacki, *J. Am. Chem. Soc.*, **70**, 2575 (1948); (d) D. P. Biddiscombe, E. A. Coulson, R. Handley, and E. F. G. Herington, *J. Chem. Soc.*, 1957 (1954); (e) Reference 3f; (f) American Petroleum Institute Research Project 44 at the Carnegie Institute of Technology, Catalog of Infrared Spectral Data, Serial No. 743, 2020, 2021, 2129, and 2190.

(5) D. W. Scott, G. B. Guthrie, J. F. Messerly, S. S. Todd, W. T. Berg, I. A. Hossenlopp, and J. P. McCullough, *J. Phys. Chem.*, **66**, 911 (1962).

(6) R. R. Randle and D. H. Whiffen, *J. Chem. Soc.*, 3497 (1955).

TABLE II

VIBRATIONAL SPECTRA OF 2-METHYLPYRIDINE, CM.$^{-1}$[a]

Raman liq.		Infrared liq.	Infrared gas	Interpretation
			188	
209 m	[0.68]	206	194.2 s	α'' fundamental
			200	
			350.4	
359 w		360.5	m	α' fundamental
			360.5	
			....	
403 vw		404 s	401 s	α'' fundamental
			409	
470 w		470 s	....[b]	α'' fundamental
546 m	0.43	547 m	550	α' fundamental
628 w	0.71	629 m	631	α' fundamental
709 vw			700 w	overtone (see text)
728 w		729 s		α'' fundamental
			732	
		751 vs	747 vs	α'' fundamental
			758	
			799	
799 m		799 m	803 w	α' fundamental
	0.11		809	
811 m		810 w		$2 \times 403 = 806$ A'
			820 vw	α'' fundamental or
				$194 + 629 = 823$ A''
886 w		885 w		α'' fundamental
939 w		942 w	928 w	combination (see text)
980 w		975 m	972 m	α'' fundamental
			984	
996 s	0.07	996 s	993 m	α' fundamental
			1004	
1044 w		1040 sh		α' & α'' fundamentals
			1047	
1049 s	0.08	1049 s	s	α' fundamental
			1056	
			1095	
1101 w	dp?	1100 m	w	α' fundamental
			1107	
			1142	
1147 w	0.75	1145 s	m	α' fundamental
			1155	
			1241	
1234 m	0.14	1236 m	m	α' fundamental
			1251	
1284 w				$403 + 886 = 1289$ A'
			1291	
1291 w	0.54	1292 s	1299 m	α' fundamental
			1305	
		1346 vw		α' fundamental
		1357 sh		$550 + 803 = 1353$ A'
			1381	
1374 m	0.41	1375	m	α' fundamental
			1389	
1426 w	dp?			α' fundamental
		1432 s	1436 s	α'' fundamental
		1451 s		α' fundamental
1458 w				$2 \times 729 = 1458$ A'
1479 w		1477 s	1468 s	α' fundamental
1567 m		1570 s		α' fundamental
	0.77			
1589 m		1591 s	1594 s	α' fundamental
1591 m				$360 + 1235 = 1595$ A'
1600 m				$2 \times 803 = 1606$ A'

Region above 1600 cm.$^{-1}$ omitted.

[a] Abbreviations: s, strong; m, medium; w, weak; vw, very weak; sh, shoulder. The depolarization factors of the Raman bands are listed after the intensity designations. [b] Not investigated.

and two methyl bending frequencies, some of which may interact with nearby overtones and combinations. The assignment of frequencies in this range is by no means certain, but is still satisfactory in a statistical sense for calculating thermodynamic functions. Between 2800 and 3200 cm.$^{-1}$ occur the seven C–H stretching frequencies, some of which also may interact with nearby overtones and combinations. Moreover, the infrared spectra in that region are not well resolved. No attempt at individual assignments of the C–H stretching frequencies was made, and average or conventional values were used (2950 cm.$^{-1}$ for methyl and 3050 cm.$^{-1}$ for aromatic). The C–H stretching frequencies are unimportant thermodynamically except at higher temperatures.

TABLE III

FUNDAMENTAL VIBRATIONAL FREQUENCIES OF 2-METHYLPYRIDINE COMPARED WITH CORRESPONDING FREQUENCIES OF TOLUENE AND 3-METHYLPYRIDINE, CM.$^{-1}$[a]

	Toluene	2-Methylpyridine	3-Methylpyridine	
	519	550	536	
	785	803	803	
	1003	993	1029	
	1031	1052	1041	
	1177	1148	1119	
	1209	1246	1231	
a_1	1385	1385	1381	
	1501	1468	1472	
	1611	1594	1593	
	2922	[2950]	[2950]	
	3058			
	3076	[3050 (2)]	[3050 (2)]	
	3110			
	342	355.4	336.5	a'
	623	631	625	
	1041	1042	(1041)	
	1081	1101	1104	
	1155	....	1193	
	1278	1299	....	
b_1	1329	1346	1333	
	1436	1426	1419	
	1460	1451	1452	
	1585	1568	1581	
	2954	[2950]	[2950]	
	3040			
	3090	[3050 (2)]	[3050 (2)]	
	405	401	404	
a_2	842	820	....	
	966	....	942	
	205	194.2	205.6	
	462	470	455	
	694	729	711	a''
	728	747	782	
b_2	893	886	920	
	981	972	984	
	(1041)	(1042)	(1041)	
	1456	1436	(1452)	
	2930	[2950]	[2950]	

[a] Parentheses denote frequencies used more than once; brackets denote average or conventional values.

The weak infrared band at 820 cm.$^{-1}$ observed only in the spectrum of the gas is assigned as a fundamental frequency, although there is an alternative assignment as a sum-combination. The vapor heat capacity data indicate a fundamental at about 820 cm.$^{-1}$.

As with toluene,[5] the two lowest frequencies shift significantly between the liquid and gas states (206 to 194.2 cm.$^{-1}$ and 360.5 to 355.4 cm.$^{-1}$). Using the two liquid-state frequencies instead of gas-state frequencies for calculating the entropy to compare with the observed values would introduce an error of 0.16 cal. deg.$^{-1}$ mole^{-1}. That error is as great as the uncertainty in the observed values. Customarily, when gas state values of frequencies are lacking, the liquid state values are assumed to be the same and are used instead. However, with 2-methylpyridine, that procedure gave an entropy discrepancy too large to dismiss as experimental uncertainty, and the discrepancy was explained and resolved only when Miller and Fateley's gas state

TABLE IV

THE MOLAL THERMODYNAMIC PROPERTIES OF 2-METHYLPYRIDINE[a]

T, °K.	$(F° - H°_0)/T$, cal. deg.$^{-1}$	$(H° - H°_0)/T$, cal. deg.$^{-1}$	$H° - H°_0$, kcal.	$S°$, cal. deg.$^{-1}$	$C_p°$, cal. deg.$^{-1}$	$\Delta Hf°$,[b] kcal.	$\Delta Ff°$,[b] kcal.	log Kf[b]
0	0	0	0	0	0	29.04	29.04	Infinite
273.15	− 62.25	13.43	3.669	75.68	21.89	24.05	40.77	−32.62
298.15	− 63.46	14.22	4.241	77.68	23.90	23.65	42.31	−31.02
300	− 63.55	14.28	4.286	77.83	24.05	23.62	42.43	−30.91
400	− 68.12	17.72	7.090	85.84	31.92	22.16	48.93	−26.73
500	− 72.46	21.27	10.64	93.73	38.82	21.00	55.76	−24.37
600	− 76.64	24.69	14.82	101.33	44.55	20.11	62.80	−22.88
700	− 80.69	27.87	19.51	108.56	49.27	19.44	69.97	−21.85
800	− 84.61	30.80	24.65	115.41	53.21	18.97	77.22	−21.10
900	− 88.39	33.48	30.13	121.87	56.52	18.67	84.52	−20.52
1000	− 92.05	35.93	35.93	127.98	59.34	18.53	91.85	−20.07
1100	− 95.58	38.17	41.99	133.75	61.75	18.53	99.18	−19.70
1200	− 98.99	40.22	48.27	139.21	63.82	18.63	106.50	−19.40
1300	−102.28	42.11	54.74	144.39	65.60	18.79	113.81	−19.13
1400	−105.47	43.84	61.38	149.31	67.16	19.00	121.12	−18.91
1500	−108.55	45.44	68.17	153.99	68.51	19.26	128.40	−18.71

[a] To retain internal consistency, some values are given to one more decimal place than is justified by the absolute accuracy. [b] For the reaction 6 C(c, graphite) + 7/2 H_2(g) + 1/2 N_2(g) = C_6H_7N(g).

spectrum was obtained. Confirmatory evidence for the shifts is obtained from overtone and combination bands. The sum-combination of the lowest frequency with 729 cm.$^{-1}$ shifts by about the expected amount from 940 cm.$^{-1}$ for the liquid to 928 cm.$^{-1}$ for the gas. Also the overtone of the second lowest frequency shifts by about the expected amount from 709 cm.$^{-1}$ for the liquid to 700 cm.$^{-1}$ for the gas.

Moments of Inertia.—As the structure of the 2-methylpyridine molecule has not been determined, the bond distances and angles were assumed to be the same as in related molecules. The pyridyl part of the molecule was taken to have the same dimensions as in pyridine.[7] The CH_3–C part of the molecule was taken to have tetrahedral angles and bond distances the same as in acetaldehyde.[8] For this assumed structure, the product of the principal moments of inertia is 2.137×10^{-113} g.^{3} cm.^{6} and the reduced moment of inertia for internal rotation is 5.076×10^{-40} g. cm.^{2}.

Internal Rotation.—To obtain agreement with the observed values of entropy, internal rotation in the 2-methylpyridine molecule must be considered as free or very nearly so. In the related molecule, toluene, internal rotation also is essentially free.[5] However, in toluene, a very low barrier is expected because of the sixfold symmetry of the internal rotation. In 2-methylpyridine, the internal rotation can have a threefold as well as a sixfold component. That the internal rotation is nearly free implies that the threefold component is unimportant.

Thermodynamic Functions.—The molecular parameters discussed in the previous paragraphs were used in calculating the thermodynamic functions of 2-methylpyridine. An empirical anharmonicity function[9] with ν = 1130 cm.$^{-1}$ and Z = 0.75 cal. deg.$^{-1}$ mole^{-1} was used to obtain better agreement with the vapor heat capacity data. The contributions of anharmonicity (in cal. deg.$^{-1}$ mole^{-1} at temperatures in °K.) according to this empirical function, are: for $C_p°$, 0.04 at 388.25, and 0.13 at 500.20 (the extremes of the experimental range), 0.01 at 298.15 and 1.27 at 1500; for $S°$, 0.001 at 298.15 and 0.70 at 1500. The calculated values of entropy and heat capacity are compared with the observed values in Table I. The satisfactory agreement is evidence of nearly free internal rotation and of the essential correctness of the vibrational assignment. Calculated values of the thermodynamic functions for selected temperatures up to 1500°K. are listed in columns 2–6 of Table IV.[10]

Heat, Free Energy, and Logarithm of Equilibrium Constant of Formation.—The calculated values of the thermodynamic functions, the experimental value of $\Delta Hf°_{298.15}$ (Table I), and values of the thermodynamic functions of C(c, graphite), H_2(g), and N_2(g)[11] were used in computing the values of $\Delta Hf°$, $\Delta Ff°$, and log Kf given in columns 7–9, Table IV.

Experimental

The basic experimental techniques are described in published accounts of apparatus and methods for low temperature calorimetry,[12] vapor flow calorimetry,[13] comparative ebulliometry,[14] and combustion calorimetry.[15] The reported values are based on a molecular weight of 93.124 g. mole^{-1} (1951 International Atomic Weights[16]), the 1951 values of fundamental physical constants,[17] and the relations: 0° = 273.15°K.[18] and 1 cal. = 4.184 (exactly) joules. Measurements of temperature were made with platinum resistance thermometers calibrated in terms of the International

(7) B. Bak, L. Hansen, and J. Rastrup-Andersen, *J. Chem. Phys.*, **22**, 2013 (1954).

(8) R. W. Kilb, C. C. Lin, and E. B. Wilson, Jr., *ibid.*, **26**, 1695 (1957).

(9) J. P. McCullough, H. L. Finke, W. N. Hubbard, W. D. Good, R. E. Pennington, J. F. Messerly, and G. Waddington, *J. Am. Chem. Soc.*, **76**, 2661 (1954).

(10) The vibrational and anharmonicity contributions were computed by the Bureau of Mines Electronic Computer Service, Pittsburgh, Pa.

(11) D. D. Wagman, J. E. Kilpatrick, W. J. Taylor, K. S. Pitzer, and F. D. Rossini, *J. Res. Natl. Bur. Std.*, **34**, 143 (1945).

(12) H. M. Huffman, *Chem. Rev.*, **40**, 1 (1947); H. M. Huffman, S. S. Todd, and G. D. Oliver, *J. Am. Chem. Soc.*, **71**, 584 (1949); D. W. Scott, D. R. Douslin, M. E. Gross, G. D. Oliver, and H. M. Huffman, *ibid.*, **74**, 883 (1952).

(13) G. Waddington, S. S. Todd, and H. M. Huffman, *ibid.*, **69**, 22 (1947); J. P. McCullough, D. W. Scott, R. E. Pennington, I. A. Hossenlopp, and G. Waddington, *ibid.*, **76**, 4791 (1954).

(14) G. Waddington, J. W. Knowlton, D. W. Scott, G. D. Oliver, S. S. Todd, W. N. Hubbard, J. C. Smith, and H. M. Huffman, *ibid.*, **71**, 797 (1949).

(15) W. N. Hubbard, F. R. Frow, and G. Waddington, *J. Phys. Chem.*, **65**, 1326 (1961).

(16) E. Wichers, *J. Am. Chem. Soc.*, **74**, 2447 (1952). Use of 1962 atomic weights (*Chem. Eng. News*, Nov. 20, 1961, p. 43) would increase all molal values given herein by 0.006%.

(17) F. D. Rossini, F. T. Gucker, Jr., H. L. Johnston, L. Pauling, and G. W. Vinal, *ibid.*, **74**, 2699 (1952).

(18) Some of the results originally were computed with constants and temperatures in terms of the relation 0° = 273.16°K. Only results affected significantly by the newer definition of the absolute temperature scale (H. F. Stimson, *Am. J. Phys.*, **23**, 614 (1955)] were recalculated. Therefore, numerical inconsistencies, much smaller than the accuracy uncertainty, may be noted in some of the reported data.

Temperature Scale[19] between 90 and 500°K. and the provisional scale[20] of the National Bureau of Standards between 11 and 90°K. All electrical and mass measurements were referred to standard devices calibrated at the National Bureau of Standards. The energy equivalent of the combustion calorimetric system, ε (Calor.), was determined by combustion of benzoic acid (NBS Sample 39 g).

The Material.—The sample of 2-methylpyridine used for low temperature calorimetry, comparative ebulliometry, and combustion calorimetry was part of the Standard Sample of Organic Nitrogen Compound API-USBM 52-4, prepared at the Laramie (Wyo.) Petroleum Research Center of the Bureau of Mines.[21] Samples were dried in the liquid state with calcium hydride before use in the experimental measurements and were always transferred and handled without exposure to air. The purity, determined by calorimetric studies of melting point as a function of fraction melted, was 99.90 mole %. A sample of somewhat lower purity was used for vapor flow calorimetry.

Heat Capacity in the Solid and Liquid States.—Low temperature calorimetric measurements were made with 0.56395 mole of sample sealed in a platinum calorimeter with helium (35 mm. pressure at room temperature) added to promote thermal equilibration. The temperature increments used in the measurements were small enough that corrections for non-linear variation of C_s with temperature were unnecessary. The observed values of heat capacity, C_s, are listed in Table V. Above 30°K., the accuracy uncertainty is estimated to be no greater than 0.2%. The heat capacity values for the liquid may be represented within 0.12% between 230 and 370°K. by the empirical equation

$$C_s = 42.247 - 0.13335T + 5.4547 \times 10^{-4}T^2 - 4.9479 \times 10^{-7}T^3, \text{ cal. deg.}^{-1}\text{ mole}^{-1} \quad (1)$$

TABLE V

THE MOLAL HEAT CAPACITY OF 2-METHYLPYRIDINE IN CAL. DEG.$^{-1}$

T, °K.[a]	C_s[b]	T, °K.[a]	C_s[b]	T, °K.[a]	C_s[b]
Crystal		55.51	9.740	168.99	20.622
12.37	0.810	60.43	10.503	171.77	20.844
12.65	.873	60.92	10.579	171.77	20.855
13.78	1.070	66.38	11.350	178.21	21.371
14.04	1.132	72.02	12.053	180.25	21.580[d]
15.20	1.347	77.84	12.751	184.52	21.920[d]
15.40	1.394	83.73	13.459	188.56	22.335[c,d]
16.52	1.619	86.95	13.829	Liquid	
16.97	1.722	89.68	14.099	209.90	33.881
18.11	1.972	92.76	14.393	211.97	33.911
18.87	2.144	95.38	14.647	215.52	34.017
20.10	2.424	98.35	14.913	221.09	34.159
20.84	2.592	101.41	15.191	231.03	34.487
22.24	2.928	104.28	15.459	240.87	34.881
22.85	3.071	107.77	15.769	250.59	35.294
24.56	3.493	110.54	16.005	260.64	35.776
24.94	3.584	113.91	16.289	270.98	36.321
27.24	4.132	119.89	16.785	281.19	36.883
27.26	4.133	126.18	17.301	291.24	37.456
29.89	4.759	127.54	17.399	301.16	38.051
30.38	4.875	132.78	17.814	306.24	38.363
33.64	5.623	134.91	17.973	317.13	39.043
37.20	6.403	142.07	18.512	327.84	39.725
41.16	7.208	149.05	19.074	338.37	40.413
45.29	7.988	155.85	19.601	348.75	41.089
49.89	8.809	162.49	20.110	358.95	41.828
54.97	9.652	165.22	20.323	369.01	42.442

[a] T is the mean temperature of each heat capacity measurement. [b] C_s is the heat capacity of the condensed phase at saturation pressure. [c] Values of C_s for crystal are *not* corrected for the effects of premelting caused by impurities. [d] The temperature increments of these measurements are in order of increasing T, °K.: 10.502, 6.250, and 6.127°.

Heat and Temperature of Fusion.—Three determinations of the heat of fusion, ΔHm, gave the average value 2324.1 ± 0.8 cal. mole^{-1} with the maximum deviation from the mean taken as the uncertainty. The results of a study of the melting temperature, T_F, as a function of the fraction of total sample melted, F, are listed in Table VI. Also listed in Table VI are values obtained for the triple-point temperature, T_{tp}, the mole fraction of impurity in the sample, N_2*, and the cryoscopic constants[22] $A = \Delta Hm/RT_{tp}^2$ and $B = 1/T_{tp} - \Delta Cm/2\Delta Hm$, calculated from the observed values of T_{tp}, ΔHm, and ΔCm (10.29 cal. deg.$^{-1}$ mole^{-1}).

Thermodynamic Properties in the Solid and Liquid States.—Values of thermodynamic functions for the condensed phases were computed from the calorimetric data for selected temperatures between 10 and 370°K. The results are given in Table VII. The values at 10°K. were computed from a Debye function for 4 degrees of freedom with $\theta = 112.0°$; these parameters were evaluated from the heat capacity data between 13 and 21°K. Corrections for the effects of premelting have been applied to the "smoothed" data in Table VII.

TABLE VI

2-METHYLPYRIDINE: MELTING POINT SUMMARY

T_{tp} = 206.45 ± 0.05°K.; N_2* = $AF/(T_{tp} - T_F)$ = 0.0010 ± 0.0002; A = 0.02744 deg.$^{-1}$; B = 0.00263 deg.$^{-1}$

F	1/F	T_F, °K.	$T_{calcd.}$,[b] °K.
0.1097	9.116	206.150	206.13
.2628	3.805	206.3232	206.313
.5040	1.984[a]	206.3763[a]	206.3763
.7112	1.406[a]	206.3965[a]	206.3965
.9010	1.110	206.412	206.407
1.0000	1.000		206.411
Pure	0		206.446

[a] A straight line through these points was extrapolated to 1/F = 0 to obtain T_{tp}. [b] Temperatures from the straight line of the preceding footnote.

Vapor Pressure.—The observed values of vapor pressure are listed in Table VIII. The condensation temperature of the sample was 0.008° lower than the ebullition temperature at 1 atm. pressure. The Antoine and Cox equations selected to represent the results are

$$\log p = 7.03202 - 1415.494/(t + 211.598) \quad (2)$$

and

$$\log (p/760) = A(1 - 402.536/T) \quad (3)$$

$$\log A = 0.861242 - 6.5320 \times 10^{-4}T + 5.6758 \times 10^{-7}T^2$$

In these equations, p is in mm., t is in °C., and T is in °K. The observed and calculated vapor pressures for both the Antoine and Cox equations are compared in Table VIII. The normal boiling point is 129.39° (402.54°K.).

Heat of Vaporization, Vapor Heat Capacity, and Effects of Gas Imperfection.—The experimental values of the heat of vaporization and vapor heat capacity are listed in Tables IX and X. The estimated accuracy uncertainties of the values of ΔHv and $C_p°$ are 0.1 and 0.2%, respectively. The heat of vaporization may be represented by the empirical equation

$$\Delta Hv = 11213 + 2.861T - 2.290 \times 10^{-2}T^2, \text{ cal. mole}^{-1}\ (359\text{–}402°\text{K.}) \quad (4)$$

The effects of gas imperfection were correlated by the procedure described in an earlier paper.[23] The empirical equation for B, the second virial coefficient in the equation of state, $PV = RT \cdot (1 + B/V)$, is

$$B = -189 - 39.76 \exp(1300/T), \text{ cc. mole}^{-1}\ (359\text{–}500°\text{K.}) \quad (5)$$

(19) H. F. Stimson, *J. Res. Natl. Bur. Std.*, **42**, 209 (1949).
(20) H. J. Hoge and F. G. Brickwedde, *ibid.*, **22**, 351 (1939).
(21) R. V. Helm, W. J. Lanum, G. L. Cook, and J. S. Ball, *J. Phys. Chem.*, 62, 858 (1958).
(22) A. R. Glasgow, A. J. Streiff, and F. D. Rossini, *J. Res. Natl. Bur. Std.*, **35**, 355 (1945).
(23) J. P. McCullough, H. L. Finke, J. F. Messerly, R. E. Pennington, I. A. Hossenlopp, and G. Waddington, *J. Am. Chem. Soc.*, **77**, 6119 (1955).

TABLE VII

THE MOLAL THERMODYNAMIC PROPERTIES OF 2-METHYLPYRIDINE IN THE SOLID AND LIQUID STATES[a]

T, °K.	$-(F_s - H°_0)/T$, cal. deg.$^{-1}$	$(H_s - H°_0)/T$, cal. deg.$^{-1}$	$H_s - H°_0$, cal.	S_s, cal. deg.$^{-1}$	C_s, cal. deg.$^{-1}$
			Crystal		
10	0.036	0.110	1.097	0.146	0.435
15	.123	.357	5.355	.480	1.307
20	.274	.728	14.558	1.002	2.397
25	.484	1.180	29.500	1.664	3.593
30	.743	1.682	50.46	2.425	4.781
35	1.042	2.207	77.26	3.249	5.923
40	1.371	2.739	109.56	4.110	6.978
45	1.724	3.264	146.87	4.988	7.930
50	2.094	3.776	188.78	5.870	8.826
60	2.870	4.754	285.26	7.624	10.438
70	3.672	5.668	396.7	9.340	11.799
80	4.485	6.510	520.7	10.995	13.012
90	5.298	7.297	656.7	12.595	14.128
100	6.104	8.028	802.8	14.132	15.070
110	6.902	8.709	957.9	15.611	15.956
120	7.688	9.348	1121.7	17.036	16.796
130	8.460	9.952	1293.7	18.412	17.598
140	9.219	10.525	1473.5	19.744	18.360
150	9.964	11.073	1660.9	21.037	19.121
160	10.695	11.600	1855.9	22.295	19.881
170	11.414	12.109	2058.5	23.523	20.646
180	12.120	12.605	2268.8	24.725	21.413
190	12.815	13.089	2486.8	25.904	22.198
200	13.499	13.564	2712.8	27.063	22.999
206.45	13.934	13.868	2863.1	27.802	23.52
			Liquid		
206.45	13.934	25.125	5187.2	39.059	33.81
210	14.363	25.272	5307	39.63	33.88
220	15.548	25.668	5647	41.21	34.12
230	16.697	26.043	5989	42.74	34.45
240	17.813	26.401	6336	44.21	34.84
250	18.898	26.747	6686	45.64	35.27
260	19.953	27.084	7041	47.03	35.74
270	20.982	27.414	7401	48.39	36.26
273.15	21.302	27.517	7516	48.81	36.43
280	21.985	27.740	7767	49.72	36.81
290	22.963	28.063	8138	51.02	37.38
298.15	23.746	28.324	8445	52.07	37.86
300	23.921	28.383	8514	52.30	37.97
310	24.856	28.703	8897	53.55	38.59
320	25.772	29.022	9286	54.79	39.22
330	26.671	29.340	9682	56.01	39.86
340	27.552	29.659	10084	57.21	40.52
350	28.416	29.979	10492	58.39	41.19
360	29.265	30.300	10908	59.56	41.87
370	30.099	30.622	11330	60.72	42.52

[a] The values tabulated are the free energy function, enthalpy function, enthalpy, entropy, and heat capacity of the condensed phases at saturation pressure.

Observed values of B and $-T(d^2B/dT^2) = \lim_{P\to 0}(\partial C_p/\partial P)_T$ and the values calculated from eq. 5 are compared in Tables IX and X.

The heat of vaporization at 298.15°K. was calculated by extrapolation of eq. 4 (10.03 kcal. mole^{-1}), by use of the Clapeyron equation with eq. 3 and 5 (10.12 kcal. mole^{-1}), and by use of a thermodynamic network with the thermodynamic functions of Table IV (10.14 kcal. mole^{-1}). The last value was selected as most reliable. By use of eq. 5, the standard heat of vaporization (to the hypothetical ideal gas) is calculated to be 0.01 kcal. mole^{-1} greater than the heat of vaporization (to the real gas); thus $\Delta Hv°_{298.15} = 10.15$ kcal. mole^{-1}.

Entropy in the Ideal Gas State.—The entropy in the ideal gas state at 1 atm. pressure was calculated as shown in Table XI.

TABLE VIII

VAPOR PRESSURE OF 2-METHYLPYRIDINE

Boiling point, °C. Water	Boiling point, °C. 2-Methyl pyridine	p(obsd.),[a] mm.	p(obsd.) − p(calcd.), mm. Antoine eq. 2	p(obsd.) − p(calcd.), mm. Cox eq. 3
60.000	79.794	149.41	+0.02	0.00
65	85.853	187.57	− .04	− .04
70	91.942	233.72	− .02	− .01
75	98.074	289.13	+ .01	+ .03
80	104.252	355.22	+ .01	+ .03
85	110.472	433.56	+ .02	+ .03
90	116.736	525.86	− .01	.00
95	123.038	633.99	+ .02	+ .03
100	129.387	760.00	− .03	− .03
105	135.773	906.06	+ .03	+ .05
110	142.207	1074.6	.0	.0
115	148.683	1268.0	− .1	.0
120	155.201	1489.1	− .2	− .1
125	161.761	1740.8	− .1	− .2
130	168.356	2026.0	+ .2	.0

[a] From the vapor pressure data for water given by N. S. Osborne, H. F. Stimson, and D. C. Ginnings, *J. Res. Natl. Bur. Std.*, **23**, 261 (1939).

TABLE IX

THE MOLAL HEAT OF VAPORIZATION AND SECOND VIRIAL COEFFICIENT OF 2-METHYLPYRIDINE

T, °K.	P, atm.	ΔHv, cal.	B, cc. Obsd.	B, cc. Calcd.[a]
359.35	0.250	9284 ± 3[b]	−1673	−1670
379.48	0.500	9001 ± 1	−1399	−1411
402.54	1.000	8654 ± 4	−1204	−1194

[a] Calculated from eq. 5. [b] Maximum deviation from the mean of three or more determinations.

TABLE X

THE MOLAL VAPOR HEAT CAPACITY OF 2-METHYLPYRIDINE IN CAL. DEG.$^{-1}$

T, °K.	388.25	413.20	438.20	468.20	500.20
C_p (1.000 atm.)		33.792	35.351	37.229	39.200
C_p (0.500 atm.)	31.686	33.343			
C_p (0.250 atm.)	31.345	33.111	34.871	36.876	38.926
$C_p°$	31.02	32.91	34.72	36.76	38.84
$-T(d^2B/dT^2)$, obsd.[a]	1.28	0.83	0.60	0.44	0.35
$-T(d^2B/dT^2)$, calcd.[b]	1.26	.85	.63	.44	.31

[a] Units: cal. deg.$^{-1}$ mole^{-1} atm.$^{-1}$. [b] Calculated from eq. 5.

TABLE XI

THE MOLAL ENTROPY OF 2-METHYLPYRIDINE IN THE IDEAL GAS STATE IN CAL. DEG.$^{-1}$

T, °K.	359.36	379.49	402.55
S_s(liq.)[a]	59.49	61.80	64.40
$\Delta Hv/T$	25.84	23.72	21.50
$S^* - S$[b]	0.09	0.14	0.20
$R \ln P$[c]	−2.76	−1.38	0.00
$S°$(obsd.) ± 0.17[d]	82.66	84.28	86.10

[a] By interpolation in Table VII or extrapolation by use of eq. 1. [b] The entropy in the ideal gas state less that in the real gas state, calculated from eq. 5. [c] Entropy of compression, calculated from eq. 3. [d] Estimated accuracy uncertainty.

Heat of Combustion and Formation.—Results of a typical determination of the heat of combustion of 2-methylpyridine are given in detail in Table XII. The symbols and abbreviations are those of Hubbard, Scott, and Waddington.[24] In three experiments, the amount of reaction determined from the mass of sample was checked by determining the amount of CO_2 in the

(24) W. N. Hubbard, D. W. Scott, and G. Waddington, "Experimental Thermochemistry," F. D. Rossini, Ed., Interscience Publishers, Inc., New York, N. Y., 1956, Chapter 5, pp. 75–128.

products. The CO_2 recovery was 100.04 ± 0.01% of that calculated from the mass of sample. Results of six acceptable determinations are summarized in Table XIII along with derived results calculated by using literature values of the heat of formation of carbon dioxide and water and the entropy of graphite, hydrogen, and nitrogen.[11]

Comparison with Earlier Work.—The results reported here are compared with those of earlier investigators in the following paper (II).[2]

TABLE XII

SUMMARY OF A TYPICAL COMBUSTION CALORIMETRIC EXPERIMENT WITH 2-METHYLPYRIDINE[a]

m' (2-methylpyridine), g.	.84185
$\Delta t_c = t_f - t_i - \Delta t_{cor}$, deg.	2.00078
ε(Calor.) $(-\Delta t_c)$, cal.	−7788.30
ε(Cont.)$(-\Delta t_c)$,[b] cal.	−9.70
ΔE_{ign}, cal.	2.70
ΔE^f_{dec} (HNO_3 + HNO_2), cal.	13.16
ΔE, corr. to st. states,[c] cal.	3.81
$-m''\Delta Ec°/M$ (auxiliary oil), cal.	384.78
$-m'''\ \Delta Ec°/M$ (fuse), cal.	15.42
$m'\Delta Ec°/M$ (2-methylpyridine), cal.	−7378.13
$\Delta Ec°/M$ (2-methylpyridine), cal. g.$^{-1}$	−8764.19

[a] Auxiliary data: ε(Calor.) = 3892.63 cal. deg.$^{-1}$; V(Bomb) = 0.344 l.; $\Delta Ec°/M$(auxiliary oil) = −10983.7 cal. g.$^{-1}$; $\Delta Ec°/M$(fuse) = −3923 cal. g.$^{-1}$. [b] ε^i(Cont.)$(t_i - 25°) + \varepsilon^f$(Cont.)$(25° - t_f + \Delta t_{corr.})$. [c] Items 81–85, 87–90, 93, and 94 of the computation form of ref. 24.

TABLE XIII

SUMMARY OF RESULTS OF COMBUSTION CALORIMETRY AT 298.15°K.

$\Delta Ec°/M$ (2-Methylpyridine), cal. g.$^{-1}$:

−8762.87, −8766.10, −8764.19, −8763.05, −8765.52, −8764.99

Mean and std. dev.: −8764.45 ± 0.54

Derived Results for the Liquid State[a]:

$\Delta Ec°$, kcal. mole^{-1}	−816.18 ± 0.16
$\Delta Hc°$, kcal. mole^{-1}	−816.92 ± 0.16
$\Delta Hf°$, kcal. mole^{-1}	13.50 ± 0.18
$\Delta Sf°$, cal. deg.$^{-1}$ mole^{-1}	− 88.22
$\Delta Ff°$, kcal. mole^{-1}	39.80
log Kf	− 29.18

[a] With uncertainty interval equal to twice the final "over-all" standard deviation [F. D. Rossini, ref. 24, Chapter 14, pp. 297–320].

Acknowledgment.—The assistance of W. T. Berg, J. P. Dawson, F. R. Frow, and T. C. Kincheloe in some of the experimental measurements is gratefully acknowledged. The authors thank Drs. F. A. Miller and W. G. Fateley of the Mellon Institute for obtaining the far-infrared (grating) spectrum.

CHEMICAL THERMODYNAMIC PROPERTIES AND INTERNAL ROTATION OF METHYLPYRIDINES. II. 3-METHYLPYRIDINE[1]

BY D. W. SCOTT, W. D. GOOD, G. B. GUTHRIE, S. S. TODD, I. A. HOSSENLOPP, A. G. OSBORN, AND J. P. MCCULLOUGH

Contribution No. 122 from the Thermodynamics Laboratory of the Bartlesville Petroleum Research Center, Bureau of Mines, U.S. Department of the Interior, Bartlesville, Okla.

Received September 19, 1962

Thermodynamic properties of 3-methylpyridine were measured and the results were correlated by use of spectral and molecular-structure data to obtain values of the chemical thermodynamic properties in the ideal gas state (0 to 1500°K.). Internal rotation of the methyl group was found to be free or nearly so. Experimental studies provided the following information: values of heat capacity for the solid (12°K. to the triple point), liquid (triple point to 393°K.), and the vapor (404 to 500°K.); the triple point temperature; the heat of fusion; thermodynamic functions for the solid and liquid (0 to 390°K.); heat of vaporization (372 to 417°K.); parameters of the equation of state; vapor pressure (347 to 458°K.); and the standard heat of formation at 298.15°K.

The thermodynamic studies of 3-methylpyridine (β-picoline) reported in this paper parallel the ones of 2-methylpyridine reported in the accompanying paper,[2] hereafter referred to as I. Results of the same kinds of experimental work were correlated by use of molecular data and used in calculating tables of chemical thermodynamic properties. The calorimetric data that were used in these calculations are collected in Table I. As in I, an assignment of the fundamental vibrational frequencies was obtained, and internal rotation was found to be free or nearly so.

The order of presentation here is the same as in I; the calculations by methods of statistical mechanics are discussed in the next section, and the detailed experimental results are presented in the Experimental section.

TABLE I

OBSERVED AND CALCULATED THERMODYNAMICS PROPERTIES OF 3-METHYLPYRIDINE

	Entropy, $S°$, cal. deg.$^{-1}$ mole^{-1}			Heat capacity, $C_p°$, cal. deg.$^{-1}$ mole^{-1}	
T, °K.	Obsd.	Calcd.	T, °K.	Obsd.	Calcd.
372.45	83.71	83.61	404.20	32.14	32.13
393.36	85.34	85.28	429.20	33.93	33.96
417.29	87.18	87.17	452.20	35.60	35.59
			475.20	37.14	37.14
			500.20	38.74	38.75

$Hf°_{298.15}$(gas) = 25.37 ± 0.17 kcal. mole^{-1}

Calculations by Methods of Statistical Mechanics

Vibrational Assignment.—As in I, the interpretation of the molecular spectra will be considered first. Bands observed in the Raman[3] and infrared[4] spectra

(1) This investigation was performed as part of American Petroleum Institute Research Project 52 on "Nitrogen Constituents of Petroleum," which is conducted at the University of Kansas in Lawrence, Kansas, and at the Bureau of Mines Petroleum Research Centers in Laramie, Wyoming, and Bartlesville, Oklahoma.

(2) D. W. Scott, W. N. Hubbard, J. F. Messerly, S. S. Todd, I. A. Hossenlopp, W. D. Good, D. R. Douslin, and J. P. McCullough, *J. Phys. Chem.*, **67**, 680 (1963).

(3) (a) E. Herz, L. Kahovec, and K. W. F. Kohlrausch, *Z. physik. Chem.*, **B53**, 124 (1943); (b) D. A. Long, F. S. Murfin, J. L. Hales, and W. Kynaston, *Trans. Faraday Soc.*, **53**, 1171 (1957).

are listed in Table II. Raman polarization data[3a] are included. Results of four investigations of the Raman spectrum reported before 1943 were ignored; the samples used in those earlier investigations are now known to have been badly contaminated, mostly with 2,6-dimethylpyridine. Included in Table II are unpublished results for the far-infrared (grating) spectra obtained at the authors' request by Drs. F. A. Miller and W. G. Fateley of the Mellon Institute.

TABLE II

VIBRATIONAL SPECTRA OF 3-METHYLPYRIDINE, CM.$^{-1}$[a]

Raman liq.		Infrared liq.	Infrared gas	Interpretation
			196	
217 m	0.88	216	205.6 m	α'' fundamental
			....	
			328	
338 w	dp ?	340.8 m	336.5 w	α' fundamental
			....	
			....	
398 w		399 s	404 s	α'' fundamental
			....	
454 w		456 m	....[b]	α'' fundamental
535 m	.62?	536 m		α' fundamental
575 vw				?
627 m	.87	629 s	625	α' fundamental
			702	
710 w		708 s	711 m	α'' fundamental
			718	
		723 sh	726 sh	?
			776	
		785 s	782 s	α'' fundamental
			790	
795 m	0.15			Fermi resonance
810 m				α' fundamental & $2 \times 399 = 798$ A'
919 vw		920 w	920 w	α'' fundamental
942 vw		942 w		α'' fundamental
984 w		986 m	984 w	α'' fundamental
			1023	
1025 m		1028 s	m	α' fundamental
			1035	
1035 w				
1041 s	0.13	1041 s		α' & α'' fundamentals
1046 w				
			1097 w	
1102 w		1104 s		α' fundamental
			1111	
1124 w		1124 s	1119 w	α' fundamental
			1130	
1154 w	dp?	1163 sh		$536 + 625 = 1161$ A'
			1186	
1189 m		1187 s	1193 w	α' fundamental
			1198	
1227 m	0.28	1226 m	1231 w	α' fundamental
		1245 w		$216 + 1026 = 1242$ A''
		1330 m		Fermi resonance
1337 w			1333 w	α' fundamental &
		1341 m		$536 + 803 = 1339$ A'
1380 m	0.45	1382 s	1381 sh	α' fundamental
1409 w		1411 s	1419 m	α' fundamental
1453 w		1452 s		α' & α'' fundamentals
1477 w		1478 s	1472 m	α' fundamental
1575 m	0.62	1576 s	1581 m	α' fundamental
1594 m		1593 s		α' fundamental

Region above 1600 cm.$^{-1}$ omitted.

[a] Abbreviations: s, strong; m, medium; w, weak; vw, very weak; sh, shoulder. The depolarization of the Raman bands are listed after the intensity designation. [b] Not investigated.

The interpretation of the spectra of 3-methylpyridine was very similar to that for 2-methylpyridine, and most of the discussion in I applies. The fundamental vibrational frequencies assigned here are given in I, Table III. Shifts of the two lowest frequencies between liquid and gas states also are found for 3-methylpyridine (216 to 205.6 cm.$^{-1}$ and 340.8 to 336.5 cm.$^{-1}$); the thermodynamic consequences of these shifts are about the same as those for 2-methylpyridine.

Moments of Inertia and Internal Rotation.—For the same assumptions about the molecular structure as were made in I, the product of the principal moments of inertia of the 3-methylpyridine molecular is calculated to be 2.210×10^{-113} g.^{3} cm.^{6} and the reduced moment of inertia for internal rotation to be 5.076×10^{-40} g. cm.^{2}. Again, internal rotation must be considered free or very nearly so to obtain agreement with the observed values of entropy. The environment of the methyl group in 3-methylpyridine is intermediate between that of the methyl group in toluene and in 2-methylpyridine. As internal rotation is very nearly free in both the other molecules, the result for 3-methylpyridine is the expected one.

Thermodynamic Properties.—Thermodynamic functions of 3-methylpyridine were calculated with the values of molecular parameters just given. The empirical anharmonicity function used to obtain better agreement with the vapor heat capacity data had $\nu = 1130$ cm.$^{-1}$ and $Z = 0.65$ cal. deg.$^{-1}$ mole^{-1}. This function contributes 0.9 as much to the thermodynamic functions as the function used for 2-methylpyridine in I (for $C_p°$ at the extremes of the experimental range, 404.20 and 500.20°K., 0.04 and 0.11 cal. deg.$^{-1}$ mole^{-1}, respectively). The calculated values of entropy and heat capacity are compared with the observed values in Table I. The satisfactory agreement is evidence for nearly free internal rotation and for the essential correctness of the vibrational assignment. Calculated values of the thermodynamic functions for selected temperatures up to 1500°K. are listed in columns 2–6 of Table III.

Values of $\Delta Hf°$, $\Delta Ff°$, and log Kf were calculated for 3-methylpyridine as described in I. The results are given in columns 7–9, Table III.

Experimental

Methods and Material.—The experimental methods were the same as those in I. The sample of 3-methylpyridine used for all studies except vapor flow calorimetry was Standard Sample of Organic Nitrogen Compound API-USBM 52-7, prepared at the Laramie (Wyo.) Petroleum Research Center of the Bureau of Mines.[5] The purity was 99.88 mole %. A sample of somewhat lower purity was used for vapor flow calorimetry.

Low Temperature Calorimetry.—The observed values of heat capacity, C_s, are listed in Table IV, the results of a study of the melting temperature as a function of the fraction melted in Table V, and values of thermodynamic functions for the condensed phases in Table VI. The empirical equation for the heat capacity of the liquid

$$C_s = 47.514 - 0.17283T + 6.4766 \times 10^{-4}T^2 - 5.8958 \times 10^{-7}T^3, \text{ cal. deg.}^{-1} \text{ mole}^{-1} \quad (1)$$

fits the observed values within 0.05% between 257 and 388°K. The average of triplicate determinations of the heat of fusion was 3389.2 ± 0.1 cal. mole^{-1} with the maximum deviation from the mean taken as the uncertainty. The Debye function used to compute values of the thermodynamic functions at 10°K. was for 5.5 degrees of freedom with $\theta = 134.3°$; these parameters were evaluated from the heat capacity data between 12 and 20°K. The smoothed data in Table VI have been corrected for the effects of premelting.

(4) (a) J. Lecomte, *Compt. rend.*, **207**, 395 (1938); (b) C. G. Cannon and G. B. B. M. Sutherland, *Spectrochim. Acta*, **4**, 373 (1951); (c) D. P. Biddiscombe, E. A. Coulson, R. Handley, and E. F. G. Herington, *J. Chem. Soc.*, 1957 (1954); (d) Reference 3b; (e) American Petroleum Institute Research Project 44 at the Carnegie Institute of Technology, Catalog of Infrared Spectral Data, Serial No. 2191, 2204, and 2205; (f) Manufacturing Chemists Association Research Project, *ibid.*, Serial No. 1 and 2.

(5) J. S. Ball, C. R. Ferrin, and R. V. Helm, unpublished.

TABLE III

THE MOLAL THERMODYNAMIC PROPERTIES OF 3-METHYLPYRIDINE[a]

T, °K.	$(F° - H°_0)/T$, cal. deg.$^{-1}$	$(H° - H°_0)/T$, cal. deg.$^{-1}$	$H° - H°_0$, kcal.	$S°$, cal. deg.$^{-1}$	$C_p°$, cal. deg.$^{-1}$	$\Delta Hf°$,[b] kcal.	$\Delta Ff°$,[b] kcal.	log Kf[b]
0	0	0	0	0	0	30.76	30.76	Infinite
273.15	− 62.26	13.42	3.665	75.68	21.80	25.77	42.49	−33.99
298.15	− 63.47	14.20	4.235	77.67	23.80	25.37	44.03	−32.28
300	− 63.56	14.26	4.280	77.82	23.94	25.34	44.15	−32.16
400	− 68.12	17.68	7.072	85.80	31.82	23.87	50.64	−27.67
500	− 72.45	21.22	10.61	93.67	38.74	22.70	57.48	−25.12
600	− 76.62	24.63	14.78	101.25	44.47	21.80	64.52	−23.50
700	− 80.66	27.82	19.47	108.48	49.19	21.13	71.70	−22.38
800	− 84.57	30.74	24.59	115.31	53.12	20.65	78.95	−21.57
900	− 88.34	33.42	30.07	121.76	56.43	20.34	86.26	−20.95
1000	− 92.00	35.86	35.86	127.86	59.23	20.19	93.60	−20.46
1100	− 95.52	38.10	41.91	133.62	61.62	20.18	100.94	−20.06
1200	− 98.92	40.15	48.17	139.07	63.68	20.26	108.28	−19.72
1300	−102.21	42.03	54.63	144.24	65.46	20.41	115.62	−19.44
1400	−105.39	43.76	61.26	149.15	67.00	20.61	122.94	−19.19
1500	−108.47	45.35	68.03	153.82	68.34	20.85	130.26	−18.98

[a] To retain internal consistency, some values are given to one more decimal place than is justified by the absolute accuracy. [b] For the reaction 6C(c, graphite) + 7/2 H_2(g) + 1/2 N_2(g) = C_6H_7N(g).

TABLE IV

MOLAL HEAT CAPACITY OF 3-METHYLPYRIDINE IN CAL. DEG.$^{-1}$

T, °K.[a]	C_s[b]	T, °K.[a]	C_s[b]	T, °K.[a]	C_s[b]
Crystal		50.57	9.549	214.51	23.188
11.94	0.591	55.45	10.332	221.71	23.849
12.43	.657	61.15	11.145	226.84	24.345
13.35	.808	66.78	11.830	228.77	24.527
13.70	.876	72.70	12.430	234.58	25.187
14.79	1.077	78.95	13.035	235.68	25.319
15.22	1.176	85.19	13.593	242.35	26.561[c]
16.52	1.459	85.77	13.665	Liquid	
17.00	1.562	91.81	14.125	257.52	35.890
18.55	1.934	98.07	14.564	264.80	36.212
18.92	2.018	104.27	14.998	271.36	36.518
20.56	2.443	110.00	15.400	280.04	36.954
20.78	2.529	116.50	15.851	289.85	37.471
22.53	2.968	123.15	16.308	299.52	38.013
22.89	3.067	130.00	16.780	300.24	38.050
24.73	3.575	136.67	17.238	310.42	38.633
25.40	3.766	143.46	17.710	316.65	39.026
27.29	4.287	150.38	18.192	326.20	39.590
28.13	4.514	157.15	18.678	336.52	40.233
30.20	5.075	164.18	19.198	347.12	40.890
31.06	5.305	171.44	19.737	357.57	41.549
34.10	6.100	178.54	20.279	367.85	42.228
37.25	6.876	185.48	20.808	377.97	42.880
40.98	7.717	192.64	21.372	387.93	43.511
45.58	8.642	199.99	21.983		
50.13	9.475	207.18	22.599		

[a] T is the mean temperature of each heat capacity measurement. [b] C_s is the heat capacity of the condensed phase at saturation pressure. [c] Values of C_s for crystal are *not* corrected for the effects of premelting caused by impurities.

TABLE V

3-METHYLPYRIDINE: MELTING POINT SUMMARY

T_{tp} = 255.01 ± 0.05°K.; N_2* = AF(T_{tp} − T_F) = 0.0012 ± 0.0002; A = 0.02623 deg.$^{-1}$; B = 0.00258 deg.$^{-1}$

F	1/F	T_F, °K.	$T_{calcd.}$, °K.[a]
0.1530	6.536	254.7190	254.7172
.3430	2.915	254.8775	254.8786
.6691	1.495	254.9387	254.9410
.9052	1.105	254.9599	254.9580
1.0000	1.000		254.9626
Pure	0		255.006[b]

[a] Temperatures from a straight line through observed results. [b] The triple-point temperature.

Vapor Pressure.—The observed values of vapor pressure are listed in Table VII. The condensation temperature of the sample was 0.001° lower than the ebullition temperature at 1 atm. pressure. The Antoine and Cox equations selected to represent the results are

$$\log p = 7.05375 - 1484.208/(211.532 + t) \quad (2)$$

and

$$\log (p/760) = A(1 - 417.286/T) \quad (3)$$

$$\log A = 0.854888 - 6.05879 \times 10^{-4}T + 5.03864 \times 10^{-7}T^2$$

In these equations, p is in mm., t is in °C., and T is in °K. Observed and calculated values are compared in Table VII. The normal boiling point is 144.14° (417.29°K.).

Heat of Vaporization, Vapor Heat Capacity, and Effects of Gas Imperfection.—The experimental values of the heat of vaporization and vapor heat capacity are given in Tables VIII and IX. The heat of vaporization may be represented by the empirical equation

$$\Delta Hv = 13264 - 5.3443T - 1.2068 \times 10^{-2}T^2 \text{ cal. mole}^{-1} \text{ (372–417°K.)} \quad (4)$$

The empirical equation for B, the second virial coefficient in the equation of state, $PV = RT(1 + B/V)$, obtained as in I, is

$$B = -620 - 21.0 \exp(1500/T) \text{ cc. mole}^{-1} \text{(372–500°K.)} \quad (5)$$

Observed values of B and $-T(d^2B/dT^2) = \lim_{P\to 0} (\partial C_p/\partial P)_T$ and the ones calculated from eq. 5 are compared in Tables VIII and IX.

The heat of vaporization at 298.15°K. was calculated by extrapolation with eq. 4 (10.60 kcal. mole^{-1}), by use of the Clapeyron equation with eq. 3 and 5 (10.59 kcal. mole^{-1}), and by use of a thermodynamic network with the thermodynamic functions of Table III (10.61 kcal. mole^{-1}). The last value was selected as most reliable. By use of eq. 5, the standard heat of vaporization (to the hypothetical ideal gas) is calculated to be 0.01 kcal. mole^{-1} greater than the heat of vaporization (to the real gas); thus $\Delta Hv°_{298.15}$ = 10.62 kcal. mole^{-1}.

Entropy in the Ideal Gas State.—The entropy in the ideal gas state at 1 atm. pressure was calculated as shown in Table X.

Heat of Combustion and Formation.—Results of a typical determination of the heat of combustion of 3-methylpyridine are given in detail in Table XI. In three experiments in which CO_2 was determined in the products, the recovery was 100.00 ± 0.01% of the amount calculated from the mass of sample. Results of

TABLE VI

THE MOLAL THERMODYNAMIC PROPERTIES OF 3-METHYLPYRIDINE IN THE SOLID AND LIQUID STATES[a]

T, °K.	$-(F_s - H°_0)/T$, cal. deg.$^{-1}$	$(H_s - H°_0)/T$, cal. deg.$^{-1}$	$H_s - H°_0$, cal.	S_s, cal. deg.$^{-1}$	C_s, cal. deg.$^{-1}$
			Crystal		
10	0.029	0.088	0.88	0.117	0.351
12	.051	.151	1.81	.202	.595
14	.080	.237	3.32	.317	.925
16	.119	.348	5.57	.467	1.339
18	.168	.483	8.70	.651	1.801
20	.226	.641	12.81	.867	2.318
25	.418	1.107	27.68	1.525	3.653
30	.666	1.647	49.40	2.313	5.023
35	.963	2.223	77.81	3.186	6.326
40	1.298	2.811	112.45	4.109	7.504
45	1.663	3.391	152.59	5.054	8.532
50	2.049	3.952	197.59	6.001	9.450
60	2.864	5.002	300.1	7.866	10.990
70	3.707	5.946	416.2	9.653	12.166
80	4.557	6.784	542.7	11.341	13.132
90	5.401	7.538	678.4	12.939	13.985
100	6.231	8.219	821.9	14.450	14.700
110	7.044	8.840	972.4	15.884	15.400
120	7.838	9.416	1129.9	17.254	16.092
130	8.613	9.956	1294.3	18.569	16.780
140	9.369	10.468	1465.5	19.837	17.469
150	10.108	10.958	1643.7	21.066	18.165
160	10.831	11.431	1828.9	22.262	18.888
170	11.538	11.891	2021.5	23.429	19.630
180	12.230	12.342	2221.6	24.572	20.389
190	12.909	12.786	2429.3	25.695	21.164
200	13.576	13.224	2644.8	26.800	21.935
210	14.232	13.658	2868.2	27.890	22.742
220	14.876	14.091	3100	28.967	23.553
230	15.515	14.517	3339	30.03	24.392
240	16.142	14.946	3587	31.09	25.246
250	16.761	15.376	3844	32.14	26.159
255.01	17.066	15.595	3977	32.66	26.661
			Liquid		
255.01	17.066	28.885	7366	45.95	35.78
260	17.628	29.019	7545	46.65	36.00
270	18.728	29.285	7907	48.01	36.45
273.15	19.069	29.368	8022	48.44	36.61
280	19.798	29.550	8274	49.35	36.95
290	20.840	29.814	8646	50.65	37.48
298.15	21.669	30.03	8954	51.70	37.93
300	21.854	30.08	9024	51.93	38.04
310	22.840	30.35	9407	53.19	38.61
320	23.816	30.61	9796	54.43	39.21
330	24.761	30.88	10191	55.64	39.83
340	25.680	31.16	10593	56.84	40.45
350	26.591	31.43	11000	58.02	41.07
360	27.477	31.71	11414	59.19	41.71
370	28.349	31.99	11835	60.34	42.37
380	29.207	32.27	12261	61.48	43.01
390	30.050	32.55	12695	62.60	43.64

[a] The values tabulated are the free energy function, enthalpy function, enthalpy, entropy, and heat capacity of the condensed phases at saturation pressure.

six acceptable determinations are summarized in Table XII along with various derived results.

Comparison with Earlier Work.—Investigators at the National Chemical Laboratory, Teddington, England, have reported experimental or calculated values of some of the properties of 2- and 3-methylpyridine given in this and the preceding paper I: namely, freezing points[4c]; heats of fusion,[4c] vaporization,[6-8] and combustion[9]; vapor pressures[6]; and second virial coefficients.[7,8] Other earlier results for the methylpyridines are not of comparable precision and accuracy. In general, the NCL and Bureau of Mines results agree for most practical purposes. However, the values for some properties differ by slightly more than the sum of the stated accuracy uncertainties. The values

(6) E. F. G. Herington and J. F. Martin, *Trans. Faraday Soc.*, **49**, 154 (1953).

TABLE VII

VAPOR PRESSURE OF 3-METHYLPYRIDINE

Boiling point, °C. Ref. compd.[b]	Boiling point, °C. 3-Methylpyridine	p(obsd.),[a] mm.	p(obsd.) − p(calcd.), mm. Antoine eq. 2	p(obsd.) − p(calcd.), mm. Cox eq. 3
19.061	74.036	71.87	+0.03	0.00
21.720	77.115	81.64	+ .02	.00
24.388	80.202	92.52	+ .01	.00
27.068	83.303	104.63	− .02	− .01
29.757	86.403	118.06	.00	+ .02
32.460	89.524	132.95	− .02	+ .01
		Change of reference compound		
60.000	92.658	149.41	−0.05	−0.02
65	98.946	187.57	− .08	− .04
70	105.270	233.72	− .04	− .01
75	111.640	289.13	− .02	.00
80	118.052	355.22	+ .02	.00
85	124.508	433.56	+ .06	+ .01
90	131.008	525.86	+ .08	.00
95	137.551	633.99	+ .10	− .02
100	144.135	760.00	+ .15	+ .02
105	150.767	906.06	+ .09	− .04
110	157.441	1074.6	+ .1	.0
115	164.156	1268.0	.0	.0
120	170.918	1489.1	− .1	− .1
125	177.721	1740.8	− .1	.0
130	184.568	2026.0	− .2	.0

[a] From vapor pressure data for benzene [F. D. Rossini, K. S. Pitzer, R. L. Arnett, R. M. Braun, and G. C. Pimentel, "Selected Values of Physical and Thermodynamic Properties of Hydrocarbons and Related Compounds," Carnegie Press, Pittsburgh, Pa., 1953, Table 21-k] and for water [N. S. Osborne, H. F. Stimson, and D. C. Ginnings, *J. Res. Natl. Bur. Std.*, **23**, 261 (1939)]. [b] The reference compound from 71.87 to 132.95 mm. was pure benzene and that from 149.41 to 2026.0 mm. was pure water.

TABLE VIII

THE MOLAL HEAT OF VAPORIZATION AND SECOND VIRIAL COEFFICIENT OF 3-METHYLPYRIDINE

T, °K.	P, atm.	ΔHv, cal.	B, cc. Obsd.	B, cc. Calcd.[a]
372.45	0.250	9599 ± 5[b]	−1799	−1798
393.36	0.500	9294 ± 3	−1600	−1571
417.29	1.000	8932 ± 4	−1355	−1385

[a] Calculated from eq. 5. [b] Maximum deviation from the mean of three or more determinations.

TABLE IX

THE MOLAL VAPOR HEAT CAPACITY OF 3-METHYLPYRIDINE IN CAL. DEG.$^{-1}$

T, °K.	404.20	429.20	452.20	475.20	500.20
C_p (1.000 atm.)		34.794	36.177	37.544	39.053
C_p (0.500 atm.)	32.697	34.343			
C_p (0.250 atm.)	32.411	34.138	35.738	37.236	38.818
$C_p°$	32.14	33.93	35.60	37.14	38.74
$-T(d^2B/dT^2)$, obsd.[a]	1.06	0.80	0.54	0.38	0.29
$-T(d^2B/dT^2)$, calcd.[b]	1.09	.75	.55	.41	.31

[a] Units: cal. deg.$^{-1}$ mole^{-1} atm.$^{-1}$. [b] Calculated from eq. 5.

(7) R. J. L. Andon, J. D. Cox, E. F. G. Herington, and J. F. Martin, *ibid.*, **53**, 1074 (1957).

(8) J. D. Cox and R. J. L. Andon, *ibid.*, **54**, 1622 (1958).

(9) J. D. Cox, A. R. Challoner, and A. R. Meetham, *J. Chem. Soc.*, 265 (1954).

of $\Delta Ec°$ for 3-methylpyridine differ significantly. The reason for these discrepancies is not apparent.

TABLE X

THE MOLAL ENTROPY OF 3-METHYLPYRIDINE IN THE IDEAL GAS STATE IN CAL. DEG.$^{-1}$

T, °K.	372.45	393.36	417.29
S_s(liq.)[a]	60.62	62.98	65.61
$\Delta Hv/T$	25.77	23.63	21.40
$S^* - S$[b]	0.08	0.11	0.17
$R \ln P$[c]	−2.76	−1.38	0.00
$S°$ (obsd.) ± 0.17[d]	83.71	85.34	87.18

[a] By interpolation in Table VI or extrapolation by use of eq. 1. [b] The entropy in the ideal gas state less that in the real gas state, calculated from eq. 5. [c] Entropy of compression, calculated from eq. 3. [d] Estimated accuracy uncertainty.

TABLE XI

SUMMARY OF A TYPICAL COMBUSTION CALORIMETRIC EXPERIMENT WITH 3-METHYLPYRIDINE[a]

m' (3-methylpyridine), g.	0.86940
$\Delta t_c = t_f - t_i - \Delta t_{cor}$, deg.	1.99846
ε (Calor.) $(-\Delta t_c)$, cal.	−8028.73
ε (Cont.) $(-\Delta t_c)$,[b] cal.	−8.92
ΔE_{ign}, cal.	1.16
$\Delta E'_{dec}$ (HNO_3 + HNO_2), cal.	16.19
ΔE, cor. to st. states,[c] cal.	3.94
$-m''\Delta Ec°/M$ (auxiliary oil), cal.	380.83
$-m'''\Delta Ec°/M$ (fuse), cal.	3.89
$m'\Delta Ec°/M$ (3-methylpyridine), cal.	−7631.64
$\Delta Ec°/M$ (3-methylpyridine), cal. g.$^{-1}$	−8778.05

[a] Auxiliary data: ε(Calor.) = 4017.46 cal. deg.$^{-1}$; V(bomb) = 0.344 l.; $\Delta Ec°/M$(auxiliary oil) = −10984.1 cal. g.$^{-1}$; $\Delta Ec°/M$ (fuse) = −4050 cal. g.$^{-1}$. [b] ε'(Cont.) $(t_i - 25°)$ + ε'(Cont.) $(25° - t_f + \Delta t_{corr.})$. [c] Items 81–85, 87–90, 93, and 94 of the computation form (I, ref. 24).

TABLE XII

SUMMARY OF RESULTS OF COMBUSTION CALORIMETRY AT 298.15°K.

$\Delta Ec°/M$ (3-methylpyridine), cal. g.$^{-1}$:
−8778.07, −8776.79, −8778.05
−8776.84, −8779.20, −8778.47
Mean and std. dev.: −8777.90 ± 0.42

Derived Results for the Liquid State[a]

$\Delta Ec°$, kcal. mole^{-1}	−817.43 ± 0.12
$\Delta Hc°$, kcal. mole^{-1}	−818.17 ± 0.12
$\Delta Hf°$, kcal. mole^{-1}	14.75 ± 0.14
$\Delta Sf°$, cal. deg.$^{-1}$ mole^{-1}	−88.59
$\Delta Ff°$, kcal. mole^{-1}	41.16
log Kf	−30.17

[a] With uncertainty interval equal to twice the final "over-all" standard deviation.

Acknowledgment.—The assistance of W. T. Berg and J. L. Lacina in some of the experimental measurements is gratefully acknowledged. The authors thank Drs. F. A. Miller and W. G. Fateley of the Mellon Institute for obtaining the far-infrared (grating) spectrum.

DIFFUSION IN THE WATER–METHANOL SYSTEM AND THE WALDEN PRODUCT

BY L. G. LONGSWORTH

Rockefeller Institute, New York, N.Y.

Received September 21, 1962

The recent work of Harned and associates affords convincing experimental evidence for the Nernst postulate that the mobility of a particle in a liquid is independent of the nature of the force responsible for the motion. From measurements, with the aid of Rayleigh interferometry, of the diffusion coefficients of non-electrolytes in dilute solutions in water, methanol, and their mixtures the limiting mobilities, λ_0, of uncharged particles thus have been obtained. The variation, with the solvent composition, of the Walden product, $\lambda_0\eta$, where η is the viscosity of the solvent, is less for a non-electrolyte than for a monatomic ion of comparable mobility and decreases with increasing size of the particle. Modification of the Stokes–Einstein relation with the extension, to methanol, of Robinson and Stokes' suggestion that the tetraalkylammonium ions are unhydrated permits computation of solvation numbers for other solutes in both solvents. For a given non-electrolyte, this number is slightly less in methanol than in water, indicating that the low value of $\lambda_0\eta$ for small particles in methanol is due primarily to the relatively large volume of the alcohol molecule in the solvation shell. In no case does the solvation number exceed the number of hydrogen bonding sites on the solute molecule.

The failure of Walden's rule when applied to the alkali halide ions in water, methanol, and their mixtures has been the subject of several investigations.[1-3] The low values of $\lambda_0\eta$ in methanol relative to those in water are usually ascribed to increased solvation. The decrease of some 20 ml. in the apparent molal volumes of the alkali halides[4] on transfer from H_2O to CH_3OH implies electrostriction of the solvent near the ions but could result from the higher compressibility of methanol without significant alteration in the solvation number. There also is the quantitative failure of Stokes' relation, on which Walden's rule is based, when the solute particles are comparable in size with the solvent molecules, in which case the numerical factor is less than 6π. This is observed in both polar[5,6] and non-polar systems,[7] a striking example being afforded by the observation of Grun and Walz[8] that tetrabromoethane diffuses five times as rapidly in glycerol trioleate as may be computed from the molal volume of the solute with the aid of the Stokes–Einstein relation. In self-diffuson,

(1) L. G. Longsworth and D. A. MacInnes, *J. Phys. Chem.*, **43**, 239 (1939).

(2) R. E. Jervis, D. R. Muir, J. P. Butler, and A. R. Gordon, *J. Am. Chem. Soc.*, **75**, 2855 (1953).

(3) N. G. Foster and E. S. Amis, *Z. physik. Chem.* (Frankfurt), **3**, 365 (1955); **7**, 360 (1956).

(4) W. C. Vosburgh, L. C. Connell, and J. A. V. Butler, *J. Chem. Soc.*, 933 (1933).

(5) S. Glasstone, K. J. Laidler, and H. Eyring, "The Theory of Rate Processes," McGraw–Hill Book Co., Inc., New York, N. Y., 1941.

(6) L. G. Longsworth, "Electrochemistry in Biology and Medicine," T. Shedlovsky, Ed., John Wiley and Sons, Inc., New York, N. Y., 1955, chapter 12.

(7) B. R. Hammond and R. H. Stokes, *Trans. Faraday Soc.*, **51**, 1641 (1955).

(8) F. Grun and D. Walz, *Helv. Chim. Acta*, **44**, 1883 (1961).

the particles are similar in size and Ottar[9] used, in effect, a factor of 2.9π in his computation of the viscosities of several pure liquids from their self-diffusion coefficients and molal volumes. Assuming the tetraalkylammonium ions to be unhydrated and of known size, Robinson and Stokes[10] have suggested that these be used to evaluate the numerical factor in Stokes relation, and Nightingale[11] adopted this procedure in a review of ion hydration.

Although primary solvation probably results from ion–dipole interaction, hydrogen bonding doubtless contributes to secondary solvation. It appeared of interest, therefore, to compare the mobilities of ions in the water–methanol system with this property of non-electrolytes, where the solute–solvent friction is restricted to that resulting from dipole–dipole interaction in the form of hydrogen bonding. Diffusion measurements of non-electrolytes afford much the same information concerning solute mobility as do conductance and transference measurements on electrolytes. Moreover, the simple dependence of the diffusion coefficient of a non-electrolyte on concentration facilitates extrapolation to infinite dilution.

Experimental

The experimental procedure for the diffusion measurements was the same as in the work with heavy water[12] except that evaporation from the reservoirs during the diffusion period was minimized by displacing most of the air therein with loosely fitting tubes whose lower ends were closed. Densities were also measured as in that work. The methanol was the middle fraction of a synthetic material and was used without further treatment since its density at 25°, the temperature at which all measurements were made, was that of the anhydrous alcohol, 0.78655. Although the solvent mixtures were prepared by direct weighing of both components into glass-stoppered flasks, the subsequent de-aeration in an oven at 45°, and occasional brief exposures to the atmosphere made it preferable to determine the composition of a solvent from a density measurement at the time the solutions were prepared. The density–composition data of Gibson[13] were used for this purpose. With only a few exceptions, the solvent composition differed insignificantly from the round values given in Table II and where necessary the diffusion coefficients have been corrected to the tabulated mole fraction of methanol. Solute concentrations, m, are expressed as moles of solute per thousand grams of solvent.

The solutes were of reagent grade and, in the case of the solids, were used without further purification except for vacuum desiccation. The formamide and glycerin were distilled under reduced pressure and the fractions having densities of 1.12929 and 1.25787, respectively, were used. The ethylene glycol had a density of 1.10982, whereas that of the polyethylene glycol of average molecular weight 600 (PEG 600) was 1.12212. The polyethylene glycol of average weight 3350 (PEG 3350) was a solid. In all cases where comparison with diffusion data of modern precision is possible, *i.e.*, aqueous urea,[14] formamide,[15] acetamide,[16] glycolamide,[17] dextrose,[18] and sucrose,[19] the present results agree within 0.1% or better.

If the solutes were sufficiently soluble, diffusion measurements were made over three or more concentration intervals to permit linear extrapolation. A concentration difference was used that gave approximately 50 fringes in a 2.5 cm. channel. A solution of about the same concentration as that below the boundary in one experiment was the dilute solution above the boundary in the experiment at the next higher mean concentration. The small departures from ideal diffusion in the mixed solvents were not significantly different from those in the pure ones and no attempt has been made to correct for possible flow coupling in the three-component systems. Unless limited by the solubility, *e.g.*, erythritol and dextrose, the apparent molal volumes, ϕ, were determined at a molality of 0.5.

Results

The experimental results in water and methanol are summarized in Table I, whereas those in the mixed solvents are given in Table II, together with the pertinent values from Table I for completeness. In Table I the limiting value of the diffusion coefficient, D, is given together with the slope, $\Delta D/\Delta m$, of the line through the experimental points. The figure in parentheses to the right of each slope in Table I is 100 times the highest mean molality at which diffusion measurements were made. The slopes for aqueous urea,[14] formamide,[15] and glycolamide[17] are taken from the more complete work of Gosting and associates, whereas the values for H_2O in water are those of HDO,[12] the isotope effect found by Wang, Robinson, and Edelman[20] being neglected. The "solvation" numbers, n, in the last two columns of Table I are considered in the discussion. There the Stokes radius, r_s, which is inversely proportional to the Walden product, frequently will be used for convenience in comparison with other estimates of particle size. The relations[10] are

$$r_s = kT/6\pi\eta D = zF^2/6\pi N\eta\lambda_0$$

where z is the valence of the ion whose limiting equivalent conductance is λ_0, F is the Faraday equivalent and the other quantities have their usual significance. For interconversion of a volume and a radius the relation $V = 4\pi N r_v^3/3$ has been used, V being the molal volume of the pure component.

Discussion

In Fig. 1 the logarithm of the Stokes radius in methanol is plotted as ordinate against the same function of this radius in water as abscissa. The values for non-electrolytes were computed from the data of Table I, whereas those for ions were taken from the compilations of Robinson and Stokes[10] and Evers and Knox.[21] On this plot any solute on the left of the diagonal line through the origin has a larger Stokes radius, *i.e.*, a smaller Walden product, in methanol than in water. It will be noted that the alkali halide ions are farther to the left of this line than the non-electrolytes, only the higher tetraalkylammonium ions having larger Stokes radii in water than in methanol. The electrical screening effect of the large alkyl groups and their inability to form hydrogen bonds justifies the assumption that these ions are unhydrated.

From estimates of the radii, r_h, of the tetraalkylammonium ions, and a plot of r_h against their Stokes radii, r_s, in water, Robinson, and Stokes[10] have computed hydration numbers, n, for the monatomic cations having comparable r_s values with the aid of the relation

$$n = (V_h - V)/V_0$$

Here $V_h = 4\pi N r_h^3/3$, V is the molar volume of the solute and V_0 that of the solvent, 18 cc./mole for water

(9) B. Ottar, "Self-diffusion and Fluidity in Liquids," Oslo University Press, 1958; *cf.*, *Acta Chem. Scand.*, **9**, 344 (1955).
(10) R. A. Robinson and R. H. Stokes, "Electrolytic Solutions," 2nd Edition, Butterworths Scientific Publications, London, 1959, p. 125.
(11) E. R. Nightingale, *J. Phys. Chem.*, **63**, 1381 (1959).
(12) L. G. Longsworth, *ibid.*, **64**, 1914 (1960).
(13) R. E. Gibson, *J. Am. Chem. Soc.*, **57**, 1551 (1935).
(14) L. J. Gosting and D. F. Akeley, *ibid.*, **74**, 2058 (1952).
(15) J. G. Albright and L. J. Gosting, *J. Phys. Chem.*, **64**, 1537 (1960).
(16) A. Biancheria and G. Kegeles, *J. Am. Chem. Soc.*, **79**, 5908 (1957).
(17) P. J. Dunlop and L. J. Gosting, *ibid.*, **75**, 5073 (1953).
(18) L. G. Longsworth, *ibid.*, **75**, 5705 (1953).
(19) L. J. Gosting and M. S. Morris, *ibid.*, **71**, 1998 (1949).
(20) J. H. Wang, C. V. Robinson, and I. S. Edelman, *ibid.*, **75**, 466 (1953).
(21) E. C. Evers and A. G. Knox, *ibid.*, **73**, 1739 (1951).

TABLE I

DIFFUSION COEFFICIENTS AND APPARENT MOLAL VOLUMES IN WATER AND METHANOL AT 25°

Solute	10^5D, cm.²/s		$10^5\Delta D/\Delta m$		ϕ, ml./mole		η	
	H_2O	CH_3OH	H_2O	CH_3OH	H_2O	CH_3OH	H_2O	CH_3OH
Water	2.272	2.176		0.077(280)	18.1	14.4	2.7[a]	2.2
Formamide	1.608	2.070	0.039	.172(54)	38.6	36.7	2.5	1.8
Acetamide	1.252	1.729	.105(18)	.175(42)	55.4	53.0	3.0	2.3
Propionamide	1.093	1.660	.160(32)	.222(40)	71.3	69.6	2.7	2.0
Thiourea	1.331	1.657	.195(8)	.450(13)	54.9	44.2	2.8	2.4
Urea	1.382	1.597	.077	.355(16)	44.2	37.6	2.8	2.8
Methylurea	1.168	1.593	.143(27)	.292(31)	62.0	57.4	2.8	2.4
1,3-Dimethylurea	.998	1.539	.271(22)	.185(29)	80.0	77.7	3.0	2.2
Glycolamide	1.142	1.533	.096	.360(17)	56.2	50.5	3.4	2.9
Ethylene glycol	1.153	1.641	.072(27)	.180(35)	54.7	52.0	3.2	2.4
Glycerol	0.938	1.305	.094(30)	.347(30)	71.7	64.9	3.7	3.5
Erythritol	.805	1.153	.142(8)	.720(8)	86.6	77.9	4.6	4.4
Dextrose	.6765	0.938	.168(20)	.850(6)	111.9	93.7	5.2	6.7[a]

[a] Modified Stokes–Einstein relation used outside of range of calibration.

TABLE II

DIFFUSION COEFFICIENTS AND APPARENT MOLAL VOLUMES IN WATER–METHANOL MIXTURES AT 25°

	Mole fraction methanol	0.0	0.1	0.2	0.3	0.4	0.6	0.8	1.0
10^5D	Urea ($m = 0$)	1.382	1.004	0.846	0.800	0.810	0.905	1.142	1.597
	Thiourea ($m = 0$)	1.331	0.955	.805	.772	.794	.928	1.181	1.658
	Dextrose ($m \simeq 0.022$)	0.6730	.4835	.4082	.3876	.3951	.4617	0.6130	0.9225
	Sucrose ($m \simeq 0.012$)	.5200	.3648	.3092	.2938	.3045	.3630	.4823	.7303
	PEG 600 ($m \simeq 0.019$)	.3638	.2642	.2298	.2284	.2424	.3015	.4121	.6339
	PEG 3350 ($m \simeq 0.003$)	.1568	.1110	.0956	.0946	.1007	.1223	.1706	.2756
$-10^5\Delta D/\Delta m$	Urea ($m \rightarrow 0.35$)	.077	.041	.039	.040	.065	.103	.187	.355
	Thiourea ($m \rightarrow 0.15$)	.195	.113	.053	.040	.051	.124	.208	.465
ϕ, ml./mole	Urea ($m \simeq 0.5$)	44.2	44.5	45.0	44.9	44.6	43.1	40.8	37.6
	Thiourea ($m \simeq 0.5$)	54.9	55.5	56.3	56.2	55.5	53.1	49.4	44.2
η, centipoise		0.895	1.321	1.566	1.596	1.493	1.165	0.828	0.542

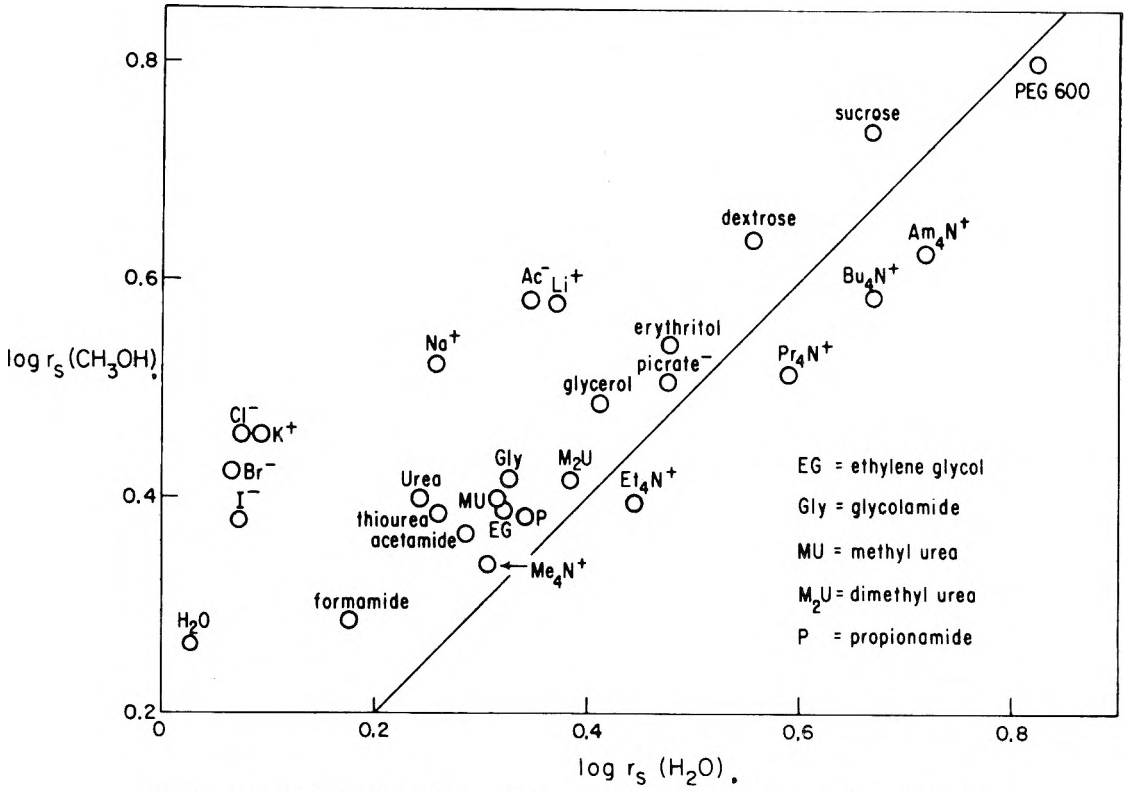

Fig. 1.—The Stokes radii of ions and of non-electrolytes in water and in methanol.

or 40 cc./mole for methanol. This procedure effectively modifies the Stokes factor for small solutes. Over the range in r_s covered by the alkylammonium ions in water, *i.e.*, 2.0–5.2 Å., the relation is

$$r_h \pm 0.04 = 0.546r_s + 2.408 \text{ Å.} \quad (1)$$

and this has been used in lieu of a graph for estimating the solvation numbers in column 8 of Table I. In methanol, column 9 of Table I, the relation for the reference ions is

$$r_h \pm 0.07 = 0.75r_s + 2.10 \text{ Å.} \quad (2)$$

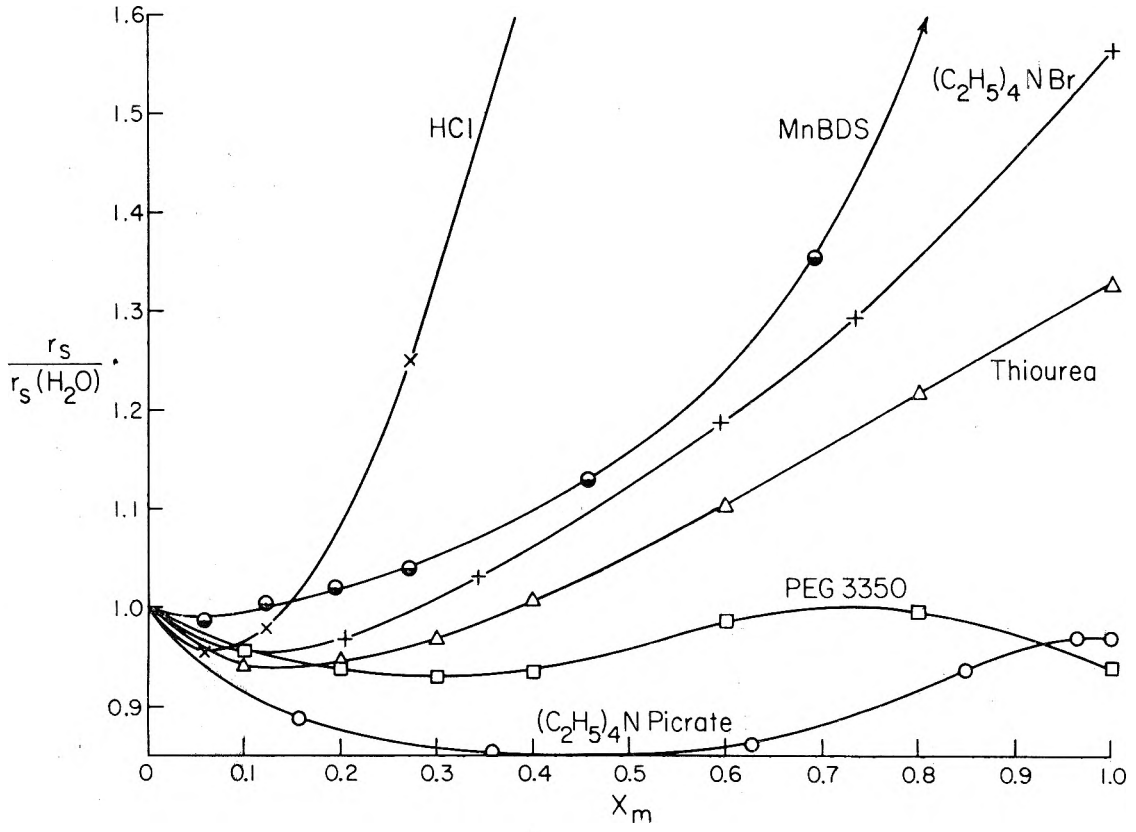

Fig. 2.—The Stokes radii, normalized to unity in water, of representative electrolytes and non-electrolytes as a function of the mole fraction of the alcohol in water–methanol mixtures

and the interval is $1.7 < r_s < 4.2$. In this solvent carbon tetrachloride, with $r_s = 1.745$, $r_v = r_h = 3.37$ and a scattering radius of 3.2 Å., affords an additional reference particle and was used in obtaining eq. 2. In both solvents the tetramethylammonium ion exhibits the largest deviations from eq. 1 and 2 and accounts for much of the indicated uncertainty in r_h. This uncertainty is reduced appreciably if r_v for $(CH_3)_4C$ replaces r_h for $(CH_3)_4N^+$.

In most cases the value of n for a solute in methanol is somewhat less than in water, from which it is clear that the low value of the Walden product in alcohol is due to the volume of this molecule in the solvation shell. In no instance does n exceed the number of hydrogen bonding sites on a solute molecule if both proton donor and acceptor sites are counted.

However, the correlation of n with the volume contraction, columns 6 and 7 of Table I, is poor. Over the size range of the reference ions the Stokes factor in water is nearer 6π for a given solute than in methanol. Moreover, eq. 1 indicates that 6π becomes the appropriate factor at $r_h = r_s = 5.3$ in water, whereas in methanol, eq. 2 must be extrapolated to $r_h = r_s = 8.4$. For small polar solutes in a polar solvent the Stokes factor is clearly not a simple function of the size of the solute particle relative to that of the solvent.

The solvation numbers of Table I are less than those of monatomic ions of comparable size. In the case of the alkali halide ions the modified Stokes relation leads to a fairly consistent set of numbers. In water, n decreases monotonely with increasing crystal radius from 7.0 for Li^+ to 3.3 for Cs^+[10] and from 3.2 for Cl^- to 2.6 for I^-, whereas in methanol the decrease is from 7.5 to 3.6 for the cations and from 4.5 to 3.1 for the anions. The higher values for the anions in methanol than in water may not be significant since eq. 1 has been used somewhat outside of its range of validity for these ions in water but there is also the possibility that the methyl group of the alcohol has enhanced the affinity of the proton for anions.

Two-Component Solvents.—The variation of the Walden product in the mixed solvents cannot be considered independently of the non-ideal behavior of the viscosity. As the mole fraction of methanol, x_m, is increased the viscosity at first increases from the value for water at 25°, 0.00895 poise, to a maximum of 0.0160 at $x_m \simeq 0.27$ and then decreases to 0.00542 for methanol. The positive departure of the viscosity from additivity is accompanied by a contraction in volume on mixing the components that reaches a maximum value of 1 cc. per mole of mixture at $x_m = 0.48$. This negative departure of the solvent volume from additivity is accompanied, in turn, by positive deviations of the volumes of the two solutes that were studied, urea and thiourea, Table II.

In Fig. 2 the Stokes radii, normalized to unity in water, for a large and a small non-electrolyte from Table II are compared, as a function of x_m, with those for representative electrolytes, *i.e.*, hydrochloric acid,[22] tetraethylammonium bromide[3] and picrate,[23] and manganese(II) benzene disulfonate.[24] Since transference data are not available for computation of limiting ion conductances in the mixed solvents the values of r_s for the electrolytes are a harmonic mean of the anion and cation. The minimum change in the Walden product is that for the large non-electrolyte and amounts to 7%,

(22) T. Shedlovsky and R. L. Kay, *J. Phys. Chem.*, **60**, 151 (1956).
(23) F. Accascina, A. D'Aprano, and R. M. Fuoss, *J. Am. Chem. Soc.*, **81**, 1058 (1959).
(24) C. J. Hallada and G. Atkinson, *ibid.*, **83**, 3759 (1961).

whereas the variation in solvent viscosity is nearly 300%.

No exceptions have been noted to the observation, illustrated in Fig. 2, that on the addition of methanol to water the initial effect is a decrease in the Stokes radius. This is in accord with the results of Stokes[25] on the limiting mobilities of ions in aqueous solutions whose viscosity has been raised by the addition of non-electrolytes of relatively large molal volume. Invariably, the depression of the ion mobility is less than the increase in the bulk viscosity but exceeds that to be expected if the added molecule is considered as an obstruction that increases the length of the path taken by the solute particle but not the viscosity of the medium in which this particle moves. This model is a stage in the transition from a fluid continuum to a porous medium and thus makes available the literature on tortuosity for the interpretation of experimental results. The model is applicable to ions and non-electrolytes and provides, as Stokes has noted, an explanation for the modified Walden relation, $\lambda_0\eta^a$ = constant, where a is less than unity. In the water–methanol system, however, the Stokes radius of small particles also decreases when water is added to methanol. Here the decrease could be attributed to replacement of methanol in the solvation shell by the smaller water molecules.

Fuoss[26] has interpreted the variation of the Walden product for an ion in a two-component solvent, only one of which is polar, as a braking effect resulting from the orientation of the solvent dipoles ahead of, and their subsequent relaxation behind, the advancing ion. The effect increases with decreasing dielectric constant. If this braking effect also operates in the case of a moving dipole it would contribute to the observed change in the Stokes radius for the methanol-rich mixtures, since the dielectric constant in this system decreases monotonely with x_w. In this system, however, both solvent components are polar and the non-ideality of their mixtures implies that other effects also are operating.

The cathodic transfer of water by hydrochloric acid and the alkali chlorides in the presence of a reference substance implies not only that the cation solvation exceeds that of the anion but that the solvation shell is rich in water. The assumption is tacit here that the anion is not preferentially solvated by the reference material. With the aid of an e.m.f. method, Feakins[27] has obtained Washburn numbers for these electrolytes, with methanol at $x_m = 0.06$ as the reference, that are comparable with the values derived from electrophoretic methods using other reference materials. As $x_m \rightarrow 1$ at what solvent composition, then, is the water in the solvation shell replaced by methanol? The curves of Fig. 2 suggest that the water content of this shell exceeds x_w over the entire range of composition. In the case of the hydronium ion of HCl, the water shell essential for its abnormal conductance remains intact up to $x_m \simeq 0.15$, whereas only a trace of water destroys the methanol shell that is required for the Grotthus mechanism at $x_m = 1$. From a comparison of MnBDS and $(Et)_4NPic$ in Fig. 2, it is clear that the monatomic ions are chiefly responsible for the variation in the Walden product. In pure methanol $r_s/r_s(H_2O) = 3.04$ for MnBDS and 90% of the increase in the ratio occurs above $x_m = 0.7$, these high concentrations being required to replace the tightly bound water around the compact divalent manganese ion with the larger methanol molecules. Although the Walden product for a small non-electrolyte varies less with x_m than that for a monatomic ion of the same mobility, the parallel behavior of the curves in Fig. 2 implies that the water content of the non-electrolyte solvation also exceeds x_w. Insofar as the solvation numbers represent a preferential interaction of the solute with one component of a mixed solvent, it should be possible to relate them eventually to the cross-term diffusion coefficients in these three-component systems.

There remains the possibility that the solvation numbers afford a measure of hydrogen bonding. The clearest evidence for such bonding is afforded, however, by work in progress on N,N-dimethylacetamide and the parent amide in methanol. Although the volume of the dimethyl compound is 82% greater than that of acetamide it diffuses 10% faster. In methanol the solvation numbers are 0.8 and 2.3, respectively. Elimination, by N-methylation, of the only two proton donor sites on acetamide has thus reduced the solvation number by 1.5 and methanol is too weakly acidic to take advantage of the proton acceptor sites on the amide oxygen. In water the effect is somewhat less, dimethylation reducing the numbers from 3.0 to 1.9. The weakly acidic character of methanol is also apparent in the case of a related solute, acetone, that is not a proton donor. The solvation numbers for this solute are 1.6 and 0.0 in water and methanol, respectively. Other factors that contribute to the strength of the hydrogen bonds in these systems have been reviewed recently by Huggins.[28]

Acknowledgment.—The author is indebted to D. A. MacInnes for a review of this manuscript and to Emilia Jurevicius for the analysis of the Rayleigh fringe patterns.

(25) R. H. Stokes, in "The Structure of Electrolytic Solutions," W. J. Hamer, Ed., John Wiley and Sons, Inc., New York, N. Y., Chapter 20, pp. 298–307.

(26) R. M. Fuoss, *Proc. Nat. Acad. Sci. U.S.*, **45**, 807 (1959).

(27) D. Feakins, *J. Chem. Soc.*, 5308 (1961).

(28) M. L. Huggins, *American Scientist*, **50**, 485 (1962).

TEMPERATURE DEPENDENCE OF THE CARBON ISOTOPE EFFECT IN THE DECARBONYLATION OF LIQUID FORMIC ACID

BY PETER E. YANKWICH AND RUDY H. HASCHEMEYER

Noyes Laboratory of Chemistry, University of Illinois, Urbana, Ill.

Received September 22, 1962

The C^{13} kinetic isotope fractionation in the decarbonylation of liquid formic acid was studied over the range 59.8–100.0°; (k_{12}/k_{13}) lay in the range 1.05–1.04. The observed temperature dependence was examined by the "gamma-bar" method of Bigeleisen and Wolfsberg, the "semi-empirical" method of Yankwich, Weber, and Ikeda, and several "two-center" approaches. Of the approximately 4.5% isotope effect, only a few tenths of a per cent is temperature independent; the calculated sums of the differences upon activation of the diagonal cartesian force constants correspond especially well with the value expected for C–O bond rupture, and indicate strongly that this rupture is a major component of the reaction coördinate motion.

Introduction

A reinvestigation[1] of the influence of temperature on the kinetic carbon isotope effect in the dehydration of formic acid by concentrated sulfuric acid[2] has shown that the temperature independent factor in the ratio of the isotope specific rate constants is very close to unity, and that the temperature dependence of the isotope effect, though large, is compatible with C–O bond rupture being the major component of the reaction coördinate motion. The latter finding is consistent with the evidence recorded by Gel'bshtein, Shcheglova, and Temkin[3] in support of the acid-catalyzed carbonium ion mechanism for the decarbonylation of formic acid in concentrated sulfuric and phosphoric acids. The research reported in this paper was undertaken in an effort to expose possible similarities in the mechanisms of decarbonylation of formic acid in concentrated sulfuric acid and in the pure liquid state. The formic acid employed in the study contained C^{13} at the natural abundance level.

Experimental

Formic Acid.—Reagent grade formic acid (Mallinckrodt, "98–100%") was dried for storage by distillation *in vacuo* at 25°, first from anhydrous copper sulfate, then from anhydrous magnesium perchlorate; before each distillation the acid stood in contact with the drying agent for two or three days. The dried formic acid was stored *in vacuo* over anhydrous magnesium perchlorate.

Samples of the formic acid used in the experiments were 99.9% pure, or better, as indicated by titration with standard base, and by close agreement between specific rate constants for the decomposition at several temperatures and those found with formic acid of this purity by Barham and Clark,[4] who investigated the negative catalytic effect of water on the rate of decarbonylation.

Apparatus and Procedure.—The reaction vessel consisted of a 30-ml. Pyrex bulb fitted with a breakoff tube and side arm, both terminating in standard taper joints to permit connection to the vacuum system. After the bulb was weighed and evacuated, 2–6 ml. of formic acid was distilled into it through the side arm, which was then sealed[5]; the bulb and contents were weighed.

Reaction was initiated by placing the vessel in a constant (±0.05°) temperature oil bath. After 1–3% decarbonylation had occurred,[6] the bulb was removed from the oil bath and cooled in ice-water.

After being cooled, the reaction vessel was connected to a vacuum combustion system consisting of the following, in sequence: stopcock A; a trap, filled with glass wool and glass beads and cooled in liquid nitrogen[7]; stopcock B; a tubular combustion furnace packed with copper oxide wire; a collection trap cooled in liquid nitrogen; stopcock C; the vacuum manifold. First, the reaction vessel was cooled in liquid nitrogen and the combustion system evacuated; with all stopcocks closed, the breakoff seal was shattered. By manipulation of stopcocks A and B, carbon monoxide was "dosed" into the first trap, then through the furnace, and the product carbon dioxide collected in the second trap. The progress of the combustion of each "dose" was followed by means of a thermocouple gage; the next manipulative cycle was started when the pressure in the system had fallen to a low value, and the cycling of operations repeated until no significant pressure increase was noted upon opening stopcock A. With stopcock A closed, the contents of the reaction vessel were warmed to room temperature for a few moments, then re-frozen. Two or three freeze–thaw cycles were sufficient to liberate all the carbon monoxide product from the reaction solution.

The carbon dioxide was distilled to the vacuum manifold through stopcock C (stopcock B closed) for manometric quantity determination[8] and final transfer to a mass spectrometer sample tube.

Isotope Analyses.—The procedures employed have been described in detail in earlier publications from this Laboratory.[8–11]

Notation and Calculations.—The isotopic rate constant ratio sought was (k_{12}/k_{13}) in the notation

$$HC^{12}OOH \xrightarrow{k_{12}} C^{12}O + H_2O \qquad (1)$$

$$HC^{13}OOH \xrightarrow{k_{13}} C^{13}O + H_2O \qquad (2)$$

Since the reaction was stopped at 3% decomposition or less, the following expression was employed in the calculation of results[12–14]

$$(k_{12}/k_{13})_{obsd} = (R_F/R_C) \qquad (3)$$

where R_F is the ratio ($HC^{13}OOH/HC^{12}OOH$) derived from measurements on carbon dioxide obtained by combustion (in a standard Pregl apparatus) of samples of the original dried formic acid,[15] and R_C is the ratio ($C^{13}O/C^{12}O$) from measurements on carbon dioxide obtained from combustion of the samples of prod-

(1) J. Bigeleisen, R. H. Haschemeyer, M. Wolfsberg, and P. E. Yankwich, *J. Am. Chem. Soc.*, **84**, 1813 (1962).

(2) G. A. Ropp, A. J. Weinbergber, and O. K. Neville, *ibid.*, **73**, 5573 (1951).

(3) A. I. Gel'bshtein, G. G. Shcheglova, and M. I. Temkin, *Zh. Fiz. Khim.*, **30**, 2267 (1956).

(4) H. N. Barham and L. W. Clark, *J. Am. Chem. Soc.*, **73**, 4638 (1951).

(5) It was established that inappreciable isotope fractionation occurred under the conditions of this distillation transfer of part of the stock formic acid.

(6) Times for 1% decarbonylation ranged from about 5 hr. at 100° to 13 days at 60°.

(7) This trap prevented combustion of a small amount of formic acid "fog" which apparently formed during the freeze–thaw cycles (*vide infra*).

(8) Carbon dioxide determinations by manometric measurement and estimates calculated from rate constants obtained from experiments with freshly dried formic acid were compared at intervals during the use of a given sample of formic acid. The agreement was always within the estimated manometric errors, which is indicative of the constancy of composition of the stock formic acid over a period of several weeks.

(9) P. E. Yankwich and R. L. Belford, *J. Am. Chem. Soc.*, **75**, 4178 (1953).

(10) P. E. Yankwich and R. L. Belford, *ibid.*, **76**, 3067 (1954).

(11) P. E. Yankwich and J. L. Copeland, *ibid.*, **79**, 2081 (1957).

(12) J. Bigeleisen, *Science*, **110**, 14 (1949).

(13) J. Bigeleisen, *J. Chem. Phys.*, **17**, 425 (1949).

(14) J. Y.-P. Tong and P. E. Yankwich, *J. Phys. Chem.*, **61**, 540 (1957).

(15) These samples of carbon dioxide were purified by several distillations between traps at −150 and −196°.

uct carbon monoxide; for the formic acid used in these experiments, $R_F \times 10^6 = 10923 \pm 2$.

Results

The corrected[9-11] carbon isotope ratio for each sample is given in Table I, along with the value of $(k_{12}/k_{13})_{obsd}$ to which it corresponds. The appended errors in the last column are average deviations from the mean; the mean precision of individual $(k_{12}/k_{13})_{obsd}$ values is estimated to be ± 0.0003. Values of $L(k_{12}/k_{13}) = 100 \ln (k_{12}/k_{13})$ calculated from the last column of Table I are plotted *vs.* $(1000/T)$ in Fig. 1; the solid vertical rectangles encompass the average deviations, while the open rectangle for the single experiment at 80.5° has a length equal to twice the estimated mean precision of a single datum. Least-squares fitting of the results recorded in Table I yields the equations

$$L(k_{12}/k_{13}) = 2.531(10^3/T) - 2.834 \quad (4)$$

$$L(k_{12}/k_{13}) = 0.483\ (10^6/T^2) + 0.446 \quad (5)$$

TABLE I

CORRECTED ISOTOPE RATIOS OF EXPERIMENTAL SAMPLES; CALCULATED INTERMOLECULAR ISOTOPE EFFECTS

Temp., °C.	Expt. no.	Decarb., %	$R_C \times 10^6$	$(k_{12}/k_{13})_{obsd}$	Av. $(k_{12}/k_{13})_{obsd}$
59.8	16	1.0	10426	1.0492	
	17	1.0	10432	1.0486	
	23	3.0	10427	1.0491	
	24	2.1	10425	1.0493	
	25	1.7	10429	1.0489	1.0490 ± 0.0002
69.5	13	1.0	10449	1.0469	
	14	1.0	10466	1.0451	
	15	1.0	10454	1.0464	1.0461 ± .0007
80.5	34	2.4	10472	1.0446	...
89.0	7	1.6	10495	1.0423	
	28	1.6	10498	1.0420	
	29	1.6	10497	1.0421	1.0421 ± .0001
100.0	4	2.0	10516	1.0402	
	5	2.0	10526	1.0392	
	18	1.3	10507	1.0411	
	20	1.3	10511	1.0407	
	21	1.3	10509	1.0409	1.0404 ± .0006

the standard error of the equation being 0.06 and the average deviation from the least-squares curve 0.04 in both cases. A line corresponding to eq. 4 is drawn through the plot of results in Fig. 1.

Discussion

The slope of the least-squares line in Fig. 1 is about twice that which would be associated, in this temperature range, with an isotope effect having a temperature-independent factor (TIF)[16] of normal magnitude; apparently, TIF here, as in the decarbonylation in concentrated sulfuric acid,[1] lies very near unity (upper limit, TIF = 1.0045). Small-vibration theory, as customarily applied to the transition state, affords no generally satisfactory explanation of such TIF values.[17]

Bigeleisen and Wolfsberg[20] have found that correspondence between experimental results and those obtained from calculations often can be achieved if *molecular fragment* masses are used with the Slater[21] two-center coördinate; on this basis, TIF = 1.0062 for the isotope effect under consideration.[22] To apply the Slater coördinate notion to TDF, one assumes that the transition state differs from the normal state only by loss of a single vibration, the C–O stretch in the case at hand; further, the isotopic frequency shift in that vibration is assumed given by the *diatomic* reduced mass relationship. The normal mode frequency most nearly characteristic of the C–O bond in formic acid has a value in the range 1393–1200 cm.$^{-1}$ [23-25]; the TDF calculated for loss of a frequency in this range is too small to produce agreement with the experiments for TIF = 1.0062.[26] The best fit which can be secured with this model requires that the frequency "lost" be 1330 cm.$^{-1}$; (k_{12}/k_{13}) calculated for this frequency is shown in Fig. 1.

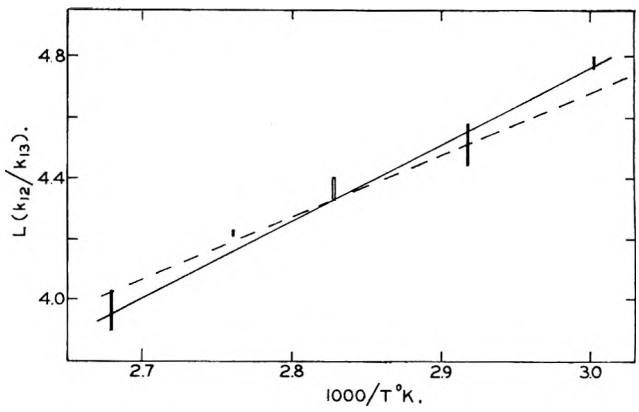

Fig. 1.—Influence of temperature on the intermolecular carbon isotope effect: ———, linear least-squares fit; – – – –, best 2-center model.

A theoretical analysis of small isotope effects can be made without detailed knowledge of the vibrations of the isotopic normal molecules and the transition states by use of the "gamma-bar" method of Bigeleisen and Wolfsberg[20]; the natural logarithm of TDF is given by

$$\ln (\mathrm{TDF}) = 0.1464(10^6/T^2)\bar{\gamma} \times \sum_{j}^{3n} \left[\frac{1}{m_{1j}} - \frac{1}{m_{2j}}\right] (a_{jj} - a^*_{jj}) \quad (6)^{27}$$

The value of $\bar{\gamma}$ to be employed in a particular calculation is estimated from an approximate knowledge of the frequencies of the normal and activated molecules. If it can be assumed that the principal change in vibration frequencies upon activation is associated with the

(16) $(k_{12}/k_{13}) = (\mathrm{TIF})(\mathrm{TDF})$. (TIF) is the ratio (ν_{12L}/ν_{13L}) of the imaginary frequencies associated with the reaction coördinate motion; (TDF), the temperature dependent factor, arises in the mass dependence of the genuine vibrations of the normal and activated species.

(17) However, introduction of an abnormally large bend-stretch interaction force constant, after Johnston, *et al.*,[18] results in TIF values much nearer unity than seems normal.[19]

(18) H. S. Johnston, W. A. Bonner, and D. J. Wilson, *J. Chem. Phys.*, **26**, 1002 (1957).

(19) M. Wolfsberg and P. E. Yankwich, unpublished calculations.

(20) J. Bigeleisen and M. Wolfsberg, *Advan. Chem. Phys.*, **1**, 15 (1958).

(21) N. B. Slater, *Trans. Roy. Soc.* (London), **246A**, 57 (1953).

(22) The original Slater calculation, which employs only the C and O atomic masses, leads to TIF = 1.0227. The dependence of $L(k_{12}/k_{13})$ on temperature is as $1/T$ at "low" temperatures and as $1/T^2$ at "high" temperatures.[20] Equations 4 and 5 yield, respectively, 0.9721 and 1.0045 as minimum and maximum values for TIF.

(23) L. G. Bonner and R. Hofstadter, *J. Chem. Phys.*, **6**, 531 (1938).

(24) R. Hofstadter, *ibid.*, **6**, 540 (1938).

(25) J. K. Wilmshurst, *ibid.*, **25**, 478 (1956).

(26) At the mid-temperature of the experiments, and with $\omega = 1200$ cm.$^{-1}$, $(k_{12}/k_{13})_{calcd} = 1.0392$, while $(k_{12}/k_{13})_{obsd} = 1.0446$.

(27) n is the number of atoms in the molecule, m is the mass of an atom in a.m.u., the subscripts 1 and 2 refer to the light and heavy isotopic species, respectively, and the a_{jj} are diagonal cartesian force constants in md. Å.$^{-1}$; $\bar{\gamma}$ is a suitably weighted average value, for the particular reaction under discussion, of the quantity $12G(u_i)/u_i$, where $u_i = hc\omega_i/kT$, and $G(u_i)$ is the function of Bigeleisen and Mayer.[28]

(28) J. Bigeleisen and M. G. Mayer, *J. Chem. Phys.*, **15**, 261 (1947).

normal mode which becomes the reaction coördinate, the most important component of $\bar{\gamma}$ arises in that single frequency.

In their original application of this method,[20] Bigeleisen and Wolfsberg calculated TIF using molecular fragment masses; TDF was then computed using an estimated single critical frequency and sum of force constant differences by means of eq. 6. The resulting k/k' was then compared with experiment. We shall employ a somewhat different approach. First, let TIF be calculated using molecular fragment masses, and TDF then computed from the experimental values of k/k'. Second, let there be assumed a range of values for a single critical frequency and, therefrom, appropriate ranges of $\bar{\gamma}$[29] over the span of temperatures covered by the experiments. Third, let the experimental TDF be matched at the mid-temperature, this resulting, for each assumed frequency, in an estimate of

$$\sum_j (a_{jj} - a_{jj}^*) = \Delta_c \qquad (7)$$

Finally, one can test the applicability of the method thus employed by comparison of the values of Δ_c with force constants typical of the C–O bond stretch and related bending vibrations, and by comparison of the slope of a plot of $L(k_{12}/k_{13})_{calcd}$ *vs.* $1000/T$ with that of the experimental plot.

The plots of such calculated $L(k_{12}/k_{13})$ differ insignificantly from that for the "best" 2-center model, shown in Fig. 1; for assumed frequencies in the 1100 to 1200 cm.$^{-1}$ range, the values of Δ_c are 5.1–5.3 md. Å.$^{-1}$, whereas values of 6–7 md. Å.$^{-1}$ seem more reasonable. Improvement of the calculated Δ_c would require the assumption of frequencies much higher than those characteristic of the C–O stretching vibration, TIF being taken as 1.0062; to secure better slope agreement, one would have to use a different (and smaller) TIF.

An experimental estimate of TIF can be obtained by employing the semi-empirical method described in earlier publications[30,31] from this Laboratory. If formic acid is treated as a three particle system, the experimental temperature dependence corresponds to TIF = 1.0014 ± 0.002. Repetition using this TIF of the "gamma-bar" method calculations described above does not improve significantly the agreement between calculated and observed slopes of the plot of $L(k_{12}/k_{13})$ *vs.* $(1000/T)$; but, the Δ_c values, again for frequencies in the 1100–1200 cm.$^{-1}$ range, are 5.9–6.1 md. Å.$^{-1}$, a definite improvement.

Another experimental estimate of TIF can be obtained by eliminating Δ_c between a pair of expressions (k_{12}/k_{13}) = (TIF)(TDF), where TDF at two different temperatures is computed from eq. 6; similarly, TIF can be eliminated to yield values for Δ_c. To illustrate this procedure, calculations were carried out for average stretching frequencies (corrected for loss of bending vibrations)[29] of 800, 1000, 1200 cm.$^{-1}$; in the same order, the values of Δ_c (in md. Å.$^{-1}$) and TIF are: 6.4, 1.0021; 7.1, 1.0001; 7.8, 0.9982. The values of these parameters are in reasonable agreement with expectation except at the highest frequency.

This application of the "gamma-bar" method seems to require a low C–O frequency to explain the observed isotope effect, while the "best" 2-center model involves a high C–O frequency estimate. The former situation is due undoubtedly to the fact that values for $\bar{\gamma}$ must be assumed for two temperatures according to some simple idea; in the discussion above, $\bar{\gamma}$ was evaluated on the asumption that the C–O stretching vibration was the major component of the reaction coördinate motion, due regard being had for the fact that bending motions are "lost" when C–O bond rupture occurs. A more sophisticated estimate of the values of $\bar{\gamma}$ involves the same additional complications as are associated with solution of the small vibration problem for multiple-particle representations of the normal molecules and activated complexes, or the Monte Carlo approach which is the basis of the "semi-empirical" method. In its higher approximations, the "gamma-bar" method is equivalent to the "semi-empirical" method; unlike other "single frequency" approaches to the explanation of small isotope effects, the simplest "gamma-bar" method application yields for many systems results in agreement with experiment which do not require an arbitrary estimate of TIF.

The several calculations described above have involved very similar models for the reaction coördinate motion; in one extreme it was assumed that the motion consisted entirely of the C–O bond stretch (which disappears upon activation); in the other, that bond-stretch was assumed to be "the most important component" of the motion. A more detailed specification of the reaction coördinate would require additional assumptions. The utility of the "gamma-bar" and "semi-empirical" methods lies in the fact that TIF need not be known or assumed in order to win useful information from the temperature dependence of experimental kinetic isotope effects.

Comparison of the results reported here with those obtained for the decarbonylation in concentrated sulfuric acid[1] shows only that in both situations the major component of the reaction coördinate motion is as indicated above. In neither case do the calculations provide an explanation for the fact that TIF differs so little from unity.

Acknowledgments.—This research was carried out under the auspices of the U. S. Atomic Energy Commission. Mrs. Beverly Thomas and Mrs. Eulah Ihnen performed the mass spectrometric analyses.

(29) In the computations, the following weighting was employed

$$\bar{\gamma} = \gamma_{stretch} \times \frac{a_{stretch}}{a_{stretch} + 2a_{bend}} + \gamma_{bend} \times \frac{2a_{bend}}{a_{stretch} + 2a_{bend}}$$

with $\nu_{stretch} = 3\nu_{bend}$.

(30) P. E. Yankwich and H. S. Weber, *J. Am. Chem. Soc.*, **78**, 564 (1956).

(31) P. E. Yankwich and R. M. Ikeda, *ibid.*, **81**, 1532 (1959).

THE HEATS OF FUSION AND TRANSITION OF ALKALINE EARTH AND RARE EARTH METAL HALIDES

BY A. S. DWORKIN AND M. A. BREDIG

Chemistry Division, Oak Ridge National Laboratory,[1] Oak Ridge, Tennessee

Received September 22, 1962

The heats of fusion of fifteen rare earth and alkaline earth halides have been measured by means of a copper block drop calorimeter. The salts and their heats of fusion in kcal. mole^{-1} are $LaCl_3$, 13.0; $PrCl_3$, 12.1; $NdCl_3$, 12.0; CeI_3, 12.4; PrI_3, 12.7; NdI_3, 9.7; $CaCl_2$, 6.78; $CaBr_2$, 6.95; CaI_2, 10.0; $SrCl_2$, 3.88; $SrBr_2$, 2.50; SrI_2, 4.70; $BaCl_2$, 3.90; $BaBr_2$, 7.63; and BaI_2, 6.34. The four salts which showed a transition, their temperatures of transition in °K., and their heats of transition in kcal. mole^{-1} are NdI_3, 847, 3.4; $SrCl_2$, 1003, 1.65; $SrBr_2$, 918, 2.90; and $BaCl_2$, 1193, 4.10. The high temperature forms of $SrBr_2$ and $BaCl_2$ are believed to have the fluorite type of structure characterized similarly as in CaF_2 and $SrCl_2$ by an unusually low entropy of fusion, probably because a high degree of disorder occurs in that structure at elevated temperatures.

Heats of fusion of the alkaline earth and rare earth metal halides are of considerable interest in connection with the interpretation of the phase equilibria and electrical conductance measurements in metal–metal halide systems.[2a] Since very few calorimetrically measured values are available in the literature, the heats of fusion of some chlorides and iodides of lanthanum, cerium, praseodymium, and neodymium, as well as the chlorides, bromides, and iodides of calcium, strontium, and barium, have been measured.

Experimental

The copper block calorimeter used for the measurements and the experimental procedure were previously described in detail.[2b]

The rare earth chlorides and the alkaline earth halides were prepared in a manner similar to that described previously.[2a] The rare earth iodides were prepared from the elements by the method of Druding and Corbett.[3] The rare earth halides contained less than 0.5% of other rare earth ions. No insoluble matter or alkalinity was found on dissolving them in water or in alcohol. All the salts used were free of other foreign metals as determined spectrographically. The alkaline earth halides also showed no alkalinity from pyrohydrolysis.

Results and Discussion

Table I lists the heats and entropies of fusion and transition, the heat content of the solid salts at their melting points, and the heat capacities of the solid and liquid in the vicinity of the melting and transition temperatures. The heat contents were measured with a precision of 0.1–0.2%, the heats of fusion to at least ±1–2%, and the heat capacities to about ±5%.

The entropies of fusion, ΔS_m, for $LaCl_3$, $PrCl_3$, and $NdCl_3$ do not differ much from each other nor from that of $CeCl_3$, 11.7 e.u., reported by Walden and Smith.[4] ΔS_m of CeI_3 and PrI_3 is slightly higher than that of the chlorides. NdI_3, distinguished above the transition temperature by a crystal structure different from CeI_3 and PrI_3, has an entropy of fusion lower than that of the other iodides by an amount approximately equal to the entropy of the transition taking place in the solid state approximately 200° below the melting point.

Since the alkaline earth halides possess a variety of crystal structures, they do not exhibit the simple regularities in ΔH_m and ΔS_m apparent in the alkali metal halides.[2b] However, $SrBr_2$ and $BaCl_2$, with transitions just below their melting points, and $SrCl_2$ which has a CaF_2 type of structure and, according to the present results, a second order transition about 140° below its melting point have unusually low entropies of fusion. (CaF_2, too, has an unusually low ΔS_m of 4.2 e.u. and what also appears to be a second order transition about 270° below its melting point.[5]) Although the temperature of transition for $SrCl_2$ is given as 1003°K. in Table I, this is merely the temperature of maximum heat capacity as the transition occurs over the temperature range 940–1040°K. with no discontinuity in the heat content curve. The heat of transition was obtained by extrapolation of the heat contents of α and β $SrCl_2$ to 1003°K. The heat content data for $SrCl_2$ from 298–1210°K. will be published elsewhere.

Table I also shows considerably larger heat capacities for the high temperature modifications of $SrCl_2$, $SrBr_2$, and $BaCl_2$, which also are formed with a rather large heat of transition. This may support the assumption that the low entropies of fusion of these compounds are connected with relatively high entropies of the solids possibly due to considerable disorder in connection with the special geometry of the fluorite type of structure in which there are lattice vacancies equal in size and number to the sites occupied by the cations.

CaI_2 with its layer type structure has a ΔS_m much higher than any of the other alkaline earth halides reported here. It thus resembles the cadmium dihalides (excluding the fluoride) of similar layer type crystal structure (ΔS_m = 7.5–9.5 e.u.).

The heats of fusion of $CaCl_2$ and $SrBr_2$ have been measured calorimetrically by other investigators. Moore's[6] value of ΔH_m for $CaCl_2$ of 6.78 kcal. and ($H_{1045} - H_{298}$) of 14.21 kcal. is in good agreement with that reported here. Taylor and Smith[7] reported the ΔH_m of $SrBr_2$ as 5.25 kcal., but apparently missed the transition reported by Eastman, *et al.*,[8] at 915°K. However, their value of 5.25 kcal. is in good agreement with the sum of our values ΔH_{tr} and ΔH_m equal 5.4 kcal. While their values for ($H_T - H_{298}$) for liquid $SrBr_2$ agree with ours to better than 0.4%, their values for the solid in the vicinity of the transition temperature are about 2.5% higher than ours. Figure 1 shows our heat con-

(1) Operated by the Union Carbide Corporation for the U. S. Atomic Energy Commission.

(2) (a) A. S. Dworkin, H. R. Bronstein, and M. A. Bredig, *Discussions Faraday Soc.*, **32**, 188 (1961); (b) A. S. Dworkin and M. A. Bredig, *J. Phys. Chem.*, **64**, 269 (1960).

(3) L. F. Druding and J. D. Corbett, *J. Am. Chem. Soc.*, **83**, 2462 (1961).

(4) G. E. Walden and D. F. Smith, U. S. Bur. Mines, Rept. Invest. No. 5859, U. S. Govt. Printing Office, Pittsburgh, Pa., 1961.

(5) B. F. Naylor, *J. Am. Chem. Soc.*, **67**, 150 (1945).

(6) G. E. Moore, *ibid.*, **65**, 1700 (1943).

(7) A. R. Taylor and D. F. Smith, U. S. Bur. Mines, Rept. Invest. No. 5967, U. S. Govt. Printing Office, Pittsburgh, Pa., 1962.

(8) E. D. Eastman, D. D. Cubicciotti, and C. D. Thurmond, in L. L. Quill, "Chemistry and Metallurgy of Miscellaneous Materials: Thermodynamics," National Nuclear Energy Series IV-19B, McGraw-Hill Book Co., New York, N. Y., 1950, pp. 6–12.

TABLE I

HEAT CAPACITY AND HEAT AND ENTROPY OF FUSION AND TRANSITION OF SOME ALKALINE EARTH AND RARE EARTH METAL HALIDES

	T_m, °K.	C_p solid cal. mole^{-1} deg.$^{-1}$	C_p liquid cal. mole^{-1} deg.$^{-1}$	$H_{T_m(solid)} - H_{298}$ kcal. mole^{-1}	ΔH_m kcal. mole^{-1}	ΔS_m e.u. mole^{-1}	T_{tr}, °K.	ΔH_{tr} kcal. mole^{-1}	ΔS_{tr} e.u. mole^{-1}	Struct. type 25°
$LaCl_3$	1131	34.7	37.7	22.8	13.0	11.5				UCl_3
$PrCl_3$	1059	32.3	32.0	21.5	12.1	11.4				UCl_3
$NdCl_3$	1032	35.4	35.0	20.3	12.0	11.6				UCl_3
CeI_3	1033	36.5	36.5	20.8	12.4	12.0				$PuBr_3$
PrI_3	1011	31.3	34.2	19.5	12.7	12.6				$PuBr_3$
NdI_3	1060	α 27.6	36.3	24.3	9.7	9.2	847	3.4	4.0	$PuBr_3$
		β 30.4								
$CaCl_2$	1045	23.6	23.6	14.3	6.78	6.49				SnO_2
$CaBr_2$	1015	23.0	27.0	14.0	6.95	6.85				SnO_2
CaI_2	1052	23.2	24.7	15.1	10.0	9.5				$Cd(OH)_2$
$SrCl_2$	1146	α 22.5	27.2	20.3	3.88	3.39	1003[a]	1.65	1.65	α CaF_2
		β 28.5								
$SrBr_2$	930	α 20.9	27.8	15.6	2.50	2.70	918	2.90	3.16	$SrBr_2$
		β 27.5								
SrI_2	811	22.9	26.3	10.4	4.70	5.80				SrI_2
$BaCl_2$	1233	α 23.1	26.3	23.5	3.90	3.17	1193	4.10	3.44	$PbCl_2$
		β 25.5								
$BaBr_2$	1130	21.7	25.6	16.9	7.63	6.75				$PbCl_2$
BaI_2	984	21.8	27.0	13.9	6.34	6.44				$PbCl_2$

[a] Temperature of maximum heat capacity. No discontinuity in heat content curve.

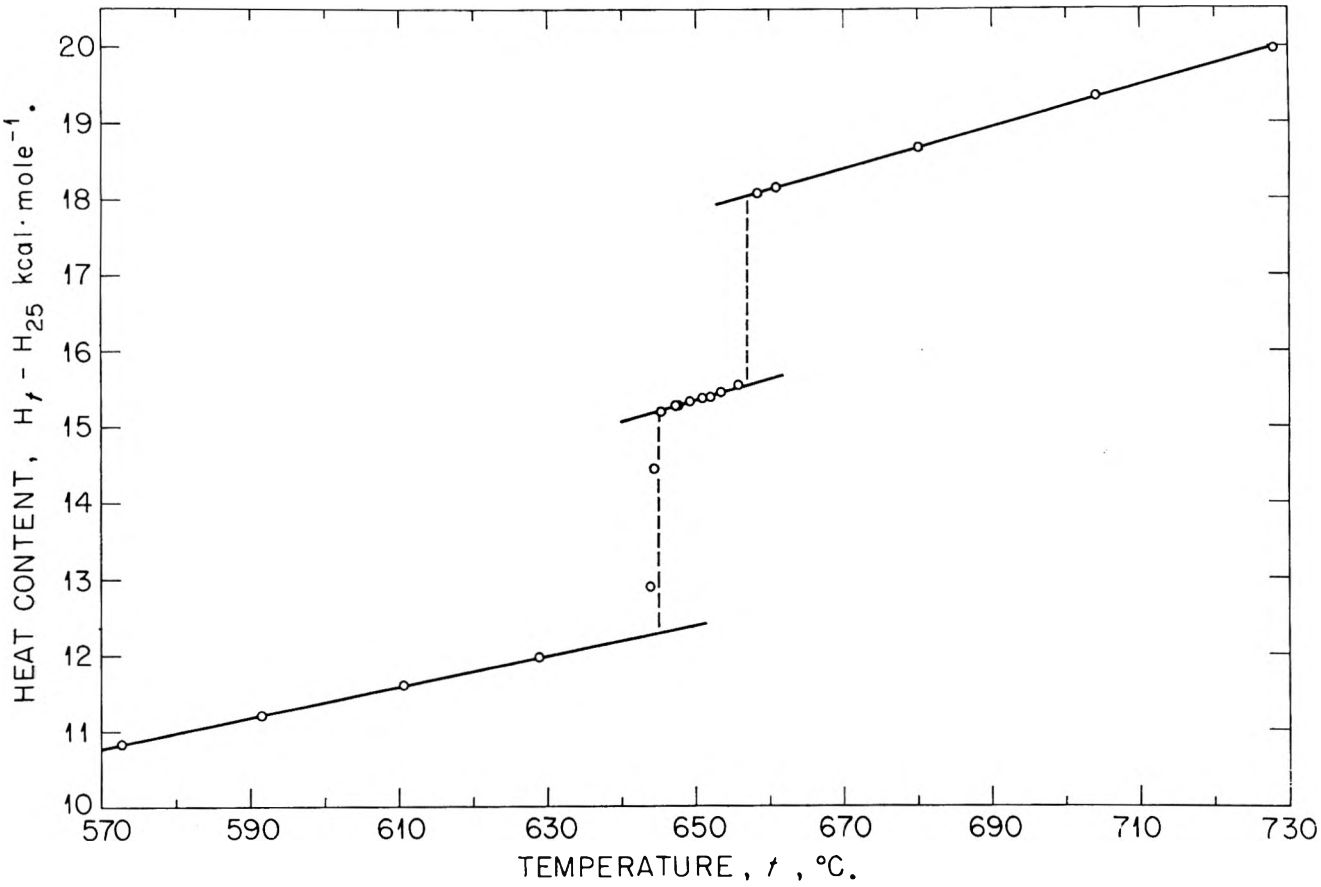

Fig. 1.—Heat content of $SrBr_2$ as a function of temperature.

tent data for $SrBr_2$ from which the heats of transition and melting were obtained.

Acknowledgment.—We wish to acknowledge the assitsance of D. E. LaValle and R. B. Quincy of this Laboratory, who prepared the samples of the anhydrous salts used in this work.

THE TRANSFERENCE NUMBERS OF D-TARTARIC ACID AND THE LIMITING EQUIVALENT CONDUCTANCE OF THE BITARTRATE ION IN WATER AT 25°

BY K. N. MARSH,[1] M. SPIRO,[2] AND M. SELVARATNAM[2]

Department of Chemistry, University of Melbourne, Melbourne N.2, Australia, and Department of Chemistry, Imperial College of Science and Technology, London S.W.7, England

Received September 25, 1962

The anion constituent transference numbers of 0.01–0.1 *M* aqueous solutions of D-tartaric acid have been measured at 25° with the direct moving-boundary method using acetic acid as indicator. The reasons for the variation of the results with current were investigated. The transference numbers at zero current were almost independent of concentration and led to a value of 27.6 for the limiting equivalent conductance of the bitartrate ion. A figure of 27.0 was derived from the conductances of ammonium bitartrate measured by Topp and Davies[3] when the large hydrolysis corrections were recalculated.

Introduction

In the past, two main methods have been employed to determine the limiting equivalent conductance (λ^0) of the anion HA^- of a weak diprotic acid H_2A. One approach has been to measure the equivalent conductances of solutions of H_2A, a procedure which necessitated a long extrapolation to infinite dilution A further loss in accuracy resulted because

$$\lambda_{HA^-}{}^0 = \lambda_{H_2A}{}^0 - \lambda_{H^+}{}^0 \qquad (1)$$

which involved taking the small difference between two large quantities. In general, an error of 0.1% in $\lambda_{H_2A}{}^0$ produced an error of the order of 1% in $\lambda_{HA^-}{}^0$. For these reasons many workers have preferred the second method of measuring the equivalent conductances of an alkali metal salt (MHA), only to encounter the hazards of hydrolysis. The closer the solutions were to infinite dilution the greater were the relative concentrations of H_2A and A^{--}, and the appropriate corrections required much ancillary information on dissociation constants, activity coefficients, and conductances. For example, Topp and Davies[3] calculated from their conductances of ammonium bitartrate at 25° that $\lambda_{HT^-}{}^0 = 45.5$ (T stands for the tartrate radical OOC.CHOH.CHOH.COO). Using more recent values of dissociation constants, we have recalculated below their hydrolysis corrections and find $\lambda_{HT^-}{}^0 = 27.0$, more than 40% below the original estimate.

Neither of these conductance methods is therefore very satisfactory, and we suggest that it is better to measure instead the transference numbers of the HA^- constituent of the acid. This procedure has three advantages:

(1) Use of the acid itself largely prevents further dissociation to A^{--} and the hydrolysis correction, if any, is small. To a first approximation H_2A can then be treated as a 1:1 electrolyte and[4]

$$T_{HA^-}{}^{H_2A} = \frac{m_{HA^-}\lambda_{HA^-}}{m_{H^+}\lambda_{H^+} + m_{HA^-}\lambda_{HA^-}} = \frac{\lambda_{HA^-}}{\lambda_{H^+} + \lambda_{HA^-}} \qquad (2)$$

where m_i is the molarity of species i. The effect of further dissociation is discussed later (eq. 7) and is usually negligible.

(2) The extrapolation of the transference numbers to infinite dilution is shorter for H_2A than for a strong electrolyte because the degree of dissociation cancels out between numerator and denominator in eq. 2 and the electrophoretic and relaxation terms are smaller. For conductances, on the other hand, the extrapolation is longer the weaker the electrolyte.

(3) Since $\lambda_{H^+} \gg \lambda_{HA^-}$, the quantity sought ($\lambda_{HA^-}$) is almost directly proportional to the quantity measured (T_{HA^-}). There is therefore no loss of accuracy in the final calculations as there is with eq. 1.

The present paper reports measurements of the anion constituent transference numbers of D-tartaric acid, with a falling moving-boundary cell and acetic acid as following (indicator) electrolyte.

Experimental

The apparatus was similar to that used for the determination of the transference numbers of iodic acid.[5] The equipment and technique have also been described in some detail in reference 6, where the cell used is depicted in Fig. 14, the circuit of the semi-constant current regulator in Fig. 20, and the optical assembly in Fig. 12. Since the leading solution in the present work was optically active, it proved helpful to place a piece of Polaroid sheet in front of the lamp bulb of the moving light source. Vibration in the oil-filled thermostat was avoided by mounting the stirring motor on a framework separate from the tank. The temperature of 25 ± 0.01° was constant to ±0.001°.

Preliminary work by Mr. J. A. McFarlane showed that indicator solutions of citric, furoic, malic, mandelic, phenoxyacetic, or succinic acids gave no visible boundaries with a leading tartaric acid solution. Only acetic or propionic acids were suitable indicators. The anode was a gassing platinum electrode while the closed cathode compartment contained a platinum wire electrode surrounded by some 3 ml. of a 2 *M* cadmium acetate solution. Care was taken to avoid undue mixing when the cell was filled, for the diffusion of cadmium ions into the leading solution caused the boundary to fade and eventually to slow down.

B. D. H. or Hopkin and Williams AnalaR D-tartaric acid was dried over silica gel in a vacuum desiccator. Further purification was unnecessary since the results were the same with a triply recrystallized sample. Preliminary work disclosed that an apparent gradual decrease in transference number from run to run was caused by bacterial decomposition in the stock solution, and thereafter no solution was kept for long and a small quantity (*ca.* 0.001 *M*) of B. D. H. thymol was added to each as a preservative. Even three times this amount of thymol had no effect on the velocity of the moving boundary. The other chemicals used were B. D. H. AnalaR acetic acid, B. D. H. AnalaR cadmium acetate, and B. D. H. propionic acid.

The volume correction is $-m(\Delta V/1000)$, where m is the stoichiometric molarity of the tartaric acid and ΔV is the volume increase in the closed cathode compartment per faraday. It is given by eq. 3

(1) Department of Chemistry, University of New England, Armidale N.S.W., Australia.

(2) Department of Chemistry, Imperial College of Science and Technology, London S.W.7, England.

(3) N. E. Topp and C. W. Davies, *J. Chem. Soc.*, 87 (1940).

(4) M. Spiro, *J. Chem. Educ.*, **33**, 464 (1956).

(5) M. Spiro, *J. Phys. Chem.*, **60**, 976, 1673 (1956).

(6) M. Spiro, "Determination of Transference Numbers," Chapt. 46 in A. Weissberger, Ed., "Physical Methods of Organic Chemistry," 3rd Ed., Interscience Publishers, New York, N. Y., 1960.

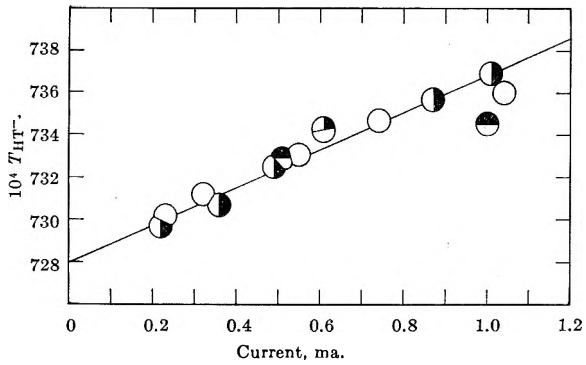

Fig. 1.—Variation with current of T_{HT^-} (solvent corrected) in 0.05 *M* tartaric acid solution, with different indicator solutions: ◑, 0.064 *M* acetic acid; ○, 0.050 *M* acetic acid, with some results at 0.045 *M* and 0.055 *M*; ◓, 0.040 *M* propionic acid.

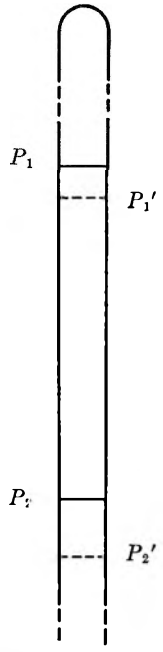

Fig. 2.—Schematic sketch of moving-boundary tube.

$$\Delta V = {}^1/_2\, V_{Cd} - {}^1/_2\, \bar{V}_{Cd(OAc)_2}{}^{Cd(OAc)_2} + \bar{V}_{HOAc}{}^{HOAc} - T_{HT^-}{}^{H_2T} \times \bar{V}_{H_2T}{}^{H_2T} \quad (3)$$

where $\bar{V}_i{}^j$ is the partial molal volume of i in solution j. Numerical values of V_{Cd} (13.0 cm.³/mole)[7] and $\bar{V}_{HOAc}$ (51.9)[8] were taken from the literature, and from our own density determinations we obtained $\bar{V}_{H_2T}$ (83) and $\bar{V}_{Cd(OAc)_2}$ (122). (The last value applies only for the 2 *M* catholyte solution whereas Longsworth's figures[7] for cadmium acetate refer to much more dilute solutions.) Hence $\Delta V = -9$ cm.³/faraday. As has recently been pointed out,[9] the volume correction calculated in this way is accurate only if there are no appreciable volume changes on mixing. Any uncertainty introduced by this is of course eliminated in the extrapolation to infinite dilution.

The small solvent correction was calculated as for iodic acid,[6] account being taken of the repression by the tartaric acid of the ionization of dissolved carbon dioxide.

The reproducibility of the transference numbers was *ca.* ±0.0001 and the results are therefore quoted to 4 decimal places only.

Results and Discussion

Variation with Current.—There is evidence in the literature[10,11] that, even with strong electrolytes, transference numbers change when the current becomes too high. Comparison of the results of strong electrolytes with those of the HIO_3–H_3PO_4 system[5] and the H_2T–CH_3COOH values in Fig. 1 showed clearly that the variation with current became the more pronounced the more associated the electrolytes used. Joule heating seemed to be the most likely explanation and a number of experiments were carried out to investigate the effect further.

In several blank runs, the whole cell was filled with either 0.05 *M* H_2T or 0.04 *M* CH_3COOH solution and the temperature inside the moving-boundary tube was measured at various currents with a chromel–alumel thermocouple. The latter was sealed into a glass sheath to insulate it from the high voltage in the tube. The results in Table I have been roughly corrected for the increased resistance caused by the presence of the thermocouple sheath (diameter 1 mm.) inside the 2.4 mm. diameter tube. A qualitative indication of the high temperature generated in the indicator solution was furnished by the observation that the Vaseline grease (softening point *ca.* 34°) on the main stopcock melted if the thermostat stirrer was switched off during a run.

TABLE I

JOULE HEATING INSIDE MOVING BOUNDARY TUBE

Solution	Current, ma.	Temp. (cor.), °C.
0.05 *M* H_2T	1.05	25.6
0.04 *M* HOAc	0.08	25.0
0.04 *M* HOAc	0.22	25.4₅
0.04 *M* HOAc	0.86	28.4
0.04 *M* HOAc	1.05	29.8

The increases in solution temperature affect the transference numbers in two ways:

(i) The indicator solution expands and, confined at one end by the closed electrode compartment, pushes the boundary forward. Let us suppose that in the absence of a temperature rise the boundary moves per faraday from a position P_1 near the top of the tube to P_2 near the bottom (Fig. 2), so sweeping out a volume $(P_2 - P_1)A$ where A is the (uniform) cross-sectional area of the tube. With Joule heating present (a "hot" run), the movement will be instead from P_1' to P_2' through a volume $(P_2' - P_1')A$. If the density of the indicator solution decreases from ρ at 25° to ρ' in the hot solution then its volume increases in the inverse proportion, and thus

$$T_{HT^-}(\text{hot})/T_{HT^-} = (P_2' - P_1')/(P_2 - P_1) = \rho/\rho'$$

It follows that a rise of (29.8 − 25)° in the acetic acid solution will increase the anionic transference number by 0.0001.

(ii) The tartaric acid transference number itself changes with temperature. It is easily shown that if t_1 and t_2 are two temperatures not very far apart, then

$$(T_{HT^-})_2 - (T_{HT^-})_1 \approx (T_{HT^-})_1\,(T_{H^+})_1\,(\beta - \gamma)\,(t_2 - t_1)$$

where

$$\beta = \frac{1}{\lambda_{HT^-}} \times \frac{d\lambda_{HT^-}}{dt}, \qquad \gamma = \frac{1}{\lambda_{H^+}} \times \frac{d\lambda_{H^+}}{dt}$$

In the present case $\gamma = 0.0138$[12] but β is unknown. In the absence of other information we can use instead the

(7) L. G. Longsworth, *J. Am. Chem. Soc.*, **57**, 1184 (1935).
(8) O. Redlich and L. E. Nielsen, *ibid.*, **64**, 761 (1942).
(9) R. J. Bearman, *J. Chem. Phys.*, **36**, 2432 (1962).
(10) E. R. Smith and D. A. MacInnes, *J. Am. Chem. Soc.*, **46**, 1398 (1924).
(11) H. P. Cady and L. G. Longsworth, *ibid.*, **51**, 1656 (1929).
(12) R. A. Robinson and R. H. Stokes, "Electrolyte Solutions," Butterworths, London, 2nd Ed., 1959, p. 465.

β value for the acetate ion (0.0206[12]), and hence with 0.05 M H_2T at 1.05 ma.

$$T_{HT^-}(25.6°) - T_{HT^-}(25.0°) \approx 0.0003$$

According to Fig. 1, the increase in T_{HT^-} caused by Joule heating at 1.05 ma. is 0.0009 whereas the sum of effects (i) and (ii) is only 0.0004. However, in an actual run the tartaric acid solution *just ahead of the boundary* will be warmer than 25.6° because of heat transfer from the hotter indicator solution, and if the latter raised the temperature to 26.6° then experiment and theory would agree exactly. The above analysis has therefore provided a fairly clear picture of the consequences of Joule heating and this should be of value in future work with weak electrolyte solutions.

Variation with Concentration and Type of Indicator.—Figure 1 shows that the transference numbers in 0.05 M H_2T solutions were virtually unaltered when the acetic acid concentration was varied, and the same was true for the other tartaric acid solutions.

Attention has sometimes been directed[6] to the importance of checking moving-boundary results by changing the indicator substance or by measuring both the cationic and the anionic transference numbers. The results obtained with propionic acid (Fig. 1) confirm that the bitartrate transference numbers were substantially independent of the indicator electrolyte. Moving-boundary determination of the H^+ constituent transference number, by a system such as H_2T–MHT, would not have been theoretically reliable because hydrolysis of the HT^- ions in the indicator solution would have produced some hydrogen ions there also. Attempts to check this point experimentally were unsuccessful, no boundaries being visible with lithium, sodium, or cadmium hydrogen tartrate as indicator to 0.01 M tartaric acid solutions.

Extrapolation of Transference Numbers.—The bitartrate transference numbers at zero current are listed in Table II with solvent and volume corrections incorporated. For the calculation of the degrees of dissociation of tartaric acid (α), we employed the dissociation constant of Bates and Canham[13] (9.17×10^{-4} mole/l.) and the Güntelberg expression for the mean ionic activity coefficients $f_\pm$

$$\log f_\pm = -Az_+ |z_-| \sqrt{\alpha m}/(1 + \sqrt{\alpha m}) \quad (4)$$

where z is the algebraic charge number and A is equal to 0.5098.[14]

The second dissociation constant of tartaric acid (4.30×10^{-5} mole/l.[13]) is not so much less than the first that the presence of tartrate ions can be altogether ignored. In 0.01 M solution 2% of HT^- ions are dissociated to T^{--} and in 0.1 M solution, 0.7%. In order to treat the problem quantitatively we must view the acid as a 1:2 electrolyte and choose as constituents the ions H^+ and T^{--}. Then[4]

$$T_{T^{--}} = \frac{2m_{HT^-}\lambda_{HT^-} + 2m_{T^{--}}\lambda_{T^{--}}}{m_{H^+}\lambda_{H^+} + m_{HT^-}\lambda_{HT^-} + 2m_{T^{--}}\lambda_{T^{--}}} = 2mV_F \quad (5)$$

The last term shows that $T_{T^{--}}$ is determined experimentally by multiplying V_F, the volume traversed by the boundary per faraday, by the equivalent concentration of the 1:2 electrolyte, *i.e.*, by twice the acid molarity. Thus the experimental transference numbers listed in Table II, which were obtained on the assumption that the acid was a 1:1 electrolyte, are really equal to

$$T_{expt} = mV_F = {}^1/_2 T_{T^{--}} \quad (6)$$

The relationship between T_{expt} and T_{HT^-} becomes clearer if we take the equilibrium concentrations in an m molar solution of tartaric acid as

$$[H_2T] = (1 - \alpha)m,\ [HT^-] = (\alpha - \beta)m,\ [T^{--}] = \beta m,\ [H^+] = (\alpha + \beta)m$$

Then from equations 5 and 6

$$T_{expt} = \frac{(\alpha - \beta)\lambda_{HT^-} + \beta\lambda_{T^{--}}}{(\alpha + \beta)\lambda_{H^+} + (\alpha - \beta)\lambda_{HT^-} + 2\beta\lambda_{T^{--}}} = \frac{\lambda_{HT^-} + \left(\frac{\beta}{\alpha - \beta}\right)\lambda_{T^{--}}}{\lambda_{H^+} + \lambda_{HT^-} + \left(\frac{2\beta}{\alpha - \beta}\right)(\lambda_+ + \lambda_{T^{--}})} \quad (7)$$

Obviously T_{HT^-} (eq. 2) is equal to T_{expt} when β/α is very small (*i.e.*, no appreciable dissociation of HT^- ions into T^{--}) or when the tartrate terms in the numerator and in the denominator of eq. 7 just balance each other so that

$$\frac{\lambda_{T^{--}}}{\lambda_{HT^-}} = \frac{2(\lambda_+ + \lambda_{T^{--}})}{\lambda_{H^+} + \lambda_{HT^-}} \quad (8)$$

In the present case condition (8) applies in dilute solutions if $\lambda_{T^{--}}{}^0 = 59.9$ (int. ohm)$^{-1}$ cm.^{2} equiv.$^{-1}$, and it so happens that values of 59.6[3] and 63.2[15] have been reported on the basis of conductance studies of tartrate salts. Unfortunately neither paper gives the original experimental figures nor details of the fairly important hydrolysis correction, and we therefore accept a value of about 60 with some reservations. Should future work lead to a significantly different value the appropriate corrections will have to be made to convert T_{expt} into T_{HT^-}, but on present indications the two transference numbers are numerically identical.

The most surprising aspect of the concentration variation of T_{HT^-} is its absence. The transference numbers of strong mineral acids in water approach the Debye–Hückel–Onsager limiting slope from above or below, but the deviation from theory is never large at

TABLE II

BITARTRATE CONSTITUENT TRANSFERENCE NUMBERS

m	α	Current range, ma.	T_{HT^-} [a]	T_{HT^-} [b] cor.	λ_{H_2T}
0.01	0.274	0.4 –0.6[c]	0.073_2	0.073_3	+0.52
.02	.205	0.2_5–0.7	.0732	.0734	+ .45
.05	.138	0.2 –1.0	.0728	.0733	+ .35
.10	.101	0.5 –1.0	.0729	.0738	+ .32

[a] At zero current and with solvent correction applied. [b] With volume correction applied also. [c] The boundary was too faint for visual observation at low currents and it became skew at high currents.

(13) R. G. Bates and R. G. Canham, *J. Res. Natl. Bur. Std.*, **47**, 343 (1951).

(14) M. Spiro, *Trans. Faraday Soc.*, **55**, 1746 (1959).

(15) J. F. J. Dippy, S. R. C. Hughes, and A. Rozanski, *J. Chem. Soc.*, 2492 (1959).

TABLE III[a]

ANALYSIS OF CONDUCTANCES OF AMMONIUM BITARTRATE[3]

$10^4 \times$ molarity of						$10^6 \times$ specific conductivity of						
Soln.	H^+	H_2T	T^{--}	HT^-	$10^4\mu$	Soln.	H^+	$(NH_4)_2T$	NH_4^+	HT^-	λ_{HT^-}	$\lambda_{HT^-}{}^0$
10.24	1.438	0.984	2.422	6.834	14.100	166.5	49.72	62.15	38.76	15.87	23.22	24.52
13.93	1.594	1.479	3.073	9.378	18.596	213.7	55.02	78.38	55.74	24.56	26.19	27.70
15.20	1.638	1.655	3.293	10.252	20.131	231.0	56.51	83.86	61.61	29.02	28.31	29.90
17.14	1.698	1.929	3.627	11.584	22.466	249.5	58.56	92.12	70.60	28.22	24.36	26.00
											Mean:	27.03

[a] To avoid cumulative errors of calculation, the computed results are all given to one decimal place more than is justified by the precision of the experimental data.

an ionic strength of 0.01 or less.[16] By analogy the value of T_{HT^-} at 0.1 M should have been *ca.* 0.007 less than that at infinite dilution. It seems reasonable to ascribe this difference in behavior of tartaric acid to the presence of H_2T molecules and these might be expected to give rise to two effects. First, the viscosity of the solution would be raised by a factor of

$$[1 + B_u(1 - \alpha)m]^n$$

over and above the interionic terms[14] and the equivalent conductance of the HT^- ion would thereby be decreased to a greater extent than that of the H^+ ion.[17] The influence of viscosity is therefore in the wrong direction to account for the experimental results and, since B_u and n are of the order of 0.1 and 1, respectively, the effect is rather small numerically. Second, H_2T molecules could migrate to some extent in an electric field, being carried along with the ions by complex formation, solvation, or momentum transfer. Equation 2 then becomes[4]

$$T_{HT^-}{}^{H_2T} = \frac{m_{HT^-}\lambda_{HT^-} \pm m_{H_2T}\lambda_{H_2T}}{m_{H^+}\lambda_{H^+} + m_{HT^-}\lambda_{HT^-}} = \frac{\lambda_{HT^-} \pm \left(\frac{1-\alpha}{\alpha}\right)\lambda_{H_2T}}{\lambda_{H^+} + \lambda_{HT^-}} \quad (9)$$

although strictly speaking a molecular species cannot be said to possess an equivalent conductance but only a mobility in an electric field. On the assumption that both λ_{H^+} and λ_{HT^-} obey the limiting Debye–Hückel–Onsager theory, we obtain, to a first approximation

$$(1 - \alpha)\lambda_{H_2T} = \pm\alpha\,[(\lambda_{H^+}{}^0 + \lambda_{HT^-}{}^0)(T_{HT^-} - T_{HT^-}{}^0) + (1 - 2T_{HT^-}{}^0)\,\sigma\sqrt{\alpha m}] \quad (10)$$

where $\sigma = 30.3$[14] (*cf.* eq. 13). The last column in Table II contains the λ_{H_2T} values so calculated. These show qualitatively that there is a small net transfer of H_2T molecules toward the anode but we cannot interpret at present the decrease in λ_{H_2T} with increasing concentration. A different trend might result if a future redetermination of $\lambda_{T^{--}}{}^0$ required a small tartrate correction (eq. 7).

Taking $T_{HT^-}{}^0$ as 0.0732 and $\lambda_{H^+}{}^0$ as 349.81,[12] we get $\lambda_{HT^-}{}^0 = 27.6$ (int. ohm)$^{-1}$ cm.^{2} equiv.$^{-1}$.

Recalculation of Literature Conductance Data.—Published figures for the limiting equivalent conductance of the bitartrate ion at 25° vary widely. The International Critical Tables select a value of 32 from data obtained around the turn of the century while more recent estimates are 38.9[15] and 45.5[3] derived, respectively, from the conductances of sodium and ammonium bitartrates. Only in the last case are experimental details available to enable a reassessment to be made of the crucial hydrolysis correction referred to in the Introduction. The calculations fall into two parts. First, with the Güntelberg equation 11 for the activity coefficient of any species i at an ionic strength μ (in mole/l.)

$$\log f_i = -0.5098z_i{}^2\sqrt{\mu}/(1 + \sqrt{\mu}) \quad (11)$$

and with $K_1 = 9.17 \times 10^{-4}$, $K_2 = 4.30 \times 10^{-5}$ mole/l. as the dissociation constants of tartaric acid[13] (Topp and Davies[3] used $K_1 = 3.0 \times 10^{-3}$, $K_2 = 6.9 \times 10^{-5}$), we calculated by successive approximations the molar concentrations of the species H^+, H_2T, T^{--}, and HT^- in the solutions (Table III). Association between ammonium and tartrate ions was presumed absent in the very dilute solutions used. Second, the specific conductivities (κ) produced by the H^+ ions, $(NH_4)_2T$, and the remaining NH_4^+ ions were worked out separately (Table III) from

$$1000\kappa = \lambda c \quad (12)$$

where c is the *equivalent* concentration, and from the Robinson and Stokes[18] conductance equation in the modified form

$$\lambda_i = \lambda_i{}^0 - (\theta\lambda_i{}^0 + \sigma)\sqrt{\mu}/(1 + \sqrt{\mu}) \quad (13)$$

We took $\lambda_{H^+}{}^0 = 349.81$,[12] $\lambda_{NH_4^+}{}^0 = 73.55$,[12] $\lambda_{T^{--}}{}^0 = 60$ (int. ohm)$^{-1}$ cm.^{2} equiv.$^{-1}$ (see comments made above), and θ and σ as 0.2292[14] and 30.3[14] for single univalent ions and as 0.4064 and 90.9 for $(NH_4)_2T$, respectively. The differences between the observed specific conductivities and the sums of the effects due to H^+, NH_4^+, and T^{--} ions were attributed to the HT^- ions, the small solvent conductivity being neglected because of the suppression of the carbon dioxide hydrolysis by the acidic solute. The implicit assumption that the specific conductivities are additive should hold well at these low ionic strengths. The last two columns in Table III then were obtained in turn from eq. 12 and eq. 13.

Inspection of Table III shows that the bitartrate ions contribute only 11% to the over-all conductances of the solutions and the estimate of $\lambda_{HT^-}{}^0$ is accordingly very sensitive to any errors in the hydrolysis corrections and in the experimental measurements themselves. This explains both the spread of the values in the last column of Table III and the drastic change from 45.5

(16) A. K. Covington and J. E. Prue, *J. Chem. Soc.*, 1567 (1957).

(17) B. J. Steel, J. M. Stokes, and R. H. Stokes, *J. Phys. Chem.*, **62**, 1514 (1958); **63**, 2089 (1959); L. A. Woolf, *ibid.*, **64**, 500 (1960).

(18) R. A. Robinson and R. H. Stokes, *J. Am. Chem. Soc.*, **76**, 1991 (1954).

to 27.0 brought about by the present recalculation. Finally, in view of the uncertainties inherent in the conductance method, the figure of 27.0 is in surprisingly good agreement with the value of 27.6 obtained from the transference determinations.

Acknowledgments.—We wish to thank the University of Ceylon for providing study leave for M. Selvaratnam, Professor A. S. Buchanan for his interest, and Mr. J. A. McFarlane for some preliminary experiments.

THE THERMODYNAMIC AND PHYSICAL PROPERTIES OF BERYLLIUM COMPOUNDS. II. HEAT OF FORMATION AND ENTROPY OF BERYLLIUM(I) FLUORIDE(g)[1]

BY MICHAEL A. GREENBAUM, R. E. YATES, M. LOUIS ARIN, MOHAMMED ARSHADI, JUSTINE WEIHER, AND MILTON FARBER

Rocket Power, Inc. Research Laboratories, Pasadena, California

Received September 26, 1962

The molecular flow effusion method has been employed to obtain second and third law heats of formation of BeF(g) from a study of the reaction $BeF_2(g) + Be(s,l) = 2BeF(g)$ over the temperature range 1425–1675°K. The ΔH of reaction was found to be 91.5 ± 3.8 kcal./mole, while the corresponding entropy of reaction was found to be 44.3 ± 2.4 cal./deg./mole. Employing recent experimental data together with available thermal functions for the constituents, a value of −48.3 ± 1.9 kcal./mole is obtained for ΔH_{f298} BeF(g) and 51.1 ± 1.2 cal./deg./mole for the S_{298} BeF. The third law value for ΔH_{f298} of BeF(g) was found to be −52.6 ± 0.6 kcal./mole.

Introduction

Increasing interest in beryllium and its compounds has prompted the undertaking of a program to obtain accurate thermodynamic and physical data for these compounds. The first phase of this program, the determination of the enthalpy and entropy of vaporization of BeF_2, was reported in the first of this series of articles.[2] This second phase of the program has been concerned with the determination of the heat of formation and entropy of BeF(g).

Inasmuch as the heat of formation of BeF(g) has not been reported previously, estimates of this property have been based on the dissociation energy, for which several values have been reported. Herzberg[3] obtained a D_0^0 value of 124 ± 23 kcal./mole by a linear extrapolation of the vibrational quanta. Gaydon,[4] after applying several corrections to the linear extrapolation, obtained D_0^0 = 92 ± 23 kcal./mole. In 1958 Tatenskii, *et al.*,[5] reinvestigated the BeF spectrum and reported a value of 184 ± 11.5 kcal./mole based on a non-linear extrapolation.

The wide variation in the dissociation energy of BeF results in a correspondingly wide variation in its heat of formation. Thus, using the heat of sublimation of beryllium of 78 kcal./mole[6] and the dissociation energy of fluorine of 38 kcal./mole,[7] the values obtained for the heat of formation of BeF are: −28 kcal./mole (Herzberg), +4 kcal./mole (Gaydon), and −88 kcal./mole (Tatenskii).

Since all previous work on BeF has been spectroscopic, the present determination of the heat of formation and entropy of BeF has been undertaken by a thermochemical method. The reaction of gaseous beryllium fluoride with a condensed phase of beryllium according to the equation

$$BeF_2(g) + Be(s,l) = 2BeF(g) \qquad (1)$$

has been studied in the 1425–1675°K. temperature range using a molecular flow effusion technique.

Experimental

A. Apparatus.—The molecular flow effusion method of Farber,[8] in combination with the Knudsen effusion method, was employed to determine the experimental data on the reaction of gaseous beryllium fluoride with solid or liquid beryllium at high temperatures. This procedure, in essence, consists of allowing the BeF_2 to pass over the Be, which is heated to the desired temperature, and allowing the resulting vapor species to escape through an effusion orifice into a high vacuum.

The experimental apparatus consisted of a three-part cell; a container for the BeF_2, a container for the Be, and a connecting tube. The cell was heated by a specially designed resistance furnace, allowing separate control of the BeF_2 and Be temperatures. The furnace containing the cell was placed inside a vacuum system where all experiments were carried out.

The container for the BeF_2 was constructed of high purity, high density graphite. It measured 20 × 20 × 22 mm. with a hole 18 mm. in diameter and 20 mm. deep drilled in it from the top. A 5-mm. diameter hole was drilled in one side of the block. The top was fitted with a tight-fitting graphite stopper. A 1-mm. hole was drilled a short way into one side of the cell to serve as a receptacle for a thermocouple. The container for the Be samples was constructed of high purity BeO. It was a tube 50 mm. in length with an outside diameter of 12.5 mm. and 1.5 mm. walls. One end of the tube was sealed off flat and a 1.1-mm. hole was drilled in the tube wall approximately 3 mm. from the closed end. The BeF_2 and Be containers were connected by a 125-mm. high purity graphite tube, approximately 15 mm. in diameter.

A resistance furnace was employed to heat the reaction cells to the desired temperatures. Heating of the tungsten coil surrounding the BeO tube was accomplished with a 40 amp., 270 v. variable auto transformer. The tungsten coil for heating the graphite cell was connected to an 8 amp., 120 v. powerstat. An alumina core, wrapped with two separate tungsten coils to provide separate heating control for the Be and BeF_2 containers,

(1) This research was supported by the Air Research and Development Command of the United States Air Force.

(2) M. A. Greenbaum, J. N. Foster, M. L. Arin, and M. Farber, *J. Phys. Chem.*, **67**, 36 (1963).

(3) G. Herzberg, "Molecular Spectra and Molecular Structures I, Spectra of Diatomic Molecules," 2nd Ed., D. Van Nostrand Co., New York, N. Y., 1950.

(4) A. G. Gaydon, "Dissociation Energies and Spectra of Diatomic Molecules," Chapman and Hall, Ltd., London, 1953.

(5) V. M. Tatenskii, L. N. Tunitskii, and M. M. Novikov, *Opt. i Spektroskopiya*, **5**, 520 (1958); *Chem. Abstr.*, **53**, 2774 (1959).

(6) G. T. Armstrong, H. W. Wooley, W. H. Evans, and L. A. Krieger, Natl. Bur. Std. Rept. 6928, July 1, 1960.

(7) D. R. Stull and G. C. Sinke, "Thermodynamic Properties of the Elements," American Chemical Society, Washington, D. C., 1956.

(8) M. Farber, *J. Chem. Phys.*, **36**, 1101 (1962).

was surrounded by four concentric radiation shields. The inner two shields were constructed of molybdenum while the outer were of stainless steel. Aligned holes were drilled through each of the four shields to allow measurement of the temperature of the BeO cell with an optical pyrometer. The temperature of the graphite cell containing the BeF_2 was measured with a chromel–alumel thermocouple.

The vacuum chamber in which the resistance furnace and cells were placed consisted of a 6-in. diameter Pyrex pipe, 18 in. in length. A 2-in. sidearm on the pipe was connected to a high vacuum gate valve. The ends of the pipe were closed with brass plates, one readily removable. A 10 mm. Kovar seal was soldered into the center of the stationary brass plate to provide for a roughing system and connection of an ionization gage tube. The other brass plate was fitted with connections for two electrical circuits and thermocouple connections.

B. Experimental Procedure.—The carbon container was filled with BeF_2[9] and was weighed. A sample of flake Be[10] was placed in the BeO container and this then was weighed The connecting graphite tube was weighed and the three sections of the cell joined together. The BeO section of the cell was placed in the closed end of the furnace, surrounded by the four radiation shields. In general, it was found advisable to place several molybdenum radiation shields between the BeO and graphite containers. This was accomplished by fitting some 7-mil molybdenum disks over the carbon connecting tube. The graphite container was placed toward the open end of the alumina core with the thermocouple receptacle facing out. An alumina-shielded chromel–alumel thermocouple, supported between steel plates mounted on a post fastened to the steel base plate, was inserted in this hole.

The entire assembly was placed in the vacuum chamber, the electrical connections were made to the inside of the brass end-plate, and the plate then was fastened tightly by means of a series of nuts and bolts. Electrical circuits were checked and the chamber was evacuated. When a vacuum of 1×10^{-4} mm. was reached, heating was commenced.

The chromel–alumel thermocouple was connected to a Leeds and Northrup recorder–controller for constant monitoring of the BeF_2 temperature. The BeF_2 and Be containers were heated simultaneously. The BeF_2 temperatures were generally in the 925–975° K. region, while the Be was maintained at a temperature in the range of 1425–1675°K. Independent control of the BeF_2 temperature was essential to the control of partial pressures of BeF_2. The temperature of the BeO cell containing the Be was measured with a Leeds and Northrup optical pyrometer.

The length of the runs varied from 1–6 hours. The BeF_2 temperature was continuously monitored to ensure that big fluctuations did not occur and produce too high or too low BeF_2 pressure. Temperature fluctuations in the BeF_2 container were always less than 5° and usually no more than 1–2°. The BeO cell temperature was constantly monitored with the pyrometer and readings were recorded. Fluctuation in this temperature was usually 10° or less. (The average temperature obtained from the series of readings during each run was taken as the actual temperature.) At the conclusion of a run, the BeF_2 heating was discontinued first to allow removal of all BeF_2 vapor in the system. From time to time some BeF_2 was found to have condensed in the graphite connecting tube, but never in the BeO cell when the above procedure was followed. The temperature of the BeO cell was lowered slowly and then the entire system was allowed to cool under vacuum. The vacuum during the course of a run was generally in the range of $1.0–5.0 \times 10^{-5}$ mm., measured with an ionization gage.

After the cell had cooled, it was removed from the vacuum chamber and the three sections were weighed individually. The loss in weight of the graphite cell minus any weight the graphite connecting tube might have gained (on some occasions when shielding between BeO and graphite containers was very efficient, the carbon tube was sufficiently cool so that some BeF_2 deposited in it) was taken as the weight loss of BeF_2. This value generally agreed very well with the weight loss predicted for the observed BeF_2 temperature and the previously reported vapor pressure curve for BeF_2.[2] Weight loss of the BeO container was considered to be due to loss of Be only.

The Clausing factor, W_0, of the effusion hole in the BeO cell was determined by measurement of the orifice dimensions by means of a traveling microscope. The measurements were made to ±0.001 mm., thus assuring a highly accurate W_0 value.

The optical pyrometer was calibrated with chromel–alumel thermocouples. It was found that over the experimental temperature range the outside cell temperature as read by the optical pyrometer corresponded within 5–10° of the inside cell temperature as measured by the thermocouple.

To establish the weight of beryllium lost due to simple vaporization of the metal at the experimental temperatures, blank runs were carried out. The beryllium sample was placed in the BeO tube which was in turn connected to a blank carbon tube supported at the far end with a graphite block. The cell was heated in the usual manner for the length of time corresponding to the experimental run, cooled *in vacuo*, and weighed. During these runs some beryllium generally condensed on the face of the carbon tube. The weight gain of the graphite tube was thus added to the weight of BeO cell and Be, the resulting total weight being subtracted from the original value to yield net Be weight loss resulting from effusion through the orifice in the BeO tube. The vapor pressure curve resulting from these runs (employing the measured Clausing factor for the effusion orifice) was in excellent agreement with the available literature curves.[11]

Treatment of Experimental Data

The reduction of the experimentally determined weight loss data to equilibrium constants was accomplished by combining a modified effusion equation with the equilibrium constant equation. The basic effusion equation[12] is

$$P = 17.4 \frac{G'}{W_0 A t} \sqrt{\frac{T}{M}} \qquad (2)$$

where P is the pressure of the effusing compound (mm.), G' is the total weight loss (grams) of the compound due to effusion through an orifice of area A (cm.^{2}) during t seconds, W_0 is the Clausing factor, T is the temperature (°K.), and M is the molecular weight of the effusing material.

In the present work A was found to be 9.51×10^{-3} cm.^{2}, W_0 was 0.1380 by direct measurement. Substituting these values into the equation and converting the equation to pressure in atmospheres, G in mg., and t in hours, the expression becomes

$$P_{(atm)} = 4.771 \times 10^{-6} \left(\frac{G}{t} \sqrt{\frac{T}{M}} \right) \qquad (3)$$

At equilibrium, according to eq. 1, two moles of BeF are formed as the result of the reaction of one mole of Be; thus, if G_r represents the weight loss of Be due to reaction, $56/9G_r$ or $6.22G_r$ represents the weight of BeF effusing from the cell at equilibrium. Also, for each mole of Be reacting one mole of BeF_2 reacts; thus, if G_0 represents the total weight loss of BeF_2 during an experiment, $(G_0 - (47/9)G_r)$ represents the weight of BeF_2 effusing from the cell at equilibrium. The partial pressures of BeF and BeF_2 at equilibrium, then, are given by the equations

$$P_{BeF} = 5.55 \times 10^{-6} \frac{\sqrt{T}}{t} G_r \qquad (4)$$

$$P_{BeF_2} = 6.96 \times 10^{-7} \frac{\sqrt{T}}{t} (G_0 - 5.22G_r) \qquad (5)$$

(9) Brush Beryllium Company, 99.7% purity.

(10) General Astrometals Corp., 99.97% purity.

(11) (a) E. H. Gulbransen and K. J. Andrew, *J. Electrochem. Soc.*, **97**, 383 (1950); (b) R. B. Holden, R. Spieser, and H. L. Johnston, *J. Am. Chem. Soc.*, **70**, 3897 (1948).

(12) S. Dushman, "Scientific Foundations of Vacuum Techniques," John Wiley and Sons, Inc., New York, N. Y., 1960.

The equation for the equilibrium constant

$$K = \frac{P^2_{BeF}}{P_{BeF_2}} \quad (6)$$

on substituting the above expression for P_{BeF} and P_{BeF_2}, becomes

$$K = 4.524 \times 10^{-5} \frac{\sqrt{T}}{t}\left(\frac{G_r^2}{G_0 - 5.22G_r}\right) \quad (7)$$

and

$$\log K = -4.345 + \log \frac{\sqrt{T}}{t} + \log\left(\frac{G_r^2}{G_0 - 5.22G_r}\right) \quad (8)$$

At temperatures in excess of 1500°K. the rate of weight loss of Be due to simple vaporization and effusion became significant. Therefore, it was necessary to subtract a blank correction from the total beryllium weight loss, G_t, to obtain the weight loss due to reaction, G_r. These blank corrections were determined experimentally for each of the temperatures above 1500°K.

The data obtained in the blank experiments were also used to calculate the vapor pressure of beryllium in the experimental temperature range, using the Clausing factor obtained from traveling microscope measurements. Table I shows the vapor pressures calculated from these data and those obtained from the literature.[11]

TABLE I

VAPOR PRESSURE OF BERYLLIUM, ATM.

T, °K.	This work	Reference 11
1670	3.1×10^{-4}	2.7×10^{-4}
1625	1.6×10^{-4}	1.5×10^{-4}
1570	6.8×10^{-5}	6.0×10^{-5}
1575	6.1×10^{-5}	6.6×10^{-5}
1575	5.9×10^{-5}	6.6×10^{-5}
1530	2.1×10^{-5}	3.1×10^{-5}

Validity of the Reaction.—The reaction occurring between beryllium and beryllium fluoride in the effusion cell has been assumed to be that represented by eq. 1. If this assumption is valid and the equilibrium constant is given by eq. 6, then a plot of log P_{BeF} *vs.* log P_{BeF_2} should result in a straight line with a slope of 2. Inasmuch as the G_r and $G_0 - 5.22G_r$ are proportional to P_{BeF} and P_{BeF_2}, respectively, a log–log plot of these data was used. The data for the experiments at 1525 and 1575°K. have been represented graphically in Fig. 1, which shows the least squares lines along with the data points. The slopes of these lines were found to be 1.74 ± 0.32 and 1.94 ± 0.30 for T = 1525 and 1575°K., respectively, indicating that the assumed reaction is valid within the experimental accuracy.

The possibility that reactions other than the desired one were taking place was investigated. Initially it was shown that no weight loss of either graphite or BeO occurred at the temperatures of interest. The available literature data likewise predict no measurable vaporization of either graphite or BeO at these temperatures. The absence of any reaction between BeF_2 and graphite at temperatures up to 1275°K. was demonstrated in a previous publication.[2] The reaction

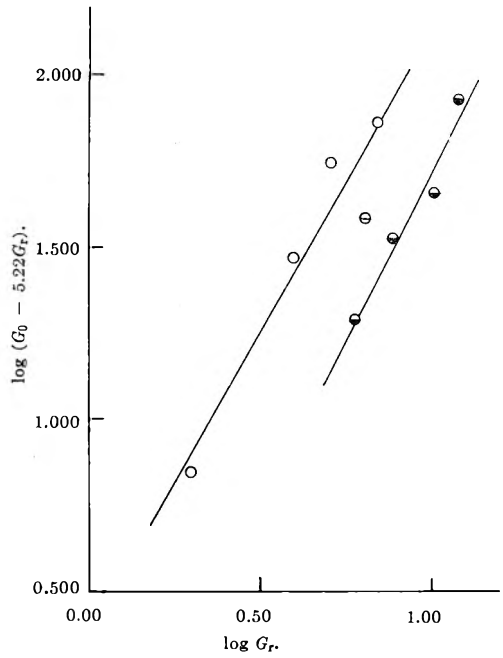

Fig. 1.—Relationship of equilibrium pressures of BeF_2 and BeF: ○, T = 1525°K.; ◒, T = 1575°K.

of BeF_2(g) and BeO(s) was investigated over the temperature range 1425–1675°K. by using the experimental apparatus without the Be sample. The BeO tube was heated to constant weight and then appreciable quantities of BeF_2 were passed through the tube. Heating of the BeF_2 container was stopped while the BeO container was heated for an additional 30 min. No change in weight of the BeO container was observed at either temperature. In agreement with published thermodynamic data,[6] BeO and graphite were found to be unreactive at the experimental temperatures.

One reaction was found to occur, however. The formation of Be_2C from reaction of Be(s,l,v) with carbon at temperatures in the neighborhood of 1250°K. takes place. Reaction of solid Be with carbon was very slow, the liquid Be reacted faster, and the Be(v) reaction with solid carbon was quite fast. The first blank runs with Be resulted in formation of Be_2C on the face of the carbon connecting tube in the BeO container as evidenced both by the formation of a brownish color on the carbon face and a small weight gain of the tube. However, subsequent blank runs using the same tube produced no further weight change apparently due to passivation of the carbon surface. It should be emphasized that the extent of reaction during these preliminary runs was very slight and during an actual experiment no such reaction was observed. All runs, however, did employ a previously passivated carbon tube.

A check was made on the possibility of diffusion of Be vapor back into the connecting graphite tube. This was accomplished by using one tube with a 1-mm. opening and a second tube with a 3-mm. opening. Runs were made with both tubes over the entire temperature range during which Be partial pressures varied between 10^{-1} and 10^{-3} mm. and BeF_2 pressures varied over a similar range. The BeF_2 pressure was always greater than that of the Be partial pressure. If Be were being lost by diffusion into the carbon tube, then it should have varied as the orifice of the carbon tube was varied and as the ratio of partial pressures was

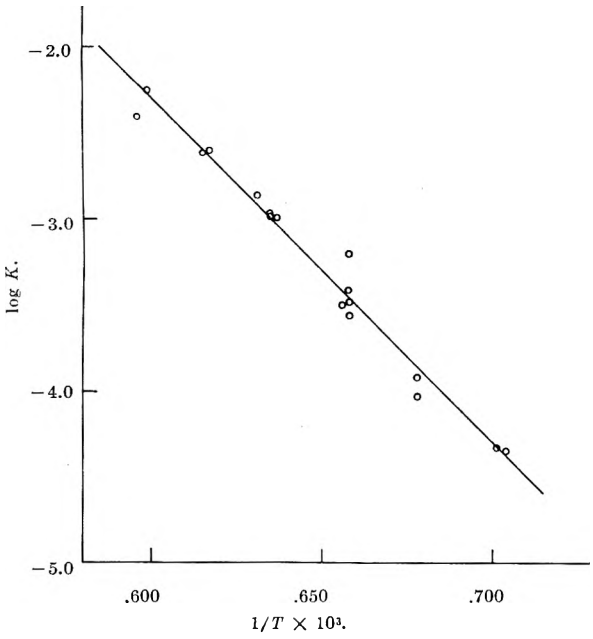

Fig. 2.—Equilibrium constant of BeF_2–Be reaction as a function of temperature.

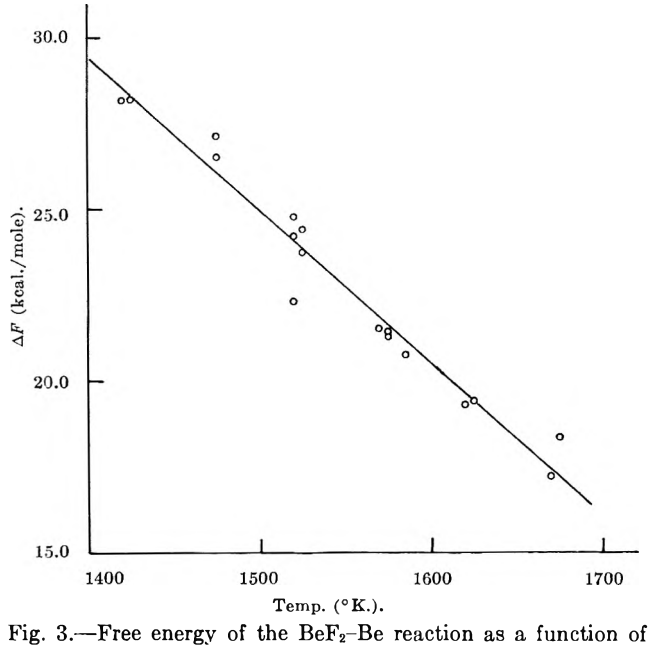

Fig. 3.—Free energy of the BeF_2–Be reaction as a function of temperature.

varied. The calculated thermodynamic values in all cases were found to be completely independent of the orifice area of the graphite tube as well as the ratio of partial pressures.

Thermodynamic Data.—The results obtained in the present study for reaction 1 have been summarized in Table II, and Fig. 2 and 3 show graphs of log K *vs.* $1/T$ and ΔF *vs.* T from which the second law heat and entropy of reaction were determined. Least squares analyses of the experimental data lead to a heat of reaction in the 1425–1675°K. temperature range of 91.5 ± 3.8 kcal./mole and an entropy of reaction of 44.3 ± 2.4 e.u. Employing this heat for the reaction and a value of −191.3 kcal./mole for ΔH_{f298} of BeF_2(g) recently obtained at this Laboratory,[13] together with estimated theoretical heat capacity data[14] for the species involved, BeF_2(g), Be(s,l), and BeF(g), a value of −48.3 ± 1.9 kcal./mole is obtained for ΔH_{f298} of BeF(g). The entropy of reaction combined with a value of 52.4 cal./deg./mole for BeF_2(g),[13] and 2.3 cal./deg./mole for Be(s),[15] together with theoretical entropy data[14] yields a value of 51.1 ± 1.2 cal./deg./mole for S_{298} of BeF(g). This compares with a theoretical entropy value of 49.2 cal./deg./mole.[14] The third law ΔH_{f298} for BeF(g) is −52.6 ± 0.6 kcal./mole, employing the same thermal data for Be and BeF_2(g),[13,15] which is in good agreement with that obtained from the Van't Hoff equation.

TABLE II

SUMMARY OF DATA FOR THE Be–BeF_2 REACTION

T, °K.	Time, hr.	G_0 BeF_2 wt. loss, mg.	G_t Be wt. loss, mg.	G_r,[a] mg.	log K	ΔF, kcal./mole	ΔH_f,[b] kcal./mole
1420	6.0	215.1	5.4	5.4	−4.354	28.2	−52.5
1425	6.0	197.0	5.3	5.3	−4.327	28.2	−52.4
1475	3.0	102.8	4.1	4.1	−3.923	26.4	−52.3
1475	3.0	126.0	4.1	4.1	−4.031	27.2	−51.9
1520	3.0	72.0	7.4	6.4	−3.204	22.2	−53.4
1520	3.0	17.5	3.0	2.0	−3.480	24.2	−52.4
1520	3.0	82.1	6.1	5.1	−3.559	24.8	−52.1
1525	3.0	110.0	8.0	7.0	−3.406	23.8	−52.5
1525	3.0	50.4	5.0	4.0	−3.496	24.4	−52.2
1575	3.0	73.7	10.7	7.7	−2.975	21.4	−52.8
1585	3.0	98.4	13.2	10.2	−2.860	20.7	−53.0
1570[c]	3.0	147.3	15.0	12.0	−2.992	21.5	−52.8
1575	3.0	51.0	9.0	6.0	−2.959	21.3	−52.9
1620	2.0	105.7	16.3	11.3	−2.604	19.3	−53.0
1625	2.0	109.3	16.5	11.5	−2.611	19.4	−52.8
1670	1.0	81.6	14.4	9.7	−2.251	17.2	−53.0
1675	1.0	76.4	13.1	8.4	−2.396	18.4	−52.4

[a] G_r is Be wt. loss (mg.) due to reaction. [b] ΔH_f [BeF(g)] at 298°K. calculated from third law. [c] Melting point of Be is 1556°K.

It should be noted that in the second law evaluation of the heat and entropy of reaction the data of experiments below the melting point of beryllium have not been treated separately from those at temperatures above the melting point. The heat and entropy of fusion of the metal (2.8 kcal./mole and 1.8 e.u.)[7] will result in small differences in the heats and entropies of the reaction in the two regions. These small differences, however, are within the limits of accuracy of the experiments and have been neglected. Although the values for the heat and entropy of fusion of Be are of the same order of magnitude as the reported uncertainties in our values, the precision of the available experimental points (±3.8 kcal. obtained from a least squares analysis of the data) was not great enough to allow the determination of a break in the curve corresponding to the heat of fusion. It should be pointed out that third law treatment has taken account of the fusion process in the calculations presented in Table II.

Previous estimates of the heat of formation of BeF(g) have been based on spectroscopically determined dissociation energies. These dissociation energies are inherently of a low order of accuracy as a result of the

(13) M. A. Greenbaum, M. L. Arin, and M. Farber, *J. Phys. Chem.*, to be published.

(14) JANAF Thermochemical Tables, USAF Contract No. AF 33(616)-6149, Advanced Research Projects Agency, Washington 25, D. C.

(15) T. D. Rossini, *et al.*, "Selected Values of Chemical Thermodynamic Properties," Natl. Bur. Std. Circ. 500, Washington, D. C., 1952.

very long extrapolations of vibrational quanta required for their calculations. The magnitude of the uncertainties involved in this procedure are well illustrated by the divergence of values which have been reported. Therefore, it is not surprising that the more precise, thermochemically determined value of ΔH_{f298} of BeF, −48.3 kcal./mole, does not agree well with any of these estimated values. It is of interest to note, however, that the thermochemical value lies between the extremes of the spectroscopic values. In addition, a re-examination of the BeF spectrum will be conducted in an effort to clarify the apparent discrepancies.

NOTES

FORMATION CONSTANTS OF WEAK COMPLEXES: THE 1:1 COMPLEXES OF MALATE WITH ALKALI METAL CATIONS IN AQUEOUS SOLUTION[1]

By Luther E. Erickson and Jay A. Denbo

Department of Chemistry, Dickinson College, Carlisle, Pa.

Received June 28, 1962

Recent nuclear magnetic resonance studies of aqueous solutions of α- and β-hydroxycarboxylic acid salts indicate that there is appreciable association between the alkali metal cation and the anion.[2,3] Jardetzky and Wertz based their conclusions on the significant broadening of the Na^{23} resonance signal, which they attributed to interaction of the Na^{23} nuclear quadrupole moment with the asymmetric electric field of the complex. Erickson and Alberty drew a similar conclusion on the basis of the concentration dependence of the high-resolution proton n.m.r. spectra of the five alkali metal malates. The latter investigation revealed, furthermore, that all of the alkali metal cations form complexes with malate and that tetramethylammonium ion is much less strongly bound by malate than is any of the alkali metal cations.

This research was undertaken in order to test the interpretation of the n.m.r. results and, if possible, to obtain accurate numerical values for the formation constants of the alkali metal–malate complexes.

Experimental

Materials.—Reagent grade chemicals (Fisher Scientific Co.) were used in all experiments. These were used without further purification. Stock solutions of the alkali metal chlorides (0.50 *M*) and tetramethylammonium bromide (0.50 *M*) were prepared by weight as needed. In each case, recently boiled, deionized water was used in preparing the solutions. A fresh malic acid solution (~0.10 *M*) was prepared and standardized with $(CH_3)_4NOH$ prior to each run.

Apparatus.—A Beckman Model GS pH meter, readable to 0.005 pH unit and reproducible to 0.01 pH unit, was used in all the work. Small glass and calomel electrodes were employed and all measurements were made in the electrically shielded compartment of the instrument. Temperature control to ±0.1° was provided by circulating water from a well stirred constant temperature bath to an auxiliary bath equipped with spaces for 50-ml. beakers, which contained samples to be determined.

Procedure.—A series of 12-solutions (100 ml. of each) was prepared for each determination. For each solution, the proper amounts of stock solutions of malic acid (10.0 ml.), $(CH_3)_4NOH$ (~16.0 ml.), alkali metal chloride (0–50.0 ml.), and $(CH_3)_4NBr$ (50.0–0 ml.) were added so as to have identical total malic acid concentration (~0.01 *M*), extent of neutralization (~1.8 equiv. base/mole acid), and ionic strength (0.28), but at least six different alkali metal ion concentrations (0–0.25 *M*). The pH of each solution was determined after temperature equilibrium had been attained.

Results

In preliminary experiments, 0.010 *M* malic acid was titrated with 0.1 *N* $(CH_3)_4NOH$ in the presence of 0.25 *M* $(CH_3)_4NBr$ or 0.25 *M* $NaClO_4$. The titration curve was slightly, but significantly, lower in the presence of $NaClO_4$, indicating that some association does occur.[4] Because of the experimental difficulty of obtaining reproducible results to the desired degree of accuracy when the full titration curve was plotted, formation constants were ultimately evaluated by pH measurements under more restrictive conditions, *i.e.*, by varying the metal ion concentration at constant extent of neutralization and ionic strength.

Mathematical Treatment.—In order to treat the system quantitatively, the following assumptions were made. (1) The concentration of undissociated acid is negligible. This restricts the validity of our equations to pH > 5, since $pK_1 = 3.26$ at $\mu = 0.20$.[5] (2) The OH^- concentration is negligible compared to the H^+ concentration, *i.e.*, pH < 6. (3) The only complex that need be considered is the 1:1 complex, MA^-, of the metal ion, M^+, and the malate anion, A^{-2}. (4) $(CH_3)_4N^+$ forms no complexes with malate[3] or with other anions. Tetramethylammonium bromide then can be used to control the ionic strength. (5) There is no significant concentration of alkali metal halide complex.

The following five equations, in which ( ) denotes concentration and $[H^+]$ denotes the conventional hydrogen ion activity, describe the state of affairs in a solution of malic acid which has been partially neutralized with $(CH_3)_4NOH$ and which, in addition, contains an appreciable concentration of MA^- as a result of the presence of added MCl

$$K_2' = [H^+](A^{-2})/(HA^-) \quad (1)$$

$$K_f = (MA^-)/(M^+)(A^{-2}) \quad (2)$$

$$t_a = (HA^-) + (MA^-) + (A^{-2}) \quad (3)$$

$$t_M = (M^+) + (MA^-) \quad (4)$$

(1) This article is based on the thesis submitted by Jay A. Denbo in fulfillment of the requirements for Chemistry 83-84, Dickinson College, 1962. Requests for reprints should be addressed to Luther E. Erickson, Grinnell College, Grinnell, Iowa.

(2) O. Jardetzky and J. E. Wertz, *J. Am. Chem. Soc.*, **82**, 318 (1960), and earlier reference cited therein.

(3) L. E. Erickson and R. A. Alberty, *J. Phys. Chem.*, **66**, 1702 (1962).

(4) Good discussions of the effect of complex formation on pH can be found in A. E. Martell and M. Calvin, "Chemistry of the Metal Chelate Compounds," Prentice-Hall, Inc., Englewood Cliffs, N. J., 1952, pp. 78–94, and in F. J. C. Rossotti and H. Rossotti, "The Determination of Stability Constants and other Equilibrium Constants in Solution," McGraw-Hill Book Co., New York, N. Y., 1961, pp. 127–160.

(5) K. Cannan and A. Kibrick, *J. Am. Chem. Soc.*, **60**, 2314 (1938).

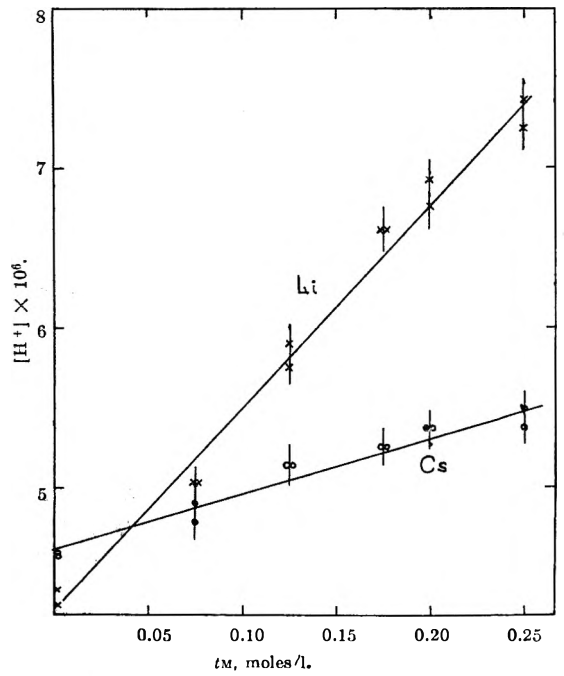

Fig. 1.—Graphical determination of K_f for the complexes of malate with alkali metal cations. Upper line obtained with added LiCl; lower line, CsCl.

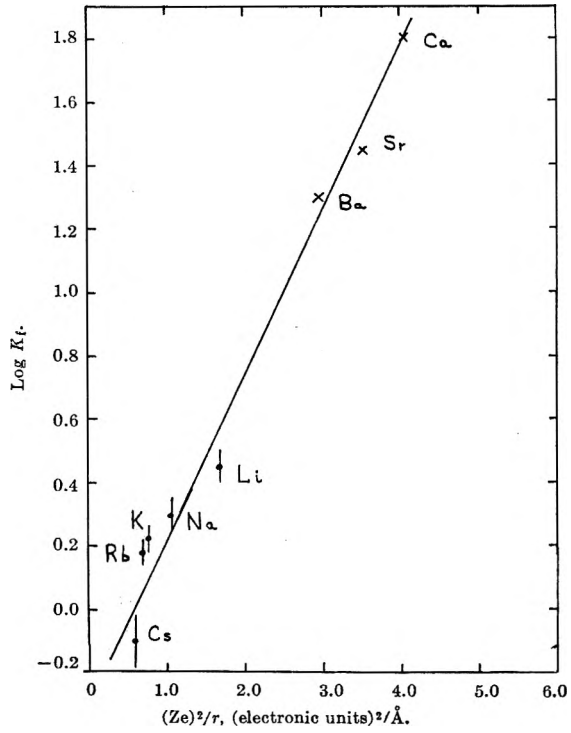

Fig. 2.—Dependence of formation constants of malate complexes on charge and radius of metal ion.

$$a + (M^+) + (H^+) = (Cl^-) + (MA^-) + (HA^-) + 2(A^{-2}) \quad (5)$$

The meanings of K_2' and K_f are obvious from the equations above, while t_a, t_m, and a denote total molar concentrations of acid, metal, and tetramethylammonium ion, respectively.

Under carefully restricted experimental conditions, these relations can be combined to enable graphical evaluation of K_f. Combining (1) and (2) with (3) and (1), (2), and (4) with (5) yields two expressions involving terms in (A^{-2}). Upon elimination of (A^{-2}) and regrouping terms, recognizing that $t_M = (Cl^-)$, we obtain

$$[a/t_a - 1 + (H^+)/t_a][H^+]/K_2' + [a/t_a - 2 + (H^+)/t_a](M^+)K_f = [2 - a/t_a - (H^+)/t_a] \quad (6)$$

Under the conditions employed in these experiments, $(H^+)/t_a \ll a/t_a - 1$ or $2 - a/t_a$. Therefore, to a very good approximation, (6) can be rewritten in the form

$$[H^+] = [(2t_a - a)/(a - t_a)]K_fK_2'(M^+) - [(2t_a - a)/(a - t_a)]K_2' \quad (7)$$

Furthermore, for these experiments, $(M^+) \gg t_a$, so that $(M^+) \sim t_M$. Therefore, a plot of hydrogen-ion activity *vs.* t_M should be linear. The ratio of slope to intercept is just K_f, the formation constant of the 1:1 complex.

Summary of Results.—Figure 1 shows the plots obtained with added LiCl and CsCl. For the other alkali metals, the slopes were intermediate between these two extremes. Vertical lines indicate the reproducibility of the individual points, 0.01 pH unit. In every case, the plot was satisfactorily linear within the estimated maximum uncertainty. It should be emphasized that the *maximum* change in pH, which occurred for 0.25 *M* added LiCl, amounted to only 0.24 unit. Therefore, there is still considerable uncertainty in the slopes.

The formation constants and K_2' calculated from these plots, along with significant experimental details and the formation constants of the alkaline earth–malate complexes, are summarized in Table I. The estimated limits of error shown in Table I correspond to an uncertainty of 10^{-6} in the slope of each line, which is equivalent to an uncertainty of 0.01 pH unit at $t_M = 0$ and 0.25 *M*.

TABLE I

FORMATION CONSTANTS AND SUMMARY OF EXPERIMENTAL DETAILS

Cation	t_a, moles l.$^{-1}$	a, moles l.$^{-1}$	K_2', moles l.$^{-1}$	K_f, l. mole^{-1}
Li^+	0.00988	0.0175	1.36×10^{-5}	2.8 ± 0.3
Na^+	.00986	.0175	1.36×10^{-5}	$2.0 \pm .3$
K^+	.00995	.0175	1.37×10^{-5}	$1.7 \pm .2$
Rb^+	.01000	.0175	1.43×10^{-5}	$1.5 \pm .2$
Cs^+	.00998	.0173	1.38×10^{-5}	$0.8 \pm .2$
Ca^{+2}	...	...	...	63.[5]
Sr^{+2}	...	...	...	28.[5]
Ba^{+2}	...	...	...	20.[5]
			Av. 1.38×10^{-5}	

Discussion

Comparison with Alkaline Earth Complexes.—In agreement with the trend usually observed for alkali metal complexes,[6] the stability of the malate complexes increases as the ionic radius of the cation decreases. According to Born's model,[7] log K_f should be linearly dependent on $(Ze)^2/r$, where Ze is the cation charge

(6) For example, G. Schwarzenbach and H. Ackermann, *Helv. Chim. Acta*, **30**, 1798 (1947); R. M. Smith and R. A. Alberty, *J. Phys. Chem.*, **60**, 180 (1956).

(7) M. Born, *Z. Physik*, **1**, 45 (1920) and the discussion thereof in A. E. Martel and M. Calv n, ref. 4, pp. 191–205.

and r is the cation radius, if the interaction is essentially ionic.

A plot of $(Ze)^2/r$ *vs.* log K_f is shown in Fig. 2. Considering the uncertainties in K_f (indicated on the graph) and the ionic radii,[8] these data all fit the line reasonably well. It is possible that there also may be very weak complexing by $(CH_3)_4N^+$. This would be most significant in the determination of K_f for the very weak cesium complex. If this were the case, K_f should be somewhat larger for the cesium complex.

K_2' of Malic Acid.—It should be noted that the apparent second dissociation constant of malic acid reported in this work (1.38×10^{-5}) differs considerably from that reported by Cannan and Kibrick, 2.09×10^{-5}. Although their ionic strength is slightly lower (0.20 *vs.* 0.28), the difference very likely reflects their use of $NaClO_4$ to control the ionic strength in their determinations and their assumption that there is no association between malate anion and sodium cation. In this connection, it should be pointed out that the K_f values for the alkaline earth complexes are probably also low, for the same reason.

Relation to N.m.r. Results.—To the extent that the formation constants obtained in this research are applicable at different ionic strengths, they can be used to calculate the fraction of malate ion present as the complex species at various total concentrations of alkali metal malate. The calculation shows that the fraction present in the complex is roughly the same at each concentration for *all* the alkali metal malates. For example, in a 2 *M* solution, the fraction in the 1:1 complex is 0.85 for lithium malate at one extreme and 0.67 for cesium malate at the other. As the total concentration is decreased, the extent of complex formation of course decreases in accord with the mass action expression. These calculations are probably more reliable than the semiquantitative estimate of 0.5 for the fraction present as the 1:1 complex in 2 *M* malate solutions, derived from the concentration dependence of the high-resolution proton n.m.r. spectra of alkali metal malates.[3] The n.m.r. estimate was based on relatively small changes in the spectra resulting from dilution and the assumption of similar chemical shifts and spin coupling constants for HA^- and MA^-. The latter assumption is open to question in view of the fact that the carboxyl group adjacent to the H–C–OH group is the group which has lost the proton in HA^-, but it is very likely (but not necessarily exclusively) the carboxyl group involved in complex formation.

The Na^{23} line-broadening observed by Jardetzky[2] for sodium malate solutions is less than that observed for solutions of some of the other sodium salts of organic acids. It therefore seems extremely likely that the stability constants of complexes of these anions with alkali metal cations can be determined with good accuracy by potentiometric pH measurements. On the basis of Jardetzky's work, other likely candidates include lactate, citrate, the tartrates, pyruvate, and α- and β-hydroxy butyrates.

Acknowledgment.—This work was supported by a grant from Research Corporation, whose assistance is gratefully acknowledged.

(8) L. Pauling, "The Nature of the Chemical Bond," 3rd Ed., Cornell Univ. Press, Ithaca, N. Y., 1960, p. 514.

THE ACTIVATION ENERGY FOR THE PYROLYSIS OF METHANE[1]

BY HOWARD B. PALMER AND THOMAS J. HIRT

Department of Fuel Technology, College of Mineral Industries, Pennsylvania State University, University Park, Pa.

Received December 22, 1962

The recent work of Bell and Kistiakowsky[2] allows one to compute ΔH^0_{298} for the reaction

$$CH_4 \longrightarrow CH_2 + H_2 \qquad (1)$$

with fair accuracy. It is 103 kcal., with an uncertainty of 3 or 4 kcal. This may be compared with the ΔH^0_{298} of about 102 kcal.[3] for the reaction

$$CH_4 \longrightarrow CH_3 + H \qquad (2)$$

It further appears that the energy barrier for the reverse of reaction 1 is not high; and it is a virtual certainty that the radical–atom recombination represented by the reverse of reaction 2 has at most an activation energy below 1 kcal. Hence in the high temperature decomposition of CH_4, both reactions 1 and 2 should be significant.

In the past few years, three shock tube studies of the decomposition of methane have been reported[4,5] which have covered wide temperature ranges with reasonable precision in the rate constant data obtained, but which have produced controversy over the activation energy for the first step in the pyrolysis. Glick[4a] and Kevorkian, *et al.*,[4b] suggested that the first step is reaction 1, the ΔH^0_{298} of which was accepted as about 85 kcal. at the time of their work.[3] The experimental activation energies obtained by these workers were in the neighborhood of this figure, when their high temperature results were used in conjunction with data obtained at much lower temperatures. The results of Kassel[6] and of Shantarovich and Pavlov[7] were relied upon particularly.

Skinner and Ruehrwein,[5] on the other hand, suggested reaction 2 as the first step. Their unusually precise shock tube data yielded an activation energy for CH_4 pyrolysis of 101 kcal. without recourse to data from other studies.

A technique recently developed in this Laboratory[8-10] for studying the kinetics of formation of carbon films during the decomposition of various compounds has produced some additional kinetic data on CH_4 at temperatures far below the shock tube studies. In our view, these additional results provide unequivocal evidence for an activation energy in essential agreement with the result of Skinner and Ruehrwein. The study of CH_4 is an extension from a study of carbon formation

(1) Work supported by the Atomic Energy Commission under Contract AT(30-1)-1710.

(2) J. A. Bell and G. B. Kistiakowsky, *J. Am. Chem. Soc.*, **84**, 3417 (1962).

(3) B. E. Knox and H. B. Palmer, *Chem. Rev.*, **61**, 247 (1961).

(4) (a) H. S. Glick, "Seventh Symposium (International) on Combustion," Butterworths, London, 1959, p. 98; (b) V. Kevorkian, C. E. Heath, and M. Boudart, *J. Phys. Chem.*, **64**, 964 (1960).

(5) G. B. Skinner and R. A. Ruehrwein, *ibid.*, **63**, 1736 (1959).

(6) L. S. Kassel. *J. Am. Chem. Soc.*, **54**, 3949 (1932).

(7) P. S. Shantarovich and B. V. Pavlov, *Zhur. Fiz. Khim.*, **30**, 811 (1956).

(8) D. B. Murphy, H. B. Palmer, and C. R. Kinney, "Industrial Carbon and Graphite," Society of Chemical Industry, London, 1958, p. 77.

(9) T. J. Hirt and H. B. Palmer, "Proceedings of the Fifth Conference on Carbon," Pergamon Press, Oxford, 1962, p. 406 and *errata*, p. 639.

(10) T. J. Hirt, Ph.D. dissertation, The Pennsylvania State University, 1962.

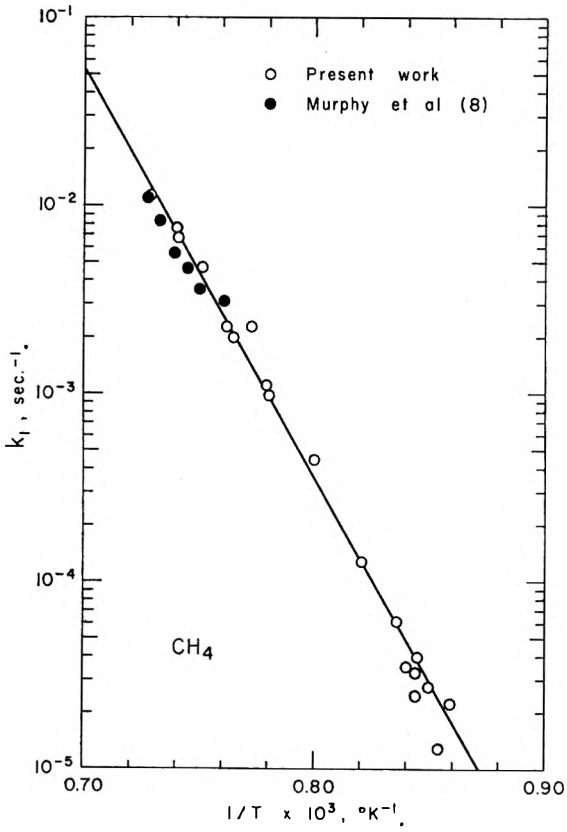

Fig. 1.—Arrhenius plot of effective decomposition rate constants for methane computed from carbon deposition rates.

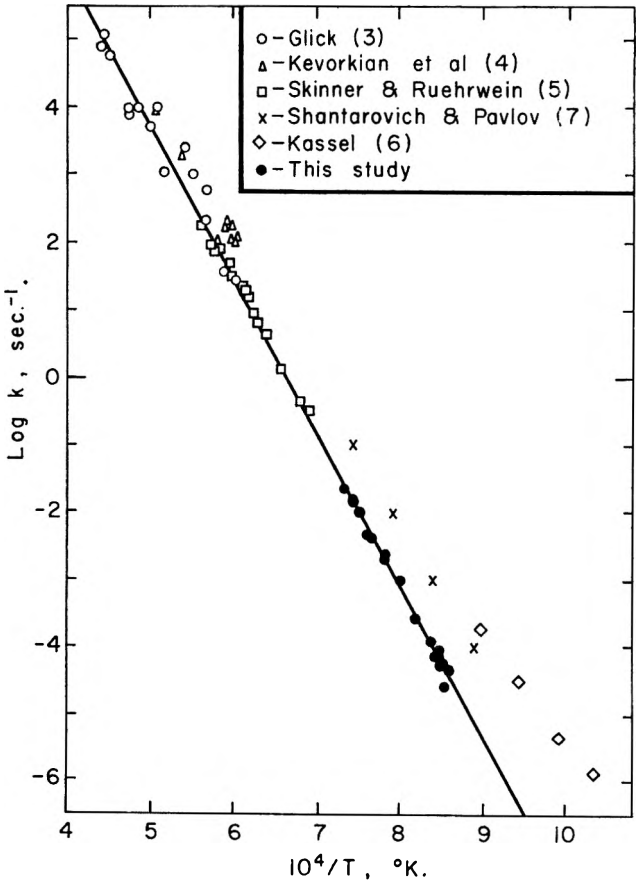

Fig. 2.—Summary of available rate constant data for methane decomposition.

from C_3O_2. The latter produced gas-phase kinetic data that have been reported earlier.[11]

(11) H. B. Palmer and T. J. Hirt, *J. Am. Chem. Soc.*, **84**, 113 (1962).

The experimental method consists of measuring the rate of carbon film formation on a specified portion of the length of a glazed porcelain rod, located centrally in a pyrolysis tube. The electrical resistance of the film is used as a measure of its thickness. The gas to be pyrolyzed enters the annular reactor in a helium carrier. After a short induction period, carbon deposits within the reactor at a steady rate. Conditions are carefully maintained so that sooting is avoided.

A mathematical analysis[9] of the steady-state deposition process in the flow system shows that the deposition rate is directly proportional to the rate of gas-phase decomposition of the starting material, provided: (a) that the characteristic diffusion time, $\beta^2/2D$ (β is the half-width of the annulus) is much less than the reciprocal of the first-order rate constant for the gaseous decomposition; and (b) that the (one or several) depositing species produce carbon on the wall with much higher efficiency than does the starting material. When these conditions are no longer satisfied, one should observe a curvature in the Arrhenius plot computed from the deposition rate data. When the conditions are satisfied, the proportionality constant that relates the deposition rate to the gaseous decomposition rate is a computable function[9] of apparatus geometry and of the density and resistivity of the carbon film. Thus absolute values of gaseous rate constants can be obtained from carbon deposition rates

Our results for CH_4 are shown in Fig. 1, together with the earlier results of Murphy, *et al.*,[8] which have been recalculated using the revised analysis.[9] The present work includes a variation of the CH_4 concentration by a factor of 20, which has established good first-order dependence upon (CH_4). The dependence upon (He) has not been determined. It is assumed to be zero-order, in keeping with the shock tube studies. The results define a straight line given by

$$k = 10^{14.1} \exp(-101 \text{ kcal.}/RT) \text{ sec.}^{-1}$$

In Fig. 2 is shown a collection of pertinent rate constant data for CH_4 decomposition, spanning a temperature range of about 1400°K. The present results have been multiplied by a factor of 2 for inclusion in the figure. The reason is that, whereas in the shock tube studies a chain length of 2 was undoubtedly present as a result of either

$$H + CH_4 \longrightarrow CH_3 + H_2 \qquad (3)$$

or

$$CH_2 + CH_4 \longrightarrow C_2H_6 \text{ or } 2CH_3 \qquad (4)$$

in the present work the dominant fate of H or CH_2 probably is removal at the walls of the annulus. This is established for H atoms by an order-of-magnitude comparison of the mean diffusion time for H atoms from the middle of the annulus to the walls, *vs.* the time required to remove 10% of the H atoms by reaction 3. The rate constant for reaction 3 is known.[12] Reaction 4 is not so well understood, and we cannot be so sure of the argument in this case.

The inclusion of the present results in Fig. 2 appears to provide the necessary low-temperature evidence

(12) S. Benson, "The Foundations of Chemical Kinetics," McGraw-Hill Book Co., Inc., New York, N. Y., 1960.

for determining the line that best describes the shock tube results. The data of Glick[4a] scatter appropriately about this line, while those of Kevorkian, *et al.*,[4b] seem somewhat high. There is a systematic uncertainty in the absolute values of k from the present study that amounts to a factor of about 1.5. It is a consequence of an inadequate knowledge of the specific resistivity of the carbon films. The uncertainty does not, however, reconcile our results with those of Shantarovich and Pavlov, nor with Kassel.

The best line through the present data and those of Skinner is given by

$$k = 10^{14.88} \exp(-103 \text{ kcal.}/RT) \text{ sec.}^{-1}$$

The rate constant for the initial step then should be

$$k_1 = 10^{14.58} \exp(-103 \text{ kcal.}/RT) \text{ sec.}^{-1}$$

The frequency factor is reasonable, while the activation energy, which is uncertain by about 2 kcal., is consistent with either or both reactions 1 and 2 as the first steps in pyrolysis. It seems likely that both reactions occur.

We conclude that the three shock tube studies were all without serious errors, the study of Skinner and Ruehrwein being the most accurate. The controversy over the activation energy would not have arisen if accurate low-temperature data had been available earlier.

THE SORPTION OF WATER VAPOR AND THE HYDROGEN–DEUTERIUM EXCHANGE EFFECT ON POLY-L-GLUTAMIC ACID[1]

BY WASYL S. HNOJEWYJ[2] AND LLOYD H. REYERSON

School of Chemistry, University of Minnesota, Minneapolis 14, Minnesota

Received August 31, 1962

Studies, in this Laboratory, of the sorption of H_2O and D_2O by lyophilized and completely dried solid natural proteins[3-5] revealed a number of interesting properties. Sigmoid isotherms were obtained at 17 and 27° and at times for the isotherms at 37°. Extrapolation of the upper straight line segments of any of these isotherms for a given protein to the ordinate for the saturated vapor pressure of H_2O at the respective temperatures crossed these ordinates at the same amounts adsorbed. Furthermore, these amounts adsorbed by the several proteins just equalled the amounts of D_2O that had to be adsorbed to account for the maximum deuterium exchange found for the proteins studied.[4] This must mean a monosite occupation. It seems to rule out any use of BET theory to obtain what many then call a monolayer of adsorbed H_2O. The theory itself was never based on assumptions that could apply to the disordered surface of proteins due to the wide variation in the character of the side chains. These variations must produce a number of sites having different energies of adsorption. In fact, a number of the isotherms show two to three straight line segments in their mid-portions which might suggest adsorption sites of different energies. At higher temperatures, *i.e.*, 47 and 57°, these segments disappear and the isotherms are smooth curves.

It was felt desirable to extend the studies in this Laboratory to a synthetic polymer of an amino acid as well as to synthetic polymers of the same acid having different substituents on the side chains. This paper presents the results of a study on poly-L-glutamic acid. Isotherms were obtained at 17, 27, 37, and 57° and these showed that this polymer of glutamic acid was not as good an adsorbent of water as was the poly-γ-Na-L-glutamate, but was a better adsorbent than the polybenzyl derivative.[6]

Experimental

The amounts of H_2O and D_2O sorbed were determined gravimetrically by using a quartz helical spring balance having a sensitivity of 1.2580 mg./mm. The spring extension was measured by a traveling microscope having an accuracy of ±0.003 mm. The equilibrium vapor pressures were read from a silicone oil manometer by a cathetometer to a precision of ±0.01 mm. The actual experimental procedure was similar to the work previously reported.[3-5] The poly-L-glutamic acid had a degree of polymerization of about 650 while the deuterium oxide was 99.5% pure.[7] The water used was triply distilled and then degassed by a series of freezings, thawings, and evacuations.

The sample, in a light glass bucket attached to the lower hook of the quartz helical spring, was first degassed and dried under a vacuum for ten days at 57 ± 0.05°. The first drying produced a loss of 6.245% of the original weight. Some of this loss was due to moisture and the remainder possibly consisted of impurities. Successive adsorptions of H_2O by the sample, up to a gain of 26% in weight at 17° or lower, were followed by tempering at 57°. Complete desorptions at 57° then showed a declining weight loss as given in Table I.

TABLE I

WEIGHT LOSS OF THE POLYMER (PGAc) AT 57° FOLLOWING SUCCESSIVE ADSORPTION–DESORPTIONS

No. of saturation–desorptions	Wt. loss, %
1	2.4720
2	0.223
3	.055
4	.032
5	.035

Thus it appears that a weight loss of 0.035% is to be expected for each adsorption–desorption of H_2O after the first four of such operations have been completed. Desorptions, carried out at reported experimental temperatures lower than 57°, showed no loss of weight. Following the above treatment, 212.4 mg. of the sample was used to determine isotherms for H_2O vapor in this given order: one at 57°, two at 37°, two at 17°, two at 27°, and one at 57°.

The sample then was desorbed to a constant weight at 57°. Relatively large amounts of D_2O then were successively adsorbed, often at lower temperatures in order to more rapidly reach a larger amount of D_2O sorbed. This then was desorbed at 57° after careful tempering at that temperature. Each of these operations took a long time, often as much as 8 to 12 days for a complete desorption. The polymer gained weight due to the exchange of deuterium for a labile hydrogen but the gain diminished with each successive adsorption–desorption of D_2O.

Results and Discussion

Isotherms for the adsorption of H_2O vapor on poly-glutamic acid at 17, 27, 37, and 57° are shown in Fig. 1. It should be noted that the time required for equilibrium to be reached for the first point of the isotherm

(1) This study was supported in part by Research Grant No. H-2972 from the National Institutes of Health.

(2) Research Associate.

(3) W. S. Hnojewyj and L. H. Reyerson, *J. Phys. Chem.*, **63**, 1653 (1959).

(4) L. H. Reyerson and W. S. Hnojewyj, *ibid.*, **64**, 811 (1960).

(5) W. S. Hnojewyj and L. H. Reyerson, *ibid.*, **65**, 1964 (1961).

(6) Reported in a paper submitted for publication in *J. Phys. Chem.*

(7) The poly-L-glutamic acid was obtained from Pilot Chemicals, Inc., Watertown, Mass., and the D_2O from Stuart Oxygen Co., San Francisco, Calif.

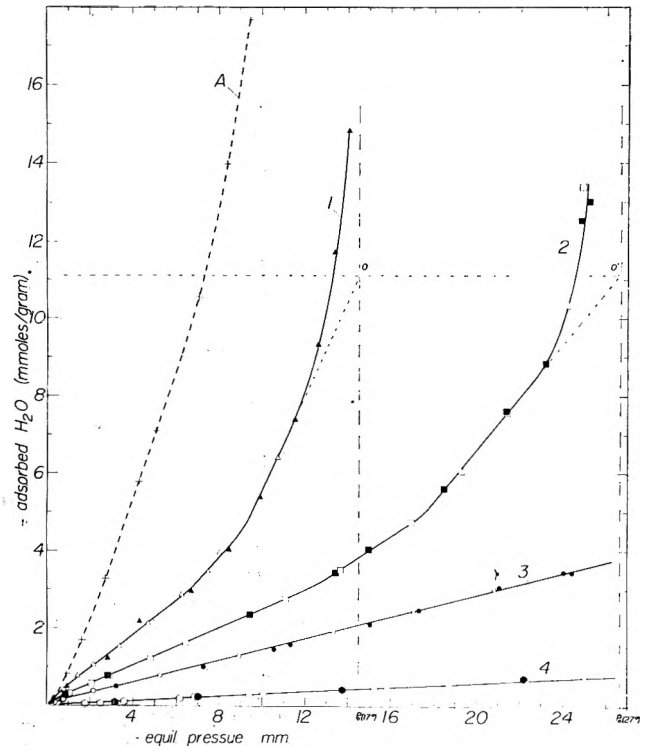

Fig. 1.—Adsorption isotherms of water vapor on poly-L-glutamic acid at various temperatures: solid points, second runs: 1, at 17°; 2, at 27°; 3, at 37°; 4, at 57°; A, adsorption of H_2O on the poly-L-glutamic ammonium salt at 17°.

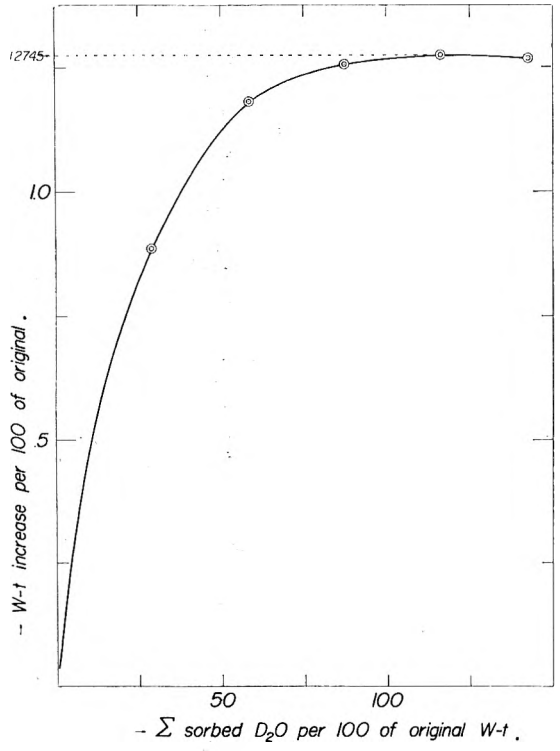

Fig. 2.—Weight increase of poly-L-glutamic acid due to hydrogen–deuterium exchange (PGAc-H + D_2O → PGAc-D + HOD) during the repeated adsorptions-desorptions at 57°.

at 17° was about 12 hr. Each successive point required more and more time until it took about 96 hr. to reach the point on the isotherm where the curve broke upward toward saturation. Less and less time was needed for equilibrium as the temperature for the isotherm was increased until at 57° only about one-third of the time was required as compared to 17°.

The isotherms at 17 and 27° have three distinct straight line segments following the first initial uptake of H_2O molecules.

One might naïvely assume that these segments are due to the adsorption of H_2O on three kinds of sites whose activity toward H_2O differs slightly. However the formula for PGAc indicates only two sites per unit that are hydrophilic, one on the peptide group and the other on the side chain

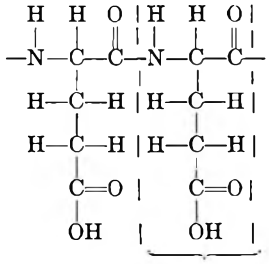

$n \backsimeq 650$ (n = degree of polymerization)

Unit

Possible formula for poly-glutamic acid

The above assumption cannot be correct because 15.4 mmoles of H_2O ought to be adsorbed if each unit of the polymer adsorbs two H_2O molecules. However, extrapolations of upper straight line segments of the isotherms at 17 and 27° cross the ordinates for the saturated vapor pressures of H_2O at these two temperatures at a value of 11.2 mmoles/g. adsorbed (see Fig. 1). This value is 72.7% of the amount that could be adsorbed if each of the two hydrophilic sites adsorbed a water molecule. In addition the maximum deuterium exchange was found to be 1.2745% of the original weight of the polymer as shown in Fig. 2. This amounts to 81.7% of the available labile hydrogens. It is evident from these results that the structure of PGAc is of such a character that only a little more than 80% of the labile hydrogens are structurally situated so that D_2O molecules, when adsorbed, are able to exchange a D for H during the adsorption–desorption process. During the successive adsorptions of D_2O, many times the amount of D_2O necessary for complete exchange was sorbed by the polymer. Once the maximum exchange had been reached, further sorption of D_2O produced no additional gain in weight of the sample. Thus this synthetic poly-amino acid behaved in a manner somewhat similar to the natural proteins studied in this Laboratory. However, the extrapolations of the upper straight line portions of the water isotherms, at 17 and 27°, crossed the saturated vapor pressure ordinates at points that were the same for the two temperatures, as shown in Fig. 1. In the previous studies on the natural proteins, these intersections indicated monosite occupation by water molecules since the moles of water sorbed at this point approximately equaled the moles of D_2O required for the maximum exchange. In the present case the two values were not the same. The indicated number of moles of H_2O sorbed at the extrapolated intersections was found to be less than the moles of D_2O required for the complete exchange. Thus the extrapolations of the H_2O isotherms may not indicate monosite occupation. However, if they do mean such occupation on the unaltered surface and structure of the polymer then, as the isotherms turn upward, the adsorbed molecules must affect the structure so that more D_2O molecules are sorbed in ways

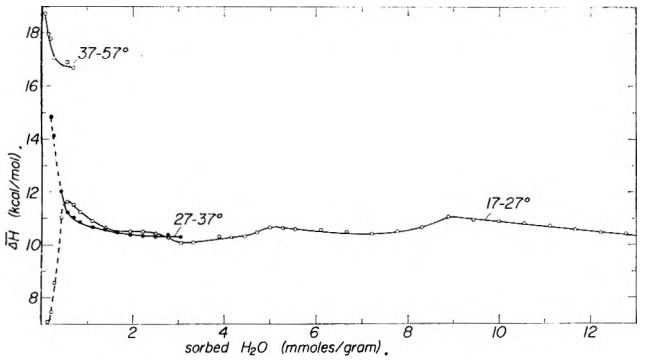

Fig. 3.—Differential heats of water vapor adsorption on poly-L-glutamic acid.

that permit exchange than would be the case if they were only able to exchange on the equivalent number of monosites holding water molecules.

Differential heats of adsorption for H_2O on this polyglutamic acid were calculated by the Clausius–Clapeyron equation and the results are sown in Fig. 3. The values for the temperature intervals 17–27° and 27–37° are in relatively good agreement except in the range of the lowest amounts adsorbed. In this range the precision of the isotherm data is not good enough to be certain of the calculated heat values. The values obtained for the temperature interval 37–57° are much higher. The amounts adsorbed at 57° have become so small that the character of the adsorption might well have changed in this temperature interval, leading to these higher values.

Finally, as a result of a study (to be published later) of the adsorption of NH_3 on a sample of this same polymer one or two interesting observations may be made. Ammonia gas was found to be very weakly adsorbed and it could be readily desorbed by evacuation. However, if H_2O vapor is adsorbed up to about 10% gain in weight, then NH_3 gas is spontaneously adsorbed up to a certain amount. The H_2O and NH_3 molecules, or their combination NH_4OH, were desorbed at a pressure of 10^{-6} mm. for a long time. The polymer showed a weight gain equivalent to the binding of one NH_4^+ group per unit of the polymer. This suggests the exchange of an NH_4^+ for the H^+ of the carboxyl group on the side chain. If an isotherm for the adsorption of H_2O vapor at 17° on this new polymer containing the NH_4^+ groups is determined, then the H_2O is adsorbed to a far greater degree than on the PGAc. This is shown as dotted curve A in Fig. 1. Here extrapolation of the straight line portion of this isotherm until it crosses the ordinate for the vapor pressure of H_2O at this temperature gives a value of adsorption of about two H_2O molecules per unit of this ammoniated polymer. Thus the presence of the NH_4^+ on the carboxyl group makes the polymer about as hydrophilic as does the sodium ion.

Conclusion

This investigation has shown that this polyglutamic acid material is able to exchange only a little more than 80% of its so-called labile hydrogens. Isotherms for the adsorption of H_2O at 17 and 27° also show a monosite occupation of less than this fraction of the total number of hydrophilic sites. Thus both the structure of the polymer plus the nature of the side chains determine its capacity for adsorbing H_2O as well as its ability to exchange its labile hydrogens. These results are quite similar to the behavior of lysozyme[5] as found in this Laboratory.

OZONE FORMATION AT −196°[1]

By J. A. Wojtowicz, H. B. Urbach, and J. A. Zaslowksy

Olin Mathieson Chemical Corporation, Organics Division, New Haven, Connecticut

Received September 10, 1962

The low temperature reaction of oxygen atoms with molecular oxygen to form ozone has long been known. Although Harteck and Kopsch[2] indicated that the reaction proceeds to a large extent at −190°, they did not indicate that the reaction was quantitative. Broida and co-workers,[3] Ruhrwein and Hashman,[4] and Harvey and Bass[5] have studied the reaction at liquid helium temperature. The quantitative formation of ozone at these low temperatures was not indicated. The above studies were concerned with the trapping of oxygen radicals in frozen matrices.

It was of interest in connection with studies on the thermal decomposition of ozone and the reaction of ozone with oxygen atoms to determine what percentage of the oxygen atoms which are present in a dissociated oxygen stream at 1 mm. pressure are converted to ozone at −196°.

Since this work was performed prior to the development of the so-called "absolute" nitrogen dioxide titration method,[6] a calorimetric method for oxygen atom assay based upon total conversion of oxygen atoms to molecular oxygen was developed. An ice-calorimetric technique was chosen for the thermal measurements.

The absence of significant quantities of ozone in a stream of oxygen atoms at ambient temperature and about 1 mm. pressure has been established.[2,7]

Experimental

Electrolytic oxygen (less than 20 p.p.m. total impurities[8]) was used in all experiments. The apparatus consisted of a Wood discharge tube connected to a vacuum system consisting of a 20 cm. length of 12 mm. i.d. tubing and a detachable U-tube. The detachable U-tube could be replaced by a Bunsen ice-calorimeter of conventional design (Fig. 1) which contained a U-tube of the same dimensions as the detachable U-tube. The oxygen flow rate of 2 mmoles/min. at 1 mm. was controlled by capillary tubing. A Welch Duo-Seal pump was used for evacuating the system. The discharge tube was activated by two neon sign transformers rated at 15 kv. and 30 ma. which were connected in parallel. With the U-trap in place ozone could be condensed from the oxygen atom stream by cooling the trap with liquid nitrogen. After several minutes the discharge was turned off and the dewar removed. The product ozone was swept with gaseous nitrogen into a potassium iodide scrubber as the condensate was allowed to warm. The ozone production rate was determined by titration of the scrubber solution with sodium thiosulfate. The experiment was repeated with the same oxygen pressure setting until a statistically significant mean rate of ozone productivity

(1) This work was performed under Contract No. AF 24 (645)-72; presented at the 136th National Meeting of the American Chemical Society, Atlantic City, N. J., September, 1959. Inquiries should be directed to J. A. Zaslowsky.

(2) P. Harteck and U. Kopsch, *Z. physik. Chem.*, **12**, 327 (1931).

(3) H. P. Broida and J. R. Pellam, *J. Chem. Phys.*, **23**, 409 (1955); H. P. Broida and O. S. Lutes, *ibid.*, **24**, 484 (1956); H. P. Broida, *Ann. N. Y. Acad. Sci.*, **67**, 530 (1957).

(4) R. A. Ruhrwein and J. S. Hashman, *J. Chem. Phys.*, **30**, 823 (1959).

(5) K. B. Harvey and A. M. Bass, *J. Mol. Spectry.*, **2**, 405 (1958).

(6) "Progress in Reaction Kinetics," G. Porter, Ed., Pergamon Press, 1961, Chapter 1 by F. Kaufman.

(7) J. T. Herron and H. I. Schiff, *Can. J. Chem.*, **36**, 1159 (1958).

(8) H. B. Urbach, E. Fisher, and J. A. Zaslowsky, unpublished data.

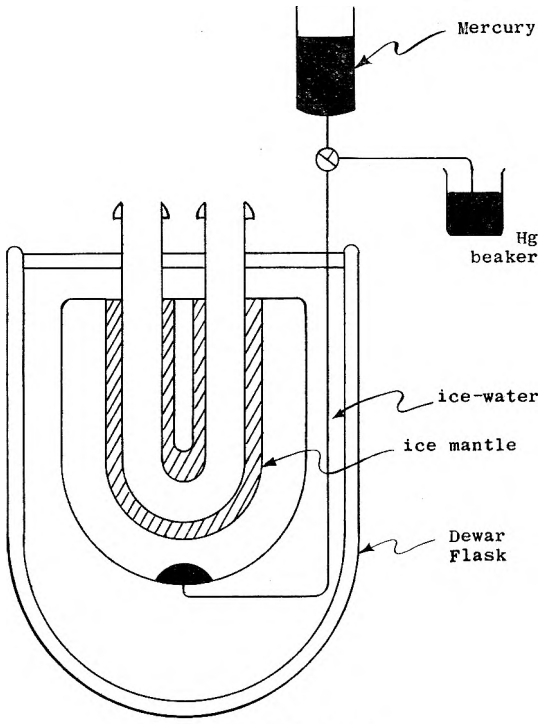

Fig. 1.—Ice calorimeter.

was attained. The ozone productivity indicated a minimum oxygen atom concentration of about 5%. The U-trap was replaced by the ice-calorimeter, which contained about 1 g. of palladium black. The calorimeter required several hours to attain thermal equilibrium. The heat leak was determined to be insignificant over the period of each experiment. The discharge was started with the same oxygen flow rate which was used previously. It was shown that all the atoms recombined in the calorimeter since cooling the exit stream with liquid nitrogen did not produce any detectable quantities of ozone. The beaker of mercury was weighed prior to and after each experiment of 5 min. duration. It required about 30 min. to reattain thermal equilibrium. The oxygen atom flow was determined by means of the equation

$$\text{mmoles O/min.} = (64.6)(W_{Hg})/58.9t$$

where 64.6 is the absolute calibration factor in cal./g. of mercury drawn into the system, 58.9 cal./mmole is the heat of recombination of oxygen atoms, and W_{Hg} is the weight of mercury drawn into the system in time t (minutes) due to the melting of the ice-mantle.

The oxygen atom flow (mmoles/min.) was

$$0.094 \pm 0.008 \text{ (90\% confidence level)} \quad \text{(a)}$$

by the ozone condensation method ($O + O_2 \rightarrow O_3$) and

$$0.092 \pm 0.010 \text{ (90\% confidence level)} \quad \text{(b)}$$

by the calorimetric procedure.

Discussion

Since the precision of the iodimetric method for ozone assay is considerably greater than that indicated in (a), the variation noted within each series of experiments is attributed to the variation of oxygen atom output by the discharge apparatus. It was noted that when the discharge was operated continuously (longer than 30 min.), the variation in ozone output by the condensation method was ±1.7%. Unfortunately it was not possible with the present calorimeter to achieve this steady-state condition with the calorimeter in place due to the large quantity of ice that would melt during the approach to the steady-state condition. The conclusion is warranted, within the precision of these measurements, that in the low-temperature condensation (−196°) of a stream of oxygen atoms (about 5%) in oxygen a quantitative yield of ozone is obtained. It is not known at what concentration of oxygen atoms this conclusion would have to be modified due to possible competing reactions, such as $O + O + M \rightarrow O_2 + M$.

Elias, Ogryzlo, and Schiff[9] have shown that calorimetric methods such as the use of a silver probe in the gas phase give an assay value which is 25% higher than that given by the nitrogen dioxide titration method. This was attributed to the presence of metastable oxygen molecules ($^1\Delta_g$, +22.5 kcal.). Harteck and Kopsch,[2] on the other hand, have indicated that only ground state oxygen is present several centimeters from the discharge tube. The possibility of having a small percentage of metastable oxygen molecules in the present oxygen atom–oxygen molecule stream cannot be discounted but it is likely that most of the metastable molecules have degraded prior to entry into the calorimeter.

The low temperature reaction

$$O + O_2 + (M) \xrightarrow{-196^\circ} O_3 + (M)$$

discussed in this paper undoubtedly involves a heterogeneous wall reaction, where M is the cold wall. The rate constant (10^{14} cc.^{2}/mole^2 sec.) for the homogeneous reaction[10,11] would not permit the rapid reaction noted in the present research if the reaction were a homogeneous three-body reaction. The ozone condenses in a narrow ring (about 1 cm. wide) in the liquid nitrogen trap.

(9) L. Elias, E. A. Ogryzlo, and H. I. Schiff, *Can. J. Chem.*, **37**, 1690 (1959).

(10) H. B. Urbach, R. Wnuk, J. A. Wojtowicz, and J. A. Zaslowsky, Abstracts of Papers, 137th Meeting of the American Chemical Society Atlantic City, 1959. p. 47-s.

(11) S. W. Benson and A. Axworthy, *J. Chem. Phys.*, **26**, 1718 (1957).

X-RAY STUDIES ON THE PRODUCT OF THE REACTION OF ATOMIC HYDROGEN AND LIQUID OZONE[1]

BY F. MARTINEZ, J. A. WOJTOWICZ, AND J. A. ZASLOWSKY

Olin Mathieson Chemical Corporation, Organics Division, New Haven, Connecticut

Received September 10, 1962

The reaction of hydrogen atoms with liquid ozone at −196° reportedly leads to the formation of a hydrogen superoxide.[2] The product decomposes above −120° to give equimolar quantities of oxygen and hydrogen peroxide.[2] The existence of this superoxide has been questioned by Giguere[3] on the basis of infrared studies.

Hydrogen peroxide deposited from the vapor at −196 and −269° has been examined by X-ray techniques.[4] The substance is amorphous and does not exhibit the sharp lines characteristic of the crystalline material. Crystallization occurs spontaneously at −183°. The

(1) This work was supported by the Directorate of Research Analysis, Air Force Office of Scientific Research, Holloman Air Force Base, under Contract AF 49(638)-1137.

(2) N. I. Kobozev, I. I. Skorokhodov, L. I. Nekrasov, and E. I. Makarova, *Zh. Fiz. Khim.*, **31**, 1843 (1957).

(3) P. Giguere and D. Chin, *J. Chem. Phys.*, **31**, 1685 (1959).

(4) L. H. Bolz, F. A. Maner, and H. S. Peiser, unpublished data; *cf.* A. M. Bass and H. P. Broida, "Formation and Trapping of Free Radicals, Academic Press Inc., New York, N. Y., 1960, p. 322.

TABLE I

X-RAY DIFFRACTION DATA

This research						Tsentsiper[5]			
Hydrogen atom–ozone product			50% H_2O_2						
At −196°	Warmed to −183° (cooled to −196°)	Warmed to −78° (cooled to −196°	At −196°	Warmed to −183° (cooled to −196°)	Hydrogen atom–ozone product ground at −196°	Ice at −196°	H_2O_2–ice at −196°	X-Ray powder data file[a] ice $(H_2O)_2$ [b]
			[e]	4.0[1]	3.90	3.42	4.09(H_2O_2)	3.93
3.9[1]	3.9[1]	3.9[1]		3.6[6]	3.45	2.70	3.49	3.68
3.6[7]	3.6[7]	3.6[7]		3.4[2]	2.65	2.30	3.07(H_2O_2)	3.45
3.4[1]	3.4[1]	3.4[2]		3.0[6](H_2O_2)	2.26	2.10	2.63	2.68
2.6[4]	2.6[4]	3.0[6](H_2O_2)		2.9[3]	2.08	[h]	2.25	2.26
[c]	[c]	2.6[4]		2.6[9]	1.93		2.06	2.07
		[d]		2.5[7]	[g]		1.87	1.92
				2.2[1]			1.79	1.52
				2.0[6]			1.67	1.37
				[f]			1.51	1.30
							1.49	
							[i]	

[a] ASTM Powder Data File, American Society for Testing Materials, Card No. 1-0509, Philadelphia, Pa., 1960. [b] Temperature unknown. [c] Strong halo at about 3.4 Å. [d] Weak halo at about 3.4 Å. [e] No distinct lines; very weak halo at about 3.4 Å. [f] Very weak halo at about 3.4 Å. [g] Intense halo at about 3.43 Å. [h] Extremely weak halo at about 3.65 Å. [i] Extremely weak halo at about 3.21 Å.

change in crystalline structure is accompanied by a strong exothermic effect.

This paper describes the results obtained by X-ray examination of the hydrogen atom–liquid ozone product in an attempt to identify the postulated product.

Experimental

1. **Equipment. A. Electric Discharge Apparatus.**—Hydrogen atoms were prepared by subjecting a stream of molecular hydrogen at 1–2 mm. pressure to an electric discharge produced by a microwave unit (Raytheon Manufacturing Co., Waltham, Mass.). The apparatus was operated at a frequency of 2450 Mc. at 125 watts. The discharge was initiated by means of a Tesla coil.

B. X-Ray Apparatus.—A Norelco unit (North American Philips Co., Inc., Mount Vernon, N. Y.), equipped with a 1 mm. collimator and a flat plate camera, was operated at 40 kv. and 20 ma. CuKα radiation was employed as the X-ray source.

C. Cooling System.—The capillary containing the sample under examination was maintained at −196° by means of a liquid nitrogen spray (Fig. 1).

2. **Preparation of Samples.**—The product was prepared by the reaction of hydrogen atoms with a thin layer of ozone contained in a U-trap cooled to −196°.[2] When the reaction was complete, as evidenced by the disappearance of the blue color of ozone, the discharge was discontinued and dry nitrogen gas was admitted into the vacuum system to 760 mm. The U-trap was disconnected from the system and filled immediately with liquid nitrogen. The sample was removed from the walls of the U-trap by means of a spatula and transferred to a dish filled with liquid nitrogen. The thin-walled glass capillary tubes employed (Caine Scientific Co., Chicago, Ill.) were sealed at one end and coated with collodion for increased strength. The sample was ground, then introduced into the constricted portion of the capillary tube. The tube was sealed with a drop of water and transferred to the aluminum support cooled to −196°.

Samples of aqueous hydrogen peroxide (30–70 volume %) were allowed to vaporize into the vacuum system at 1 mm. pressure. The vapors were condensed in a U-trap cooled to −196° and the frozen condensate was transferred to the capillary in the manner described.

The samples were exposed to X-ray radiation for 1 hr. in all experiments.

Results and Discussion

Examination of the hydrogen atom–liquid ozone product at −196° revealed an intense halo at about 3.4 Å. in addition to low intensity ice lines at 3.9[1], 3.6[7], 3.4[1], and 2.6[4] Å.

When the product was warmed to −183°, by transferring rapidly from a liquid nitrogen refrigerant to liquid oxygen, and then recooled to −196° after about 10 min., no detectable change in the diffraction pattern was noted.

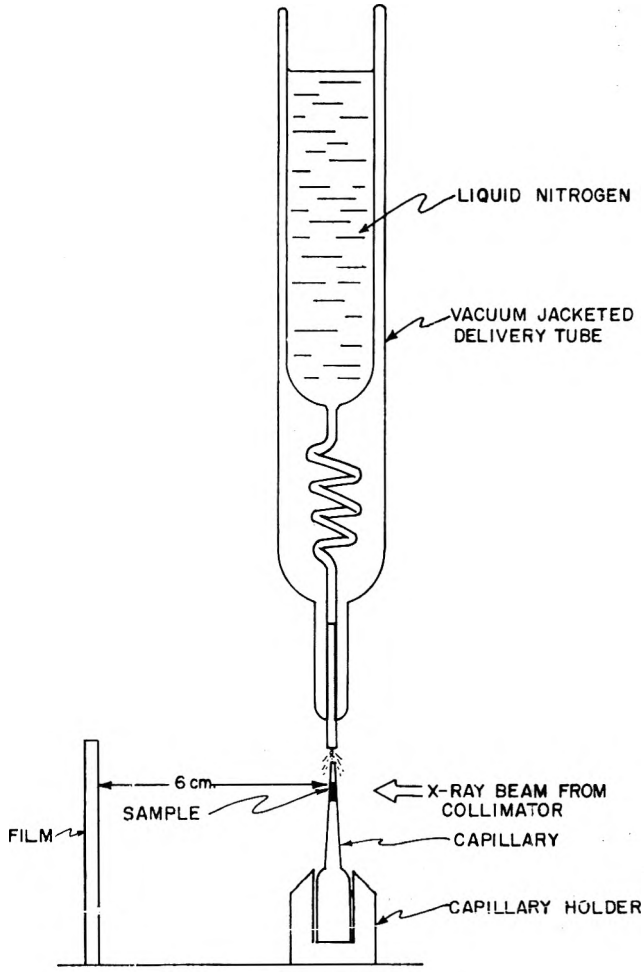

Figure 1.

In contrast to these results when the condensed water–hydrogen peroxide product was examined at −196°, no discrete lines were noted. An ill defined halo at about 3.4 Å. was visible. When this sample was warmed to −183° and recooled to −196° after 10 min. at the higher temperature, ice as well as hydrogen per-

oxide lines were noted. This result confirms the results of Bolz and co-workers.[4]

When the product of the hydrogen atom–ozone reaction was warmed to about −78° and recooled to −196°, the X-ray pattern revealed the presence of hydrogen peroxide. The data indicate that: (1) The hydrogen atom–ozone product as formed does not contain hydrogen peroxide. (2) Upon warming to −78° hydrogen peroxide is produced. (3) The product is not crystalline and its presence is most likely manifested by the intense halo at about 3.4 Å.

The data presented in this report are in general agreement with those reported by Tsentsiper[5] and support the contention that a new peroxide species is formed by the reaction of atomic hydrogen with ozone. Hydrogen peroxide forms on warming. This is in agreement with the view of Kobozev,[2] who postulates the reactions

$$H\cdot + O_3 \xrightarrow{-196^\circ} H_2O_4 \xrightarrow{-115^\circ} H_2O_2 + O_2$$

The data of Tsentsiper,[5] as well as that obtained in the present research, are summarized in Table I.[6]

The intent of these experiments was to determine if a superoxidic species could be detected in the frozen matrix of the hydrogen atom–ozone reaction product and to ascertain whether hydrogen peroxide is present. Although no proof for the presence of a new peroxide was obtained, the absence of hydrogen peroxide suggests that a higher unstable peroxide is the progenitor of the hydrogen peroxide which is detected on warming.

Acknowledgment.—The authors wish to thank G. P. Tilley of the Central Analytical Laboratories of Olin Mathieson Chemical Corporation for the interpretation of the X-ray diffraction patterns.

(5) A. B. Tsentsiper, M. A. Danilova, A. S. Kanisheva, and A. I. Gorbanev, *Russ. J. Inorg. Chem.*, **4**, 886 (1959)(in English).

(6) The concentration of hydrogen peroxide examined corresponds with ultimate concentrations of residual peroxide reported by Kobozev.[2]

THE VINYL + H SPLIT IN THE MERCURY SENSITIZED PHOTOLYSIS OF ETHYLENE

BY P. KEBARLE

Department of Chemistry, University of Alberta, Edmonton, Alberta, Canada

Received September 10, 1962

The primary reaction in the mercury sensitized decomposition of ethylene has been subject to a number of investigations. For some time there was no agreement whether the decomposition proceeds by a molecular elimination of hydrogen (1) or a split to vinyl radicals and hydrogen atoms (2). It then was shown by Cvetanovic[1,2] that the decomposition proceeds predominantly and possibly entirely by (1).

It is the purpose of the present paper to show that the split to vinyl also occurs but only to about 4% of the total decomposition.

The experiments were at 55°, done in a flow system attached to a mass spectrometer.[3,4] The general experimental procedures have been described elsewhere.[5] The ethylene was co-decomposed with an excess of mercury dimethyl-d_6. Recombination of the methyl radicals, produced by the decomposition of the mercury dimethyl,[4] with vinyl should lead to the formation of propylene-d_3. This methyl radical technique has been used with success in several cases.[5,6] Due to the relatively high ratio of radical to substrate concentrations no complicating radical attack on the substrate occurs, but the secondary reactions are predominantly radical–radical interactions.

In a typical run the decomposition of 1 μ[7] of ethylene with 10 μ of mercury dimethyl-d_6 led to the formation of 0.288 μ of acetylene and 0.02 μ of propylene, in addition to 3 μ of ethane (C_2D_6) and 0.02 μ of propane (C_3D_8). The latter two products originate from the decomposition of the mercury dimethyl.[4] The hydrogen and methane formed were not determined. The reaction products were analyzed directly with the mass spectrometer and also trapped at liquid nitrogen temperature and separated by gas chromatography. The propylene was collected and readmitted into the mass spectrometer. It was found to consist of 85% $C_3H_3D_3$, 7% $C_3H_2D_4$, and 8% $C_3H_4D_3$. The propylene-d_3 must be formed by the recombination of CD_3 with vinyl radicals. If all the vinyl radicals originate from the primary reaction 2, then the acetylene and propylene measured should give the relative rates of reactions 1 and 2. Accordingly, the primary decomposition should proceed 96% by (1) and 4% by (2). Since some of the methyl–vinyl encounters will lead to disproportionation the above 4% are rather a lower limit.

In order to show that the vinyl radicals are produced in the primary reaction the following two experiments were made.

Ethylene at a constant pressure of 1 μ was co-decomposed with variable amounts of mercury dimethyl. The propylene-d_3 formed and the ethylene decomposed were measured. The results are shown in Fig. 1. Plotted is the propylene-d_3 formed, over the ethylene decomposed *vs.* the square root of ethane formed. The latter quantity should be a measure of the methyl radical concentration. It is seen that the curve levels off at about 5%, in approximate agreement with the previous result. From the results it is evident that a fixed amount of vinyl radicals is available which is independent of the methyl radical concentration.

In the second experiment a mixture of C_2H_4 and C_2D_4 in the ratio 1:1.8 was decomposed (total pressure 1 μ), together with 10 μ of mercury dimethyl-d_6. The propylene was analyzed as described previously. The following result was obtained: C_3H_6, 2.4; C_3H_5D, 1.6; $C_3H_4D_2$, 3.3; $C_3H_3D_3$, 33.0; $C_3H_2D_4$, 4.5; C_3HD_5, 3.2; C_3D_6, 52.0%. The presence of all these isotopes is difficult to understand. Nevertheless the two major products are $C_3H_3D_3$ and C_3D_6, as expected from the proposed mechanism.

It is concluded that reaction 2 constitutes about 4% of the total primary decomposition. The results of Cvetanovic[1] are compatible with the operation of reaction 2. Thus the hydrogen obtained from a mixture of C_2H_4 and C_2D_4 contained 1.2% HD (the remainder being H_2 and D_2). Doubling this figure to take into account the recombination of H and D to H_2 and D_2

(1) R. J. Cvetanovic and A. B. Callear, *J. Chem. Phys.*, **23**, 1182 (1955).

(2) A. B. Callear and R. J. Cvetanovic, *ibid.* **24**, 873 (1956).

(3) F. P. Lossing, D. G. H. Marsden, and J. B. Farmer, *Can. J. Chem.*, **34**, 701 (1956).

(4) P. Kebarle, *J. Phys. Chem.*, **67**, 351 (1963).

(5) M. Avrahami and P. Kebarle, *ibid.*, **67**, 354 (1963).

(6) R. F. Pottie, A. G. Harrison, and F. P. Lossing, *Can. J. Chem.*, **39**, 102 (1961).

(7) μ = microns, partial pressure.

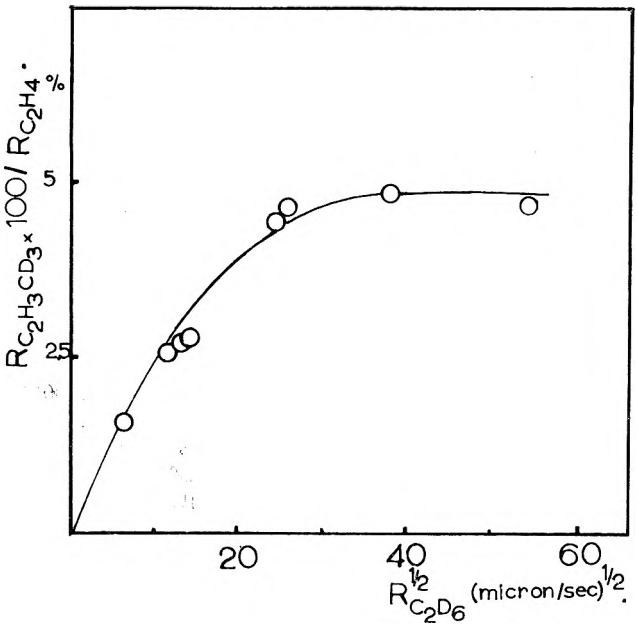

Fig. 1.—Formation of $C_2H_3CD_3$ from C_2H_3 and CD_3 radicals in function of CD_3 radical concentration.

one obtains 2.4%. Possibly some of the H and D also were lost by addition to the ethylene.

Robb and co-workers[8] in a recent investigation of the mercury sensitized decomposition of ethylene also conclude that the decomposition (2) participates as a minor reaction. A number of secondary reactions occur in the system studied by these authors and so it cannot be determined accurately to what extend (2) occurs, but an addition of the suitable products leads to a figure of about 3%.

LeRoy and Steacie[9] in an early investigation in the temperature range 25–350° suggested that at room temperature (2) occurs to a very minor extent if at all but that its importance increases with temperature so that, particularly in the range 200–350°, it begins to contribute significantly as a primary process. Since hydrogen atoms can be produced by the Hg-sensitized decomposition of hydrogen originating from reaction 1, it is not completely certain that the authors could really distinguish between (2) and ethylene disappearance initiated by H atom addition. Thus it would have been of interest to confirm LeRoy and Steacie's high temperature results. Such experiments were not attempted, however, since the present apparatus does not lend itself easily to conversion for work at such temperatures.

(8) J. R. Majer, B. Mile, and J. C. Robb, *Trans. Faraday Soc.*, **57**, 1342 (1960).

(9) D. J. LeRoy and E. W. R. Steacie, *J. Chem. Phys.*, **10**, 676 (1942).

THE IONIZATION CONSTANT OF 4-AMINO-3-METHYLBENZENESULFONIC ACID FROM 0 TO 50° BY MEANS OF ELECTROMOTIVE FORCE MEASUREMENTS

BY STANLEY D. MORRETT AND D. F. SWINEHART

Department of Chemistry, University of Oregon, Eugene, Oregon

Received September 12, 1962

The ionization constants and related thermodynamic quantities for sulfanilic acid,[1] metanilic acid,[2] and orthanilic acid[3] have been reported previously from this Laboratory. The present paper reports experimental data for the determination of the ionization constant of 4-amino-3-methylbenzenesulfonic acid. All these acids are zwitterions with large charge separations and all show a remarkably small entropy of ionization.

Using conductance measurements, Ostwald[4] has determined the ionization constant of this acid at 25° and found it to be 7.53×10^{-4}.

By analogy with the other aminobenzenesulfonic acids, we assume that this acid is a zwitterion and thus that the ionization reaction is

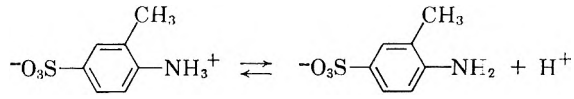

The general method of investigation is that developed by Harned and co-workers.[5] The cells were of the type Pt, H_2/HAts(m_1^0), NaAts(m_2^0), NaCl(m_3^0)/AgCl–Ag where HAts and NaAts are the acid and its sodium salt, respectively, and m_1^0, m_2^0, m_3^0 are weight molalities. By elimination of $m_{H^+}\gamma_{H^+}$ from the cell potential equation

$$E = E^0 - \frac{2.30259RT}{F} \log m_{H^+} m_{Cl^-} \gamma_{H^+} \gamma_{Cl^-} \quad (1)$$

and the thermodynamic ionization constant expression

$$K = \frac{m_{H^+} m_{Ats^-} \gamma_{H^+} \gamma_{Ats^-}}{m_{HAts} \gamma_{HAts}} \quad (2)$$

there results the relation

$$\frac{(E - E^0)F}{2.30259RT} + \log \frac{m_{HAts} m_{Cl^-}}{m_{Ats^-}} = -\log K - \log \frac{\gamma_{HAts} \gamma_{Cl^-}}{\gamma_{Ats^-}} \quad (3)$$

The ionization constant of HAts is so large (about 7×10^{-4}) that m_{Ats^-} and m_{HAts} are not equal to the stoichiometric values and these values must be corrected for the ionization of the acid

$$m_{HAts} = m^0_{HAts} - m_{H^+}$$

$$m_{Ats^-} = m^0_{NaAts} + m_{H^+}$$

where m^0 represents the stoichiometric molalities.

Values of m_{H^+} were calculated by solving eq. 1 for log m_{H^+} and using the Debye–Hückel limiting law for the activity coefficients. This procedure required two successive approximations. The left-hand side of eq. 3 was plotted as a function of ionic strength and extrapolated to zero ionic strength, yielding a first approximation for $-\log K$. Using this value of K, new values of m_{H^+} were computed from eq. 2 and again the left-hand side of eq. 3 was extrapolated to zero ionic strength using the method of least squares.

Three complete cycles of these calculations were made

(1) R. O. MacLaren and D. F. Swinehart, *J. Am. Chem. Soc.*, **73**, 1822 (1951).

(2) R. D. McCoy and D. F. Swinehart, *ibid.*, **76**, 4708 (1954).

(3) R. N. Diebel and D. F. Swinehart, *J. Phys. Chem.*, **61**, 333 (1957).

(4) W. Ostwald, *Z. physik. Chem.*, **3**, 412 (1889).

(5) H. S. Harned and B. B. Owen, "The Physical Chemistry of Electrolytic Solutions," 2nd Ed., Reinhold Publ. Corp., New York, N. Y., 1950.

TABLE I

ELECTROMOTIVE FORCE OF THE CELL

$Pt,H_2/HAts(m_1^0)$, $NaAts(m_2^0)$, $NaCl(m_3^0)/AgCl$–Ag,

ABSOLUTE VOLTS

μ (approx.)	0.01[a]	0.02	0.03[a]	0.04	0.048	0.055	0.08	0.01
m_1^0	0.0050601_0	0.010373_0	0.015571_0	0.019464_0	0.024683_0	0.026652_0	0.037584_0	0.049946_0
m_2^0	$.0050719_0$	$.010389_0$	$.015562_0$	$.019429_0$	$.024182_0$	$.028595_0$	$.037462_0$	$.050087_0$
m_3^0	$.0050346_0$	$.010418_0$	$.015595_0$	$.019426_0$	$.024133_0$	$.028653_0$	$.037482_0$	$.050141_0$
t, °C.								
0	0.55101	0.53285	0.52297	0.51750	0.51197	0.50852	0.50241	0.49605
5	.55124	.53250	.52237	.51679	.51111	.50766	.50132	.49471
10	.55134	.53199	.52165	.51585	.51009	.50659	.50008	.49336
15	.55133	.53139	.52083	.51478	.50893	.50530	.49866	.49184
20	.55125	.53061	.51981	.51370	.50766	.50392	.49721	.49016
25	.55094	.52975	.51868	.51236	.50625	.50236	.49551	.48840
30	.55064	.52870	.51751	.51109	.50484	.50071	.49384	.48652
35	.55031	.52777	.51620	.50968	.50331	.49907	.49206	.48450
40	.54998	.52687	.51490	.50825	.50169	.49730	.49012	.48240
45	.54949	.52585	.51347	.50665	.49986	.49534	.48813	.48023
50	.54912	.52469	.51203	.50509	.49813	.49345	.48596	.47800

[a] One cell only.

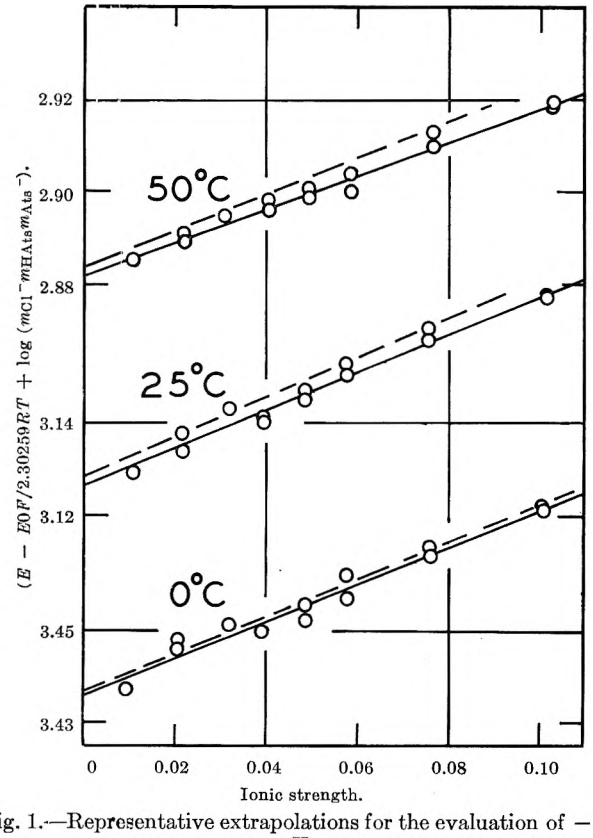

Fig. 1.—Representative extrapolations for the evaluation of $-\log K$.

at each temperature, the third being virtually identical with the second.

The values of E^0 used were those of Harned and Ehlers[6] recalculated by Swinehart,[7] along with $2.30259RT/F$, in absolute volts using the constants of Bearden and Watts.[8]

Experimental

The materials and reagents other than the aminomethylbenzenesulfonic acid were purified in a manner similar to that described by MacLaren and Swinehart.[1]

Eastman White Label 4-amino-3-methylbenzenesulfonic acid was recrystallized three times from water. The compound fresh from the bottle turned distilled water a yellowish pink color when the solution was heated to boiling. Charcoal was added and the mixture was filtered. The filtrate was colorless and the acid crystallized out as white crystals. A solution of HAts in water at room temperature appeared to be somewhat light sensitive although it did not show evidence of being air sensitive. Before each run the acid was dried in an oven for 2 hr. at 130°. Each batch of the acid was analyzed by titration with CO_2-free sodium hydroxide standardized *vs.* NBS potassium acid phthalate using a pH meter to determine the end point at pH 7.5 for the acid and 8.4 for the acid phthalate. All titrations were made with a weight buret. In general, the precision of duplicate titrations was a few parts in 10,000.

The cells, electrodes, measuring instruments, and procedure of the measurements were the same as those described by MacLaren and Swinehart.[1]

Results

The results are shown in Table I. Each potential difference is the average of 16 potential measurements obtained from two cells run in duplicate except where noted in the table by the footnote "one cell only." These latter values are the averages of eight measurements from one cell only. The average deviation of the potentials from any one cell from the mean potential was about 0.05 mv. The mean potentials of duplicate cells showed an average difference of about 0.06 mv. and no difference was greater than 0.17 mv.

The data were treated as indicated in the introduction. Representative extrapolations of the first and last approximations of the left-hand side of eq. 3 to zero ionic strength yielding thermodynamic values of $-\log K$ are shown in Fig. 1.

The resulting values of $-\log K$ were fitted by the equation

$$-\log K = A/T + CT - D \qquad (4)$$

using the method of least squares yielding the values 1363.39, 0.0043010, and 2.7280 for A, C, and D, respectively. The calculated values of $-\log K$ using these constants together with the experimental values of $-\log K$ and the values of K itself are shown in Table II. The standard deviation of the calculated values $-\log K$ from the experimental values is 0.0017 in $-\log K$. This quantity is calculated from the equation

$$\text{standard deviation} = \left(\frac{\Sigma\Delta^2}{n - c}\right)^{1/2}$$

where Δ is the deviation of the experimental point from

(6) H. S. Harned and R. W. Ehlers, *J. Am. Chem. Soc.*, **55**, 2179 (1933).
(7) D. F. Swinehart, *ibid.*, **74**, 1100 (1952).
(8) J. A. Bearden and H. M. Watts, *Phys. Rev.*, **81**, 73 (1951).

TABLE II

THE IONIZATION CONSTANT OF 4-AMINO-3-METHYLBENZENESULFONIC ACID IN WATER FROM 0 TO 50°

t (°C.)	$K \times 10^4$	$-\log K^a$ Obsd.	Calcd. (eq. 4)	$\Delta \times 10^4$
0	3.664	3.4361	3.4380	+19
5	4.261	3.3705	3.3698	− 7
10	4.944	3.3059	3.3048	−11
15	5.698	3.2443	3.2427	−16
20	6.525	3.1854	3.1836	−18
25	7.475	3.1264	3.1271	+ 7
30	8.496	3.0708	3.0732	+24
35	9.554	3.0198	3.0217	+19
40	10.642	2.9730	2.9726	− 4
45	11.869	2.9256	2.9256	0
50	13.119	2.8821	2.8808	−13

[a] Standard deviation in $-\log K = 0.0017$.

the calculated curve in the direction of the $-\log K$ axis, n is the number of experimental points and c is the number of constants in the equation.[9]

Discussion

By means of the usual relations[10] standard thermodynamic quantities for the ionization reaction may be calculated from the constants in eq. 4. In Table III a comparison is shown of the standard thermodynamic values for four aminobenzenesulfonic acids.

TABLE III

COMPARISON OF $-\log K$ AND THERMODYNAMIC VALUES FOR THE DISSOCIATION OF FOUR AMINOBENZENESULFONIC ACIDS AT 25°

Acid	$-\log K$	ΔF^0, kcal.	ΔH^0, kcal.	ΔS^0, kcal. deg.$^{-1}$	ΔC_p^0, kcal. deg.$^{-1}$
Orthanilic[3]	2.459	3353	2365	−3.32	−18.6
Metanilic[2]	3.738	5977	5960	−0.57	− 7.7
Sulfanilic[1]	3.277	4403	4295	−0.37	− 7.1
4-Amino-3-methylbenzenesulfonic	3.126	4266	4489	+0.75	−11.7

These entropies of ionization are much more positive (*i.e.*, less negative) than almost all other acids, *e.g.*, acetic,[11] $\Delta S_{298}^0 = -22.1$ e.u.; propionic,[11] $\Delta S_{298}^0 = -22.8$ e.u.; glycine,[11] $\Delta S_{298}^0 = -6.9$.

Interpreted in terms of the ideas of Frank and Evans[12] and of Powell and Latimer,[13] these entropies are negative largely because the free ions "freeze" or orient much larger members of water molecules than do the neutral molecules. As the dipole moment of the neutral molecules increases, the neutral molecules orient more water molecules and the entropy change on ionization becomes less. From simple structural considerations, the dipole moments of the three isomeric acids in Table III increase in the order orthanilic, metanilic, sulfanilic and the values of ΔS^0 increase correspondingly. In this light, it is reasonable to suppose that the dipole moment of 4-amino-3-methylbenzenesulfonic acid is larger still and the entropy increase is still more positive. This latter acid has an algebraically positive value of ΔS^0 ionization at 25° and is the only acid to show a positive value of this property that is known at this time.

(9) T. B. Crumpler and J. H. Yoe, "Chemical Computations and Errors," John Wiley and Sons, Inc., New York, N. Y., 1940, p. 222.
(10) Reference 5, p. 583.
(11) Reference 5, p. 514.
(12) H. S. Frank and M. W. Evans, *J. Chem. Phys.*, **13**, 507 (1945).
(13) R. E. Powell and W. M. Latimer, *ibid.*, **19**, 1139 (1951).

Acknowledgment.—This research was supported by a grant from the Graduate Council of the University of Oregon.

HYDROGEN IODIDE AS RADICAL ACCEPTOR IN THE THERMAL DECOMPOSITION OF GASEOUS ORGANIC IODIDES

BY R. K. BOYD, G. W. DOWNS, J. S. GOW, AND C. HORREX

Chemistry Department, St. Salvator's College, The University, St. Andrews, Fife, Scotland

Received September 12, 1962

A study of the thermal decomposition of trifluoromethyl iodide showed that the formation of C_2F_6 could not be suppressed by the use of a reasonable excess of toluene as radical acceptor. When hydrogen iodide was substituted for toluene and used in about the same concentrations, the formation of C_2F_6 ceased and the yield of iodine was greatly increased. This extra iodine production was not caused by either of the new possible reactions, $2HI \rightarrow H_2 + I_2$ or $HI + CF_3I \rightarrow CF_3H + I_2$. The former reaction was eliminated by performing appropriate blank experiments, and by calculations using well established data on the decomposition of hydrogen iodide; the second reaction was not significant in our conditions, since the yield of iodine became zero order in hydrogen iodide for sufficiently high concentrations of the latter. This can be illustrated by the following data for experiments using 0.24 mm. CF_3I in about 4.3 mm. N_2 as carrier gas, 758°K., and 0.50 sec. contact time in a flow system

Partial pressure HI, mm.	0.031	0.072	0.131	0.476	1.08	1.97	3.72
% dec. of CF_3I	2.19	3.20	3.95	5.65	6.5	6.6	6.45

Similar behavior was observed in static experiments of 3 hr. duration at 522°K. with 8 mm. CF_3I and 0–560 mm. HI. We conclude that the increased yield of iodine results from the efficient capture of the CF_3 radicals by hydrogen iodide and the prevention of their reaction with iodine. The assumption that, in the presence of excess HI, the reaction proceeds by the simple steps

$$CF_3I \longrightarrow CF_3^- + I^- \ldots \quad (1)$$

$$CF_3^- + HI \longrightarrow CF_3H + I^- \ldots \quad (2)$$

$$2I \rightleftharpoons I_2 \ldots \quad (3)$$

did not yield satisfactory kinetic data and tests showed the decomposition to be catalyzed by iodine atoms

$$I^- + CF_3I \longrightarrow CF_3^- + I_2 \ldots \quad (4)$$

This autocatalysis is masked by the reverse of (4) unless an excess of HI is present; with moderate concentrations of HI the competition of HI and I_2 for CF_3 radicals can give the appearance of a second order (CF_3I + HI) process. Using excess HI and analyzing the data in terms of the above scheme, it was found that the iodine production was due almost entirely to (4) for the lower temperature and higher pressure conditions of the static system. In the case of the flow system (1) played a much greater part particularly at high temperatures and low partial pressures. By combining data from the

flow and static systems we obtain,[1] over the large temperature range of 440–758°K.

$$\log k_4 \text{ (l. mole}^{-1} \text{ sec.}^{-1}) = 10.8 - (17{,}600/2.303RT)$$

Assuming the energy of activation for the reverse of (4) to be 0–1 kcal. we derive $D(CF_3\text{–}I) = 53.5$ kcal.; the previously published values of this quantity cover the wide range 57 ± 4,[3a] 48.5 ± 5,[3b] and 43.7[3c] kcal.

The behavior of $C_6H_5CH_2I$ was very similar[2] to that of CF_3I, but in the absence of HI the processes analogous to (1) and (4) reached approximate equilibrium positions. Under these circumstances the dimerization of benzyl radicals was rate determining for the decomposition of the iodide. With excess of HI we obtained conditions in which benzyl radicals did not reform benzyl iodide and determined the energy of activation for the process $I + C_6H_5CH_2I \rightarrow I_2 + C_6H_5CH_2-$. The use of this value of 4.1 kcal. agrees with $D(C_6H_5\text{-}CH_2\text{–}I) = 40.6$ kcal. and with an enthalpy of formation of the benzyl radical of 43 kcal.

Two recent publications[4,5] have criticized Ogg's evidence[6] for a bimolecular process (RI + HI) in the reaction of iodides and hydrogen iodide and have proposed schemes of the type quoted above for CF_3I. The recalculation of Ogg's work in these terms has proved complicated because of inadequate primary experimental data in his paper. We have extended our work above, which was done by titrimetric methods, and have applied a photometric technique capable of measuring iodine concentration down to 10^{-6} mole $l.^{-1}$ and using automatic recording of the data. Using methyl iodide and excess hydrogen iodide, this technique showed clearly the autocatalytic nature of the reaction and the data permitted the use of an integrated rate expression. The velocity constant for $I + CH_3I \rightarrow I_2 + CH_3-$ is given by $\log k$(l. mole^{-1} sec.$^{-1}$) $= 10.71 - (19{,}200/2.303RT)$, which agrees with $D(CH_3\text{–}I) = 53.6$ kcal.

The above findings show that a reaction of type (4) plays a major part in the thermal decomposition of three organic iodides, one of which has a relatively weak C–I bond while the other two have strong bonds. It seems probable that it is important for all iodides.

(1) G. W. Downs, Thesis, St. Andrews, 1959.
(2) J. S. Gow, Thesis, St. Andrews, 1961.
(3) (a) J. B. Farmer, I. H. S. Henderson, F. P. Lossing, and D. G. H. Marsden, *J. Chem. Phys.*, **24**, 348 (1956); (b) V. H. Dibeler, R. M. Reese, and F. L. Mohler, *J. Research Natl. Bur. Standards*, **57**, 113 (1956); (c) J. Marriott and J. D. Craggs, *J. Electronics*, **1**, 405 (1956).
(4) J. H. Sullivan, *J. Phys. Chem.*, **65**, 722 (1961).
(5) S. W. Benson and E. O'Neal, *J. Chem. Phys.*, **34**, 514 (1961).
(6) R. A. Ogg, Jr., *J. Am. Chem. Soc.*, **56**, 526 (1934).

COMPLEXING OF MAGNESIUM WITH BICARBONATE[1]

BY P. B. HOSTETLER

U. S. Geological Survey, Menlo Park, California

Received September 14, 1962

In 1941 Greenwald[2] noted that the pH values of mixtures of $KHCO_3$ and MCl_2 (M = Mg or Ca) were significantly lower than the pH values of mixtures of $KHCO_3$ and KCl of the same ionic strength ($\mu \sim 0.15$). Greenwald[2] suggested that the lower pH values were due to the formation of $MHCO_3^+$ and MCO_3^0, and by assuming a concentration quotient for the reaction

$$MHCO_3^+ \rightleftarrows H^+ + MCO_3^0$$

Greenwald[2] was able to derive concentration quotients for $MHCO_3^+$ and MCO_3^0. Halla and Van Tassel,[3] in a series of experiments carried out under a constant P_{CO_2} of 1 atm., were unable to detect the presence of these complexes, but Greenwald[4] has pointed out that the solutions used by Halla and Van Tassel[3] were so dilute that the amount of complexing that occurred would not be expected to indicate a sensible difference between measured pH values and pH values expected on the basis of no complexing. Recently, Garrels, *et al.*,[5] have found that all complexing of magnesium with carbonate can be accounted for as $MgCO_3^0$, and that the pK_{diss} for this complex is 3.40 ± 0.02 at 25°. Garrels, *et al.*,[5] also detected magnesium–bicarbonate complexing, but were unable to derive a specific model(s). The experimental work described here was designed to determine the nature and extent of complexing of magnesium with bicarbonate in the presence of negligible magnesium–carbonate complexing.

Experimental

In two separate experiments carbon dioxide was bubbled through 200 ml. of 0.0233 *m* $MgCl_2$ solution in a sealed glass vessel at 1 atm. Increments of carbonate-free barium hydroxide were added, as bubbling continued, to increase the solubility of carbon dioxide. Temperature within the vessel was maintained at 25 ± 0.4°. A Beckman No. 4990-72 glass electrode and a No. 19730 Ag–AgCl palladium junction reference electrode were used with a Beckman model V pH meter for pH measurements. Individual pH measurements were accurate to ±0.02 pH unit. Experimental results are shown in Table I.

TABLE I

(1) Ml. solution	(2) pH	(3) μ	(4) $2m_{Mg_t} \times 10^3$	(5) $2m_{Ba_t} \times 10^3$	(6) $m_{HCO_3^-} \times 10^3$
200	3.88	0.0700	46.6	...	0.145
202	4.00	.0695	46.2	0.0929	0.191
205	4.18	.0686	45.5	0.229	0.288
260	5.43	.0612	35.9	5.42	5.09
270	5.63	.0636	34.5	8.70	8.08
300	5.91	.0690	31.1	17.22	15.51

(7) $(2m_{Ba_t} + m_{H^+} - m_{HCO_3^-}) \times 10^3$	(8) $m_{Mg^{++}} \times 10^3$	(9) $\gamma_{Mg^{++}}$	(10) $\gamma_{HCO_3^-}$	(11) $MgHCO_3^+$ pK_{diss}
0.014	23.3	0.453	0.813	0.96
.022	23.05	.453	.813	1.05
.020	22.7	.454	.814	0.83
.344	17.60	.468	.819	0.90
.623	16.63	.464	.817	1.00
1.71	13.84	.454	.813	1.24

Results

The experimental conditions were such that there was no sensible formation of CO_3^{-2} or $MgCO_3^0$ ($pH < 6$, $MgCl_2 \sim 0.02$ *m*). In the absence of any magnesium or barium complexing

$$m_{Cl^-} = 2m_{Mg^{++}},\ m_{Ba^{++}} = m_{Ba_t} \qquad (1)$$

Ba_t represents total barium in solution. Substitution of (1) in the equation for electrostatic balance yields

$$2m_{Ba_t} + m_{H^+} - m_{HCO_3^-} = 0 \qquad (2)$$

(1) Publication authorized by the Director, U. S. Geological Survey.
(2) I. Greenwald, *J. Biol. Chem.*, **141**, 789 (1941).
(3) F. Halla and R. Van Tassel, *J. Phys. Chem.*, **62**, 1135 (1958).
(4) I. Greenwald, *ibid.*, **63**, 1328 (1959).
(5) R. M. Garrels, M. E. Thompson, and R. Siever, *Am. J. Sci.*, **259**, 24 (1961).

If magnesium or barium bicarbonate complexing occurs, and is assumed to be due to the formation of one or more complexes of the type $M(HCO_3)_n^{2-n}$ (M = Mg or Ba); the total extent of the complexing may be derived from the equation for electrostatic balance

$$\sum_{n=1}^{\infty} n m_{M(HCO_3)_n^{2-n}} = 2m_{Ba_t} + m_{H^+} - m_{HCO_3^-} \quad (3)$$

$m_{HCO_3^-}$ was calculated directly from measured pH values by assuming $P_{CO_2} = f_{CO_2} = 1$ atm., and using Latimer's[6] pK_1 value of 6.38 for carbonic acid. Activity coefficients for H^+ and Mg^{++} were calculated from published $\gamma_{\pm}$ values for KCl,[6] HCl,[7] and $MgCl_2$,[7] using the assumption that $\gamma_{\pm KCl} = \gamma_{Cl^-} = \gamma_{K^+}$. Values used for $\gamma_{HCO_3^-}$ are those determined by Walker, *et al.*,[8] from $KHCO_3$ solutions.

Complexing of magnesium with bicarbonate was found to occur because the sum expressed by the right-hand side of eq. 3 (column 7, Table I) was positive, even with the initial absence of $Ba(OH)_2$. From Table I the following data may be noted as $Ba(OH)_2$ was added: (a) No significant variations in μ, (b) m_{Ba_t}, $m_{HCO_3^-}$, and $\sum_{n=1}^{\infty} n m_{M(HCO_3)_n^{2-n}}$ increased by more than two orders of magnitude at approximately the same rate, and, (c) m_{Mg_t} decreased slightly by dilution. Since, at constant μ

$$m_{M(HCO_3)_n^{2-n}} \propto \frac{(m_{M^{++}})(m_{HCO_3^-})^n}{n} \quad (4)$$

and $m_{M^{++}} \cong m_{M_t}$ (the ratio of complex M to M_t is low), it can be seen that only an $MgHCO_3^+$ model and no $Ba(HCO_3)_n^{2-n}$ model nor $Mg(HCO_3)_n^{2-n}$ ($n > 1$) model is consistent with conditions (b) and (c) and proportionality (4) above.

The pK_{diss} values for $MgHCO_3^+$ given in Table I are calculated thermodynamic dissociation constants. It was assumed that for these relatively dilute solutions $\gamma_{MgHCO_3^+} = \gamma_{HCO_3^-}$. The six tabulated values yield an average pK_{diss} value of 1.00, but the last pK value shown ($pK = 1.24$), corresponding to the largest amount of added $Ba(OH)_2$, is significantly higher than the other five values, and may reflect the formation of a modest amount of $Ba(HCO_3)_n^{2-n}$. Averaging the five other values leads to a pK_{diss} value of 0.95 ± 0.1.

Using a pK_{diss} value of 3.40[5] for $MgCO_3^0$ yields an equilibrium constant of $10^{-7.86}$ for the reaction

$$MgHCO_3^+ \rightleftarrows MgCO_3^0 + H^+ \quad (5)$$

Greenwald's[2] experiments were conducted at a nearly constant μ of 0.15, and at this μ

$$(\alpha_{H^+})(m_{MgCO_3^0})/(m_{MgHCO_3^+}) = 10^{-8.00} \quad (6)$$

The corresponding value of (6) assumed by Greenwald[2] was $10^{-8.50}$, which he used to calculate a concentration quotient for $MgHCO_3^+$ of 0.17. If the value of $10^{-8.00}$ is used instead, the concentration quotient is 0.37. The corresponding pK value for the thermodynamic dissociation constant is 0.86; a value within the limit of error of the present determination.

(6) W. M. Latimer, "Oxidation Potentials," Second Ed., Prentice-Hall, New York, N. Y., 1952, pp. 135, 355.

(7) H. S. Harned and B. B. Owen, "The Physical Chemistry of Electrolytic Solutions," Third Edition, Reinhold Publ. Corp., New York, N. Y. 1958, pp. 252, 716, 738.

(8) A. G. Walker, V. B. Bray, and J. Johnston, *J. Am. Chem. Soc.*, **49**, 1235 (1927).

ON THE ORIGIN OF THE DIPOLE MOMENT OF TETRAZOLES

By John B. Lounsbury[1]

Department of Chemistry, Illinois Institute of Technology, Chicago 16, Illinois, and IBM Development Laboratory, Poughkeepsie, New York

Received September 24, 1962

The various substituted tetrazoles have received much attention with regard to activity upon the central nervous system.[2] In an examination of possible relationships between dipole moments of these compounds and their physiological activities, it has been remarked that " . . . the origin and nature of the tetrazole ring moment still is incompletely understood."[3] With regard to this comment, a theoretical examination of the dipole moment of tetrazole has been undertaken. A further point of consideration for the present study has been the uncertainty of the tetrazole structure.[4] The location of one of the hydrogens is not known, either of the structures I or II being possible. It is conceivable that a tautomeric equilibrium might exist between structures I and II. Both of these structures have been considered in the present study.

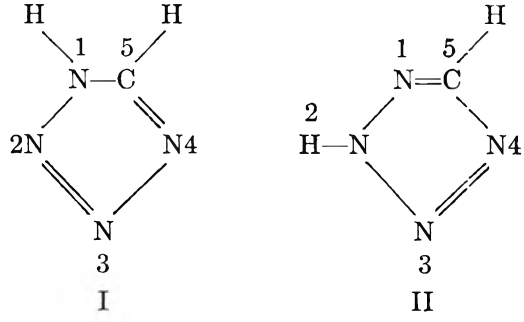

Theory

It is customary to construct molecular dipole moments by vectorial summations of dipoles associated with bonds, those associated with the polarization of non-bonding electrons and the dipoles arising from asymmetry of the distribution of delocalized (pi) electrons.[5] In this study the bond moments for the sigma bonds in the ring have been taken to be zero. This has been done previously for the C–N and C–C bonds in pyridine[6] and pyrrole.[7] This is essentially an assumption that electronegativity differences of ring atoms are accommodated exclusively by the mobile pi electrons. The moment of the C^+–H^- bond has been taken as 2.23 D., which is the value calculated by Hameka and Liquori[6] for pure sp^2 hybridization on carbon. The value of the N^+–H^- dipole moment used is the 1.64 D. value calculated by Hamano and Hameka[7] for the N–H bond in pyrrole.

(1) IBM Predoctoral Fellow at I.I.T.

(2) F. W. Schueler, S. C. Wang, R. M. Featherstone, and E. G. Gross, *J. Pharmacol. Exptl. Therapy*, **97**, 266 (1949).

(3) A. I. Popov and R. D. Holm, *J. Phys. Chem.*, **66**, 158 (1962).

(4) M. H. Kaufman, F. M. Ernsberger, and W. S. McEwan, *J. Am. Chem. Soc.*, **78**, 4197 (1956).

(5) See, for example, R. Daudel, R. Lefebvre, and C. Moser, "Quantum Chemistry," Interscience Publ., New York, N. Y., 1959, pp. 201-213.

(6) H. F. Hameka and A. M. Liquori, *Mol. Phys.*, **1**, 9 (1958).

(7) H. Hamano and H. F. Hameka, *Tetrahedron*, **18**, 985 (1962).

The lone pair dipole moments on the pyridine type nitrogens has been handled by the procedure developed by Hameka and Liquori.[6,8] If the hybridized lone pair orbital is normalized to unity and defined by eq. 1, then the lone pair dipole will point in the x-direction,

$$t_{LP} = as_N + bp_{xN} \quad (1)$$

and the moment is given by eq. 2. The functions s_N

$$\mu_{LP} = 4ab \int s_N x p_{xN}\, d\tau \quad (2)$$

and p_{xN} are the Slater type orbitals defined by eq. 3.

$$s_N = \left(\frac{\zeta_N}{\pi}\right)^{1/2} r \exp(-\zeta_N r) \quad (3)$$

$$p_{xN} = \left(\frac{\zeta_N}{\pi}\right)^{1/2} x \exp(-\zeta_N r)$$

Hameka and Liquori take $\zeta_N = 1.95$ according to the Slater–Zener rules.[9,10] Thus μ_{LP} is found to be given by eq. 4. If it is assumed that the state of hybridiza-

$$\mu_{LP} = 4ab \frac{5}{2\zeta_N \sqrt{3}} (4.80)(0.5292) = 7.521ab \text{ D.} \quad (4)$$

tion of the two bonding orbitals on the nitrogen of interest are equal and that these hybrids lie along the lines connecting this nitrogen with the two bonded neighboring nuclei X and Y, Hameka and Liquori[8] have shown how the values of a and b depend on the state of hybridization of the lone pair orbital. The values of a and b are given by eq. 5, where ϕ is the X–N–Y angle. When $\phi = 120°$ there is pure sp^2 hy-

$$a = \sqrt{\frac{-(\cos\phi + 1)}{\cos\phi - 1}} \qquad b = \sqrt{\frac{2\cos\phi}{\cos\phi - 1}} \quad (5)$$

bridization on the nitrogen and $\mu_{LP} = 3.55$ D. The largest value μ_{LP} can obtain is 3.76 D. at $\phi = 109° 28' 15''$. The value of μ_{LP} is not a very sensitive function of ϕ around this maximum, and the value may be taken as 3.69 ± 0.07 D. for $103° \leqslant \phi \leqslant 116°$.

The pi electron distributions were calculated using the I.I.T. SCF-MO Univac 1105 computer program.[11] The details of this program and the parameters it utilizes are thoroughly discussed in the indicated references and will not be repeated here. It is worthwhile to note that, using the pi electron distributions obtained by Miller, *et al.*,[11c] very good theoretical values for the dipole moments of pyridine and pyrrole are realized. In the case of pyridine, a dipole moment due to the pi electrons $\mu_\pi = 0.60$ D. is found, which points in the same direction as the lone pair moment and opposes the net C^+–H^- moment (calculated using the pyridine geometry of Bak, *et al.*[12]) of 2.18 D. Thus $\mu = \mu_\pi + \mu_{LP} - \mu_{CH} = 0.60 + 3.69 - 2.18 = 2.11$ D. This compares favorably with the experimental value[13] of 2.15 ± 0.07 D. For pyrrole $\mu_\pi = 1.25$ D. is obtained which is in the opposite direction of the N^+–H^- moment and in the same direction as the net C^+–H^- moment of 2.24 D. (calculated using the pyrrole geometry of Bak, *et al.*[14]). Thus $\mu = 1.25 - 1.64 + 2.24 = 1.85$ D., in good agreement with the measured value[15] of 1.84 ± 0.08 D.

Results and Discussion

The tetrazole geometry was approximated by a regular pentagon with sides of 1.32 Å. since no experimental information regarding the geometry of unsubstituted tetrazole was found in the literature. The molecule is assumed to be planar, although this may not be correct for the N–H bond. The pi electron distributions found for structures I and II are given in Table I. This leads to values of the pi moment of $\mu_{\pi I} = 1.17$ D. and $\mu_{\pi II} = 0.49$ D. If the x-axis selected passes through ring positions 2 and 5 and the y-axis through ring position 1, then the directions of pi moments are such that the x and y components are those given in Table II. Also given in Table II are the x and y components of the C^+–H^- moment, the net lone pair moment, and the N^+–H^- moment. The individual x and y components are summed to give those components of the total dipole moment. The total dipole moments calculated for the two tetrazole structures are $\mu_I = 5.22$ D. and $\mu_{II} = 1.63$ D. The experimental dipole moment of tetrazole is 5.11 D.[15]

TABLE I

SCF–MO PI ELECTRON DISTRIBUTIONS IN TETRAZOLE[a]

Position	Structure I	Structure II
1	1.7447	1.2489
2	1.2260	1.7050
3	0.9331	1.0767
4	1.2412	1.1367
5	0.8550	0.8328

[a] Tetrazole assumed to be planar and to have a regular pentagon geometry with 1.32 Å. sides.

TABLE II

COMPONENTS OF THE DIPOLE MOMENT OF TETRAZOLE[a]

	Structure I		Structure II	
	x-Component	y-Component	x-Component	y-Component
μ_{CH}	2.12	0.69	2.12	0.69
μ_{NH}	1.64	0	−1.56	0.51
μ_{LP}	−3.51	−4.84	0	−2.29
μ_π	−0.49	−1.06	0.45	−0.19
μ_{total}	−0.24	−5.21	1.01	−1.28

[a] x-Axis taken to pass through ring positions 2 and 5, y-axis to pass through ring position 1. Tetrazole assumed to have a regular pentagon geometry and to be planar.

It is felt that these results are of considerable value in representing the gross features of the origin of the dipole moment of tetrazole. The close agreement of the theoretical and experimental dipole moments of pyridine and pyrrole should not be taken to indicate that a similar close agreement necessarily exists between the theoretical and experimental values for tetrazole. This is especially true considering the uncertainty in the tetrazole geometry. The results show that a large

(8) H. F. Hameka and A. M. Liquori, *Proc. Koninkl. Ned. Akad. Wetenschap.*, **B59**, 242 (1956).

(9) J. C. Slater, *Phys. Rev.*, **36**, 57 (1930).

(10) C. Zener, *ibid.*, **36**, 51 (1930).

(11) (a) O. W. Adams, Ph.D. Thesis, Illinois Institute of Technology, 1961; (b) O. W. Adams and P. G. Lykos, *J. Chem. Phys.*, **34**, 1444 (1961); (c) R. L. Miller, P. G. Lykos, and H. N. Schmeising, *J. Am. Chem. Soc.*, **84**, 4623 (1962).

(12) B. Bak, K. Hansen-Nygaard, and J. Rastrip-Andersen, *J. Mol. Spectry.*, **2**, 361 (1958).

(13) B. B. DeMore, W. S. Wilcox, and J. H. Goldstein, *J. Chem. Phys.*, **22**, 876 (1954).

(14) B. Bak, D. Christensen, L. Hansen, and J. Rastrip-Andersen, *ibid.*, **24**, 720 (1956).

(15) A. D. Buckingham, B. Harris, and R. J. LeFevre, *J. Chem. Soc.*, 1623 (1953).

(16) K. A. Jensen and A. Friediger, *Kgl. Danske Videnskab. Selskab. Mat.-Fys. Medd.*, **20**, (20) 1 (1943).

part of the difference in the dipole moments of 1- and 2-substituted tetrazoles lies in the difference in the vectorial sums of the lone pair moments and the sigma bond moments, these moments more nearly canceling each other in the case of 2-substitution. A much smaller part of the difference is due to the reduced pi moment of the 2-substituted compounds. Although the accuracy of the calculated dipole moments does not warrant it, and although the existence of a tautomeric equilibrium between structures I and II has never been demonstrated, it is of interest to calculate an equilibrium constant between structures I and II, if for no other reason than it is not known that this has ever been done before for tetrazole. It is found that, for a mixture of I and II to produce an apparent dipole moment of 5.11 D., $K_{eq} = [I]/[II] = 31.3$, which corresponds to tetrazole existing as 97% in form I. Considering the probable numerical accuracy, this calculation may be considered consistent with tetrazole existing exclusively in the 1-protonated tautomer. This predominance of structure I is in agreement with the results of a recent n.m.r. study[17] of the chemical shifts of the carbon bound proton on the tetrazole ring in tetrazole and N-alkylated tetrazoles. It is also consistent with the observation[4] that 1-ethyltetrazole has a dipole moment of 5.64 while 2-ethyltetrazole has a moment of 2.64 D.

Acknowledgment.—The author is indebted to Dr. P. G. Lykos of this Laboratory for suggesting this problem and for encouragement and advice during the study. The author wishes to thank Drs. R. L. Flurry and R. L. Miller of this Laboratory for many stimulating discussions. This work was carried out with a generous grant of computer time by the Illinois Institute of Technology. The author is especially indebted to the International Business Machines Corporation for a fellowship from the IBM Special Education Program.

(17) D. W. Moore and A. G. Whittaker, *J. Am. Chem. Soc.*, **82**, 5007 (1960).

COMMUNICATION TO THE EDITOR

RELATIVE MOBILITIES OF LIKE-CHARGED IONS IN FUSED SALTS[1a]

Sir:

We wish to call attention to an observation, based on results of other workers as well as our own experimental data, that appears sufficiently general to warrant consideration in any attempt to understand the mechanism of ionic transport in fused salts.

Our experiments were initiated in an effort to throw light on the reasons for the characteristic behavior of conductivity isotherms in fused salt mixtures. The equivalent conductance generally is found to deviate negatively from additivity of the pure salt values.[1b] Because this behavior is particularly striking in the case of LiCl–KCl mixtures, we have been running Hittorf-type transference experiments to determine the relative mobilities of the two cations at various concentrations. Electrolysis between chlorine electrodes is carried out in accordance with experimental procedures analogous to those described elsewhere for this type of experiment.[2] By choosing the common ion (in this case chloride) as reference, we can use the results of such experiments to compare the two cation mobilities.[3] A useful quantity for this purpose is the per cent mobility difference $100(\mu_{13} - \mu_{23})/\mu_{23}$ which is equal to $[100(\phi_1 - E_1)/\phi_2 E_1]$, and thus independent of the conductivity of the mixture. Here E_1 is the equivalent fraction of the faster-moving ion and ϕ_2 $(= 1 - \phi_1)$ is the quantity designated ϕ by Aziz and Wetmore.[2b] The latter quantity has been represented by P elsewhere.[3]

Our preliminary results (described below) immediately recalled the corresponding observations of Duke and Victor[4] on the system $LiNO_3$–KNO_3, and prompted a search of the literature for all data indicative of relative mobilities of like-charged ions in binary fused salt mixtures. What follows is summary of our findings.

Hittorf-type experiments have yielded the following results.

LiCl–KCl.—At 2.2 mole per cent KCl Klemm and co-workers[2a] found the lithium ion more mobile than potassium by about 15%. Our results are in good agreement here, but are also consistent with the rather surprising observation of Chemla and coworkers[5] on relative cation mobilities in the LiBr–KBr and NaBr–KBr systems. These workers reported that in spite of the substantially higher conductances of the pure salts LiBr and NaBr, K^+ is the more mobile cation at concentrations greater than about 30 mole % KBr. Similarly we find that Li^+ moves faster than K^+ up to about the same concentration, after which the potassium ion becomes more mobile. Since our work permits quantitative evaluation of relative ionic mobilities, however, an even more striking observation has emerged from our results. We find that over the entire range of our measurements to date (3 to 50 mole % KCl) the relative mobility difference is never greater than about 13%. Thus, it is the similarity rather than the difference of cation mobilities that seems most noteworthy; the total conductivity of the mixture changes by more than 50% in the same region.[6]

$LiNO_3$–KNO_3.—Duke and Victor[4] reported the two cation mobilities equal within experimental error (presumably about 10%) over the entire range of composition.

$AgNO_3$–$NaNO_3$.—Although data of Aziz and Wet-

(1) (a) This work is supported by a contract with the U. S. Atomic Energy Commission. Financial assistance from a National Science Foundation pre-doctoral fellowship is also gratefully acknowledged. (b) See, for example, R. W. Laity, *J. Chem. Educ.*, **39**, 67 (1962), and references cited therein.

(2) (a) A. Klemm, H. Hintenberger, and P. Hoernes, *Z. Naturforsch.*, **2a**, 245 (1947); (b) P. M. Aziz and F. E. W. Wetmore, *Can. J. Chem.*, **30**, 779 (1952).

(3) R. W. Laity, *J. Chem. Phys.*, **30**, 682 (1959); *Ann. N. Y. Acad. Sci.*, **79**, 997 (1960).

(4) F. R. Duke and G. Victor, *J. Am. Chem. Soc.*, **83**, 3337 (1961).

(5) J. Perie, M. Chemla, and N. Gignoux, *Bull. Soc. Chim. France*, 1249 (1961).

(6) E. R. Van Artsdalen, and I. S. Yaffe, *J. Phys. Chem.*, **59**, 118 (1955).

more[2b] give silver ion mobilities up to 18 times greater than sodium, more recent work by Duke, Laity, and Owens[7] concludes that the cation mobilities are identical within experimental error over the entire range of composition. Employing improved experimental techniques, subsequent determinations carried out in this Laboratory[8] appear to confirm the latter, the greatest mobility difference observed in the range covered by Aziz and Wetmore being 7%.

$AgNO_3$–AgCl.—The results of Hill and Wetmore[9] for solutions rich in $AgNO_3$ indicated a much greater mobility (relative to Ag^+) for nitrate than for chloride ion, the difference being about 80% at 77 and at 88 mole % $AgNO_3$. This is not consistent, however, with the more recent result of Monse,[10] who reported a chloride ion mobility only 8% higher than that of nitrate at 66 mole % $AgNO_3$.

$PbCl_2$–KCl.—Lorenz and co-workers twice[11] reported figures for equimolar mixtures from which a value of ϕ can be calculated. Both results are in good agreement, and imply a potassium mobility more than three times greater than that of lead. From the data of Duke and Fleming,[12] however, K^+ moves only about 50% faster at this composition, the greatest mobility difference in the system being 77% at 63 mole % KCl. Nevertheless, compared with the other systems above these are still large differences. Although this completes the summary of Hittorf measurements, other experimental results on $PbCl_2$–KCl are discussed below.

E.m.f. measurements on concentration cells with transference are another source of relevant information.[13] When like-charged ions have equal mobilities, the "junction potentials" in such cells are equal to zero,[7b] so that e.m.f. values can be predicted from those found in cells without transference (or from suitable thermodynamic data). The following systems have been studied in this way.

AgCl–KCl, AgBr–KBr, AgBr–NaBr, AgBr–LiBr, AgBr–$PbBr_2$.—Junction potentials in every one of these systems were found to be less than 1 mv. by Murgelescu and co-workers.[14] The results indicate in each case that cation mobilities are equal within a few per cent over the entire range of composition studied (50 mole % or more). These workers deserve credit for pointing out the apparent generality of this phenomenon in the systems they studied.[14,15]

$PbCl_2$–KCl.—The junction potentials in cells containing 20 and 60 mole % KCl (measured *vs.* pure $PbCl_2$) also were found by Murgelescu and Marchidan to be zero within 1 mv.[16] This appears to contradict the results of Duke and Fleming[12] whose data predict a junction potential of about 11 mv. for the latter cell.

AgCl–NaCl, NaCl–KCl, and AgCl–KCl.—On the basis of his e.m.f. measurements Stern[17] concluded that cation mobilities are probably equal over the entire composition range in each of these systems. Unfortunately, however, the results may be invalidated by the use of a porous graphite separator that "shorts out" any potential drop across the liquid–liquid junction.[13]

The moving boundary method is known to have been attempted once in a fused-salt system, with the following results.

$PbCl_2$–LiCl.—Klemm and Monse[18] reported that Li^+ is the more mobile cation at all concentrations, the disparity reaching 140% at 95 mole % $PbCl_2$.

In summary, data reported for at least 10 different systems are consistent with the hypothesis that the mobilities of like-charged ions in fused-salt mixtures are equal within about 10 to 15% at all concentrations. If the moving-boundary results for $PbCl_2$–LiCl are valid, the latter system constitutes the only clearcut counter-example to this generalization we have found in the literature.

(7) (a) F. R. Duke, R. W. Laity, and B. Owens, *J. Electrochem. Soc.*, **104**, 299 (1957); (b) R. W. Laity, *J. Am. Chem. Soc.*, **79**, 1849 (1957).

(8) R. W. Laity, unpublished results.

(9) S. Hill and F. E. W. Wetmore, *Can. J. Chem.*, **32**, 864 (1954).

(10) E. Monse, *Z. Naturforsch.*, **12a**, 526 (1957).

(11) (a) R. Lorenz and G. Fausti, *Z. Elektrochem.*, **10**, 630 (1904); (b) R. Lorenz and W. Ruckstuhl, *Z. anorg. allgem. Chem.*, **52**, 51 (1907).

(12) F. R. Duke and R. A. Fleming, *J. Electrochem. Soc.*, **106**, 130 (1959).

(13) R. W. Laity, in "Reference Electrodes: Theory and Practice," Ed. by D. J. G. Ives and G. J. Janz, Academic Press, New York, N. Y., 1961.

(14) I. G. Murgelescu and D. I. Marchidan, *Russ. J. Phys. Chem.*, **34**, 1196 (1960).

(15) I. G. Murgelescu and S. Sternberg, *Discussions Faraday Soc.*, **32**, 107 (1961).

(16) I. G. Murgelescu and D. I. Marchidan, *Acad. rep. populare Romine, studii cercetari chim.*, **8**, 383 (1960).

(17) K. H. Stern, *J. Phys. Chem.*, **63**, 741 (1959).

(18) A. Klemm and E. Monse, *Z. Naturforsch.*, **12a**, 319 (1957).

FRICK CHEMICAL LABORATORY
PRINCETON UNIVERSITY
PRINCETON, N. J.
RICHARD W. LAITY
CORNELIUS T. MOYNIHAN

RECEIVED DECEMBER 27, 1962